NIST GCR 96-701

ENERGY-BASED METHOD FOR LIQUEFACTION POTENTIAL EVALUATION, PHASE I - FEASIBILITY STUDY

FILE COPY
DO NOT TAKE

Building and Fire Research Laboratory
Gaithersburg, MD 20899

NIST

United States Department of Commerce
Technology Administration
National Institute of Standards and Technology

NIST GCR 96-701

ENERGY-BASED METHOD FOR LIQUEFACTION POTENTIAL EVALUATION, PHASE I - FEASIBILITY STUDY

Farhang Ostadan
Nan Deng
Ignacio Arango

Bechtel Corporation
San Francisco, CA 94119

A Report to:

U.S. Department of Commerce
Technology Administration
National Institute of Standards and Technology
Building and Fire Research Laboratory
Gaithersburg, MD 20899

August 1996

U.S. Department of Commerce
Michael Kantor, *Secretary*
Technology Administration
Mary L. Good, *Under Secretary for Technology*
National Institute of Standards and Technology
Arati Prabhakar, *Director*

ABSTRACT

This report presents the results of the first phase of a three-phase study on the development and application of the energy-based method for prediction of the liquefaction potential of sandy soils. The formulation of the method is based on the convolution of the basic elements from both the "stress" and "strain" approaches and is very flexible in incorporating the special characteristics of ground motion such as the near-field effects. The feasibility phase consists of the tasks: 1) to collect and synthesize laboratory data; 2) to perform ground response analyses at the Wildlife Site, which suffered a massive ground liquefaction failure during the Superstition Hills Earthquake; and finally 3) to compare and to assess the differences between the field and the laboratory data. Even though the scope of the feasibility study did not permit cyclic testing of the soil samples from the Wildlife Site, the correlation of the field response data and the applicable laboratory data are strong. The results of this phase suggest that development of an energy-based method to evaluate liquefaction potential is feasible.

KEYWORDS: building technology; liquefaction; strain energy; earthquake; ground response; cyclic testing; laboratory measurements; ground motion; pore pressure.

ACKNOWLEDGMENT

The study was sponsored by the National Institute of Standards and Technology (NIST) under the Contract No. 50SBNB5C8640. Drs. R. Andrus and R. Chung of NIST provided support and guidance throughout the course of the study. The authors gratefully acknowledge the support and supply of laboratory data by Dr. J. Koester from the U. S. Army Corps of Engineers. Dr. S. Glaser from the Colorado School of Mines generously provided the data recorded at the Wildlife Site and made many helpful suggestions during the course of the study. The report was reviewed by Mr. M. Lewis, geotechnical manager, in Bechtel National.

TABLE OF CONTENTS

PAGE

ABSTRACT **i**

ACKNOWLEDGMENT **ii**

TABLE OF CONTENTS **iii**

LIST OF TABLES **vi**

LIST OF FIGURES **vii**

LIST OF SYMBOLS **xv**

UNITS CONVERSION FACTORS **xvi**

CHAPTER 1 **1-1 through 1-3**

INTRODUCTION **1-1**

1.1 BACKGROUND 1-1

1.2 PURPOSE 1-2

1.3 OVERVIEW OF THE REPORT 1-2

CHAPTER 2 **2-1 through 2-36**

COLLECTION AND SYNTHESIS OF LABORATORY DATA **2-1**

2.1 STRAIN ENERGY COMPUTATION 2-1

2.2 CYCLIC TRIAXIAL TESTS ON MONTEREY NO. 0 SAND, PERFORMED AT THE UNIVERSITY OF CALIFORNIA, BERKELEY (UCB) 2-2

2.3 CYCLIC TRIAXIAL TESTS ON SOIL SAMPLES FROM THE SAVANNAH RIVER SITE, PERFORMED AT THE UNIVERSITY OF CALIFORNIA, BERKELEY (UCB) 2-3

2.4 CYCLIC TORSIONAL TESTS ON SOIL SAMPLES, PERFORMED AT THE UNIVERSITY OF COLORADO (UOC) 2-4

PAGE

2.5 CYCLIC TRIAXIAL TESTS ON SOIL SAMPLES FROM THE NORTHRIDGE SITE, PERFORMED AT THE UNIVERSITY OF CALIFORNIA, BERKELEY (UCB) 2-4

2.6 CYCLIC TRIAXIAL TESTS ON CLEAN SANDS PERFORMED AT THE WAYNE STATE UNIVERSITY (WSU) 2-5

2.7 SUMMARY DATA BY FIGUEROA et al. 2-5

2.8 SUMMARY OF ALL LABORATORY DATA 2-6

CHAPTER 3 **3-1 through 3-20**

WILDLIFE SITE: SOILS AND EARTHQUAKE DATA **3-1**

3.1 BACKGROUND 3-1

3.2 WILDLIFE SITE 3-1

3.3 STRATIGRAPHY AND SOIL PROPERTIES AT THE WILDLIFE SITE 3-1

3.4 INSTRUMENTATION AT THE WILDLIFE SITE 3-2

3.5 RECORDED EARTHQUAKE DATA 3-3

CHAPTER 4 **4-1 through 4-64**

GROUND RESPONSE ANALYSES AND COMPARISON WITH THE LABORATORY DATA **4-1**

4.1 METHODS OF ANALYSES 4-1

4.2 RESULTS OF THE GROUND RESPONSE ANALYSES USING THE COMPUTER PROGRAM SHAKE 4-2

4.3 RESULTS OF THE GROUND RESPONSE ANALYSES USING THE COMPUTER PROGRAM BDESRA (MODIFIED DESRA) 4-3

PAGE

4.4 RESULTS OF THE GROUND RESPONSE ANALYSES BASED ON DIRECT INTERPOLATION OF RECORDED MOTIONS 4-4

4.5 RESULTS OF THE GROUND RESPONSE ANALYSES USING THE COMPUTER PROGRAM SHAKE AND EPRI SOIL CURVES 4-5

4.6 COMPARISON OF THE RESULTS OF GROUND RESPONSE ANALYSES 4-5

4.7 COMPARISON OF THE RESULTS OF GROUND RESPONSE ANALYSES WITH THE LABORATORY DATA 4-6

CHAPTER 5 **5-1 through 5-2**

SUMMARY AND RECOMMENDATION **5-1**

CHAPTER 6 **6-1 through 6-4**

REFERENCES **6-1**

APPENDIX A **A-1 through A-42**

LABORATORY TESTS ON MONTEREY NO. 0 SAND, PERFORMED AT THE UNIVERSITY OF CALIFORNIA, BERKELEY

APPENDIX B **B-1 through B-46**

LABORATORY TESTS ON SOIL SAMPLES FROM THE SAVANNAH RIVER SITE, PERFORMED AT THE UNIVERSITY OF CALIFORNIA, BERKELEY

APPENDIX C **C-1 through C-20**

LABORATORY TESTS ON SOIL SAMPLES, PERFORMED AT THE UNIVERSITY OF COLORADO

APPENDIX D **D-1 through D-18**

LABORATORY TESTS ON SOIL SAMPLES FROM THE NORTHRIDGE SITE, PERFORMED AT THE UNIVERSITY OF CALIFORNIA, BERKELEY

LIST OF TABLES

Table 2.1 Summary of the Cyclic Triaxial Test Data on Monterey No. 0 Sand Performed at University of California, Berkeley

Table 2.2 Average Material Properties at the SRS Site

Table 2.3 Summary of the Cyclic Triaxial Test Data on SRS Soil Samples Performed at University of California, Berkeley

Table 2.4 Summary of the Cyclic Torsional Test Data on Clean and Silty Sands Performed at University of Colorado

Table 2.5 Summary of the Cyclic Triaxial Test Data on Northridge Samples Performed at University of California, Berkeley

Table 2.6 Summary of the Cyclic Triaxial Test Data on Clean Sands Performed at Wayne State University

Table 3.1 Summary of the Wildlife Site Earthquake Data and Recorded Time Histories

Table 4.1 Summary of Strain Energy Computation from Ground Response Analyses (November 24, 1987, 1315 GMT Earthquake)

LIST OF FIGURES

Figure 1.1 Relationships Between Stress Ratio Causing Liquefaction and $(N_1)_{60}$ Values for Silty Sands for M = 7-1/2 Earthquakes (Seed et al., 1985)

Figure 2.1 Typical Time History Records of a Strain-Controlled Cyclic Triaxial Test

Figure 2.2 A Typical Plot of Shear Stress-Strain Hysteresis Loops Developed During Cyclic Triaxial Tests

Figure 2.3 Grain Size Distribution for Monterey No. 0 Sand (Arango, 1994)

Figure 2.4 Strain Energy at Liquefaction Onset as a Function of Relative Density for Monterey No. 0 Sand - UCB Data

Figure 2.5 Strain Energy at Liquefaction Onset as a Function of Frequencies of Loading for Monterey No. 0 Sand - UCB Data

Figure 2.6 Generalized Subsurface Soil Profile at the SRS Site

Figure 2.7 Typical Grain Size Distribution Curve for Tobacco Road Soil Material - SRS (Riemer and Seed, 1994)

Figure 2.8 Strain Energy as a Function of Confining Pressure for SRS Soil Samples - UCB Data

Figure 2.9 Grain Size Distribution of Silty Sands - UOC Samples (Koester, 1992)

Figure 2.10 Strain Energy at Liquefaction Onset as a Function of Relative Density for Clean Sands - UOC Data

Figure 2.11 Strain Energy at Liquefaction Onset as a Function of Confining Pressure for Silty Sands - UOC Data

Figure 2.12 Grain Size Distribution Curves for the Northridge Site Soil Samples (Arango and Migues, 1996)

Figure 2.13 Strain Energy at Liquefaction Onset as a Function of Relative Density for the Northridge Samples - UCB Data

Figure 2.14 Grain Size Distribution Curves for Monterey No. 0 and Kasumigaura Sands (Al-Khatib, 1994)

Figure 2.15 Strain Energy at Liquefaction Onset as a Function of Relative Density for Monterey No. 0 and Kasumigaura Sands - WSU Data

Figure 2.16 Effect of Cyclic Loading Types on Strain Energy at Liquefaction Onset for Monterey No. 0 Sand - WSU Data

Figure 2.17 Effect of Cyclic and Transient Loading on Strain Energy at Liquefaction Onset for Monterey No. 0 Sand - WSU Data

Figure 2.18 Grain Size Distribution Curves for Soil Samples for the Lower San Fernando Dam and the Reid Bedford Sand (Figueroa et al., 1995)

Figure 2.19 Comparison of Strain Energy at Liquefaction Onset for All Test Groups - Clean Sands

Figure 2.20 Comparison of Strain Energy at Liquefaction Onset for All Test Groups - Silty Sands

Figure 3.1 Map of California with Locations of Parkfield and Wildlife Liquefaction Arrays

Figure 3.2 Wildlife Liquefaction Array - Geotechnical Properties (Bennett et al., 1984)

Figure 3.3 Main Geological Units at the Wildlife Site and Their Geotechnical Characteristics (Bennett et al., 1984)

Figure 3.4 Comparison of Shear Wave Velocity Profiles from Crosshole and SASW Tests at Wildlife Site (Bierschwale and Stokoe, 1984)

Figure 3.5 Variation in Normalized Shear Modulus with Shearing Strain for Channel Fill Sand (Ladd, 1982)

Figure 3.6 Variation in Normalized Shear Modulus with Shearing Strain for Imperial Valley Clays (Turner and Stokoe, 1982)

Figure 3.7 Variation in Damping Ratio with Shearing Strain for Imperial Valley Soils (Ladd, 1982; Turner and Stokoe, 1982)

Figure 3.8 Instrumentation of the Wildlife Site (Bennett et al., 1984)

Figure 3.9 Location Map of the Wildlife Site and the Epicenters of the Elmore Ranch ($M_s = 6.2$) and Superstition Hills ($M_s = 6.6$) Earthquakes (Porcella et al., 1987)

Figure 3.10 Earthquake Time Histories at 1315 GMT, November 24, 1987 at Wildlife Array - Horizontal Motions in 360° Direction

Figure 3.11 Earthquake Time Histories at 1315 GMT, November 24, 1987 at Wildlife Array - Horizontal Motions in 90° Direction

Figure 3.12 Earthquake Time Histories at 1315 GMT, November 24, 1987 at Wildlife Array - Vertical Motions

Figure 3.13 Acceleration Response Spectra at 5% Damping - Wildlife Liquefaction Array, November 24, 1987, 1315 GMT Earthquake - Comparison of the Spectral Characteristics of Horizontal Motions

Figure 3.14 Acceleration Response Spectra at 5% Damping - Wildlife Liquefaction Array, November 24, 1987, 1315 GMT Earthquake - Comparison of the Spectral Characteristics of Vertical Motions

Figure 3.15 Normalized Pore Water Pressure Ratios - Wildlife Liquefaction Array, November 24, 1987, 1315 GMT Event (Matasovic et al., 1993)

Figure 4.1 Wildlife Site Soil Profile Used in Response Analysis Based on Average of SASW and Crosshole Shear Wave Velocity Measurements

Figure 4.2 Acceleration Response Spectra at 5% Damping - Wildlife Liquefaction Array, November 24, 1987, 1315 GMT Earthquake - Comparison of Horizontal Motions in 360 Degree Direction - SHAKE Output at Ground Surface Calculated Using Crosshole Shear Wave Velocity Measurements

Figure 4.3 Acceleration Response Spectra at 5% Damping - Wildlife Liquefaction Array, November 24, 1987, 1315 GMT Earthquake - Comparison of Horizontal Motions in 360 Degree Direction - SHAKE Output at Ground Surface Calculated Using SASW Shear Wave Velocity Measurements

Figure 4.4 Acceleration Response Spectra at 5% Damping - Wildlife Liquefaction Array, November 24, 1987, 1315 GMT Earthquake - Comparison of Horizontal Motions in 360 Degree Direction - SHAKE Output at Ground Surface Calculated Using Average of SASW and Crosshole Shear Wave Velocity Measurements

Figure 4.5 Acceleration Response Spectra at 5% Damping - Wildlife Liquefaction Array, November 24, 1987, 1315 GMT Earthquake - Comparison of Horizontal Motions in 360 Degree Direction - SHAKE Output at Depth of 7.5 m with Cutoff Frequency of 25 Hz

Figure 4.6 Acceleration Response Spectra at 5% Damping - Wildlife Liquefaction Array, November 24, 1987, 1315 GMT Earthquake - Comparison of Horizontal Motions in 90 Degree Direction - SHAKE Output at Ground Surface Calculated Using Average of SASW and Crosshole Shear Wave Velocity Measurements

Figure 4.7 Maximum Acceleration Distribution over Depth from SHAKE Results - Wildlife Site, November 24, 1987, 1315 GMT Earthquake in 360° Direction

Figure 4.8 Maximum Acceleration Distribution over Depth from SHAKE Results - Wildlife Site, November 24, 1987, 1315 GMT Earthquake in 90° Direction

Figure 4.9 Maximum Shear Stress Distribution over Depth from SHAKE Results - Wildlife Site, November 24, 1987, 1315 GMT Earthquake in 360° Direction

Figure 4.10 Maximum Shear Stress Distribution over Depth from SHAKE Results - Wildlife Site, November 24, 1987, 1315 GMT Earthquake in 90° Direction

Figure 4.11 Maximum Shear Strain Distribution over Depth from SHAKE Results - Wildlife Site, November 24, 1987, 1315 GMT Earthquake in 360° Direction

Figure 4.12 Maximum Shear Strain Distribution over Depth from SHAKE Results - Wildlife Site, November 24, 1987, 1315 GMT Earthquake in 90° Direction

Figure 4.13 Shear Stress Time History at Depth 4.21 m from SHAKE Output - Wildlife Site, November 24, 1987, 1315 GMT Earthquake in 360° Direction

Figure 4.14 Shear Strain Time History at Depth 4.21 m from SHAKE Output - Wildlife Site, November 24, 1987, 1315 GMT Earthquake in 360° Direction

Figure 4.15 Shear Stress-Shear Strain Hysteresis Loop at Depth 4.21 m. Calculated from SHAKE Output - Wildlife Site, November 24, 1987, 1315 GMT Earthquake in 360° Direction. Soil Properties are Based on the Average of SASW and Crosshole Shear Wave Velocity Measurements

Figure 4.16 Accumulation of Strain Energy in Liquefied Sand Layer - Wildlife Site, November 24, 1987, 1315 GMT Earthquake in 360° Direction - SHAKE Analysis Output

Figure 4.17 Accumulation of Strain Energy in Liquefied Sand Layer - Wildlife Site, November 24, 1987, 1315 GMT Earthquake in 90° Direction - SHAKE Analysis Output

Figure 4.18 Accumulation of Strain Energy in Liquefied Sand Layer - Wildlife Site, November 24, 1987, 1315 GMT Earthquake - Summation of SHAKE Analysis Output in both 360° and 90° Directions

Figure 4.19 Acceleration Response Spectra at 5% Damping - Wildlife Liquefaction Array, November 24, 1987, 1315 GMT Earthquake - Comparison of Horizontal Motions in 360° Direction - BDESRA Output, Total Stress Analysis

Figure 4.20 Acceleration Response Spectra at 5% Damping - Wildlife Liquefaction Array, November 24, 1987, 1315 GMT Earthquake - Comparison of Horizontal Motions in 90° Direction - BDESRA Output, Total Stress Analysis

Figure 4.21 Maximum Shear Stress Distribution over Depth from BDESRA Results of Total Stress Analyses - Wildlife Site, November 24, 1987, 1315 GMT Earthquake

Figure 4.22 Maximum Shear Strain Distribution over Depth from BDESRA Results of Total Stress Analyses - Wildlife Site, November 24, 1987, 1315 GMT Earthquake

Figure 4.23 Accumulation of Strain Energy in Liquefied Sand Layer - Wildlife Site, November 24, 1987, 1315 GMT Earthquake in 360° Direction - BDESRA Output, Total Stress Analysis

Figure 4.24 Accumulation of Strain Energy in Liquefied Sand Layer - Wildlife Site, November 24, 1987, 1315 GMT Earthquake in 90° Direction - BDESRA Output, Total Stress Analysis

Figure 4.25 Accumulation of Strain Energy in Liquefied Sand Layer - Wildlife Site, November 24, 1987, 1315 GMT Earthquake - Summation of BDESRA Total Stress Analysis Output in both 360° and 90° Directions

Figure 4.26 Acceleration Response Spectra at 5% Damping - Wildlife Liquefaction Array, November 24, 1987, 1315 GMT Earthquake - Comparison of Horizontal Motions in 360° Direction - BDESRA Output, Effective Stress Analysis

Figure 4.27 Acceleration Response Spectra at 5% Damping - Wildlife Liquefaction Array, November 24, 1987, 1315 GMT Earthquake - Comparison of Horizontal Motions in 90° Direction - BDESRA Output, Effective Stress Analysis

Figure 4.28 Maximum Shear Stress Distribution over Depth from BDESRA Results of Effective Stress Analyses - Wildlife Site, November 24, 1987, 1315 GMT Earthquake

Figure 4.29 Maximum Shear Strain Distribution over Depth from BDESRA Results of Effective Stress Analyses - Wildlife Site, November 24, 1987, 1315 GMT Earthquake

Figure 4.30 Accumulation of Strain Energy in Liquefied Sand Layer - Wildlife Site, November 24, 1987, 1315 GMT Earthquake in 360° Direction - BDESRA Output, Effective Stress Analysis

Figure 4.31 Accumulation of Strain Energy in Liquefied Sand Layer - Wildlife Site, November 24, 1987, 1315 GMT Earthquake in 90° Direction - BDESRA Output, Effective Stress Analysis

Figure 4.32 Accumulation of Strain Energy in Liquefied Sand Layer - Wildlife Site, November 24, 1987, 1315 GMT Earthquake - Summation of BDESRA Effective Stress Analysis Output in both 360° and 90° Directions

Figure 4.33 Normalized Pore Water Pressure Generation in Liquefied Sand Layer - Wildlife Site, November 24, 1987, 1315 GMT Earthquake in 360° Direction, BDESRA Output, Effective Stress Analysis

Figure 4.34 Normalized Pore Water Pressure Generation in Liquefied Sand Layer - Wildlife Site, November 24, 1987, 1315 GMT Earthquake in 90° Direction, BDESRA Output, Effective Stress Analysis

Figure 4.35 Methodology Adopted in Estimating the Dynamic Stress and Strain Time Histories in a Soil Layer from Field Records (After Zeghal and Elgamal, 1994)

Figure 4.36 Shear Stress Time History at Depth of 5.06 m (16.6 ft) Based on Direct Interpolation of Recorded Motions, Wildlife Site, November 24, 1987, 1315 GMT Earthquake in 360° Direction

Figure 4.37 Shear Strain Time History at Depth of 5.06 m (16.6 ft) Based on Direct Interpolation of Recorded Motions, Wildlife Site, November 24, 1987, 1315 GMT Earthquake in 360° Direction

Figure 4.38 Shear Stress-Strain Hysteresis Loop at Depth of 5.06 m (16.6 ft) Based on Direct Interpolation of Recorded Motions, Wildlife Site, November 24, 1987, 1315 GMT Earthquake in 360° Direction

Figure 4.39 Shear Stress Time History at Depth of 5.06 m (16.6 ft) Based on Direct Interpolation of Recorded Motions, Wildlife Site, November 24, 1987, 1315 GMT Earthquake in 90° Direction

Figure 4.40 Shear Strain Time History at Depth of 5.06 m (16.6 ft) Based on Direct Interpolation of Recorded Motions, Wildlife Site, November 24, 1987, 1315 GMT Earthquake in 90° Direction

Figure 4.41 Shear Stress-Strain Hysteresis Loop at Depth of 5.06 m (16.6 ft) Based on Direct Interpolation of Recorded Motions, Wildlife Site, November 24, 1987, 1315 GMT Earthquake in 90° Direction

Figure 4.42 Accumulation of Strain Energy in Liquefied Sand Layer Based on Direct Interpolation of Recorded Motions, Wildlife Site, November 24, 1987, 1315 GMT Earthquake in 360° Direction

Figure 4.43 Accumulation of Strain Energy in Liquefied Sand Layer Based on Direct Interpolation of Recorded Motions, Wildlife Site, November 24, 1987, 1315 GMT Earthquake in 90° Direction

Figure 4.44 Accumulation of Strain Energy in Liquefied Sand Layer Based on Direct Interpolation of Recorded Motions, Wildlife Site, November 24, 1987, 1315 GMT Earthquake - Summation of Strain Energy in both 360° and 90° Directions

Figure 4.45 Comparison of Shear Modulus Degradation Curves used in SHAKE Analyses

Figure 4.46 Comparison of Damping Curves used in SHAKE Analyses

Figure 4.47 Acceleration Response Spectra at 5% Damping - Wildlife Liquefaction Array, November 24, 1987, 1315 GMT Earthquake - Comparison of Horizontal Motions in 360° Direction - SHAKE Output with EPRI (1993) Soil Curves

Figure 4.48 Acceleration Response Spectra at 5% Damping - Wildlife Liquefaction Array, November 24, 1987, 1315 GMT Earthquake - Comparison of Horizontal Motions in 90° Direction - SHAKE Output with EPRI (1993) Soil Curves

Figure 4.49 Shear Stress Time History at Depth of 4.21 m (13.8 ft) from SHAKE Output with EPRI (1993) Soil Curves - Wildlife Site, November 24, 1987, 1315 GMT Earthquake in 360° Direction

Figure 4.50 Shear Strain Time History at Depth of 4.21 m (13.8 ft) from SHAKE Output with EPRI (1993) Soil Curves - Wildlife Site, November 24, 1987, 1315 GMT Earthquake in 360° Direction

Figure 4.51 Shear Stress-Strain Hysteresis Loop at Depth of 4.21 m (13.8 ft). Calculated from SHAKE Output - Wildlife Site, November 24, 1987, 1315 GMT Earthquake in 360° Direction. Soil Properties are Based on the Average of SASW and Crosshole Shear Wave Velocity Measurements. The EPRI (1993) G/Gmax and Damping Curves are used in the Calculation

Figure 4.52 Accumulation of Strain Energy in Liquefied Sand Layer - Wildlife Site, November 24, 1987, 1315 GMT Earthquake in 360° Direction - SHAKE Output Using EPRI (1993) Soil Curves

Figure 4.53 Accumulation of Strain Energy in Liquefied Sand Layer - Wildlife Site, November 24, 1987, 1315 GMT Earthquake in 90° Direction - SHAKE Output Using EPRI (1993) Soil Curves

Figure 4.54 Accumulation of Strain Energy in Liquefied Sand Layer - Wildlife Site, November 24, 1987, 1315 GMT Earthquake - Summation of Strain Energy in both 360° and 90° Directions - SHAKE Output Using EPRI (1993) Soil Curves

Figure 4.55 Total Strain Energy at Liquefaction Onset. Calculated from Ground Response Analyses

Figure 4.56 Total Strain Energy at Liquefaction Onset. Calculated from Ground Response Analyses (with All Points in Unliquefied Layers Removed)

Figure 4.57 Comparison of Total Strain Energy at Liquefaction Onset. Ground Response Analyses and Laboratory Data - Wildlife Site, November 24, 1987, 1315 GMT Earthquake

LIST OF SYMBOLS

a, a(t)	acceleration at time t in cm/sec^2
CPT	cone penetration data
d, d(t)	displacement at time t in cm
D_r	relative density - %
FC	fines content
G	soil shear modulus
G_{max}	maximum soil shear modulus
N	SPT, blow-count
N_1	blow-count normalized to 1 ksc
$(N_1)_{60}$	normalized blow-count for a 60 percent energy ratio
v, v(t)	velocity at time t in cm/sec
δE, E_{liq}	energy per volume at the onset of liquefaction, $Joules/m^3$
$\Delta\gamma(t)$	shear strain increment from time t to $t + \Delta t$
γ, $\gamma(t)$	shear strain
γ_d	dry unit weight, kN/m^3
r_u	pore pressure ratio
σ_c'	effective confining pressure, kPa
SPT	standard penetration test
Σ	summation
τ, $\tau(t)$	shear stress
$\bar{\tau}(t)$	average shear stress at times t and $t + \Delta t$

UNITS CONVERSION FACTORS

1 Joules	0.0007376 ft-kip
1 kg/cm^2	2.048 kip/ft^2
1 km	0.621 miles
1 kN	0.225 kips
1 kN/m^2	0.02088 kip/ft^2
1 kN/m^3	6.366 lb/ft^3
1 m	3.281 ft
1 m^2	10.76 ft^2
1 m^3	35.31 ft^3

CHAPTER 1

INTRODUCTION

1.1 BACKGROUND

Liquefaction failure has been and continues to be a major cause of damage during earthquakes. The direct and indirect costs associated with ground failure may far exceed the damage caused by other types of failures such as structural collapses. Due to the enormous damage potential, research in the areas of liquefaction prediction and mitigation has continued, and the respective technologies have significantly improved over the years.

Two basic methods are currently used to predict liquefaction potential. The most widely used method, based on laboratory data and field performance data, was developed by Seed et al. (1983, 1985). In this method, the cyclic stress ratio in the field is predicted based on a simple or a more detailed ground response analysis, and the demand resulting from the design earthquake is established. The cyclic shear strength of the material can be obtained from laboratory testing of the soil samples or from the penetration data (Standard Penetration Test [SPT] data or Cone Penetration Test [CPT] data) along with the index and gradation properties of the soil samples. The most widely used curves to predict the capacity of the soil in terms of cyclic shear strength are the set of curves by Seed et al. (1985), shown in Figure 1.1. From knowledge of the penetration resistance and the fines content in the soil materials, the cyclic shear strength can be determined. However, the application of this method involves several empirical factors, including the corrections for sample disturbance, earthquake magnitude, and overburden pressure. Recently, Arango (1994) presented the new developments for this method, including the effects of higher frequency of loading on the cyclic shear strength of the soil and most notably, the recommendations made for revising the correction factors for earthquake magnitudes. Another recent study (Koester, 1992) has shown that the correction for overburden pressure is also a function of the fines content and that a reduction of the cyclic shear strength due to overburden pressure will significantly decrease if the fines content of the materials increases. The recent publication by Ishihara (1993) also provides an adjustment factor to incorporate the plasticity effects of the fines on the cyclic shear strength of the materials. Over the years, the "stress" method has proved to be a conservative and reliable method for the prediction of liquefaction potential, especially for distant earthquake events, which was the basis of the data used for development of this method. However, the method lacks the flexibility to incorporate recently recognized characteristics of the earthquake ground motions such as the near-field effects. For example, the "fling" effect resulting from the source and directivity of the rupture which was recently observed in the Kobe and the Northridge earthquakes, concentrates most of the energy in a short period of time. Such effects, combined with a much higher intensity of the ground motion in excess of 1g peak ground acceleration recorded in urban areas in recent major earthquakes, require a more robust approach to investigate the liquefaction potential in such regions.

The second method for predicting liquefaction potential is based on the "strain" approach. This method was developed among others by Dobry et al. (1982). In this method, the shear strain in the field is compared with the laboratory data relating cyclic shear strain to excess pore pressure to determine the liquefaction potential. Similar to the "stress" method, the "strain" method also requires ground response analyses and laboratory testing of the soil samples. The "strain" method is fundamentally different from the "stress" method and lacks the wide range of the field and the laboratory data bases that exist for the "stress" approach.

The "strain energy" method discussed in this report incorporates the basic elements of both the stress and strain approaches in the formulation. In this method, the amount of total strain energy at the onset of liquefaction is obtained from the stress and strain time histories from laboratory testing and is compared with the same energy in the field due to the design earthquake motion. The basis for this method is the observation made on the laboratory data that the build-up of the excess pore pressure is proportional to the total strain energy in all loading cycles up to the initial liquefaction. This observation has prompted the formulation of the "energy-based" method. This method has been investigated in recent years by several researchers, including Figueroa et al. (1994, 1995) and Kagawa et al. (1990).

1.2 PURPOSE

The purpose of this study is to evaluate the feasibility of the development and application of the strain energy method for general use. The study is expected to continue with two additional phases that will develop generic "strain energy" liquefaction curves as a function of the most relevant soil properties and generic "strain energy" demand as a function of seismicity data and a wide range of site soil data and profiles. The limited scope of the feasibility study did not permit laboratory testing for the purpose of the "strain energy" computation. Available laboratory data were used for this purpose.

1.3 OVERVIEW OF THE REPORT

In this report, Chapter 1 includes the introduction and scope of the study. Chapter 2 presents the collection and synthesis of the laboratory data. Chapter 3 discusses the soil and earthquake data from the Wildlife Site. The ground response analyses and comparison of the results with the laboratory data are presented in Chapter 4. Finally, Chapter 5 presents the summary and the recommendation. The references are listed in Chapter 6. All the laboratory data used in this report are presented in Appendices A through D.

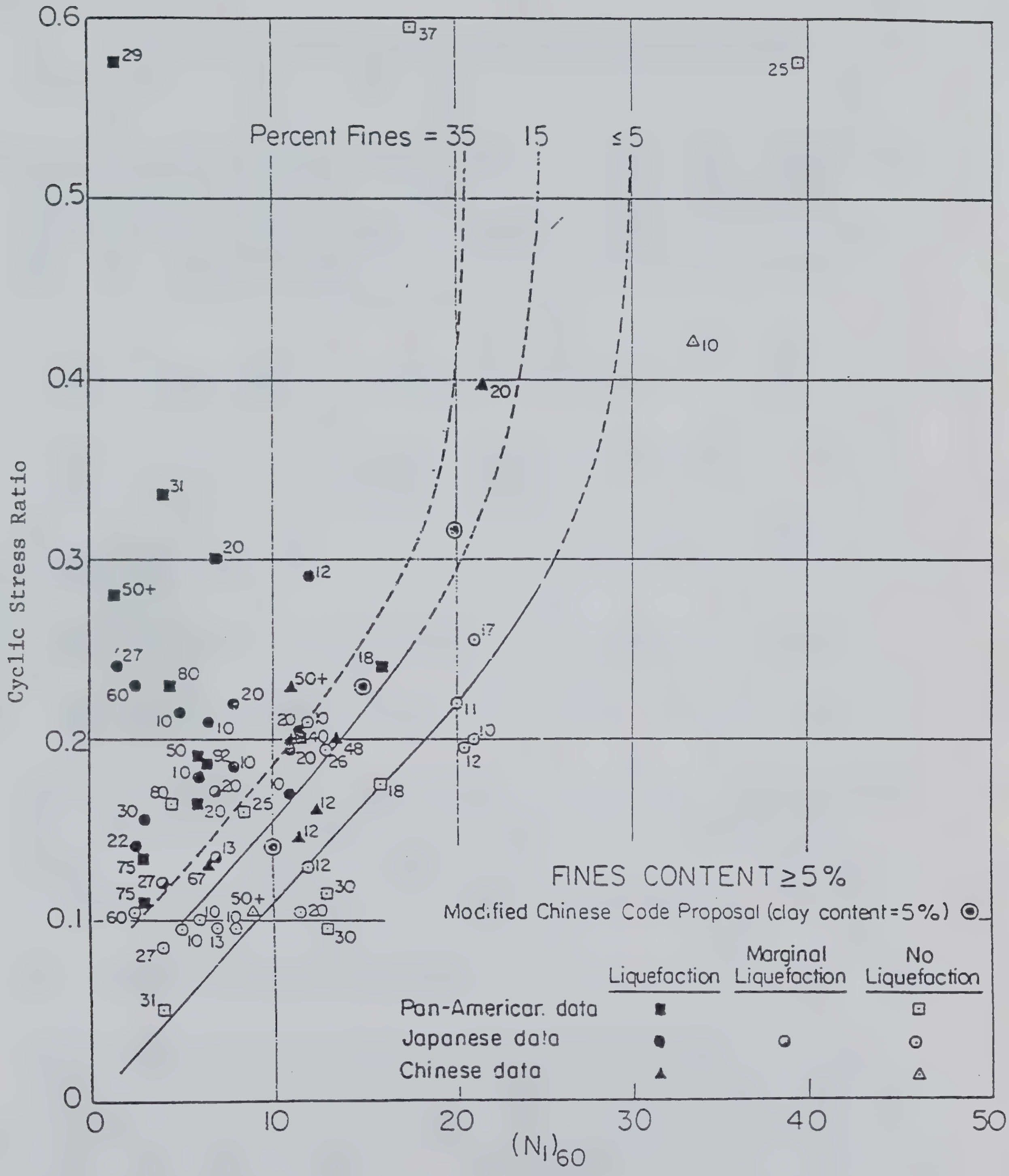

Figure 1.1 - Relationships Between Stress Ratio Causing Liquefaction and $(N_1)_{60}$ Values for Silty Sands for M = 7-1/2 Earthquakes (Seed et al., 1985)

CHAPTER 2

COLLECTION AND SYNTHESIS OF LABORATORY DATA

Computation of the strain energy requires access to the stress and strain time histories from cyclic (triaxial or simple shear) tests in the laboratory. Such data are usually computer storage-intensive and are not maintained for a long period. However, an attempt was made to collect the available and reliable data to characterize the strain energy. Most of the data were obtained in connection with various recent Bechtel projects. The laboratory data used in this study are from:

- The cyclic stress- and strain-controlled tests on Monterey No. 0 sand, performed at the University of California, Berkeley.
- The stress-controlled tests on soil samples from the Savannah River Site (SRS), performed at the University of California, Berkeley.
- The cyclic torsional shear tests on clean and silty sands, performed at the University of Colorado.
- The cyclic triaxial tests on clean sands, performed at Wayne State University.
- The summary of the laboratory data reduced to a set of relationships to compute strain energy, as developed by Figueroa et al.

Altogether, a total of 150 cyclic test data sets have been processed. A limited number of these were excluded in the process due to peculiar stress and strain patterns and incompleteness of the respective time histories. The computation of the strain energy from each data set and a discussion on the validity of each group of tests follow.

2.1 STRAIN ENERGY COMPUTATION

In a typical cyclic laboratory test, the stress, strain and pore pressure time histories are recorded. Typical recorded time histories for a strain-controlled cyclic triaxial test are shown in Figure 2.1. Hysteresis loops can be developed from the shear stress and strain time histories. The hysteresis loops corresponding to the stress and strain time histories shown in Figure 2.1 are shown in Figure 2.2. From the shear stress, $\tau(t)$, and the shear strain, $\gamma(t)$ at time t, the time history of the total strain energy up to time t, E(t), is computed from:

$$E(T) = \sum_{t=0}^{T} \bar{\tau}(t).\Delta\gamma(t) \qquad (2.1)$$

where t is the time, $\sum$ is summation over the time increment Δt up to time t, $\bar{\tau}$ (t) is the average shear stress from time t to t + Δt, and $\Delta\gamma(t)$ is the shear strain increment from time t to t + Δt. The strain energy for each cycle of loading amounts to the area inside the hysteresis loop. The computation of the instantaneous energy and its summation over time intervals were performed until the onset of the liquefaction, at which time the pore pressure ratio reached a value of unity. The summation of the energy at this time, E_{Liq}, was used as the measure of the capacity of the soil sample against initial liquefaction occurrence in terms of the strain energy.

2.2 CYCLIC TRIAXIAL TESTS ON MONTEREY NO. 0 SAND, PERFORMED AT THE UNIVERSITY OF CALIFORNIA, BERKELEY (UCB)

The data were prepared as part of the Bechtel in-house technical research led by Arango (1994). The gradation curve for Monterey No. 0 sand is shown in Figure 2.3. The tests were both stress- and strain-controlled. The samples were prepared at relative densities ranging from 40% to 60%, and the loads were applied at frequencies ranging from 0.10 Hz to 20 Hz. All tests were conducted at a confining pressure of 100 kPa. More detailed information about the testing program and the testing apparatus may be obtained from Riemer (Riemer et al., 1994). A total of 20 tests from this group were incorporated in this study. A summary of the test data, including the computed total strain energy to the onset of liquefaction for each test, is presented in Table 2.1. The recorded stress, strain, pore pressure (in terms of the pore pressure ratio r_u), and the computed time history of the strain energy for each test are shown in Appendix A. In addition to the strain energy time history, the energy time history normalized to the total energy at the time of $r_u = 1$, (E_{Liq}), is also plotted and compared with the r_u time history, e. g. see Page A-3. As shown in these plots, the normalized strain energy increase follows the pattern of the pore pressure ratio increase and, on the average, shows a very good agreement for all the tests at a wide range of frequencies and at all the relative densities tested. The agreement holds whether the data are obtained from the stress- or the strain-controlled tests. As stated earlier, this observation was the basis for formulation of the strain energy method.

A summary of the results in terms of the total energy as a function of relative density is shown in Figure 2.4. As expected, the total energy to the onset of liquefaction increases as the relative density of the sample increases. It can also be observed in this figure that the scatter in the strain-controlled test data is less severe than the scatter in the data from the stress-controlled test results.

The strain energy for each test as a function of the frequency of loading is plotted in Figure 2.5, which shows a decreasing total energy as the frequency of loading increases. In this figure, the frequency of loading has a more pronounced effect on the total energy obtained from the stress-controlled tests than the strain-controlled tests. In addition, the strain-controlled tests require lower total energy to develop initial liquefaction as compared to the stress-controlled tests. It should also be noted that for a typical strain-controlled test, the pore pressure build-up takes place at a much faster rate in the first several cycles of loading. On the other hand, in the stress-controlled test, the rate of pore pressure build-up increases towards the end of loading cycles. This observation can also be made from the shape and size of the respective hysteresis loops. In the strain-controlled tests, the largest loops are the earlier loops, and they decrease in size as the sample degrades due to the pore pressure build-up. The opposite trend takes place in a stress-controlled test, as shown in Appendix A, e. g. Pages A-4 and A-16.

2.3 CYCLIC TRIAXIAL TESTS ON SOIL SAMPLES FROM THE SAVANNAH RIVER SITE, PERFORMED AT THE UNIVERSITY OF CALIFORNIA, BERKELEY (UCB)

The laboratory program for this group of tests was developed as part of one of the Bechtel projects for the Department of Energy (DOE) at the Savannah River Site (SRS). Subsurface conditions for the site under consideration are shown in Figure 2.6. The soil layers of primary interest were the Tobacco Road (TR3 and TR4) and the Santee formations.

A comprehensive site investigation program was conducted at the site. Relevant average soil properties of each soil layer at the SRS site, shown in Figure 2.6 are summarized in Table 2.2.

Most of the cyclic load tests were conducted on undisturbed soil samples from the Tobacco Road formation from depths of 16 m to 23 m. As shown in Table 2.2, this material has an average fines content of 23%, including 9% clay content (minus 2 micron particle size) and an average plasticity index of 25%. A typical gradation curve for the Tobacco Road Materials is shown in Figure 2.7. A total of 22 cyclic stress-controlled tests at 1 Hz were performed (Riemer and Seed, 1994). The confining pressure ranged from 200 kPa to 750 kPa. A summary of the test data and of the total strain energy for each test in this group is presented in Table 2.3. Notable characteristic of this group of tests is the large confining pressure used in the tests and the relatively large fines content in the soil samples tested. The plots of shear stress, strain, total energy and normalized energy, pore pressure ratios, and the hysteresis loops for this group are shown in Appendix B. As shown in this appendix, the increase of the normalized energy in general follows the pore pressure ratio increase up to the pore pressure ratio of one. A summary of the total energy as a function of the confining pressure is shown in Figure 2.8. As expected, the total strain energy is greater for the samples tested at higher confining pressures. For the same confining pressure, tests on samples having a higher dry density resulted in the development of a larger total energy. This trend is similar to the trend observed in Figure 2.4 with respect to the relative density of the samples.

2.4 CYCLIC TORSIONAL TESTS ON SOIL SAMPLES, PERFORMED AT THE UNIVERSITY OF COLORADO (UOC)

The time histories for this group of tests were provided by Koester (1992). The test data were developed as part of the research work for a doctoral dissertation at the University of Colorado (UOC). Only the time histories from nine tests were available. The tests were performed using the stress-controlled hollow torsional simple shear test apparatus. The cyclic loading was applied at a frequency of 0.1 Hz. Both clean sands and sands with fines content up to 45% were tested.

The silty sand samples were prepared with a density such that the void ratio of the sample matched that of the parent clean sand at the selected relative densities. The confining pressure in the tests ranged from 200 kPa to 300 kPa. A summary of the soil data and the test results in terms of the total energy is shown in Table 2.4, whereas the gradation curve is shown in Figure 2.9. A more detailed description of the sample preparation and testing program can be obtained from Koester (1992).

The time histories of the stress, strain, pore pressure ratio, total energy, and hysteresis loops for this group are presented in Appendix C. In general, the hysteresis loops in this group of tests start with a few narrow loops followed by one or two large loops before reaching the initial liquefaction stage, suggesting a sudden contraction and collapse of the samples. This behavior may have been the cause of the relatively low densities of the samples. The test results in terms of the total strain energy as a function of relative density for the clean sand are shown in Figure 2.10. The results show a relatively large scatter in the energy at low relative densities. The results of the silty sand samples as a function of the confining pressure are shown in Figure 2.11. These results show relatively less scatter in the data.

2.5 CYCLIC TRIAXIAL TESTS ON SOIL SAMPLES FROM THE NORTHRIDGE SITE, PERFORMED AT THE UNIVERSITY OF CALIFORNIA, BERKELEY (UCB)

The samples for this group of tests were prepared as part of the National Science Foundation (NSF)/Bechtel research work led by Arango (Arango and Migues, 1996). As part of the test program, a total of 8 reconstituted clean sand samples were prepared and tested in a stress-controlled cyclic triaxial test device. The samples were prepared at relative densities ranging from 35% to 90%. The gradation curves for two soil samples are shown in Figure 2.12. A summary of the test data and of the computed total strain energy is presented in Table 2.5. Time history plots are included in Appendix D. Test results in terms of the total strain energy as a function of relative density is presented in

Figure 2.13. As shown previously, the total strain energy increases as the relative density increases.

2.6 CYCLIC TRIAXIAL TESTS ON CLEAN SANDS, PERFORMED AT WAYNE STATE UNIVERSITY (WSU)

The summary results of 91 cyclic triaxial stress-controlled tests on clean sands was presented in the doctoral dissertation by Al-Khatib (1994). The tests were performed at Wayne State University (WSU). All tests were performed on clean sands consisting of Monterey No. 0 and Kasumigaura sand (K-sand). The gradation curves for the two sands are shown in Figure 2.14. The breakdown of the tests is as follows:

- 28 tests on K-sand at low frequency with cyclic reversal loading (two-way cyclic loading)
- 28 tests on Monterey No. 0 sand at low frequency with cyclic reversal loading
- 25 tests on Monterey No. 0, low frequency and one-way loading
- 10 tests on Monterey No. 0 with earthquake simulated loading using the El Centro and Taft records

Time histories of the test data were not available; however, the total energy in terms of axial stress/strain has been reported by Al-Khatib (1994). The total energy was converted to the total energy in terms of the shear strain and shear stress attributes and are summarized in Table 2.6. The results in terms of the total strain energy as a function of relative density for the cyclic reversal loading cases are shown in Figure 2.15 which shows a similar trend to the one observed in the UCB data (see Figure 2.4). As shown in this figure, both the K-sand and the Monterey No. 0 sand have similar capacity in terms of total energy and consistently show an increase of the total energy with an increase in the relative density. The scatter in the data appear to be minimal.

The results in terms of the cyclic one-way and two-way loadings are compared in Figure 2.16. As shown, the two-way loading results in lower total energy capacity as compared to the one-way loading. This trend is consistent with the intuitive indication that soil resistance to liquefaction will be higher due to the less damaging effects of the one-way loading. Finally, the results of the two-way loading are compared with the earthquake loading in Figure 2.17. The earthquake loading results in the lower total energy. Altogether, the results of this group of tests appear to be more uniform with little scatter in terms of the total energy.

2.7 SUMMARY DATA BY FIGUEROA et al.

A series of torsional shear hollow cylinder tests were performed on both clean sand and silty sand by Figueroa et al. (1994, 1995). Samples from the Reid Bedford sand (clean sand) were tested at relative densities ranging from 50% to 70%. The silty sand from the

Lower San Fernando Dam (LSFD) were tested at relative densities of 57% to 92%. The gradation curves for both materials are shown in Figure 2.18. Each sample was successively tested at confining pressures of 41.4 kPa, 82.7 kPa, and 124.1 kPa. Actual data points for this group of tests are not available. However, the authors performed regression analyses of the test results in terms of total strain energy and identified the most relevant parameters affecting the results of clean sand and silty sand. Based on the test results, the authors recommended the following relationships (Figueroa et al., 1995):

Clean sand

$$\text{Log } \delta E = 2.062 + 0.0039\ \sigma_c' + 0.0124\ D_r \tag{2.2}$$

Silty sand

$$\text{Log } \delta E = 2.529 + 0.00474\ \sigma_c' \tag{2.3}$$

where δE is the total strain energy in Joules/m^3, σ_c' is the effective confining pressure in kPa, and D_r is the relative density in percent. The relationship for clean sand shows the confining pressure as one of the variables. However, the importance of this parameter is very small due to the small coefficient associated with this parameter in Equation 2.2.

2.8 SUMMARY OF ALL LABORATORY DATA

Based on the results of the five groups of tests outlined above, summary plots have been prepared to evaluate consistency between the various test groups.

For clean sand, the results of tests on Monterey No. 0 performed at the UCB (20 tests), the data on clean sands from the WSU (81 tests), the data from the Northridge samples (8 tests) also tested at the UCB, and the data from the UOC (4 tests) are compared with the relationship by Figueroa et al. in Figure 2.19. As shown in this figure, except for the data from the UOC, the remaining groups show a quite consistent pattern of the rate of energy dissipation and of the total energy absorbed. The confining pressure used in the tests at the UOC was at least 2 to 3 times larger than the pressure used for the rest of the tests. Also, the differences in the shape and size of the sand particles may have contributed to some of the differences in the results. For relative densities in the range of 40% to 70%, the data from UCB, WSU, and Figueroa et al. are in relatively good agreement.

For silty sands, the results from the Savannah River Site (SRS) are compared with the data from the UOC and the relationship by Figueroa et al. in Figure 2.20. The fines content in each group are: 28% for the samples from the lower San Fernando Dam (Figuero et al., 1995), 20% to 45% for soil samples tested at UOC (Koester, 1992), and the average 23% for samples taken from the SRS site. The Plasticity Index of the materials in the groups also varies from 10 to 25%. Unfortunately, the confining pressures used for each group of tests do not overlap. Nevertheless, each group of results follows the pattern of the previous group and a consistent trend is maintained.

All of the results indicate that for clean sands, the energy to liquefaction can be quantified in terms of the relative density and the confining pressure. However, the limited data available does not permit a study of effects of the grain size and shape on the total energy.

Summary of the results for silty sands also shows that the energy to liquefaction can be quantified in terms of the effective confining pressure. However, the effects of the plasticity index, the amount, and the type of fine need to be studied in the future.

As stated earlier in the report, the scope of this feasibility study did not include laboratory testing. However, comparison of the data available from the various researchers and practitioners at different institutes shows remarkably good agreement. This observation leads to the conclusion that development of generic total strain energy relationship as a measure of soil resistance against liquefaction by means of laboratory testing is feasible. If consistent sampling, sample handling, and testing methods and specifications are followed, the results are expected to be more consistent and vary within narrower limits.

Table 2.1 - Summary of the Cyclic Triaxial Test Data on Monterey No. 0 Sand Performed at University of California, Berkeley

No.	Test ID	Sample	D_r(%)	E_{liq} (J/m^3)	FC (%)	γ_d (kN/m^3)	Control	σ_c' (kPa)	Freq. (Hz)	Load Shape
1	MONT4	Monterey No.0	61.8	2677	2	15.6	Stress	100	1	Sinusoidal 2-way
2	MONT10	Monterey No.0	61.0	1933	2	15.5	Stress	100	1	Sinusoidal 2-way
3	MONT11	Monterey No.0	60.6	988	2	15.5	Stress	100	10	Sinusoidal 2-way
4	MONT12	Monterey No.0	61.0	2481	2	15.5	Stress	100	1	Sinusoidal 2-way
5	MONT14	Monterey No.0	60.2	1583	2	15.5	Stress	100	20	Sinusoidal 2-way
6	MONT15	Monterey No.0	60.5	1245	2	15.5	Stress	100	10	Sinusoidal 2-way
7	MONT17	Monterey No.0	61.0	1878	2	15.5	Strain	100	1	Sinusoidal 2-way
8	MONT18	Monterey No.0	61.0	1187	2	15.5	Strain	100	10	Sinusoidal 2-way
9	MONT19	Monterey No.0	60.6	1483	2	15.5	Strain	100	15	Sinusoidal 2-way
10	MONT20	Monterey No.0	40.9	851	2	15.0	Strain	100	1	Sinusoidal 2-way
11	MONT21	Monterey No.0	41.8	880	2	15.0	Strain	100	1	Sinusoidal 2-way
12	MONT22	Monterey No.0	42.3	1078	2	15.0	Strain	100	1	Sinusoidal 2-way
13	MONT24	Monterey No.0	51.8	2736	2	15.3	Stress	100	1	Sinusoidal 2-way
14	MONT25	Monterey No.0	50.4	2985	2	15.3	Stress	100	1	Sinusoidal 2-way
15	MONT26	Monterey No.0	49.9	2769	2	15.2	Stress	100	1	Sinusoidal 2-way
16	MONT30	Monterey No.0	41.9	708	2	15.0	Strain	100	10	Sinusoidal 2-way
17	MONT33	Monterey No.0	40.5	829	2	15.0	Strain	100	10	Sinusoidal 2-way
18	MONT35	Monterey No.0	61.8	4211	2	15.6	Stress	100	0.1	Sinusoidal 2-way
19	MONT37	Monterey No.0	61.6	1388	2	15.5	Strain	100	1	Sinusoidal 2-way
20	MONT38	Monterey No.0	61.8	704	2	15.6	Strain	100	10	Sinusoidal 2-way

Table 2.2 - Average Material Properties at the SRS Site

PARAMETER/SOIL LAYER	TR3/TR4 AVG	SANTEE AVG
SPT N-VALUE	15	58
SHEAR WAVE VELOCITY, m/sec (ft/s)	364 (1193)	381 (1251)
CONE TIP RESISTANCE, Qc, tsf	52	111
FRICTION RATIO	3	1
Qc/N	3.5	1.9
PERCENT FINES (<.074 mm)	23	25
PERCENT SILT	9	12
PERCENT CLAY (<.002 mm)	14	13
PLASTICITY INDEX, %	25	31
LIQUID LIMIT, %	45	55
PLASTICITY INDEX (-200 MATERIAL), %	101	78
LIQUID LIMIT (-200 MATERIAL), %	144	112
DRY DENSITY, KN/m^3 (pcf)	16 (102)	13.8 (88)
WATER CONTENT, %	22	32
WET DENSITY, KN/m^3 (pcf)	19.6 (125)	6.4 (116)
SPECIFIC GRAVITY	2.68	2.67
VOID RATIO	0.625	0.876
AT-REST LAT. EARTH PRESS. COEFF	0.46	0.44
OVERCONSOLIDATION RATIO	1.89	1.26
TOTAL COHESION, kPa (ksf)	91 (1.9)	-
TOTAL FRICTION ANGLE, degree	13	-
EFFECTIVE COHESION, kPa (ksf)	0	0
EFFECTIVE FRICTION ANGLE, degree	33	34
DILATION ANGLE, degree	1.7	1.3

Table 2.3 - Summary of the Cyclic Triaxial Test Data on SRS Soil Samples Performed at University of California, Berkeley

No.	Test ID	Sample	D_r(%)	E_{liq} (J/m^3)	FC (%)	γ_d (kN/m^3)	Control	σ_c' (kPa)	Freq. (Hz)	Load Shape
1	B23P2BCY	Santee	N/A	14675	33.7	16.0	Stress	400	1	Sinusoidal 2-way
2	B23P2MCY	Santee	N/A	16782	35.6	16.4	Stress	400	1	Sinusoidal 2-way
3	B23P2TCY	Santee	N/A	11402	32.6	16.8	Stress	400	1	Sinusoidal 2-way
4	B23P3BCY	Tobacco Rd.	N/A	4929	16.6	16.4	Stress	200	1	Sinusoidal 2-way
5	B23P3MCY	Tobacco Rd.	N/A	5585	18.5	15.2	Stress	200	1	Sinusoidal 2-way
6	B23P3TCY	Tobacco Rd.	N/A	2924	20.5	16.6	Stress	200	1	Sinusoidal 2-way
7	B12P5BCY	Tobacco Rd.	N/A	14918	27.0	15.8	Stress	300	1	Sinusoidal 2-way
8	B12P5MCY	Tobacco Rd.	N/A	49114	26.8	16.8	Stress	300	1	Sinusoidal 2-way
9	B12P5TCY	Tobacco Rd.	N/A	5450	22.3	18.0	Stress	300	1	Sinusoidal 2-way
10	B12P7BCY	Tobacco Rd.	N/A	7666	15.7	15.9	Stress	375	1	Sinusoidal 2-way
11	B12P7MCY	Tobacco Rd.	N/A	14482	17.0	16.3	Stress	375	1	Sinusoidal 2-way
12	B12P7TCY	Tobacco Rd.	N/A	3852	15.7	16.2	Stress	375	1	Sinusoidal 2-way
13	B2P5BCYC	Tobacco Rd.	N/A	11672	25.4	14.7	Stress	500	1	Sinusoidal 2-way
14	B2P5MCYC	Tobacco Rd.	N/A	23344	29.6	15.4	Stress	500	1	Sinusoidal 2-way
15	B2P5TCYC	Tobacco Rd.	N/A	8819	26.6	16.7	Stress	500	1	Sinusoidal 2-way
16	B23P4BCY	Tobacco Rd.	N/A	21667	11.4	14.6	Stress	750	1	Sinusoidal 2-way
17	B23P4MCY	Tobacco Rd.	N/A	36680	16.5	15.5	Stress	700	1	Sinusoidal 2-way
18	B23P4TCY	Tobacco Rd.	N/A	17968	28.0	N/A	Stress	750	1	Sinusoidal 2-way
19	B29P2TCY	Tobacco Rd.	N/A	23637	23.0	16.7	Stress	750	1	Sinusoidal 2-way
20	B2P6BCY	Tobacco Rd.	N/A	17985	18.9	16.7	Stress	725	1	Sinusoidal 2-way
21	B2P6MCY	Tobacco Rd.	N/A	19831	20.1	16.5	Stress	743	1	Sinusoidal 2-way
22	B2P6TCYC	Tobacco Rd.	N/A	14446	22.4	16.0	Stress	750	1	Sinusoidal 2-way

Table 2.4 - Summary of the Cyclic Torsional Test Data on Clean and Silty Sands Performed at University of Colorado

No.	Test ID	Sample	D_r(%)	E_{liq} (J/m^3)	FC (%)	γ_d (kN/m^3)	P. I.	Control	σ_c' (kPa)	Freq. (Hz)	Load Shape
1	UOFC5	F11	32.6	3728	0	14.5		Stress	199.9	0.1	Sinusoidal 2-way
2	UOFC7	F11	41.0	12495	0	14.7		Stress	204.8	0.1	Sinusoidal 2-way
3	UOFC9	F11	42.0	16997	0	14.8		Stress	304.1	0.1	Sinusoidal 2-way
4	UOFC13	F43	N/A	3450	20	15.3	10.0	Stress	299.9	0.1	Sinusoidal 2-way
5	UOFC14	F46	N/A	4753	20	15.2	25.0	Stress	199.9	0.1	Sinusoidal 2-way
6	UOFC15	F46	N/A	2485	20	15.2	25.0	Stress	201.3	0.1	Sinusoidal 2-way
7	UOFC17	F64	N/A	3427	45	16.2	15.0	Stress	203.4	0.1	Sinusoidal 2-way
8	UOFC18	F64	N/A	3993	45	16.2	15.0	Stress	190.3	0.1	Sinusoidal 2-way
9	UOFC23	F11	45.3	7437	0	14.9		Stress	199.9	0.1	Sinusoidal 2-way

Table 2.5 - Summary of the Cyclic Triaxial Test Data on Northridge Samples Performed at University of California, Berkeley

No.	Test ID	Sample	D_r(%)	E_{liq} (J/m^3)	FC (%)	γ_d (kN/m^3)	Control	σ_c' (kPa)	Freq. (Hz)	Load Shape
1	BTC2CY1	Northridge Sand	58.3	5930	5	14.5	Stress	100	1	Sinusoidal 2-way
2	BTC2CY2	Northridge Sand	78.4	2247	5	15.5	Stress	100	1	Sinusoidal 2-way
3	BTC3CY1	Northridge Sand	82.3	5146	5	15.7	Stress	100	1	Sinusoidal 2-way
4	BTC3CY2	Northridge Sand	89.9	3813	5	16.1	Stress	100	1	Sinusoidal 2-way
5	BTC3CY3	Northridge Sand	97.2	36156	5	16.5	Stress	100	1	Sinusoidal 2-way
6	BTC4CY1	Northridge Sand	93.7	7874	5	16.3	Stress	100	1	Sinusoidal 2-way
7	BTC4CY2	Northridge Sand	100.0	6647	5	16.7	Stress	100	1	Sinusoidal 2-way
8	BTC6CY1	Northridge Sand	35.2	3206	5	13.5	Stress	100	1	Sinusoidal 2-way

Table 2.6 - Summary of the Cyclic Triaxial Test Data on Clean Sands Performed at Wayne State University

No.	Test ID	Sample	D_r(%)	E_{liq} (J/m^3)	FC (%)	γ_d (kN/m^3)	Control	σ_c' (kPa)	Freq. (Hz)	Load Shape
1	WS6-1-1	K-Sand	67.0	2211	2.5	15.8	Stress	44.3	0.1	Sinusoidal 2-way
2	WS6-1-2	K-Sand	65.0	2397	2.5	15.7	Stress	56.5	0.1	Sinusoidal 2-way
3	WS6-1-3	K-Sand	59.0	1893	2.5	15.4	Stress	68.9	0.1	Sinusoidal 2-way
4	WS6-1-4	K-Sand	40.0	397	2.5	14.7	Stress	33.8	0.1	Sinusoidal 2-way
5	WS6-1-5	K-Sand	32.0	293	2.5	14.4	Stress	38.6	0.1	Sinusoidal 2-way
6	WS6-1-6	K-Sand	74.0	2163	2.5	16.1	Stress	26.2	0.1	Sinusoidal 2-way
7	WS6-1-7	K-Sand	52.0	424	2.5	15.2	Stress	22.8	0.1	Sinusoidal 2-way
8	WS6-1-8	K-Sand	66.0	1690	2.5	15.7	Stress	36.5	0.1	Sinusoidal 2-way
9	WS6-1-9	K-Sand	34.0	289	2.5	14.5	Stress	35.2	0.1	Sinusoidal 2-way
10	WS6-1-10	K-Sand	48.0	486	2.5	15.0	Stress	31.8	0.1	Sinusoidal 2-way
11	WS6-1-11	K-Sand	42.0	394	2.5	14.8	Stress	31.9	0.1	Sinusoidal 2-way
12	WS6-1-12	K-Sand	23.0	1857	2.5	14.1	Stress	35.2	0.1	Sinusoidal 2-way
13	WS6-1-13	K-Sand	29.0	223	2.5	14.3	Stress	35.3	0.1	Sinusoidal 2-way
14	WS6-1-14	K-Sand	50.0	463	2.5	15.1	Stress	27.0	0.1	Sinusoidal 2-way
15	WS6-1-15	K-Sand	38.0	320	2.5	14.6	Stress	32.5	0.1	Sinusoidal 2-way
16	WS6-1-16	K-Sand	55.0	642	2.5	15.3	Stress	32.4	0.1	Sinusoidal 2-way
17	WS6-1-17	K-Sand	51.0	615	2.5	15.1	Stress	35.2	0.1	Sinusoidal 2-way
18	WS6-1-18	K-Sand	58.0	899	2.5	15.4	Stress	35.9	0.1	Sinusoidal 2-way
19	WS6-1-19	K-Sand	37.0	309	2.5	14.6	Stress	34.5	0.1	Sinusoidal 2-way
20	WS6-1-20	K-Sand	47.0	467	2.5	15.0	Stress	33.1	0.1	Sinusoidal 2-way
21	WS6-1-21	K-Sand	39.0	379	2.5	14.7	Stress	34.5	0.1	Sinusoidal 2-way
22	WS6-1-22	K-Sand	61.0	1120	2.5	15.5	Stress	35.2	0.1	Sinusoidal 2-way
23	WS6-1-23	K-Sand	56.0	739	2.5	15.3	Stress	34.6	0.1	Sinusoidal 2-way
24	WS6-1-24	K-Sand	30.0	237	2.5	14.3	Stress	36.0	0.1	Sinusoidal 2-way
25	WS6-1-25	K-Sand	57.0	768	2.5	15.4	Stress	33.9	0.1	Sinusoidal 2-way
26	WS6-1-26	K-Sand	38.0	358	2.5	14.6	Stress	35.2	0.1	Sinusoidal 2-way
27	WS6-1-27	K-Sand	44.0	456	2.5	14.9	Stress	34.5	0.1	Sinusoidal 2-way

Table 2.6 - Summary of the Cyclic Triaxial Test Data on Clean Sands Performed at Wayne State University (Continued)

No.	Test ID	Sample	D_r(%)	E_{liq} (J/m^3)	FC (%)	γ_d (kN/m^3)	Control	σ_c' (kPa)	Freq. (Hz)	Load Shape
28	WS6-1-28	K-Sand	31.0	268	2.5	14.4	Stress	37.2	0.1	Sinusoidal 2-way
29	WS6-2-1	Monterey No. 0	62.0	1162	2	15.8	Stress	32.9	0.1	Sinusoidal 2-way
30	WS6-2-2	Monterey No. 0	57.0	802	2	15.6	Stress	33.6	0.1	Sinusoidal 2-way
31	WS6-2-3	Monterey No. 0	36.0	302	2	14.8	Stress	32.5	0.1	Sinusoidal 2-way
32	WS6-2-4	Monterey No. 0	39.0	361	2	14.9	Stress	34.3	0.1	Sinusoidal 2-way
33	WS6-2-5	Monterey No. 0	38.0	424	2	14.8	Stress	43.1	0.1	Sinusoidal 2-way
34	WS6-2-6	Monterey No. 0	52.0	710	2	15.4	Stress	41.4	0.1	Sinusoidal 2-way
35	WS6-2-7	Monterey No. 0	58.0	1083	2	15.6	Stress	42.9	0.1	Sinusoidal 2-way
36	WS6-2-8	Monterey No. 0	60.0	1264	2	15.7	Stress	39.6	0.1	Sinusoidal 2-way
37	WS6-2-9	Monterey No. 0	65.0	1747	2	15.9	Stress	42.7	0.1	Sinusoidal 2-way
38	WS6-2-10	Monterey No. 0	59.0	926	2	15.7	Stress	34.4	0.1	Sinusoidal 2-way
39	WS6-2-11	Monterey No. 0	66.0	1749	2	15.9	Stress	40.8	0.1	Sinusoidal 2-way
40	WS6-2-12	Monterey No. 0	26.0	215	2	14.4	Stress	34.5	0.1	Sinusoidal 2-way
41	WS6-2-13	Monterey No. 0	32.0	252	2	14.6	Stress	31.0	0.1	Sinusoidal 2-way
42	WS6-2-14	Monterey No. 0	30.0	239	2	14.6	Stress	31.8	0.1	Sinusoidal 2-way
43	WS6-2-15	Monterey No. 0	55.0	762	2	15.5	Stress	37.0	0.1	Sinusoidal 2-way
44	WS6-2-16	Monterey No. 0	54.0	615	2	15.5	Stress	32.4	0.1	Sinusoidal 2-way
45	WS6-2-17	Monterey No. 0	47.0	436	2	15.2	Stress	33.5	0.1	Sinusoidal 2-way
46	WS6-2-18	Monterey No. 0	44.0	413	2	15.1	Stress	32.3	0.1	Sinusoidal 2-way
47	WS6-2-19	Monterey No. 0	42.0	320	2	15.0	Stress	27.7	0.1	Sinusoidal 2-way
48	WS6-2-20	Monterey No. 0	72.0	1179	2	16.2	Stress	16.5	0.1	Sinusoidal 2-way
49	WS6-2-21	Monterey No. 0	28.0	194	2	14.5	Stress	28.1	0.1	Sinusoidal 2-way
50	WS6-2-22	Monterey No. 0	41.0	374	2	15.0	Stress	33.4	0.1	Sinusoidal 2-way
51	WS6-2-23	Monterey No. 0	35.0	251	2	14.7	Stress	28.2	0.1	Sinusoidal 2-way
52	WS6-2-24	Monterey No. 0	51.0	533	2	15.3	Stress	33.8	0.1	Sinusoidal 2-way
53	WS6-2-25	Monterey No. 0	53.0	462	2	15.4	Stress	25.9	0.1	Sinusoidal 2-way
54	WS6-2-26	Monterey No. 0	33.0	232	2	14.7	Stress	27.3	0.1	Sinusoidal 2-way

Table 2.6 - Summary of the Cyclic Triaxial Test Data on Clean Sands Performed at Wayne State University (Continued)

No.	Test ID	Sample	D_r(%)	E_{liq} (J/m^3)	FC (%)	γ_d (kN/m^3)	Control	σ_c' (kPa)	Freq. (Hz)	Load Shape
55	WS6-2-27	Monterey No. 0	49.0	532	2	15.3	Stress	35.3	0.1	Sinusoidal 2-way
56	WS6-2-28	Monterey No. 0	56.0	608	2	15.5	Stress	27.3	0.1	Sinusoidal 2-way
57	WS6-3-1	Monterey No. 0	51.0	2423	2	15.3	Stress	61.0	0.1	Sinusoidal 1-way
58	WS6-3-2	Monterey No. 0	33.0	1114	2	14.7	Stress	67.6	0.1	Sinusoidal 1-way
59	WS6-3-3	Monterey No. 0	30.0	755	2	14.6	Stress	60.4	0.1	Sinusoidal 1-way
60	WS6-3-4	Monterey No. 0	54.0	3151	2	15.5	Stress	67.1	0.1	Sinusoidal 1-way
61	WS6-3-5	Monterey No. 0	53.0	2589	2	15.4	Stress	58.8	0.1	Sinusoidal 1-way
62	WS6-3-6	Monterey No. 0	43.0	1306	2	15.0	Stress	45.3	0.1	Sinusoidal 1-way
63	WS6-3-7	Monterey No. 0	28.0	547	2	14.5	Stress	51.8	0.1	Sinusoidal 1-way
64	WS6-3-8	Monterey No. 0	71.0	4468	2	16.1	Stress	45.6	0.1	Sinusoidal 1-way
65	WS6-3-9	Monterey No. 0	46.0	1679	2	15.1	Stress	52.5	0.1	Sinusoidal 1-way
66	WS6-3-10	Monterey No. 0	61.0	1944	2	15.7	Stress	33.1	0.1	Sinusoidal 1-way
67	WS6-3-11	Monterey No. 0	62.0	2047	2	15.8	Stress	32.3	0.1	Sinusoidal 1-way
68	WS6-3-12	Monterey No. 0	38.0	633	2	14.8	Stress	29.6	0.1	Sinusoidal 1-way
69	WS6-3-13	Monterey No. 0	68.0	2952	2	16.0	Stress	34.7	0.1	Sinusoidal 1-way
70	WS6-3-14	Monterey No. 0	66.0	3813	2	15.9	Stress	48.6	0.1	Sinusoidal 1-way
71	WS6-3-15	Monterey No. 0	73.0	5014	2	16.2	Stress	44.5	0.1	Sinusoidal 1-way
72	WS6-3-16	Monterey No. 0	56.0	2148	2	15.5	Stress	43.1	0.1	Sinusoidal 1-way
73	WS6-3-17	Monterey No. 0	55.0	2031	2	15.5	Stress	42.3	0.1	Sinusoidal 1-way
74	WS6-3-18	Monterey No. 0	58.0	2622	2	15.6	Stress	48.6	0.1	Sinusoidal 1-way
75	WS6-3-19	Monterey No. 0	49.0	1184	2	15.3	Stress	31.9	0.1	Sinusoidal 1-way
76	WS6-3-20	Monterey No. 0	32.0	441	2	14.6	Stress	31.7	0.1	Sinusoidal 1-way
77	WS6-3-21	Monterey No. 0	82.0	5103	2	16.6	Stress	40.5	0.1	Sinusoidal 1-way
78	WS6-3-22	Monterey No. 0	50.0	1073	2	15.3	Stress	26.8	0.1	Sinusoidal 1-way
79	WS6-3-23	Monterey No. 0	52.0	1655	2	15.4	Stress	40.3	0.1	Sinusoidal 1-way
80	WS6-3-24	Monterey No. 0	36.0	511	2	14.8	Stress	27.5	0.1	Sinusoidal 1-way
81	WS6-3-25	Monterey No. 0	37.0	666	2	14.8	Stress	34.1	0.1	Sinusoidal 1-way

Table 2.6 - Summary of the Cyclic Triaxial Test Data on Clean Sands Performed at Wayne State University (Continued)

No.	Test ID	Sample	D_r(%)	E_{liq} (J/m^3)	FC (%)	γ_d (kN/m^3)	Control	σ_c' (kPa)	Freq. (Hz)	Load Shape
82	WS6-4-1	Monterey No. 0	49.0	51	2	15.3	Stress	42.0	Earthquake	Earthquake
83	WS6-4-2	Monterey No. 0	61.0	79	2	15.7	Stress	40.7	Earthquake	Earthquake
84	WS6-4-3	Monterey No. 0	53.0	57	2	15.4	Stress	40.1	Earthquake	Earthquake
85	WS6-4-4	Monterey No. 0	40.0	36	2	14.9	Stress	42.6	Earthquake	Earthquake
86	WS6-4-5	Monterey No. 0	89.0	105	2	17.0	Stress	15.2	Earthquake	Earthquake
87	WS6-4-6	Monterey No. 0	44.0	40	2	15.1	Stress	41.3	Earthquake	Earthquake
88	WS6-4-7	Monterey No. 0	35.0	33	2	14.7	Stress	43.2	Earthquake	Earthquake
89	WS6-4-8	Monterey No. 0	31.0	28	2	14.6	Stress	41.6	Earthquake	Earthquake
90	WS6-4-9	Monterey No. 0	71.0	71	2	16.1	Stress	23.4	Earthquake	Earthquake
91	WS6-4-10	Monterey No. 0	80.0	190	2	16.5	Stress	43.9	Earthquake	Earthquake

Test I.D.:	MONT19	**Controlled Parameter:**	Strain
Relative Density (%):	60.6	**Initial Effective Stress (kPa):**	100
Applied Shear Strain (%):	0.25	**Frequency (Hz):**	15

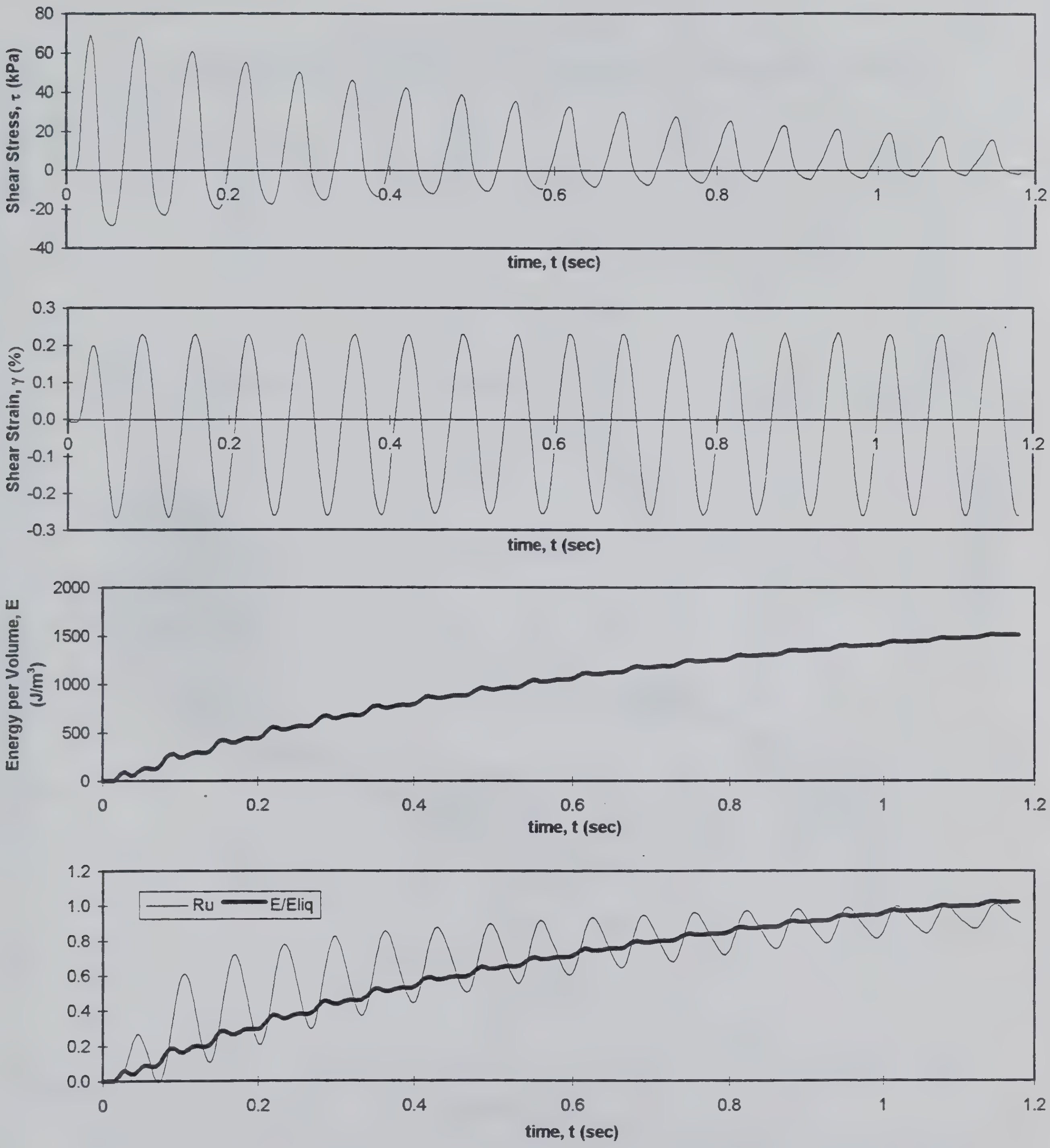

Figure 2.1 - Typical Time History Records of a Strain-Controlled Cyclic Triaxial Test

Test I.D.:	MONT19	**Controlled Parameter:**	Strain
Relative Density (%):	60.6	**Initial Effective Stress (kPa):**	100
Applied Shear Strain (%):	0.25	**Frequency (Hz):**	15

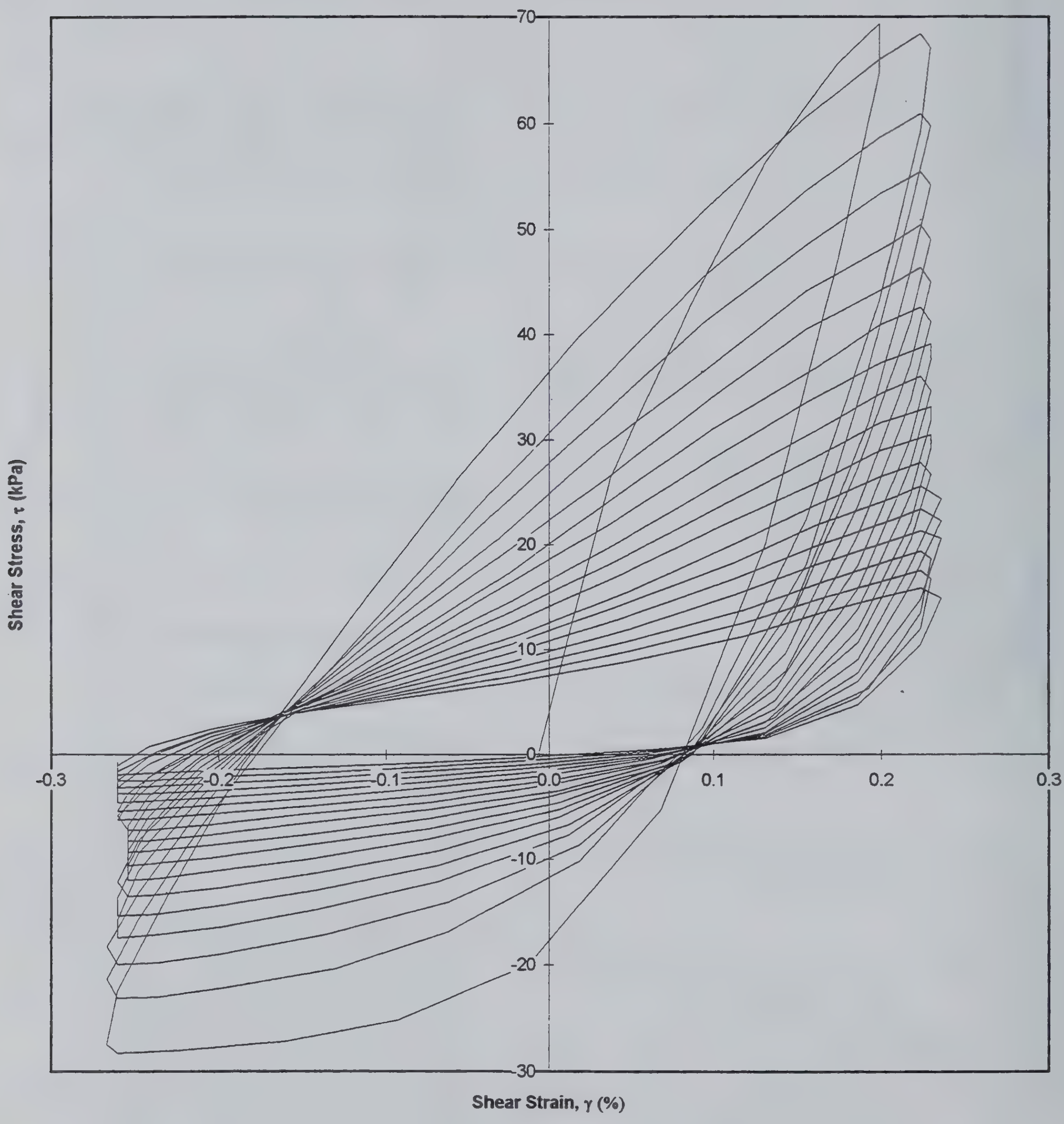
Shear Stress vs. Shear Strain

Figure 2.2 - A Typical Plot of Shear Stress - Shear Strain Hysteresis Loops Developed During Cyclic Triaxial Tests

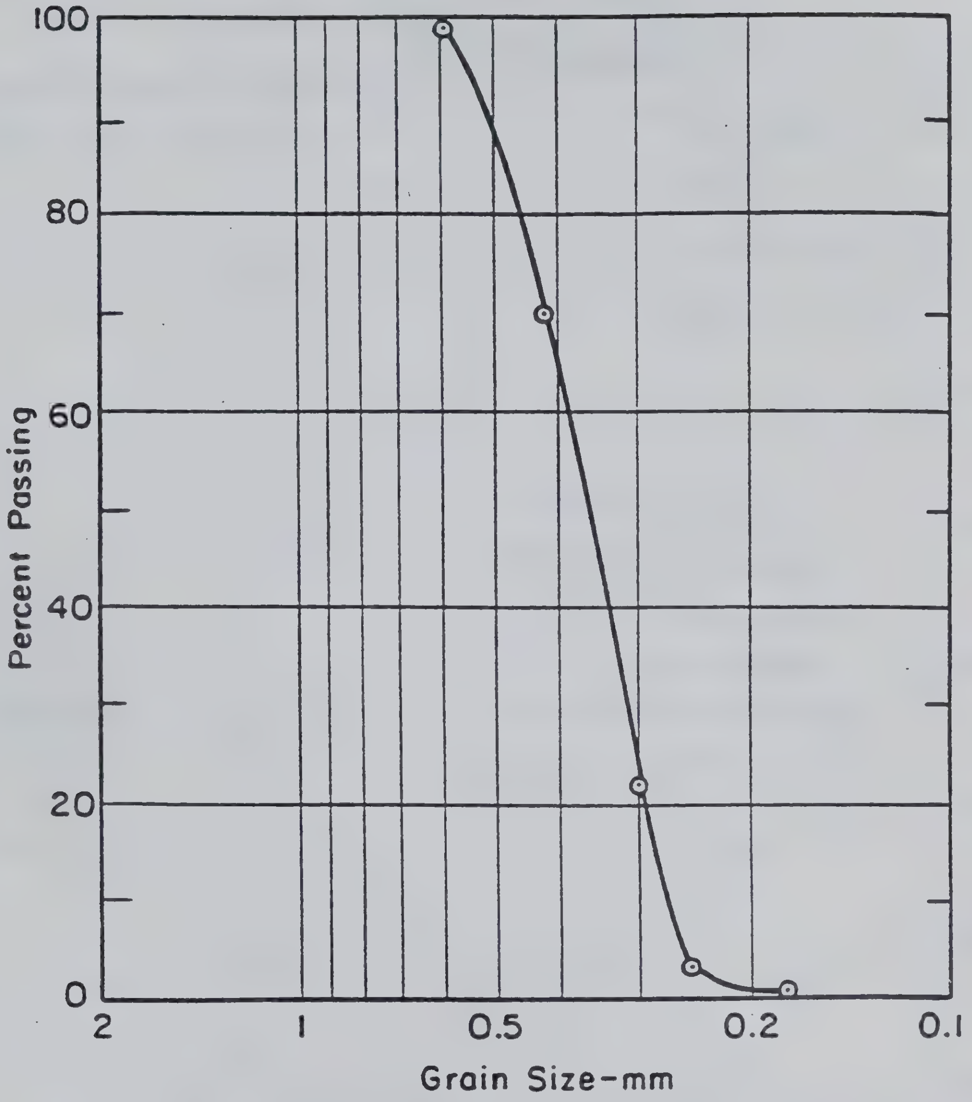

Figure 2.3 - Grain Size Distribution Curve for Monterey No. 0 Sand (Arango, 1994)

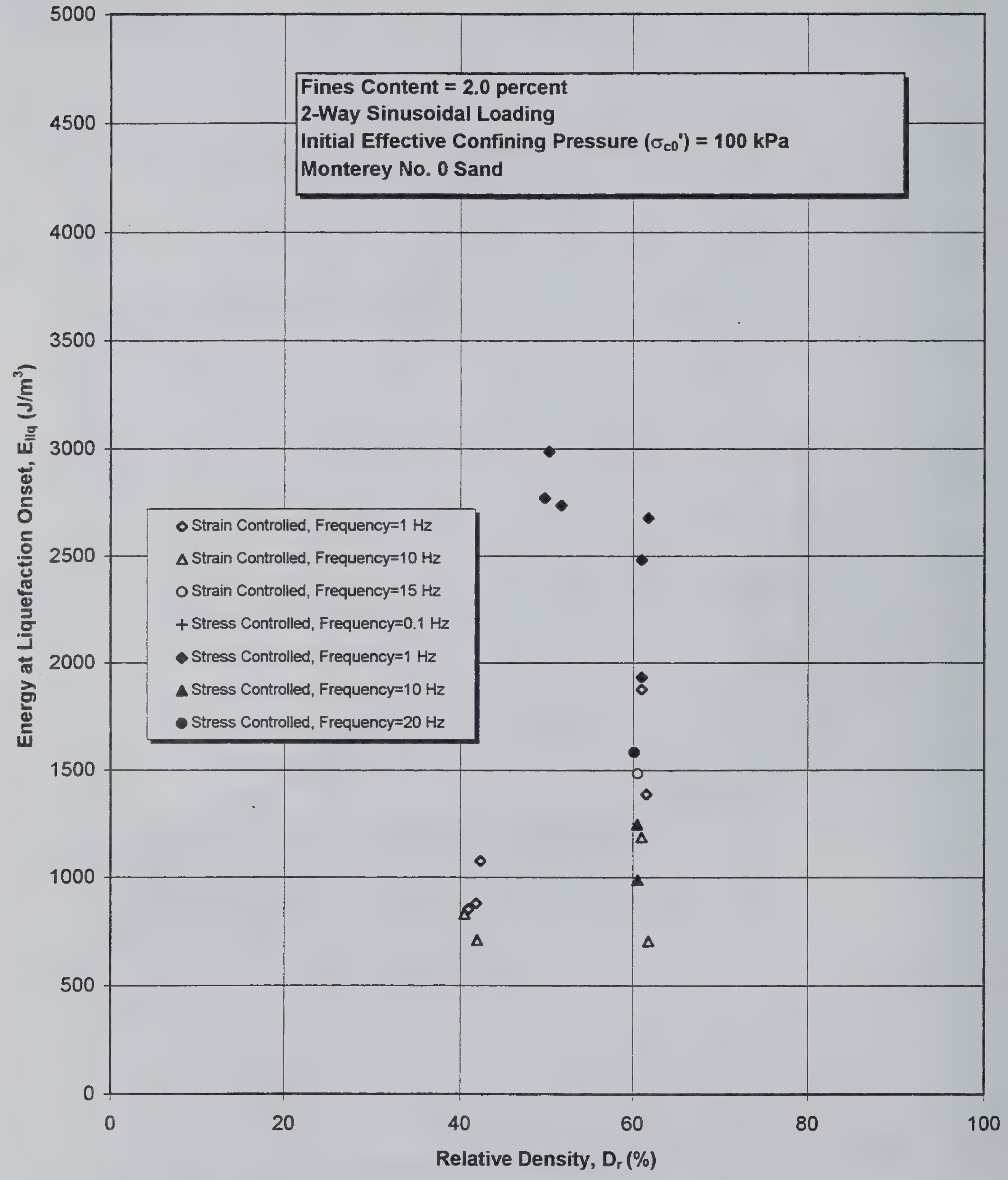

Figure 2.4 - Strain Energy at Liquefaction Onset as a Function of Relative Density for Monterey No. 0 Sand - UCB Data

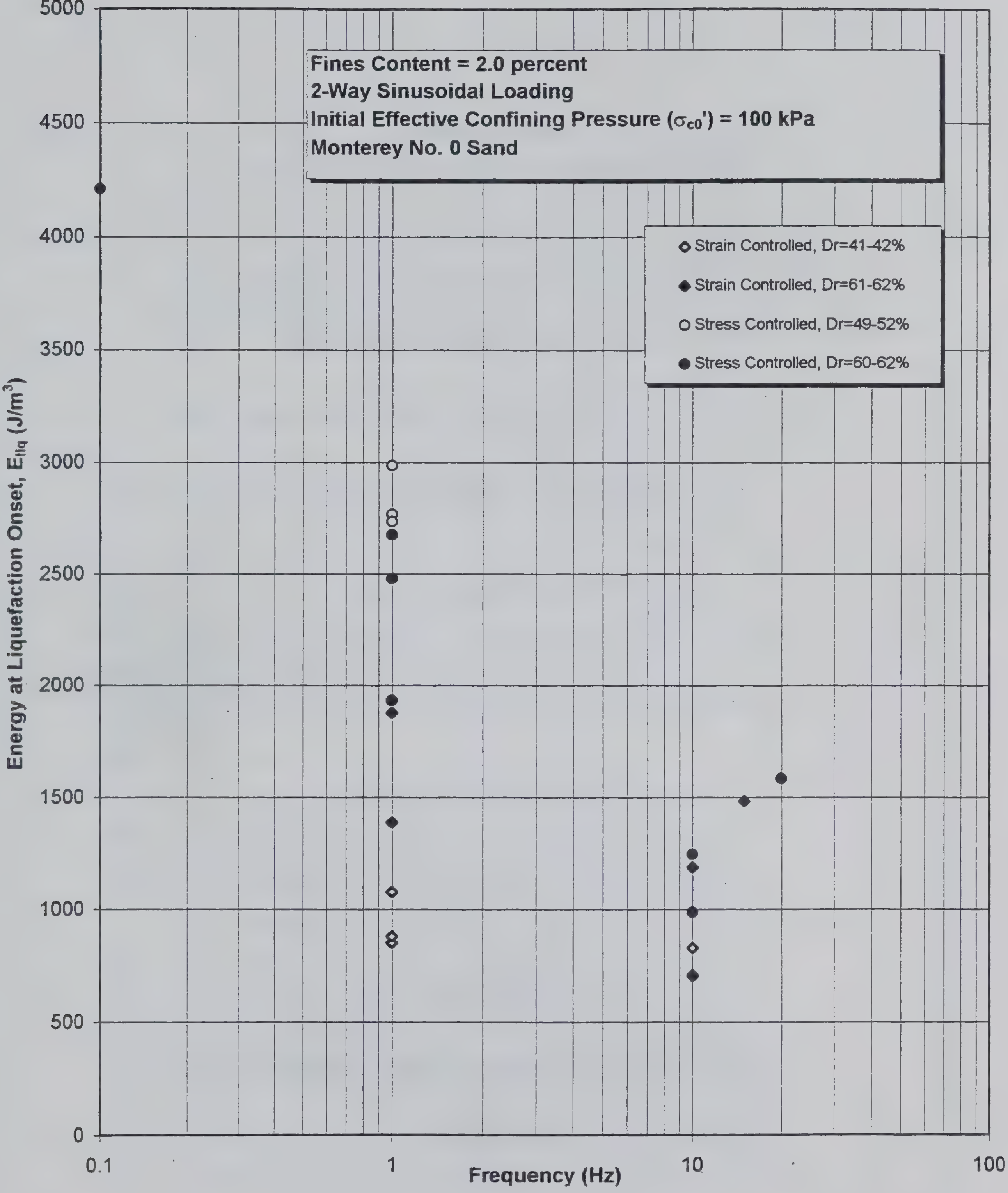

Figure 2.5 - Strain Energy at Liquefaction Onset as a Function of Frequencies of Loading for Monterey No. 0 Sand - UCB Data

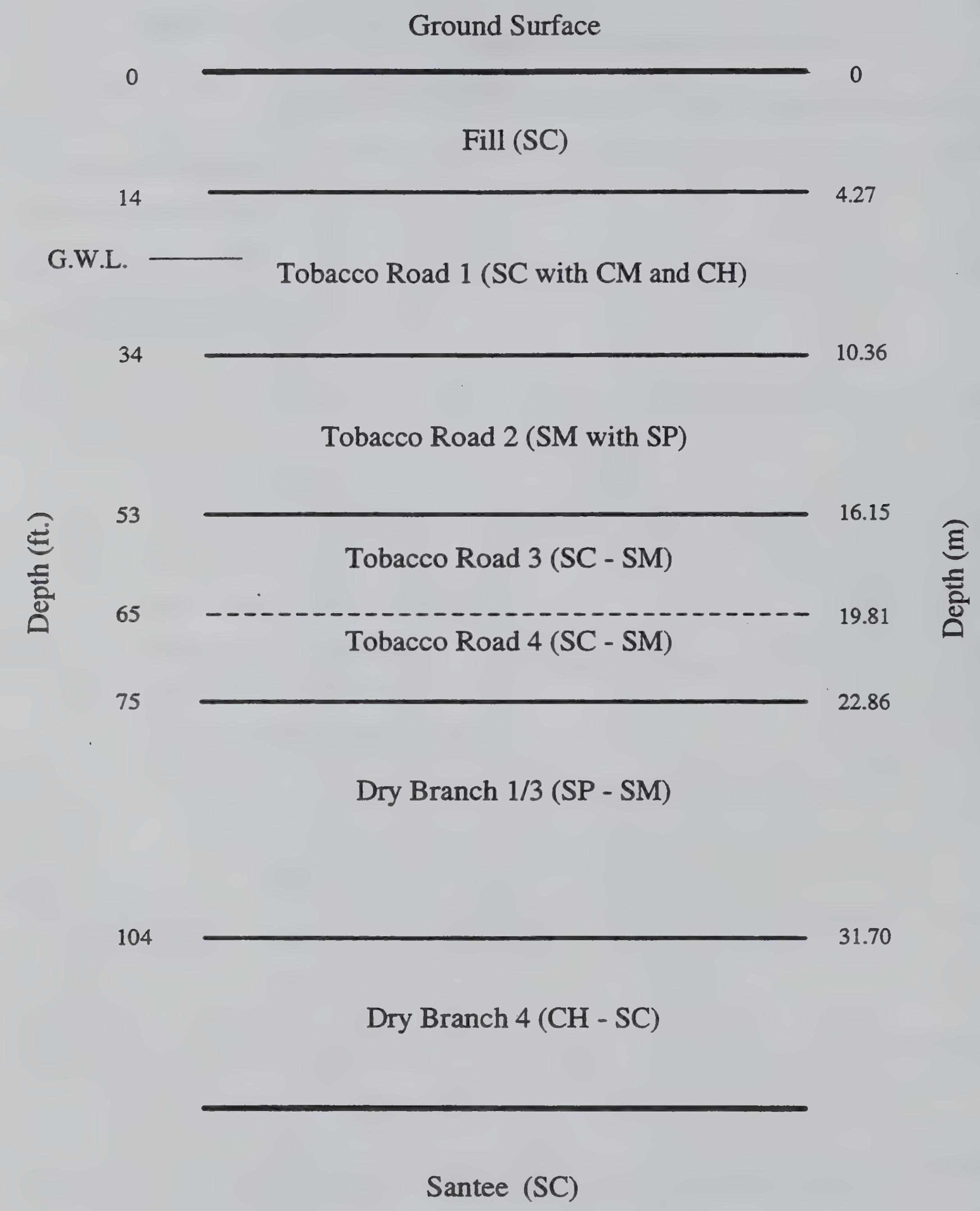

Figure 2.6 - Generalized Subsurface Soil Profile at SRS Site

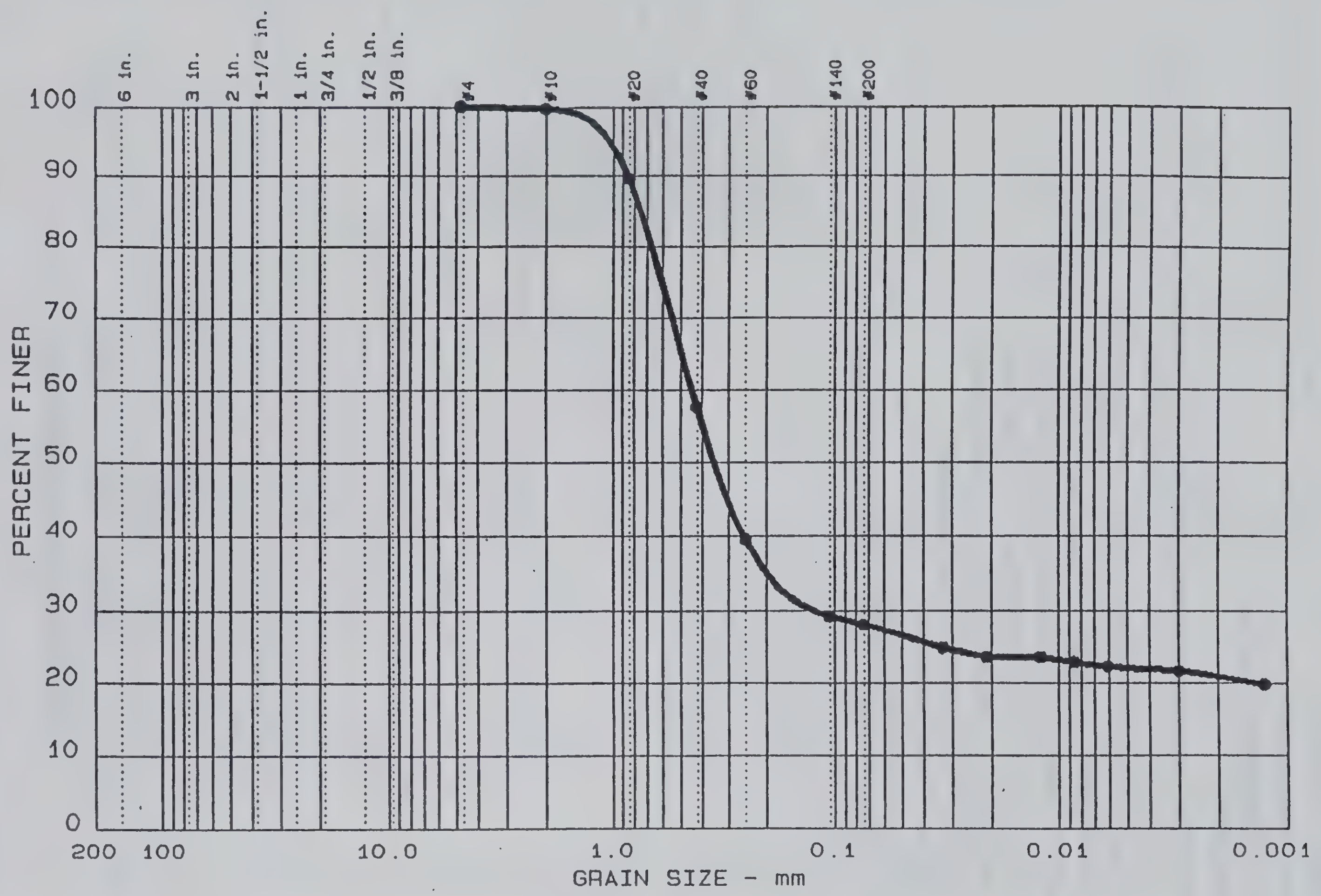

Figure 2.7 - Typical Grain Size Distribution Curve for Tobacco Road Soil Material, SRS (Riemer and Seed, 1994)

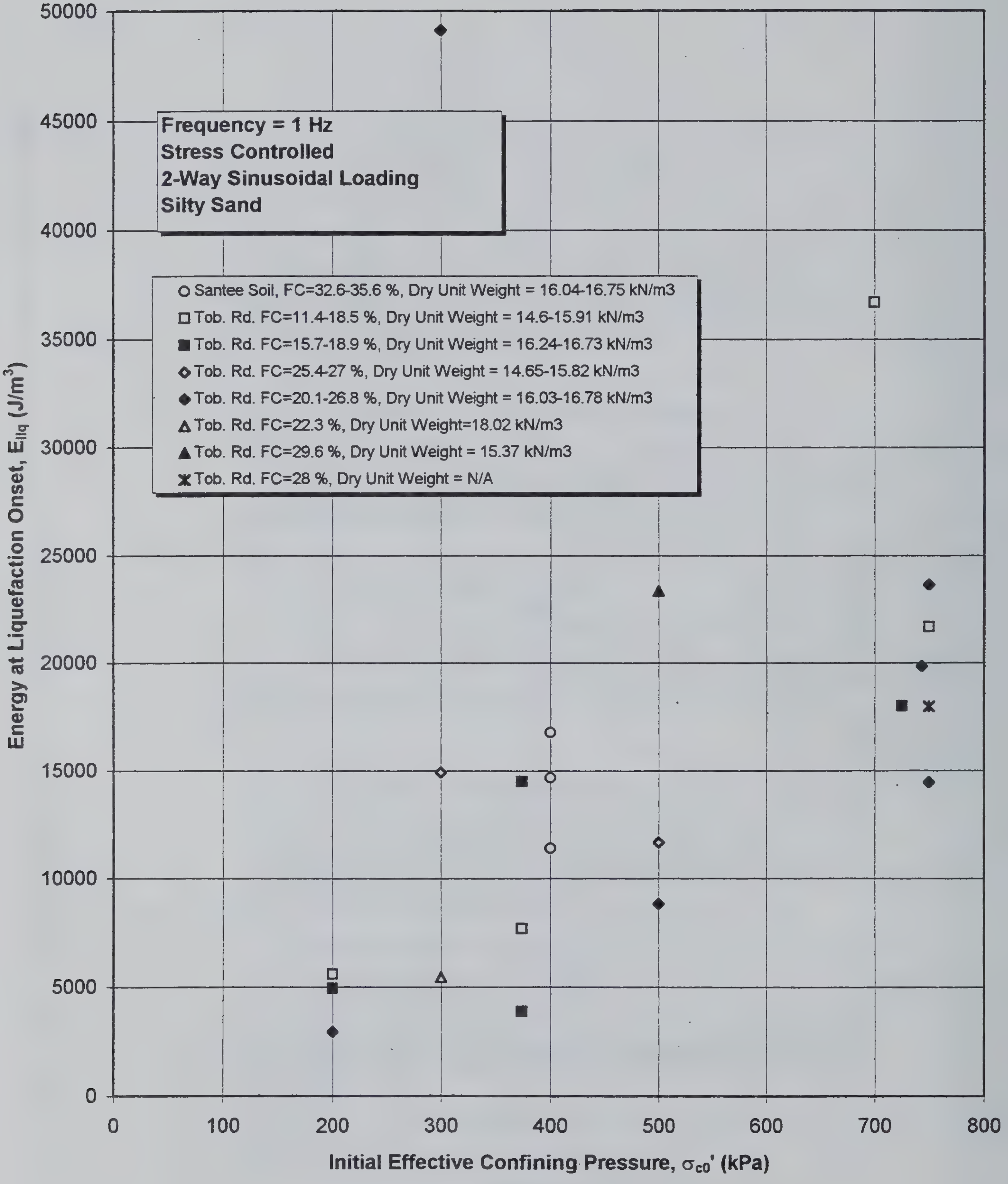

Figure 2.8 - Strain Energy at Liquefaction Onset as a Function of Confining Pressure for SRS Soil Samples - UCB Data

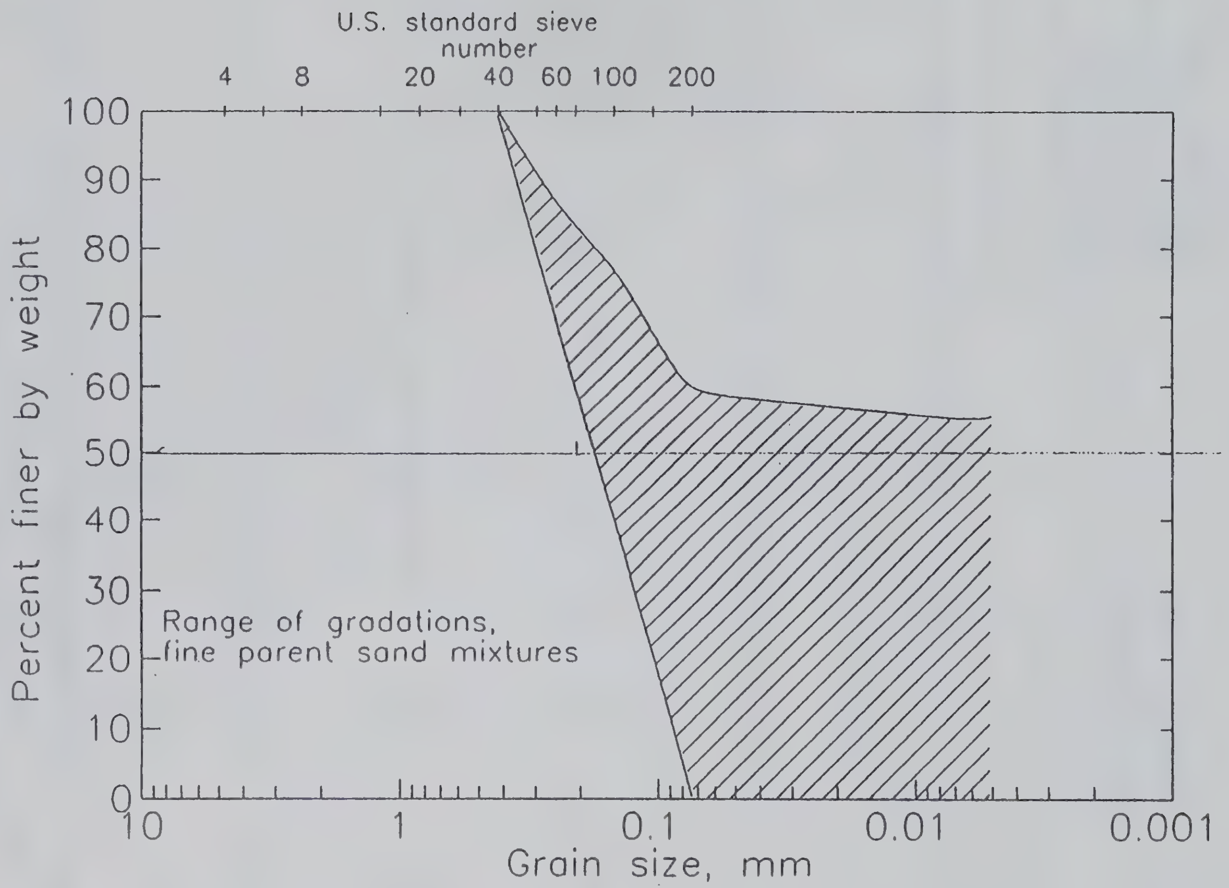

Figure 2.9 - Grain Size Distribution of Silty Sands - University of Colorado Samples (Koester, 1992)

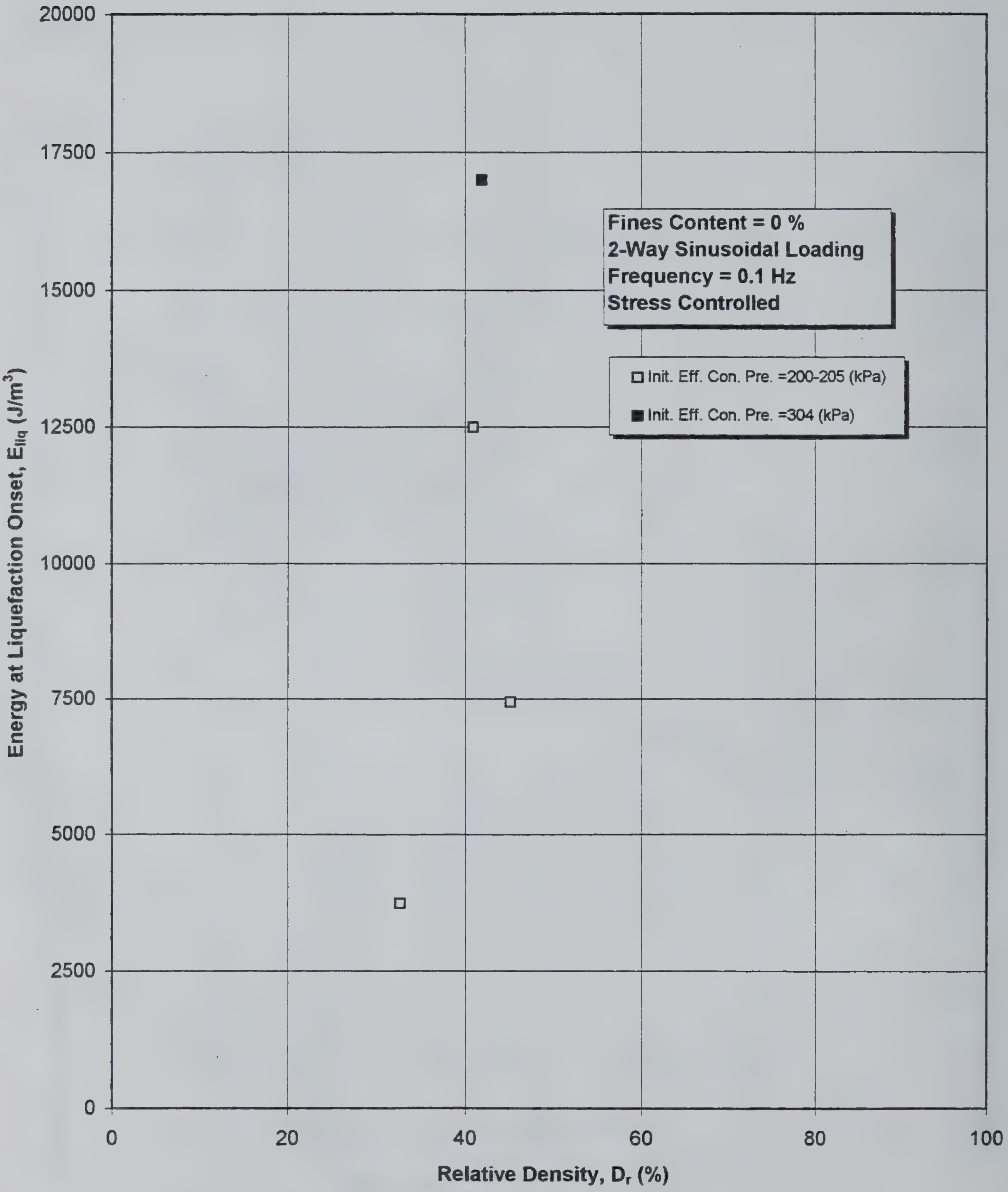

Figure 2.10 - Strain Energy at Liquefaction Onset as a Function of Relative Density for Clean Sands - University of Colorado Data

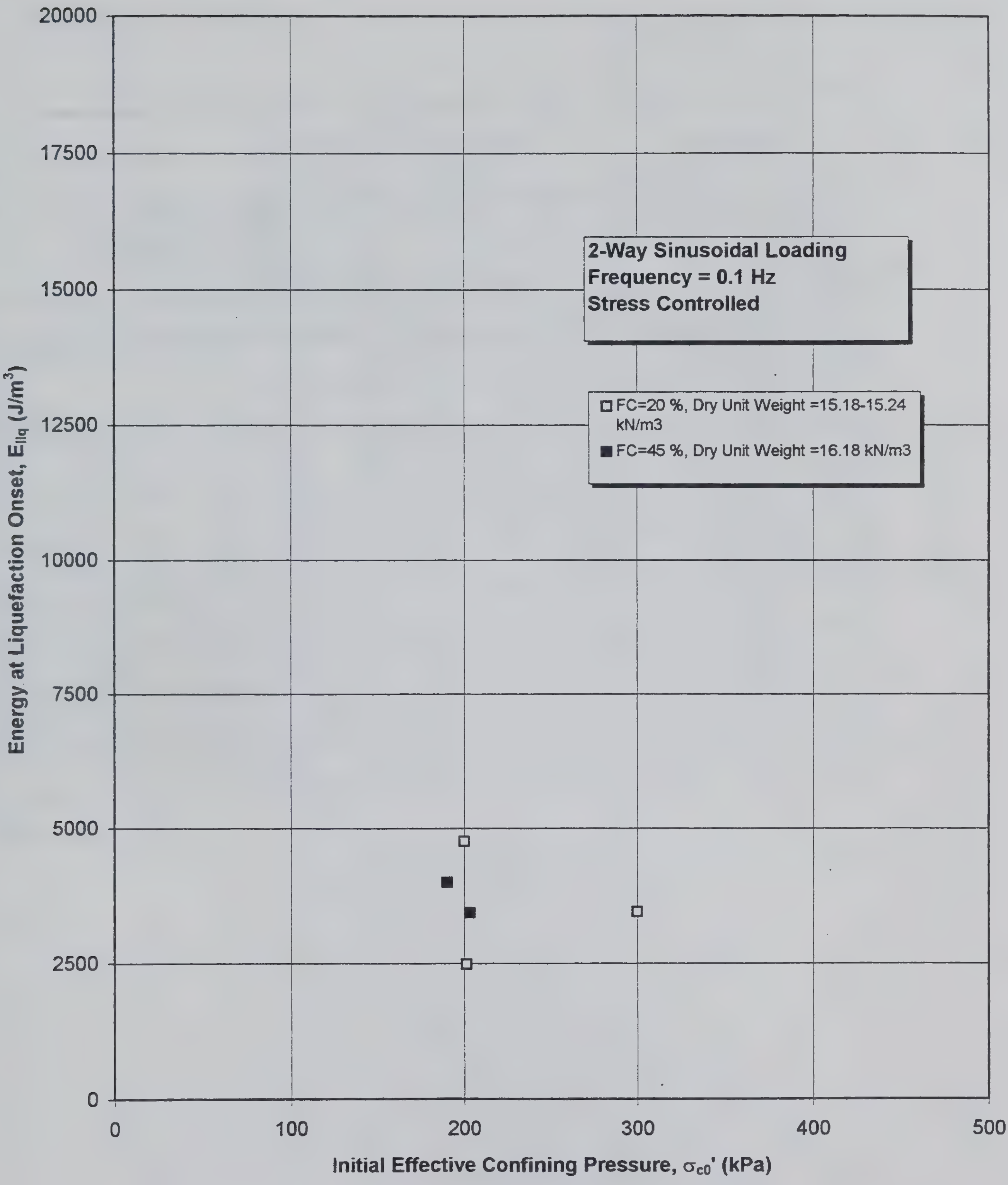

Figure 2.11 - Strain Energy at Liquefaction Onset as a Function of Confining Pressure for Silty Sands - University of Colorado Data

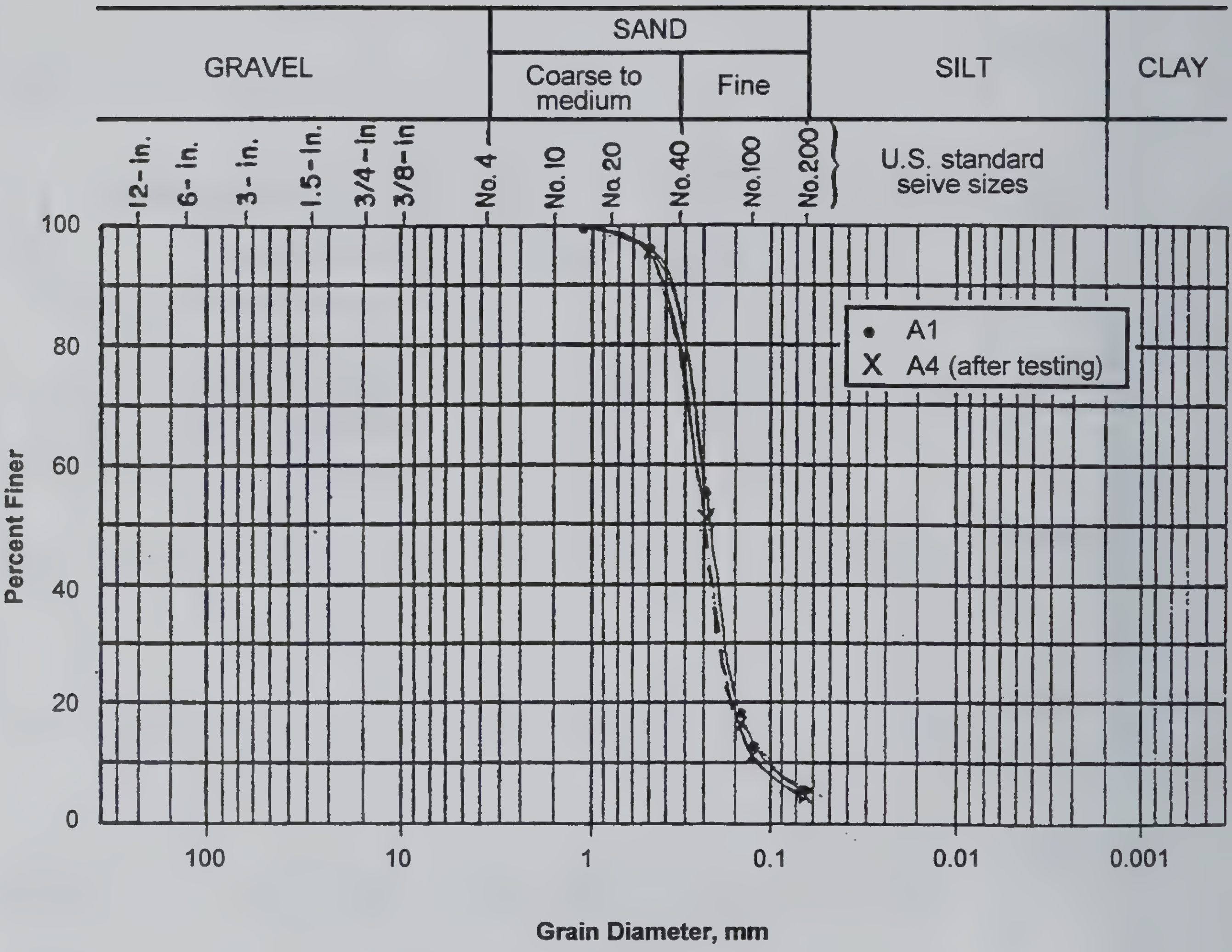

Figure 2.12 - Grain Size Distribution Curves for the Northridge Site Soil Samples (Arango and Migues, 1996)

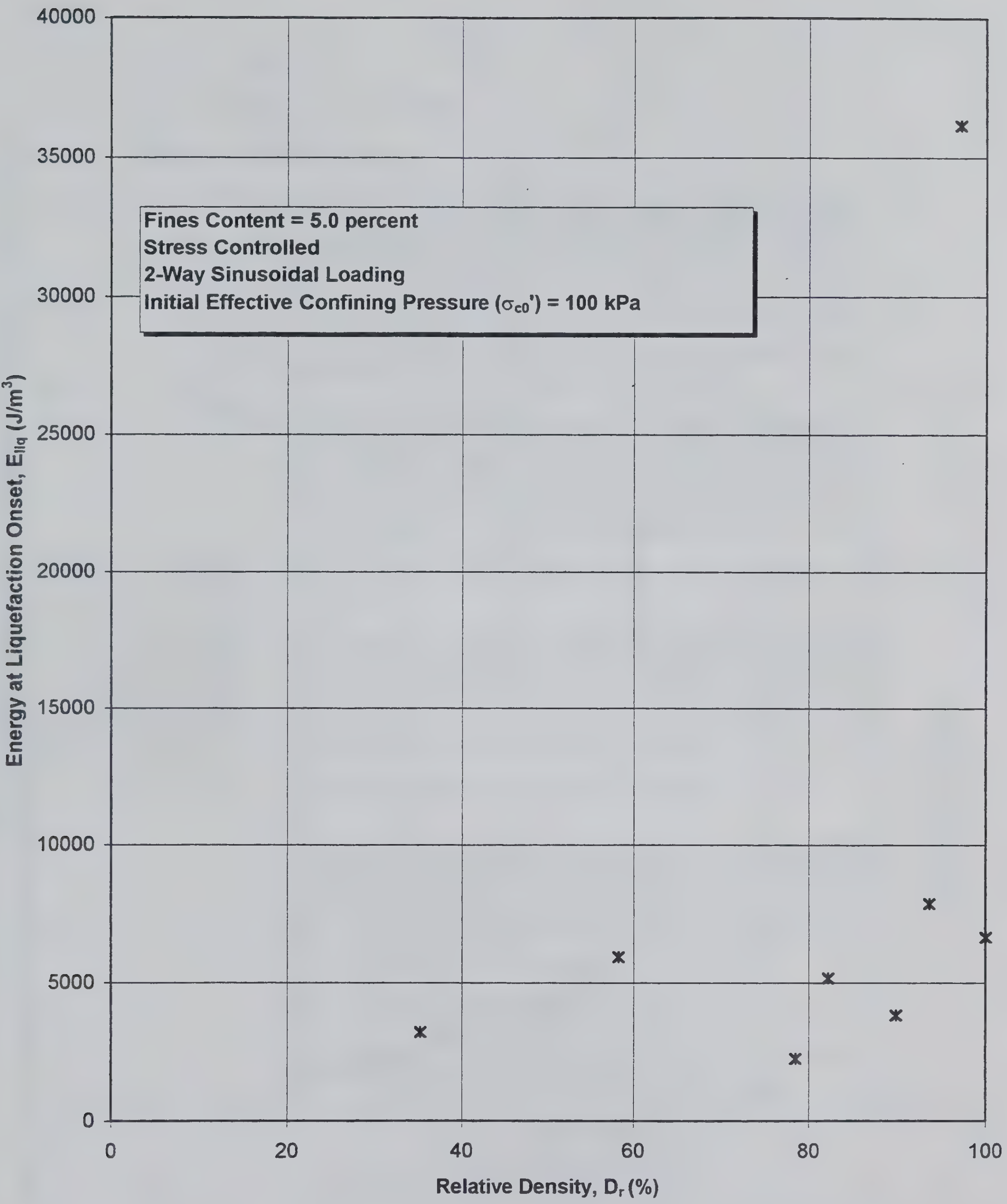

Figure 2.13 - Strain Energy at Liquefaction Onset as a Function of Relative Density for the Northridge Samples - UCB Data

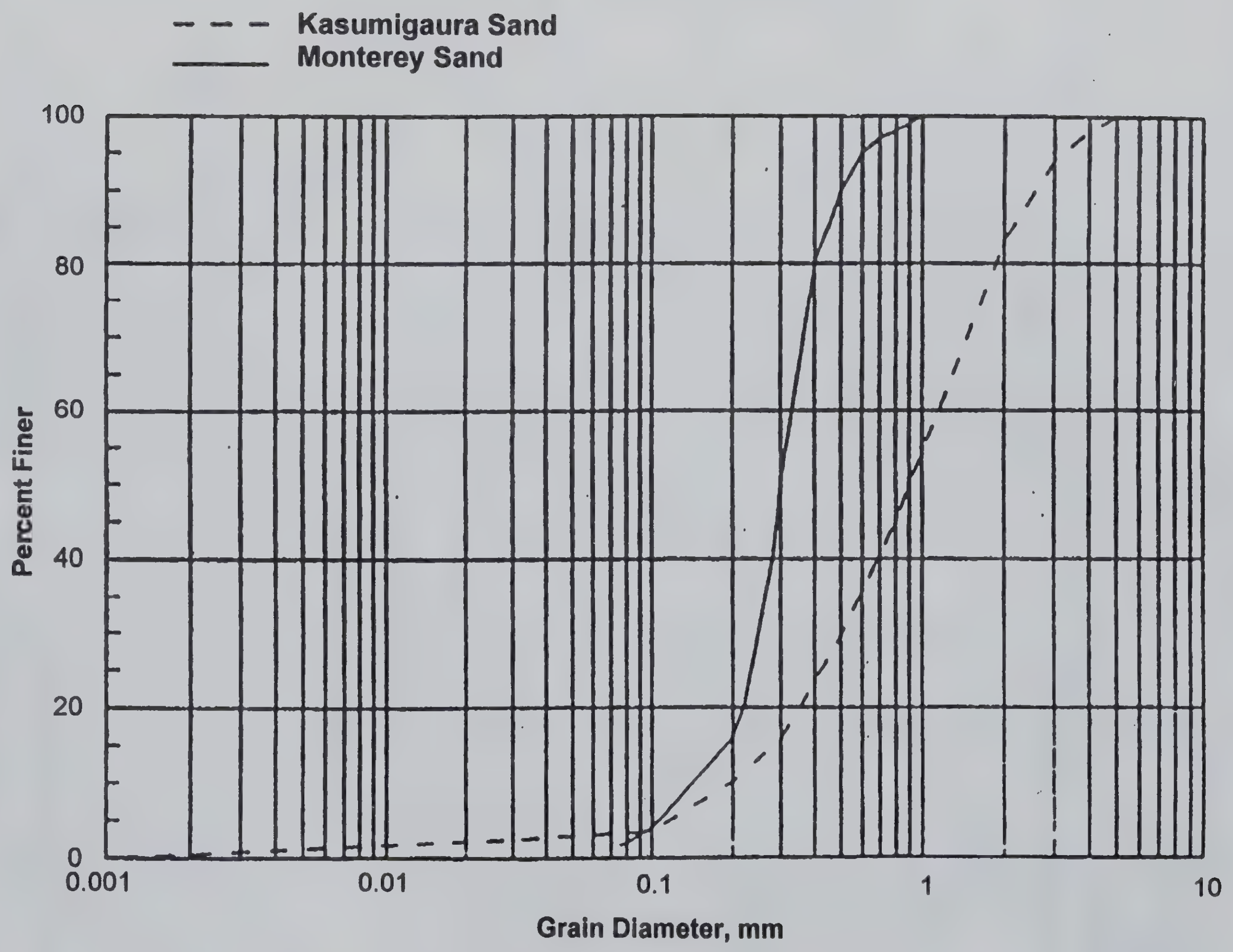

Figure 2.14 - Grain Size Distribution Curves for Monterey No. 0 and Kasumigaura Sands (AL-Khatib, 1994)

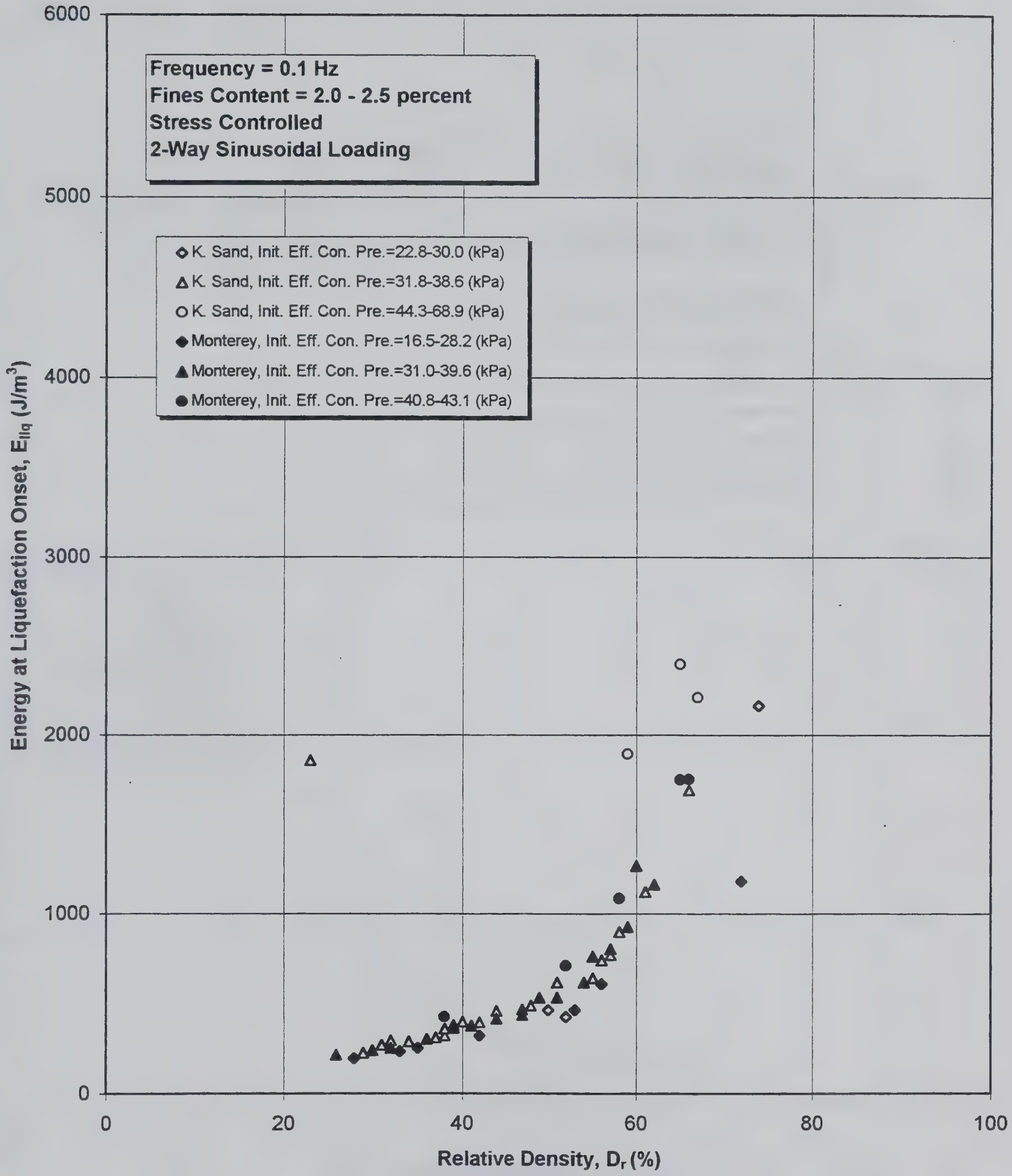

Figure 2.15 - Strain Energy at Liquefaction Onset as a Function of Relative Density for Monterey No. 0 and Kasumigaura Sands - WSU Data

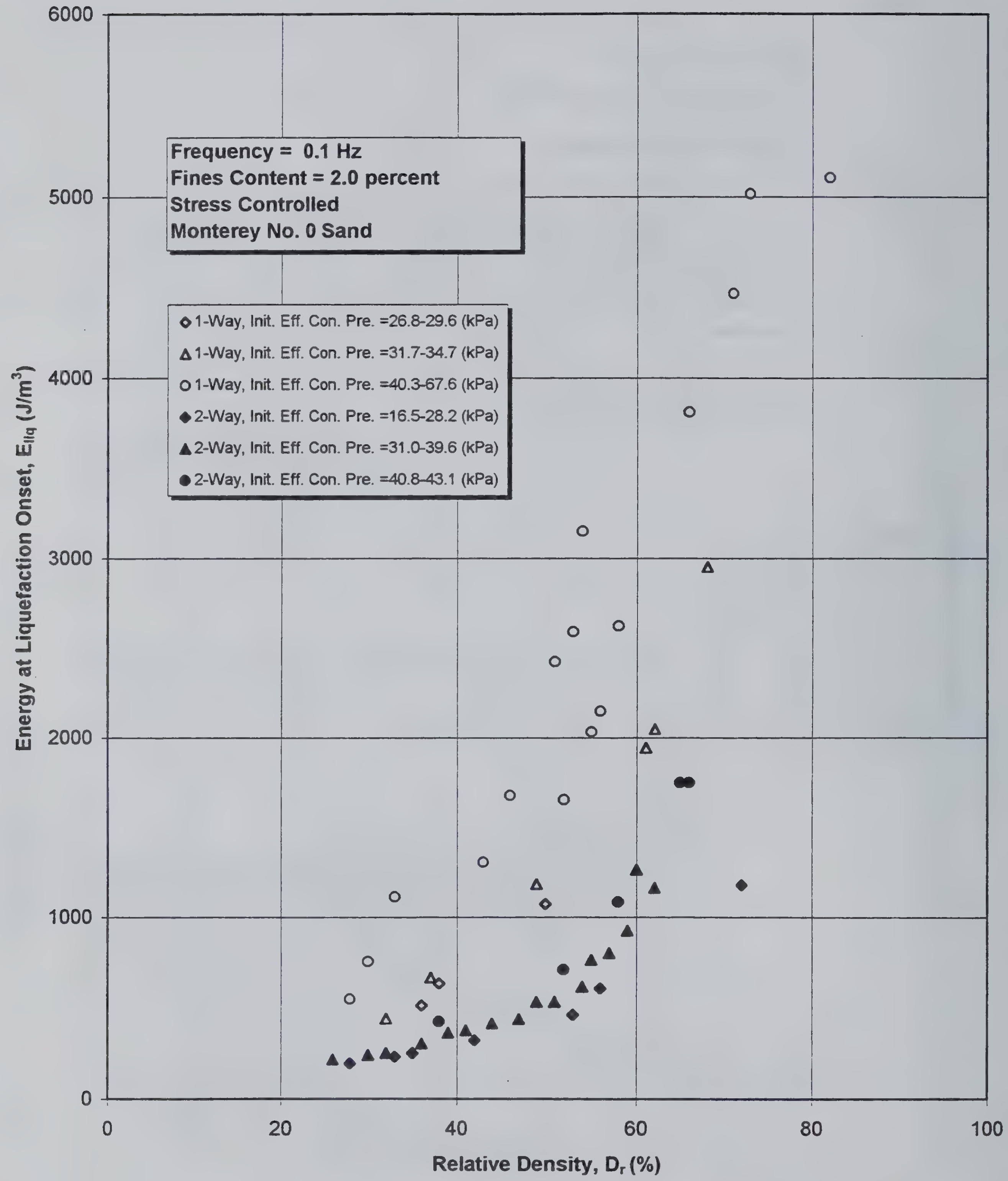

Figure 2.16 - Effect of Cyclic Loading Types on Strain Energy at Liquefaction Onset for Monterey No. 0 Sand - WSU Data

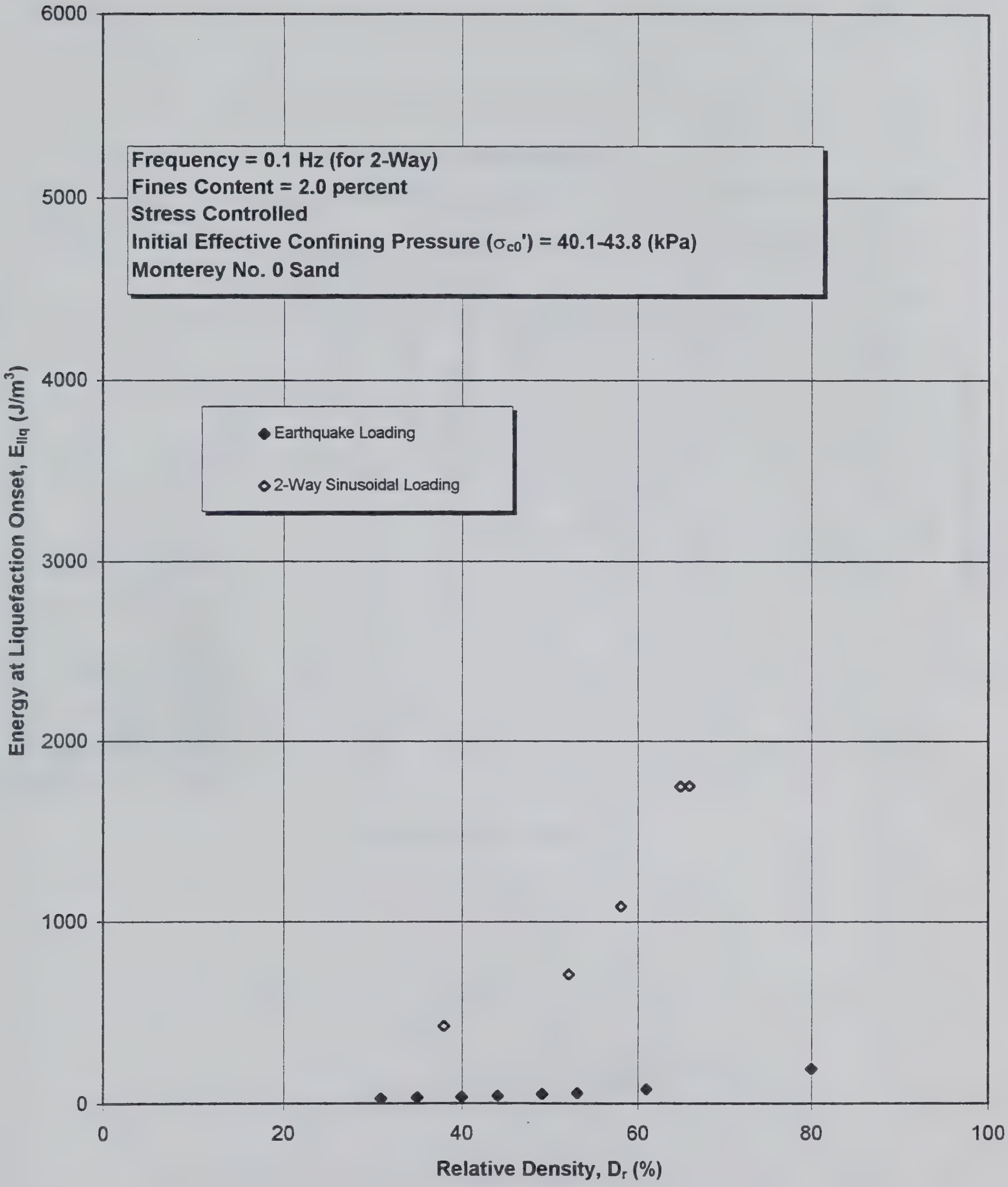

Figure 2.17 - Effect of Cyclic and Transient Loadings on Strain Energy at Liquefaction Onset for Monterey No. 0 Sand - WSU Data

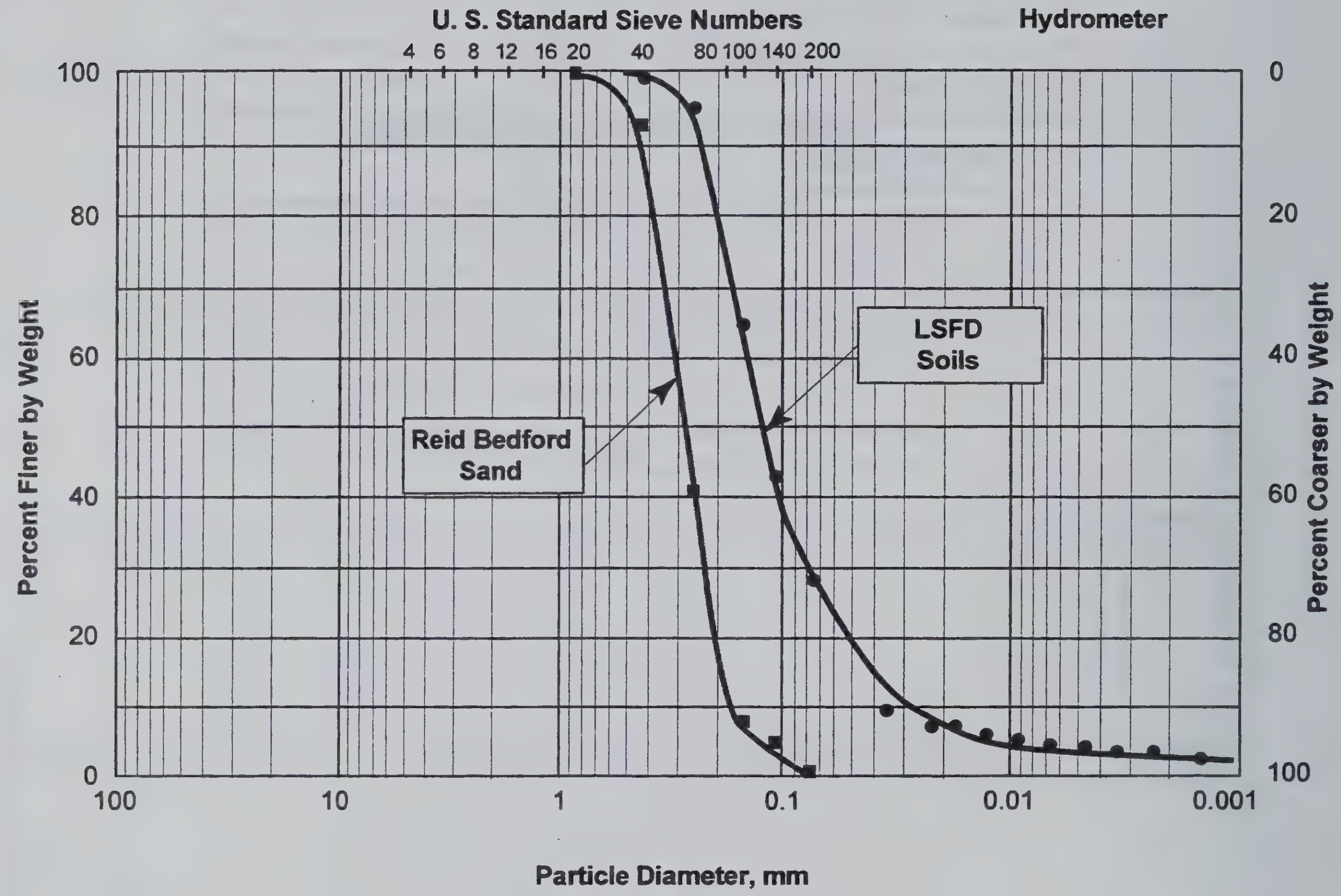

Figure 2.18 - Grain Size Distribution Curves for Soil Samples from the Lower San Fernando Dam and the Reid Bedford Sand (Figeroa et al., 1995)

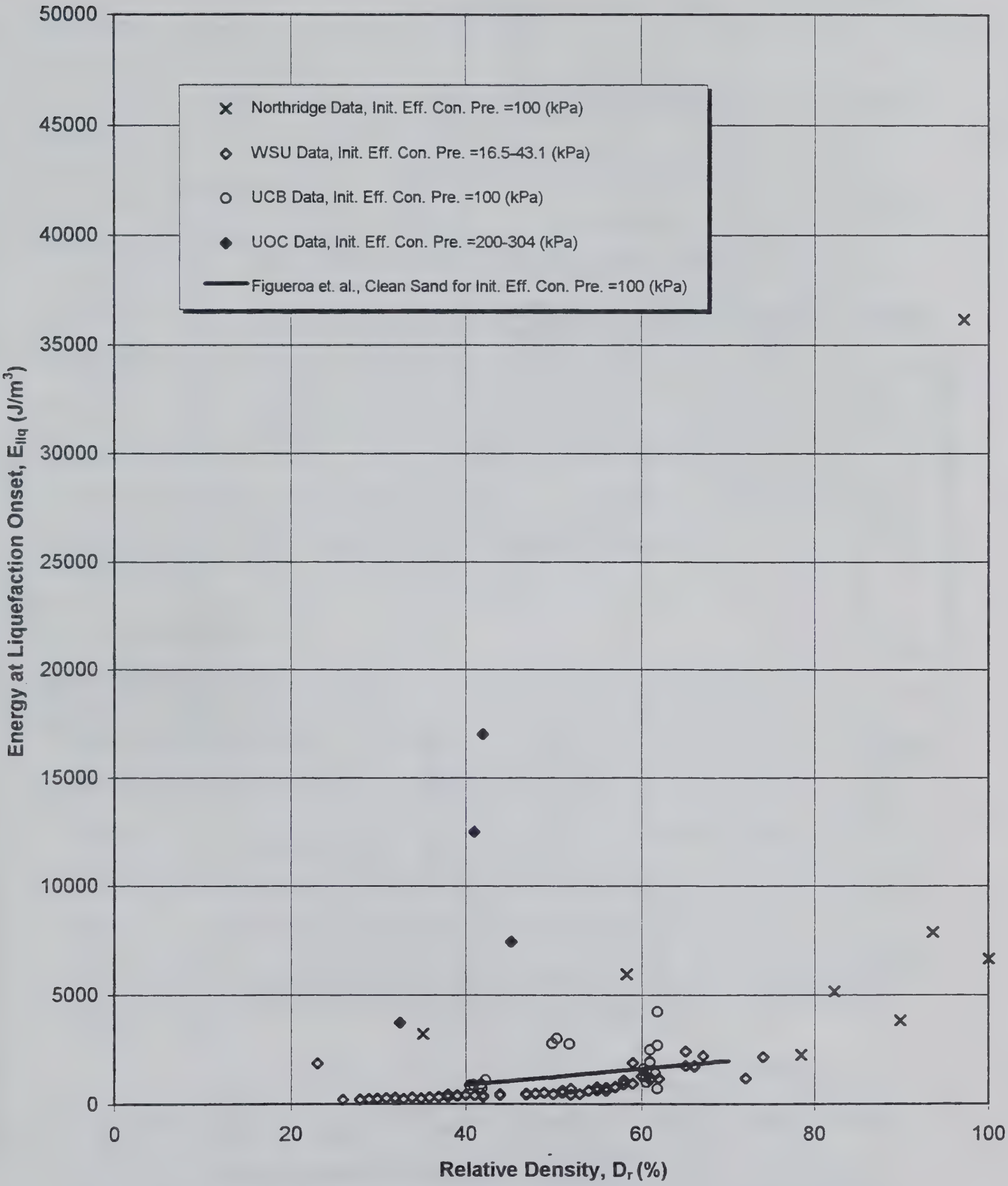

Figure 2.19 - Comparison of Strain Energy at Liquefaction Onset for All Test Groups - Clean Sands

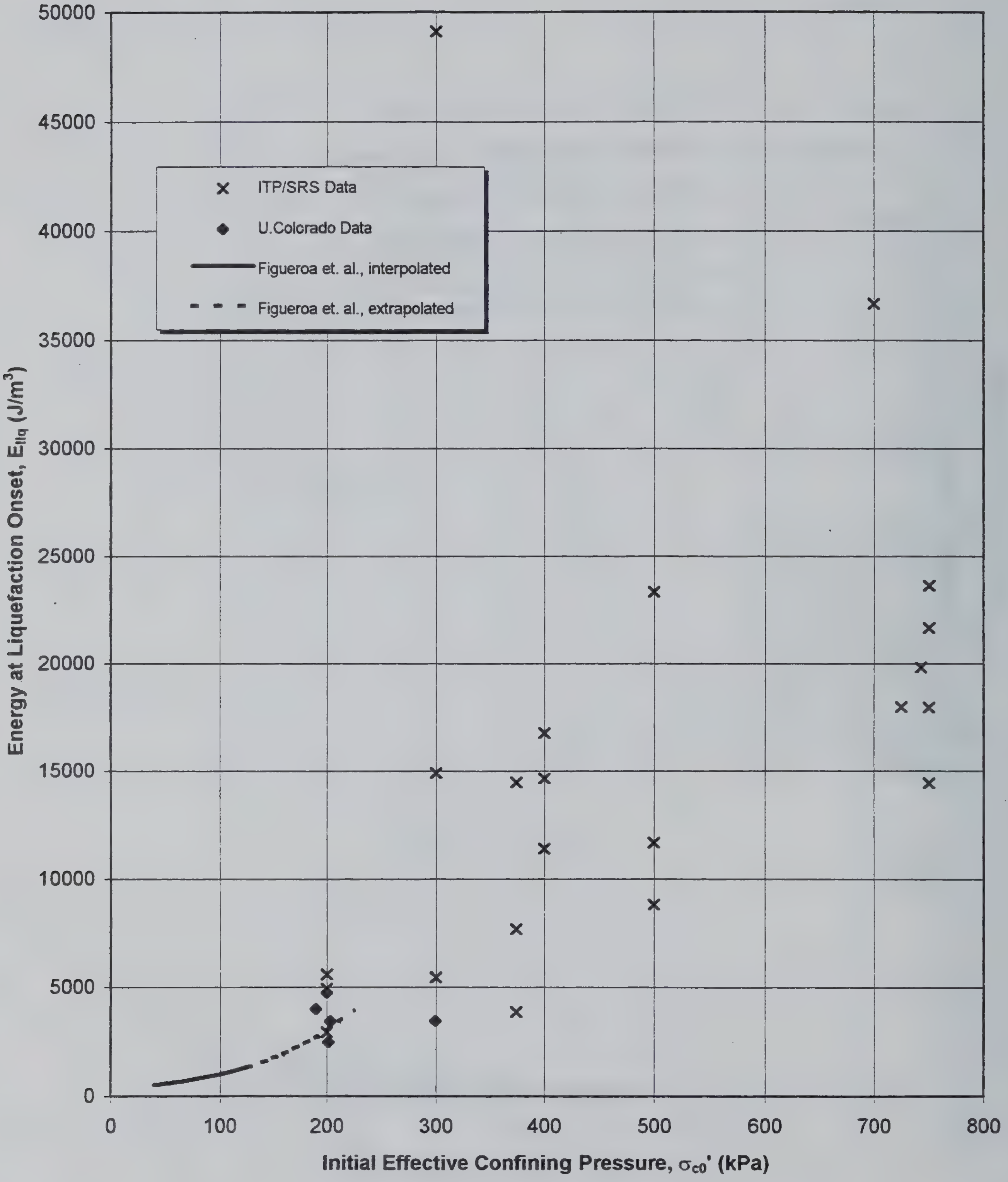

Figure 2.20 - Comparison of Strain Energy at Liquefaction Onset for All Test Groups - Silty Sands

CHAPTER 3

WILDLIFE SITE: SOILS AND EARTHQUAKE DATA

3.1 BACKGROUND

The Parkfield and Wildlife seismologic instrumentation arrays are among the few liquefaction arrays in operation in the United States. Both arrays are maintained by the United States Geological Survey (USGS). The Wildlife instrument array was established in the fall of 1982 primarily to monitor pore pressure in sand deposits undergoing earthquake loading. The site was an obvious choice since this region is seismically active and the site has repeatedly liquefied during past earthquakes. The data recorded during one of the recent earthquakes (Superstition Hills earthquake of November 24, 1987) provide a unique opportunity to perform ground response analyses and to compare predicted ground motions with recorded motions. The results of these analyses in terms of the total strain energy can in turn, be used to compare the laboratory-derived strain energy with the energy calculated to cause liquefaction in the field.

3.2 WILDLIFE SITE

The Wildlife instrument array is located in the Imperial Valley, Southern California about 36 km north of El Centro (see Figure 3.1). This is one of the most seismically active regions in the United States. Recent major earthquakes occurred in this region in 1979, 1981, and 1987. The array is on level ground and is located in the flood plain of the Alamo River, 20 m west of the river channel. Numerous articles, and several doctoral dissertations focus on the geological, geotechnical and seismological aspects of the site (Bennett et al., 1984; Bierschwale and Stokoe, 1984; Dobry et al., 1989; Etheredge et al., 1987; Haag and Stokoe, 1985; Holzer et al., 1989; Magistrale et al., 1989; Matasovic and Vucetic, 1993; Vucetic and Thilakaratne, 1989; Youd et al., 1989; Wald et al., 1990; and Zeghal and Elgamal, 1994). Lateral spreading associated with liquefaction caused by the 1987 Superstition Hills earthquake has been mapped by Holzer et al. (1989). The ground response analyses presented in this chapter was performed based on the data recorded during this event.

3.3 STRATIGRAPHY AND SOIL PROPERTIES AT THE WILDLIFE SITE

The subsurface stratigraphy at the Wildlife Site is shown in Figure 3.2 (Bennett et al., 1984). Soil properties in terms of soil classification, index properties, penetration data (CPT and SPT), water content, and fines content for each subsurface soil unit are shown in Figure 3.3. The subsurface units are defined as follows (Holzer et al., 1989; Bennett et al., 1984):

- Unit A is 2.3 m thick and consists of fine-grained flood plain deposits. The clay content in this layer is relatively high, about 16% to 65%. The water table is near the bottom of this unit, typically at a depth of 1.5 m.

- Unit B1 is a loose, moderately sorted sandy silt about 1 m thick and highly susceptible to liquefaction (note the blow count of 3 in Figure 3.3 for this unit). The grain size distribution from the sand boil materials in the 1981 magnitude 5.9 Westmoreland earthquake matched the gradation of the materials from this unit (Haag et al., 1985).

- Unit B2 is a coarser deposit of silty fine sand to very fine sand about 3.5 m thick and is moderately dense.

- Unit C consists of deposits of silty clay and clayey silt and is about 5 m thick. This unit and the layers below are very stiff and are not susceptible to liquefaction.

Both seismic crosshole and the Spectral Analyses of Surface Waves (SASW) techniques have been used to measure the shear wave velocities at the site (Bierschwale and Stokoe, 1984). The shear wave velocity profiles are shown in Figure 3.4. These profiles have been used in the ground response analyses performed for the current study as discussed below.

Strain-dependent soil properties were obtained by Ladd (1982) and Turner and Stokoe (1982) from tests on soil samples taken at the Herber Road site, located about 40 km from the Wildlife Site. These soils are believed to consist of similar materials as those at the Wildlife Site. Shear modulus reduction curves and damping curves are shown in Figures 3.5, 3.6, and 3.7. The values of G/Gmax and damping shown on the curves were selected at 10 cycles of loading to take into account the strain softening due to an earthquake loading of approximately 10 equivalent cycles (earthquake magnitude of about 6.6).

3.4 INSTRUMENTATION AT THE WILDLIFE SITE

The instrumentation at the Wildlife Site has been documented by Holzer et al. (1988) and is shown in Figure 3.8. The instrumentation consists of:

- Six pore pressure transducers installed in borings located along the circumferences of a 9.2 m diameter circle, with a horizontal spacing of 4.6 m. Two transducers are in Unit B1 (at 2.8 m and 3.0 m depths), three in Unit B2 (at 4 m, 5 m, and 6.3 m depths), and one in Unit D at 12.1 m.

- Two triaxial accelerometers located in the center of the circle. The downhole accelerometer was placed at a depth of 7.5 m in Unit C, and a surface accelerometer was mounted on a concrete pad.

3.5 RECORDED EARTHQUAKE DATA

On November 24, 1987, the Elmore Ranch earthquake with a surface wave magnitude of 6.2 occurred at 0154 GMT. No liquefaction or significant pore pressure build-up was observed during this event. Approximately 11 hours later, a second earthquake, the Superstition Hills earthquake, occurred at 1315 GMT with a surface wave magnitude of 6.6. During this event, massive liquefaction and sand boils followed by lateral spreading took place at the site. Instrumentation readings recorded during this event are described below. The epicentral distance and the duration of these two events are compared in Table 3.1. The location of the epicenters, 1987 surface rupture on the Superstition Hills fault, and their positions relative to the Wildlife Site are shown in Figure 3.9.

Following the Superstition Hills earthquake, major ground surface cracks oriented in the east-west direction and displacements towards the Alamo river were mapped. Maximum displacements up to 200 mm (8 inches) were observed (Holzer et al., 1989). The records of all pressure transducers and accelerometers were obtained and processed. As indicated in Table 3.1, the 360 degree component of the records is in the north-south direction. The 90 degree component is in the east-west direction. The acceleration, velocity, and displacement time histories of the record in the 360 degree direction from both the surface and the 7.5 m deep accelerometers are shown in Figure 3.10. The corresponding records for the 90 degree direction are shown in Figure 3.11. The vertical records are shown in Figure 3.12.

Although the records indicate low frequency characteristics of the ground surface motion towards the tail of the record, identification of the initial liquefaction from the time history records is difficult. The acceleration response spectra of the records at 5% damping calculated from the records at the surface and at 7.5 m depth are compared in Figures 3.13 and 3.14, for horizontal and vertical components, respectively. Both the horizontal components depicted in Figure 3.13 show amplification of motion within the 7.5 m soil thickness, with the main amplification taking place in the frequency range of 0.5 Hz to 3 Hz. All records show that the earthquake waves were polarized and the intensity of the motion in the 360 degree direction was much larger than the intensity in the 90 degree direction. The vertical motion at the ground surface shown in Figure 3.14 indicates a significant amplification (about 8 times) at about 20 Hz which cannot be explained.

In a study of liquefaction at the Wildlife Site, Matasovic et al. (1993) analyzed the pore pressure records and determined the soil unit weight and the location of the water table are consistent with the pore pressure records. The pore pressure ratios obtained from the records of the four pressure transducers are shown in Figure 3.15. The records show that the P5 transducer (see Figure 3.8) reached the onset of liquefaction first, and that the onset of liquefaction of the other three transducers followed. The onset of liquefaction occurred at about 35 seconds after the start of the earthquake at transducer P5 and at about 90 seconds at the other three transducers. This may be due to the procedures followed in installation of the transducers and the densification of the soils at the locations of the transducers. Holzer et al. (1988) reported that the transducers in their housings were pushed into the soil from the bottom of the bore hole and that the bore hole was filled with bentonite-cement grout, which could have disrupted hydraulic continuity and caused a delay in recording the maximum pore pressure. For transducers at the greater depths (P3 and P1), the delay in recording of the maximum pore pressure may also have been caused by the time required for migration of the express pore pressure from Unit B1, in which liquefaction occurred first, to the deeper depths in Unit B2.

Table 3.1 - Summary of the Wildlife Site Earthquake Data and Recorded Time Histories

EARTHQUAKE	DATE AND TIME	MAGNITUDE	EPICENTRAL DISTANCE (km)	DURATION (sec)	MAXIMUM ACCELERATIONS, (g)	
					0.0m (surface)	7.5m (downhole)
Elmore Ranch	November 24, 1987 0154 GMT	5.8 (M_L) 6.2 (M_S)	23	30	0.13 (360°) 0.13 (90°)	0.08 (360°) 0.07 (90°)
Superstition Hills	November 24, 1987 1315 GMT	6.1 (M_L) 6.6 (M_S)	31	97	0.21 (360°) 0.18 (90°)	0.17 (360°) 0.11 (90°)

Note that the N-S component corresponds to the 360° direction and E-W component to the 90° direction.

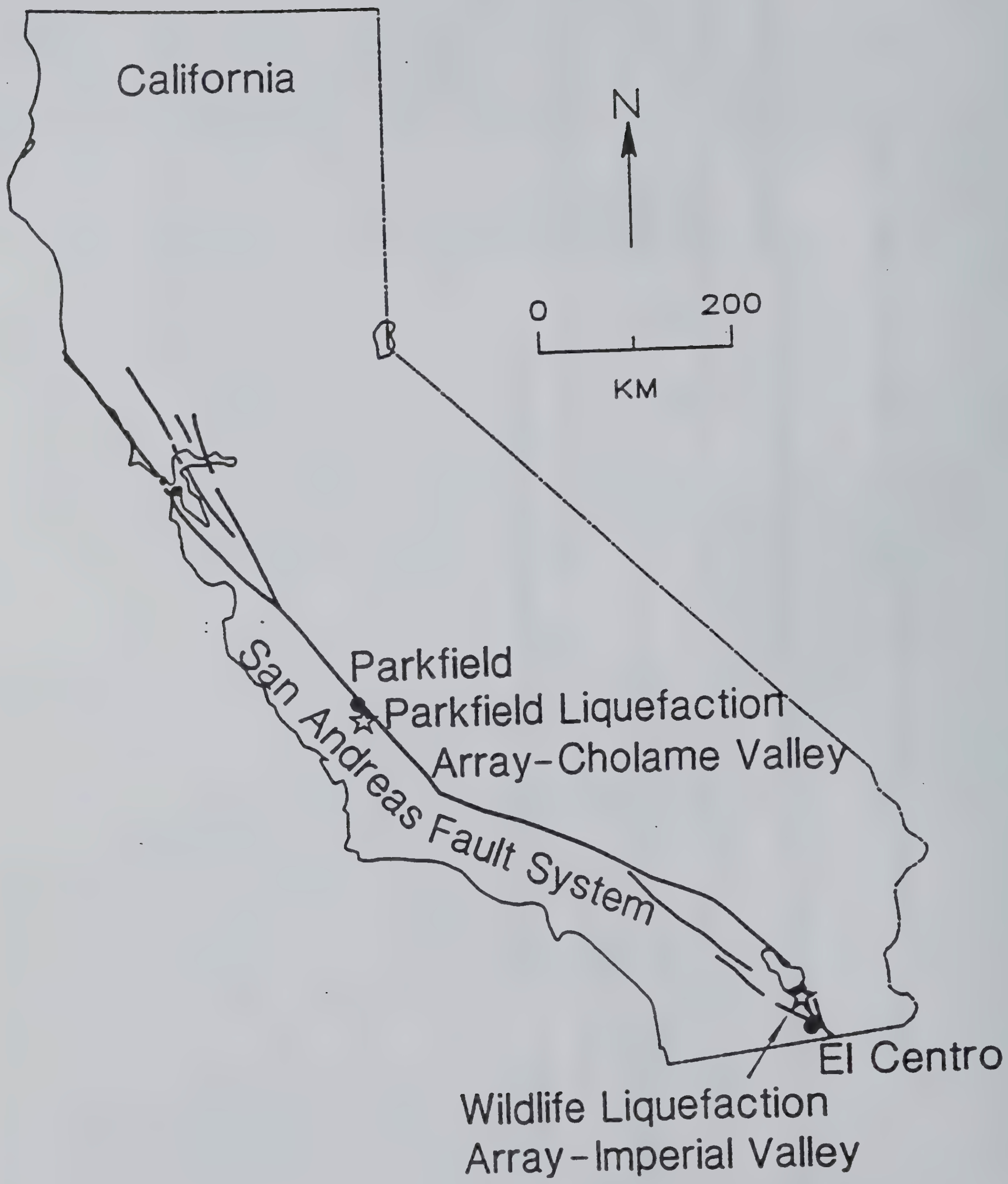

Figure 3.1 - Map of California with Locations of Parkfield and Wildlife Liquefaction Arrays

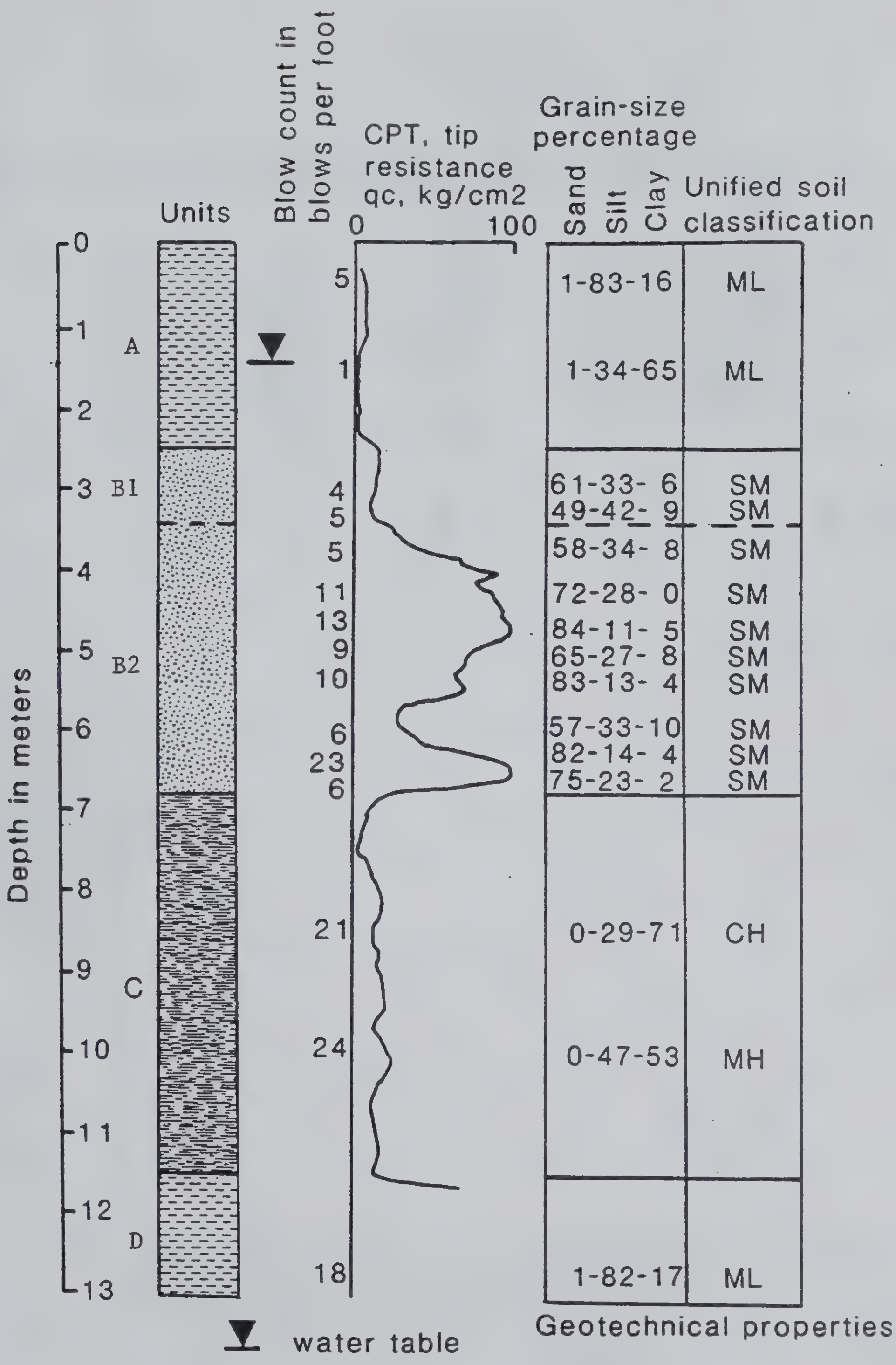

Figure 3.2 - Wildlife Liquefaction Array - Geotechnical Properties (Bennett et al., 1984)

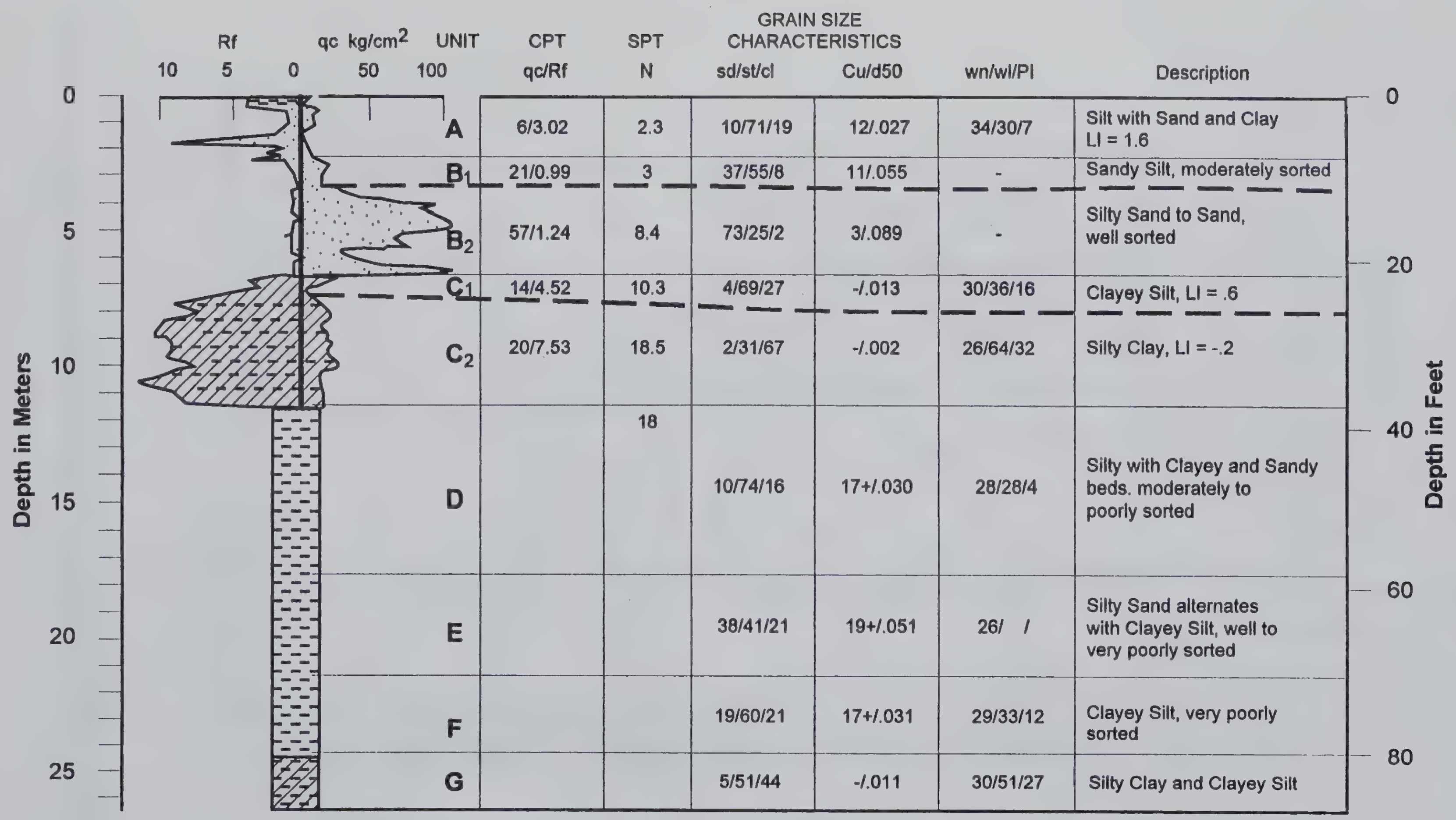

UNIT	CPT qc/Rf	SPT N	GRAIN SIZE CHARACTERISTICS sd/st/cl	 Cu/d50	wn/wl/PI	Description
A	6/3.02	2.3	10/71/19	12/.027	34/30/7	Silt with Sand and Clay LI = 1.6
B_1	21/0.99	3	37/55/8	11/.055	-	Sandy Silt, moderately sorted
B_2	57/1.24	8.4	73/25/2	3/.089	-	Silty Sand to Sand, well sorted
C_1	14/4.52	10.3	4/69/27	-/.013	30/36/16	Clayey Silt, LI = .6
C_2	20/7.53	18.5	2/31/67	-/.002	26/64/32	Silty Clay, LI = -.2
D		18	10/74/16	17+/.030	28/28/4	Silty with Clayey and Sandy beds. moderately to poorly sorted
E			38/41/21	19+/.051	26/ /	Silty Sand alternates with Clayey Silt, well to very poorly sorted
F			19/60/21	17+/.031	29/33/12	Clayey Silt, very poorly sorted
G			5/51/44	-/.011	30/51/27	Silty Clay and Clayey Silt

LEGEND:

Rf = Skin friction ratio
qc = Cone tip resistance
Cu = Coefficient of uniformity
sd = Sand
st = Silt
cl = Clay
wn = Natural moisture content
wl = Liquid limit
PI = Plasticity index
LI = Liquidity index

Figure 3.3 - Main Geological Units at the Wildlife Site and Their Geotechnical Characteristics (modified from Bennett et al., 1984)

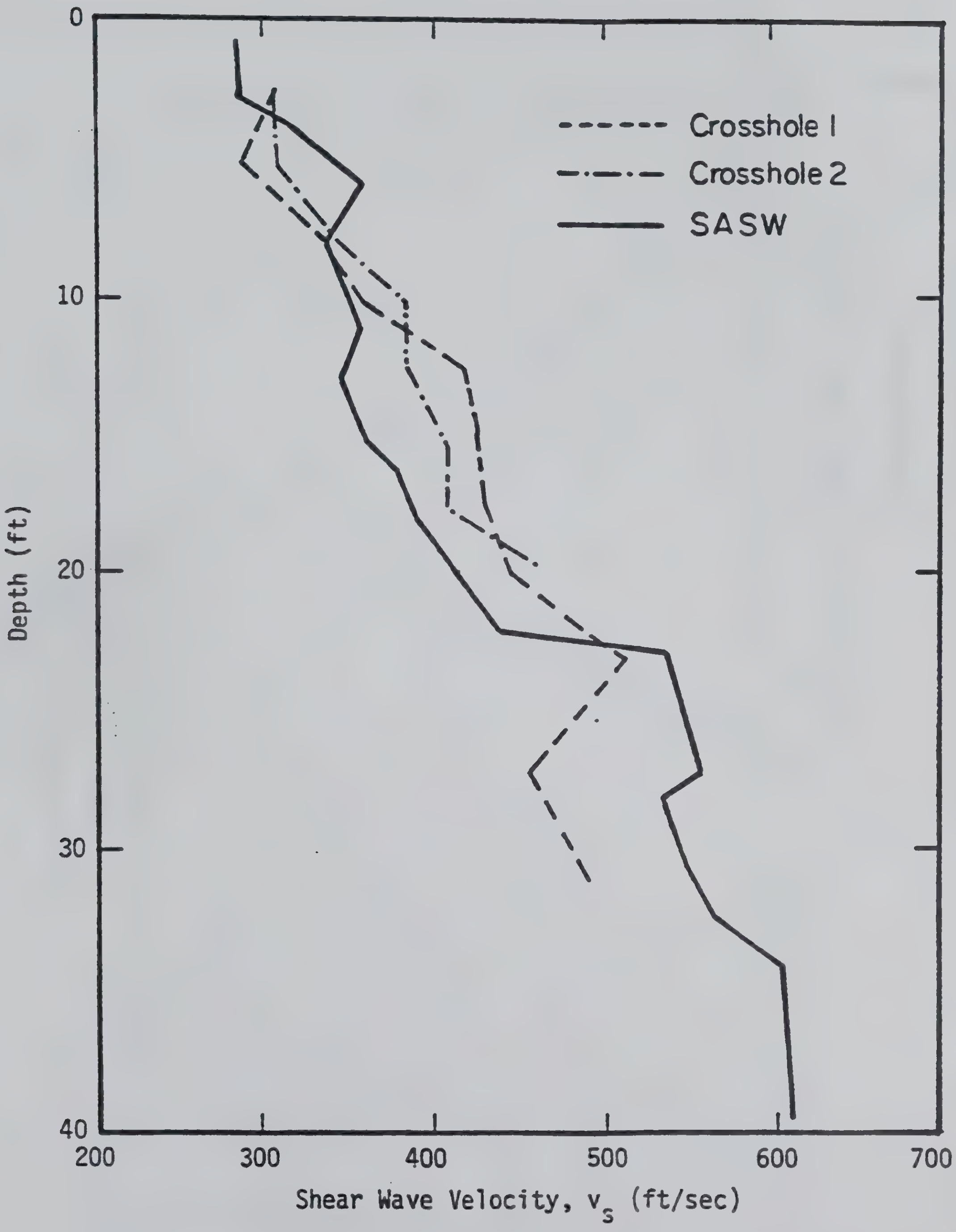

Figure 3.4 - Comparison of Shear Wave Velocity Profiles from Crosshole and SASW Tests at Wildlife Site (Bierschwale and Stokoe, 1984)

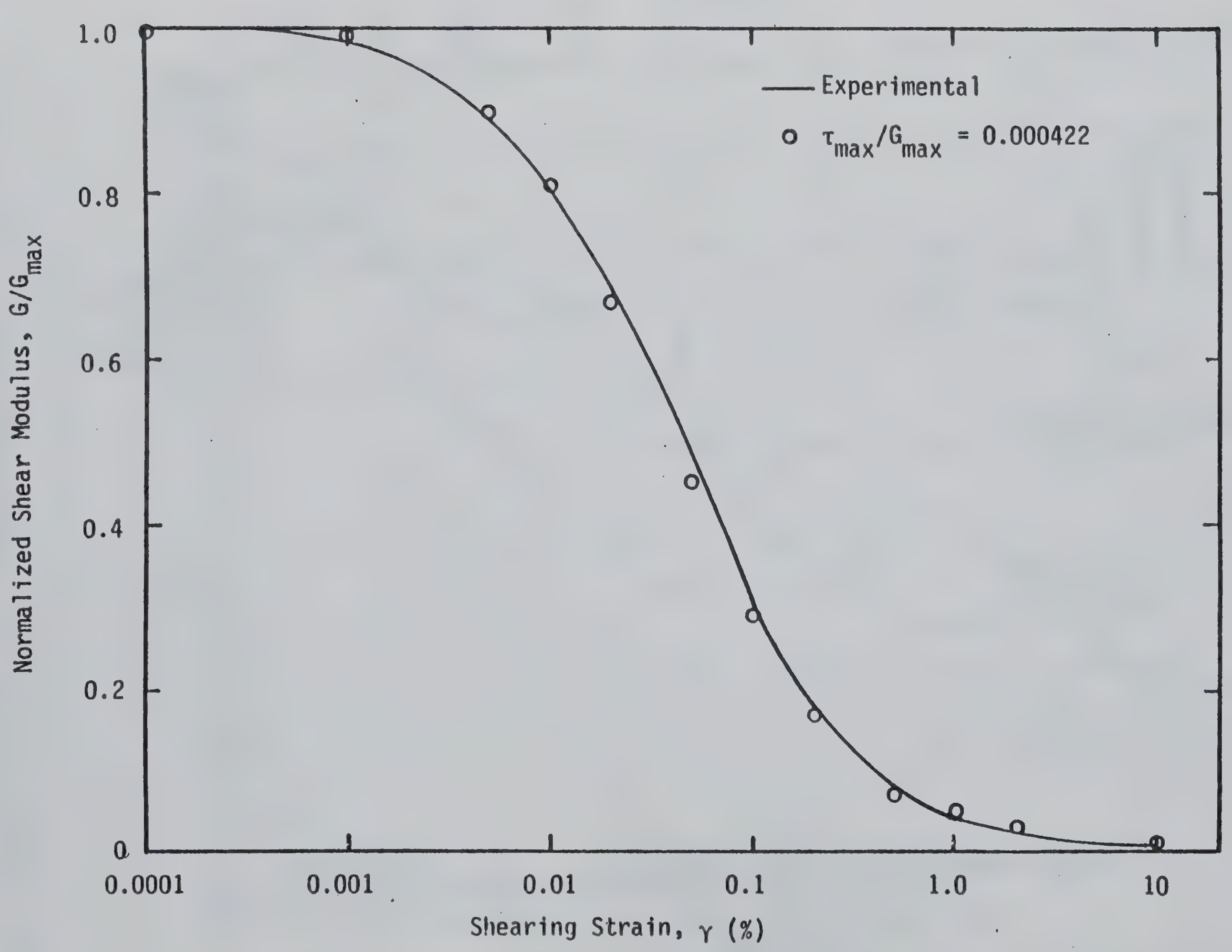

Figure 3.5 - Variation in Normalized Shear Modulus with Shearing Strain for Channel Fill Sand (Ladd, 1982)

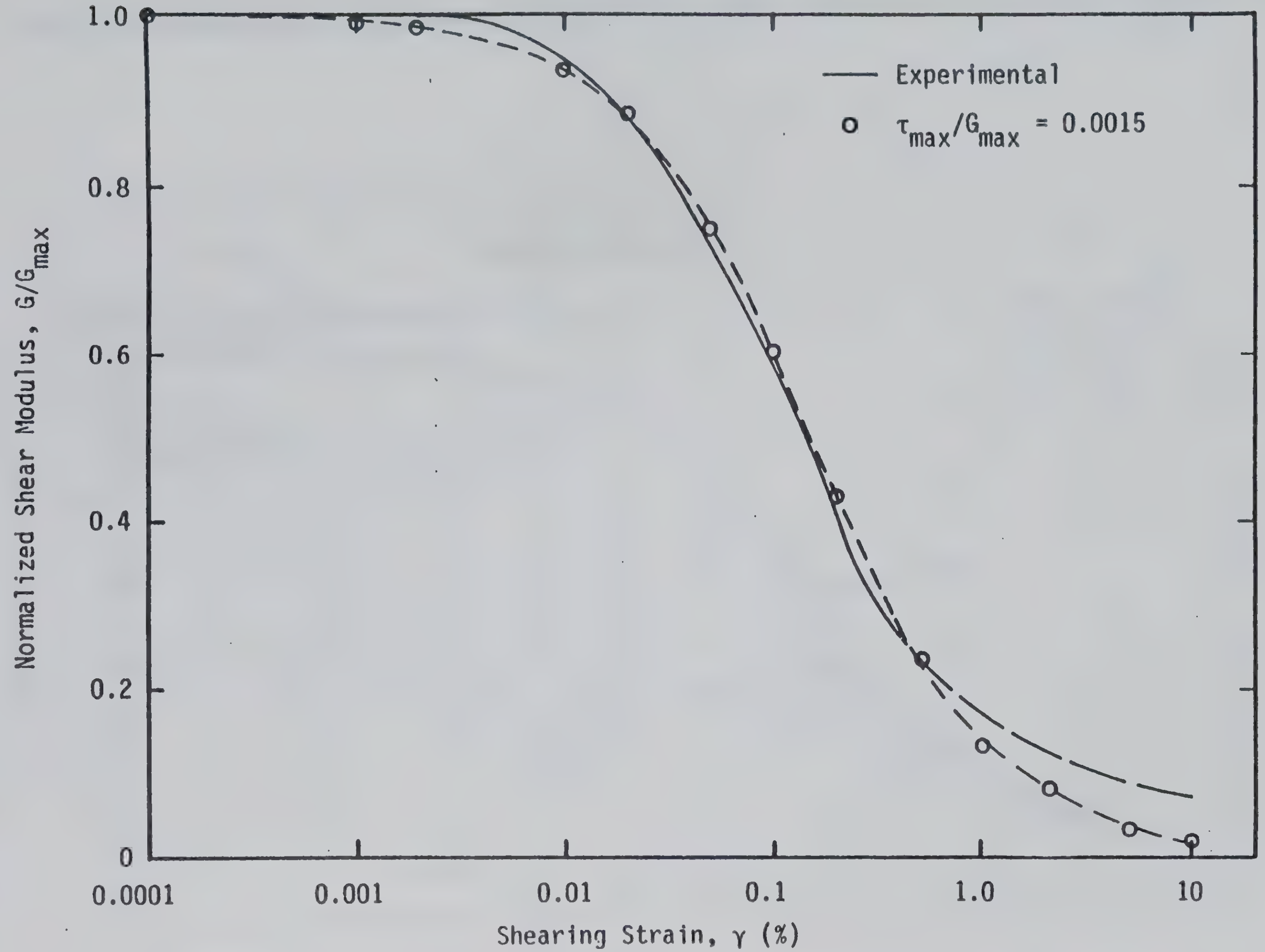

Figure 3.6 - Variation in Normalized Shear Modulus with Shearing Strain for Imperial Valley Clays (Turner and Stokoe, 1982)

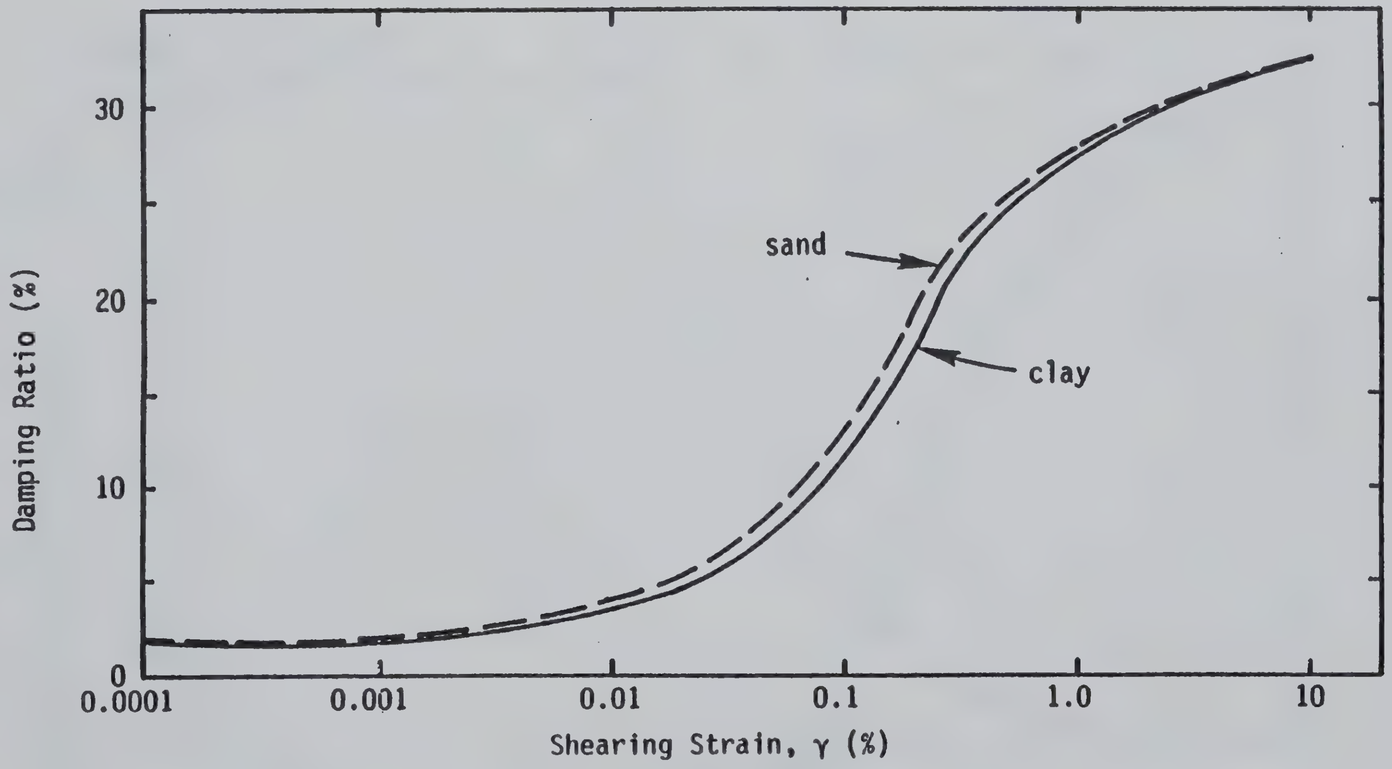

Figure 3.7 - Variation in Damping Ratio with Shearing Strain for Imperial Valley Soils (Ladd, 1982; Turner and Stokoe, 1982)

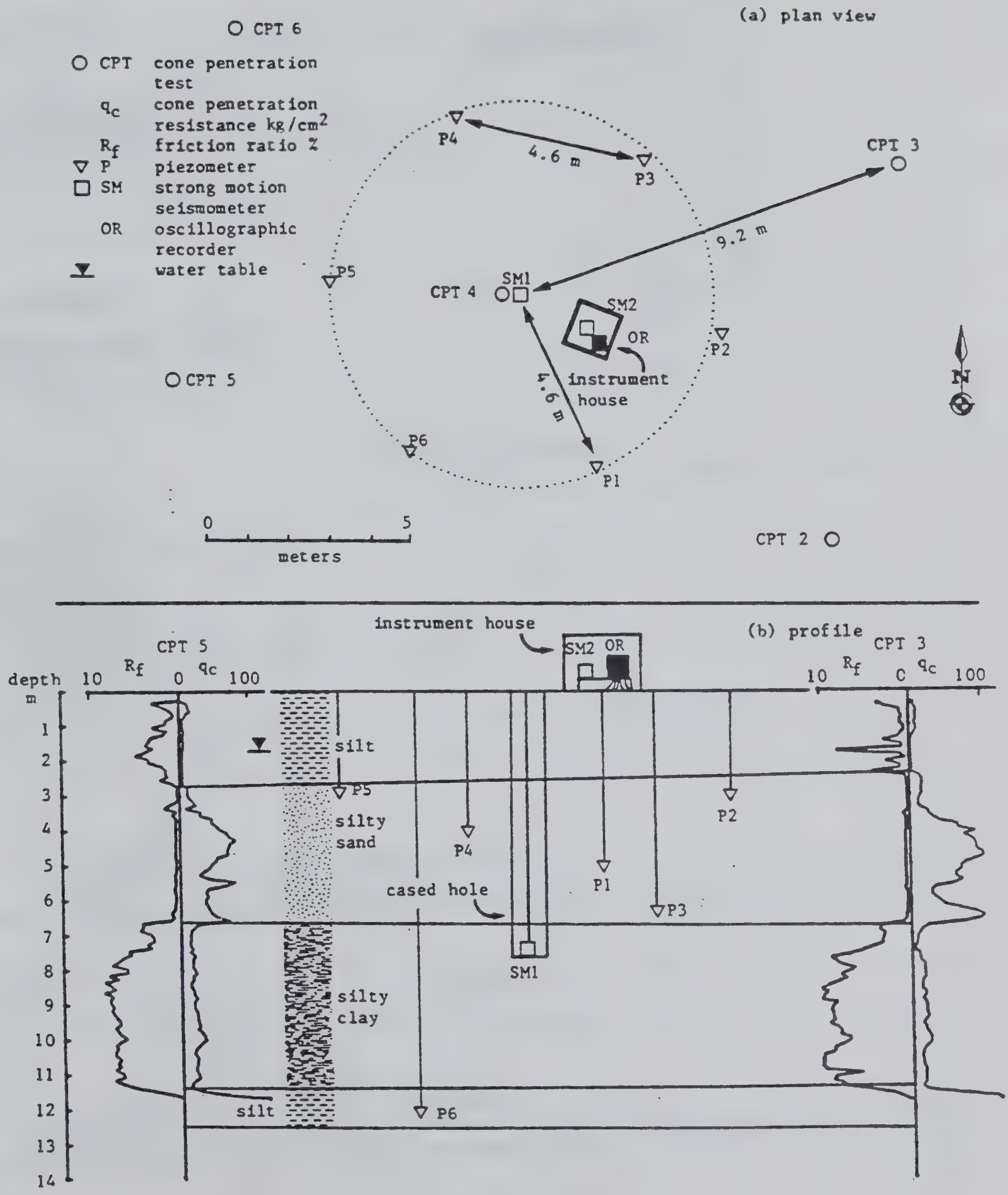

Figure 3.8 - Instrumentation of the Wildlife Site (Bennett et al., 1984)

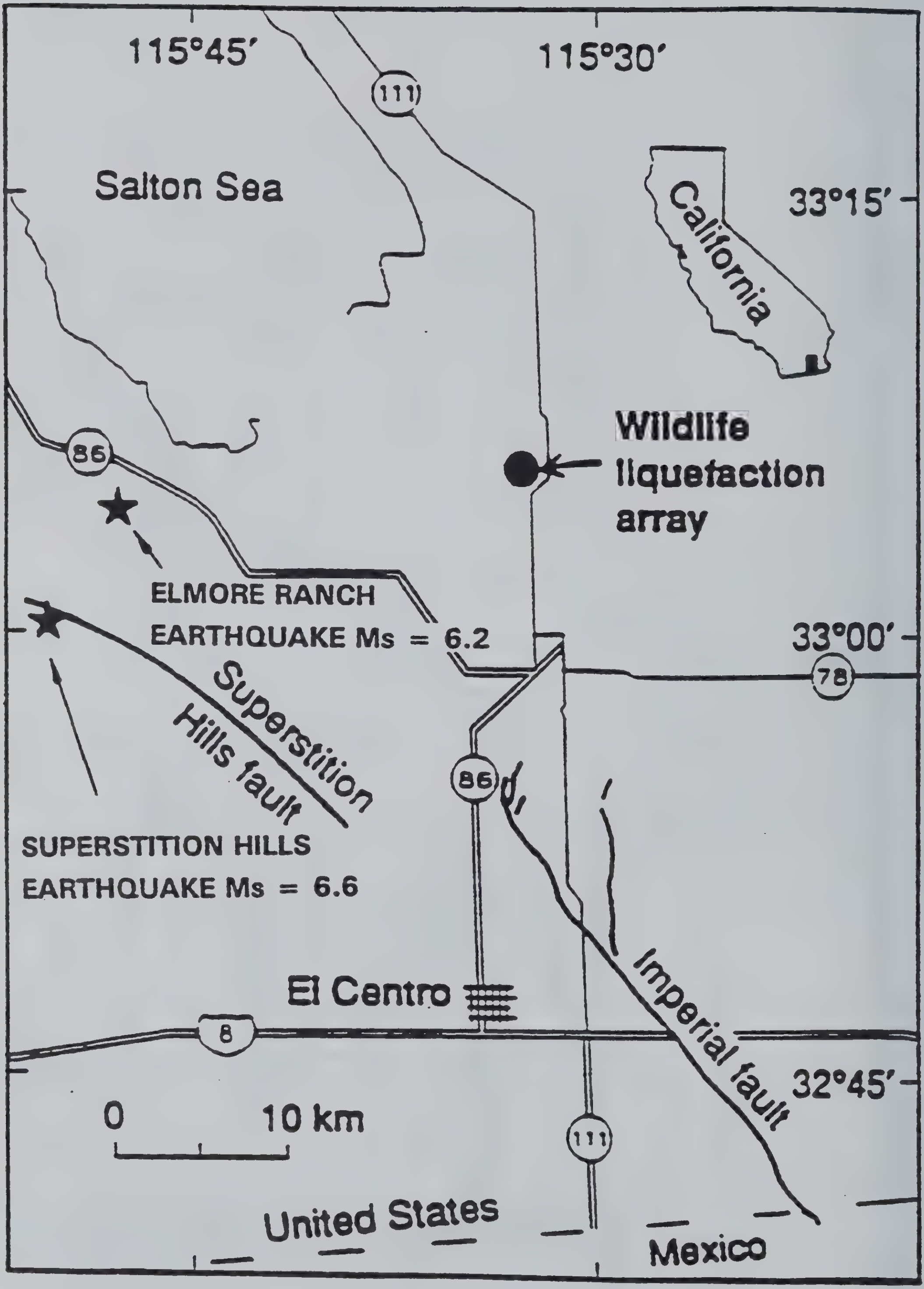

Figure 3.9 - Location Map of the Wildlife Site and the Epicenters of the Elmore Ranch (M_s = 6.2) and Superstition Hills (M_s = 6.6) Earthquakes (Porcella et al., 1987)

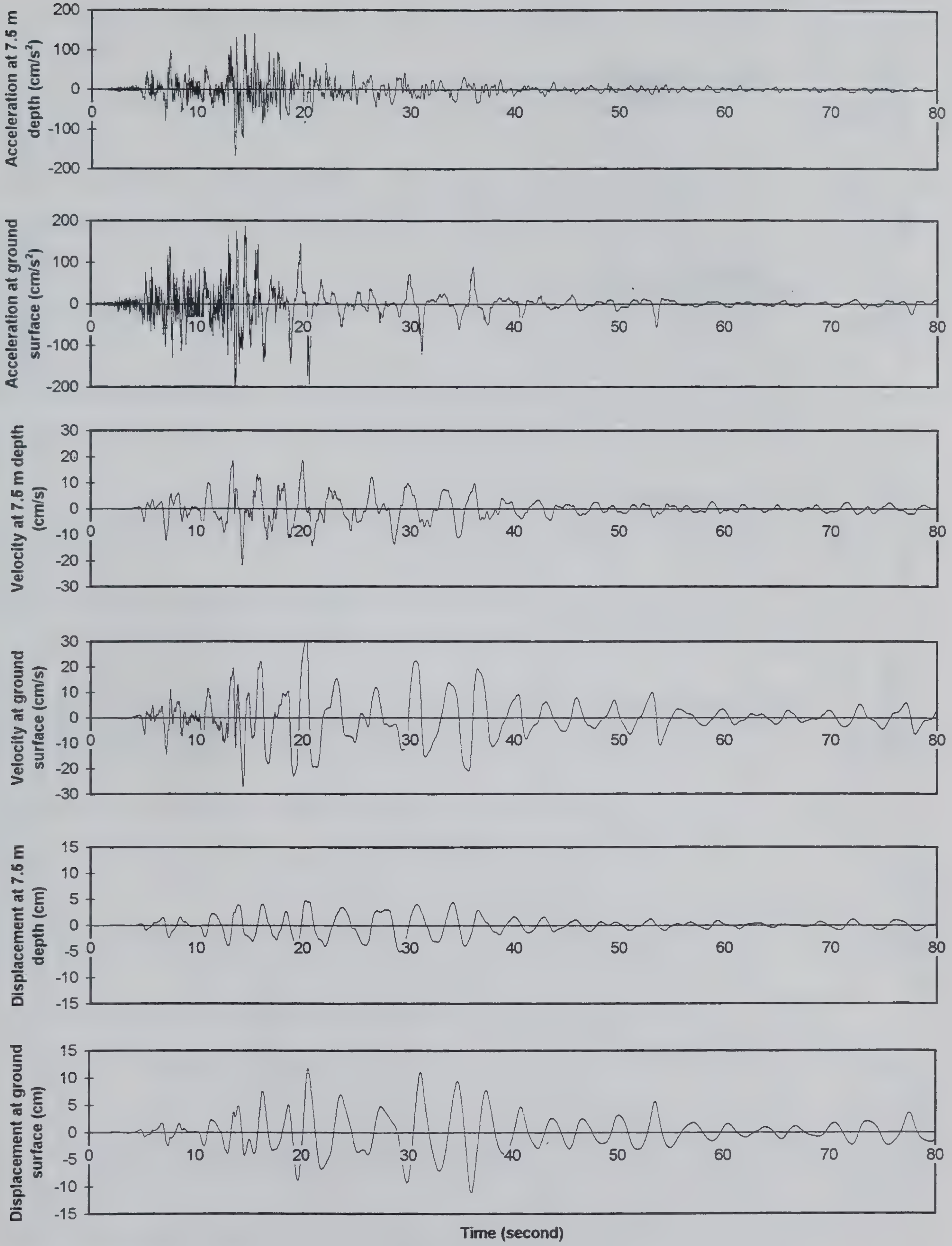

Figure 3.10 - Earthquake Time Histories at 1315 GMT, November 24, 1987 at Wildlife Array - Horizontal Motions in 360° Direction

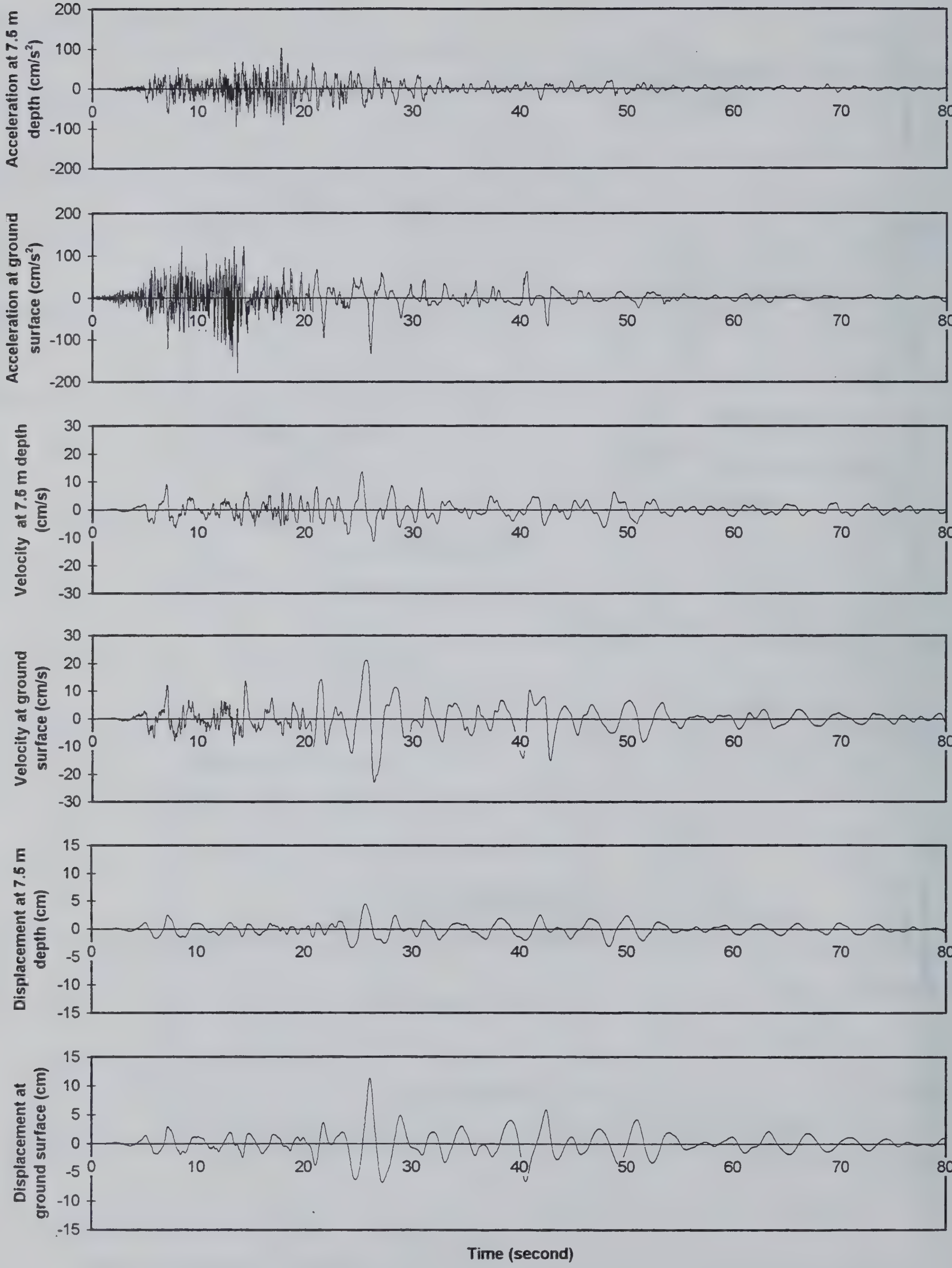

Figure 3.11 - Earthquake Time Histories at 1315 GMT, November 24, 1987 at Wildlife Array - Horizontal Motions in 90° Direction

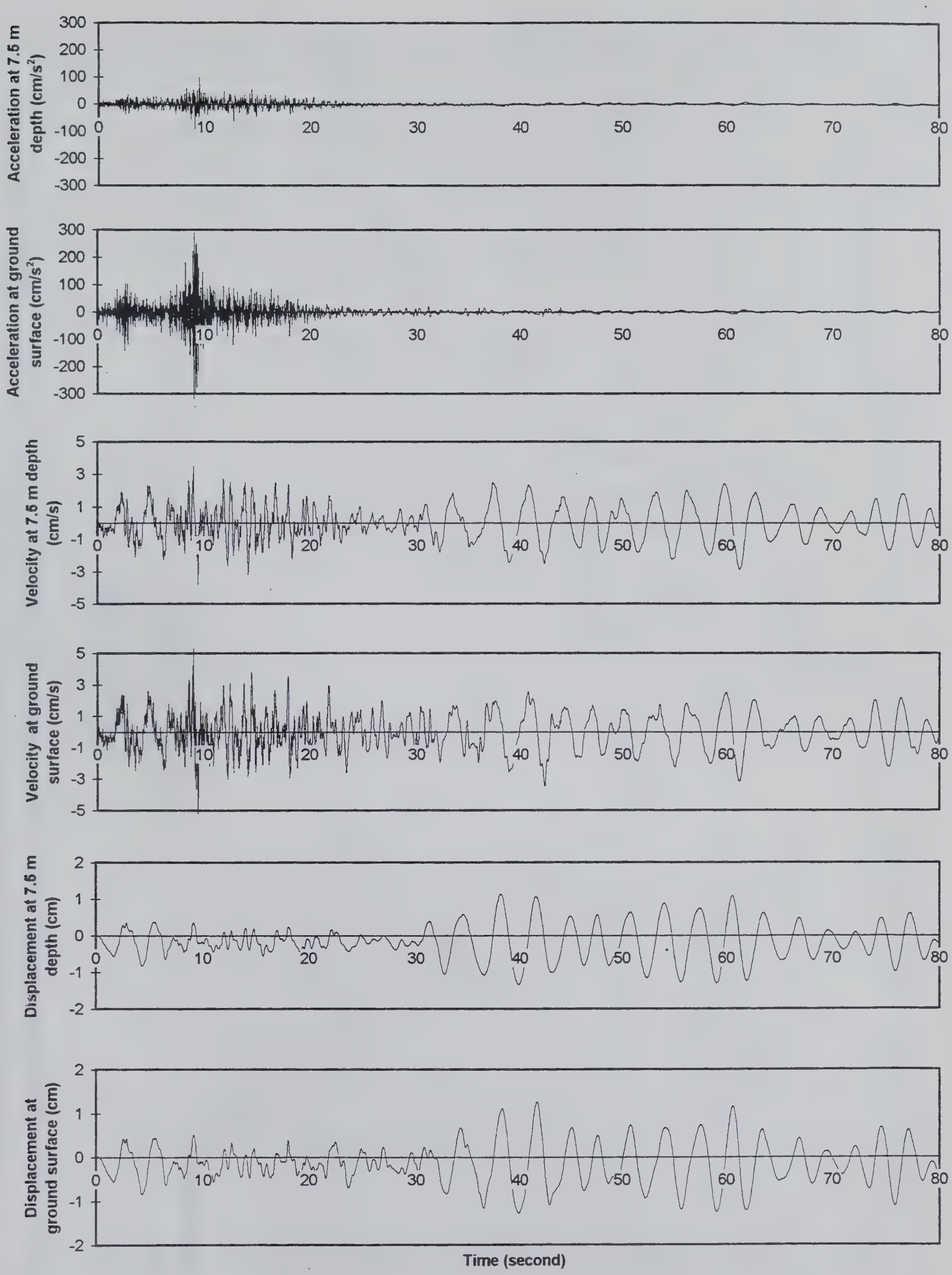

Figure 3.12 - Earthquake Time Histories at 1315 GMT, November 24, 1987 at Wildlife Site - Vertical Motions

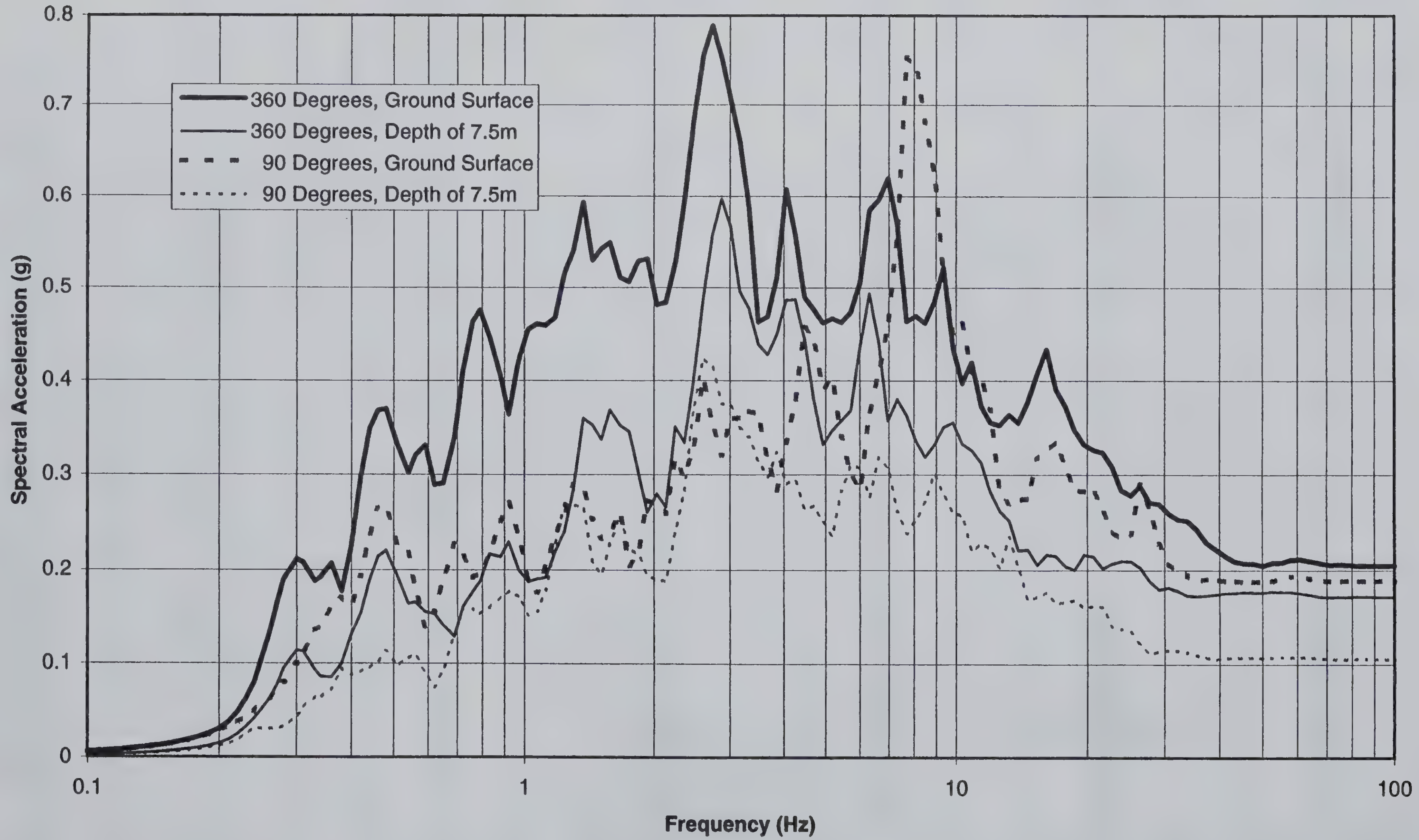

Figure 3.13 - Acceleration Response Spectra at 5% Damping - Wildlife Liquefaction Array, November 24, 1987, 1315 GMT Earthquake - Comparison of the Spectral Characteristics of Horizontal Motions

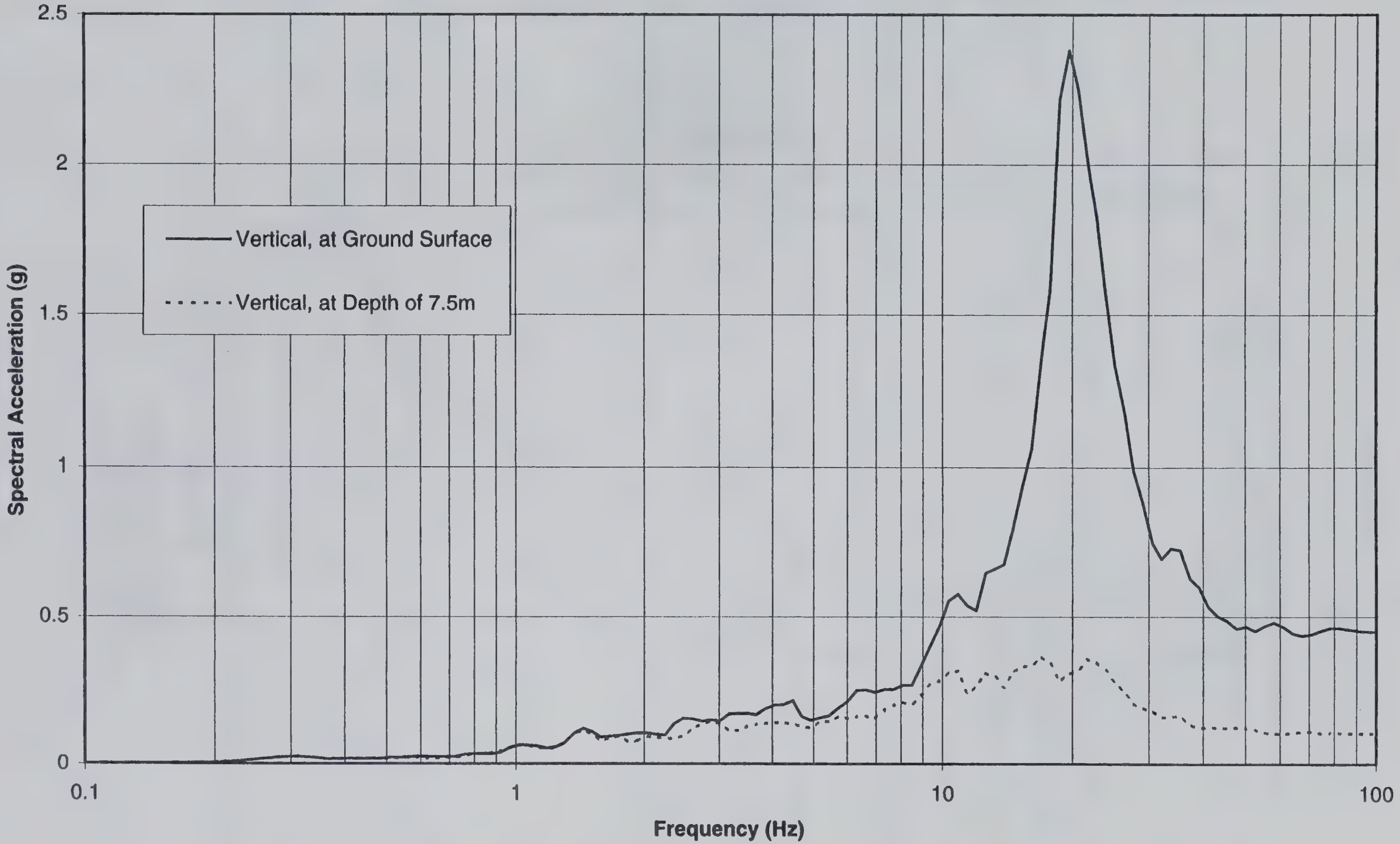

Figure 3.14 - Acceleration Response Spectra at 5% Damping - Wildlife Liquefaction Array, November 24, 1987, 1315 GMT Earthquake - Comparison of the Spectral Characteristics of Vertical Motions

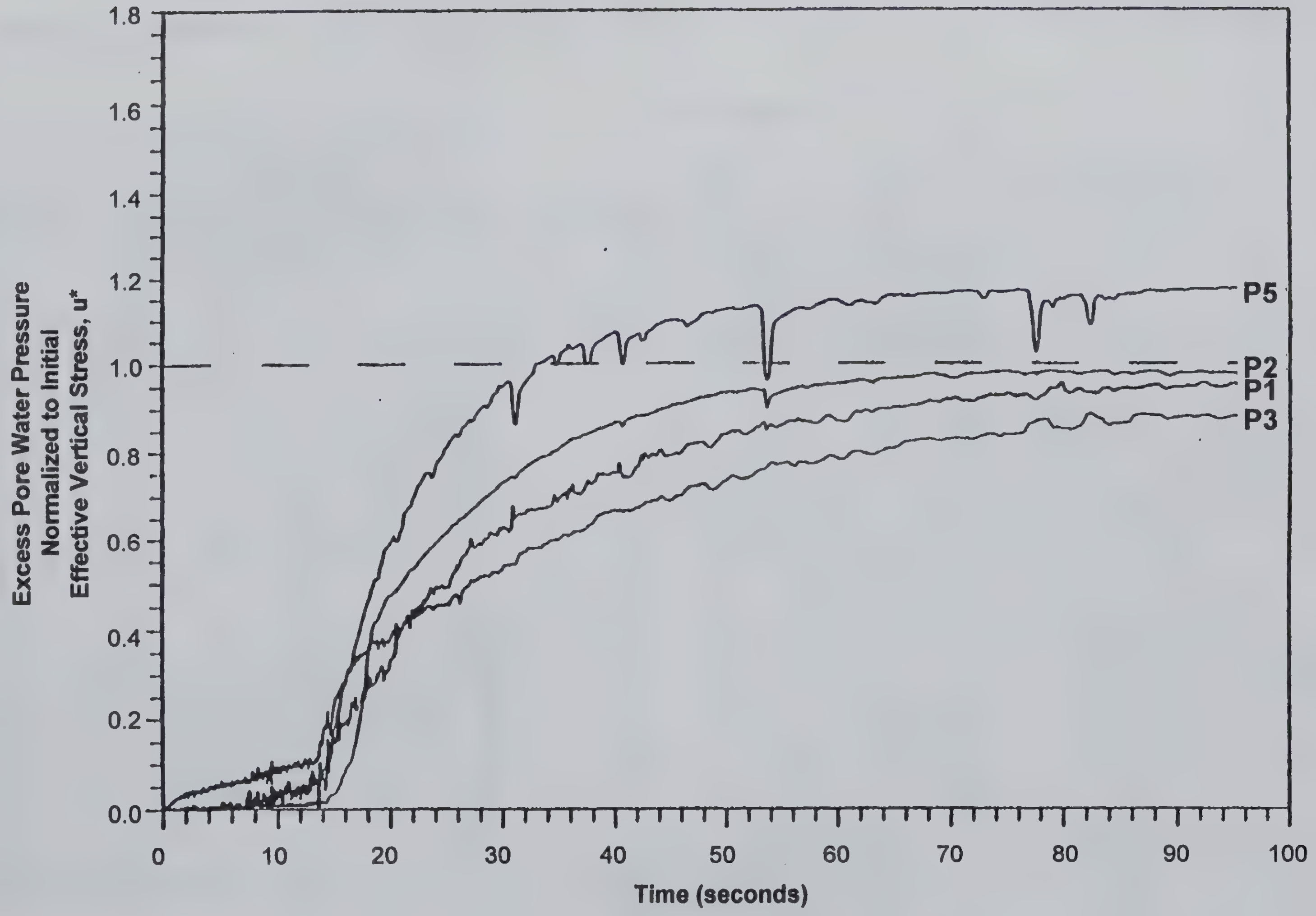

Figure 3.15 - Normalized Pore Water Pressure Ratios - Wildlife Liquefaction Array, November 24, 1987, 1315 GMT Event (Matasovic et al., 1993)

CHAPTER 4

GROUND RESPONSE ANALYSES AND COMPARISON WITH THE LABORATORY DATA

4.1 METHODS OF ANALYSES

To evaluate the strain energy induced in the soil layers by the 1987 Superstition Hills earthquake, a series of ground response analyses were performed using the computer programs SHAKE (Schnabel et al., 1972), the modified program BDESRA (DESRA, Lee and Finn, 1978), and the direct computation of the stress and strain time histories from the motions recorded at the top and bottom of the liquefied layer. The modifications to the program DESRA were performed to incorporate the Martin-Dovidenkov soil model so that the user's specified strain-dependent soil properties can be used. In the ground response analyses, the effects of variations of the shear wave velocity and the strain-dependent soil properties on the ground responses are evaluated.

The computer programs SHAKE and DESRA are widely used for ground response analysis. The computer program SHAKE works in frequency domain and uses the equivalent linear method to handle soil nonlinearity. The computer program DESRA works in time domain and uses the hyperbolic stress-strain soil model to handle soil nonlinear effects. In each method, the shear stress and the shear strain response time histories were obtained at several depths. The time history of the strain energy at time t, E(t), was obtained from the following relationship:

$$E(T) = \sum_{t=0}^{T} \bar{\tau}(t).\Delta\gamma(t) \tag{4.1}$$

where $\bar{\tau}(t)$ is the average shear stress from time t to t + Δt, and $\Delta\gamma(t)$ is the increment of the shear strain from time t to t+Δt. The summation is computed for the total duration of the motion. Due to the one-dimensional formulation of the methodologies adopted for the ground response analyses, strain energy time histories at several elevations in both 360 degrees and 90 degrees directions were first calculated separately. These two time histories at each elevation were subsequently combined at each time step to obtain the total strain energy time history at the respective elevation. All acceleration time histories used in the analytical study described in this chapter were from the November 24, 1987, 1315 GMT Superstition Hills earthquake records.

4.2 RESULTS OF THE GROUND RESPONSE ANALYSES USING THE COMPUTER PROGRAM SHAKE

A representative soil profile was modeled for the Wildlife Site using the subsurface data, the shear wave velocity profiles, and the strain-dependent soil properties discussed in Chapter 3. The resulting SHAKE model is shown in Figure 4.1. The initial shear wave velocity profile used in this model is the average of the crosshole and the Spectral Analysis of Surface Waves (SASW) velocity profiles shown in Figure 3.4.

The sensitivity of the results to the use of the crosshole, the SASW, or the average velocity profiles was first evaluated in three parallel SHAKE runs: the first with the crosshole velocity profile, the second with the SASW velocity profile, and the third with the average profile. The motion recorded at 7.5 m depth in the 360 degree direction was used as the input motion for the three runs. The responses at the ground surface from SHAKE output were then compared with the recorded surface motion. The comparisons are presented in Figures 4.2, 4.3, and 4.4, respectively, for the crosshole, SASW, and the average velocity profiles. The crosshole velocity profile significantly overpredicts the peak response. The agreement between the calculated and recorded spectral responses improve when the SASW velocity profile is used. However, generally a better agreement is obtained when the average velocity profile is used.

Having determined the more representative velocity profile, the SHAKE deconvolution simulation was then studied. The soil profile used was the average velocity profile. The input motion used was the motion recorded at the ground surface. The response calculated at the depth of 7.5 m was compared with the motion recorded which is shown in Figure 4.5. This comparison shows a relatively good agreement in the frequency range of 1.5 Hz to 10 Hz.

Third, the SHAKE simulation in the 90 degree direction was performed. The input motion used 7.5 m downhole recorded motion in the 90 degree direction. The soil properties used in this run were the strain-compatible properties obtained from the companion run using the 360 degree input motion. The calculated ground surface motion is compared with the recorded ground motions in Figure 4.6. The agreement, particularly at the peak response at 8 Hz, is very poor. However, it should be noted that as the pore pressure builds up, the ground response shifts to the low frequency range. The major contribution to the strain energy occurs at the time of the high pore pressure build-up at which time the soil stiffness is reduced significantly. Thus, the major attributes to the total strain energy are from the low frequency response of the soil layer. For this reason, good agreement at high frequencies, such as at 8 Hz for the 90 degree direction, may not be important for the purpose of the total strain energy computation.

The results of analyses in terms of maximum acceleration, maximum shear stress, and maximum shear strain for each direction of shaking using the three velocity profiles are shown in Figures 4.7 through 4.12. Depending on the velocity profile and the earthquake component, the maximum estimated shear strain in the liquefiable sand layer ranges from

0.25% to 0.6%. In general, the 90 degree component of the motion has a lower intensity and results in smaller stress and strain peak responses.

Typical shear stress and shear strain time histories at the depth of 4.2 m obtained from the SHAKE analysis from the 360 degree input motion are shown in Figures 4.13 and 4.14, respectively. The corresponding hysteresis loops are shown in Figure 4.15.

The time histories of the total strain energy at four depths obtained from the SHAKE responses using the 360 degree input motion are compared in Figure 4.16. The same results for the 90 degree input motion are shown in Figure 4.17. As shown in these two figures, the strain energy obtained from the 360 degree of input motion is approximately twice the energy using the 90 degree component of the input motion. A summation of the strain energy from both directions of shaking is shown in Figure 4.18.

4.3 RESULTS OF THE GROUND RESPONSE ANALYSES USING THE COMPUTER PROGRAM BDESRA (MODIFIED DESRA)

In order to evaluate the effects of modeling nonlinear soil behavior on ground responses, in addition to the program SHAKE, the computer program DESRA with total and effective stress options was also used. Due to the fully nonlinear formulation of this program, only the recorded motion at 7.5 m can be used as input motion.

In the total stress analysis method, the strain-dependent soil properties shown in Chapter 3 were used in the modified DESRA (BDESRA) program. The input motion was specified at the 7.5 m depth and the response at the ground surface was compared with the recorded motion. The results are compared in Figures 4.19 and 4.20 using the 360 degree and the 90 degree input motions, respectively. While the response comparisons show a better agreement in the frequency range of 2 Hz to 4 Hz in the 360 degree direction compared to the results obtained with the program SHAKE, the agreement in the 90 degree direction remains to be poor. The maximum shear stresses, and the maximum shear strains are shown in Figures 4.21 and 4.22, respectively. The time histories of the strain energy and the summation over both directions of shaking are shown in Figures 4.23, 4.24, and 4.25, respectively.

The same analyses were repeated using the effective stress capability of BDESRA which is capable of computing the pore pressure build-up and its effect on the soil properties. The comparison of the responses at the ground surface from both the 360 degree and the 90 degree input motion are shown in Figure 4.26 and 4.27, respectively. The results in the 360 degree direction under estimate the response in a wide frequency range. The agreement in the 90 degree direction is still very poor. The results in terms of the maximum shear stresses and the maximum shear strains are shown in Figures 4.28 and 4.29, respectively. The maximum shear strain in the 360 degree direction reaches the peak value of about 1.7% (see Figure 4.29), well above the values computed by the other methods. The strain energy from each direction of shaking and the total energy are shown in Figures 4.30, 4.31 and 4.32 , respectively. The strain energy computed by this method is about half the value computed by the other methods. In addition, the pore water pressure obtained from the effective stress DESRA analysis normalized to the effective overburden pressure at five depths have also been computed. The pore pressure ratios have been plotted in Figures 4.33 and 4.34 due to shaking from each direction. As shown in these figures, in the 360 degree direction, the pore pressure ratio reached the maximum value of one, while in the 90 degree direction it remains below the value one. In general, the results of the effective stress analyses are in poorer agreement with the recorded motion when compared to the total stress analyses results. This may be due to the fact that the strain-dependent soil properties used already includes the effect of the pore pressure build-up so that the use of the effective stress option double-counts the softening effect.

4.4 RESULTS OF THE GROUND RESPONSE ANALYSES BASED ON DIRECT INTERPOLATION OF RECORDED MOTIONS

In this approach, the recorded acceleration time histories at the top and bottom of the liquefied sand layer and the associated displacement time histories are used to estimate the average shear stresses and strains in the liquefied sand layer, assuming a linear distribution of the displacement and acceleration amplitudes over the thickness of the layer at each time step. The formulation of this approach is shown in Figure 4.35. It is, in essence, a linear interpolation of accelerations and displacement over the thickness of a layer based on recorded motions at the top and bottom of the layer. This approach is adopted from Zeghal and Elgamal (1994). As shown in Figure 3.8, the recording accelerometers are located at the surface and at the depth of 7.5 m below the liquefied layer. Assumptions for linear distribution of the stress and strain amplitudes may over estimate the actual amplitudes in the liquefied layer. Using this approach, the shear stress and the shear strain time histories are computed at several depths. The time histories corresponding to the depth of 5 m and the associated hysteresis loops due to the 360 degree response motions are shown in Figures 4.36, 4.37, and 4.38, respectively. The same results for the 90 degree response motion are shown in Figures 4.39 through 4.41. The time histories of the strain energy computed using the ground motion for each direction of shaking and the total strain energy are shown in Figures 4.42 through 4.44. The results in terms of total energy are generally larger than the results obtained from the SHAKE and DESRA ground response analyses. This is mainly due to the fact that the accelerometer at 7.5 m is well below the liquefied unit B1 (see Figure 3.2) which results in over estimation of shear strain in this approach.

4.5 RESULTS OF THE GROUND RESPONSE ANALYSES USING THE COMPUTER PROGRAM SHAKE AND EPRI SOIL CURVES

In a recent study, the Electric Power Research Institute (EPRI) published a set of generic soil modulus degradations and damping curves applicable to sand and clay soils under dry and submerged conditions (EPRI, 1993). The shear modulus and the damping curves used for the Wildlife ground response analysis are compared with the EPRI saturated sand curves in Figures 4.45 and 4.46, respectively. The Wildlife soil curves correspond to the upper bound of the shear modulus curves and the lower bound of the damping curves. The EPRI curves were also used in a series of SHAKE analyses using the recorded motion at the 7.5 m as the input motion. The response motions at ground surface in 360 degree and 90 degree directions are compared with recorded motions in Figures 4.47 and 4.48, respectively. No significant improvement in agreement with the recorded motions can be observed from the use of the EPRI soil curves. The shear stress and the shear strain and the associated hysteresis loops at a depth of 4.2 m are shown in Figures 4.49, 4.50, and 4.51, respectively. The strain energy for each direction of shaking and the total energy are shown in Figures 4.52 through 4.54.

4.6 COMPARISON OF THE RESULTS OF GROUND RESPONSE ANALYSES

The results of the ground response analyses in terms of total strain energy, obtained from SHAKE (using both the Wildlife soil curves and the EPRI soil modulus degradation and damping curves) and DESRA (total and effective analyses), are compared with the results derived from the recorded motions in Table 4.1 and Figure 4.55. The effective confining pressure shown in this figure is the mean effective stress at the respective depth of the response calculation. The results show a consistent trend except at a confining pressure of about 40 kPa to 50 kPa. This pressure corresponds to unit B2 (see Sections 3.3 and 3.4), which may not have reached the onset of liquefaction during the earthquake. In fact, the pore pressure ratios reported by Matasovic and Vucetic (see Figure 3.15) show that the pressure transducers P1 and P3 (at depths of 5 and 6.3 m) did not reach the pore pressure ratio of one, and that the large pore pressure ratios were developed after about 50 seconds, indicating a redistribution of pore pressure after the shaking. For these reasons, the data below the depth of 5 m (16.4 ft) have been removed from the results and the new summary plot is depicted in Figure 4.56. As shown in this figure, the results of the ground response analyses obtained from all the different methods show a consistent trend and close agreement. In general, use of the EPRI soil curves in the SHAKE analyses results in larger total energy, mainly due to the differences in the damping curves (see Figure 4.46). In general, the results from the SHAKE analyses (using Wildlife soil curves) and the results obtained from the recorded motions are in better agreement.

4.7 COMPARISON OF THE RESULTS OF GROUND RESPONSE ANALYSES WITH THE LABORATORY DATA

The results of the total strain energy for silty sands obtained from the available laboratory data are shown in Figure 2.16. As shown in this figure, the only set of data that covers the range of confining pressures less than 100 kPa are the summary results from Figueroa et al. Since the Wildlife liquefied layer is at a confining pressure lower less than 50 kPa, the relationship by Figueroa et al. (Equation 2.3) was used to extrapolate the data points to the low confining pressures. The extrapolated data points are plotted with the results from the ground response analyses in Figure 4.57. As shown in this figure, the agreement between the laboratory data and the results from the ground response analyses is good in spite of the fact that the laboratory data are not from the soil samples at the Wildlife Site. In addition, no correction factor has been applied to the laboratory data to correct for the field condition. Such factors should be evaluated once site-specific laboratory data are obtained.

Table 4.1 Summary of Strain Energy Computation from Ground Response Analyses

(November 24, 1987, 1315 GMT Earthquake)

Method of Analysis	Soil Properties		Depth from Ground Surface (m)	Total Strain Energy (J/m^3)
	Shear Wave Velocity Profile	Strain Dependence Relationships		
SHAKE	Average of SASW and Crosshole Field Measurements	Channel Fill Sand (Ladd, 1982)	3.35	340
			4.21	612
			5.06	646
			5.91	404
		EPRI (1993)	3.35	658
			4.21	739
			5.06	676
			5.91	358
BDESRA (Total Stress)	Average of SASW and Crosshole Field Measurements	Hyperbolic, Parameters adjusted to fit Channel Fill Sand (Ladd, 1982)	2.93	138
			3.78	266
			4.63	443
			5.49	581
			6.36	398
BDESRA (Effective Stress)	Average of SASW and Crosshole Field Measurements	Hyperbolic, Parameters adjusted to fit Channel Fill Sand (Ladd, 1982)	2.93	246
			3.78	360
			4.63	422
			5.49	385
			6.36	298
Direct Interpolation of Record Motions	N/A	N/A	3.35	448
			4.21	564
			5.06	677
			5.91	791

Note: The motions recorded at 7.5 m depth were used as input motion in ground response analyses.

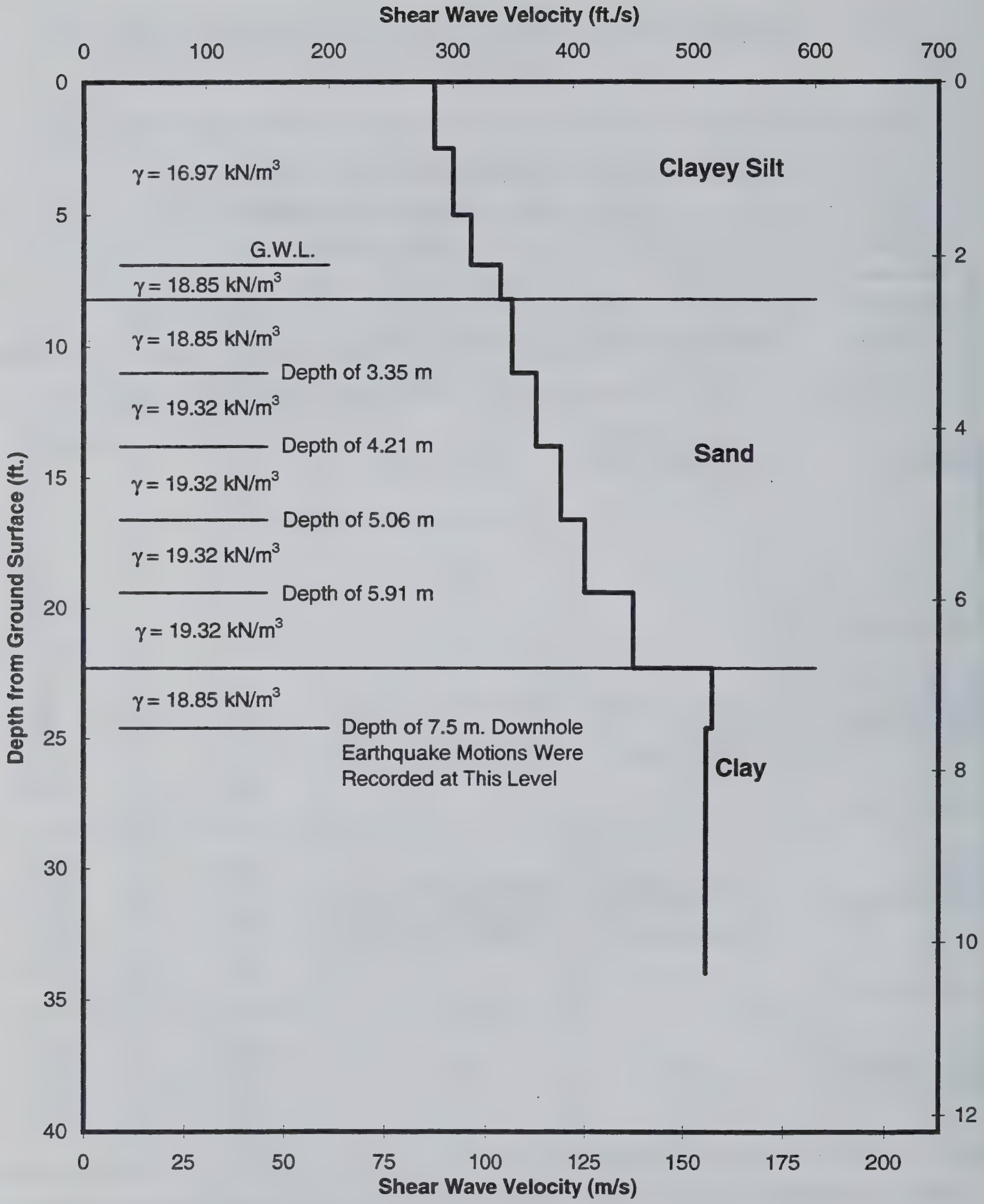

Figure 4.1 - Wildlife Site Soil Profile Used in Response Analyses Based on Average of SASW and Crosshole Shear Wave Velocity Measurements

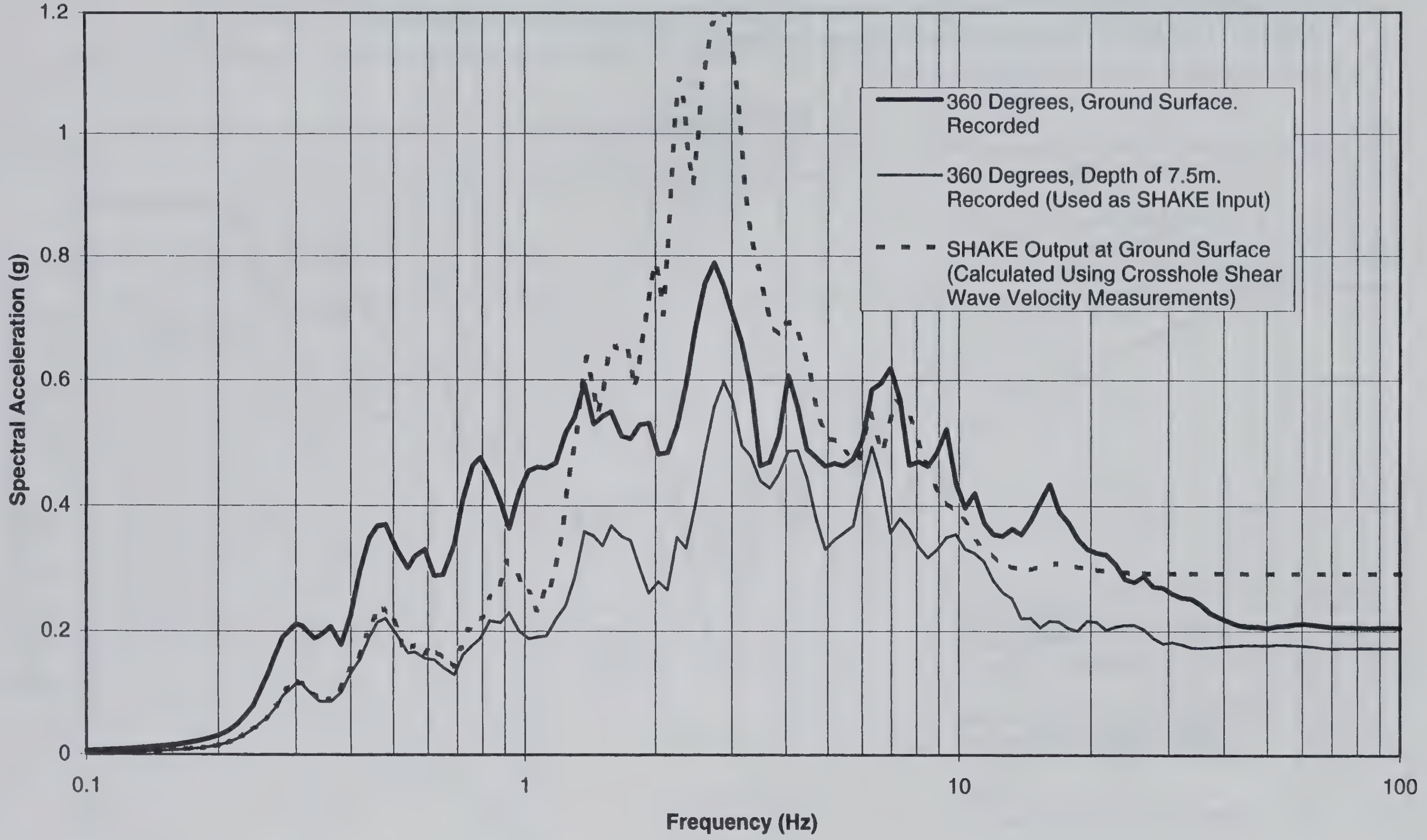

Figure 4.2 - Acceleration Response Spectra at 5% Damping - Wildlife Liquefaction Array, November 24, 1987, 1315 GMT Earthquake - Comparison of Horizontal Motions in 360° Direction - SHAKE Output at Ground Surface Calculated Using Crosshole Shear Wave Velocity Measurements

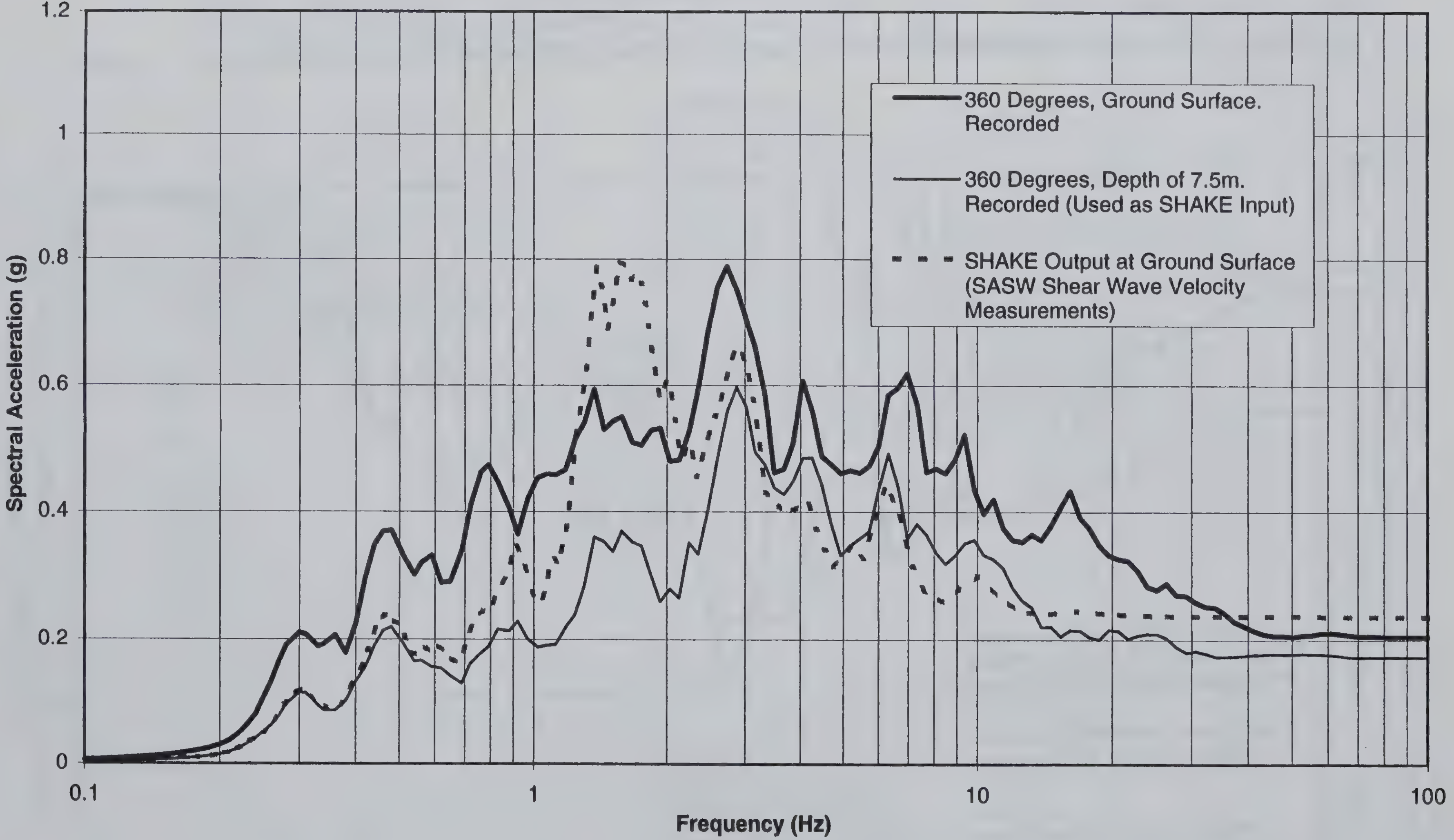

Figure 4.3 - Acceleration Response Spectra at 5% Damping - Wildlife Liquefaction Array, November 24, 1987, 1315 GMT Earthquake - Comparison of Horizontal Motions in 360° Direction - SHAKE Output at Ground Surface Calculated Using SASW Shear Wave Velocity Measurements

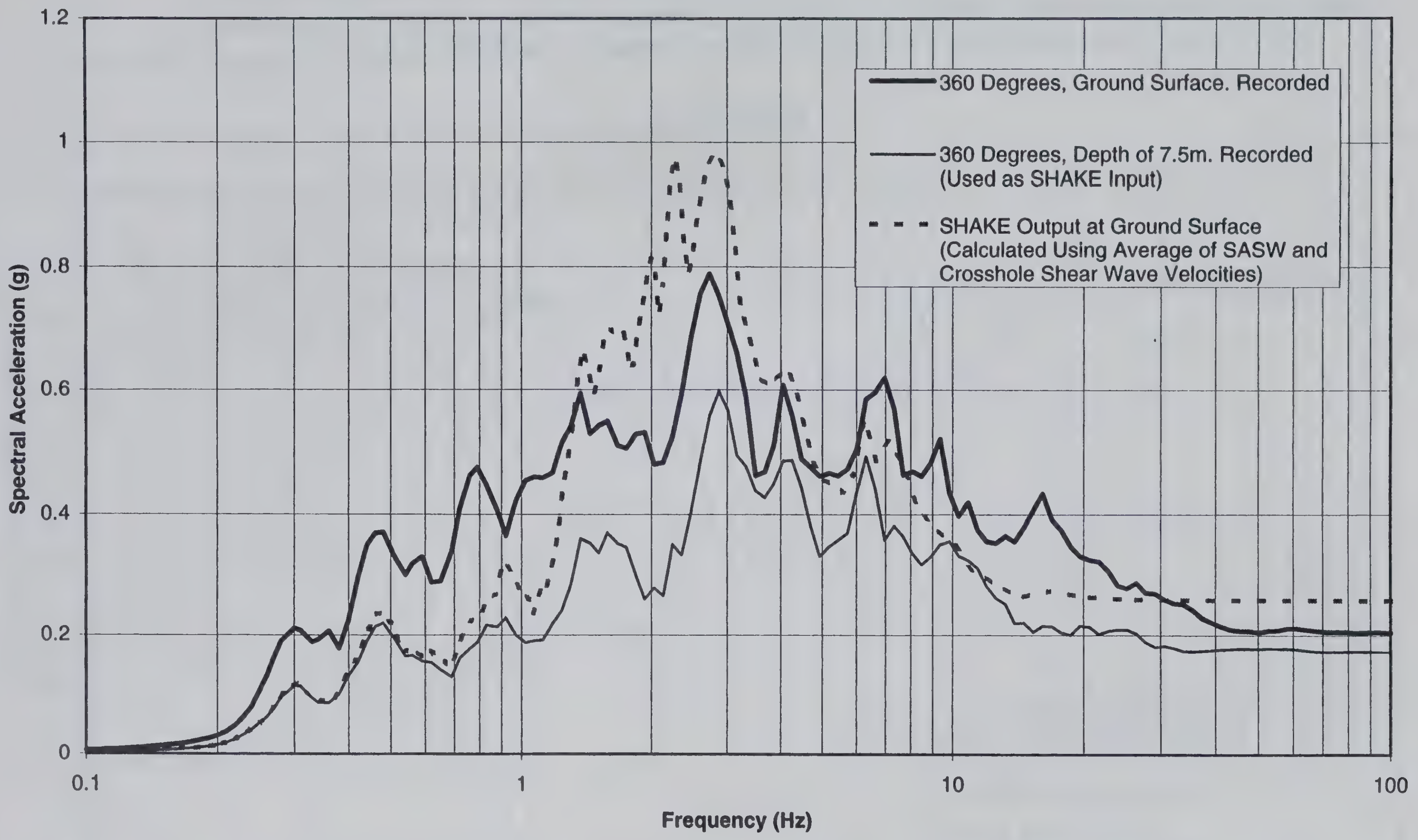

Figure 4.4 - Acceleration Response Spectra at 5% Damping - Wildlife Liquefaction Array, November 24, 1987, 1315 GMT Earthquake - Comparison of Horizontal Motions in 360° Direction - SHAKE Output at Ground Surface Calculated Using Average of SASW and Crosshole Shear Wave Velocity Measurements

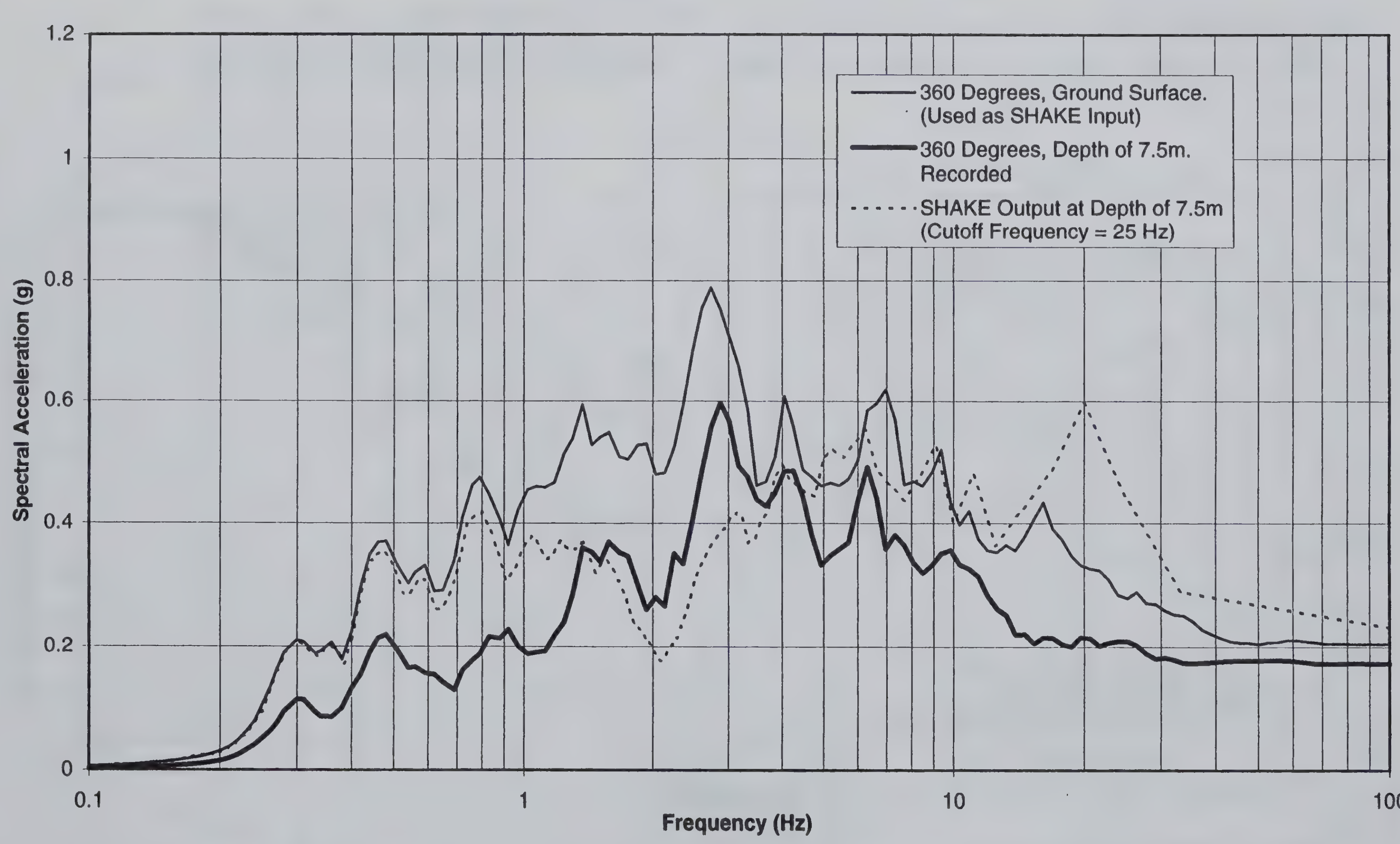

Figure 4.5 - Acceleration Response Spectra at 5% Damping - Wildlife Liquefaction Array, November 24, 1987, 1315 GMT Earthquake - Comparison of Horizontal Motions in 360° Direction - SHAKE Output at Depth of 7.5 m with Cutoff Frequency of 25 Hz.

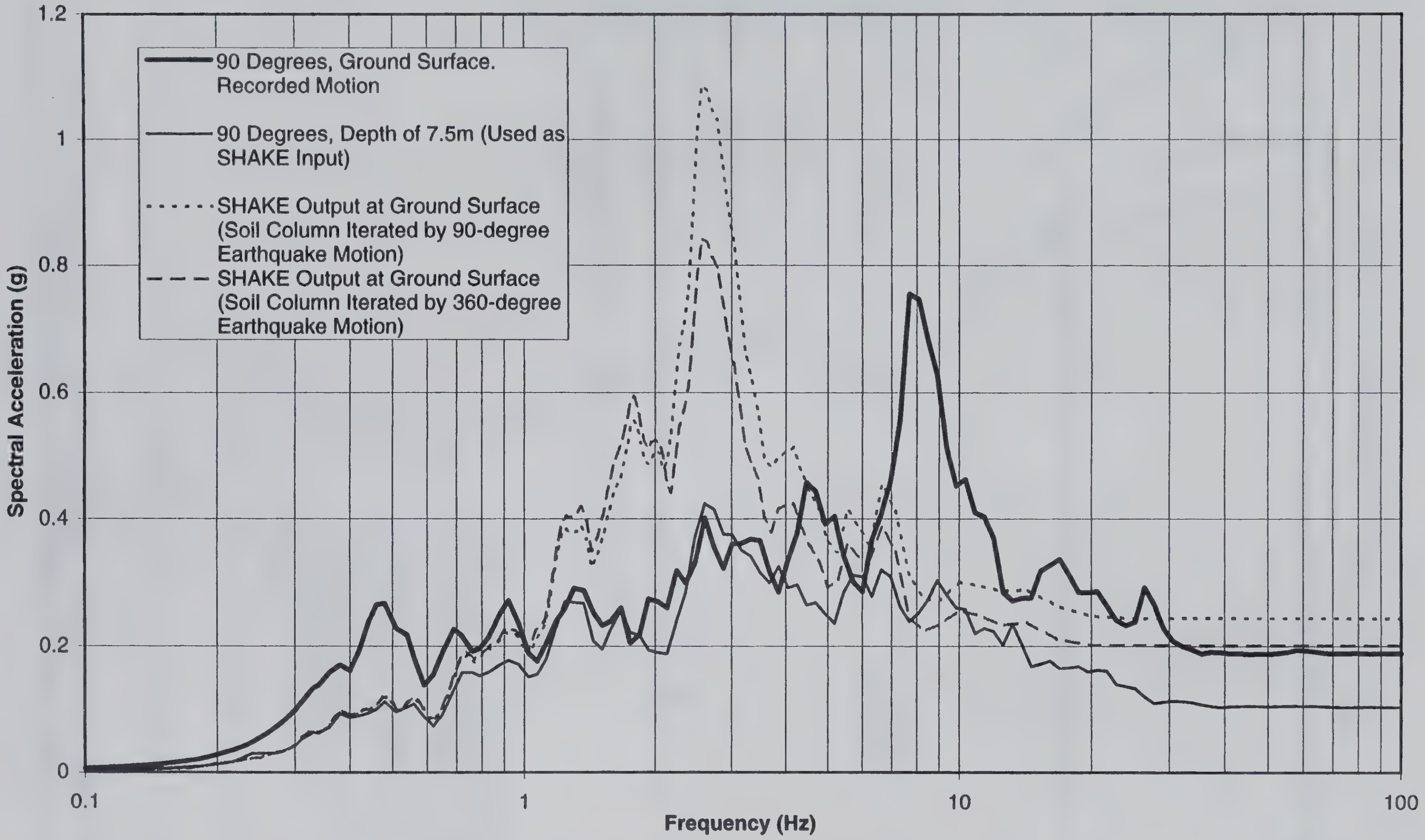

Figure 4.6 - Acceleration Response Spectra at 5% Damping - Wildlife Liquefaction Array, November 24, 1987, 1315 GMT Earthquake - Comparison of Horizontal Motions in 90° Direction - SHAKE Output at Ground Surface Calculated Using Average of SASW and Crosshole Shear Wave Velocity Measurements.

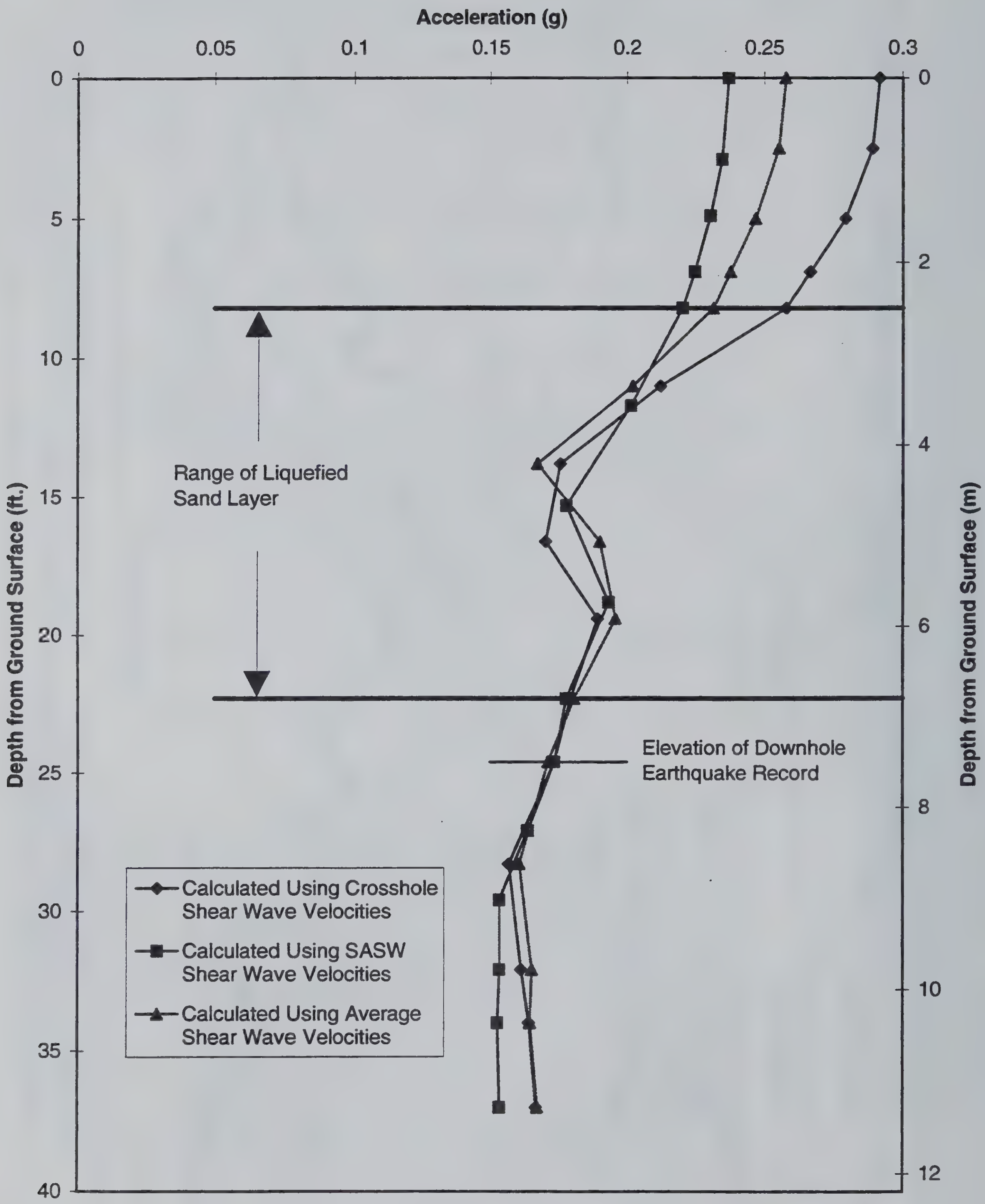

Figure 4.7 - Maximum Acceleration Distribution over Depth from SHAKE Results - Wildlife Site, NOvember 24, 1987, 1315 GMT Earthquake in 360° Direction

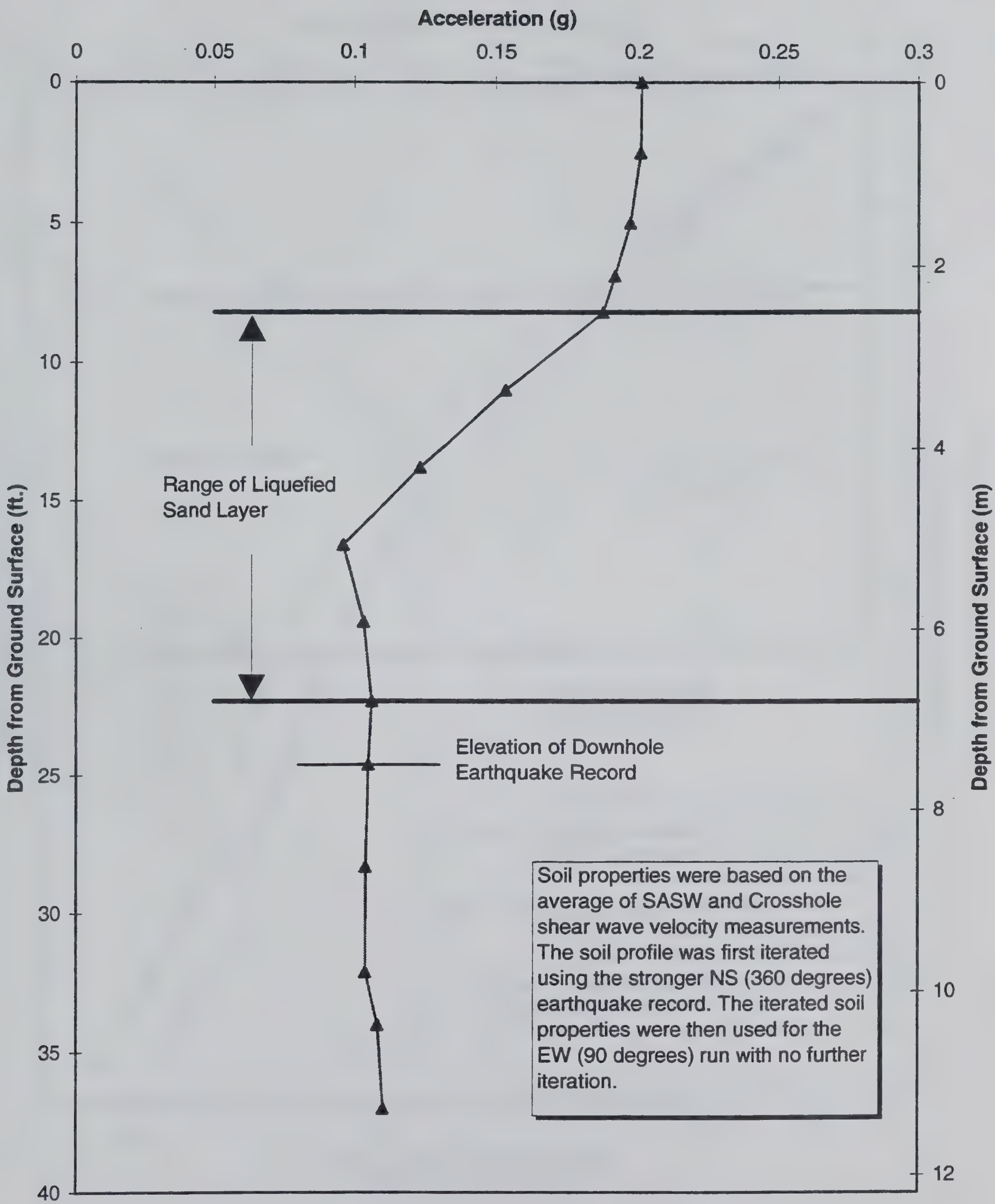

Figure 4.8 - Maximum Acceleration Distribution over Depth from SHAKE Results - Wildlife Site, November 24, 1987, 1315 GMT Earthquake in 90° Direction

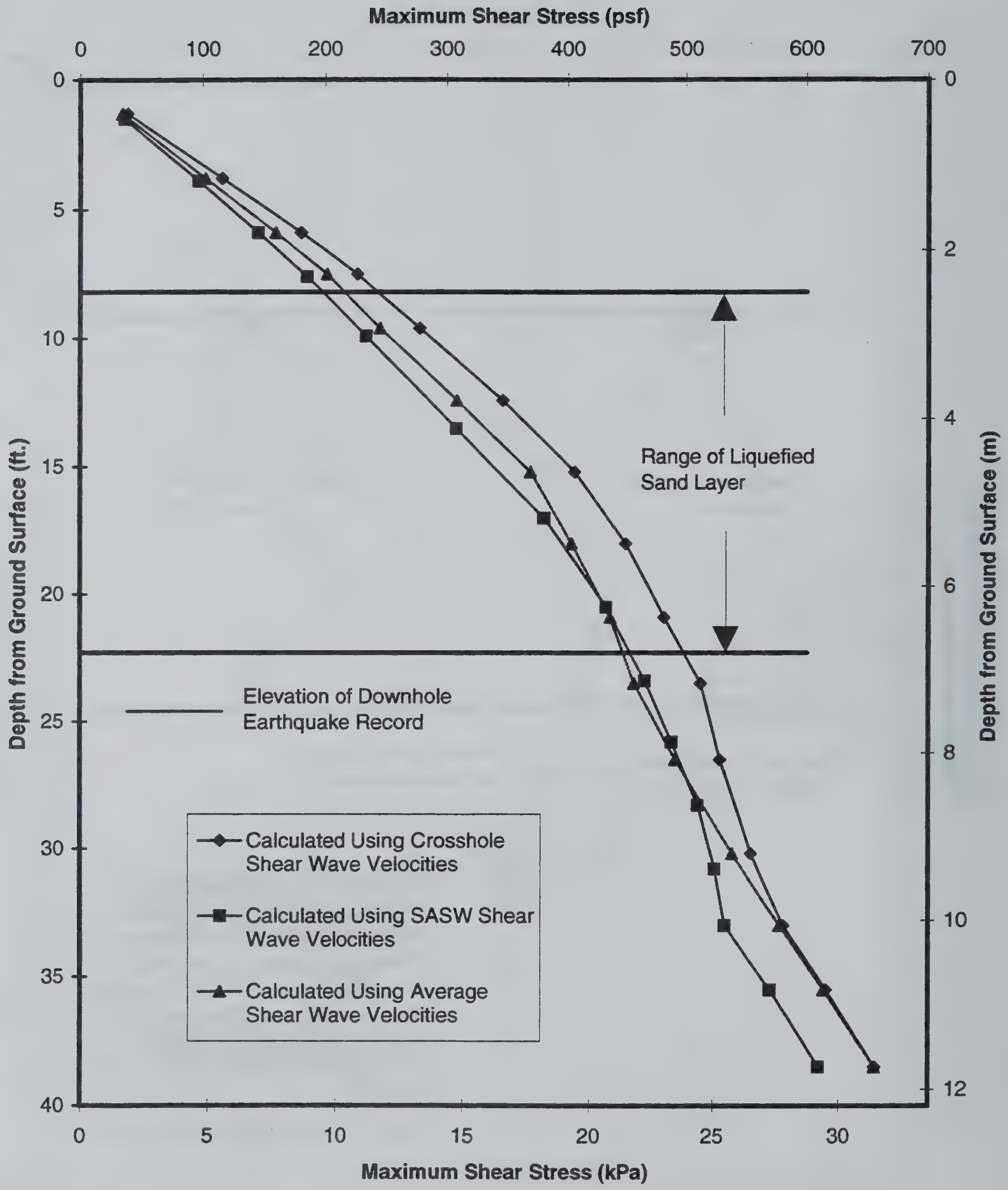

Figure 4.9 - Maximum Shear Stress Distribution over Depth from SHAKE Results - Wildlife Site, November 24, 1987, 1315 GMT Earthquake in 360° Direction

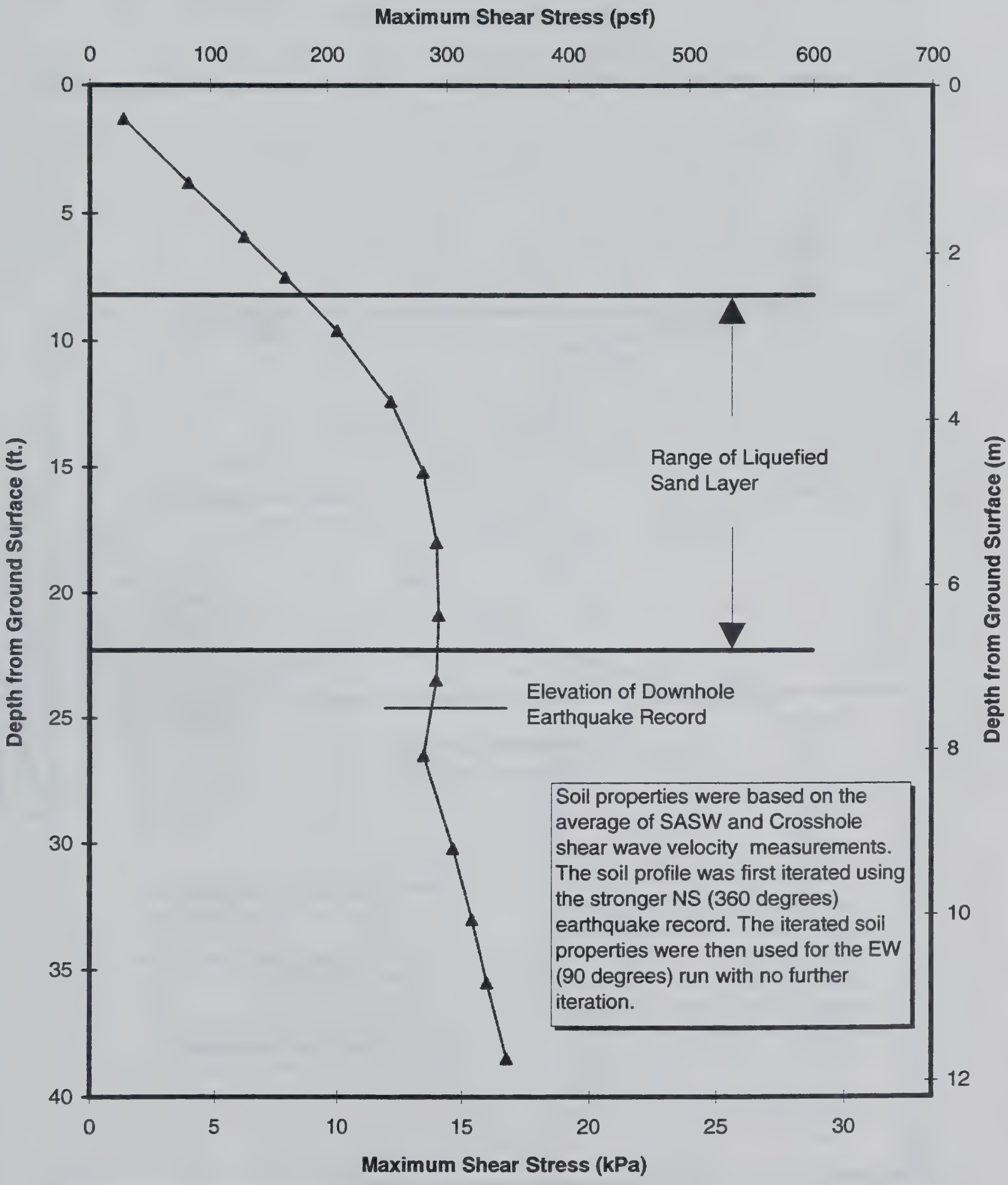

Figure 4.10 - Maximum Shear Stress Distribution over Depth from SHAKE Results - Wildlife Site, November 24, 1987, 1315 GMT Earthquake in 90° Direction

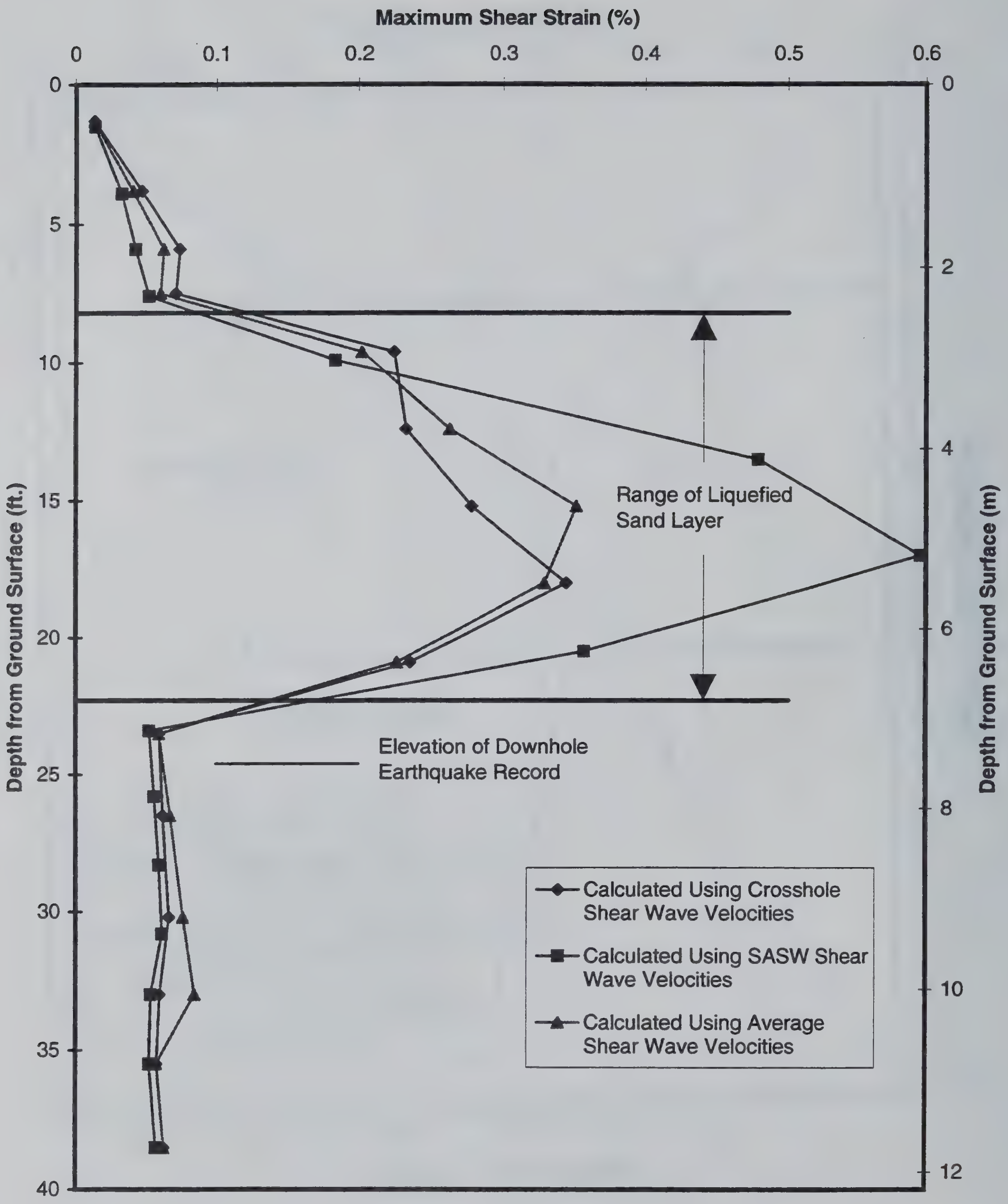

Figure 4.11 - Maximum Shear Strain Distribution over Depth from SHAKE Results - Wildlife Site, November 24, 1987, 1315 GMT Earthquake in 360° Direction

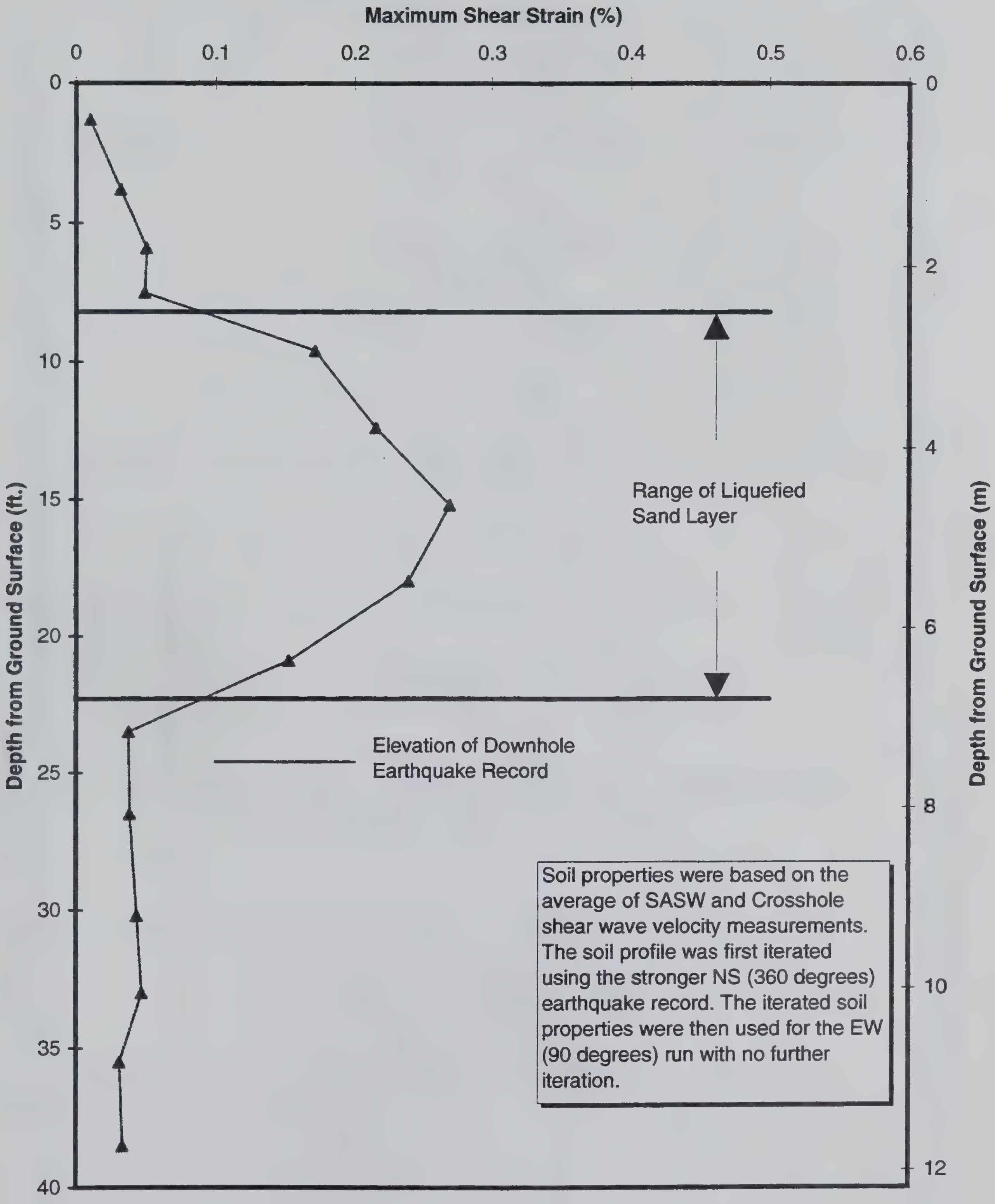

Figure 4.12 - Maximum Shear Strain Distribution over Depth from SHAKE Results - Wildlife Site, November 24, 1987, 1315 GMT Earthquake in 90° Direction

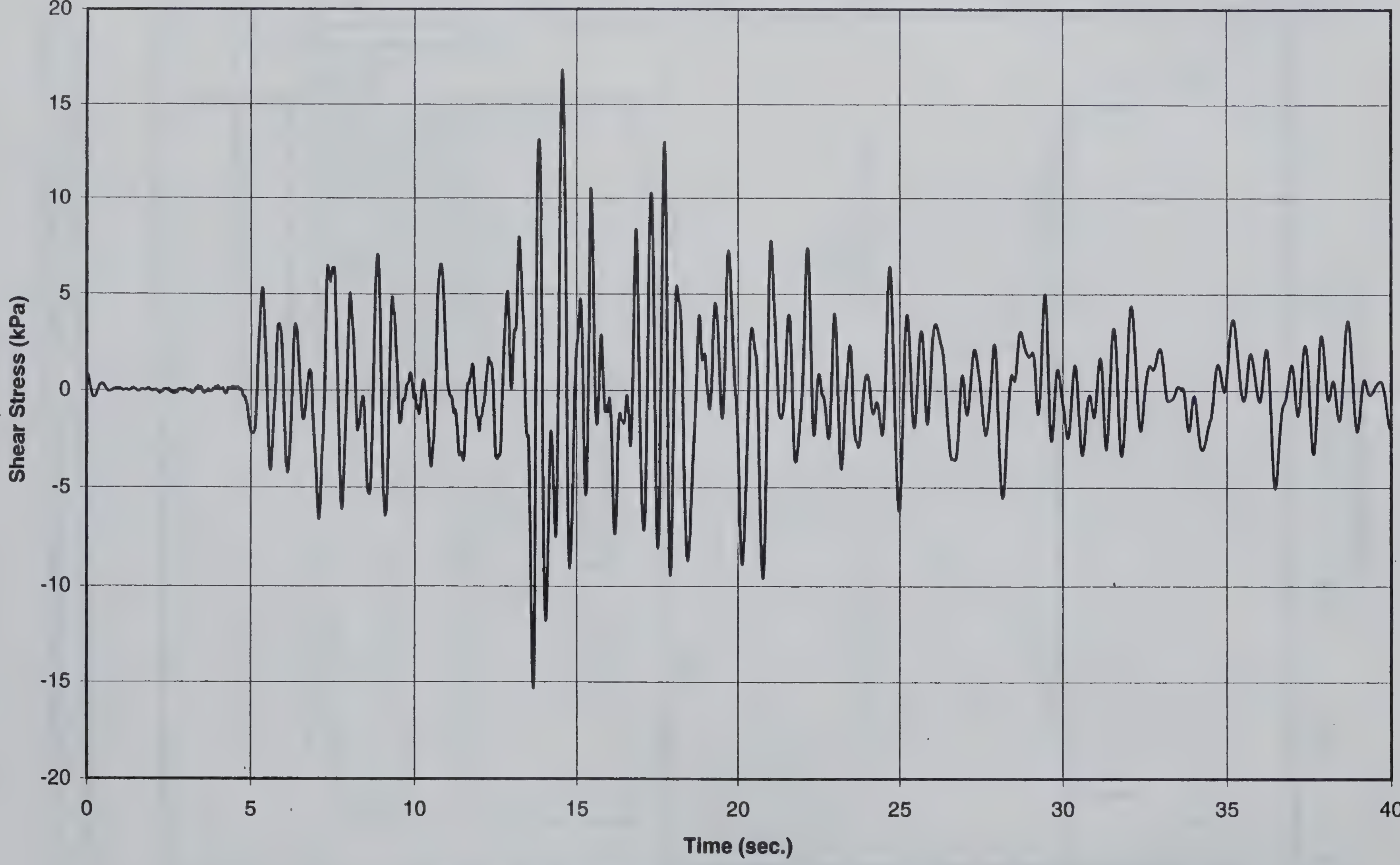

Figure 4.13 - Shear Stress Time History at Depth 4.21 m (13.8 ft.) from SHAKE Output - Wildlife Site, November 24, 1987, 1315 GMT Earthquake in 360° Direction

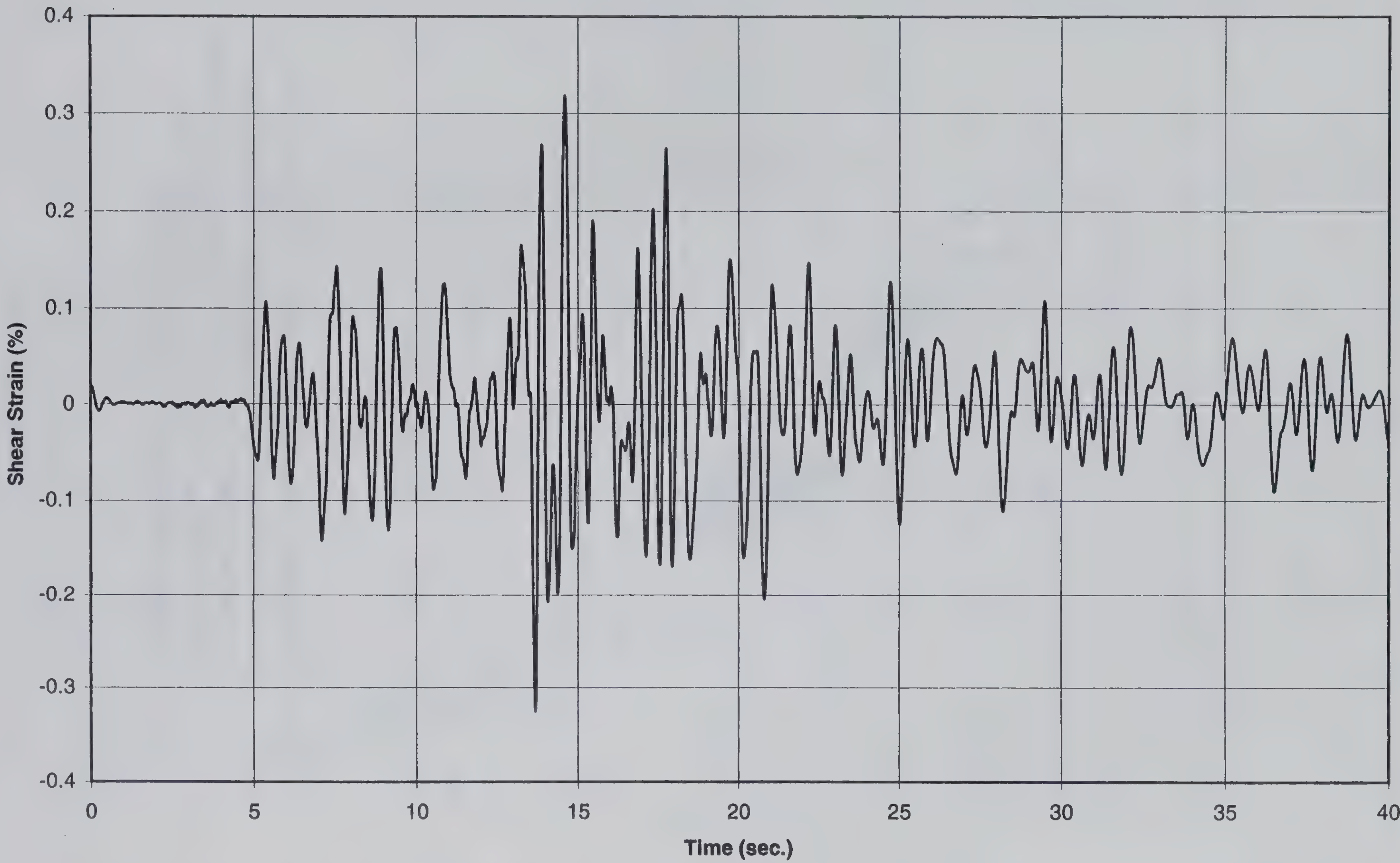

Figure 4.14 - Shear Strain Time History at Depth 4.21 m (13.8 ft.) from SHAKE Output - Wildlife Site, November 24, 1987, 1315 GMT Earthquake in 360° Direction

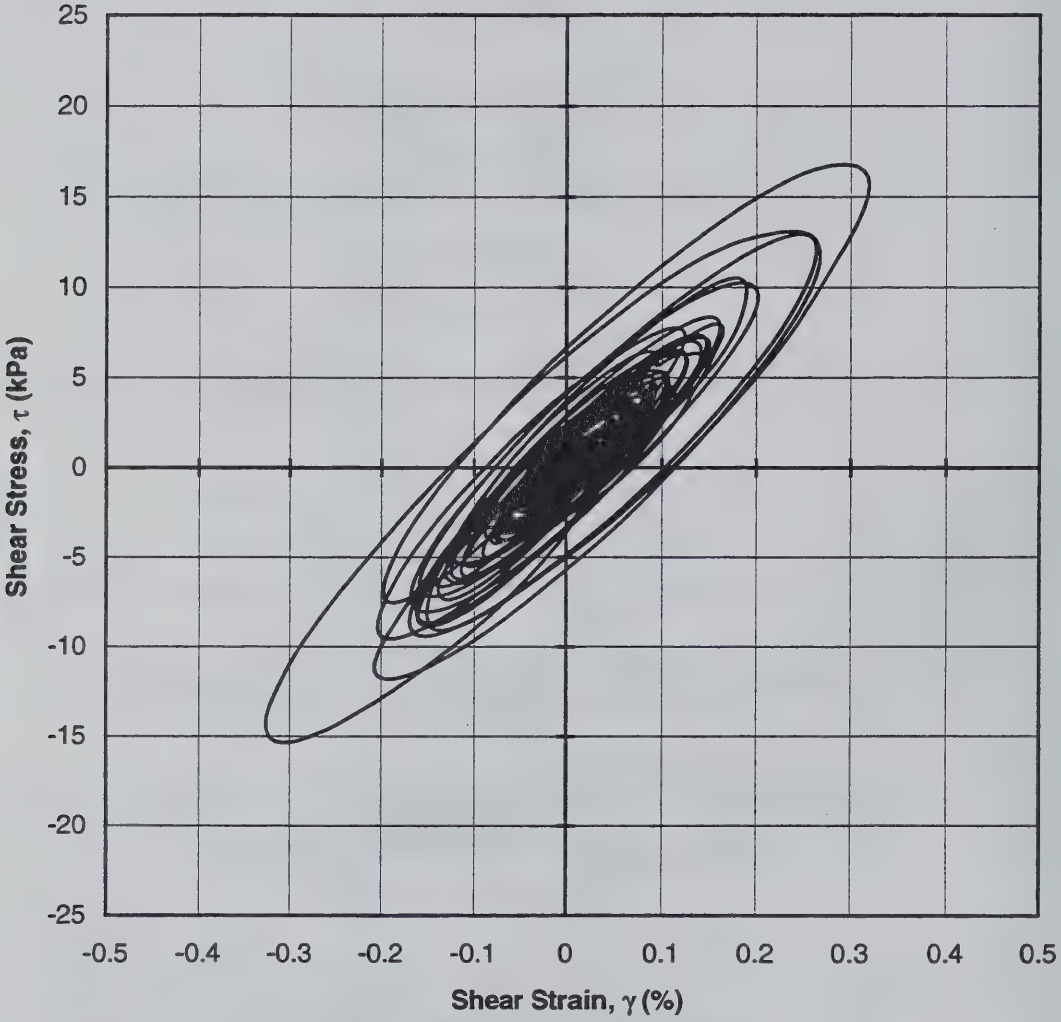

Figure 4.15 - Shear Stress - Shear Strain Hysteresis Loop at Depth 4.21 m (13.8 ft.) Calculated from SHAKE Output - Wildlife Site, November 24, 1987, 1315 GMT Earthquake in 360° Direction. Soil Properties are Based on the Average of SASW and Crosshole Shear Wave Velocity Measurements

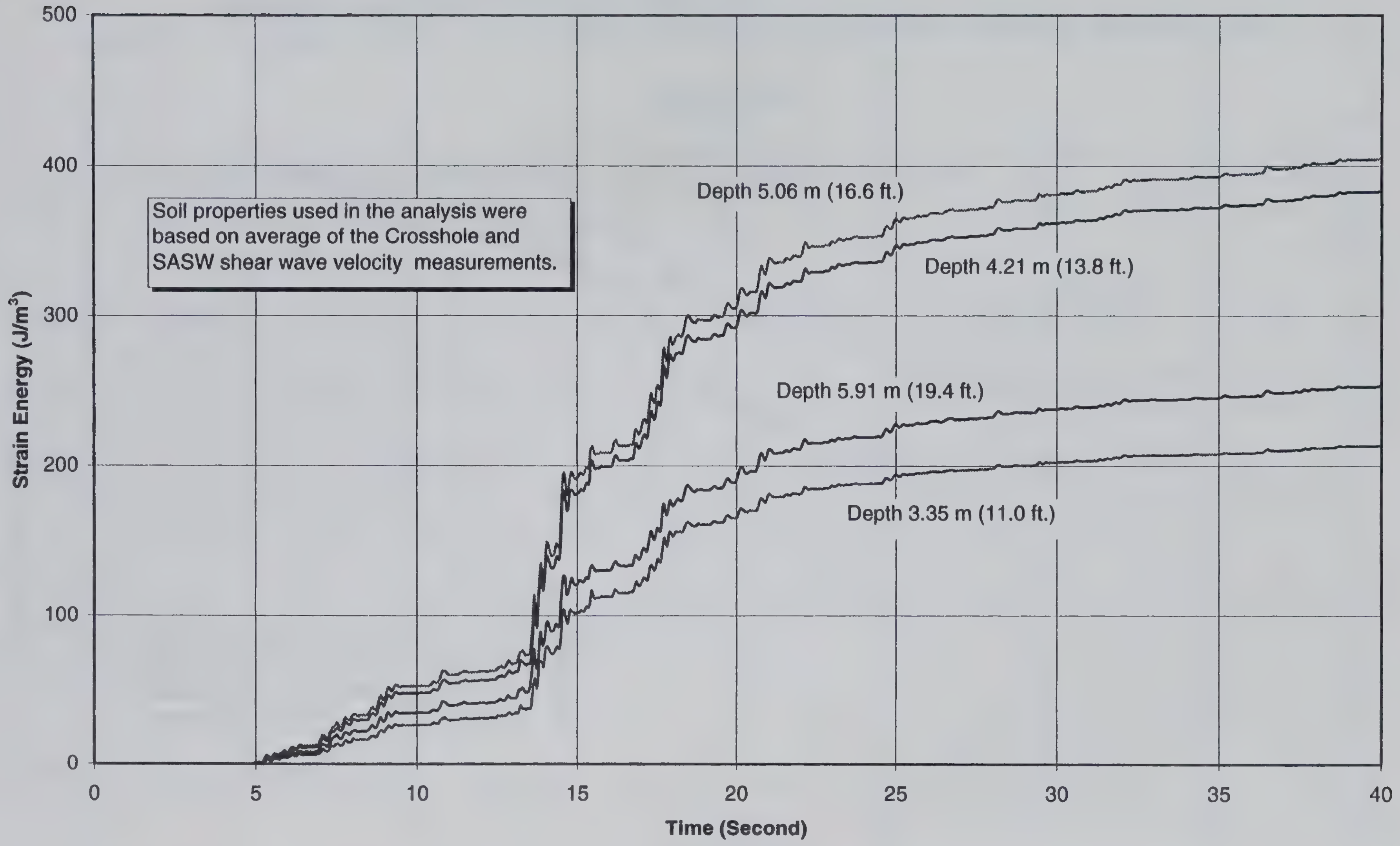

Figure 4.16 - Accumulation of Strain Energy in Liquefied Sand Layer - Wildlife Site, November 24, 1987, 1315 GMT Earthquake in 360° Direction - SHAKE Analysis Output

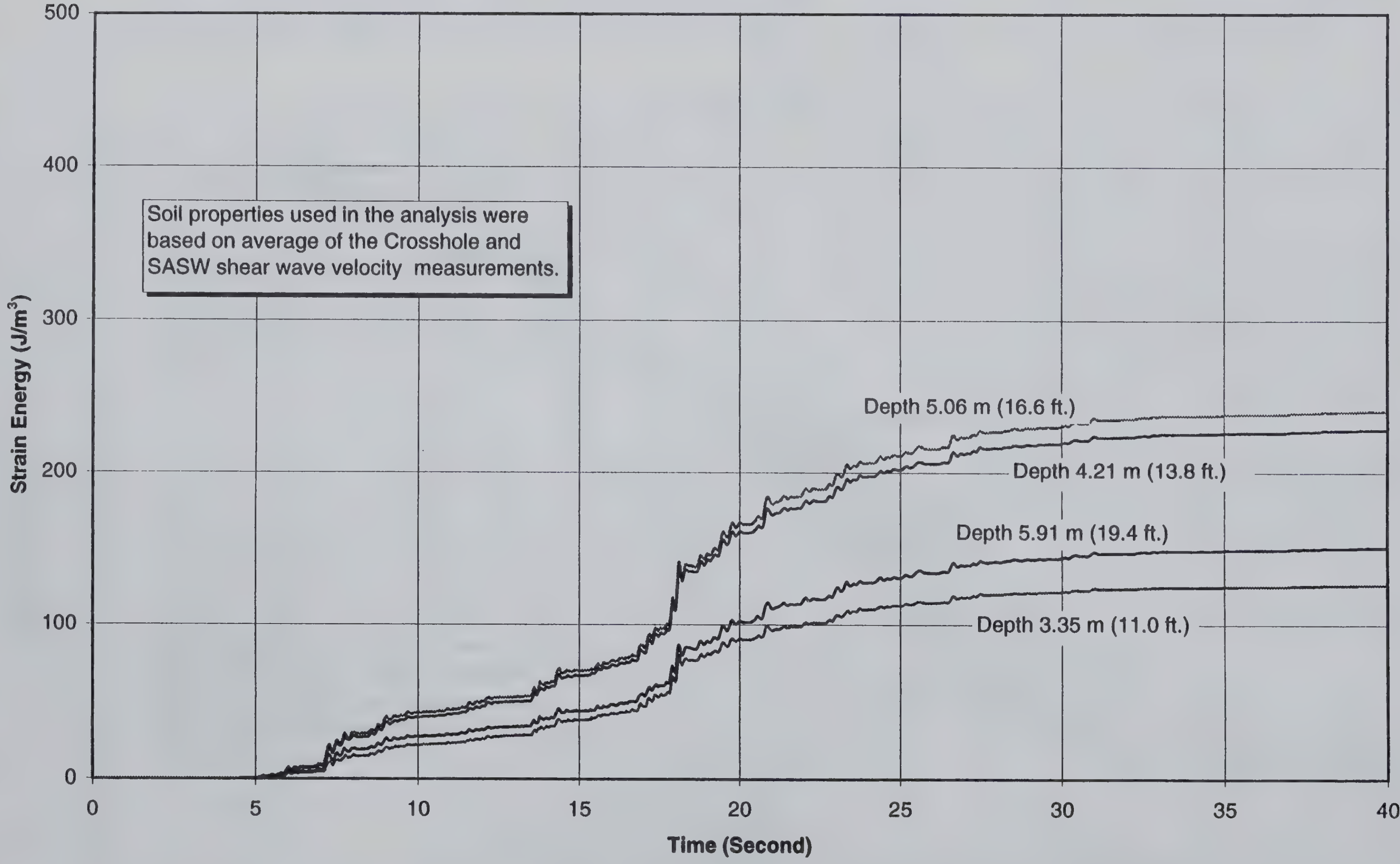

Figure 4.17 - Accumulation of Strain Energy in Liquefied Sand Layer - Wildlife Site, November 24, 1987, 1315 GMT Earthquake in 90° Direction - SHAKE Analysis Output

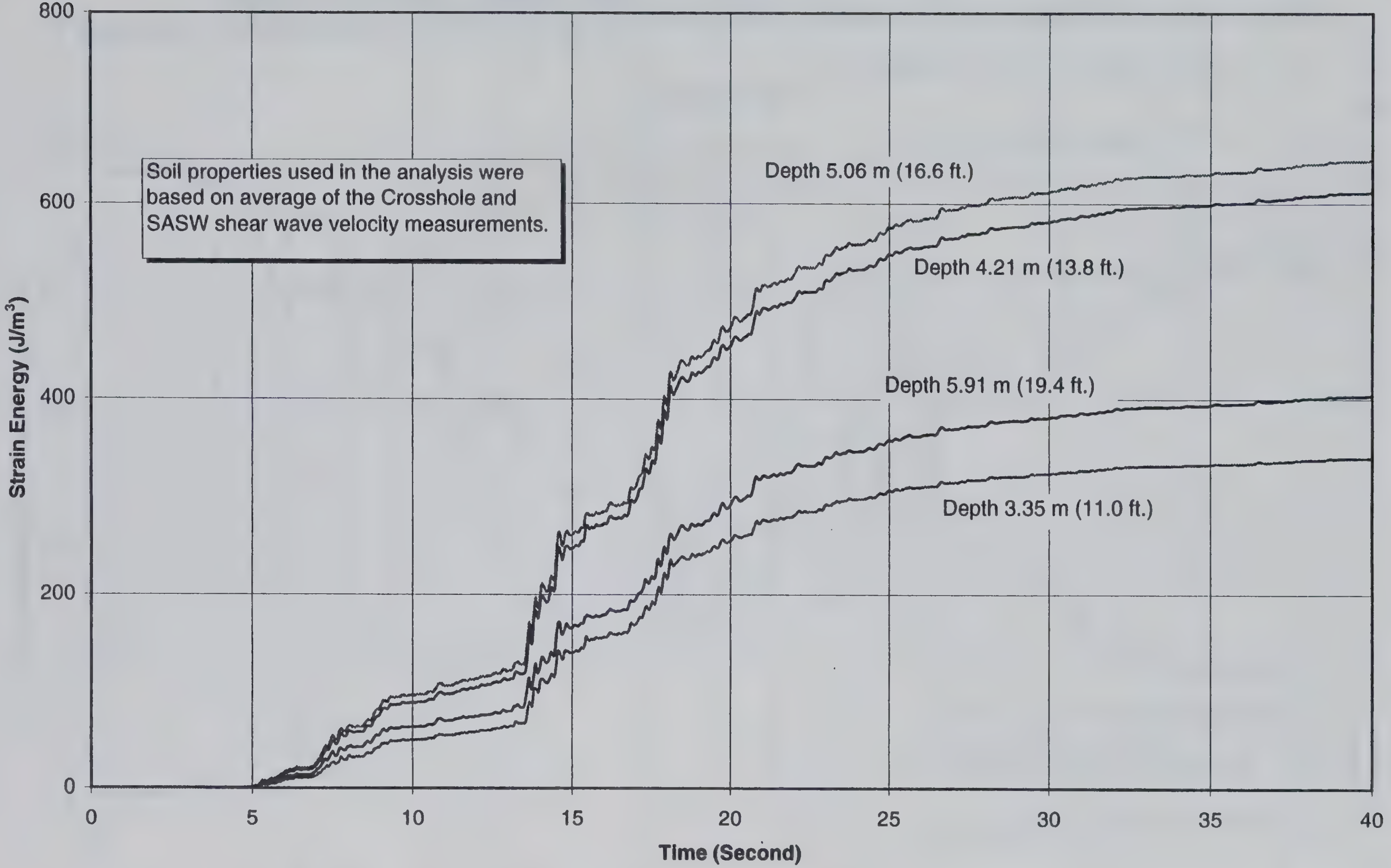

Figure 4.18 - Accumulation of Strain Energy in Liquefied Sand Layer - Wildlife Site, November 24, 1987, 1315 GMT Eathquake - Summation of SHAKE Analysis Output in both 360° and 90° Directions

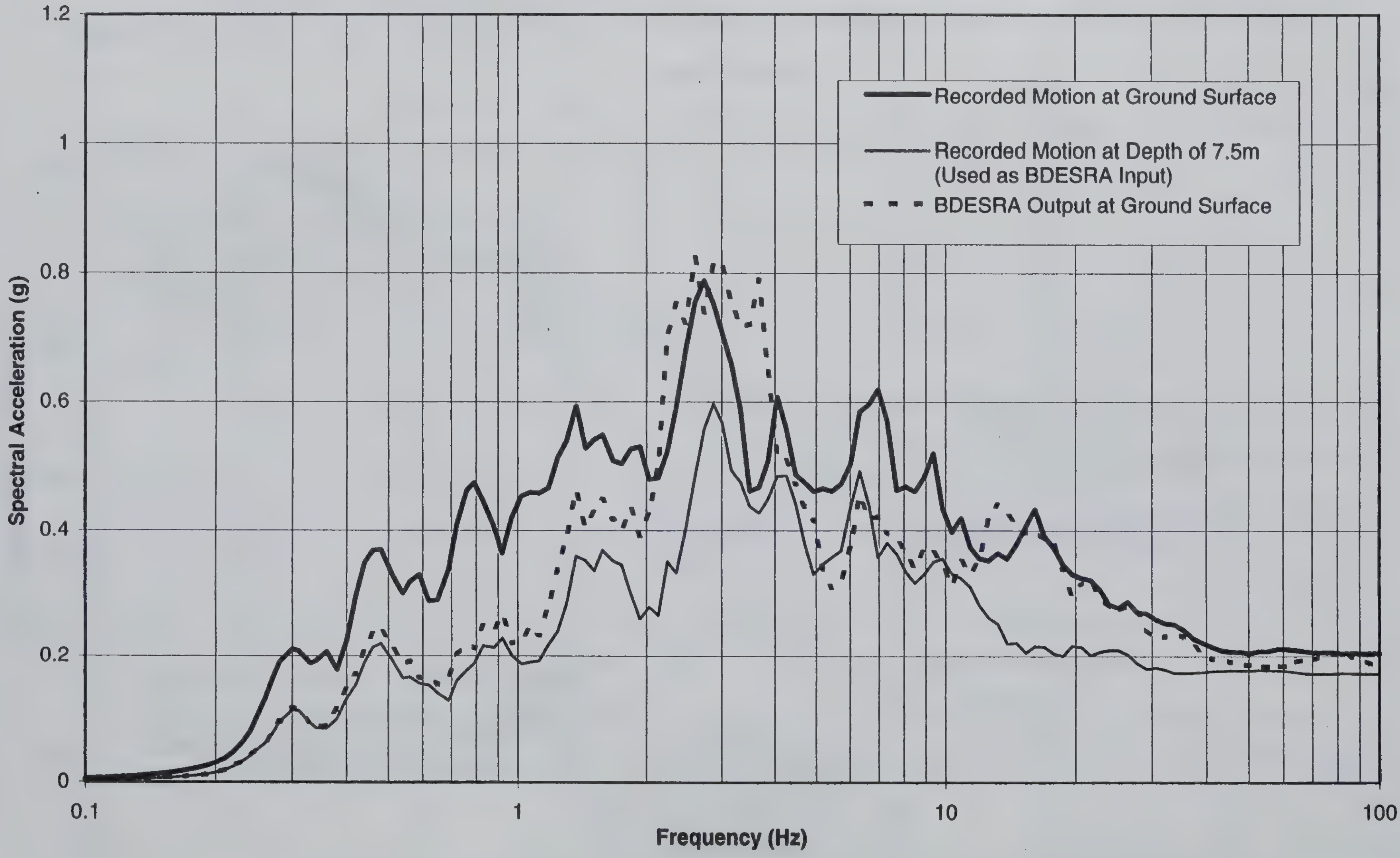

Figure 4.19 - Acceleration Response Spectra at 5% Damping - Wildlife Liquefaction Array, November 24, 1987, 1315 GMT Earthquake - Comparison of Horizontal Motions in 360° Direction - BDESRA Output, Total Stress Analysis

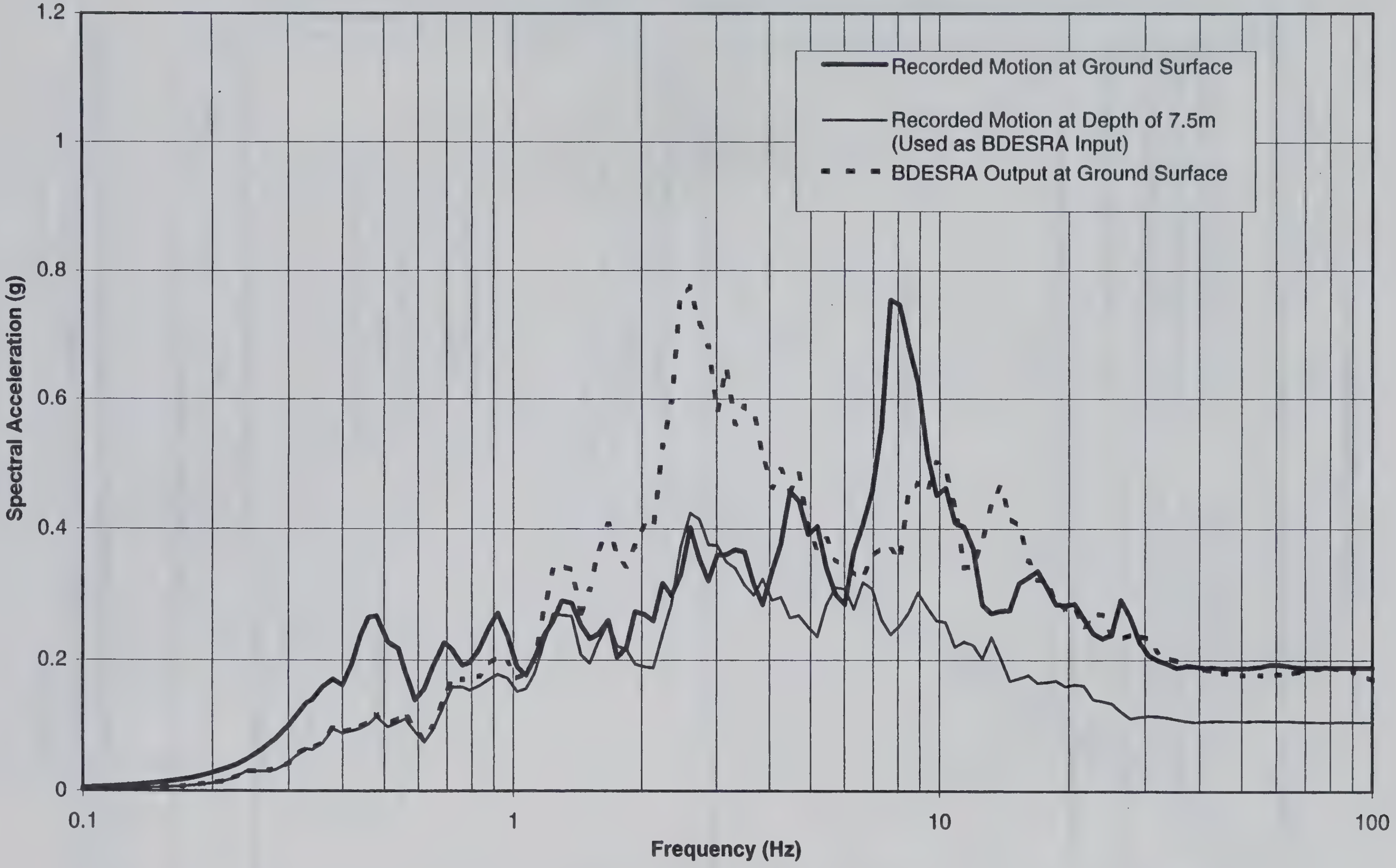

Figure 4.20 - Acceleration Response Spectra at 5% Damping - Wildlife Liquefaction Array, November 24, 1987, 1315 GMT Earthquake - Comparison of Horizontal Motions in 90° Direction - BDESRA Output, Total Stress Analysis

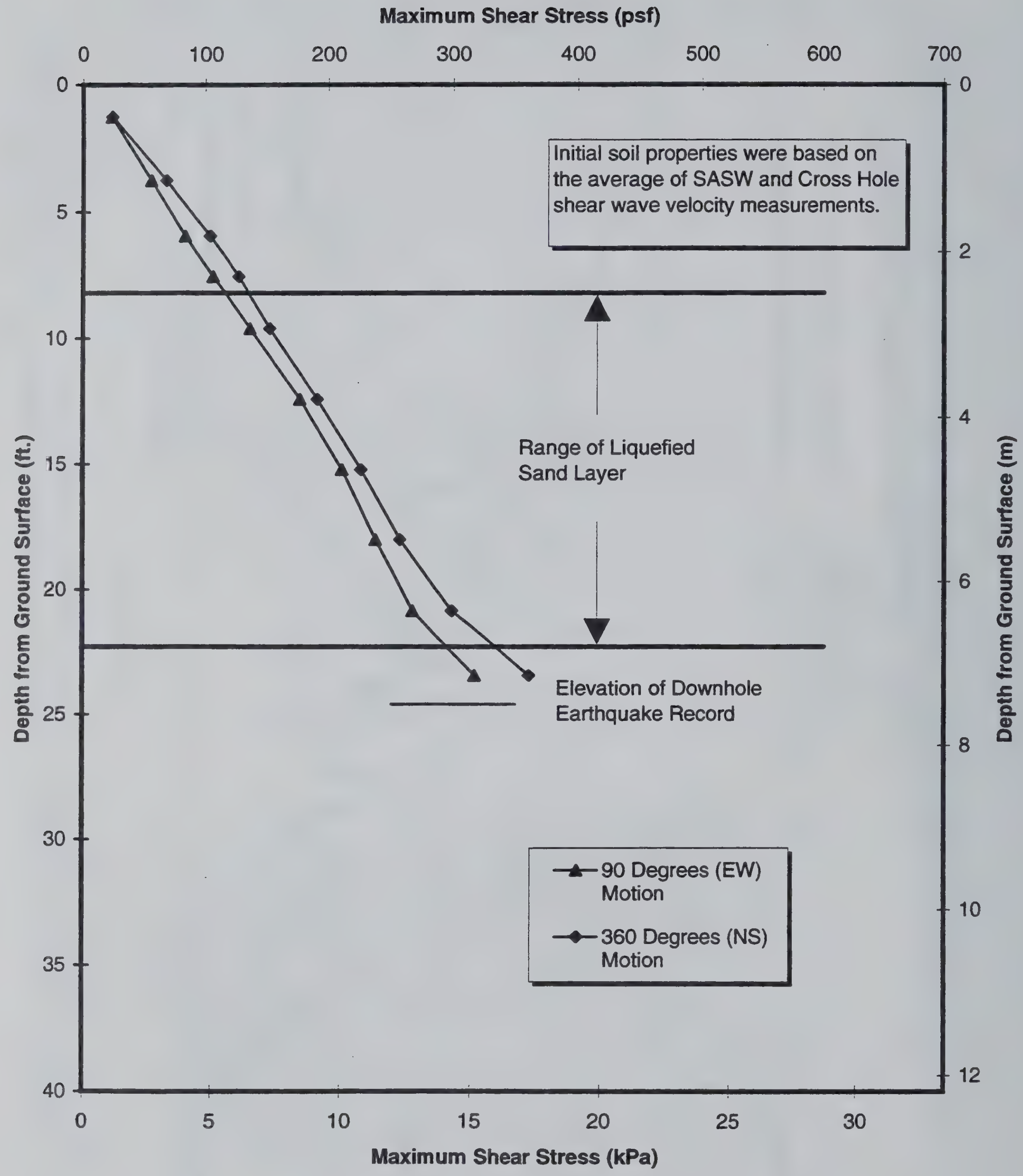

Figure 4.21 - Maximum Shear Stress Distribution over Depth from BDESRA Results of Total Stress Analyses - Wildlife Site, November 24, 1987, 1315 GMT Earthquake

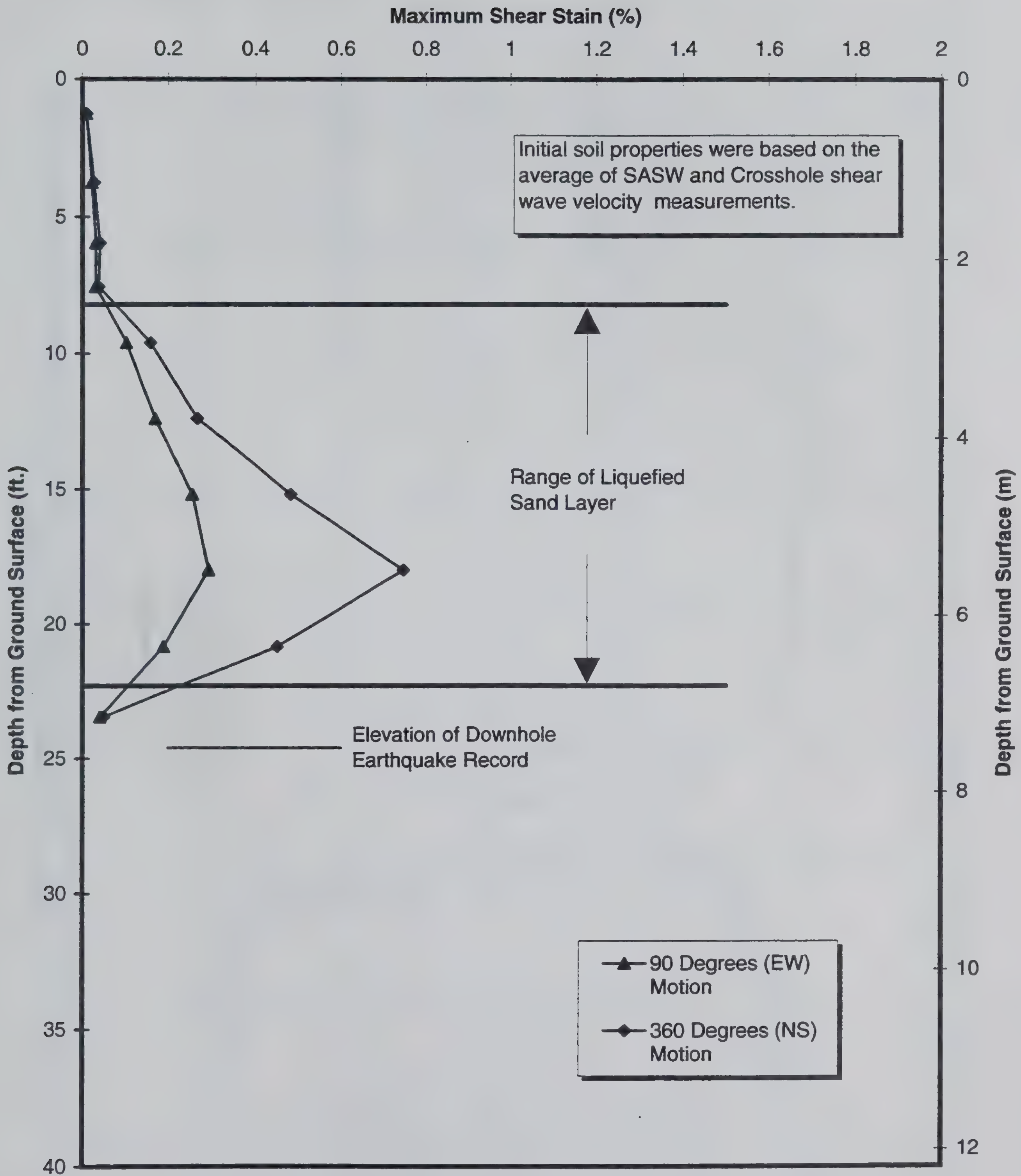

Figure 4.22 - Maximum Shear Strain Distribution over Depth from BDESRA Results of Total Stress Analyses - Wildlife Site, November 24, 1987, 1315 GMT Earthquake

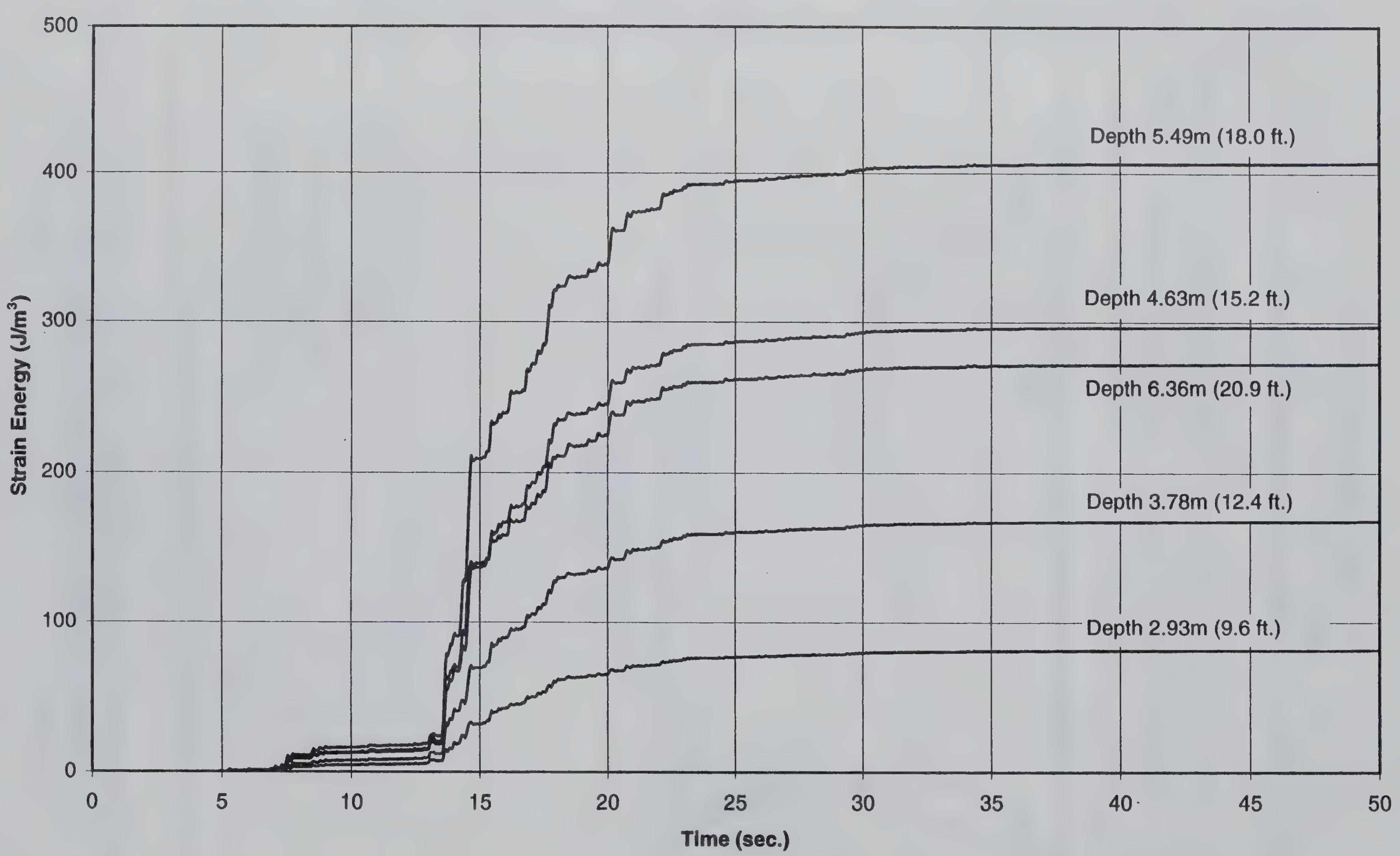

Figure 4.23 - Accumulation of Strain Energy in Liquefied Sand Layer - Wildlife Site, November 24, 1987, 1315 GMT Earthquake in 360° Direction - BDESRA Output, Total Stress Analysis

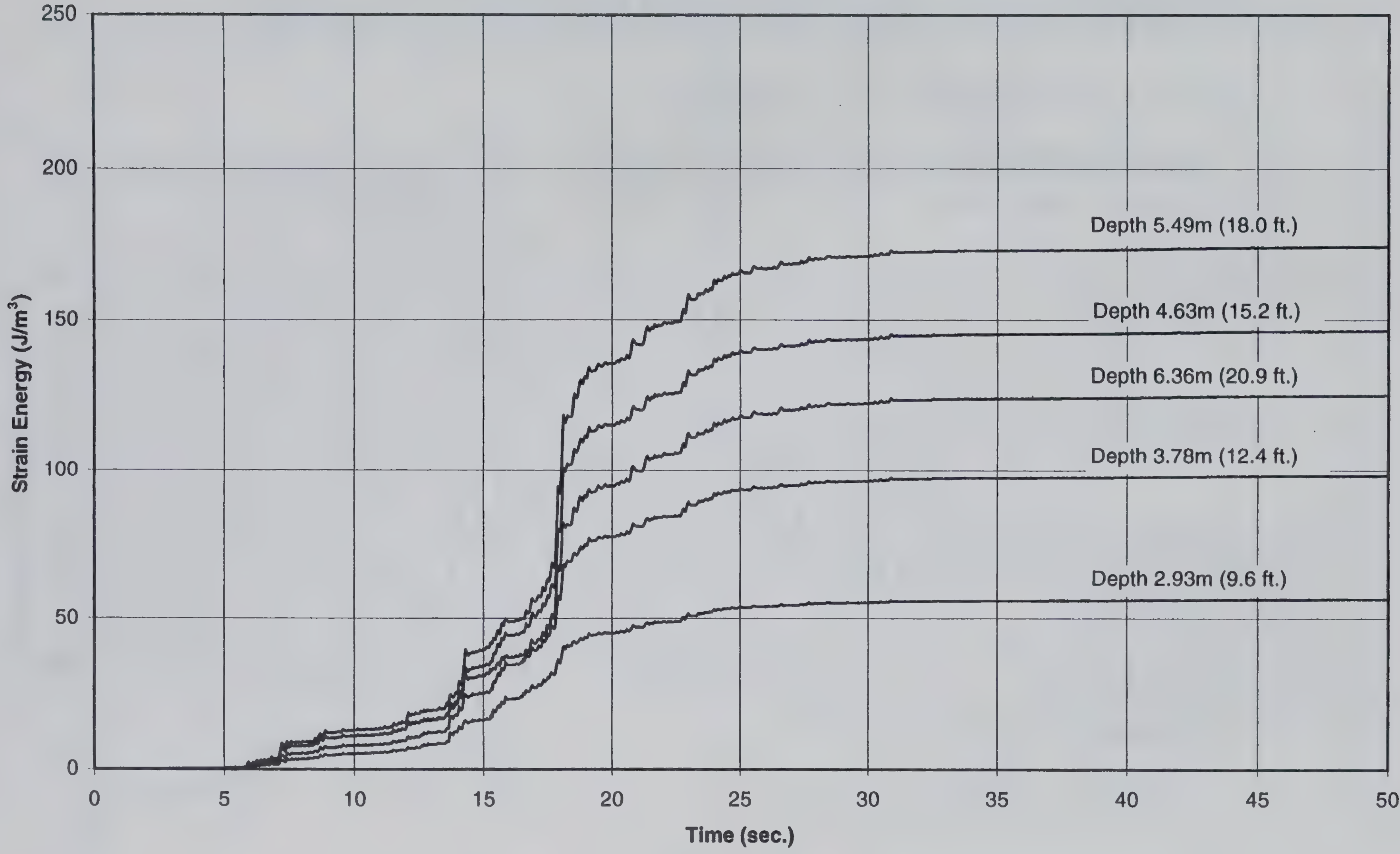

Figure 4.24 - Accumulation of Strain Energy in Liquefied Sand Layer - Wildlife Site, November 24, 1987, 1315 GMT Earthquake in 90° Direction - BDESRA Output, Total Stress Analysis

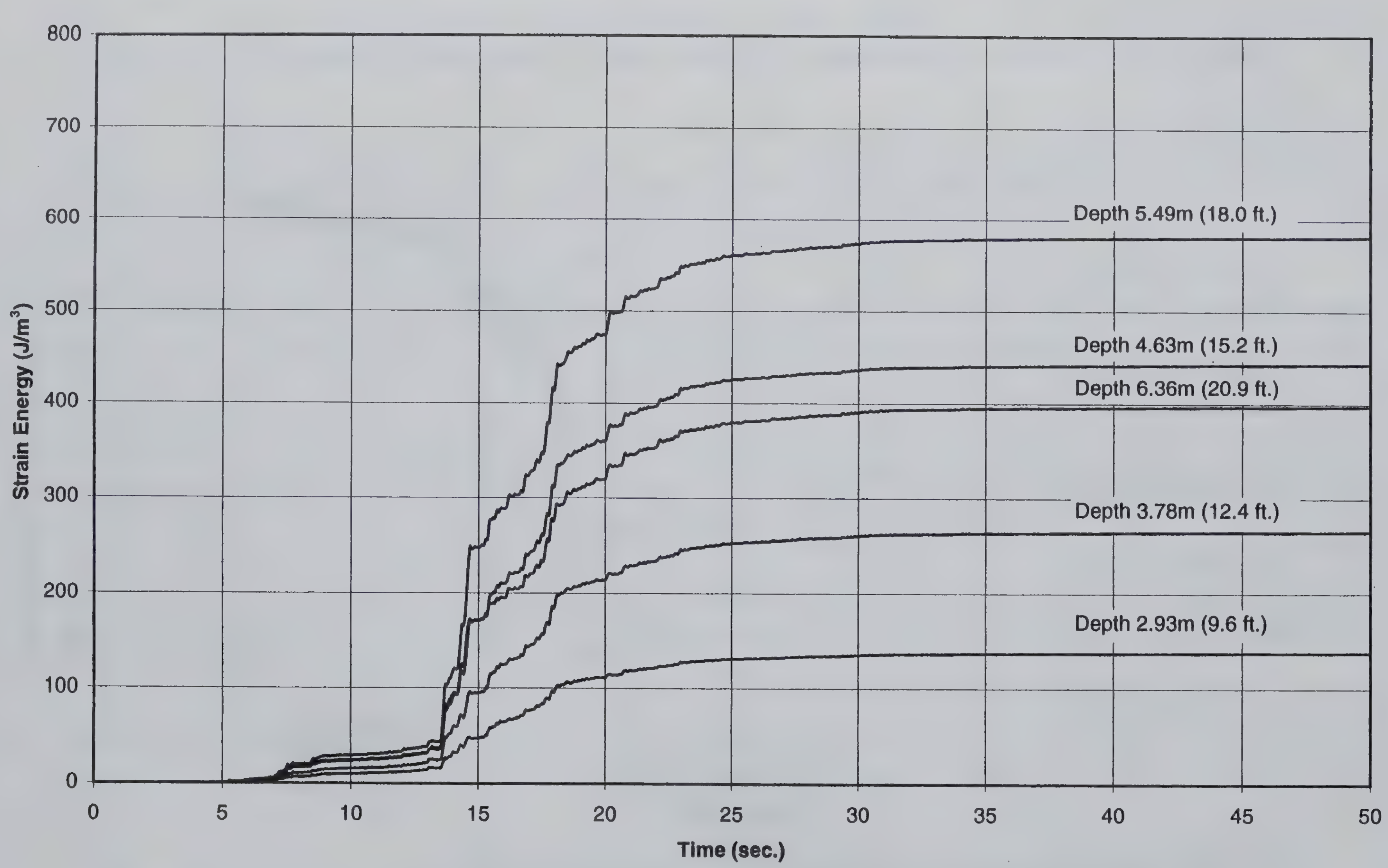

Figure 4.25 - Accumulation of Strain Energy in Liquefied Sand Layer - Wildlife Site, November 24, 1987, 1315 GMT Earthquake - Summation of BDESRA Total Stress Analysis Output in both 360° and 90° Directions

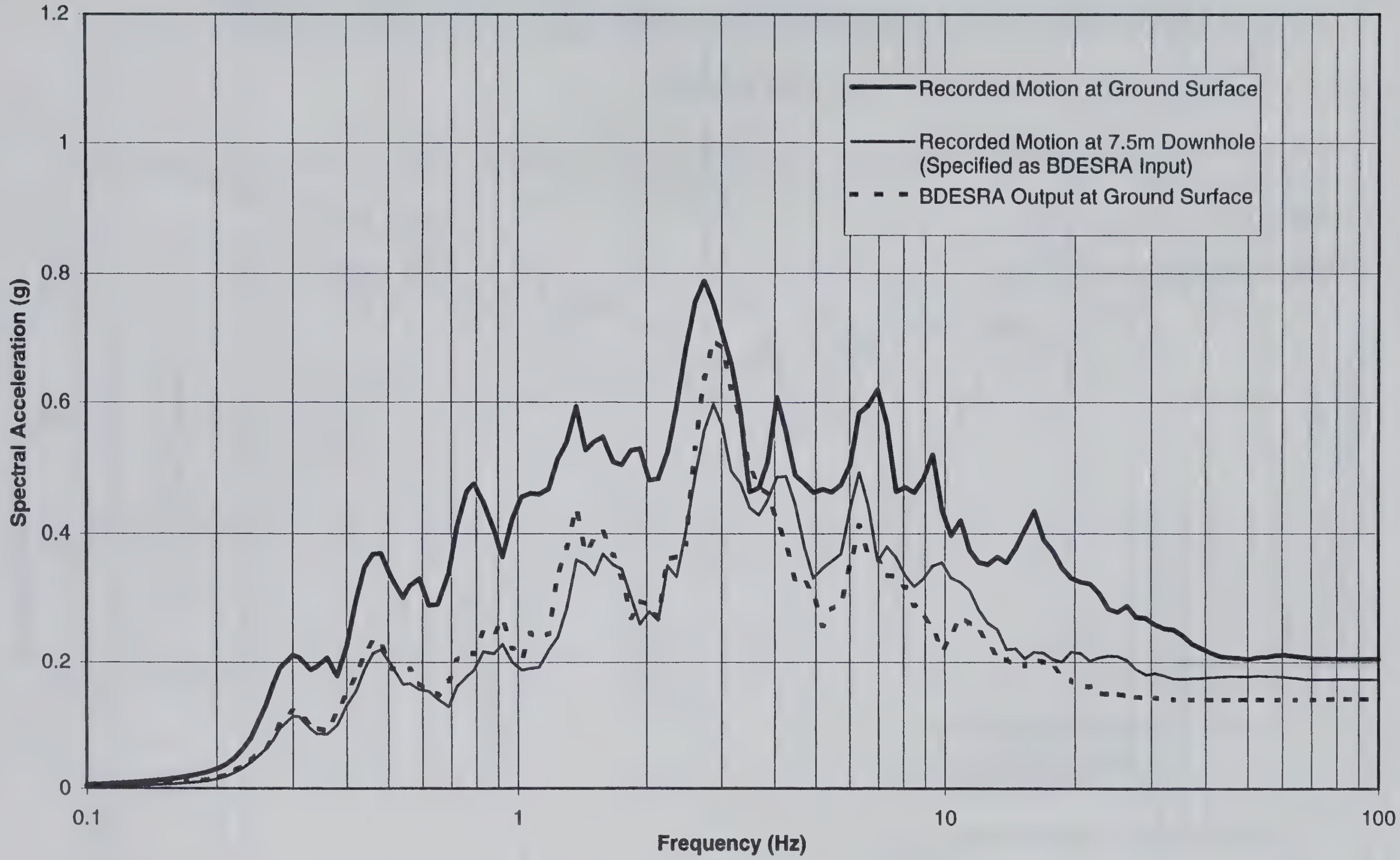

Figure 4.26 - Acceleration Response Spectra at 5% Damping - Wildlife Liquefaction Array, November 24, 1987, 1315 GMT Earthquake - Comparison of Horizontal Motions in 360° Direction - BDESRA Output, Effective Stress Analysis

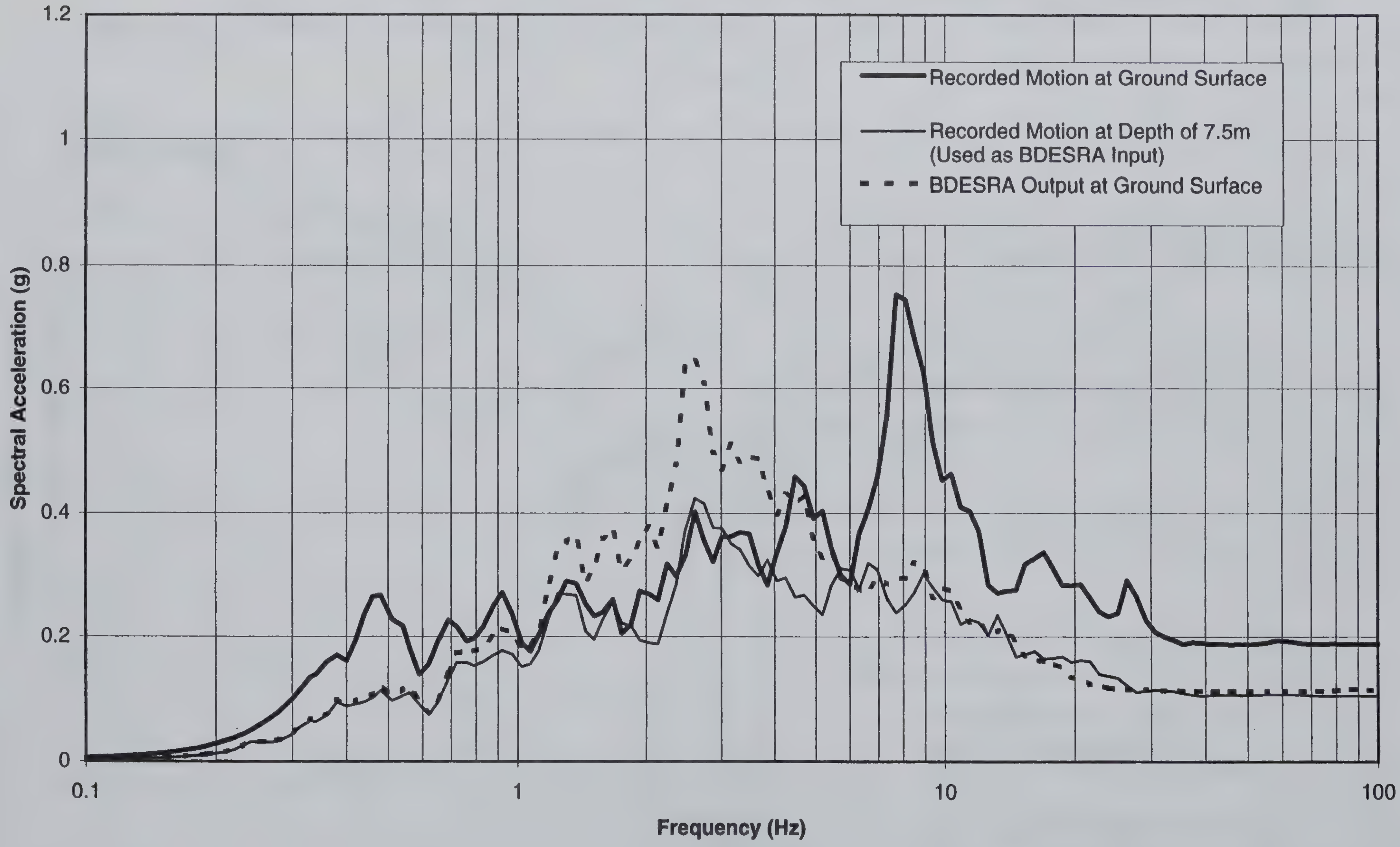

Figure 4.27 - Acceleration Response Spectra at 5% Damping - Wildlife Liquefaction Array, November 24, 1987, 1315 GMT Earthquake - Comparison of Horizontal Motions in 90° Direction - BDESRA Output, Effective Stress Analysis

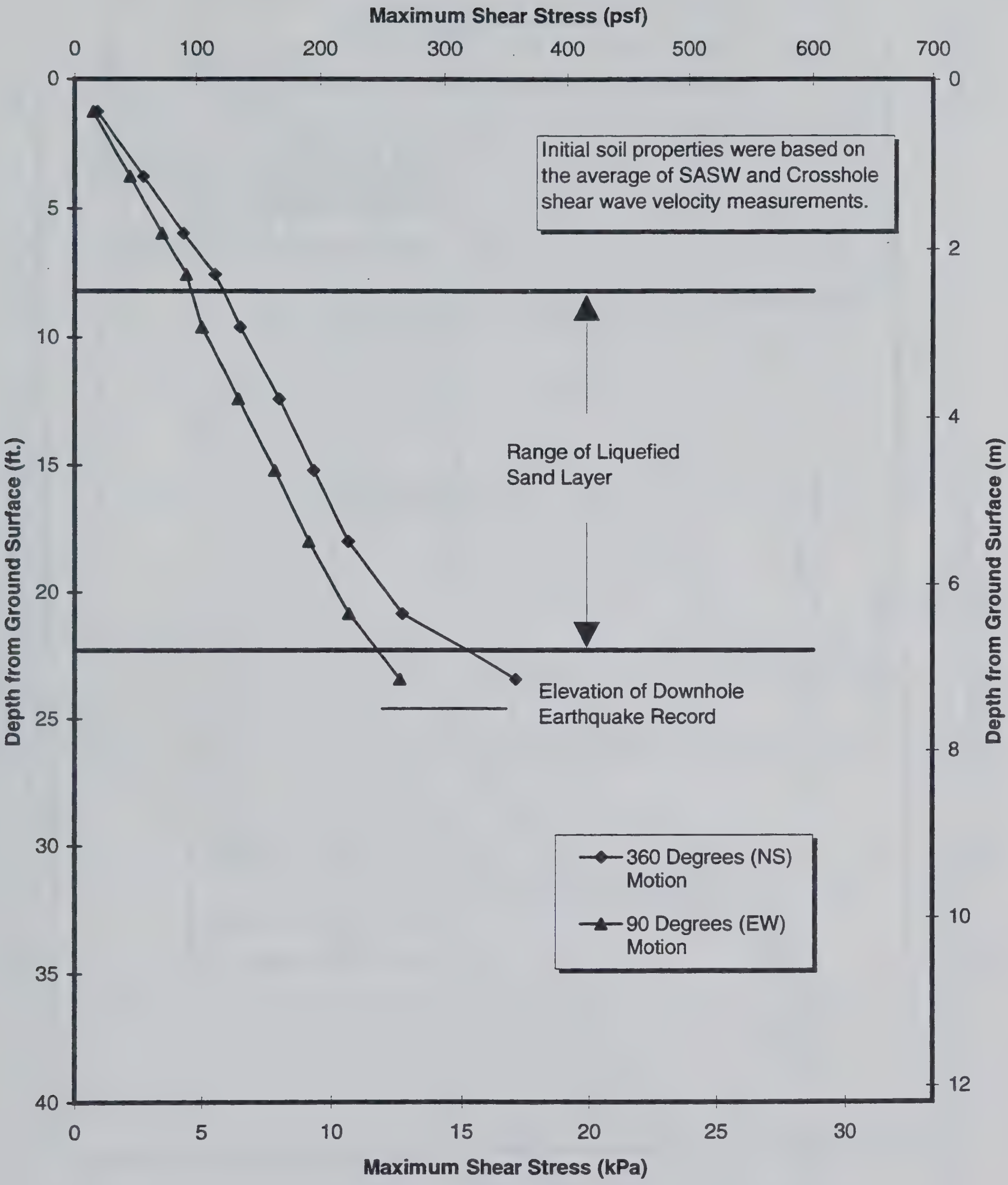

Figure 4.28 - Maximum Shear Stress Distribution over Depth from BDESRA Results of Effective Stress Analyses - Wildlife Site, November 24, 1987, 1315 GMT Earthquake

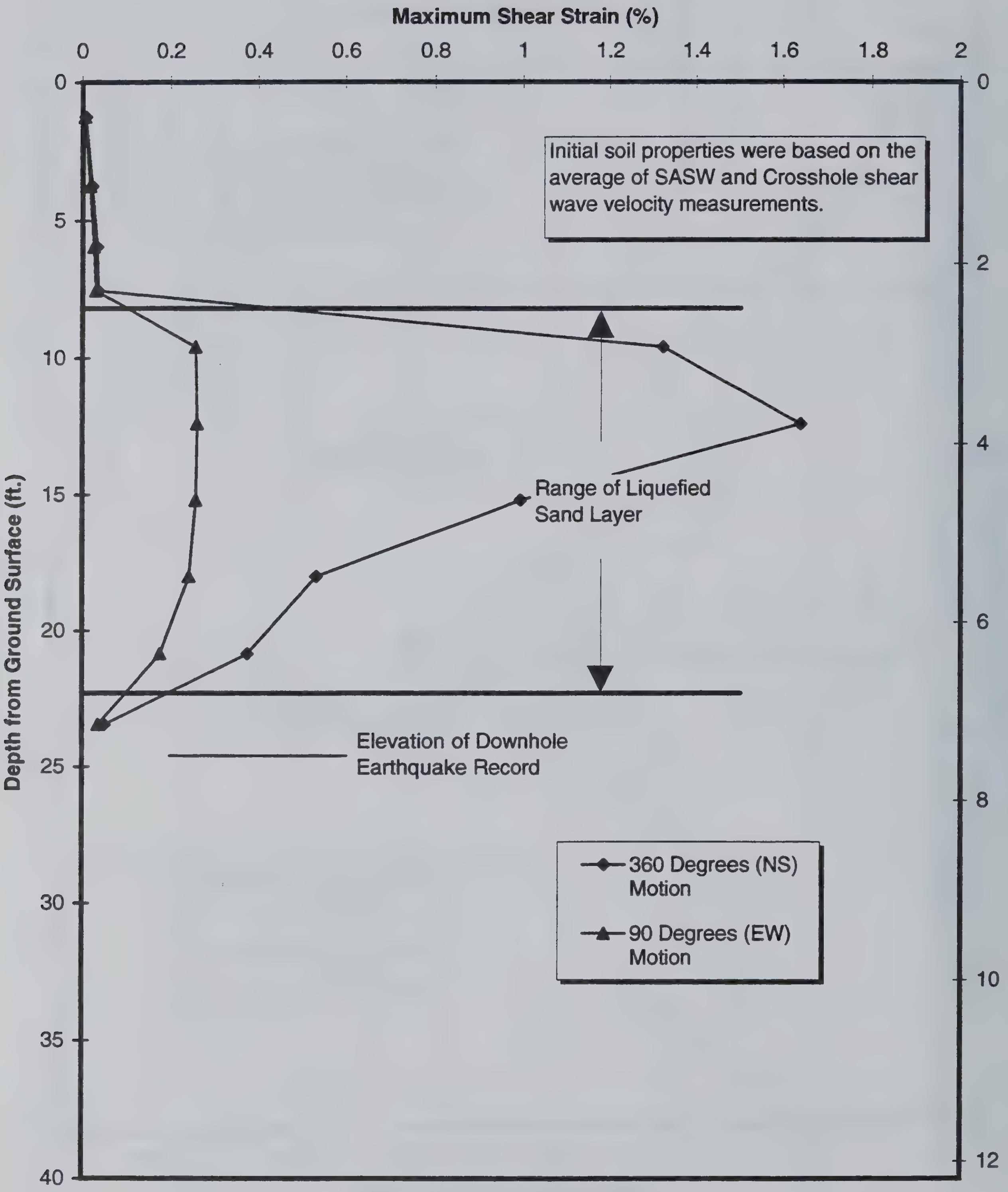

Figure 4.29 - Maximum Shear Strain Distribution over Depth from BDESRA Results of Effective Stress Analyses - Wildlife Site, November 24, 1987, 1315 GMT Earthquake

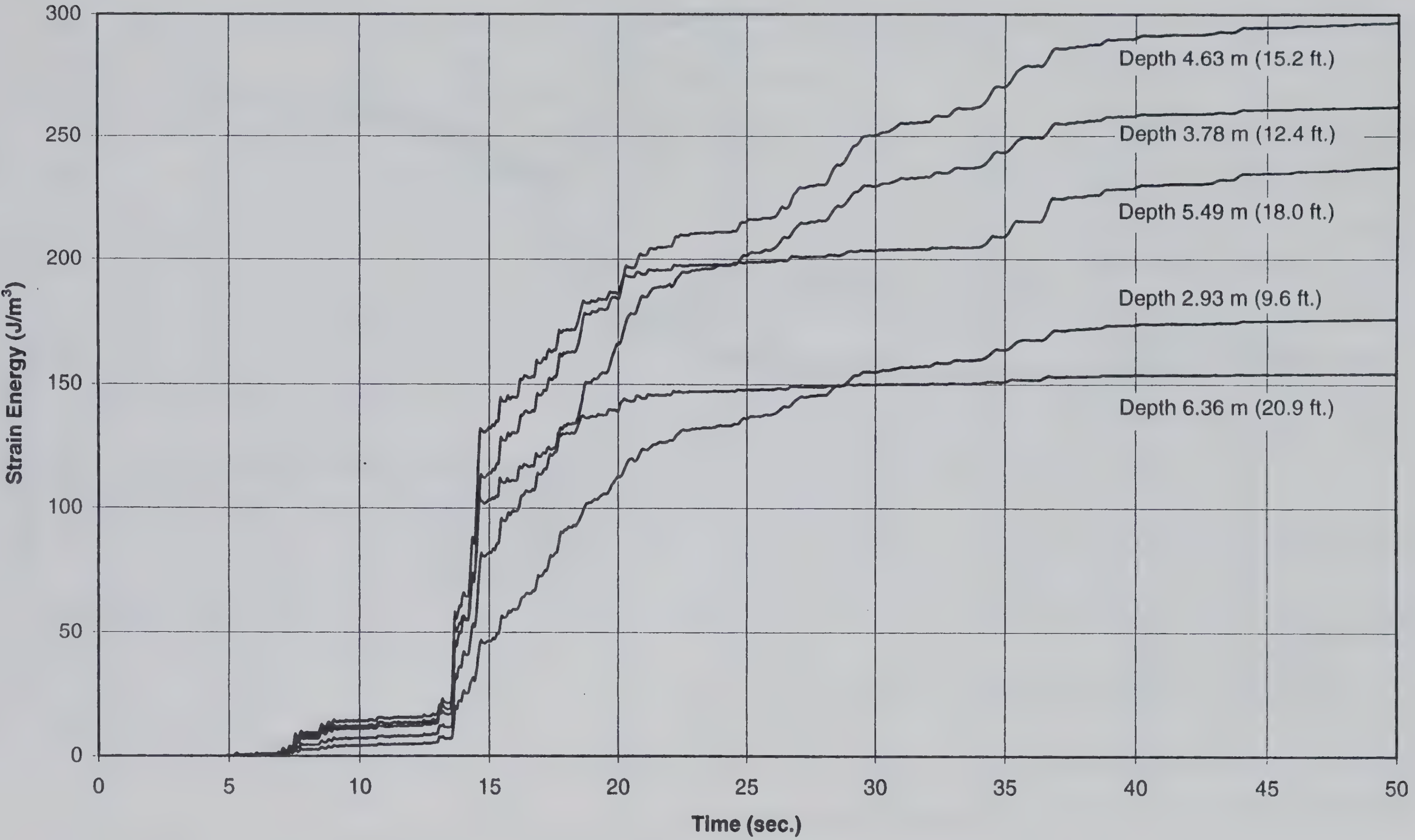

Figure 4.30 - Accumulation of Strain Energy in Liquefied Sand Layer - Wildlife Site, November 24, 1987, 1315 GMT Earthquake in 360° Direction - BDESRA Output, Effective Stress Analysis

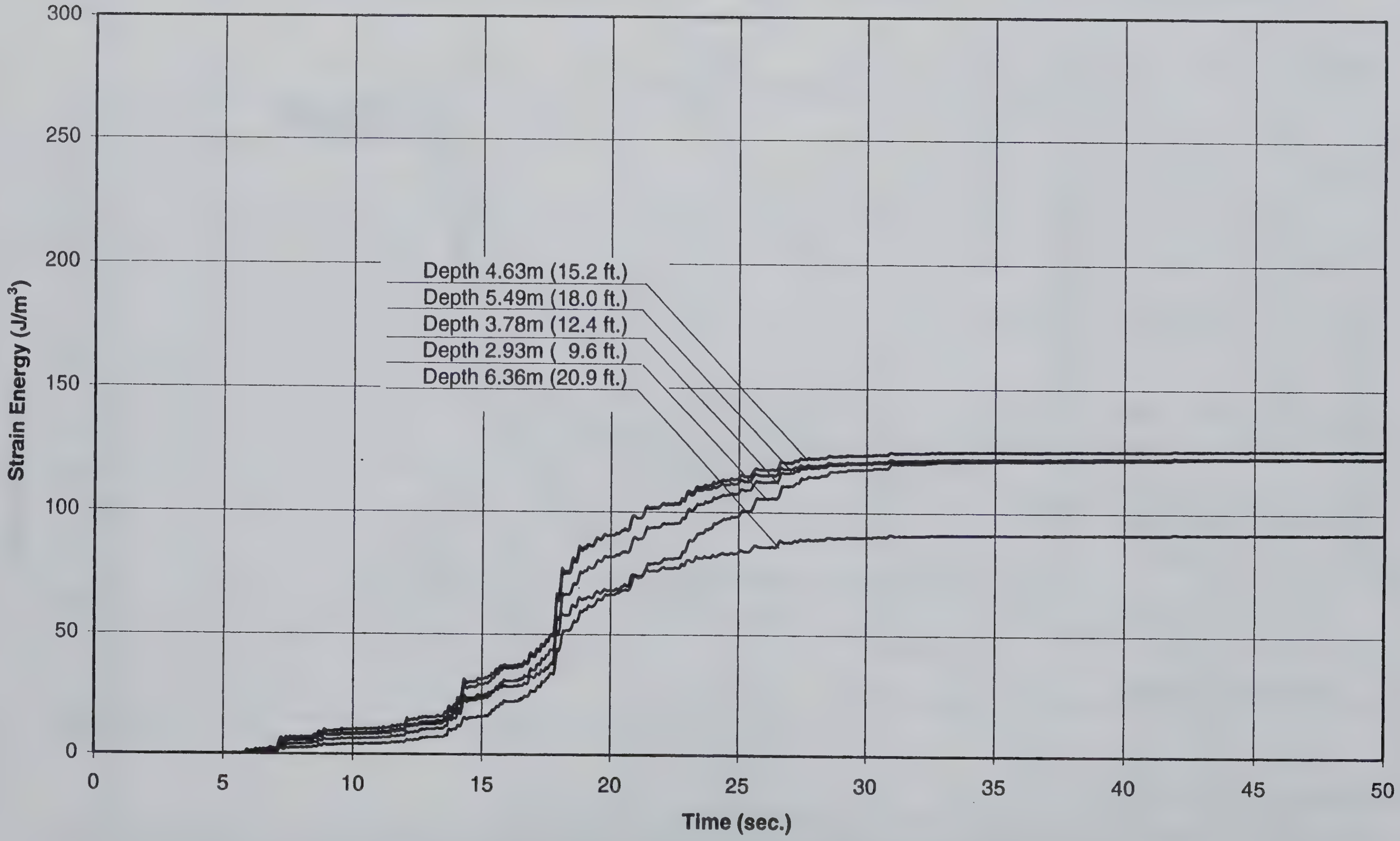

Figure 4.31 - Accumulation of Strain Energy in Liquefied Sand Layer - Wildlife Site, November 24, 1987, 1315 GMT Earthquake in 90° Direction - BDESRA Output, Effective Stress Analysis

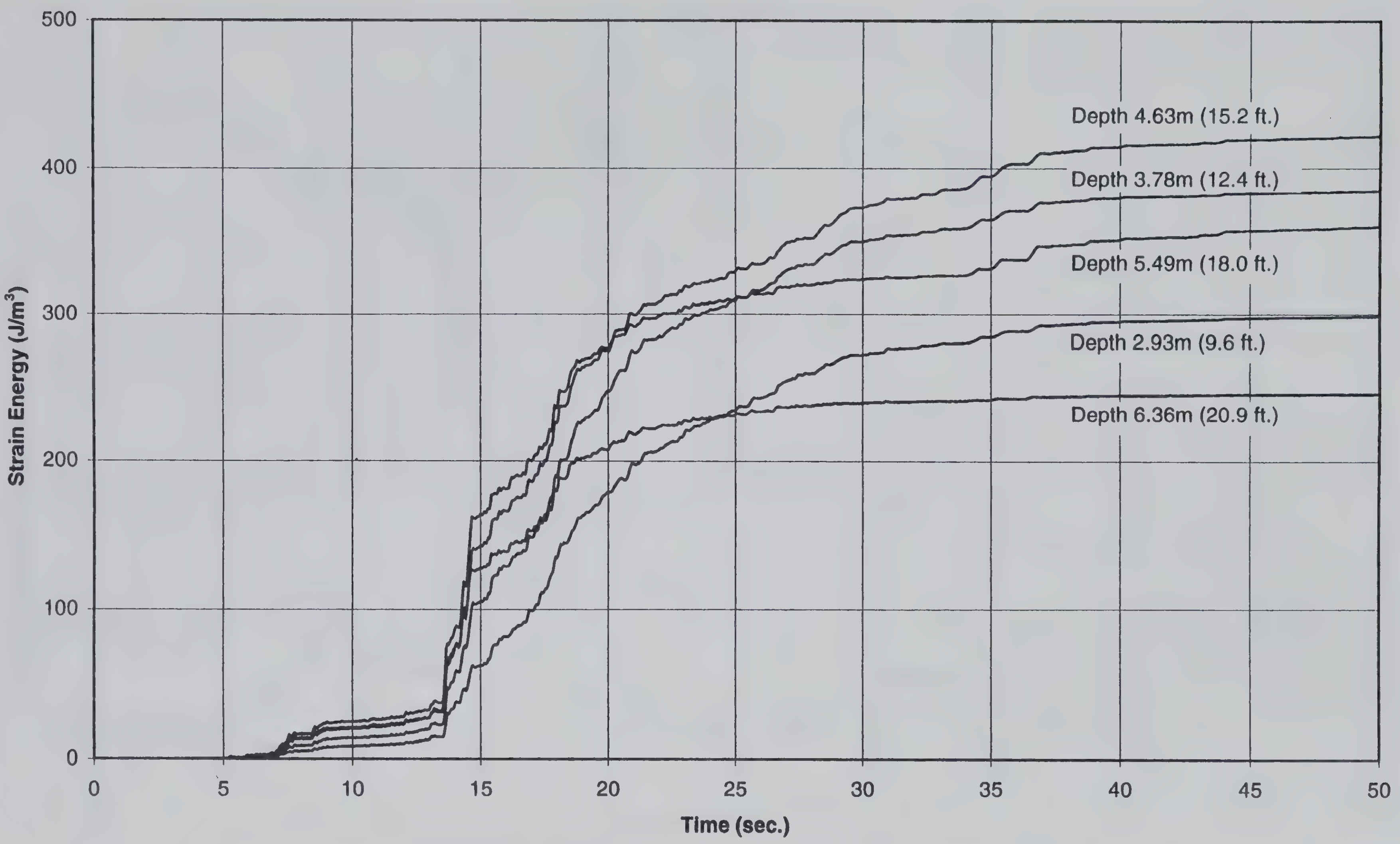

Figure 4.32 - Accumulation of Strain Energy in Liquefied Sand Layer - Wildlife Site, November 24, 1987, 1315 GMT Earthquake - Summation of BDESRA Effective Stress Analysis Output in both 360° and 90° Directions

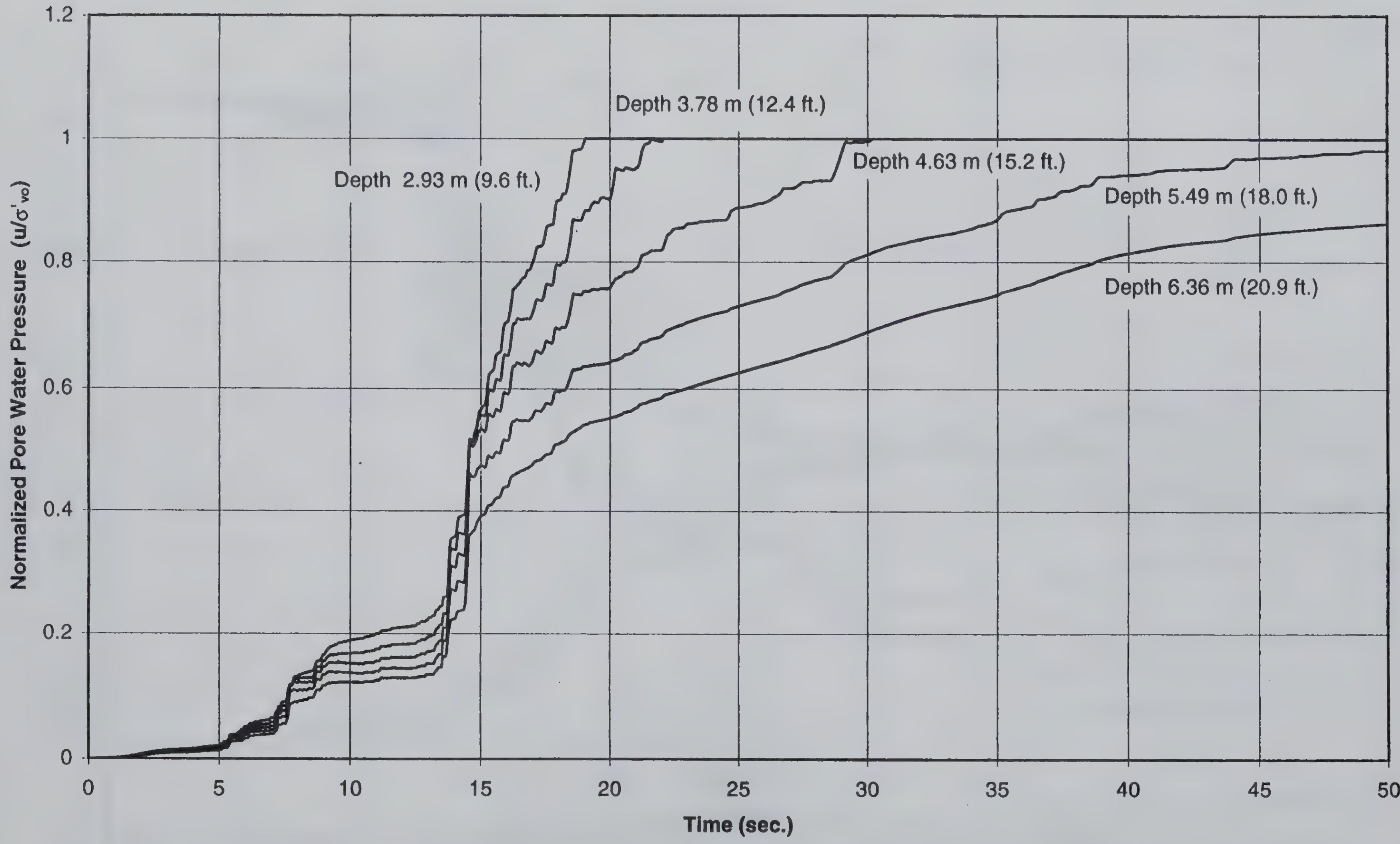

Figure 4.33 - Normalized Pore Water Pressure Generation in Liquefied Sand Layer - Wildlife Site, November 24, 1987, 1315 GMT Earthquake in 360° Direction, BDESRA Output, Effective Stress Analysis

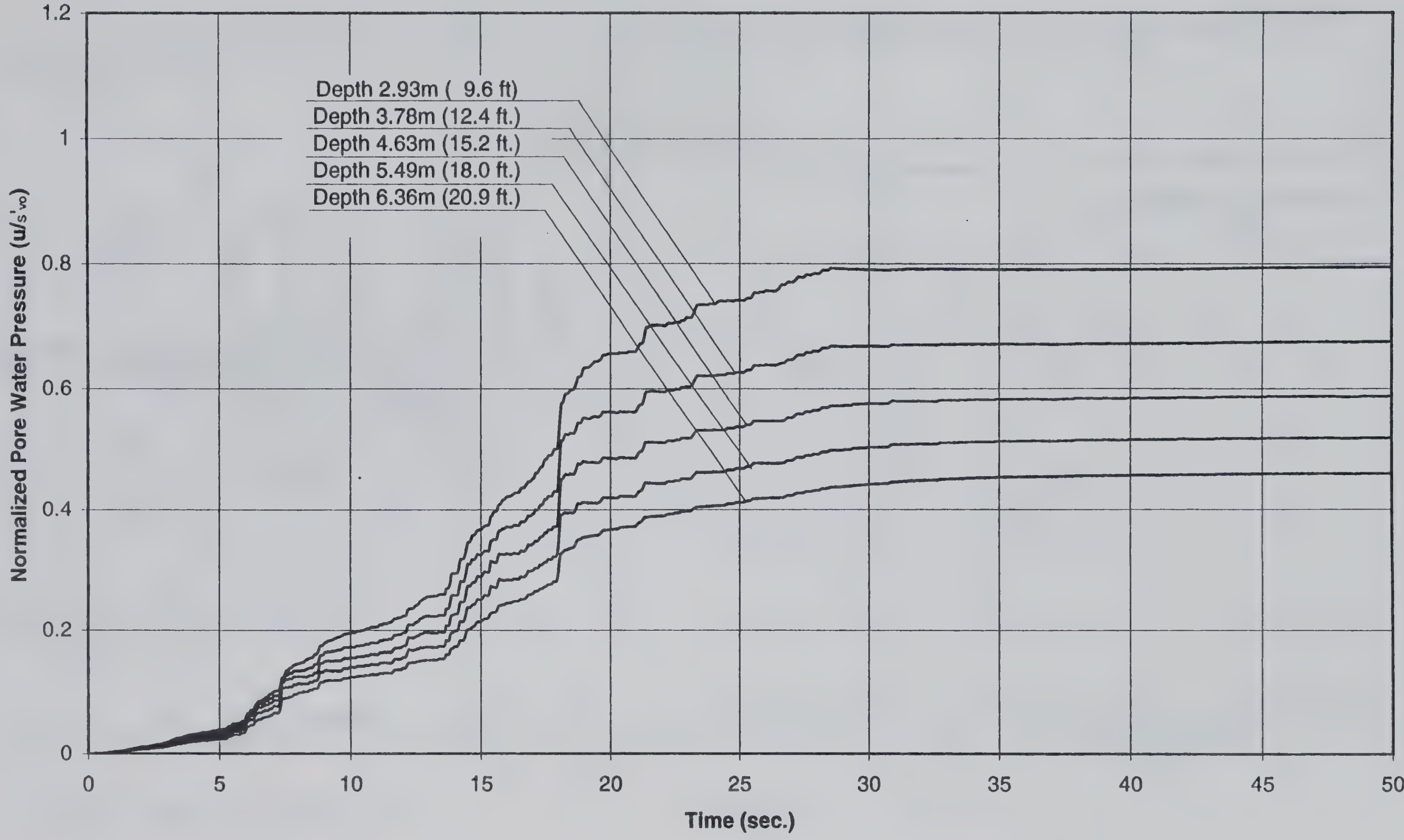

Figure 4.34 - Normalized Pore Water Pressure Generation in Liquefied Sand Layer - Wildlife Site, November 24, 1987, 1315 GMT Earthquake in 90° Direction, BDESRA Output, Effective Stress Analysis

Acceleration at Depth z:

$$a_z = a_{top} + (a_{bottom} - a_{top}) \cdot \frac{z}{h}$$

Shear Stress at Depth z:

$$\tau_z = \frac{1}{2} \cdot \rho \cdot z \cdot (a_{top} + a_z)$$

Shear Strain at Depth z:

$$\gamma = \frac{d_{top} - d_{bottom}}{h}$$

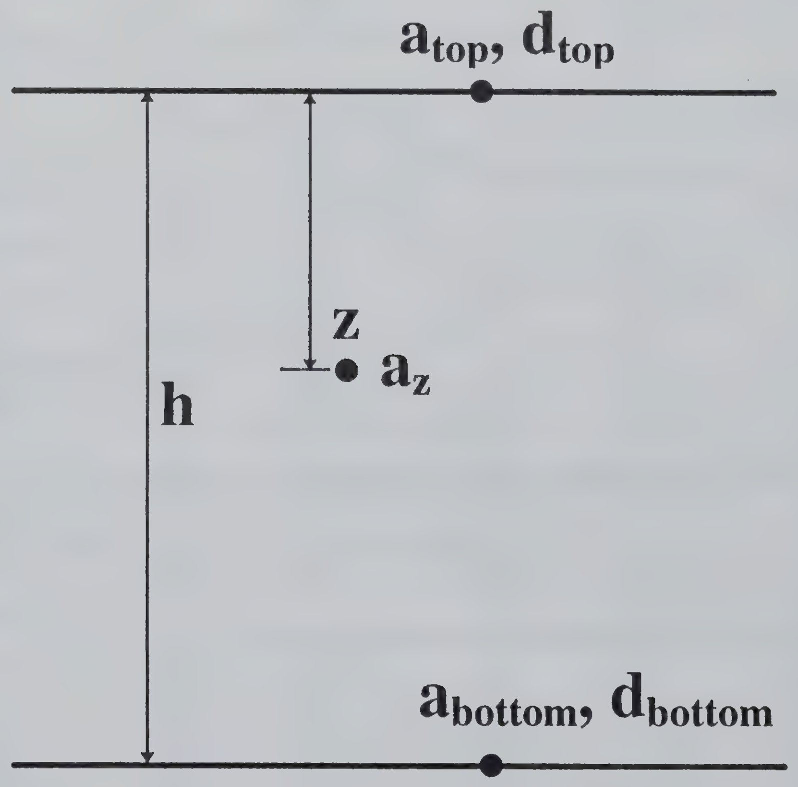

Figure 4.35 - Methodology Adopted in Estimating the Dynamic Stress and Strain Time Histories in a Soil Layer from Field Records (After Zeghal and Elgamal, 1994)

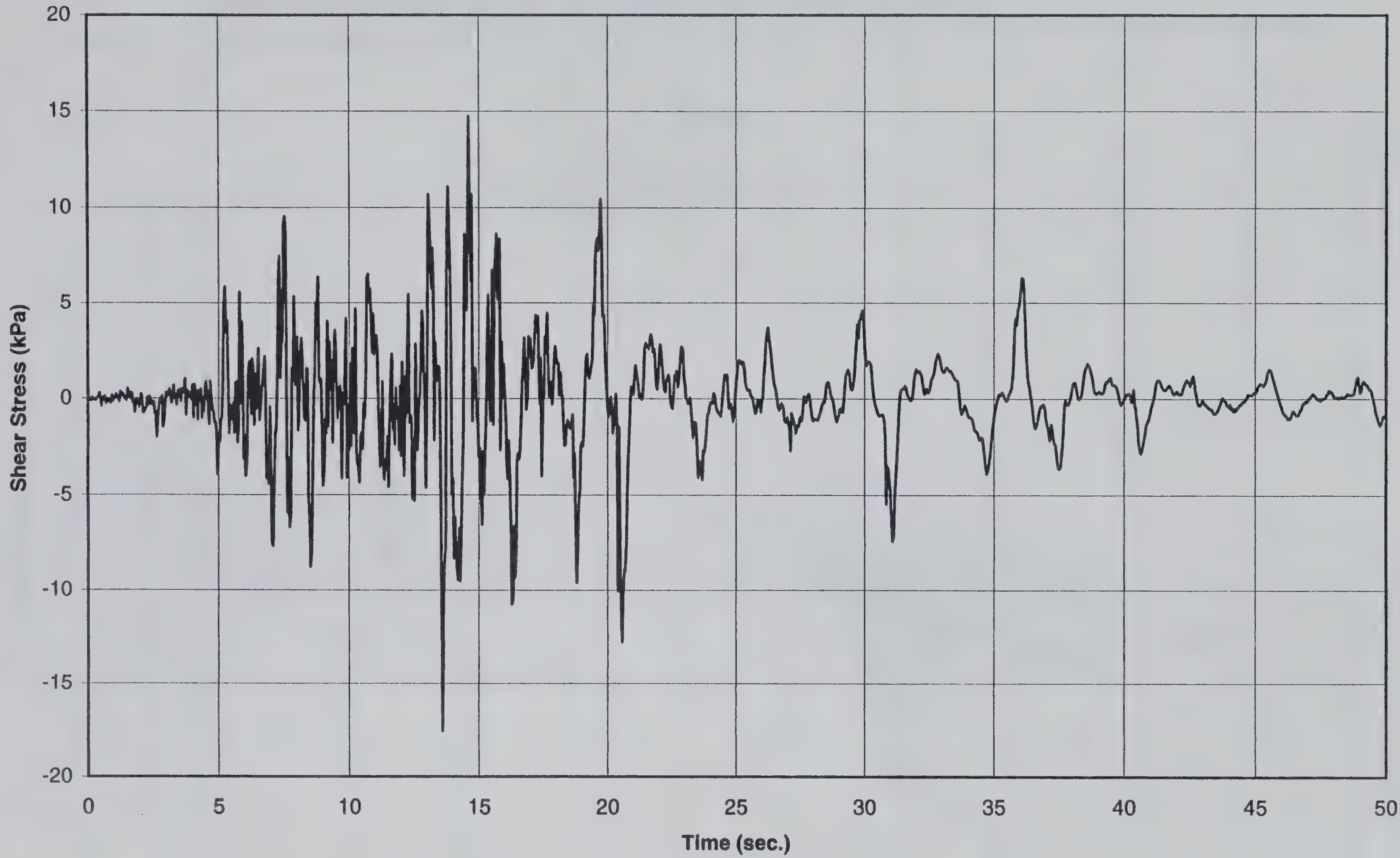

Figure 4.36 - Shear Stress Time History at Depth of 5.06 m (16.6 ft.) - Based on Direct Interpolation of Recorded Motions, Wildlife Site, November 24, 1987, 1315 GMT Earthquake in 360° Direction

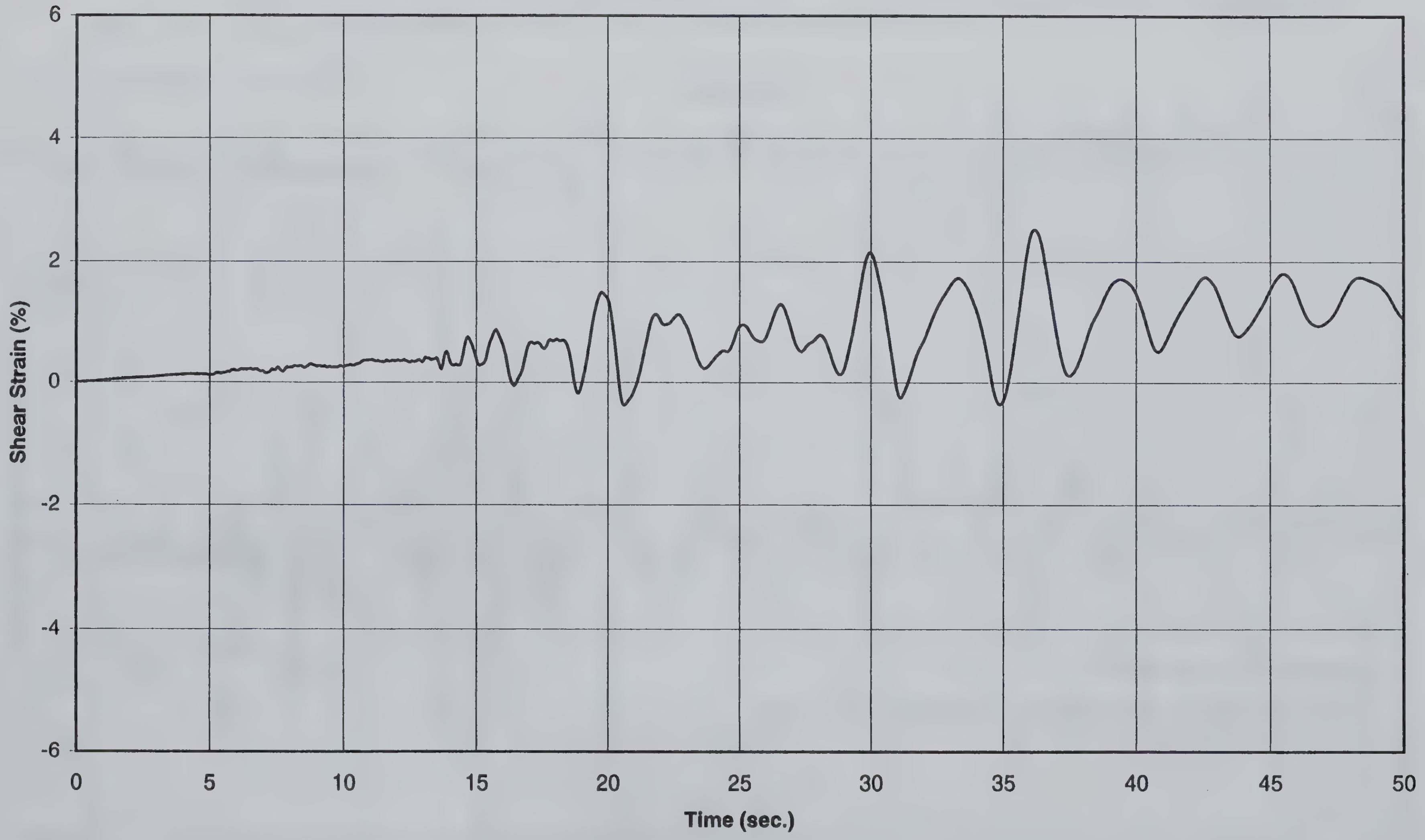

Figure 4.37 - Shear Strain Time History at Depth of 5.06 m (16.6 ft.) - Based on Direct Interpolation of Recorded Motions, Wildlife Site, November 24, 1987, 1315 GMT Earthquake in 360° Direction

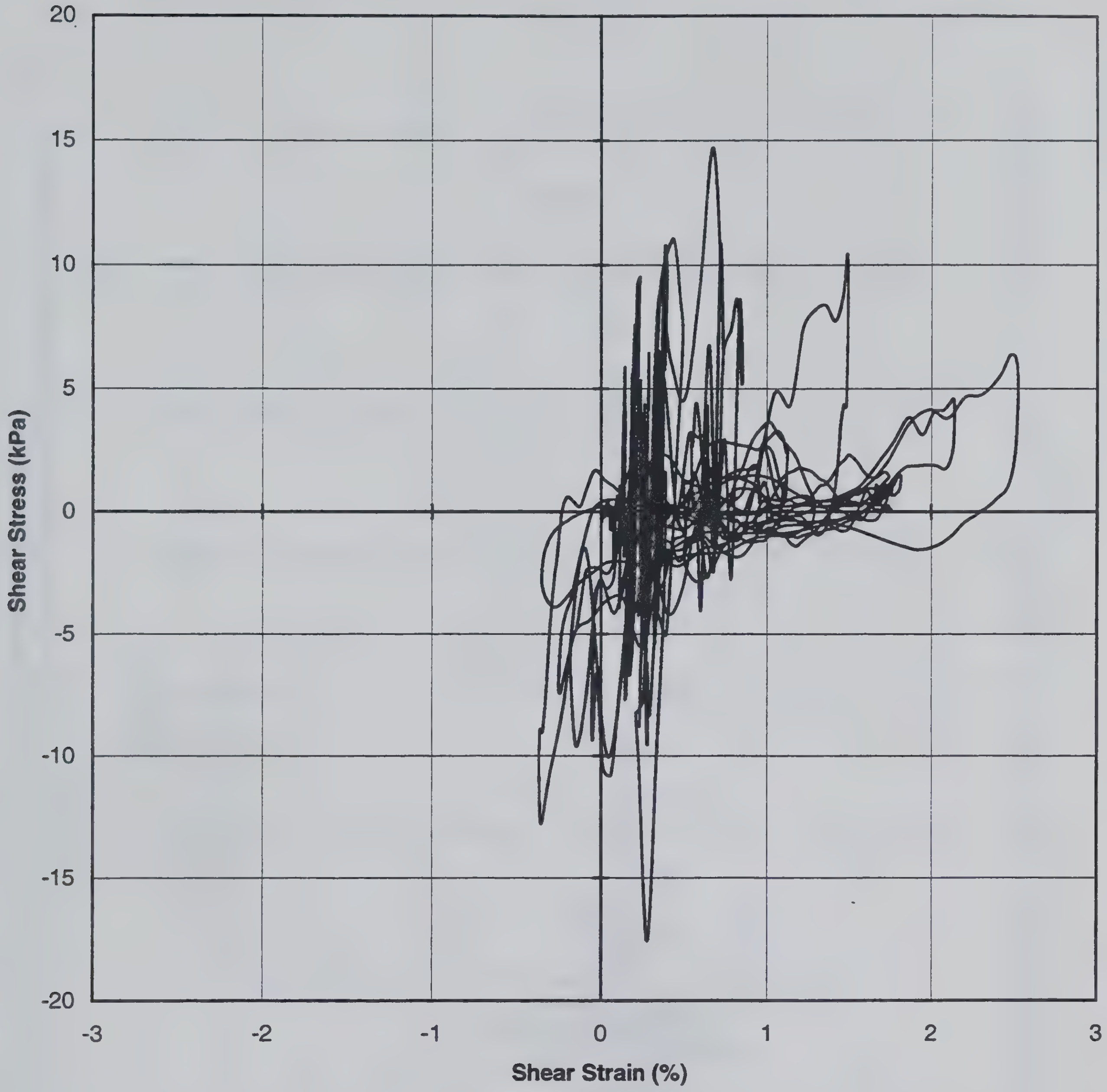

Figure 4.38 - Shear Stress - Shear Strain Hysteresis Loop at Depth of 5.06 m (16.6 ft.) - Based on Direction Interpolation of Recorded Motions, Wildlife Site, November 24, 1987, 1315 GMT Earthquake in 360° Direction.

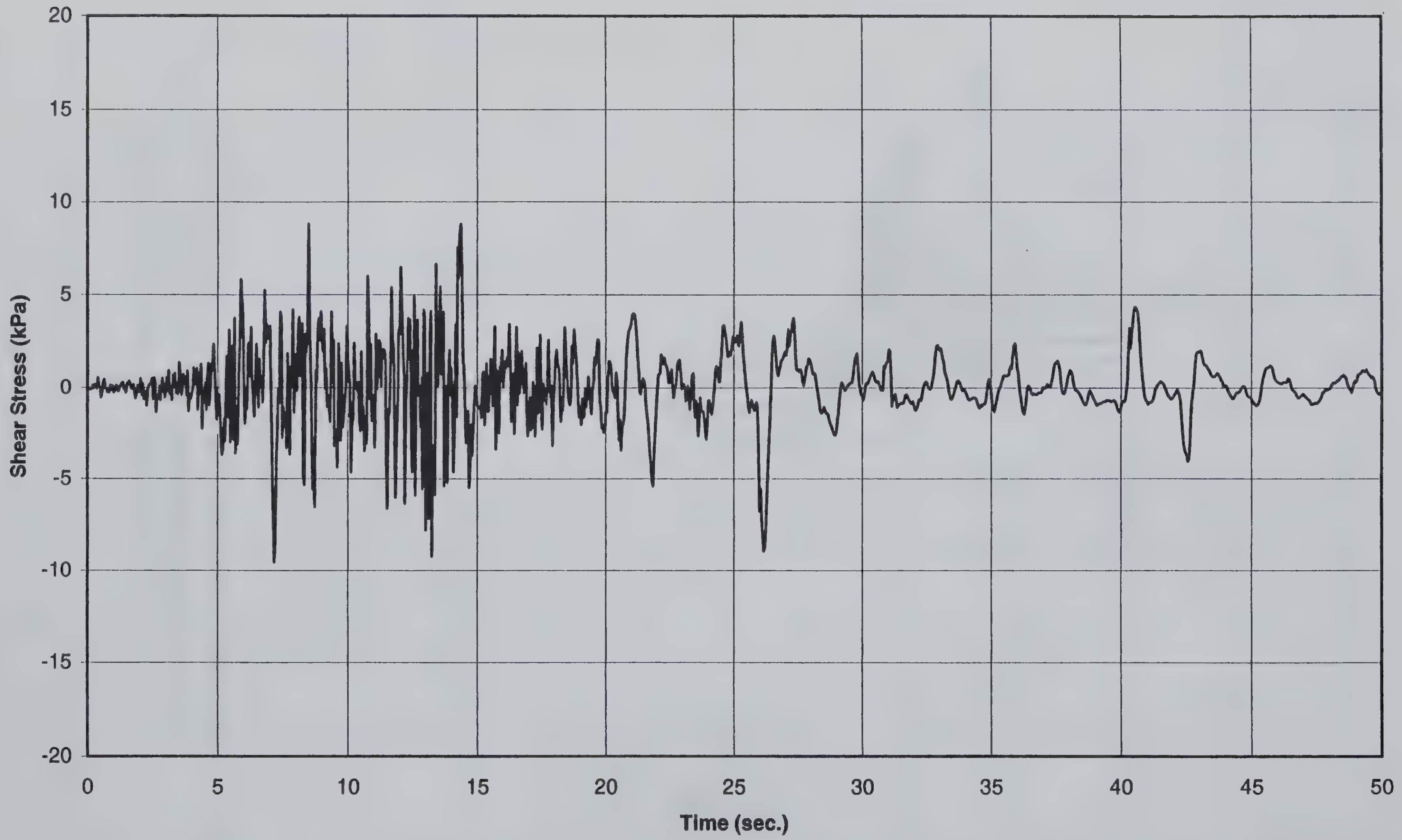

Figure 4.39 - Shear Stress Time History at Depth of 5.06 m (16.6 ft.). - Based on Direct Interpolation of Recorded Motions, Wildlife Site, November 24, 1987, 1315 GMT Earthquake in 90° Direction

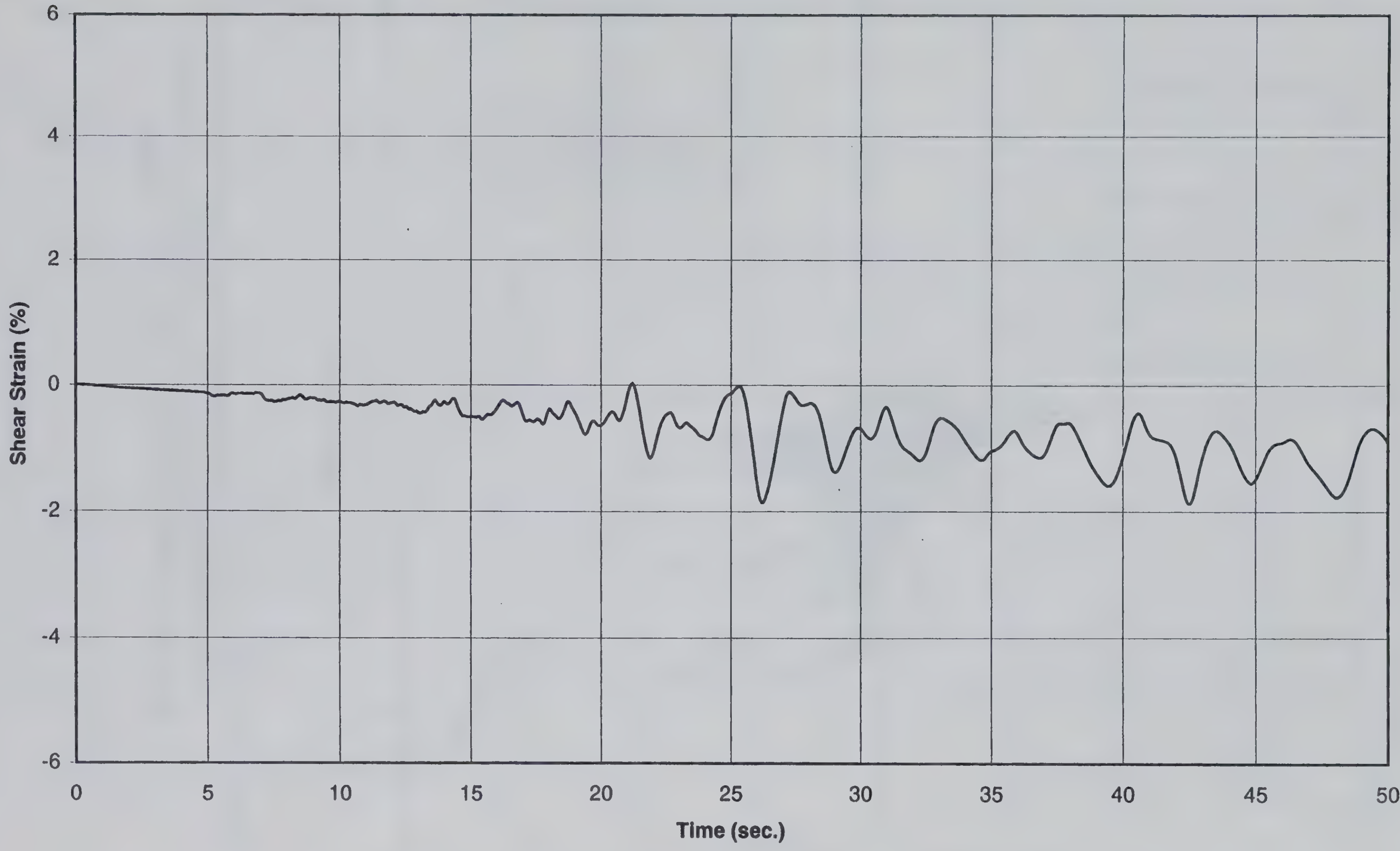

Figure 4.40 - Shear Strain Time History at Depth of 5.06 m (16.6 ft.) - Based on Direct Interpolation of Recorded Motions, Wildlife Site, November 24, 1987, 1315 GMT Earthquake in 90° Direction

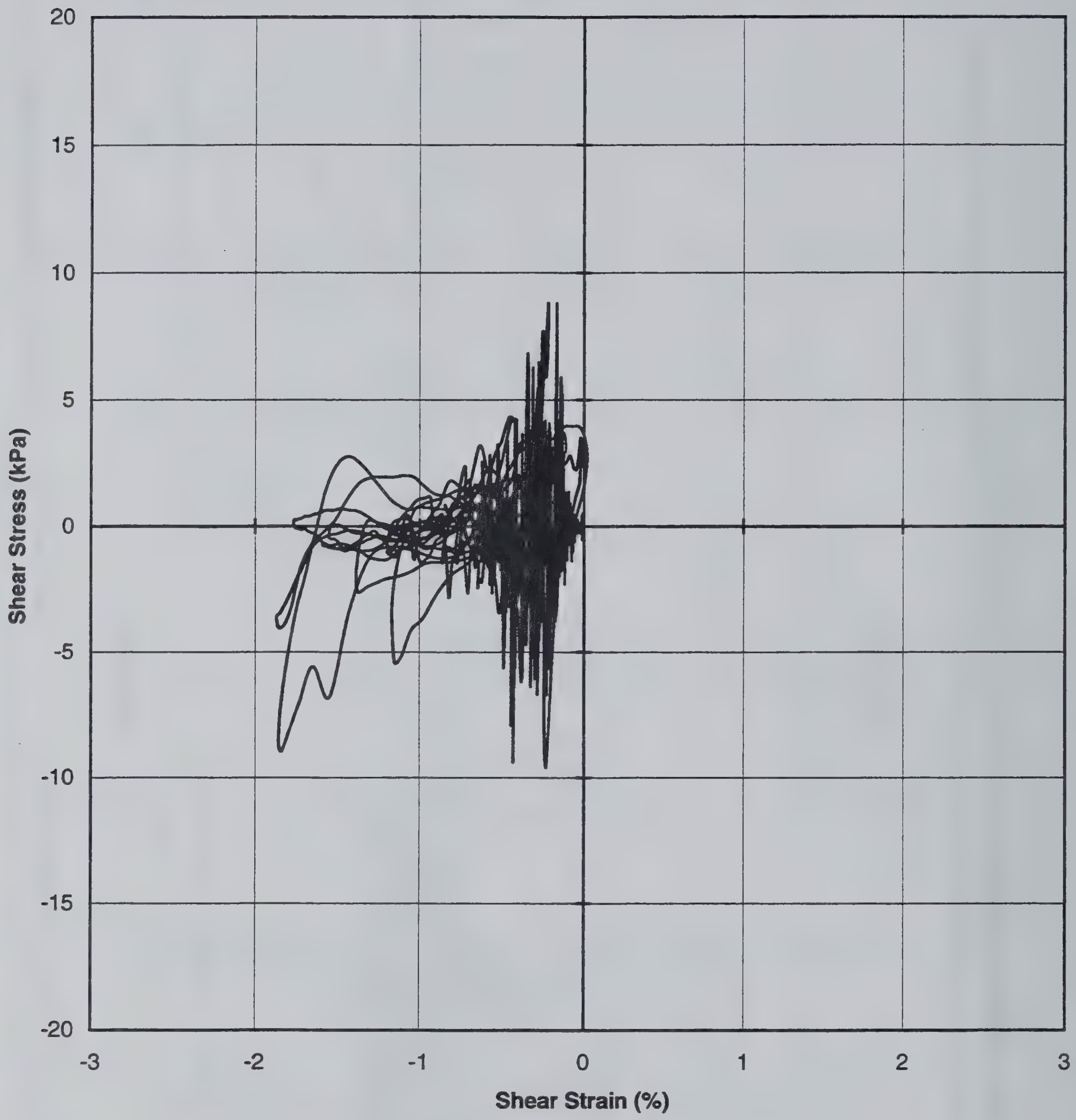

Figure 4.41 - Shear Stress - Shear Strain Hysteresis Loop at Depth of 5.06 m (16.6 ft.) - Based on Direct Interpolation of Recorded Motions, Wildlife Site, November 24, 1987, 1315 GMT Earthquake in 90° Direction

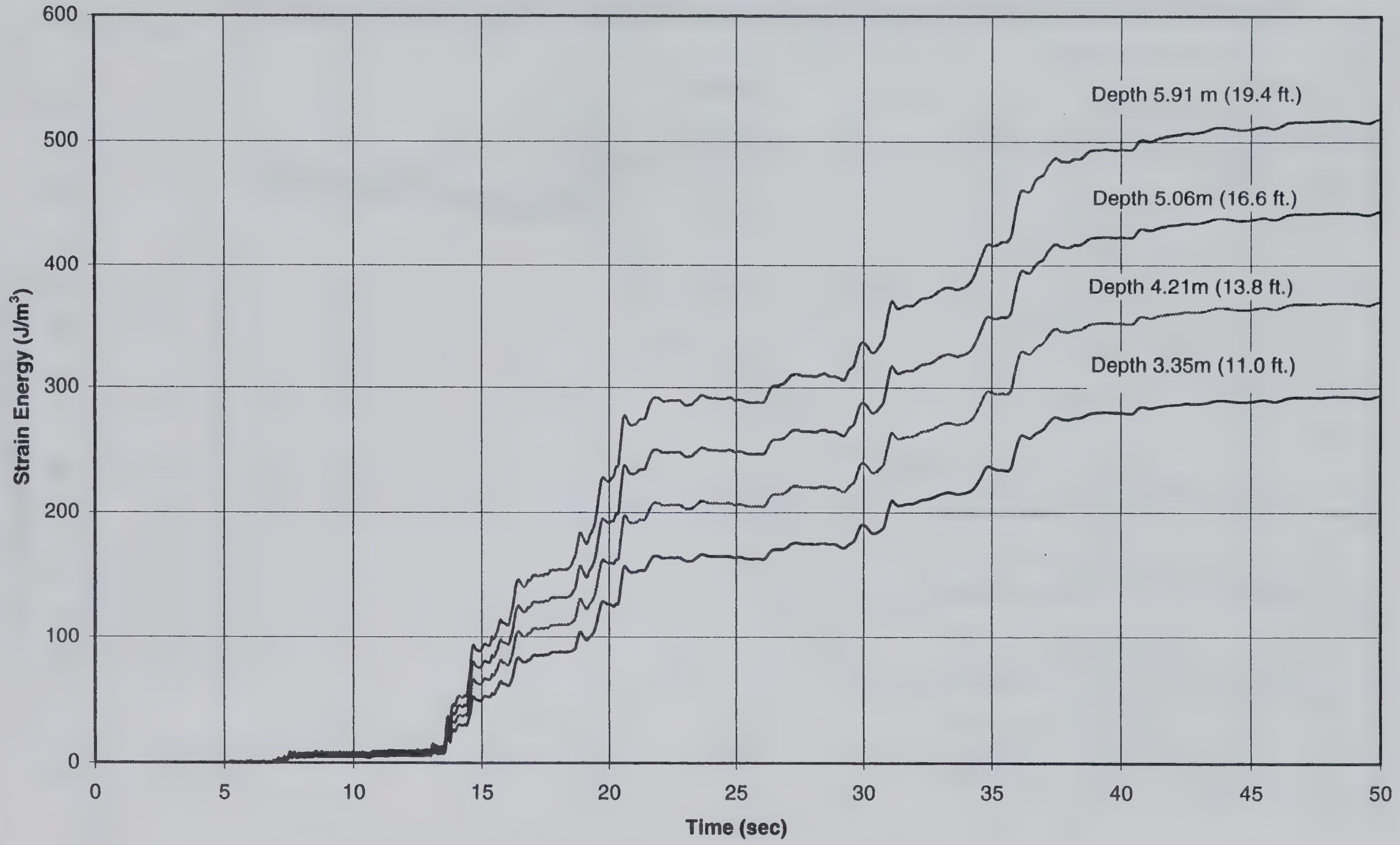

Figure 4.42 - Accumulation of Strain Energy in Liquefied Sand Layer - Based on Direct Interpolation of Recorded Motions, Wildlife Site, November 24, 1987, 1315 GMT Earthquake in 360° Direction

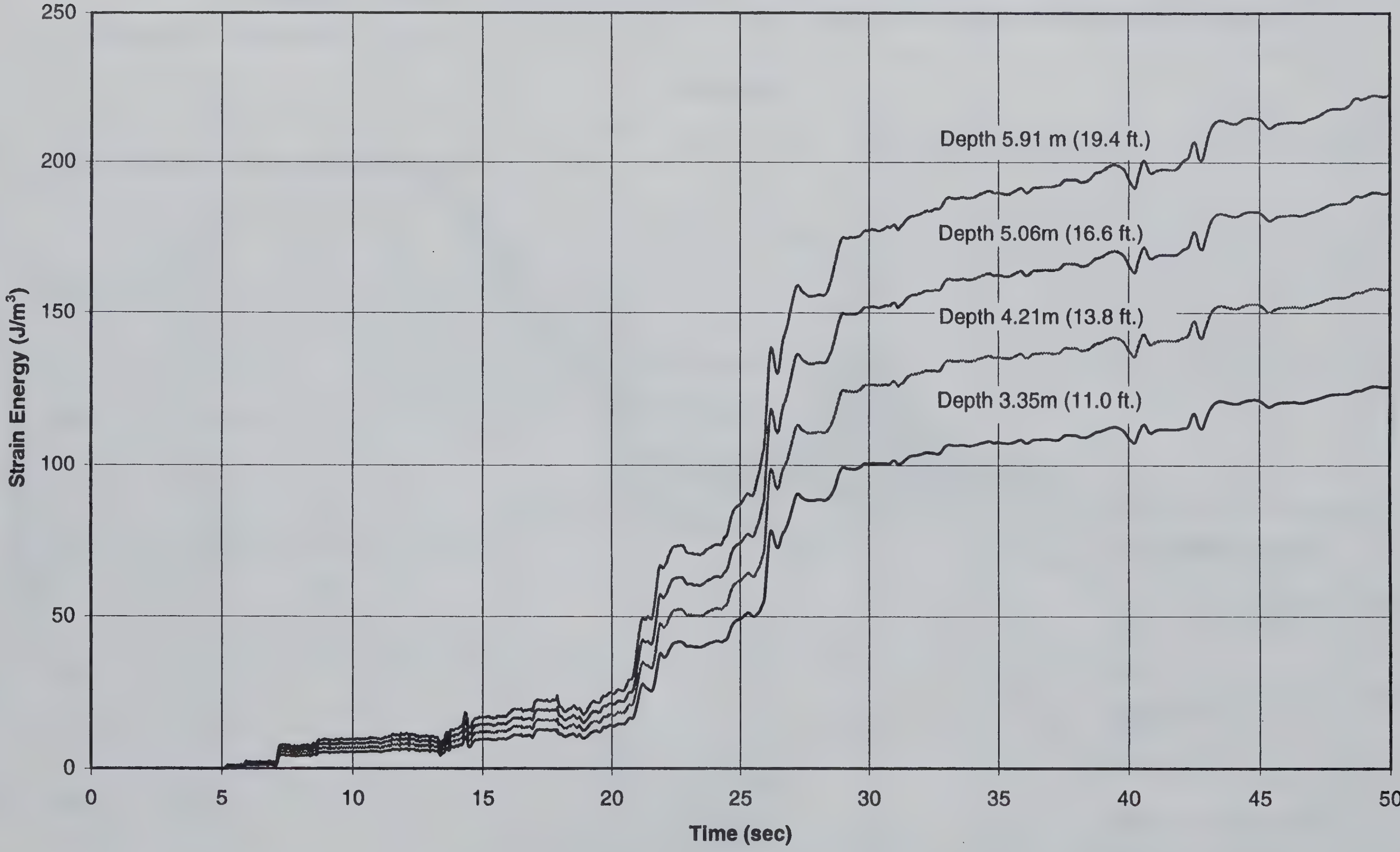

Figure 4.43 - Accumulation of Strain Energy in Liquefied Sand Layer - Based on Direct Interpolation of Recorded Motions, Wildlife Site, November 24, 1987, 1315 GMT Earthquake in 90° Direction

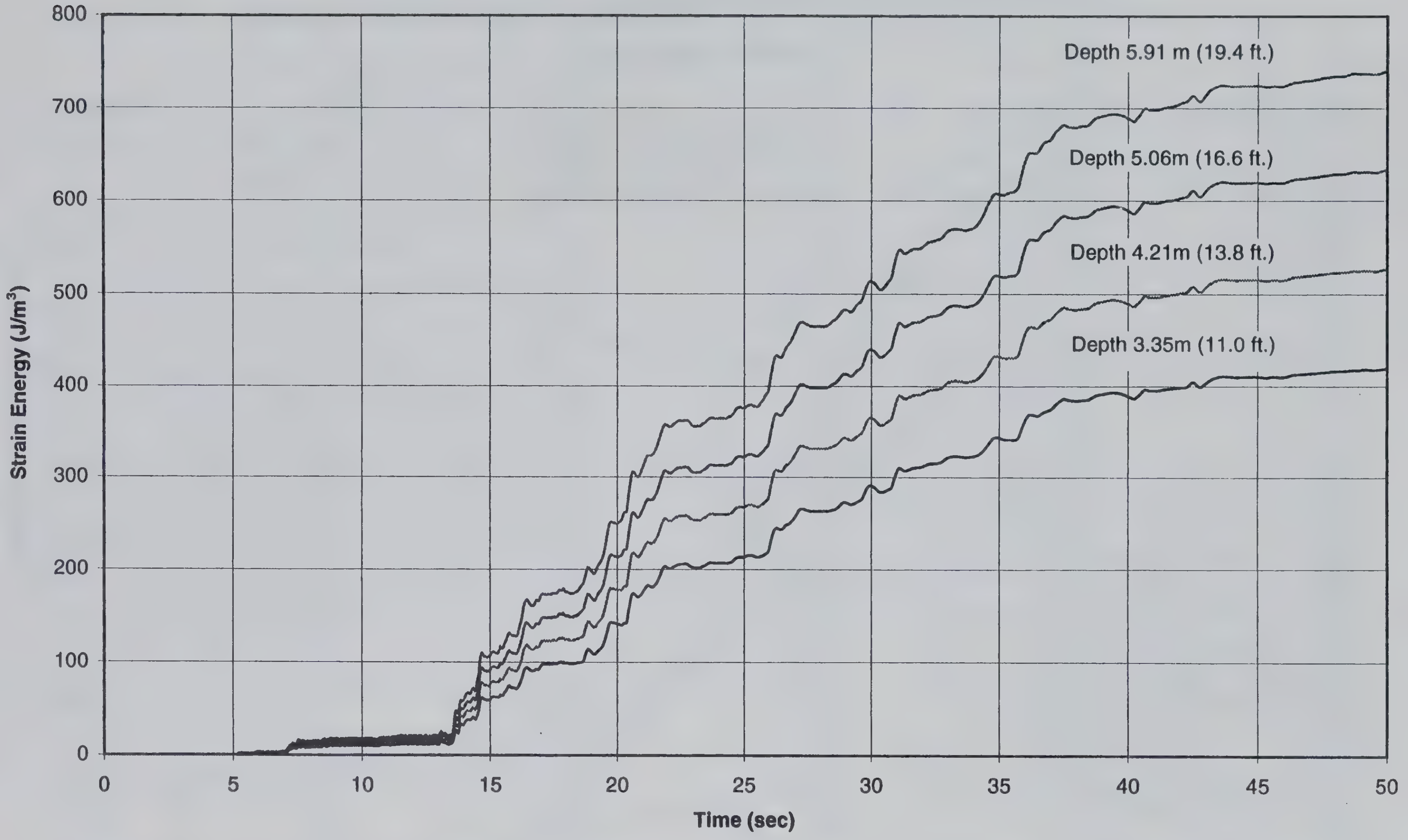

Figure 4.44 - Accumulation of Strain Energy in Liquefied Sand Layer - Based on Direct Interpolation of Recorded Motions, Wildlife Site, November 24, 1987, 1315 GMT Earthquake - Summation of Strain Energy in both 360° and 90° Directions

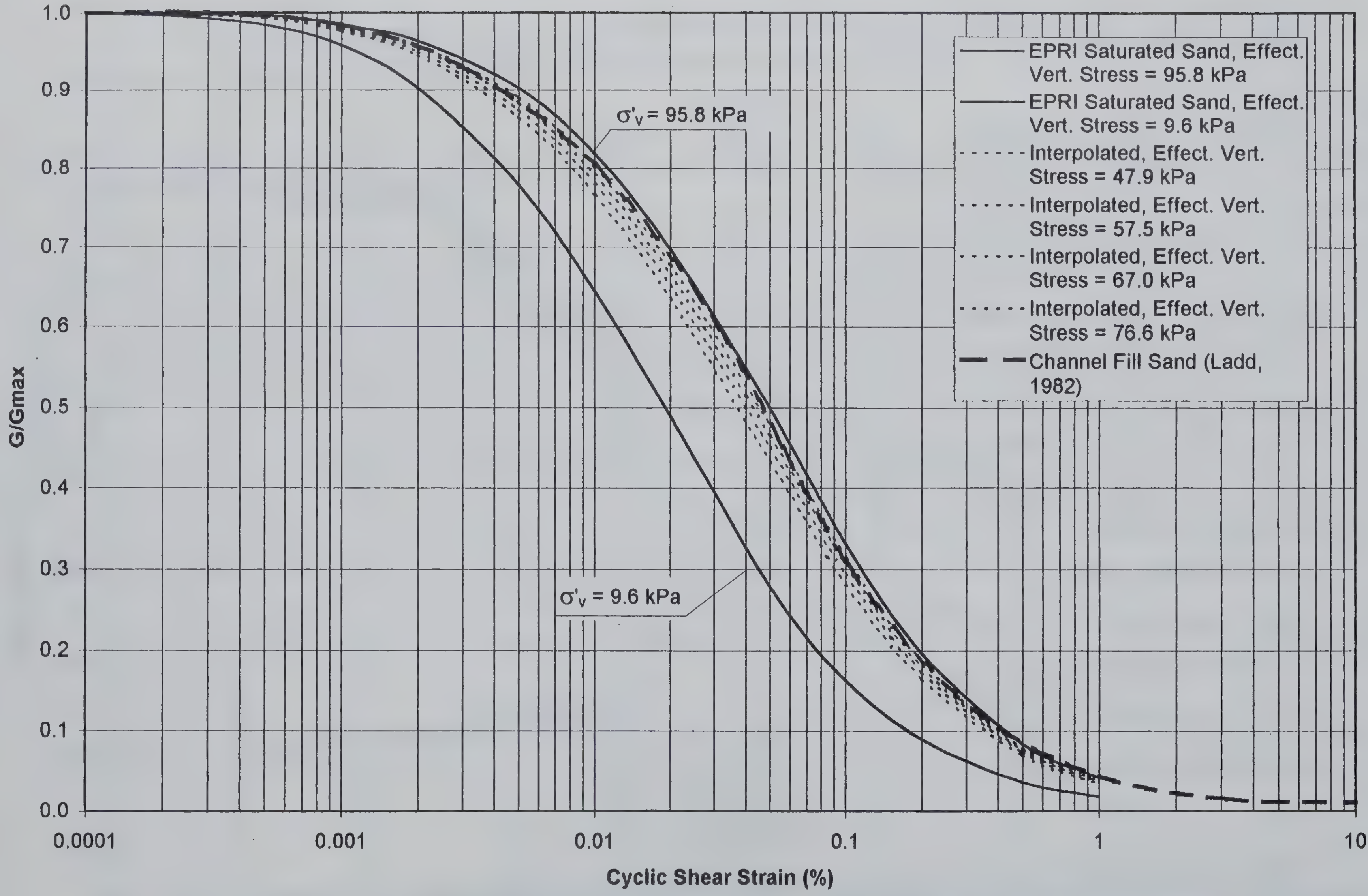

Figure 4.45 - Comparison of Shear Modulus Degradation Curves Used in SHAKE Analyses

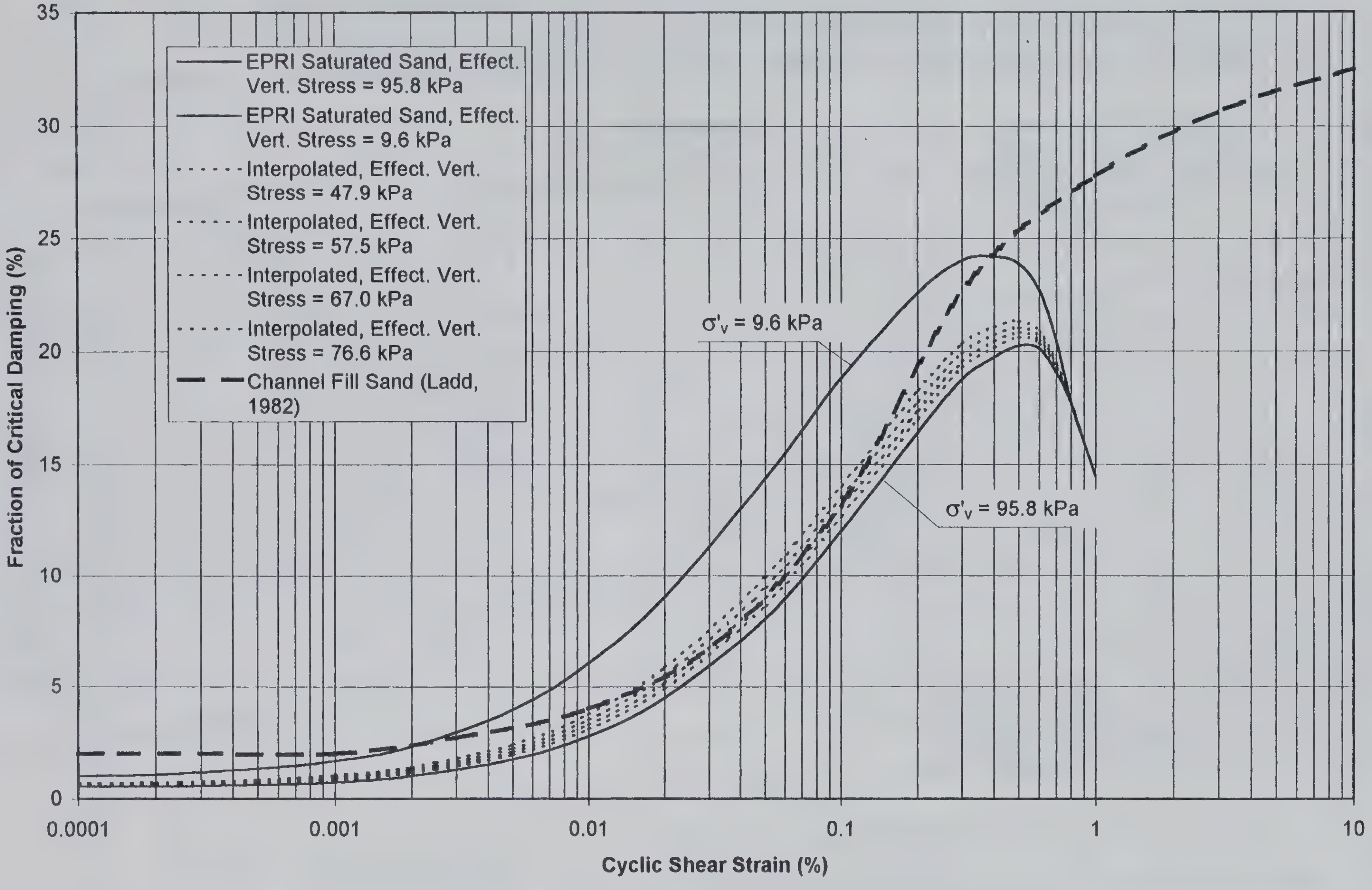

Figure 4.46 - Comparison of Damping Curves Used in SHAKE Analyses

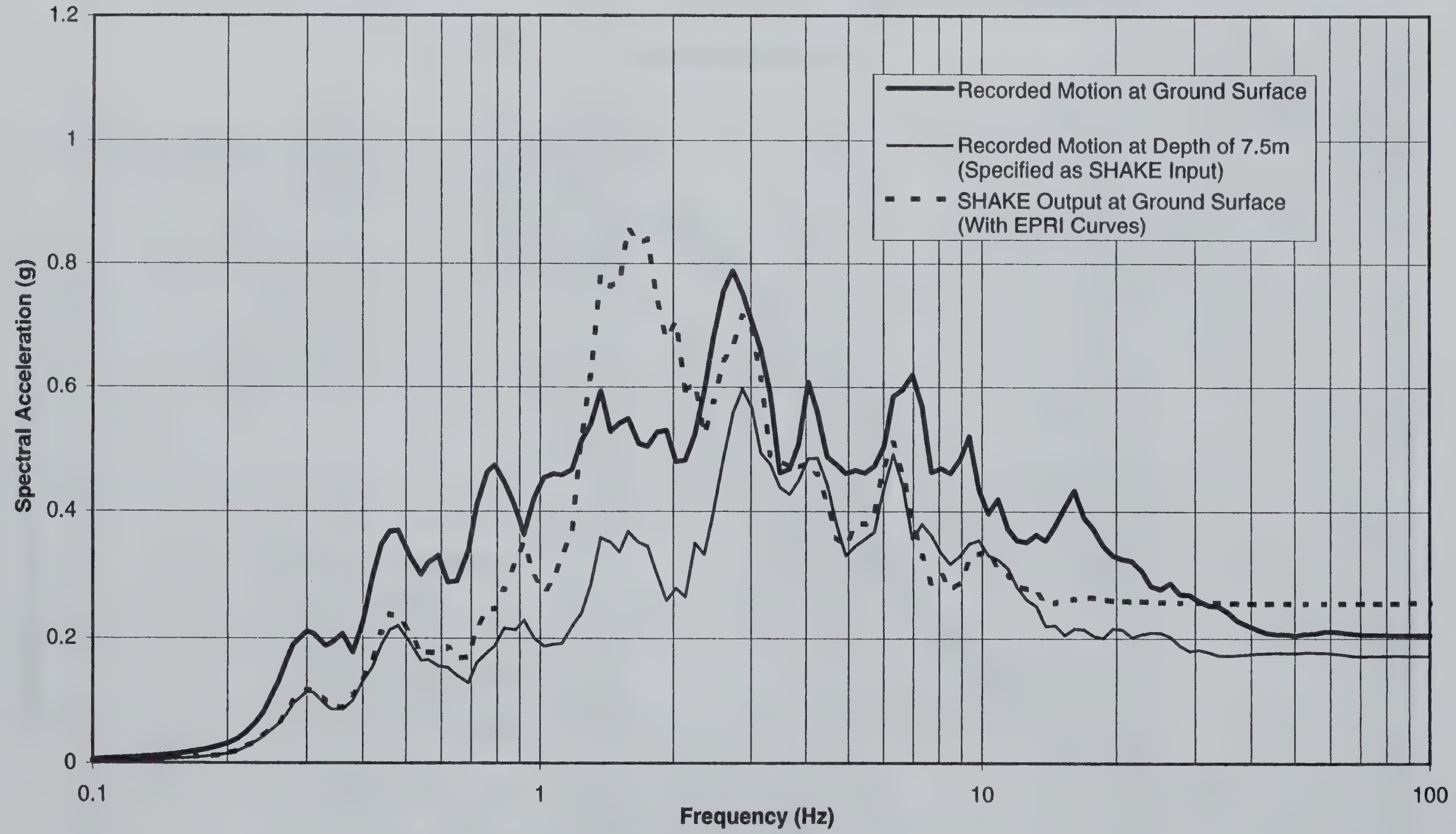

Figure 4.47 - Acceleration Response Spectra at 5% Damping - Wildlife Liquefaction Array, November 24, 1987, 1315 GMT Earthquake - Comparison of Horizontal Motions in 360° Direction - SHAKE Output with EPRI (1993) Soil Curves.

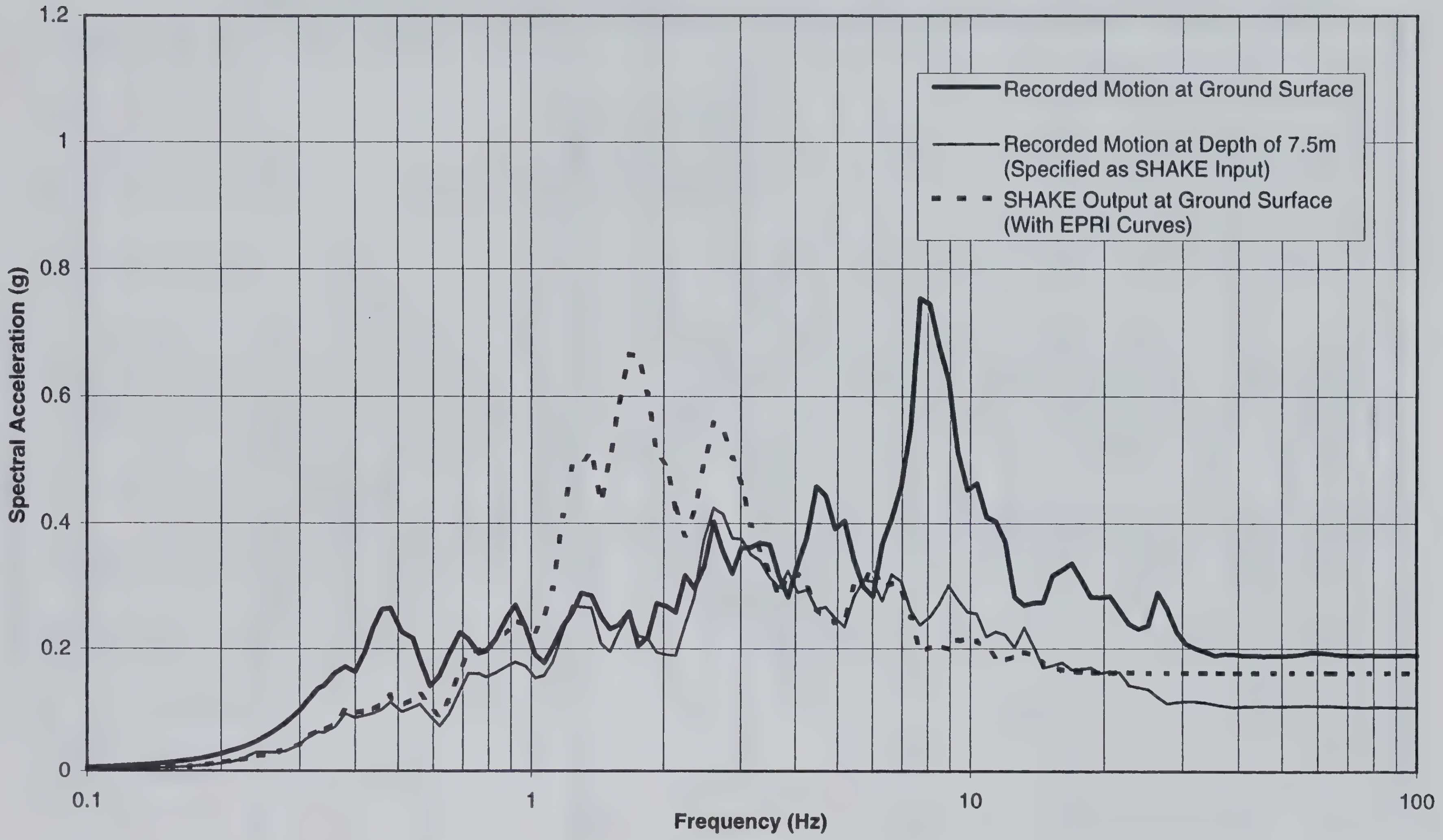

Figure 4.48 - Acceleration Response Spectra at 5% Damping - Wildlife Liquefaction Array, November 24, 1987, 1315 GMT Earthquake - Comparison of Horizontal Motions in 90° Direction - SHAKE Output with EPRI (1993) Soil Curves

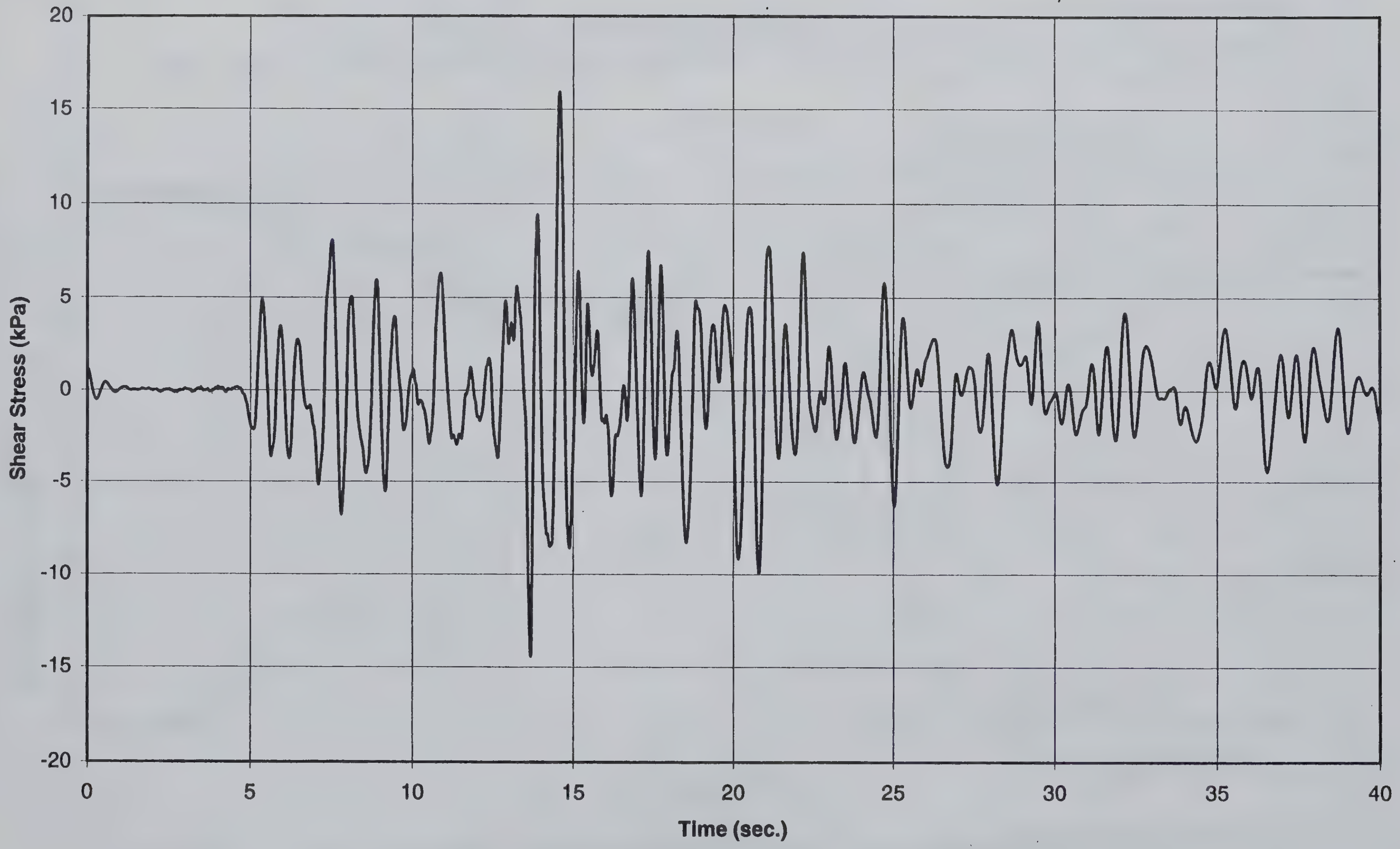

Figure 4.49 - Shear Stress Time History at Depth of 4.21 m (13.8 ft.) from SHAKE Output with EPRI (1993) Soil Curves - Wildlife Site, November 24, 1987, 1315 GMT Earthquake in 360° Direction

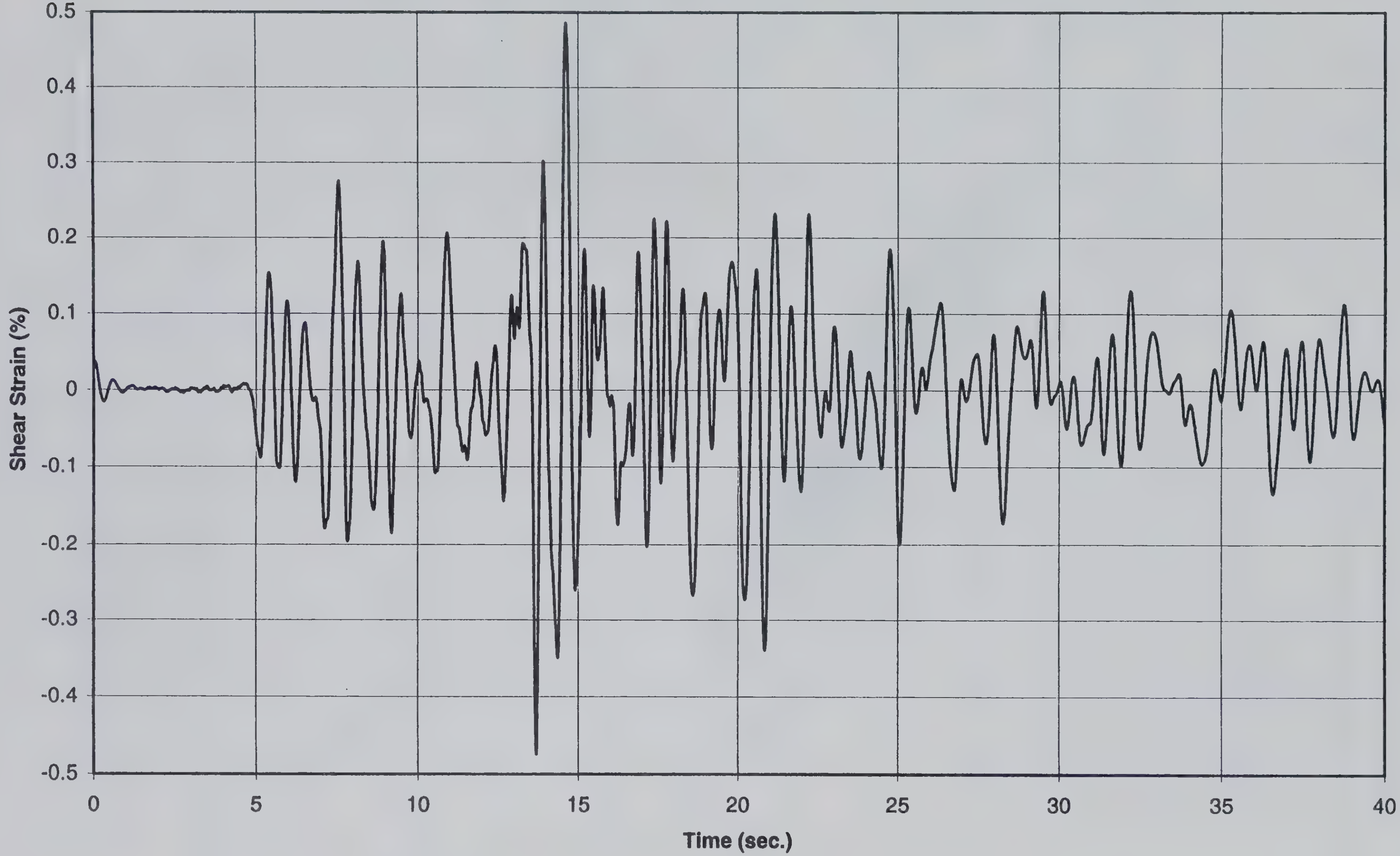

Figure 4.50 - Shear Strain Time History at Depth of 4.21 m (13.8 ft.) from SHAKE Output with EPRI (1993) Soil Curves - Wildlife Site, November 24, 1987, 1315 GMT Earthquake in 360° Direction

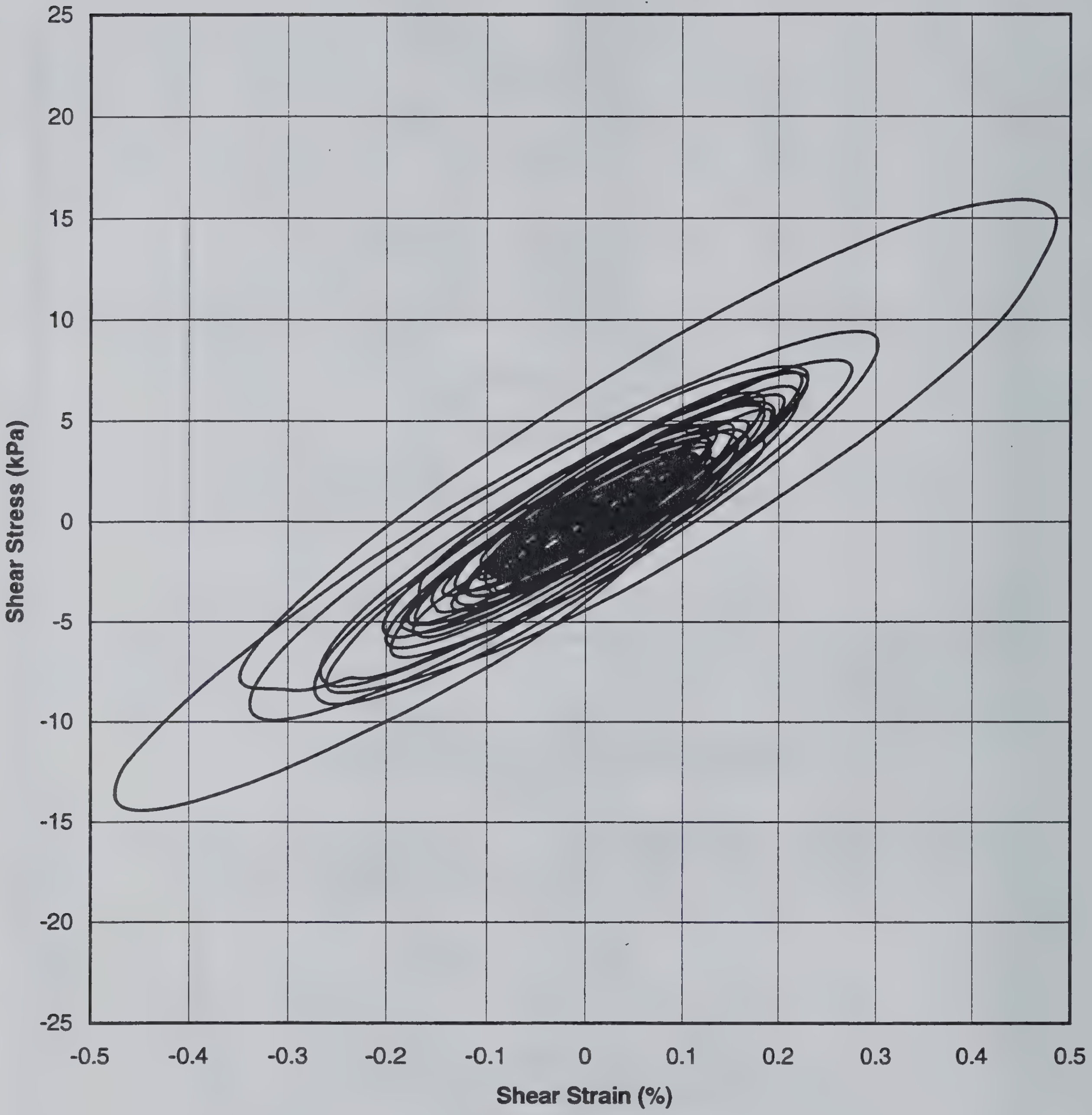

Figure 4.51 - Shear Stress - Shear Strain Hysteresis Loop at Depth of 4.21 m (13.8 ft.). Calculated from SHAKE Output - Wildlife SIte, November 24, 1987, 1315 GMT Earthquake in 360° Direction. Soil Properties Are Based on the Average of SASW and Crosshole Shear Wave Velocity Measurements. The EPRI (1993) G/Gmax and Damping Curves Are Used in the Calculation.

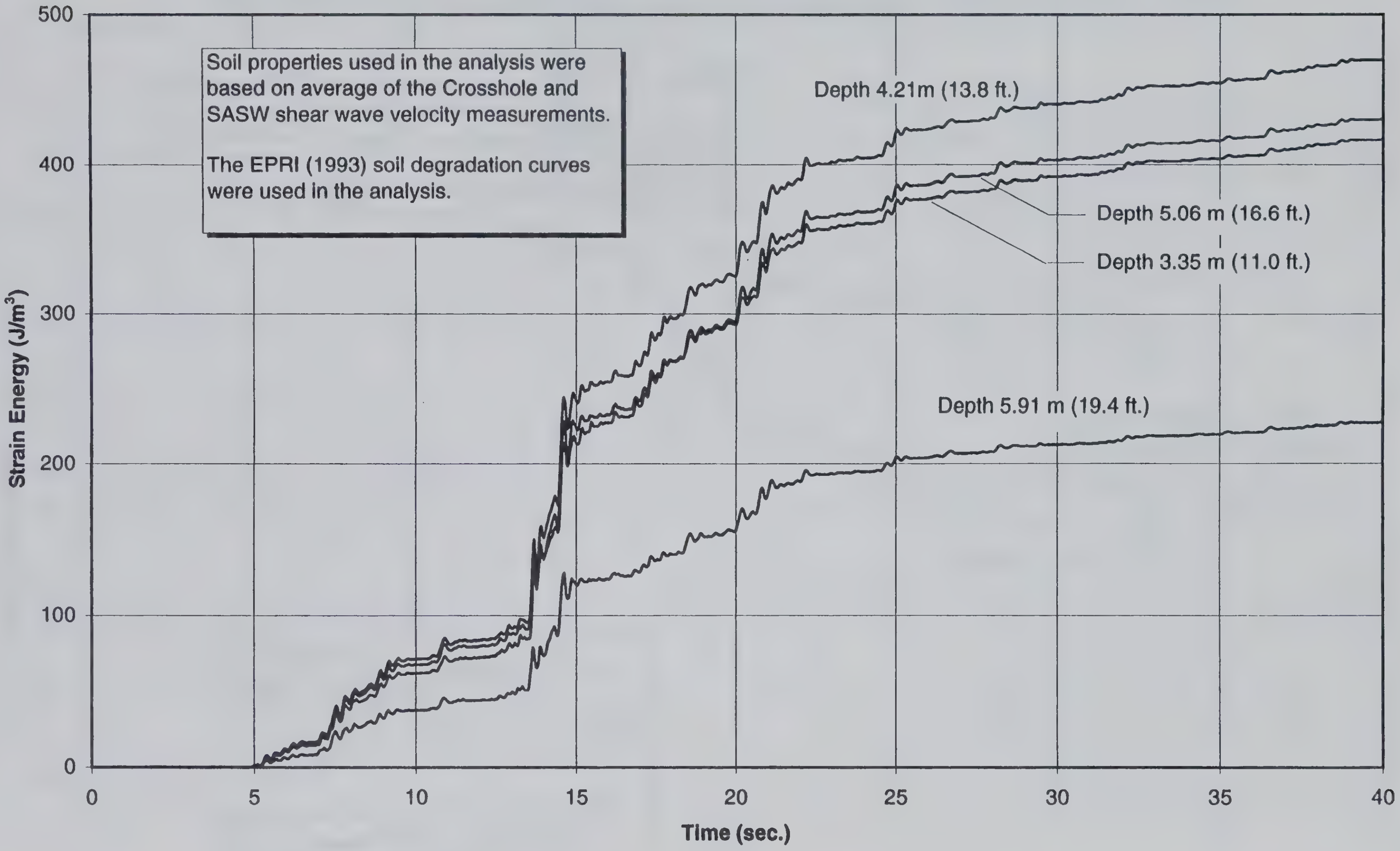

Figure 4.52 - Accumulation of Strain Energy in Liquefied Sand Layer - Wildlife Site, November 24, 1987, 1315 GMT Earthquake in 360° Direction - SHAKE Output Using EPRI (1993) Soil Curves

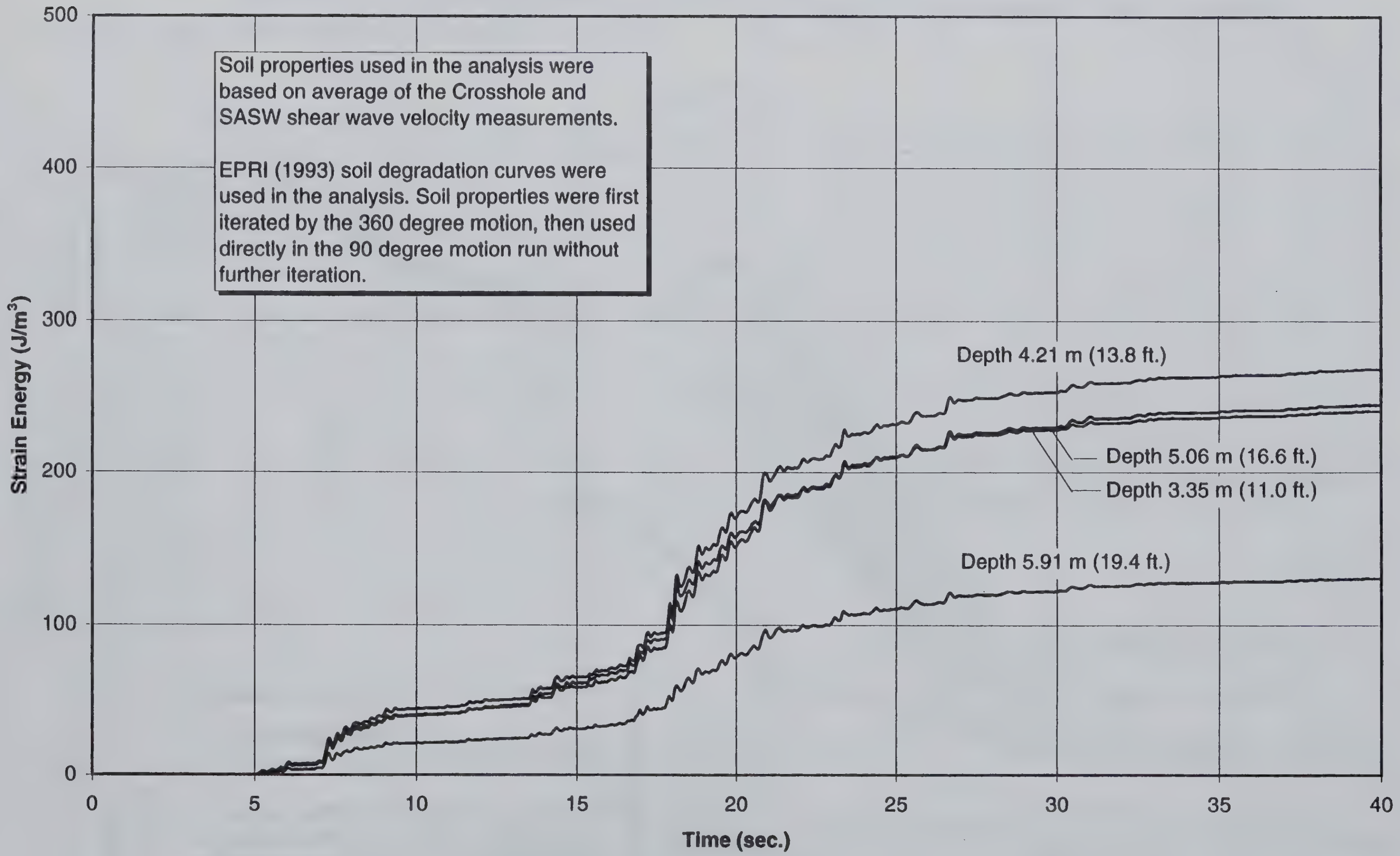

Soil properties used in the analysis were based on average of the Crosshole and SASW shear wave velocity measurements.

EPRI (1993) soil degradation curves were used in the analysis. Soil properties were first iterated by the 360 degree motion, then used directly in the 90 degree motion run without further iteration.

Figure 4.53 - Accumulation of Strain Energy in Liquefied Sand Layer - Wildlife Site, November 24, 1987, 1315 GMT Earthquake in 90° Direction - SHAKE Output Using EPRI (1993) Soil Curves

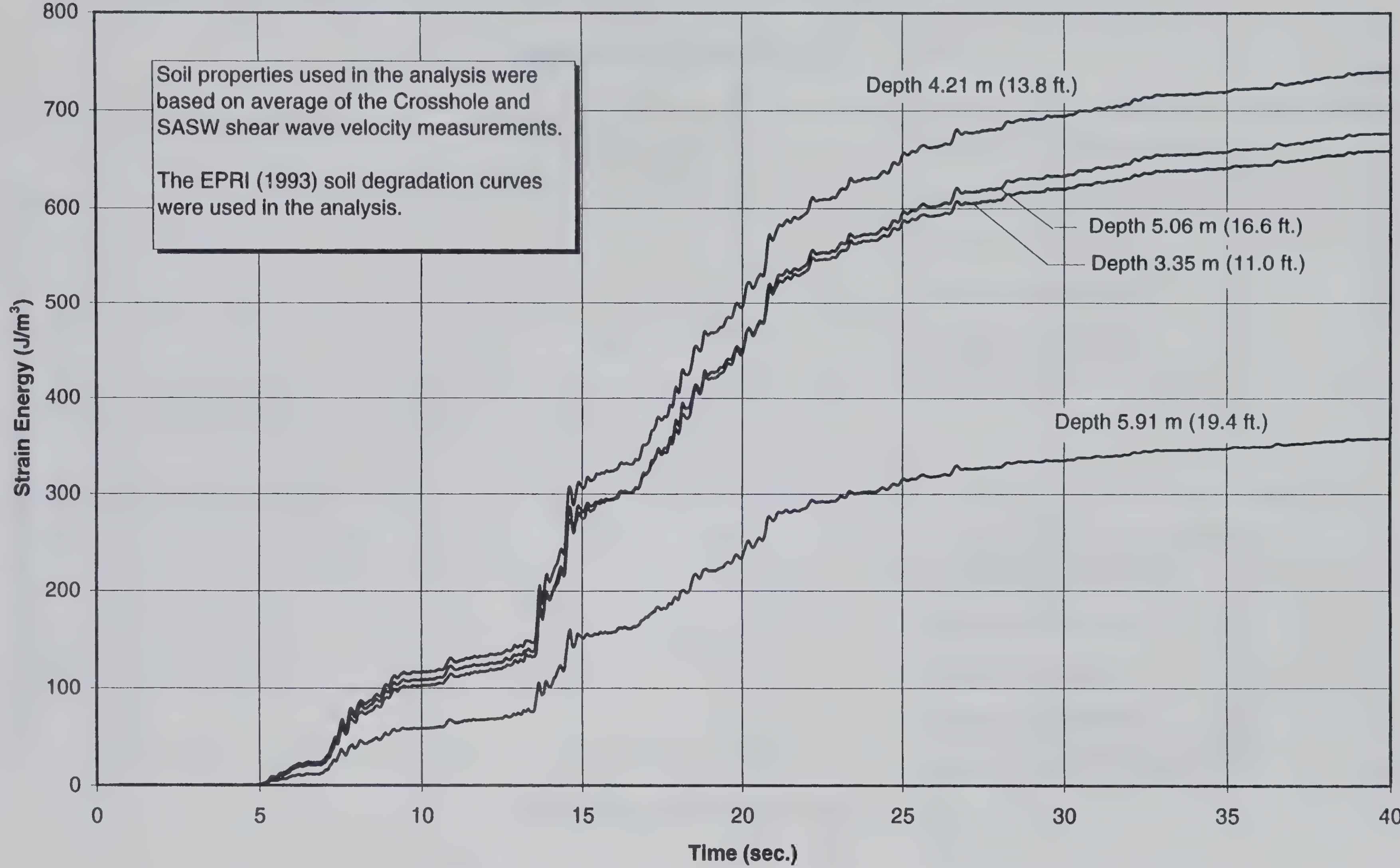

Soil properties used in the analysis were based on average of the Crosshole and SASW shear wave velocity measurements.

The EPRI (1993) soil degradation curves were used in the analysis.

Figure 4.54 - Accumulation of Strain Energy in Liquefied Sand Layer - Wildlife Site, November 24, 1987, 1315 GMT Earthquake - Summation of Strain Energy in both 360° and 90° Directions - SHAKE Output Using EPRI (1993) Soil Curves

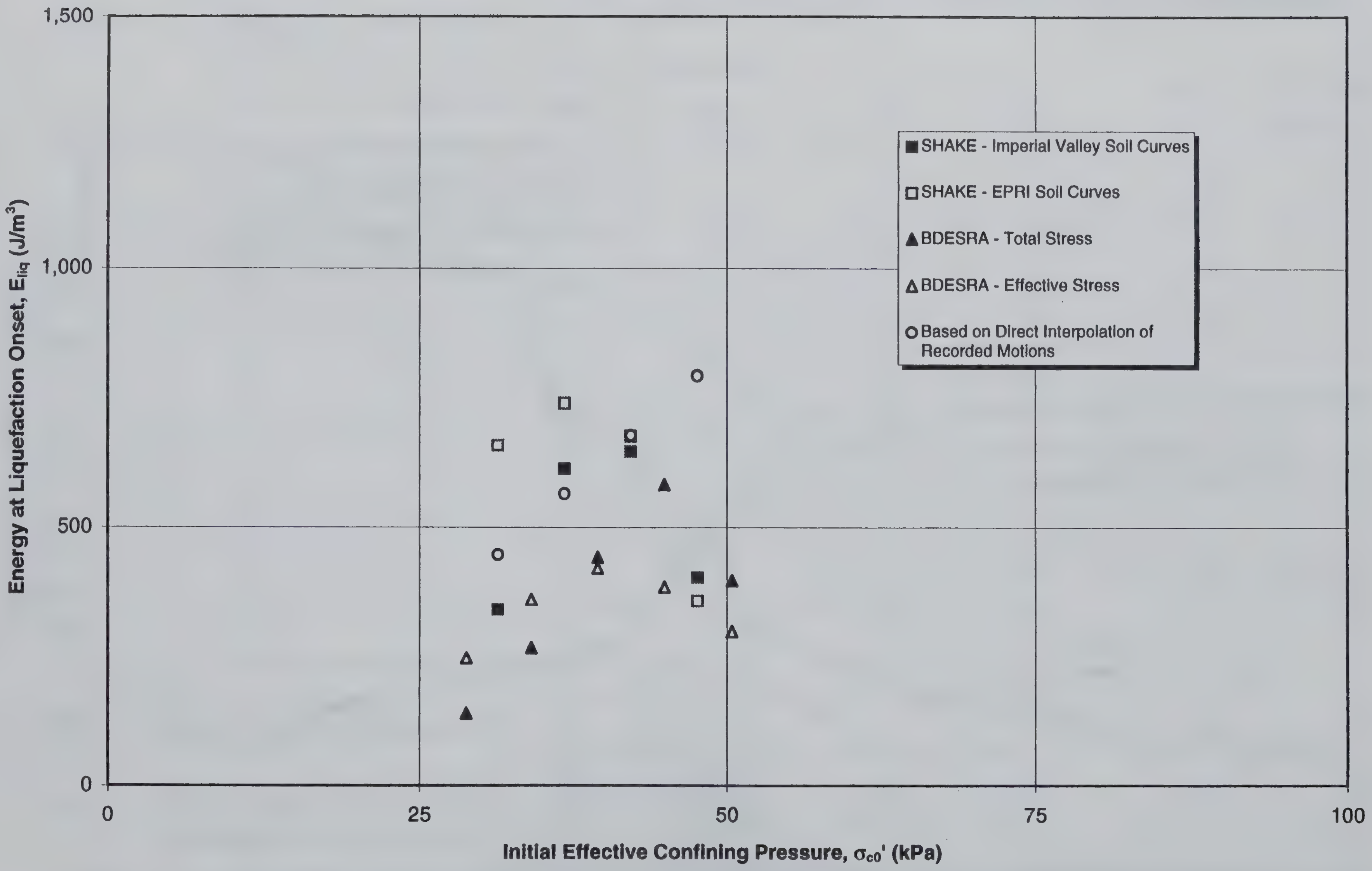

Figure 4.55 - Total Strain Energy at Liquefaction Onset. Calculated from Ground Response Analyses

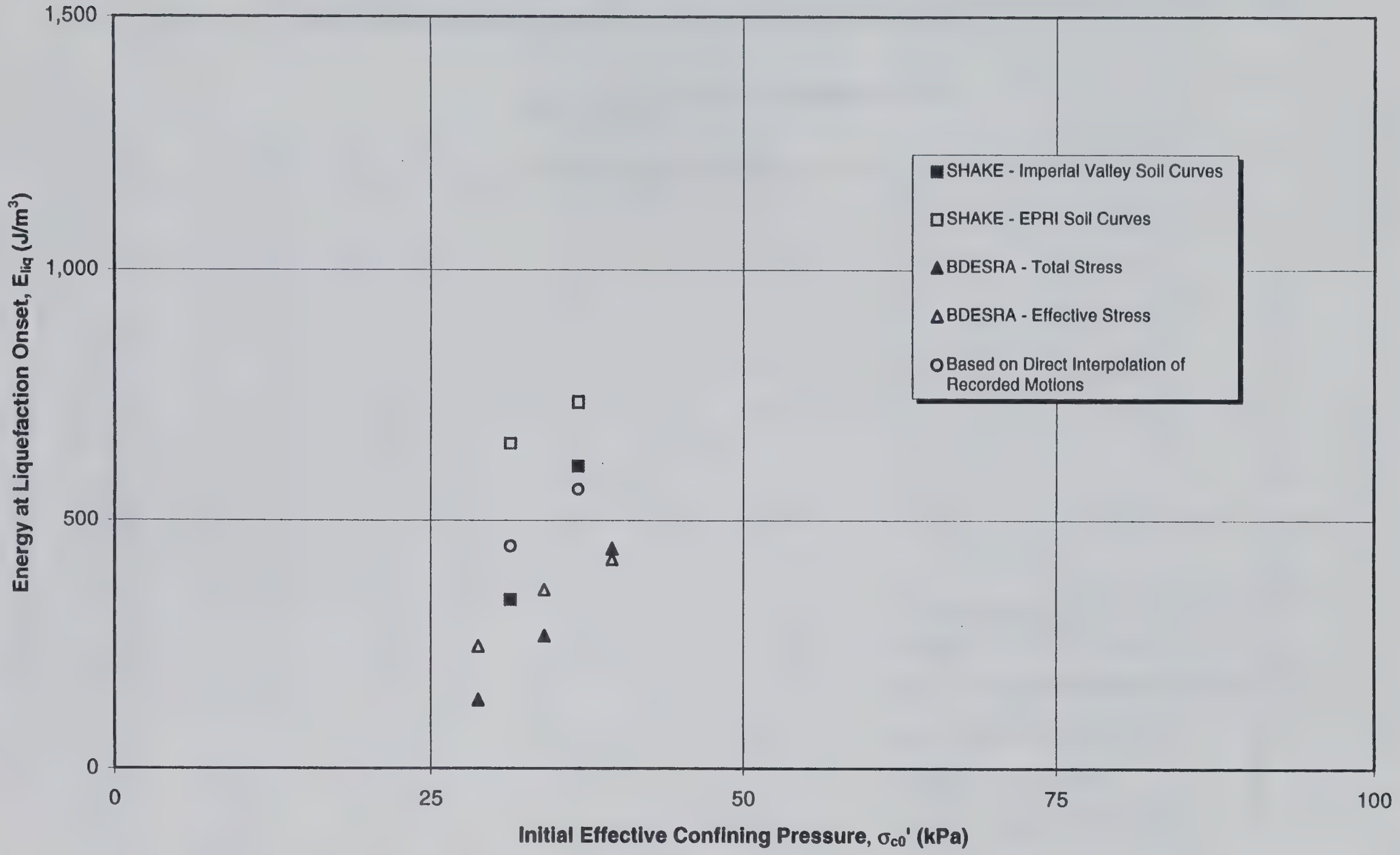

Figure 4.56 - Total Strain Energy at Liquefaction Onset. Calculated from Ground Response Analyses (All Points in Unliquefied Layers Removed)

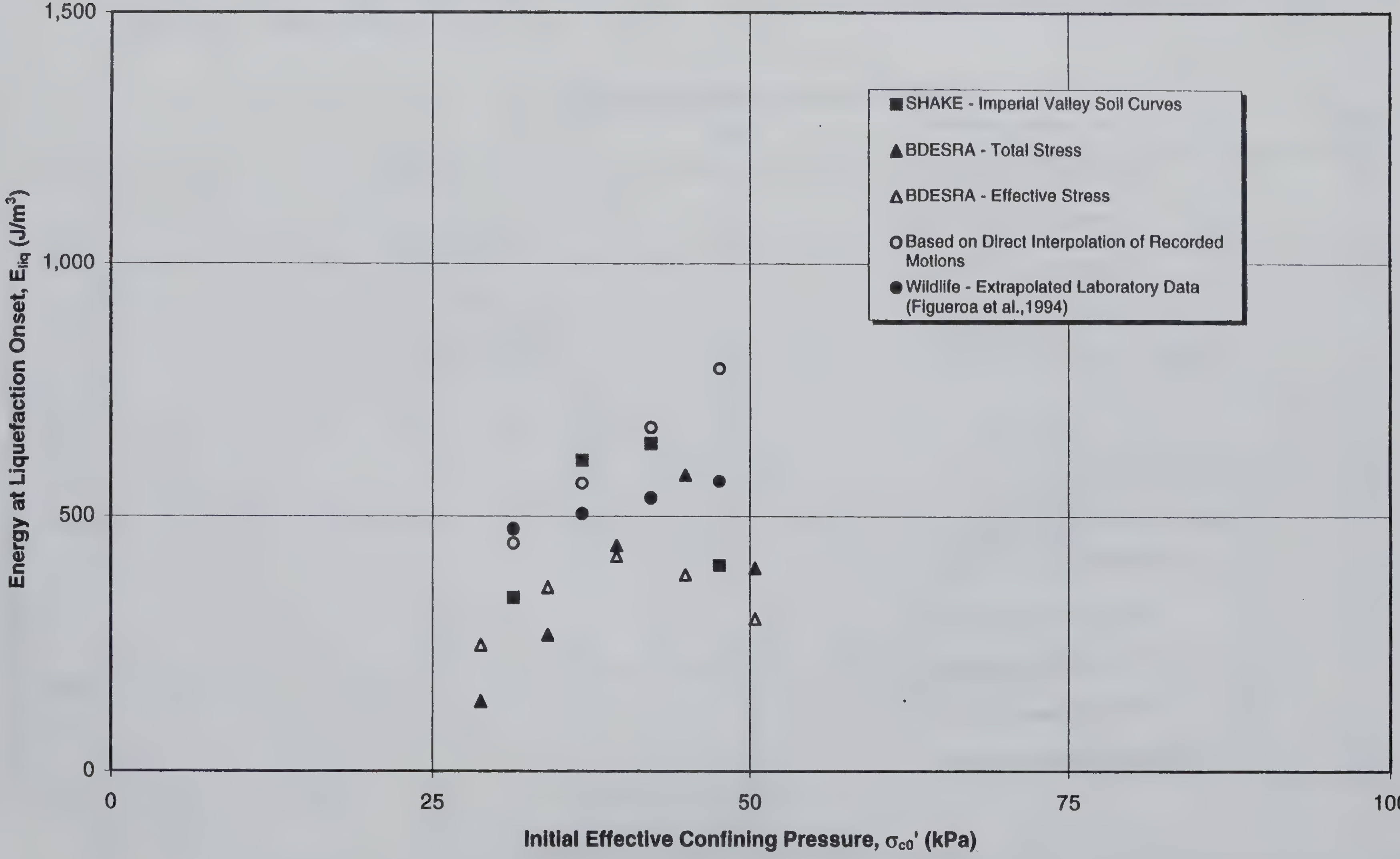

Figure 4.57 - Comparison of Total Strain Energy at Liquefaction Onset: Ground Response Analyses and Laboratory Data - Wildlife Site, November 24, 1987, 1315 GMT Earthquake.

CHAPTER 5

SUMMARY AND RECOMMENDATION

A feasibility study was conducted to determine the applicability of the strain energy method for liquefaction potential evaluation. This study consisted of collection and synthesis of available laboratory test data and evaluation of the strain energy as a measure of soil resistance to liquefaction. The data obtained by several groups of researchers confirm the observation that the strain energy (in normalized form) follows the time history of the pore pressure ratio increase up to the onset of liquefaction. The data also show that by using the relative density for clean sands and the confining pressure for silty sands, development of the generic strain energy relationships for liquefaction resistance is feasible. However, other factors such as the shape and size of the sand particles, the type and the amount of fines content, and the effect of the rate and type of loading on the strain energy need to be investigated and quantified.

The feasibility study also successfully predicts the strain energy required for liquefaction to take place in the field based on the recorded data at the Wildlife Site. The ground response analyses performed for this site, using the conventional methods of the ground response analyses, resulted in consistent results, with a scatter typically expected in such analyses. However, all methods used in the ground response analyses were one-dimensional, and the summation of the strain energy due to shaking in each direction is at best an approximation. Nevertheless, the comparison of the laboratory data with the results of ground response analyses is encouraging. Such favorable comparison suggests also that the goal of developing the strain energy approach for generic application to the evaluation of the soil liquefaction potential should be pursued in future phases of the project.

Based on the results of the feasibility study, it is recommended to:

- Perform laboratory testing, preferably on soil samples from the Wildlife Site at confining pressures in the range of 26 kPa to 50 kPa to cover the low end of the test results.

- Perform ground response analyses using a nonlinear computer program with multi-directional shaking capability to validate or modify the summation of the total strain energy calculated by the methods limited to uni-directional shaking capability as used in the current study.

- Apply the energy based method to liquefaction/no liquefaction sites at Northridge, Kobe in Japan where recorded motions are available, and at the Wildlife Site for the Elmore Ranch earthquake during which no liquefaction occurrence was observed.

The energy method provides a sound approach to the evaluation of liquefaction potential. It is based on the basic principles of the "stress" and "strain" approaches in which the soil capacity to resist liquefaction is measured in terms of the strain energy. It can also handle the special characteristics of the ground motion, such as the near-field effects. The method also has the capability of providing an estimate of the amount of pore pressure build-up before the onset of liquefaction. In this approach, the laboratory data can also be corroborated as more field data from the sites that have or have not liquefied become available.

CHAPTER 6

REFERENCES

Al-Khatib, M. A. (1994). "Liquefaction Assessment by Strain Energy Approach," Doctoral Dissertation Submitted to the Graduate School of Wayne State University, Detroit, Michigan.

Arango, I. (1994). "Methodology for Liquefaction Evaluation of Sites East of the Rockies," Bechtel Corporation, Technical Grant. San Francisco, California, June.

Arango, I., Migues, R. E. (1996), "Investigation of the Seismic Liquefaction of Old Sand Deposits," a Report Prepared for the National Science Foundation Grant No. CMS-9416169, Bechtel Corporation, San Francisco, California, March.

Bennett, M. J., McLaughlin, P. V., Sarmiento, P. V., Youd, T. L. (1984). "Geotechnical Investigation of Liquefaction Sites, Imperial Valley, California," USGS Open-File Report 84-252.

Bierschwale, J. G., Stokoe, K. H. (1984). "Analytical Evaluation of Liquefaction Potential of Sands Subjected to the 1981 Westmoreland Earthquake," Geotechnical Engineering Report GR84-15, Geotechnical Engineering Center, Civil Engineering Department, The University of Texas at Austin, Austin, Texas.

Dobry, R., Elgamal, A. W., Baziar, M. (1989). "Pore Pressure and Acceleration Response of Wildlife Site During the 1987 Earthquake," Proceedings from the 2nd US - Japan Workshop on Liquefaction, Large Ground Deformation and Their Effects on Lifelines, held at the Grand Island Holiday Inn in Grand Island, New York from September 26-28 and at the Cornell University in Ithaca, New York on September 29; also Technical Report NCEER-89-0032.

Dobry, R., Ladd, R. S., Yokel, F. Y., Chung, R. M., Powell, D. (1982). "Prediction of Pore Water Pressure Build-Up and Liquefaction of Sands During Earthquakes by the Cyclic Strain Method," NBS Building Science Series 138, National Bureau of Standards, US Department of Commerce, July.

Electric Power Research Institute (EPRI), (1993). Guidelines for Determining Design Basis Ground Motion," EPRI Report No. TR-102293, November.

Etheredge, R. P., Maley, R., Switzer, J. (1987). Strong-Motion Data from the Superstition Hills Earthquakes of 0154 and 1315 (GMT), November 24, 1987," USGS Open-File Report 87-672, December.

Figueroa, J. L., Saada, A. S., Liang, L., Dahisaria, N. M. (1994). "Evaluation of Soil Liquefaction by Energy Principles," Journal of the Geotechnical Engineering, Vol. 120, No. 9, September.

Figueroa, J. L., Saada, A. S., Liang, L., (1995). "Effect of the Grain Size on the Energy per Unit Volume at the Onset of Liquefaction," Proceedings of the 3rd International Conference on Recent Advances in Geotechnical Earthquake Engineering and Soil Dynamics, April 2-7, St. Louis, Missouri, Vol. 1.

Haag, E. D., Stokoe, K. (1985). "Laboratory Investigation of Static and Dynamic Properties of Sandy Soils Subjected to the 1981 Westmoreland Earthquake," Geotechnical Engineering Report GR85-11, Geotechnical Engineering Center, Civil Engineering Department, The University of Texas at Austin, Austin, Texas.

Holzer, T. L., Bennett, M. J., Youd, T. L. (1989). "Lateral Spreading Field Experiments by the US Geological Survey," Proceedings from the 2nd US - Japan Workshop on Liquefaction, Large Ground Deformation and Their Effects on Lifelines, held at the Grand Island Holiday Inn in Grand Island, New York from September 26-28 and at the Cornell University in Ithaca, New York on September 29; also Technical Report NCEER-89-0032.

Holzer, T. L., Youd, L., Bennett, M. J. (1988). "In Situ Measurement of Pore Pressure Build-Up During Liquefaction," Proceedings of the 20th Joint Meeting of The US - Japan Cooperative Program in Natural Resources, Panel on Wind and Seismic Effects, NIST Report SP 760.

Ishihara, K. (1993). "Liquefaction and Flow Failure During Earthquakes," 33rd Rankine Lecture, Geotechnique, Vol. 43, No. 3, pp. 351-415.

Kagawa, T., Al-Khatib, M. A. (1990). "Use of Shear-Strain Energy for Liquefaction Prediction," Proceedings of 4th US National Conference on Earthquake Engineering, May 20-24, Palm Springs, California, Vol. 3.

Koester, J. P. (1992). "Cyclic Strength and Pore Pressure Generation Characteristics of Fine-Grained Soils," A Thesis Submitted to the Faculty of the Graduate School of the University of Colorado, Denver, Colorado.

Ladd, R. S., (1982). "Geotechnical Laboratory Testing Program for Study and Evaluation of Liquefaction Ground Failure Using Stress and Strain Approaches: Heber Site, October 15, 1979 Imperial Valley Earthquake," Woodward-Clyde Consultants, Wayne, New Jersey, February.

Lee, M. K., Finn, W. L. (1978). “DESRA-2C, Dynamic Effective Stress Analysis of Soil Deposits with Energy Transmitting Boundary Including Assessment of Liquefaction Potential,” the University of British Columbia, British Columbia, Canada; Modified by Bechtel Corporation to include Martin-Davidenkov Soil Model, Bechtel Corporation, San Francisco, California.

Magistrale, H., Jones, L., Kanamori, H. (1989). “The Superstition Hills, California, Earthquake of 24 November 1987,” Bulletin of the Seismological Society of America, Vol. 79, April.

Matasovic, J., Vucetic, M. (1993). “Analyses of Seismic Records Obtained on November 24, 1987 at the Wildlife Liquefaction Array,” Research Report, Civil Engineering Department, University of California, Los Angeles, California, May.

Porcella, R., Etheredge, E., Maley, R., Switzer, J. (1987). “Strong-Motion Data from the Superstition Hills Earthquakes of 0154 and 1315 (GMT), November 24, 1987,” USGS Report, 87-672.

Riemer, M. F., Gookin, W. B., Bray, J. D, Arango, I. (1994). “Effects of Loading Frequency and Control on the Liquefaction Behavior of Clean Sands,” Geotechnical Engineering report No. UCB/GT/94-07, Geotechnical Engineering, Department of Civil Engineering, University of California, Berkeley.

Riemer, M. F., Seed. R. B. (1994). “Dynamic Testing of Soils from the SRS/ITP Facility,” Geotechnical Engineering Report No. UCB/GT/94-02, Geotechnical Engineering, Department of Civil Engineering, University of California, Berkeley, May.

Schnabel, P. B., Lysmer, J., Seed, H. B. (1972), “SHAKE, A Computer Program for Earthquake Response Analyses of Horizontally Layered Sites,” Report EERC 72-12, University of California, Berkeley; Modified by Bechtel Corporation, San Francisco, California, 1995.

Seed, H. B., Idriss, I. M., Arango, I. (1983). “Evaluation of Liquefaction Potential Using Field Performance Data,” Journal of Geotechnical Engineering, Vol. 109, No. 3, March.

Seed, H. B., Tokimatsu, K., Harder, L. F. (1985). “Influence of SPT Procedures in Soil Liquefaction Resistance Evaluations,” Journal of Geotechnical Engineering, Vol. 111, No. 12, February.

Thilakaratne, V., Vucetic, M. (1990). “Analysis of the Seismic Response at the Imperial Wildlife Liquefaction Array in 1987,” Proceedings of the 4th US National Conference on Earthquake Engineering, May 20-24, Palm Springs, California, Vol. 3.

Turner, E., Stokoe, K. H. (1982). “Static and Dynamic Properties of the Clayey Soils Subjected to the 1979 Imperial Valley Earthquake,” Geotechnical Engineering Report GR82-86, The University of Texas at Austin, Texas, October.

Vucetic, M., Thilakaratne, V. (1989). “Liquefaction at the Wildlife Site - Effect of Soil Stiffness on Seismic Responses,” Proceedings of the 4th International Conference on Soil Dynamics and Earthquake Engineering, Mexico City, October.

Wald, D J., Helmberger, D. V., Hartzell, S. H. (1990). “Rupture Process of the 1987 Superstition Hills Earthquake from the Inversion of Strong-Motion Data,” Bulletin of the Seismological Society of America, Vol. 80, No. 5, October.

Youd, T. L., Holtzer, T. L., Bennett, M. J. (1989). “Liquefaction Lessons Learned from the Imperial Valley, California,” Proceedings of the 12th International Conference on Soil Mechanics and Foundation Engineering, Rio de Janeiro.

Zeghal, M., Elgamal, A. W. (1994). “Analysis of Site Liquefaction Using Earthquake Records,” Journal of Geotechnical Engineering, Vol. 120, No. 6, June.

APPENDIX A

LABORATORY TESTS ON MONTEREY NO. 0 SAND, PERFORMED AT THE UNIVERSITY OF CALIFORNIA, BERKELEY

Table A.1 - Summary of the Cyclic Triaxial Test Data on Monterey No. 0 Sand Performed at University of California, Berkeley

No.	Test ID	Sample	D_r(%)	E_{liq} (J/m^3)	FC (%)	γ_d (kN/m^3)	Control	σ_c' (kPa)	Freq. (Hz)	Load Shape
1	MONT4	Monterey No.0	61.8	2677	2	15.6	Stress	100	1	Sinusoidal 2-way
2	MONT10	Monterey No.0	61.0	1933	2	15.5	Stress	100	1	Sinusoidal 2-way
3	MONT11	Monterey No.0	60.6	988	2	15.5	Stress	100	10	Sinusoidal 2-way
4	MONT12	Monterey No.0	61.0	2481	2	15.5	Stress	100	1	Sinusoidal 2-way
5	MONT14	Monterey No.0	60.2	1583	2	15.5	Stress	100	20	Sinusoidal 2-way
6	MONT15	Monterey No.0	60.5	1245	2	15.5	Stress	100	10	Sinusoidal 2-way
7	MONT17	Monterey No.0	61.0	1878	2	15.5	Strain	100	1	Sinusoidal 2-way
8	MONT18	Monterey No.0	61.0	1187	2	15.5	Strain	100	10	Sinusoidal 2-way
9	MONT19	Monterey No.0	60.6	1483	2	15.5	Strain	100	15	Sinusoidal 2-way
10	MONT20	Monterey No.0	40.9	851	2	15.0	Strain	100	1	Sinusoidal 2-way
11	MONT21	Monterey No.0	41.8	880	2	15.0	Strain	100	1	Sinusoidal 2-way
12	MONT22	Monterey No.0	42.3	1078	2	15.0	Strain	100	1	Sinusoidal 2-way
13	MONT24	Monterey No.0	51.8	2736	2	15.3	Stress	100	1	Sinusoidal 2-way
14	MONT25	Monterey No.0	50.4	2985	2	15.3	Stress	100	1	Sinusoidal 2-way
15	MONT26	Monterey No.0	49.9	2769	2	15.2	Stress	100	1	Sinusoidal 2-way
16	MONT30	Monterey No.0	41.9	708	2	15.0	Strain	100	10	Sinusoidal 2-way
17	MONT33	Monterey No.0	40.5	829	2	15.0	Strain	100	10	Sinusoidal 2-way
18	MONT35	Monterey No.0	61.8	4211	2	15.6	Stress	100	0.1	Sinusoidal 2-way
19	MONT37	Monterey No.0	61.6	1388	2	15.5	Strain	100	1	Sinusoidal 2-way
20	MONT38	Monterey No.0	61.8	704	2	15.6	Strain	100	10	Sinusoidal 2-way

Test Results Following the Sequence of Test ID's are Attached.

Test I.D.:	MONT4	**Controlled Parameter:**	Stress
Relative Density (%):	61.8	**Initial Effective Stress (kPa):**	100
Applied Stress Ratio:	0.31	**Frequency (Hz):**	1

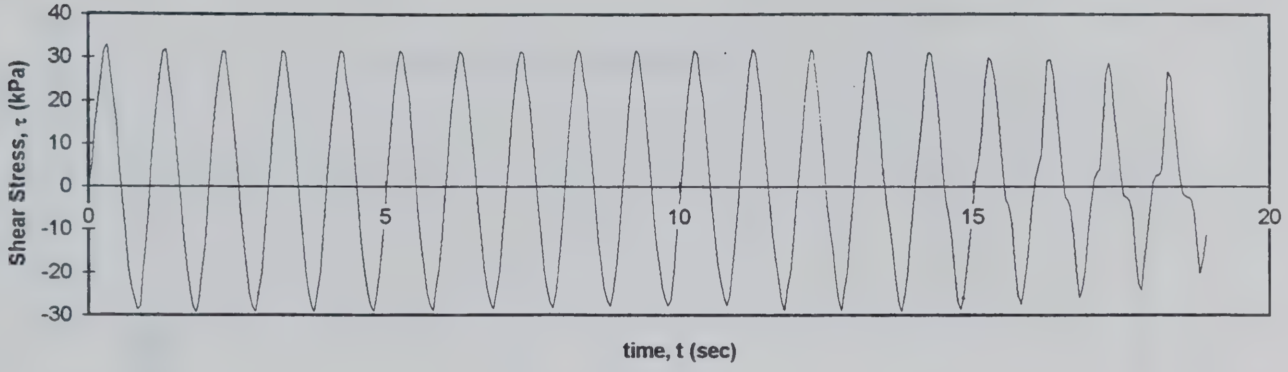

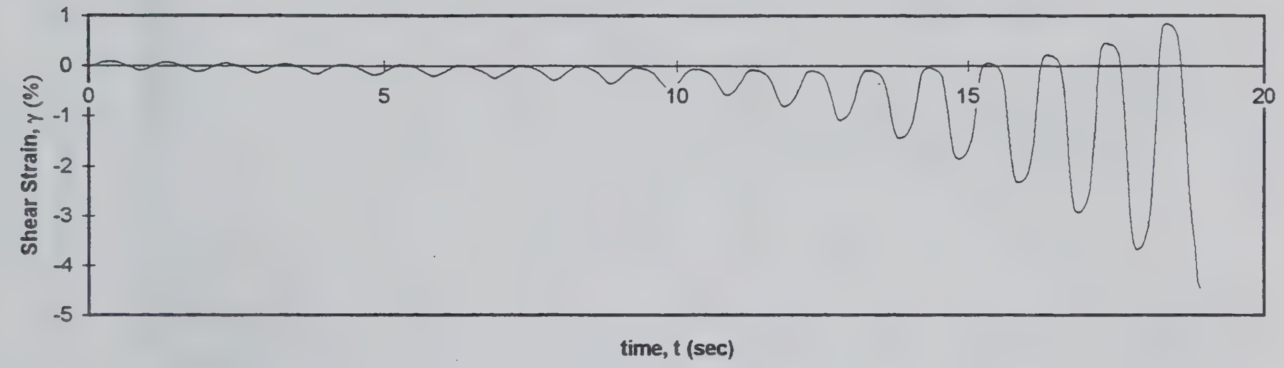

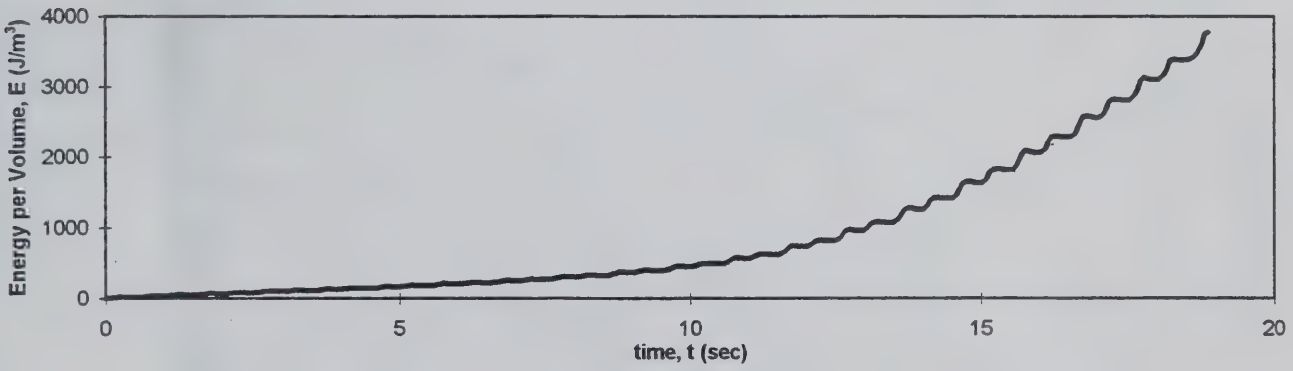

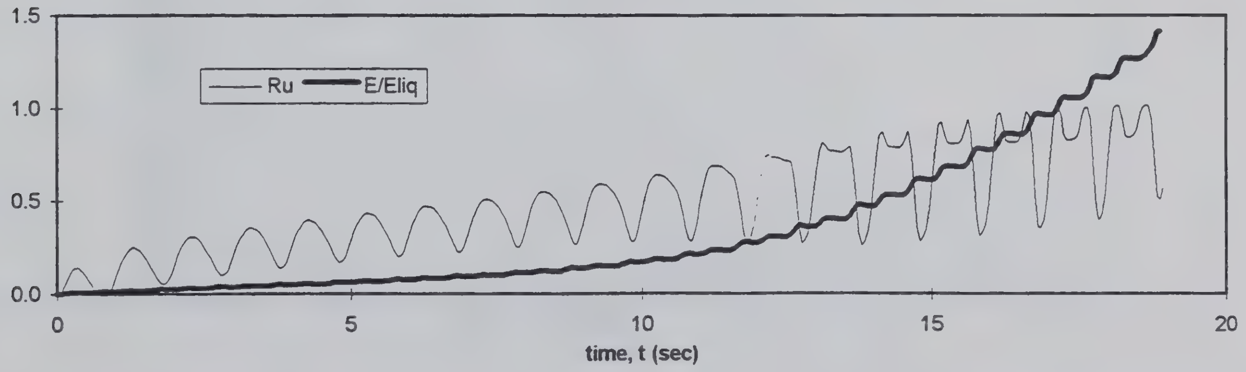

Test I.D.: MONT4
Relative Density (%) 61.8
Applied Stress Ratio: 0.31
Controlled Parameter: Stress
Initial Effective Stress (kPa): 100
Frequency (Hz): 1

Shear Stress vs. Shear Strain

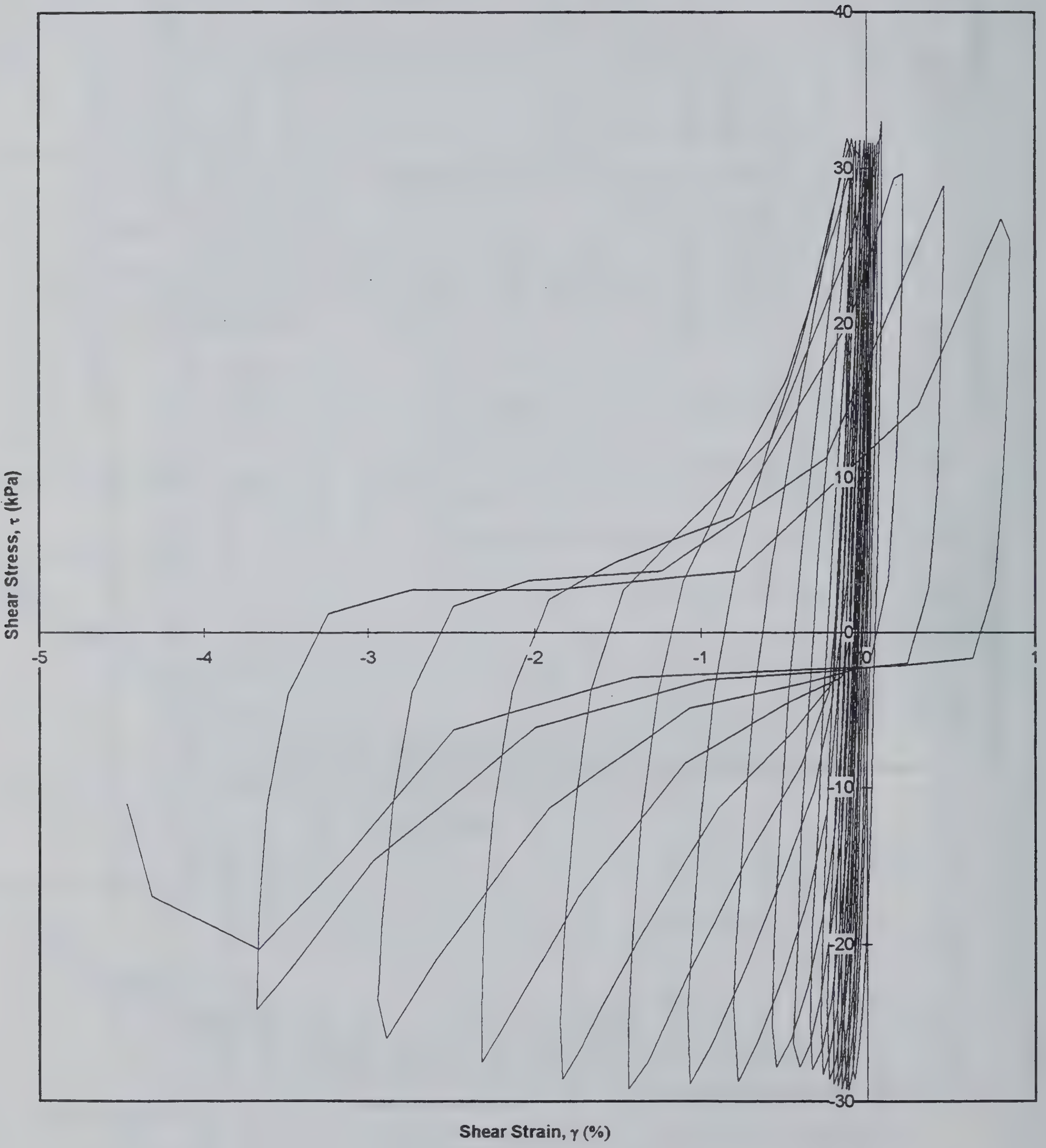

Test I.D.:	MONT10	**Controlled Parameter:**	Stress
Relative Density (%):	61	**Initial Effective Stress (kPa):**	100
Applied Stress Ratio:	0.27	**Frequency (Hz):**	1

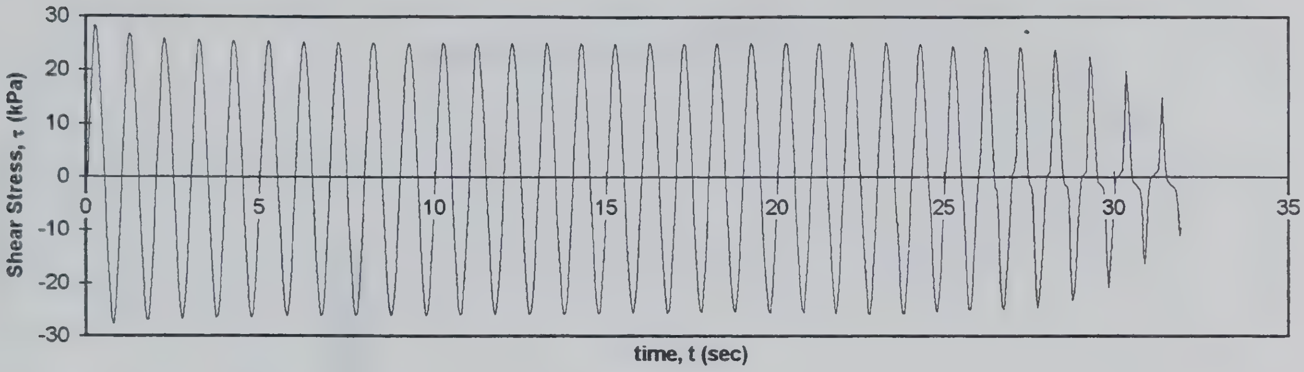

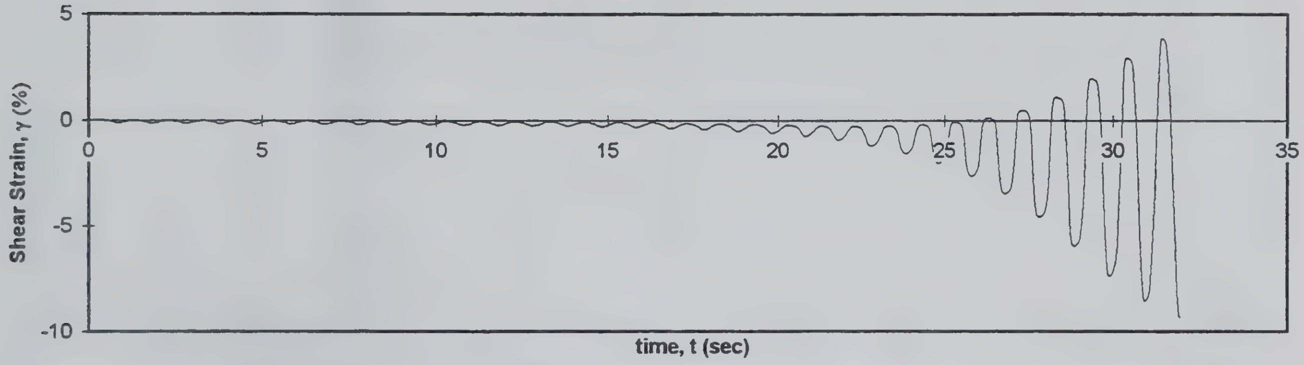

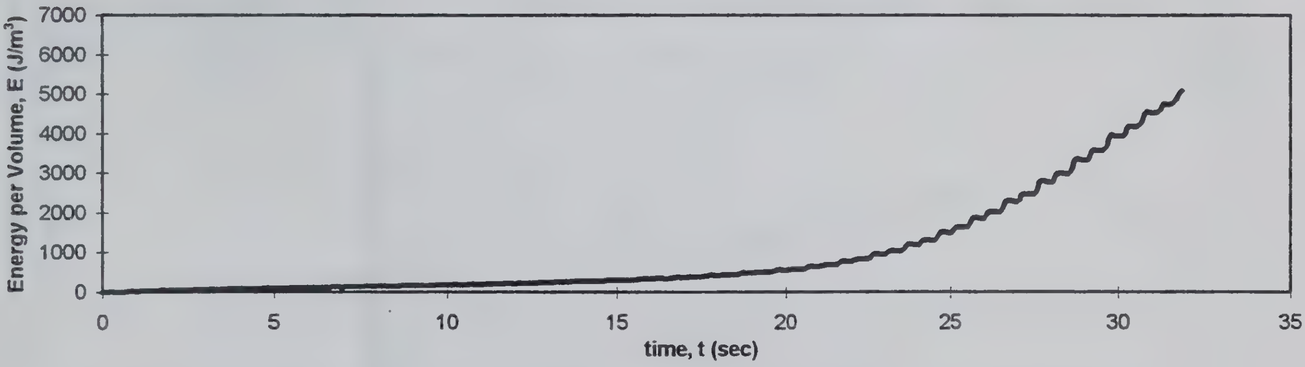

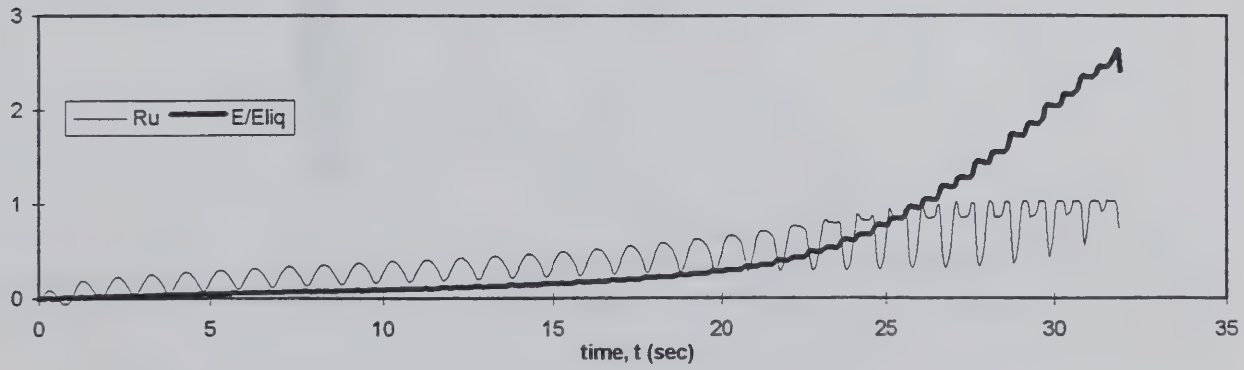

Test I.D.:	MONT10	**Controlled Parameter:**	Stress
Relative Density (%):	61	**Initial Effective Stress (kPa):**	100
Applied Stress Ratio:	0.27	**Frequency (Hz):**	1

Shear Stress vs. Shear Strain

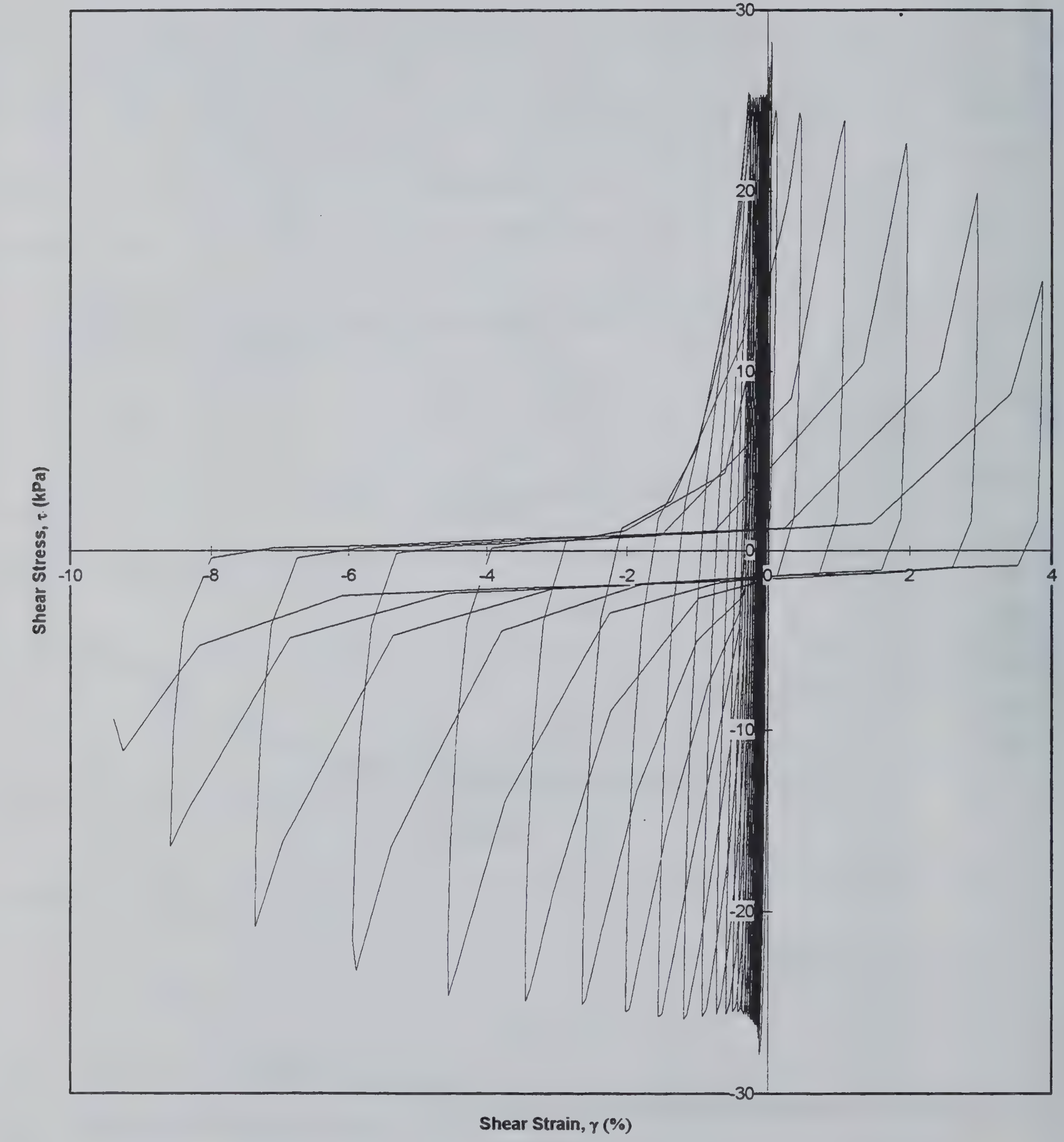

d:\nit\itp\cy_files\MONT10.XLS

8/21/96 9:46 AM

Test I.D.:	MONT11	**Controlled Parameter:**	Stress
Relative Density (%):	60.6	**Initial Effective Stress (kPa):**	100
Applied Stress Ratio:	0.3	**Frequency (Hz):**	10

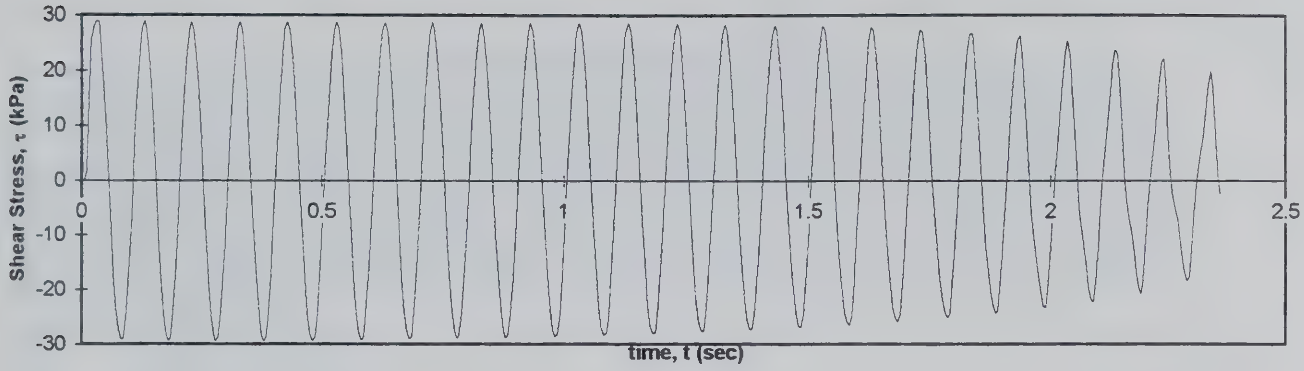

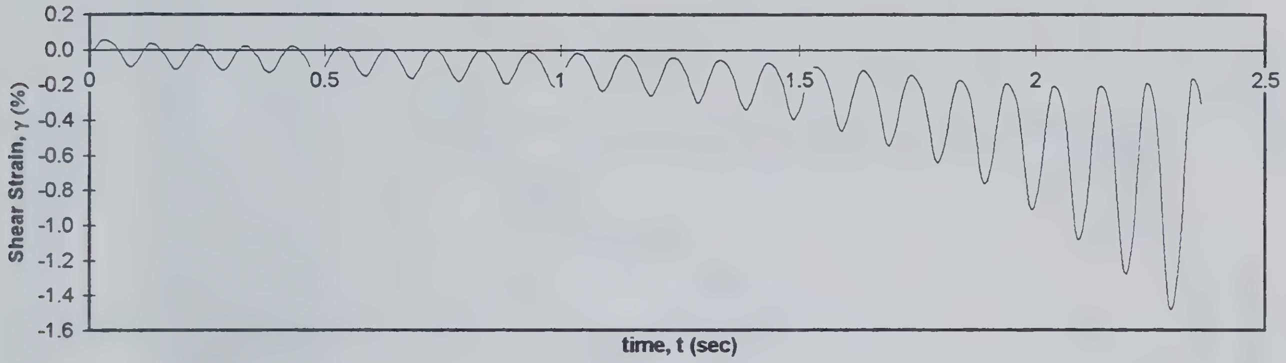

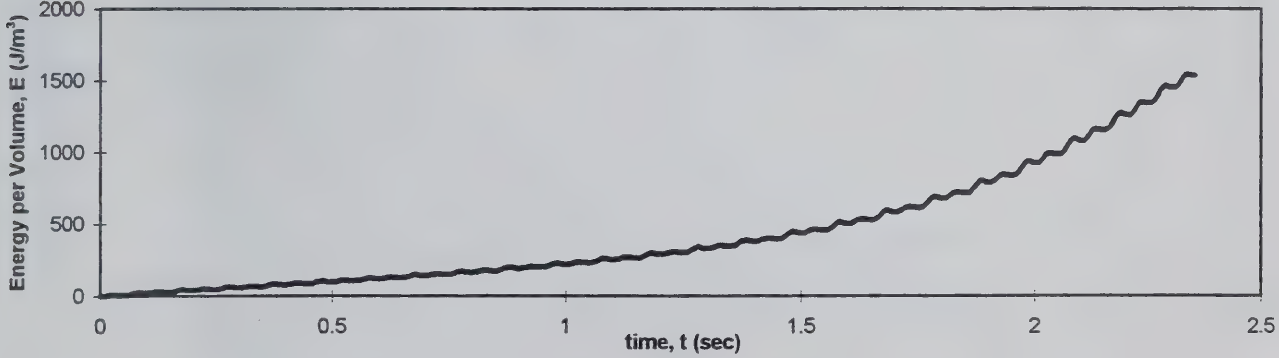

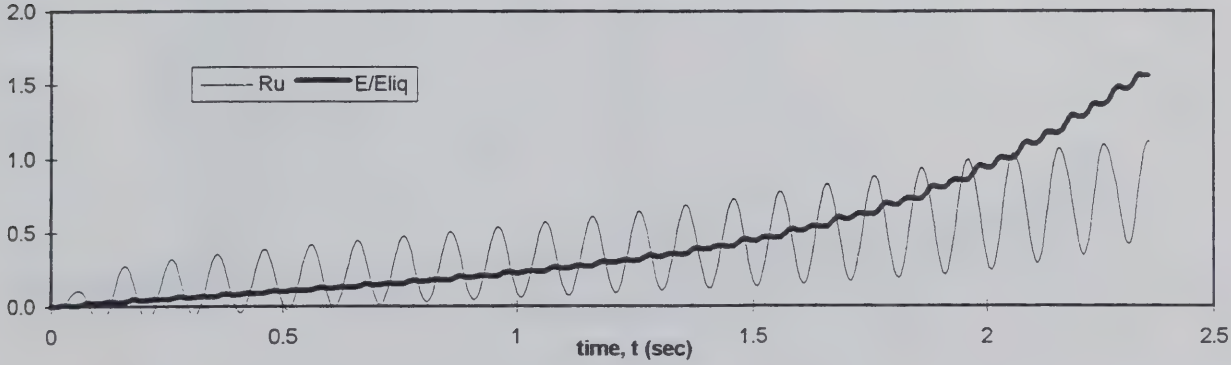

Test I.D.:	MONT11	**Controlled Parameter:**	Stress
Relative Density (%):	60.6	**Initial Effective Stress (kPa):**	100
Applied Stress Ratio:	0.3	**Frequency (Hz):**	10

Shear Stress vs. Shear Strain

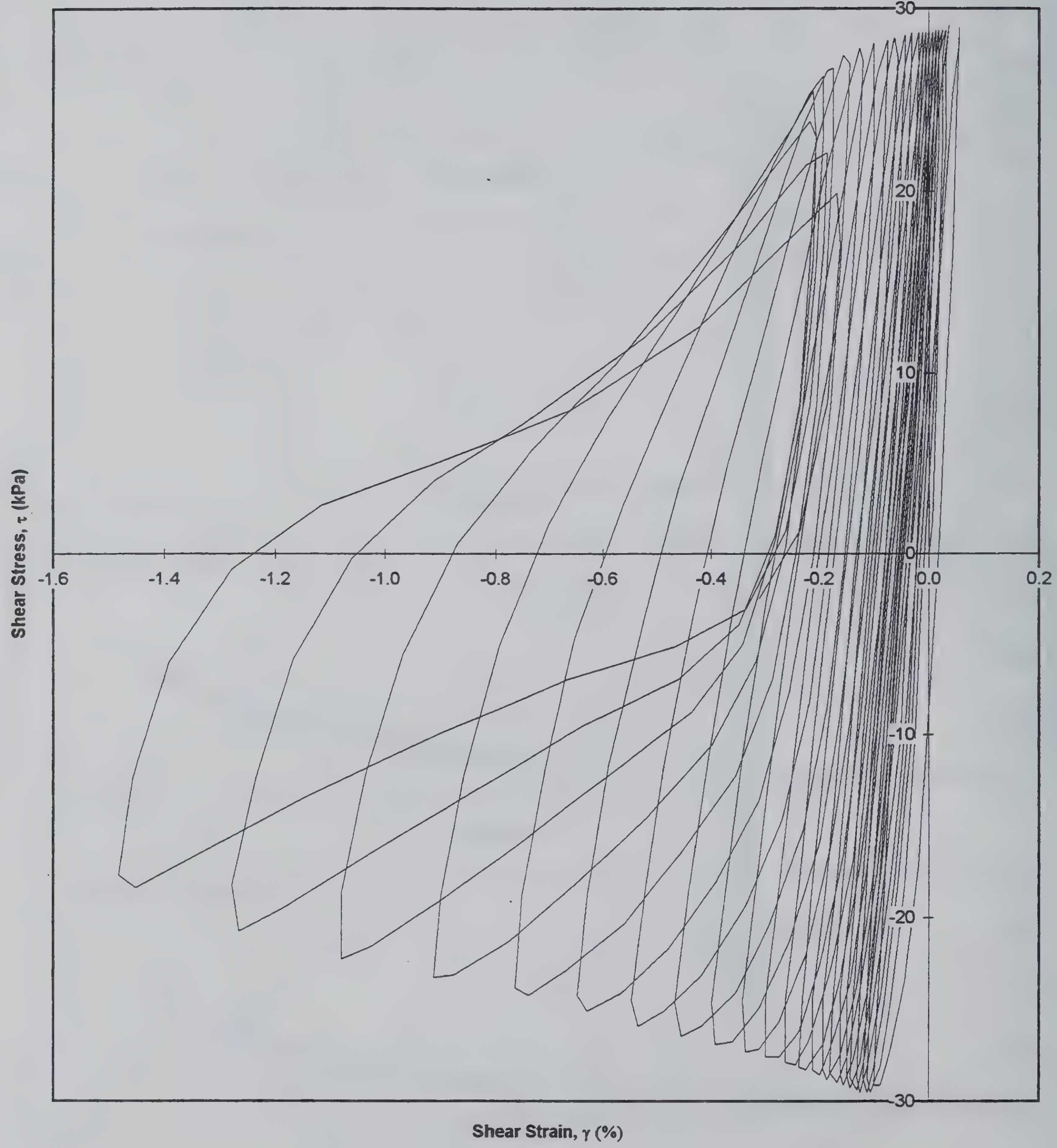

Test I.D.: MONT12
Relative Density (%): 61
Applied Stress Ratio: 0.23

Controlled Parameter: Stress
Initial Effective Stress (kPa): 100
Frequency (Hz): 1

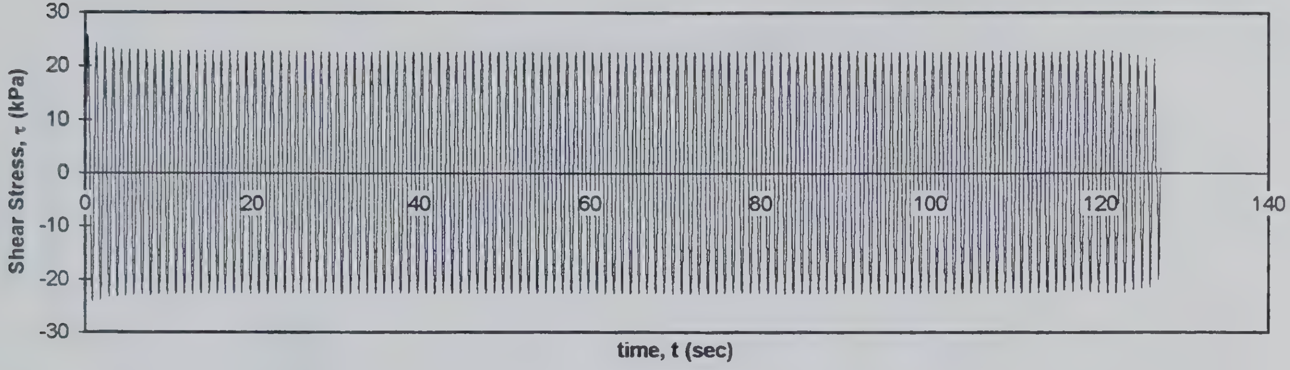

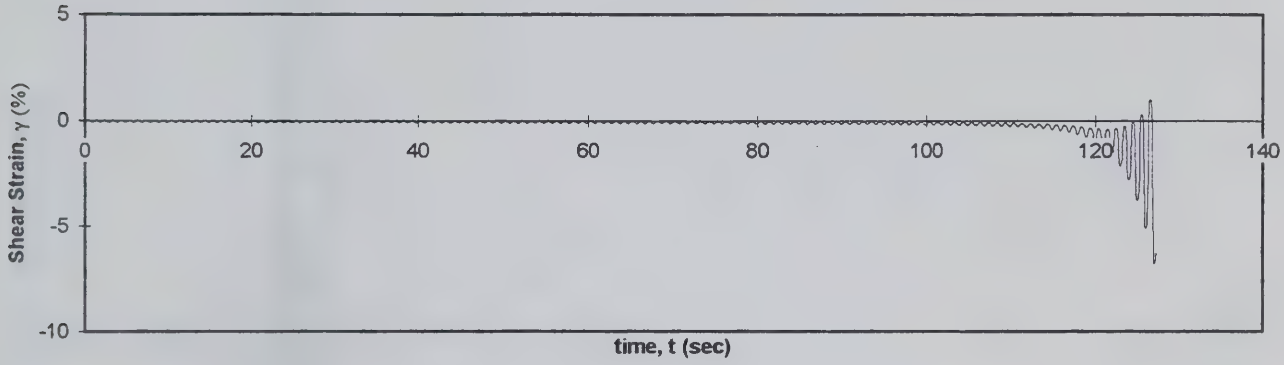

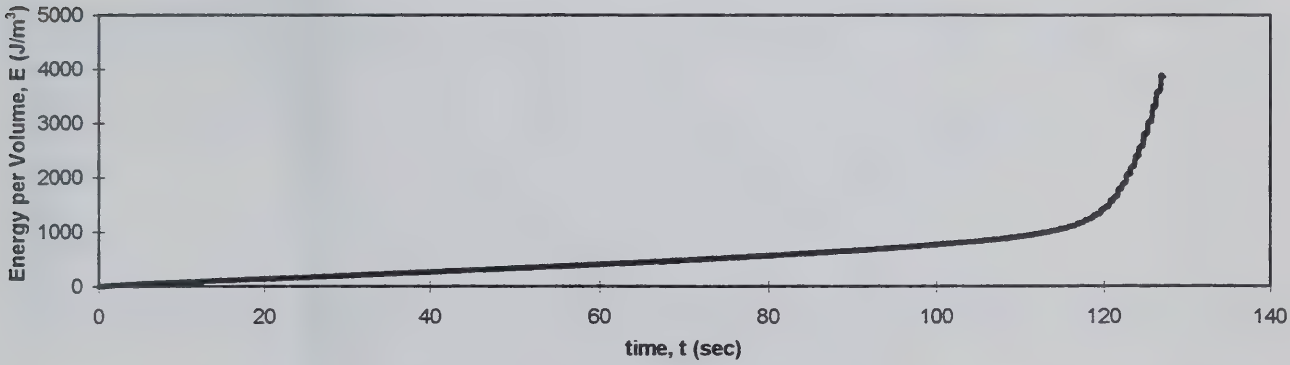

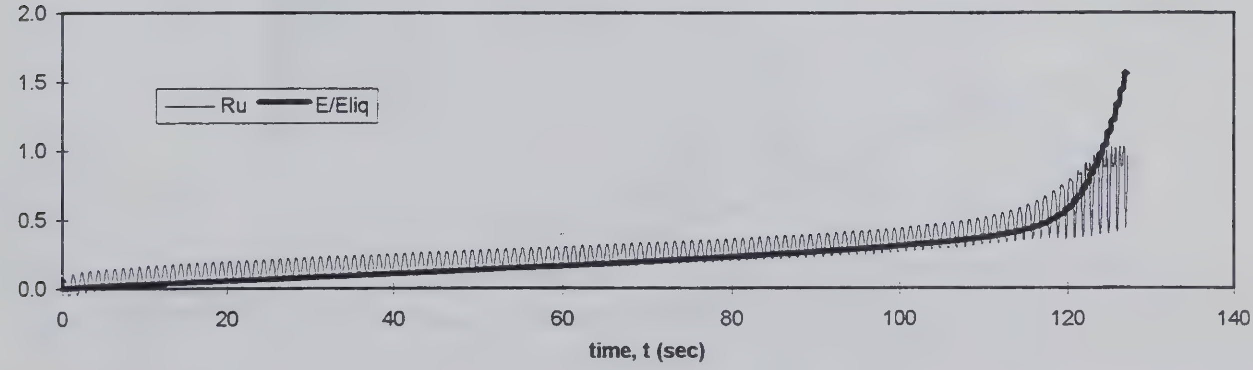

Test I.D.: MONT12
Relative Density (%): 61
Applied Stress Ratio: 0.23
Controlled Parameter: Stress
Initial Effective Stress (kPa): 100
Frequency (Hz): 1

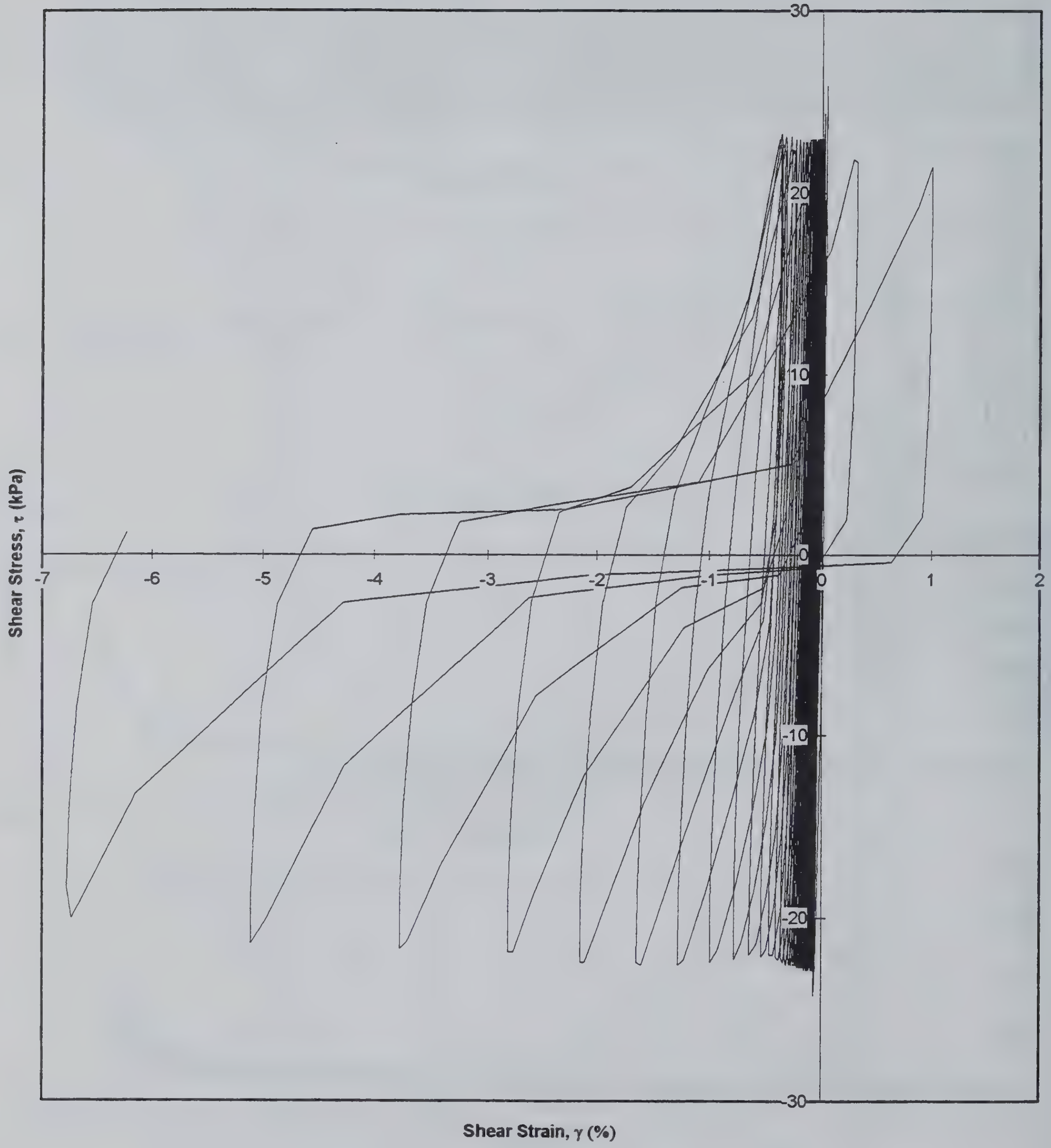

Shear Stress vs. Shear Strain

d:\nit\itp\cy_files\MONT12.XLS

8/15/96 11:22 AM

Test I.D.:	MONT14	**Controlled Parameter:**	Stress
Relative Density (%):	60.2	**Initial Effective Stress (kPa):**	100
Applied Stress Ratio:	0.3	**Frequency (Hz):**	20

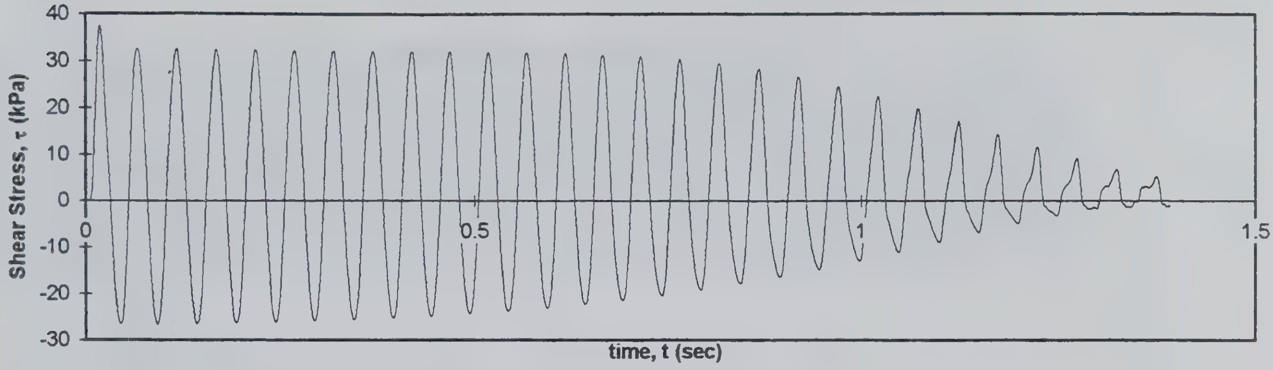

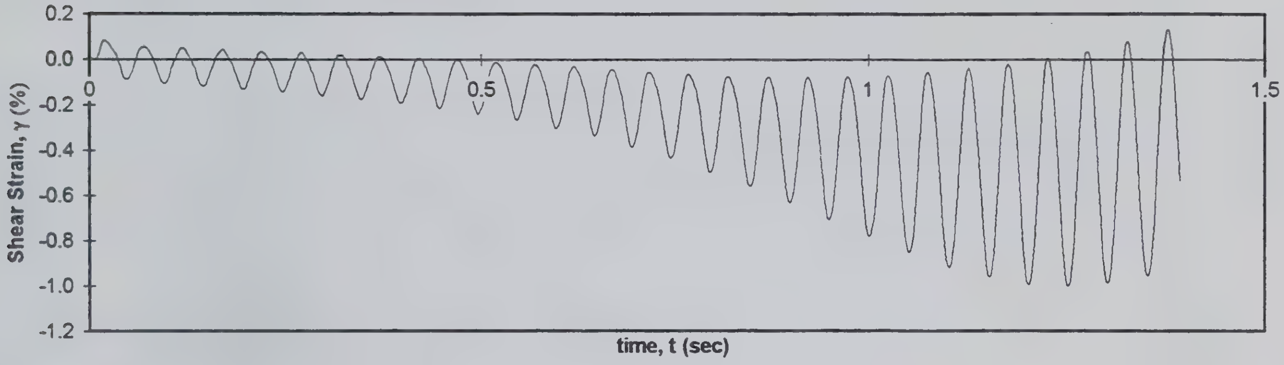

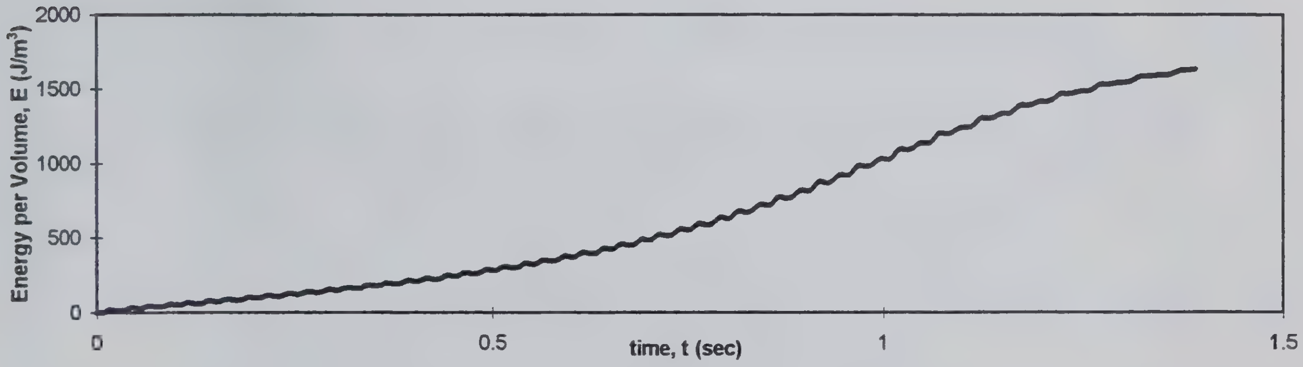

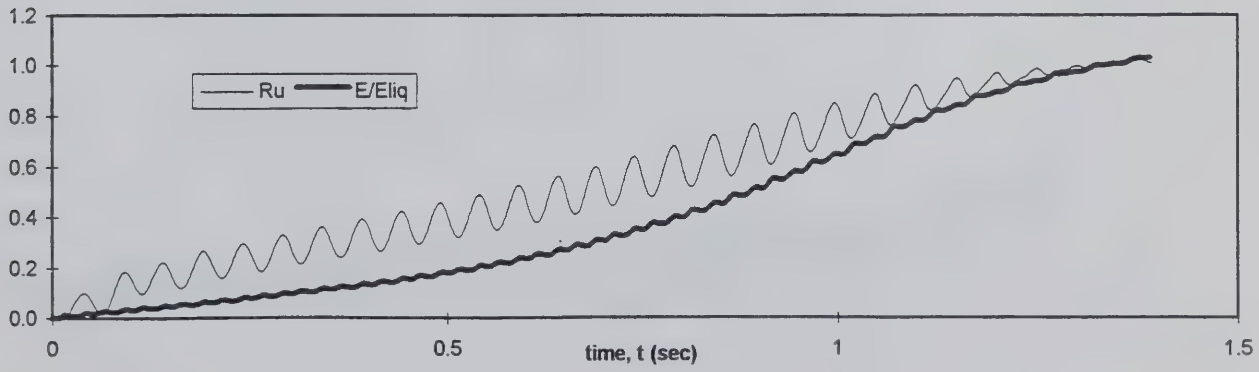

d:\nit\itp\cy_files\MONT14.XLS 8/15/96 11:24 AM

Test I.D.:	MONT14	**Controlled Parameter:**	Stress
Relative Density (%):	60.2	**Initial Effective Stress (kPa):**	100
Applied Stress Ratio:	0.3	**Frequency (Hz):**	20

Shear Stress vs. Shear Strain

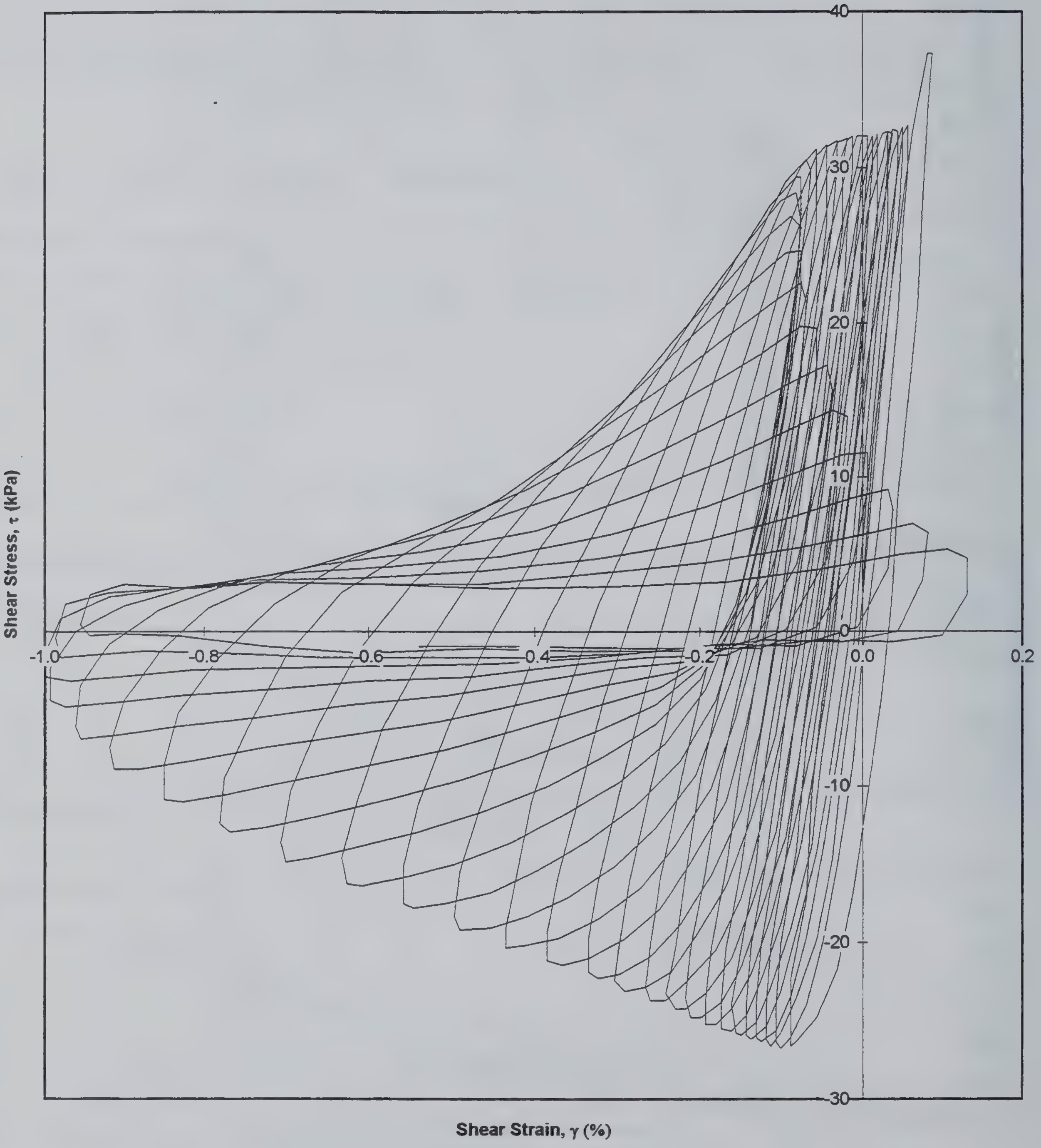

Test I.D.: MONT15
Relative Density (%): 60.5
Applied Stress Ratio: 0.22
Controlled Parameter: Stress
Initial Effective Stress (kPa): 100
Frequency (Hz): 10

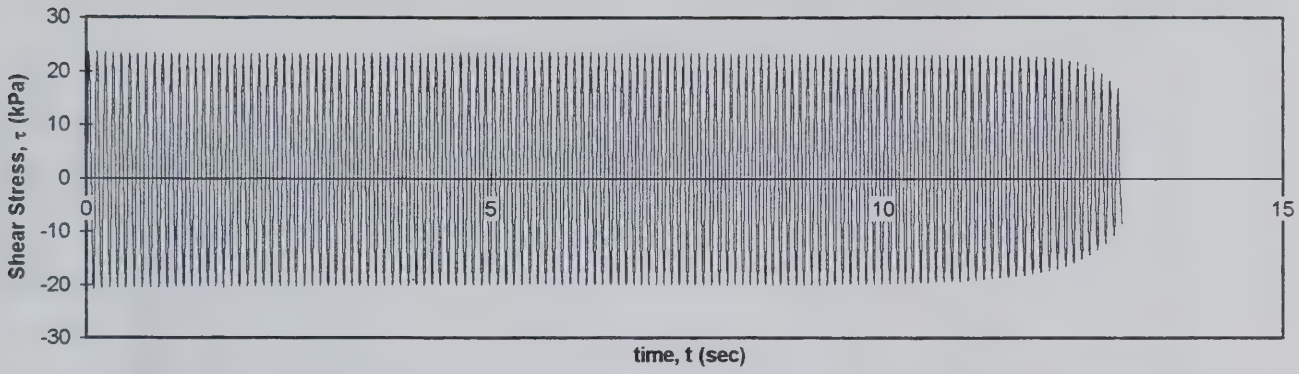

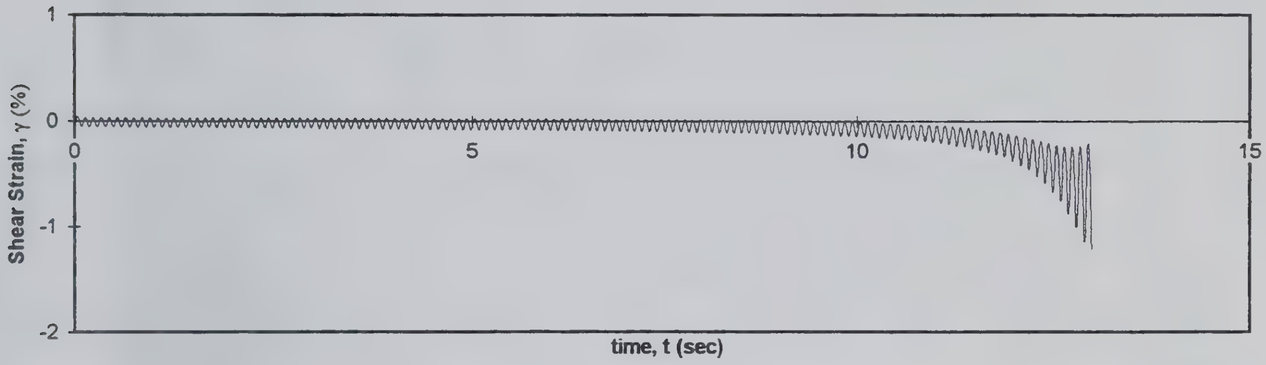

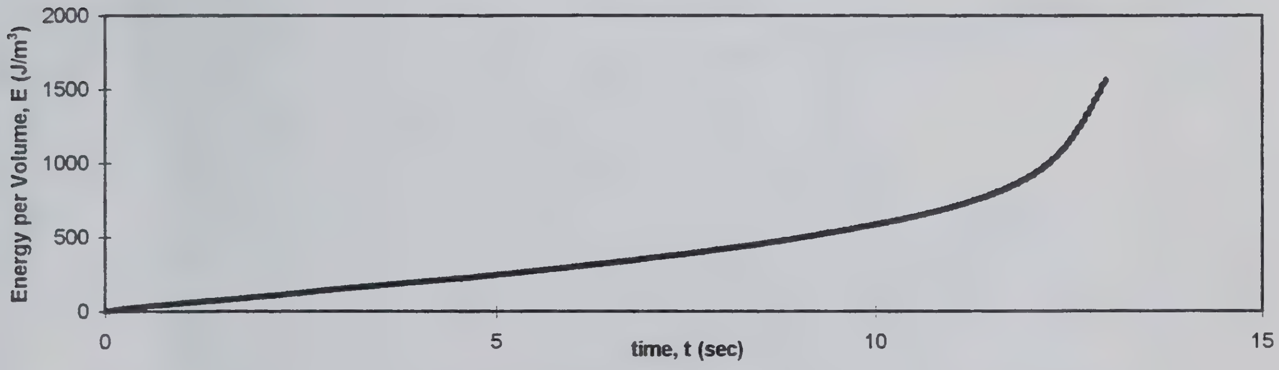

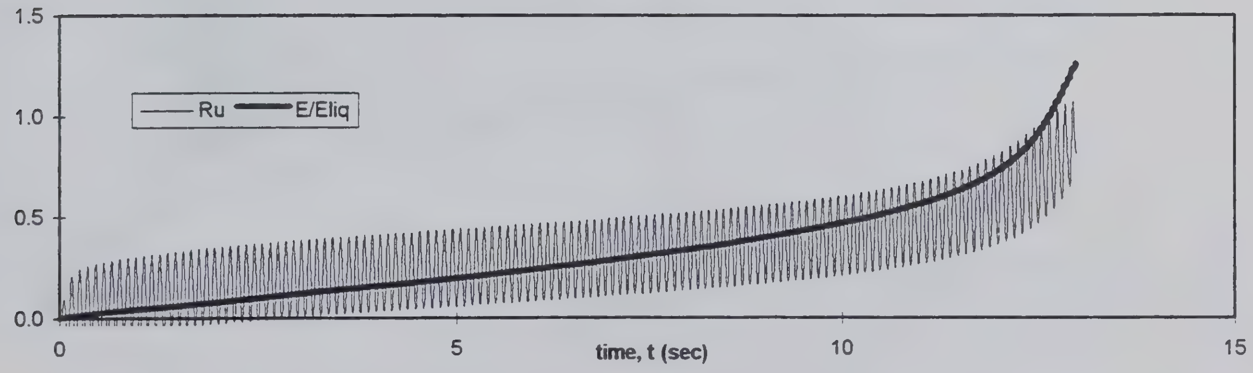

Test I.D.:	MONT15	**Controlled Parameter:**	Stress
Relative Density (%):	60.5	**Initial Effective Stress (kPa):**	100
Applied Stress Ratio:	0.22	**Frequency (Hz):**	10

Shear Stress vs. Shear Strain

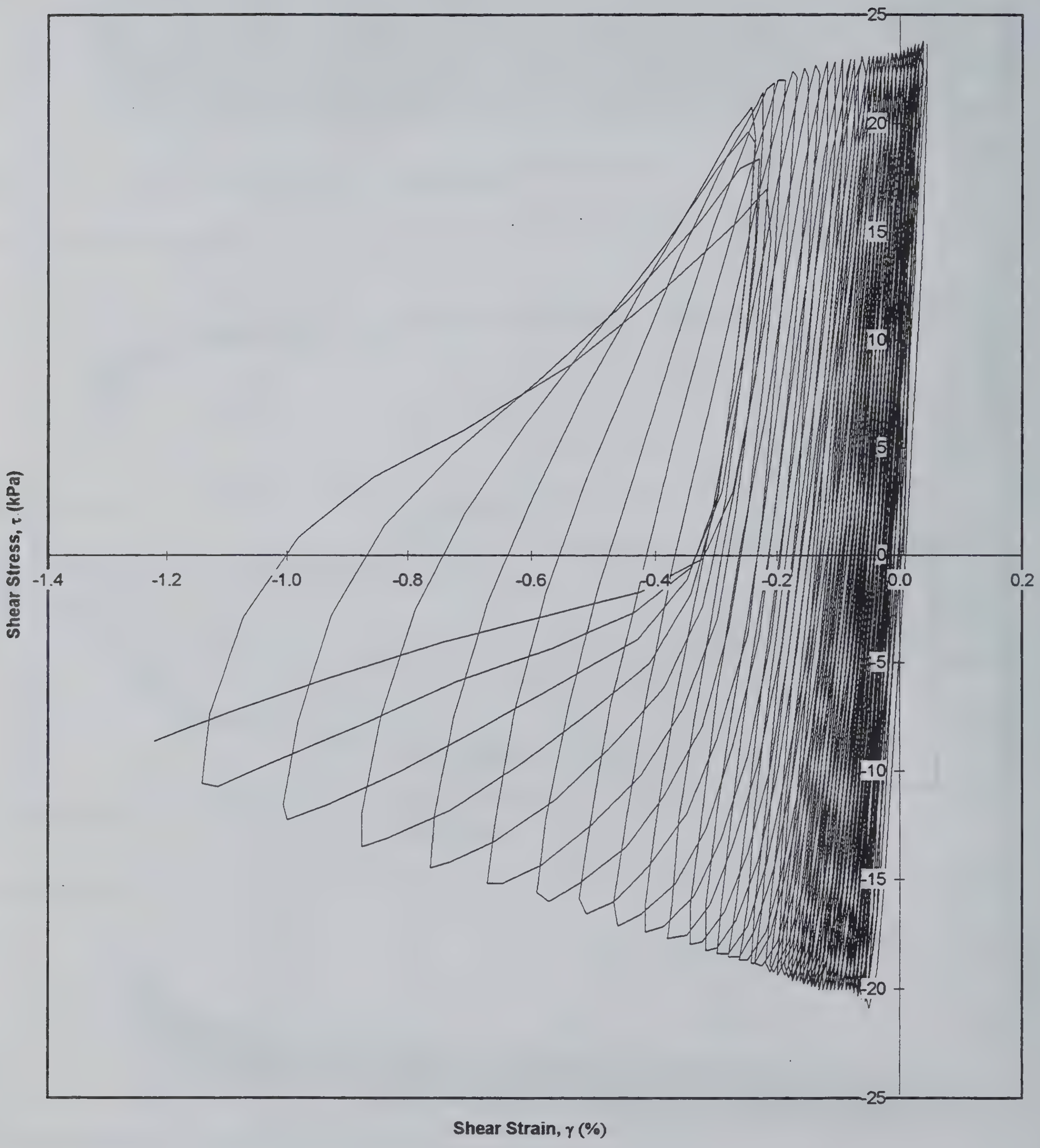

d:\nit\itp\cy_files\MONT15.XLS

8/15/96 11:28 AM

Test I.D.:	MONT17	**Controlled Parameter:**	Strain
Relative Density (%):	61	**Initial Effective Stress (kPa):**	100
Applied Shear Strain (%):	0.25	**Frequency (Hz):**	1

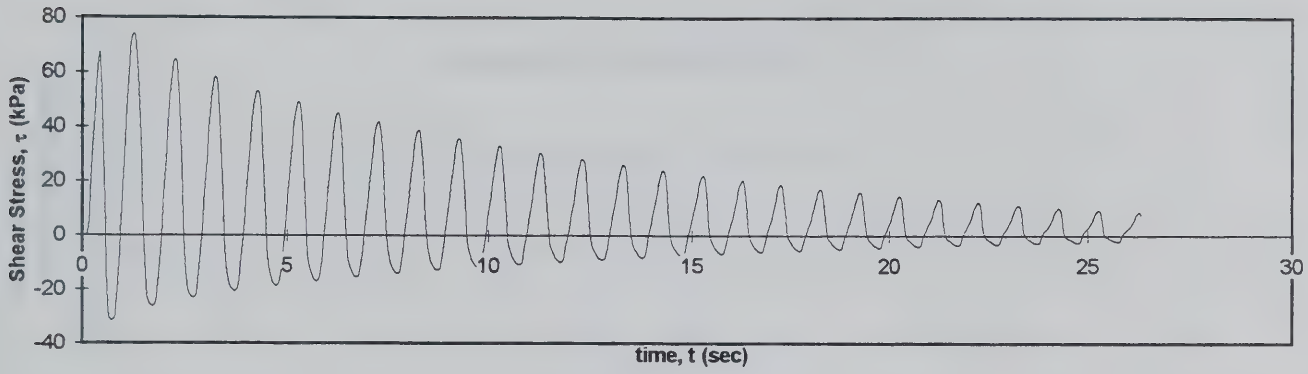

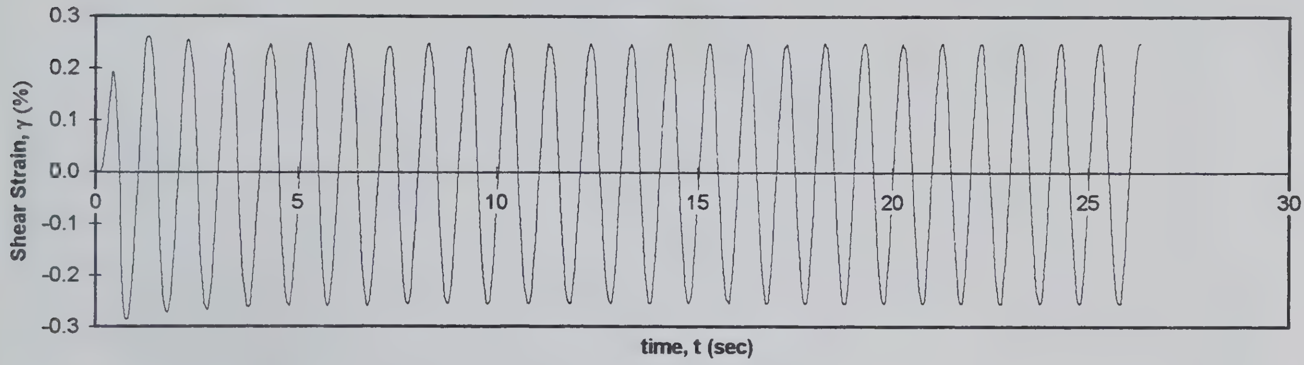

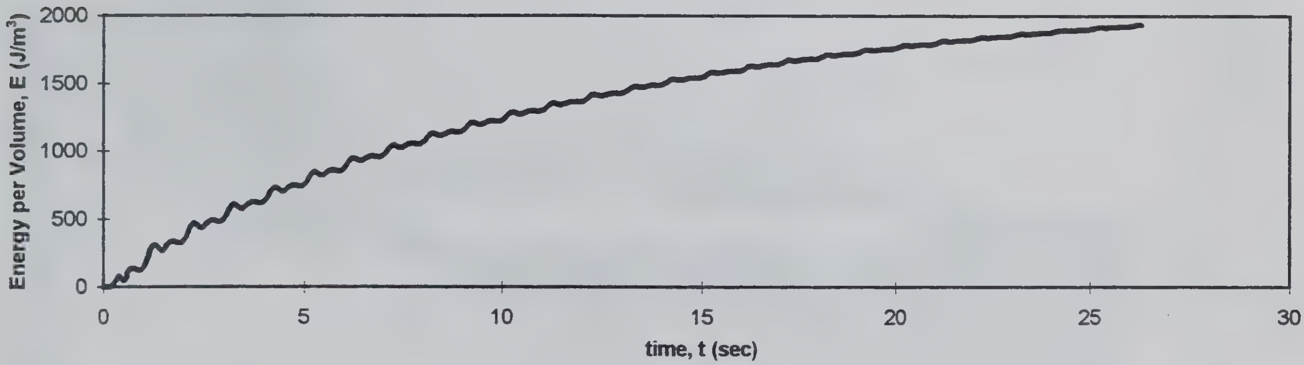

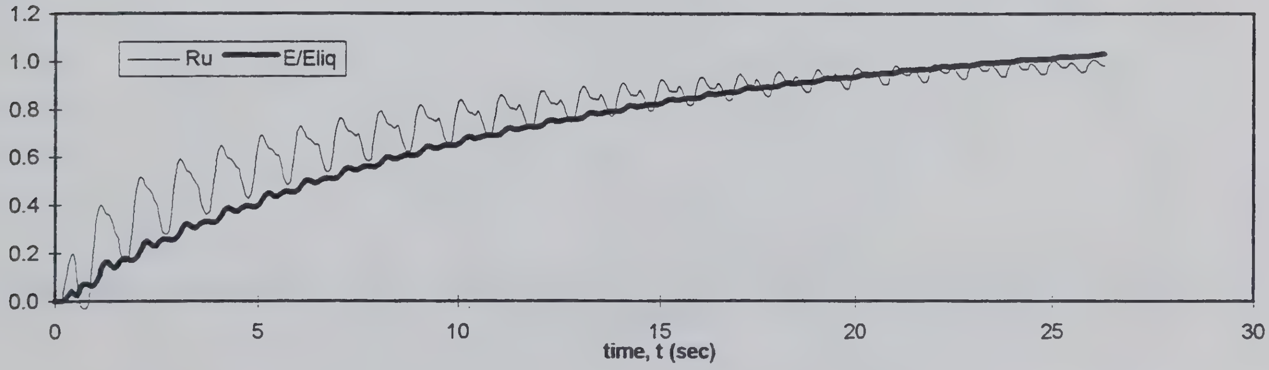

Test I.D.:	MONT17	**Controlled Parameter:**	Strain
Relative Density (%):	61	**Initial Effective Stress (kPa):**	100
Applied Shear Strain (%):	0.25	**Frequency (Hz):**	1

Shear Stress vs. Shear Strain

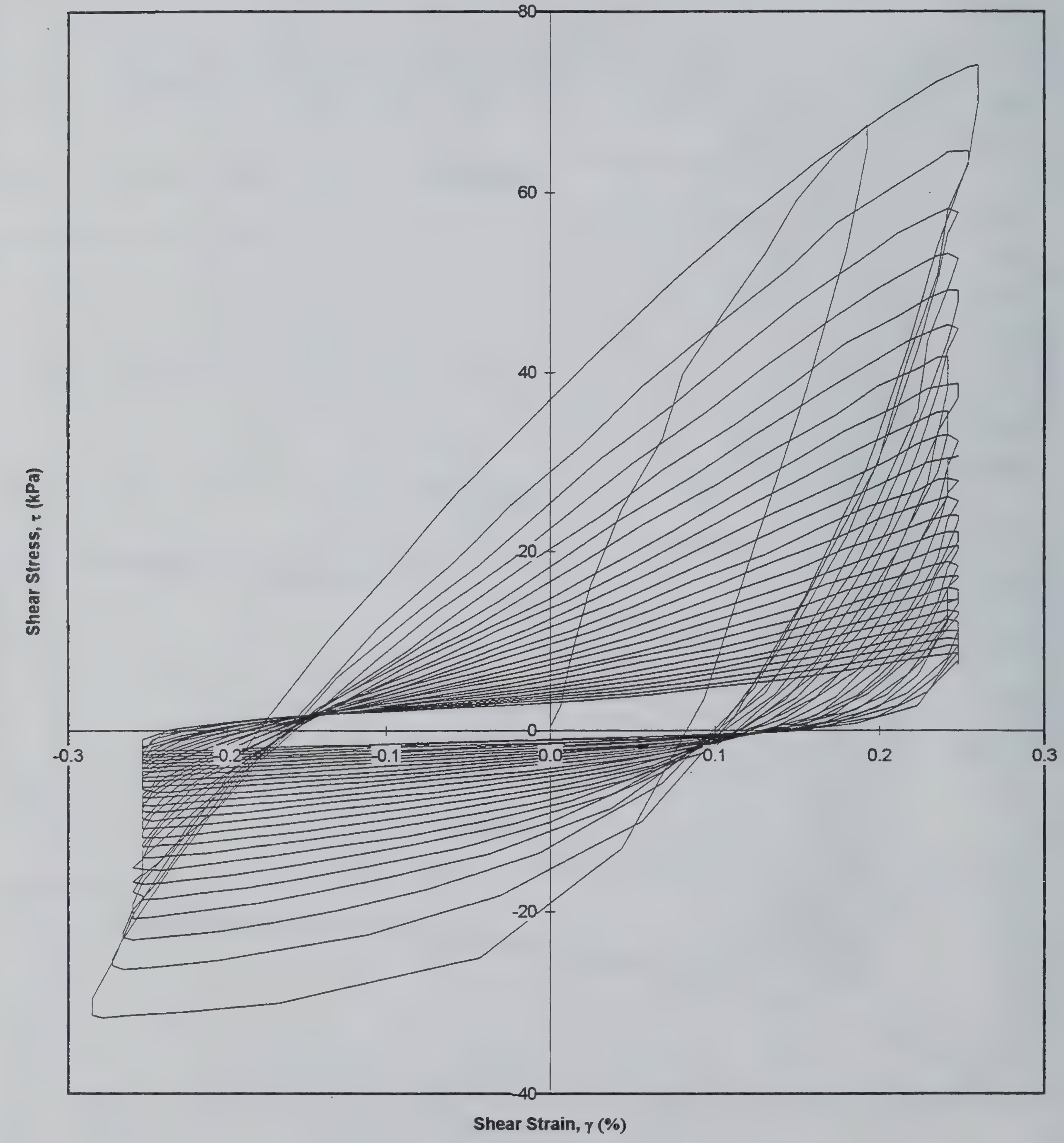

d:\nit\itp\cy_files\MONT17.XLS

8/15/96 11:31 AM

Test I.D.:	MONT18	**Controlled Parameter:**	Strain
Relative Density (%):	61	**Initial Effective Stress (kPa):**	100
Applied Shear Strain (%):	0.25	**Frequency (Hz):**	10

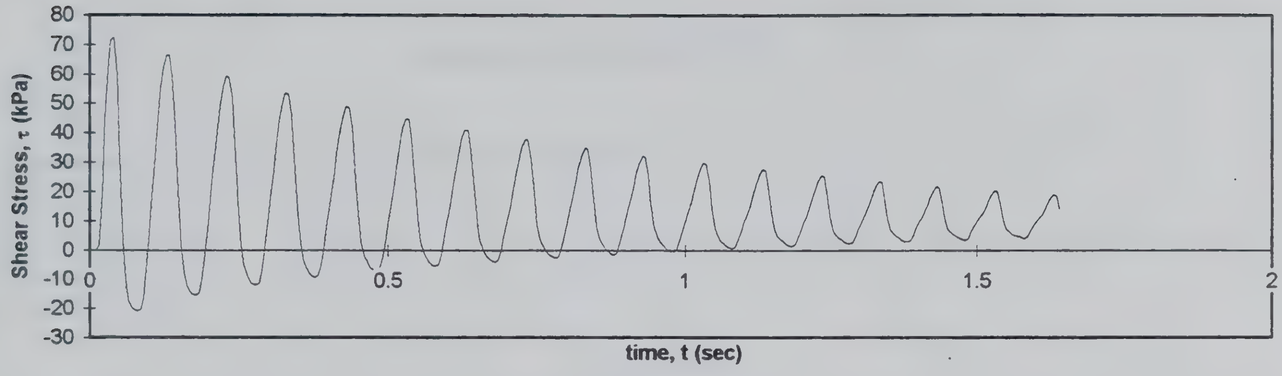

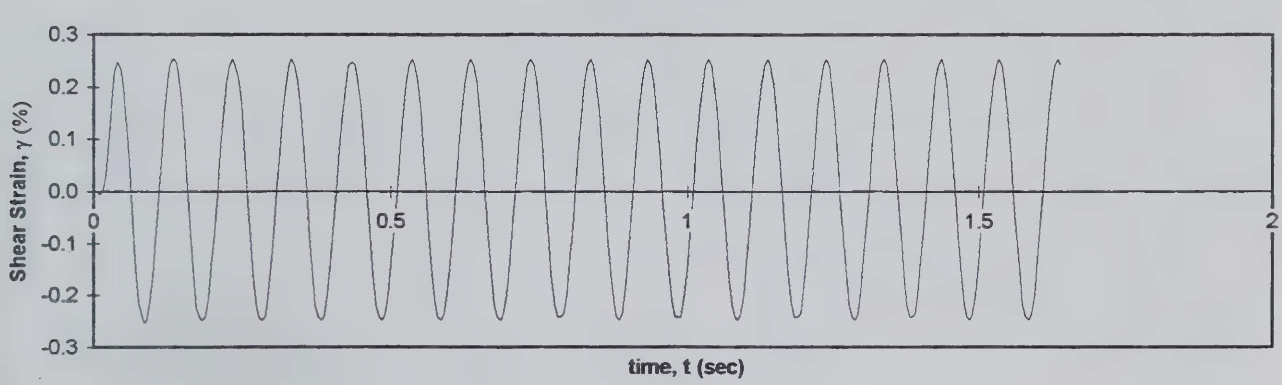

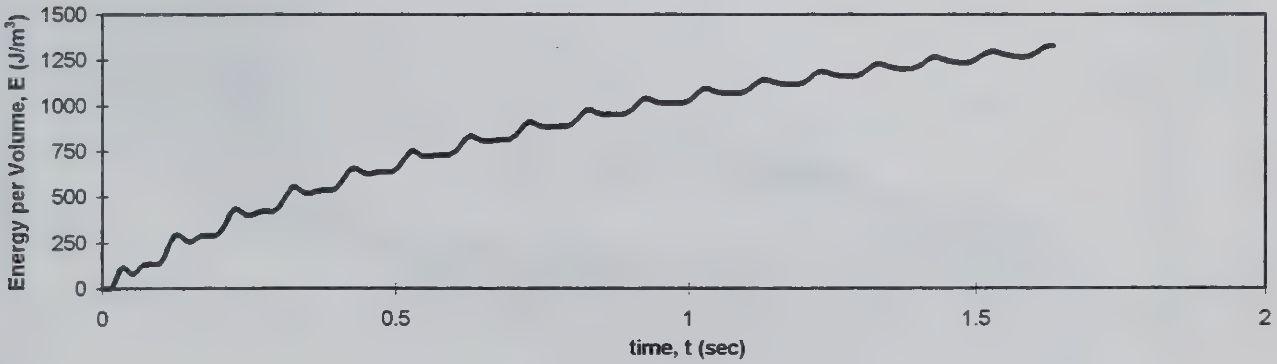

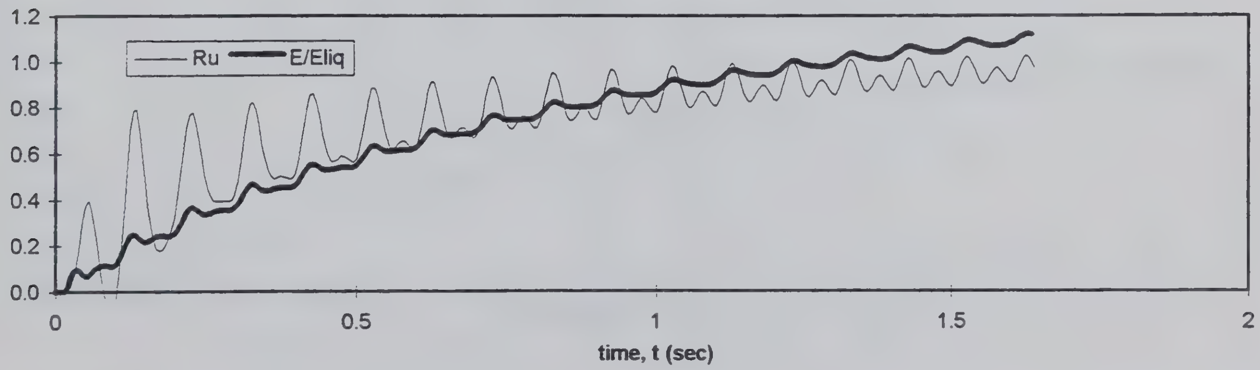

Test I.D.:	MONT18	**Controlled Parameter:**	Strain
Relative Density (%):	61	**Initial Effective Stress (kPa):**	100
Applied Shear Strain (%):	0.25	**Frequency (Hz):**	10

Shear Stress vs. Shear Strain

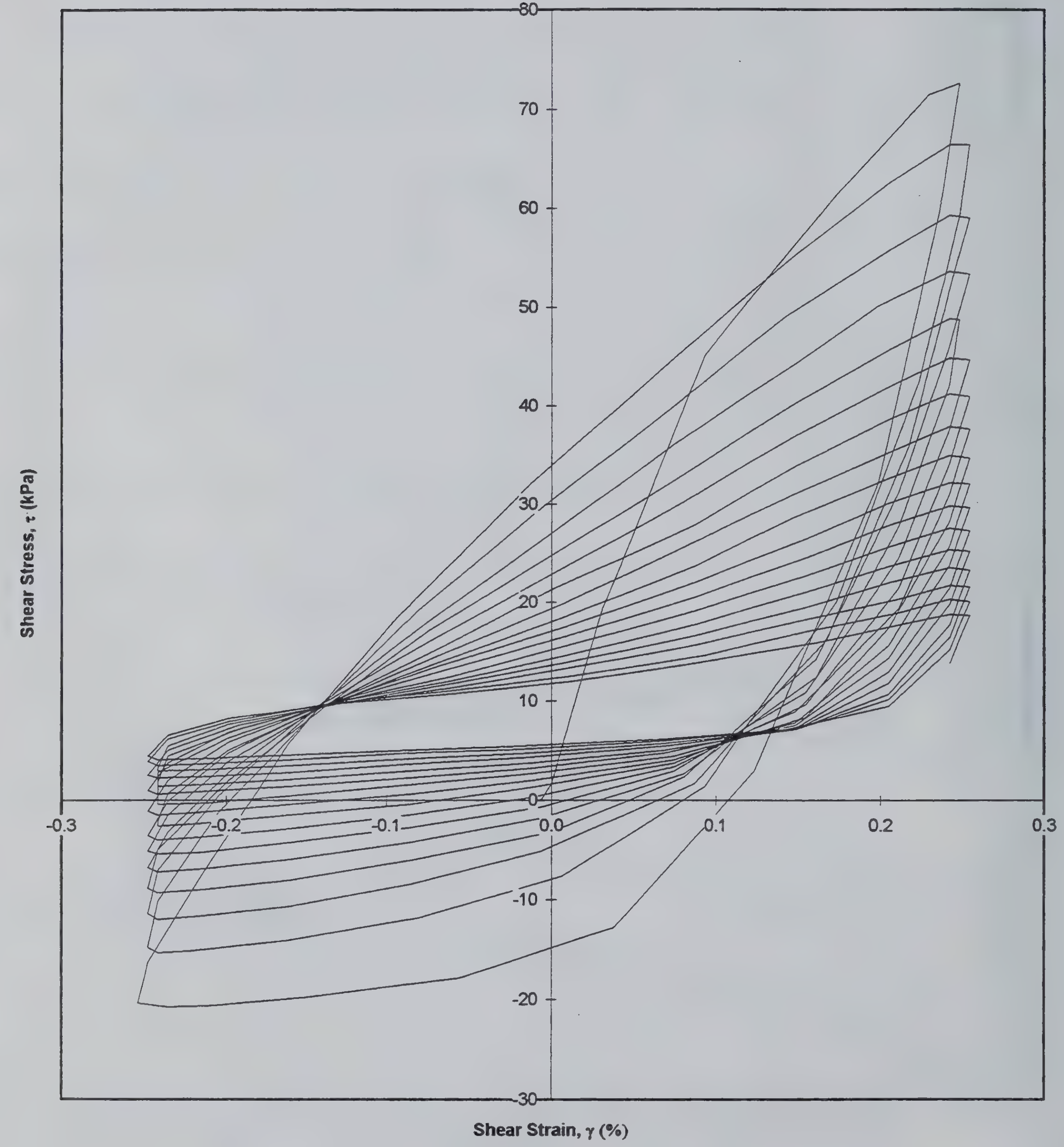

Test I.D.:	MONT19	**Controlled Parameter:**	Strain
Relative Density (%):	60.6	**Initial Effective Stress (kPa):**	100
Applied Shear Strain (%):	0.25	**Frequency (Hz):**	15

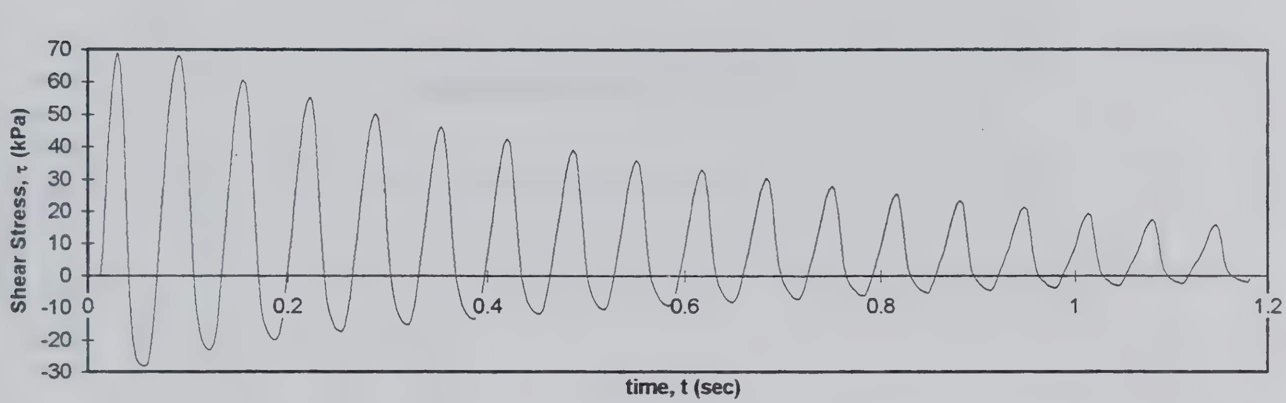

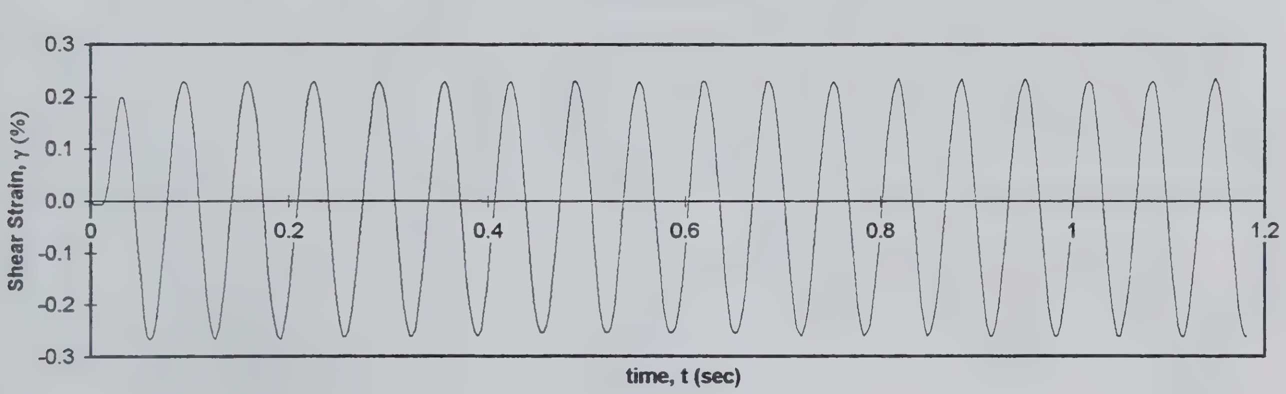

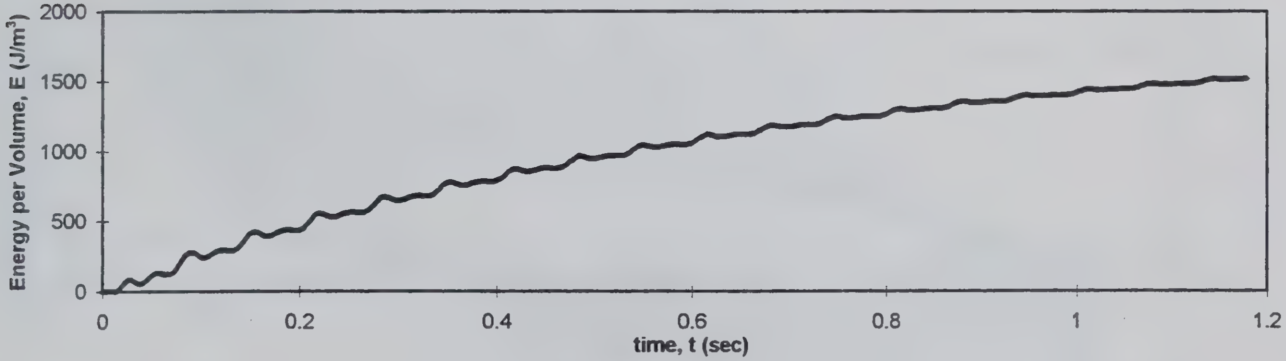

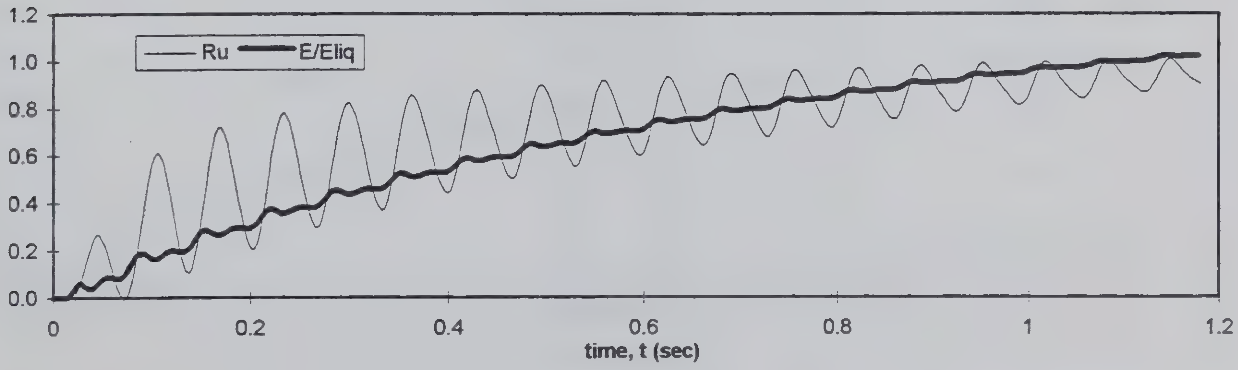

Test I.D.:	MONT19	**Controlled Parameter:**	Strain
Relative Density (%):	60.6	**Initial Effective Stress (kPa):**	100
Applied Shear Strain (%):	0.25	**Frequency (Hz):**	15

Shear Stress vs. Shear Strain

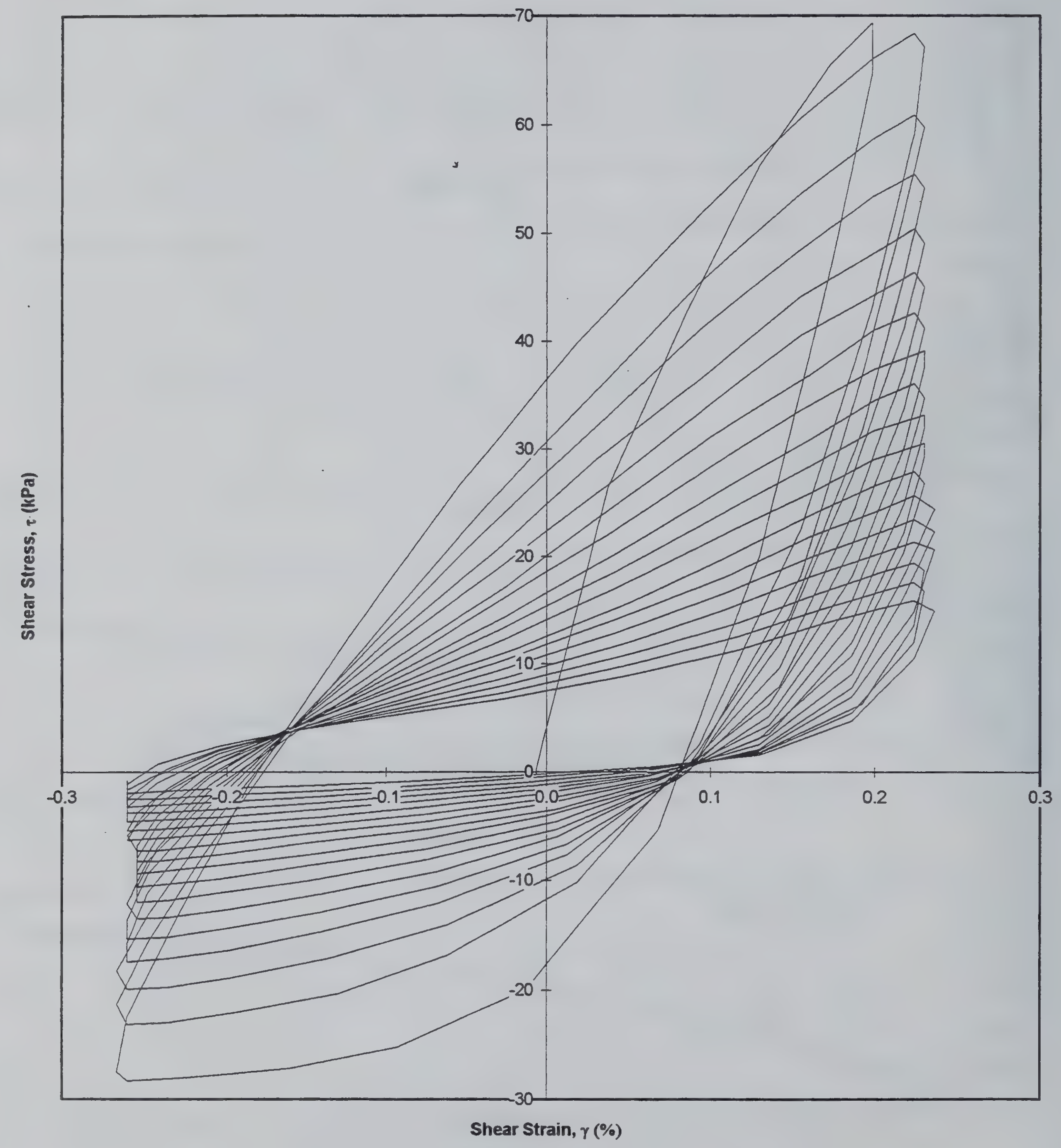

d:\nit\itp\cy_files\MONT19.XLS

8/15/96 11:42 AM

Test I.D.: MONT20
Relative Density (%): 40.9
Applied Shear Strain (%): 0.25

Controlled Parameter: Strain
Initial Effective Stress (kPa): 100
Frequency (Hz): 1

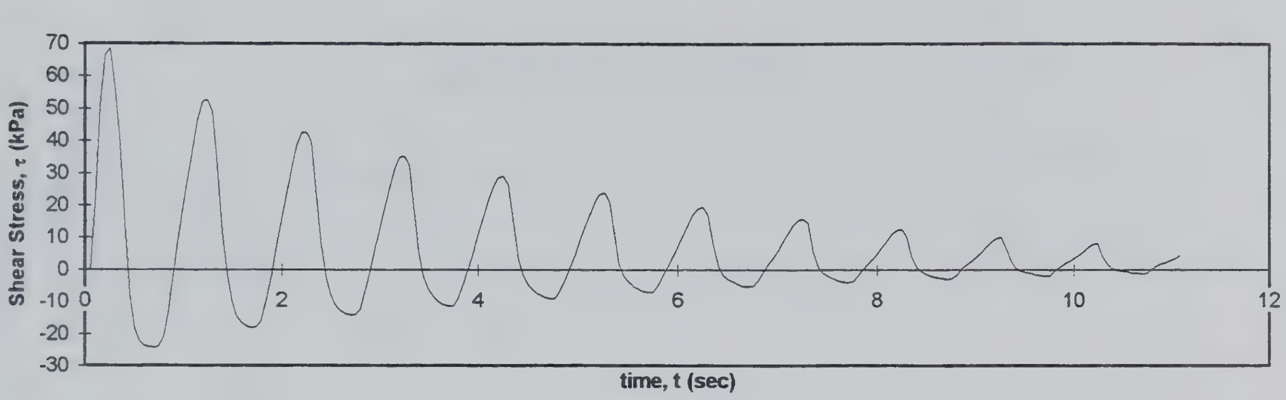

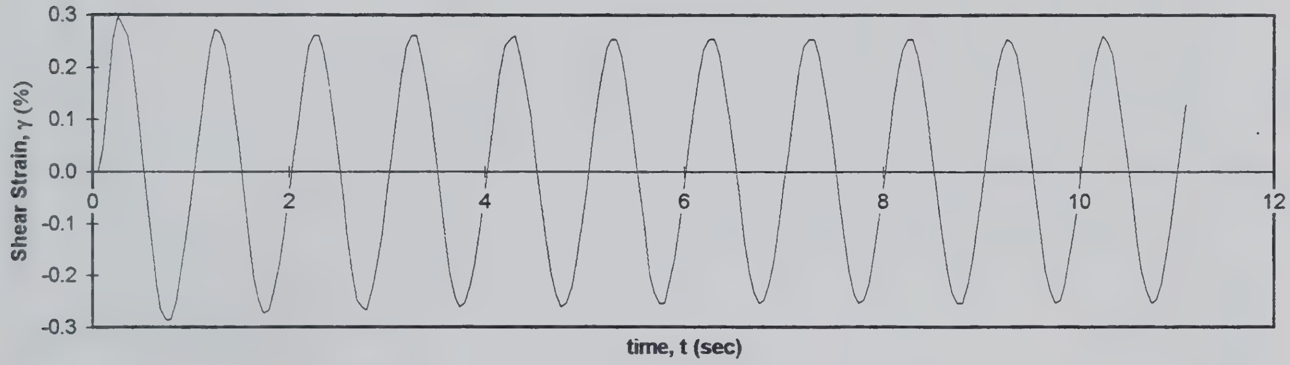

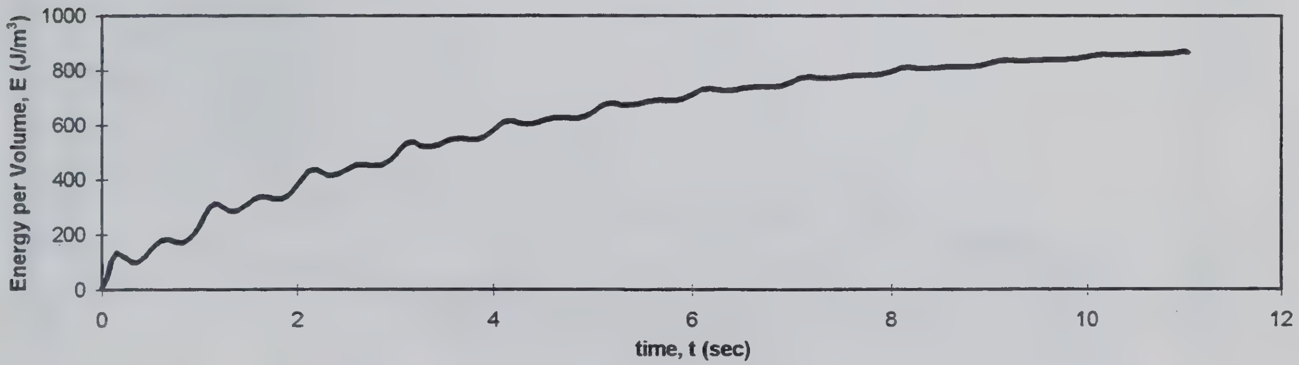

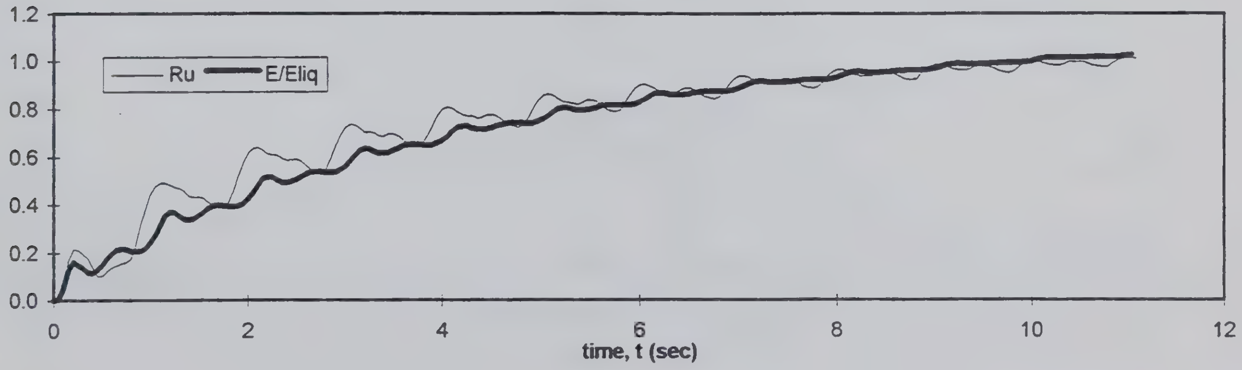

Test I.D.:	MONT20	**Controlled Parameter:**	Strain
Relative Density (%):	40.9	**Initial Effective Stress (kPa):**	100
Applied Shear Strain (%):	0.25	**Frequency (Hz):**	1

Shear Stress vs. Shear Strain

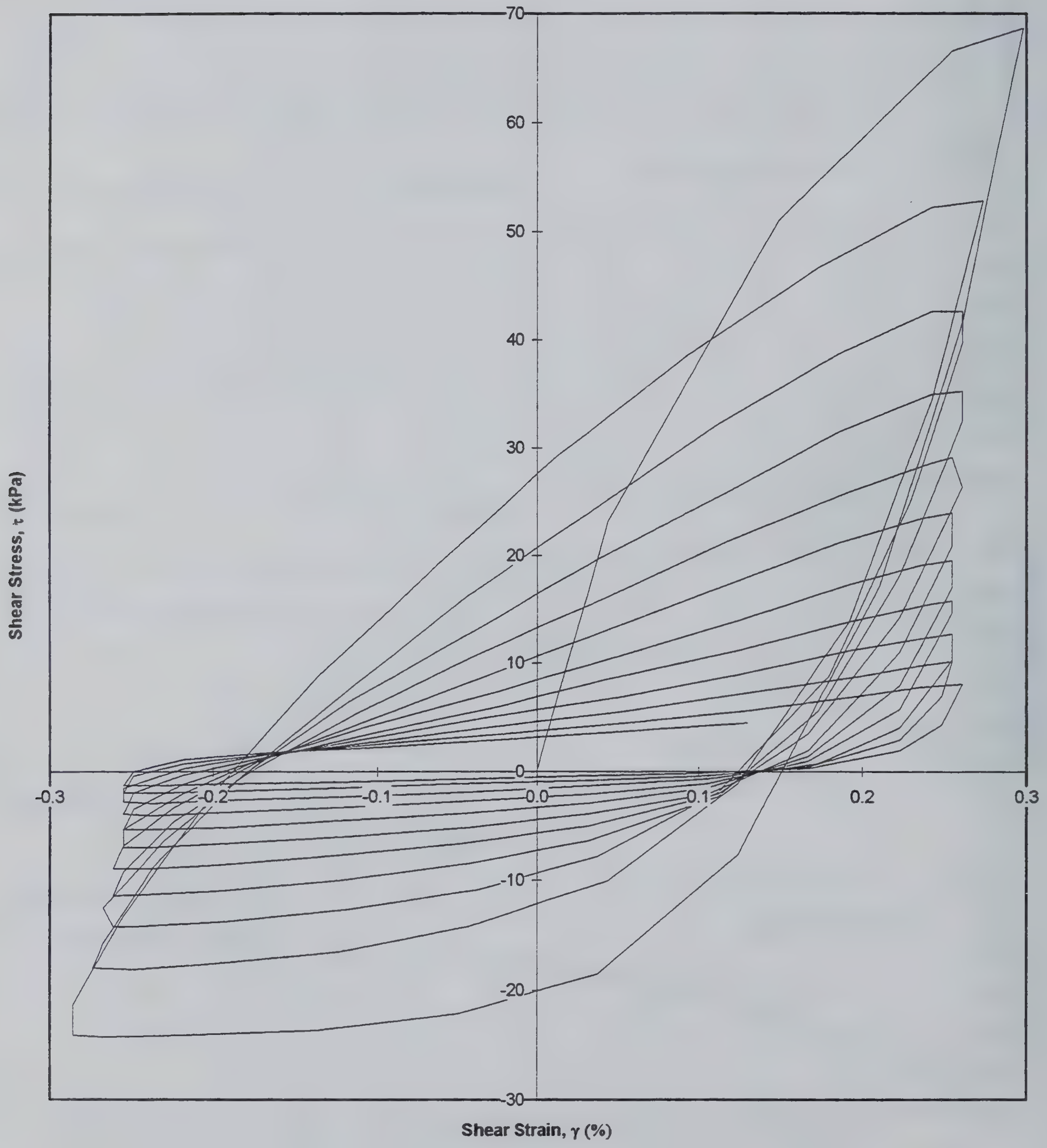

d:\nit\itp\cy_files\MONT20.XLS

8/15/96 11:47 AM

Test I.D.:	MONT21	**Controlled Parameter:**	Strain
Relative Density (%):	41.8	**Initial Effective Stress (kPa):**	100
Applied Shear Strain (%):	0.15	**Frequency (Hz):**	1

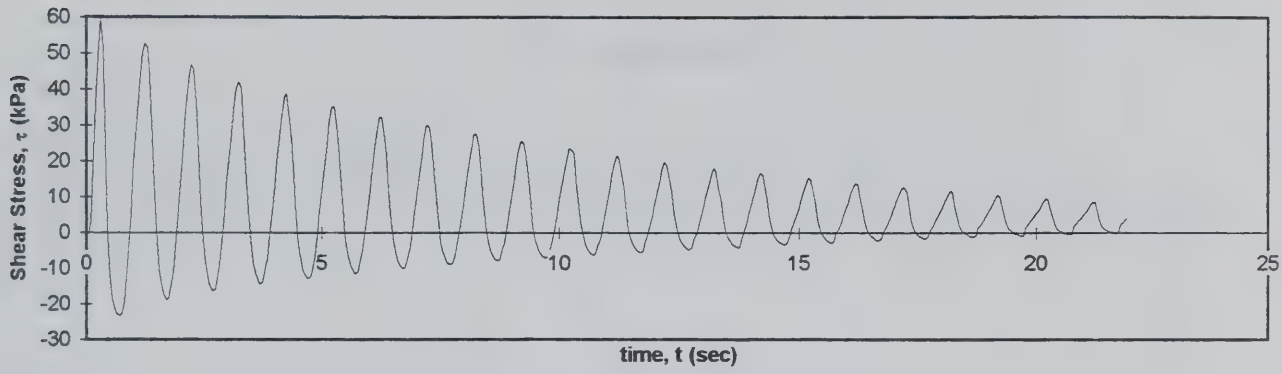

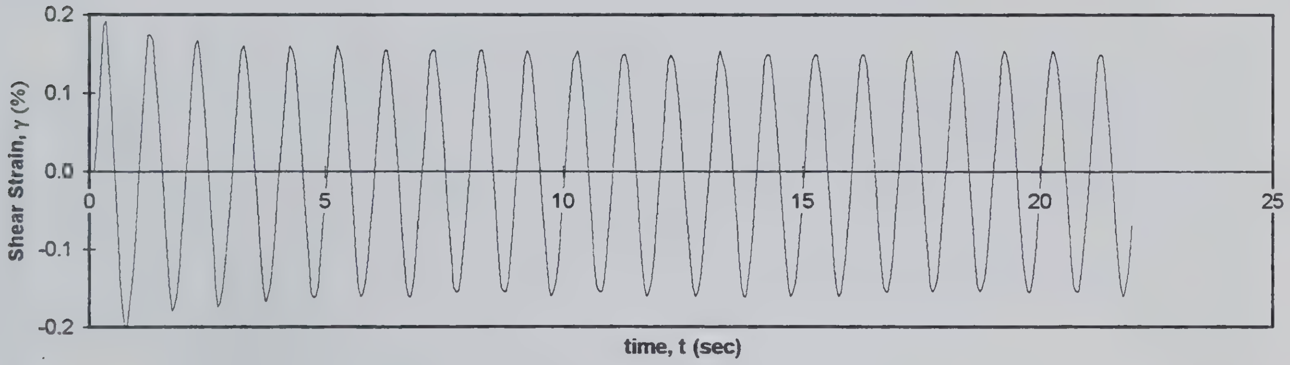

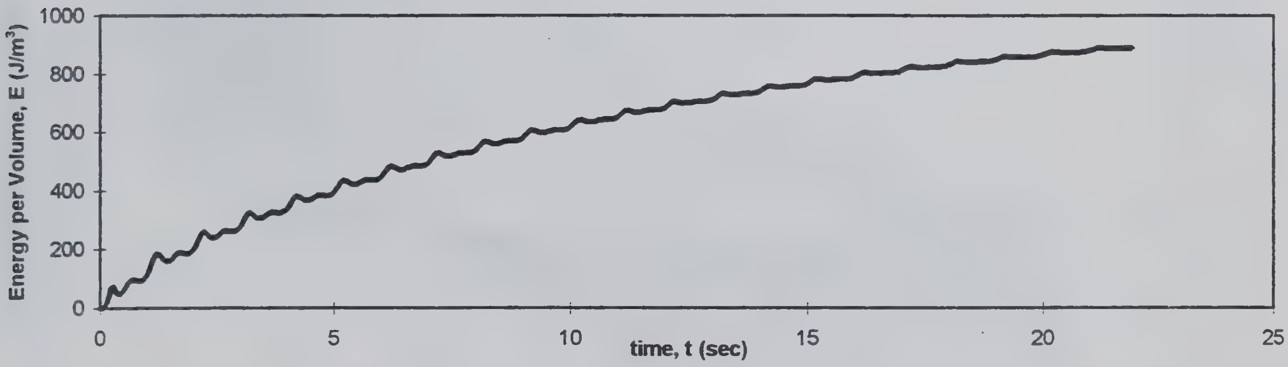

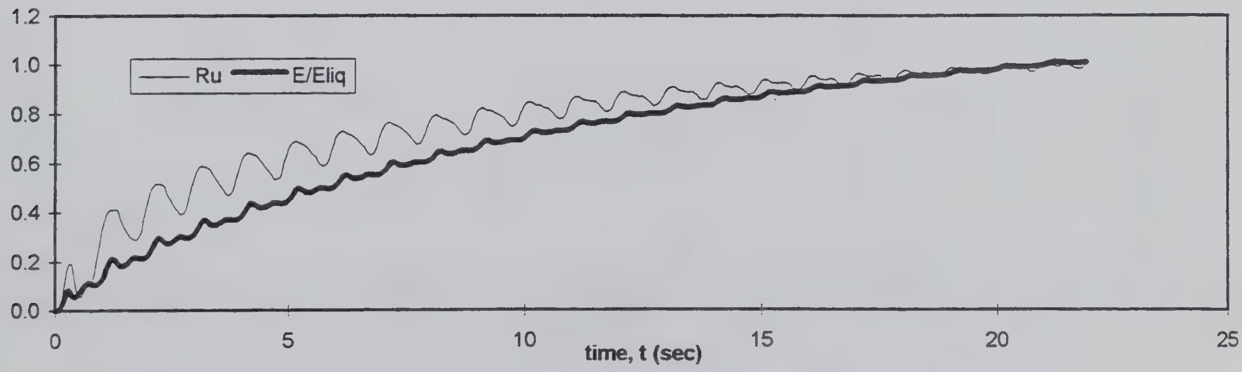

Test I.D.:	MONT21	**Controlled Parameter:**	Strain
Relative Density (%):	41.8	**Initial Effective Stress (kPa):**	100
Applied Shear Strain (%):	0.15	**Frequency (Hz):**	1

Shear Stress vs. Shear Strain

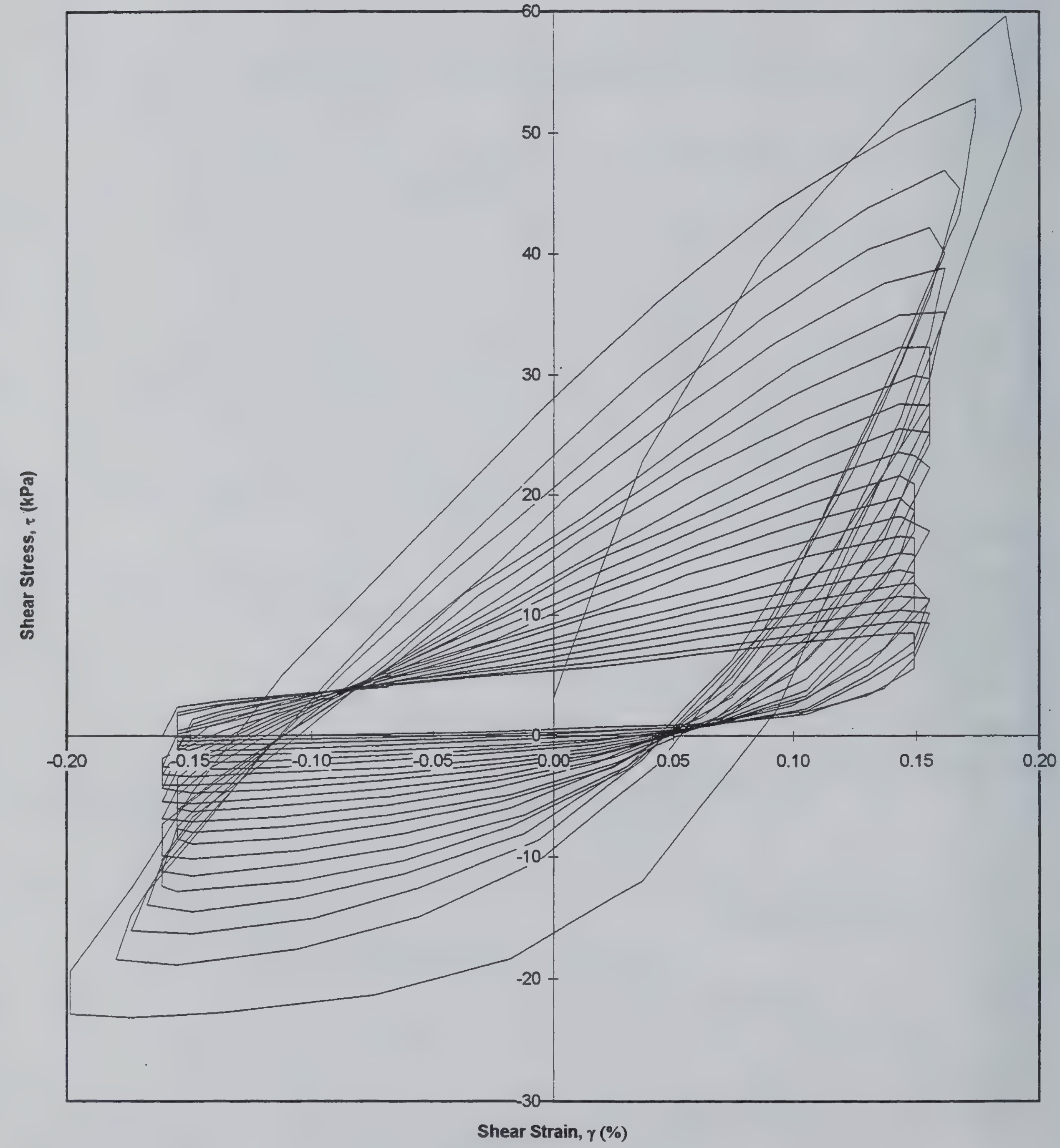

d:\nit\itp\cy_files\MONT21.XLS

8/15/96 11:53 AM

Test I.D.:	MONT22	**Controlled Parameter:**	Strain
Relative Density (%):	42.3	**Initial Effective Stress (kPa):**	100
Applied Shear Strain:	0.08%	**Frequency (Hz):**	1

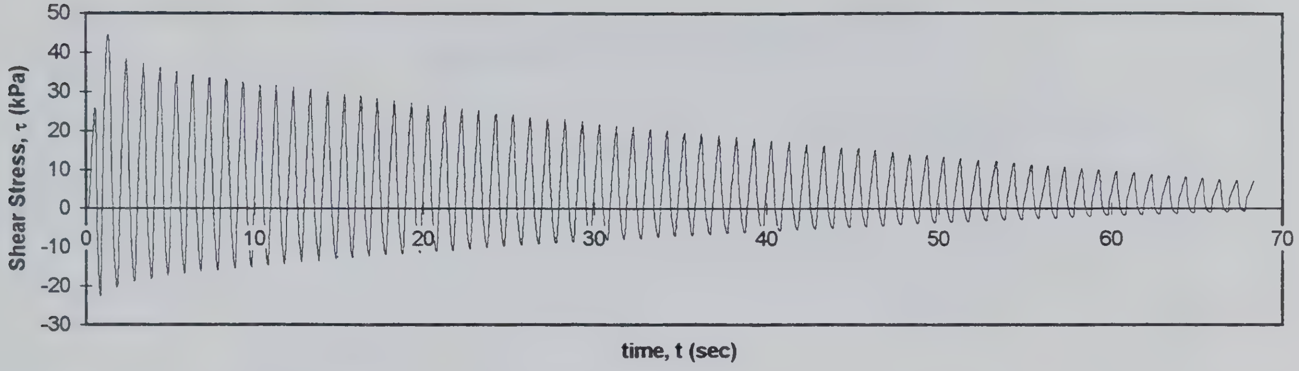

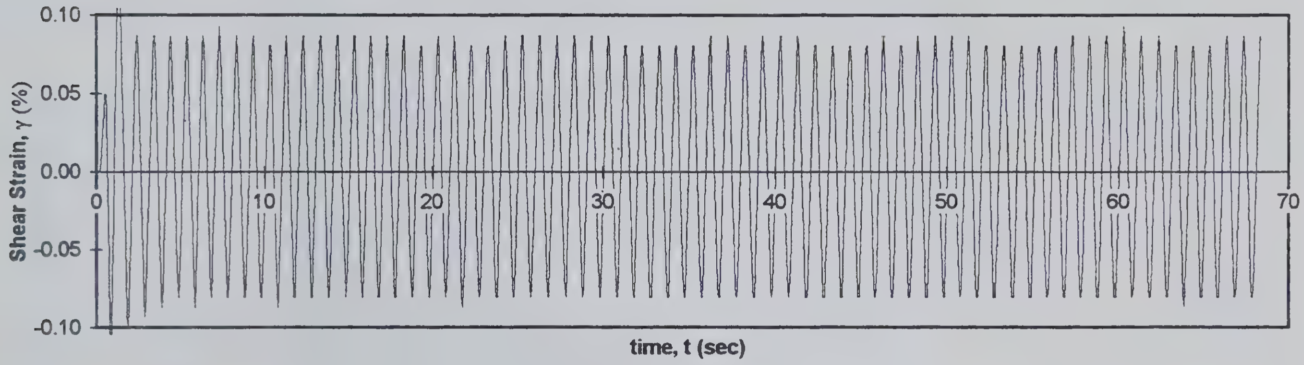

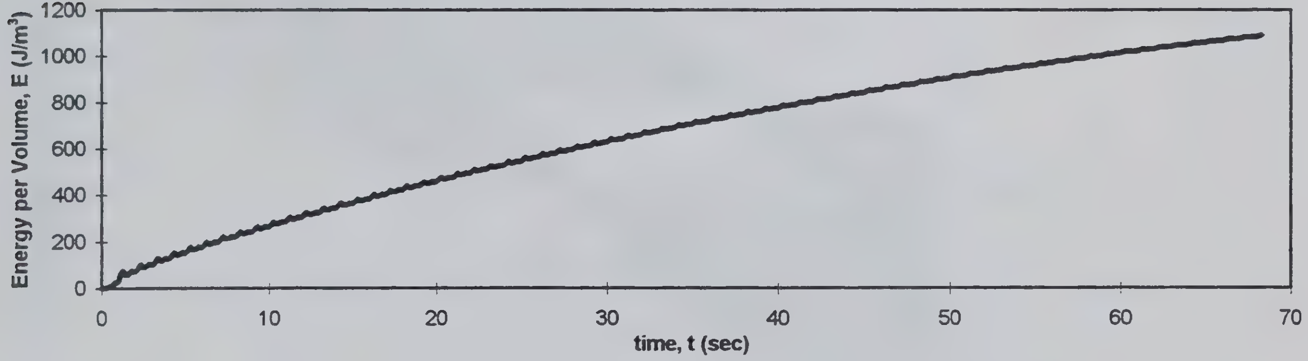

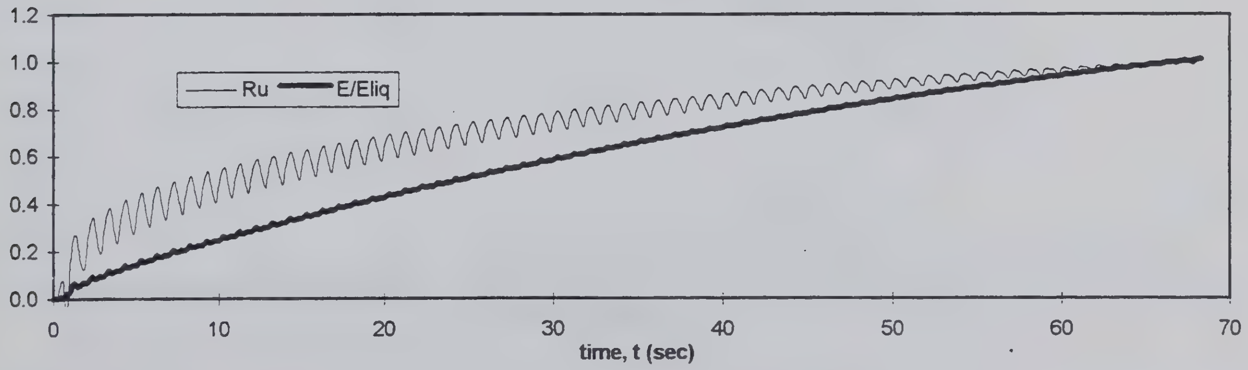

Test I.D.:	MONT22	**Controlled Parameter:**	Strain
Relative Density (%):	42.3	**Initial Effective Stress (kPa):**	100
Applied Shear Strain:	0.08%	**Frequency (Hz):**	1

Shear Stress vs. Shear Strain

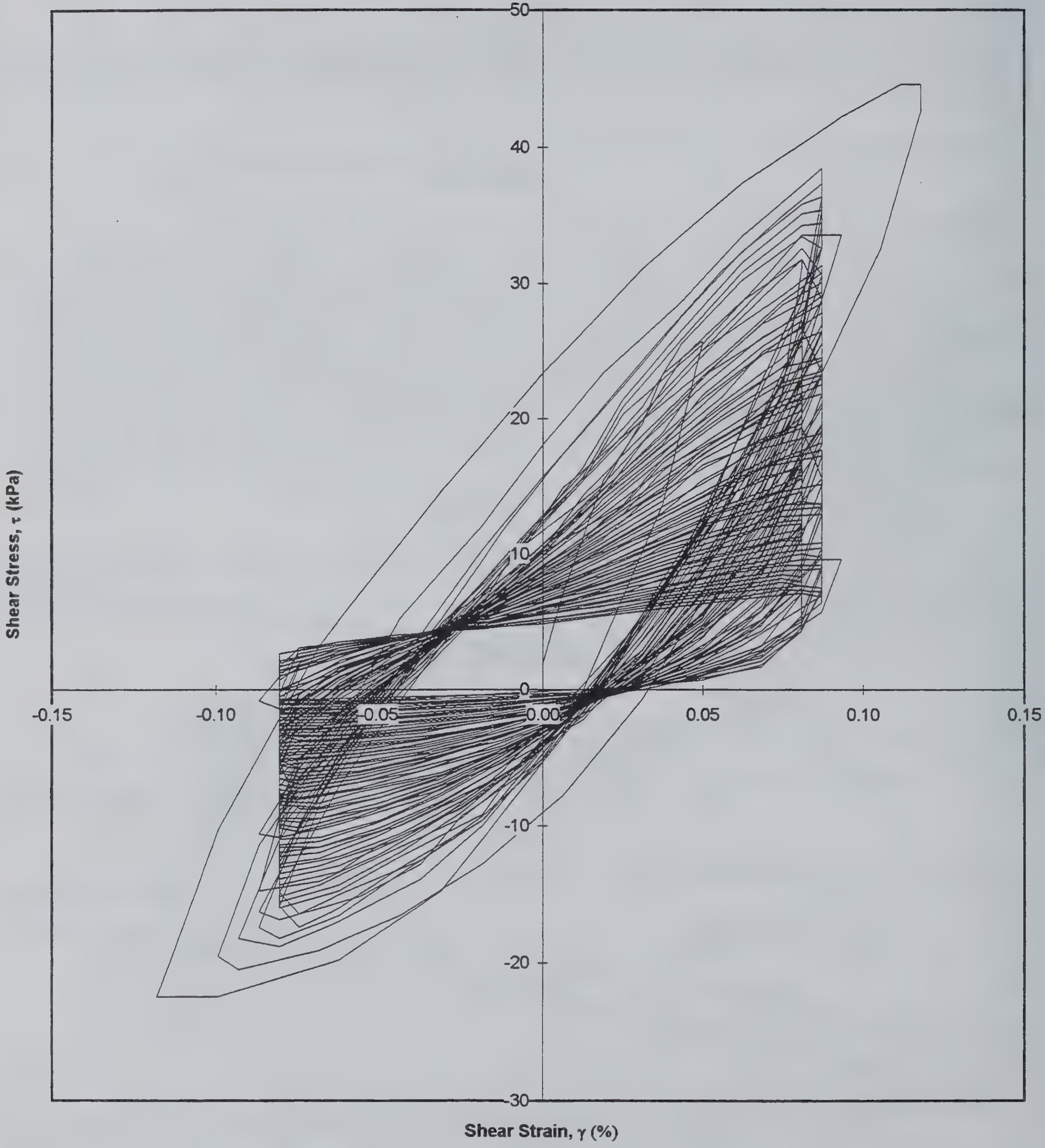

d:\nit\itp\cy_files\MONT22.XLS

8/21/96 9:47 AM

Test I.D.:	MONT24	**Controlled Parameter:**	Stress
Relative Density (%):	51.8	**Initial Effective Stress (kPa):**	100
Applied Stress Ratio:	0.31	**Frequency (Hz):**	1

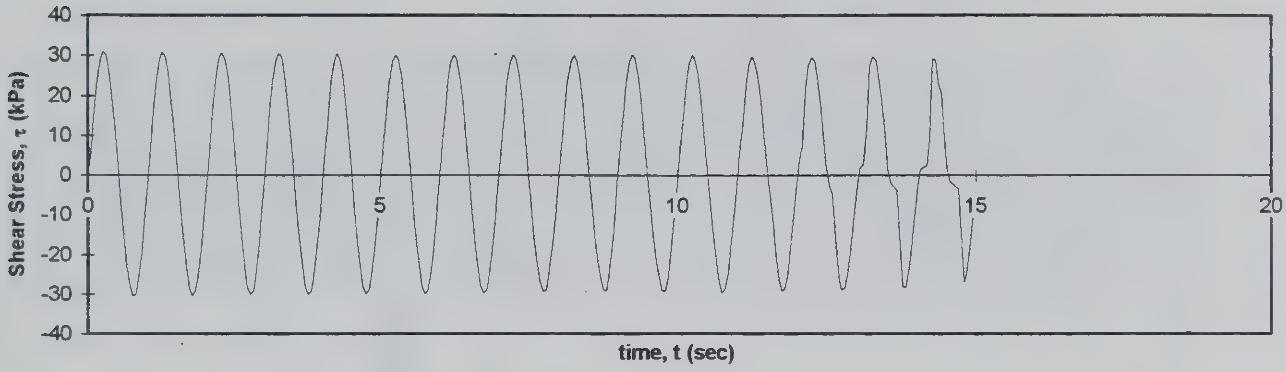

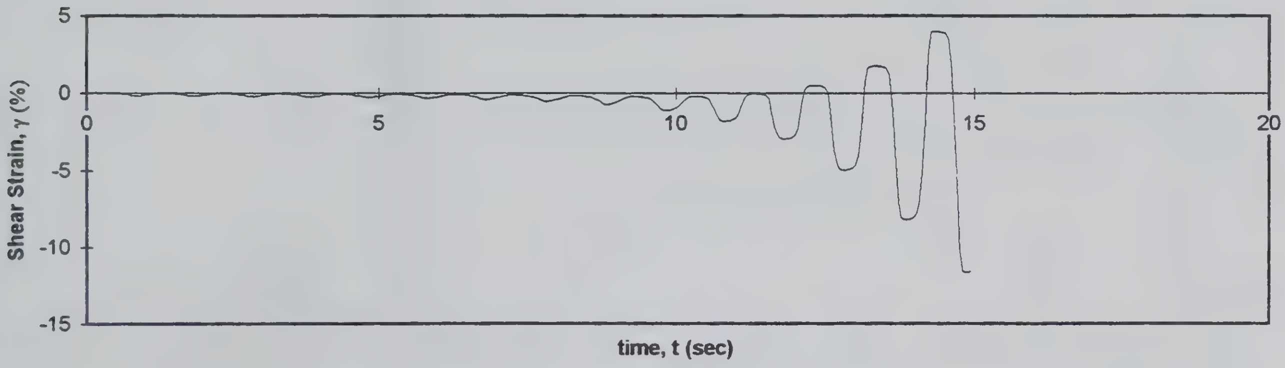

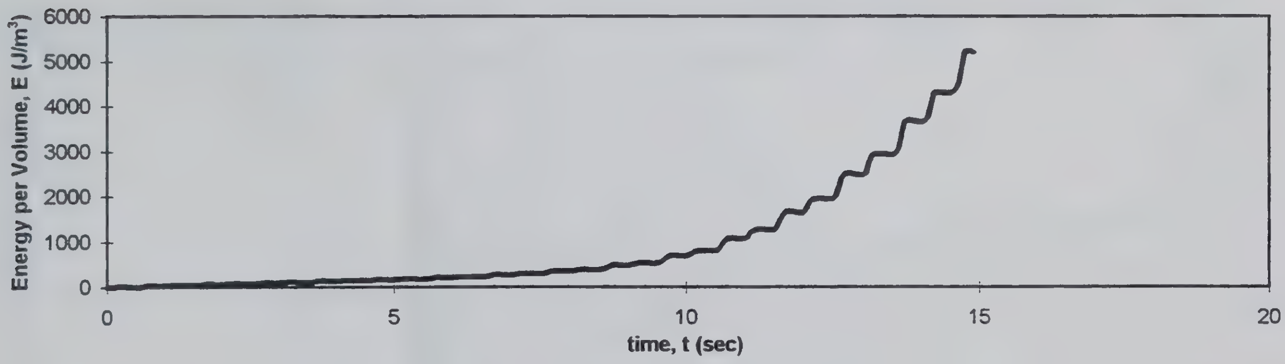

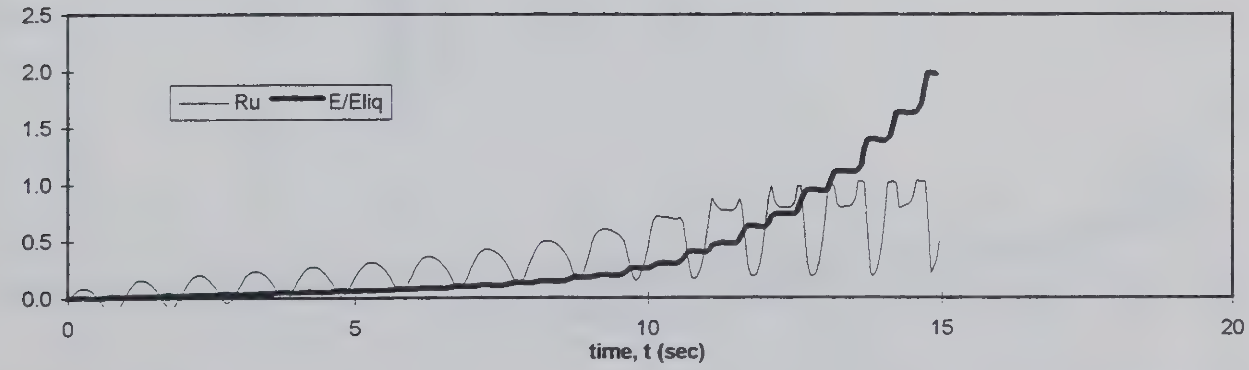

Test I.D.:	MONT24	**Controlled Parameter:**	Stress
Relative Density (%):	51.8	**Initial Effective Stress (kPa):**	100
Applied Stress Ratio:	0.31	**Frequency (Hz):**	1

Shear Stress vs. Shear Strain

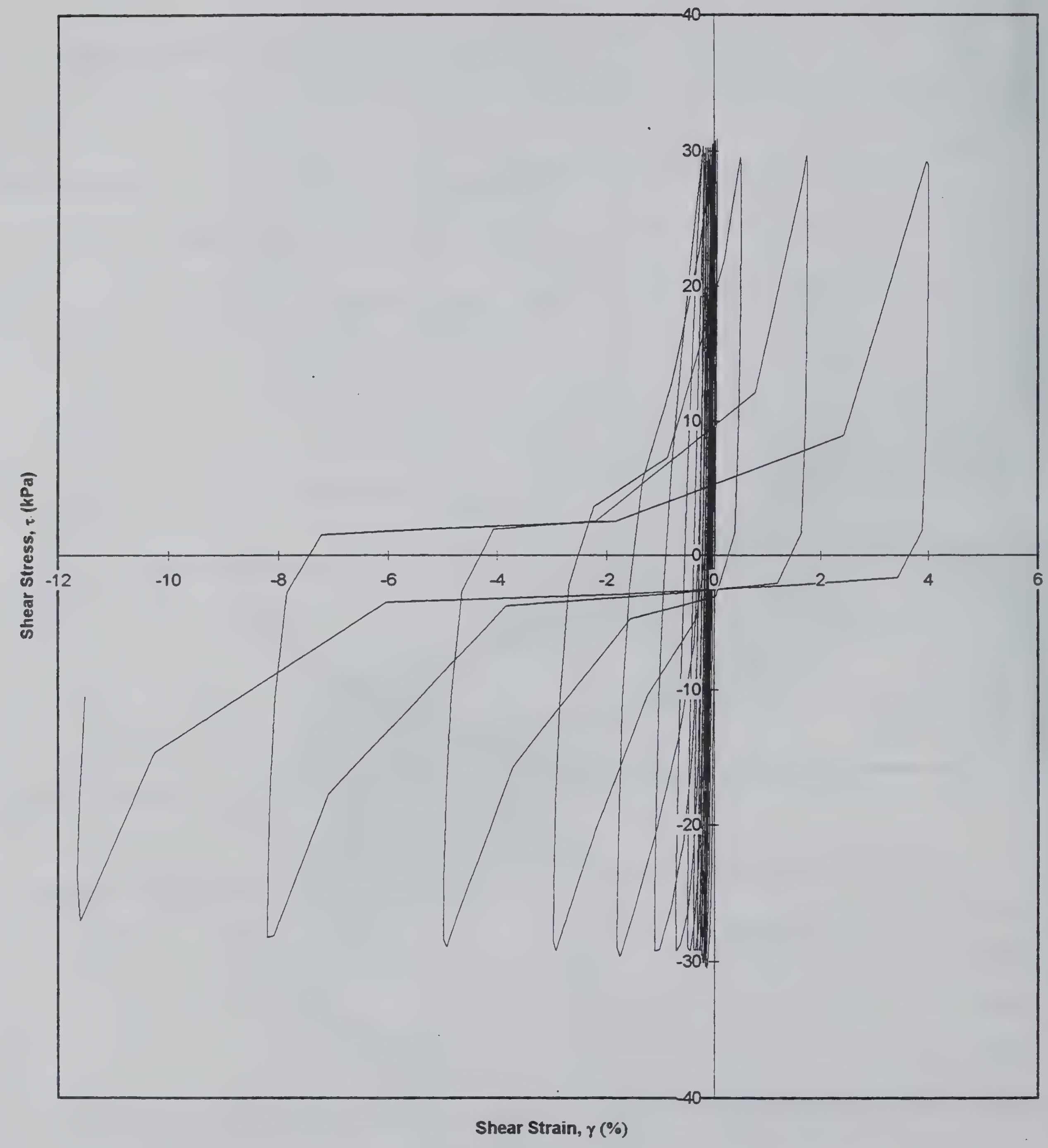

d:\nit\itp\cy_files\MONT24.XLS

8/21/96 9:48 AM

Test I.D.: MONT25
Relative Density (%): 50.4
Applied Stress Ratio: 0.25

Controlled Parameter: Stress
Initial Effective Stress (kPa): 100
Frequency (Hz): 1

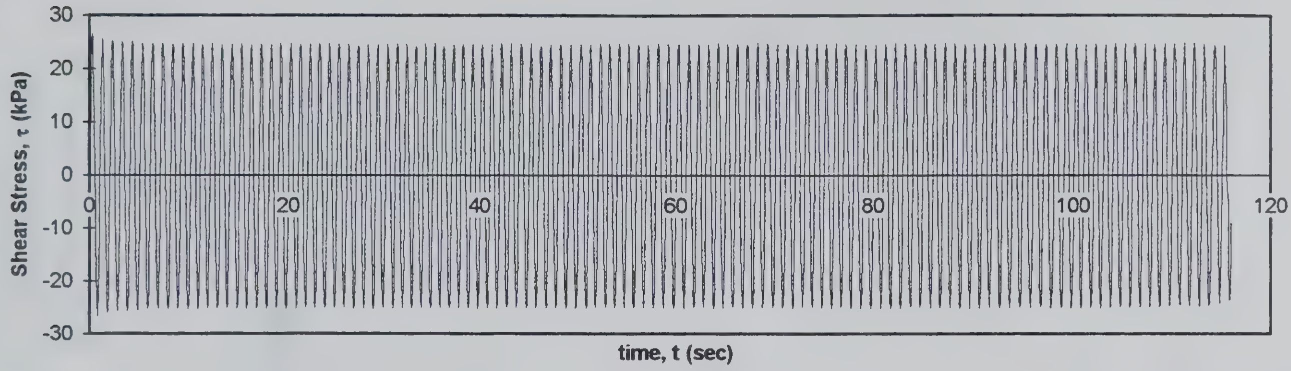

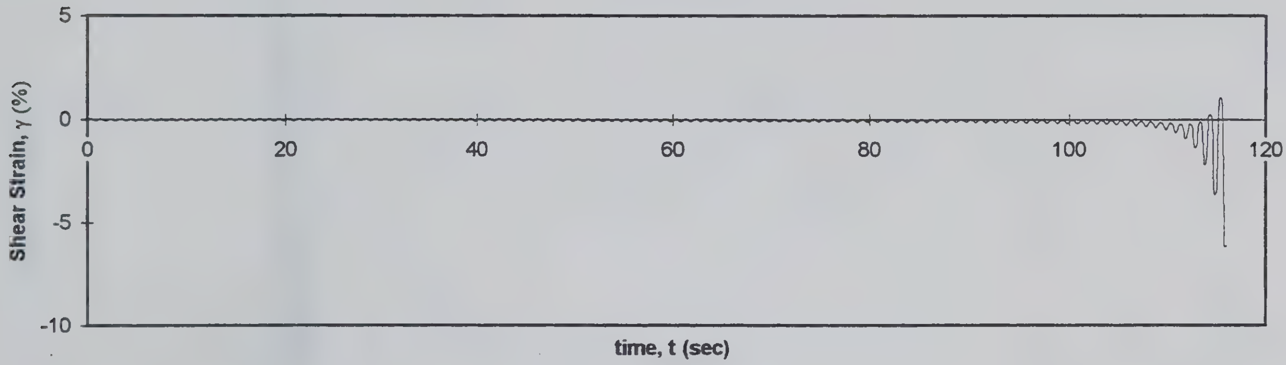

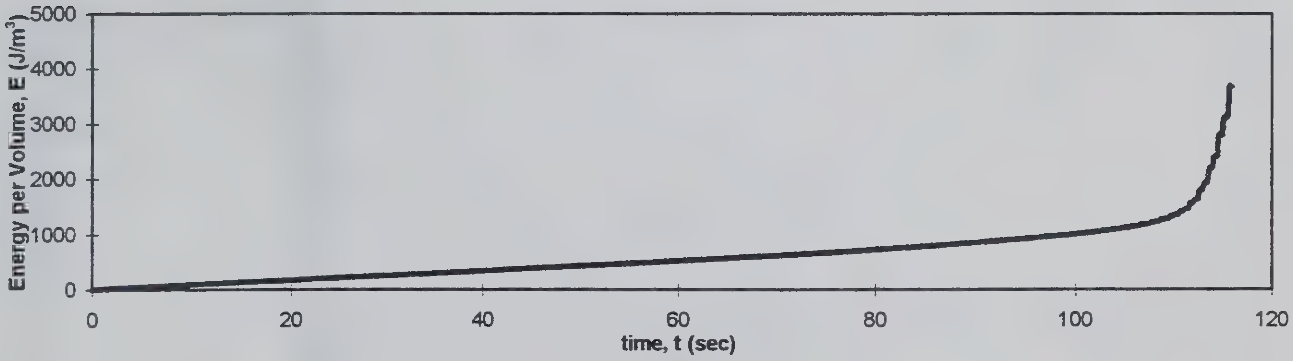

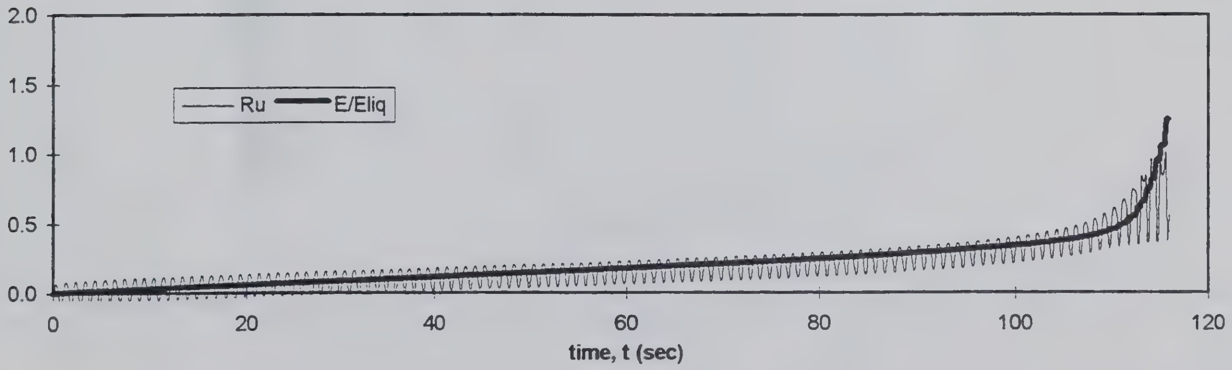

Test I.D.:	MONT25	**Controlled Parameter:**	Stress
Relative Density (%):	50.4	**Initial Effective Stress (kPa):**	100
Applied Stress Ratio:	0.25	**Frequency (Hz):**	1

Shear Stress vs. Shear Strain

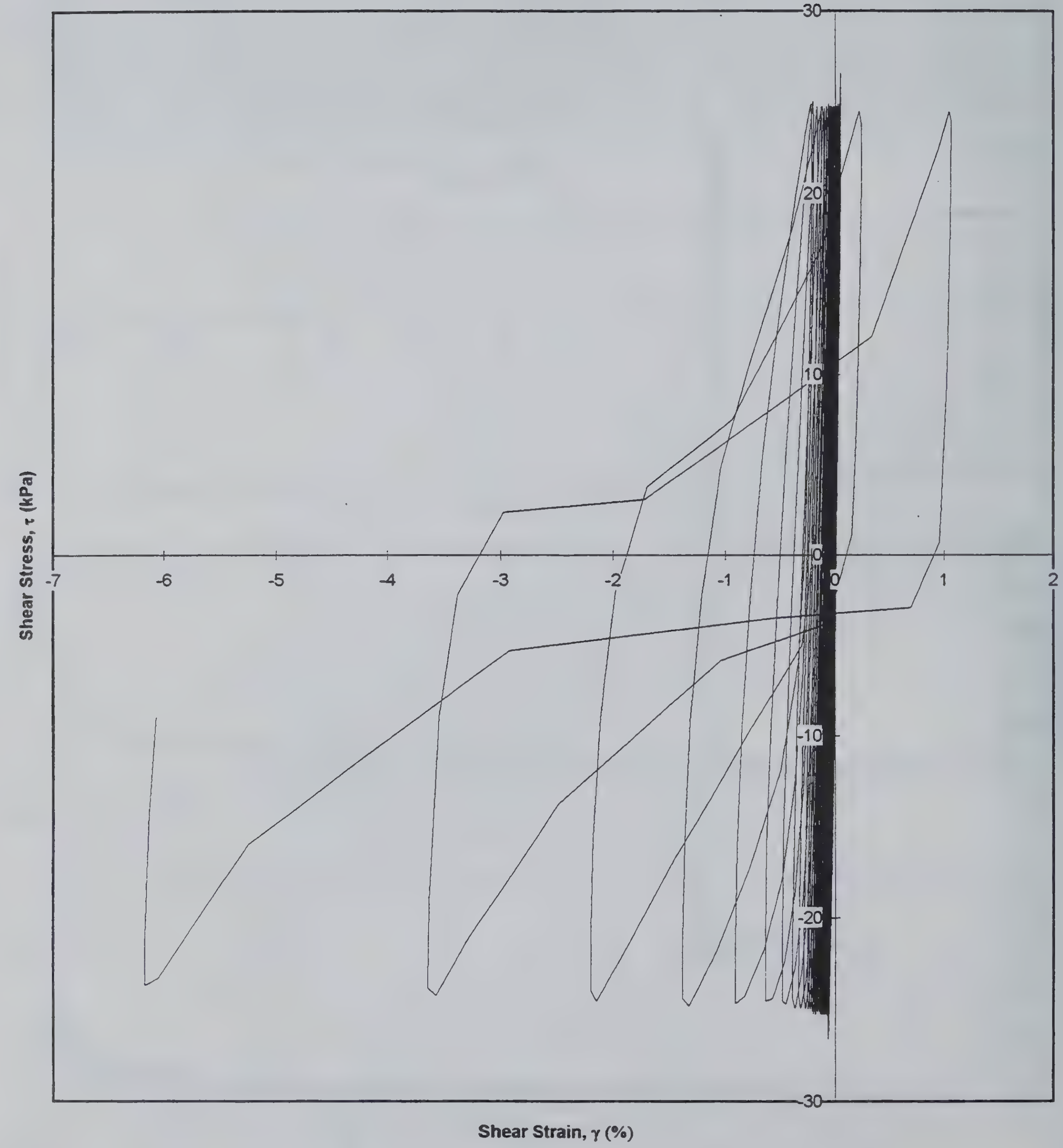

d:\nit\itp\cy_files\MONT25.XLS

8/20/96 8:23 AM

Test I.D.:	MONT26	**Controlled Parameter:**	Stress
Relative Density (%):	49.9	**Initial Effective Stress (kPa):**	100
Applied Stress Ratio:	0.35	**Frequency (Hz):**	1

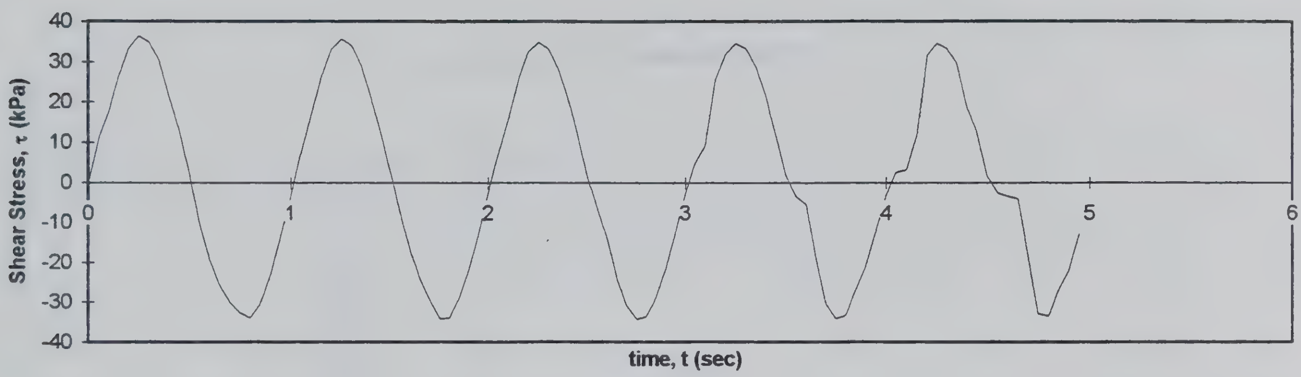

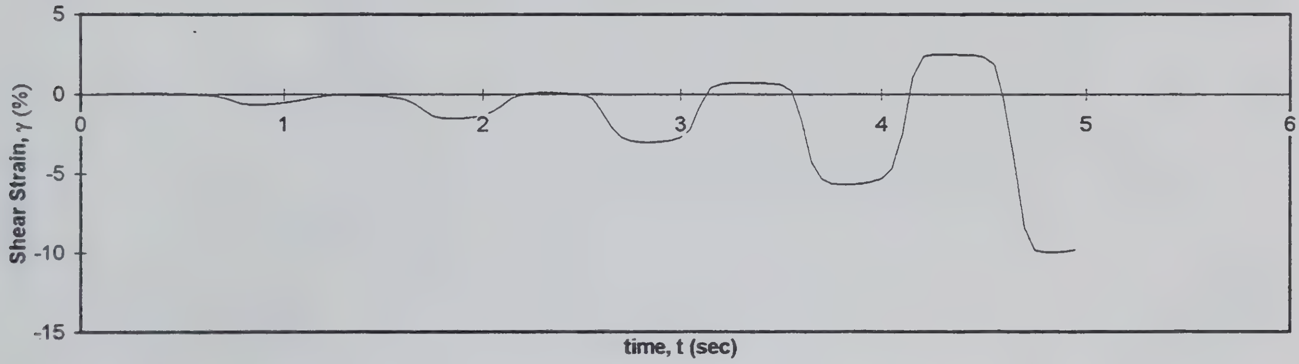

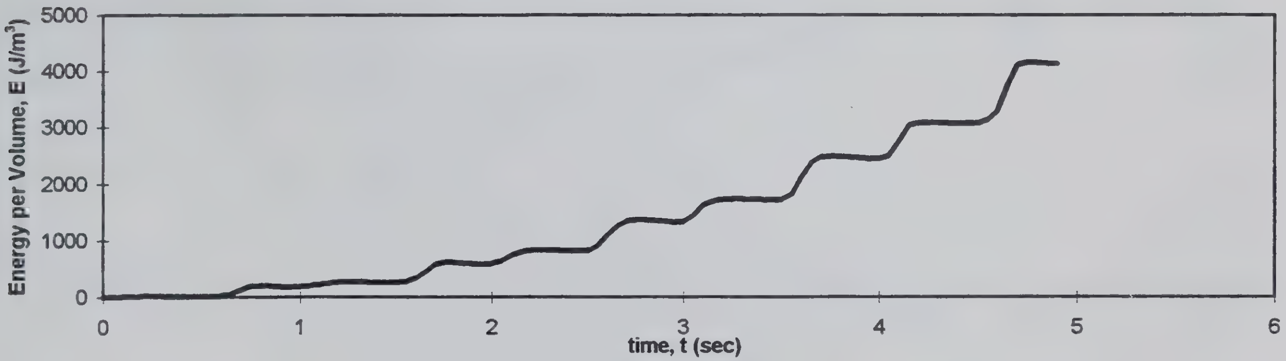

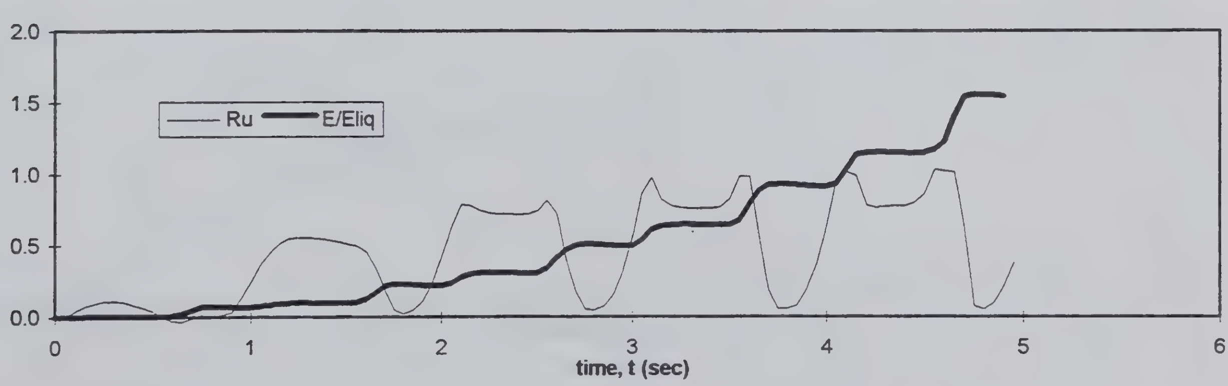

Test I.D.:	MONT26	**Controlled Parameter:**	Stress
Relative Density (%):	49.9	**Initial Effective Stress (kPa):**	100
Applied Stress Ratio:	0.35	**Frequency (Hz):**	1

Shear Stress vs. Shear Strain

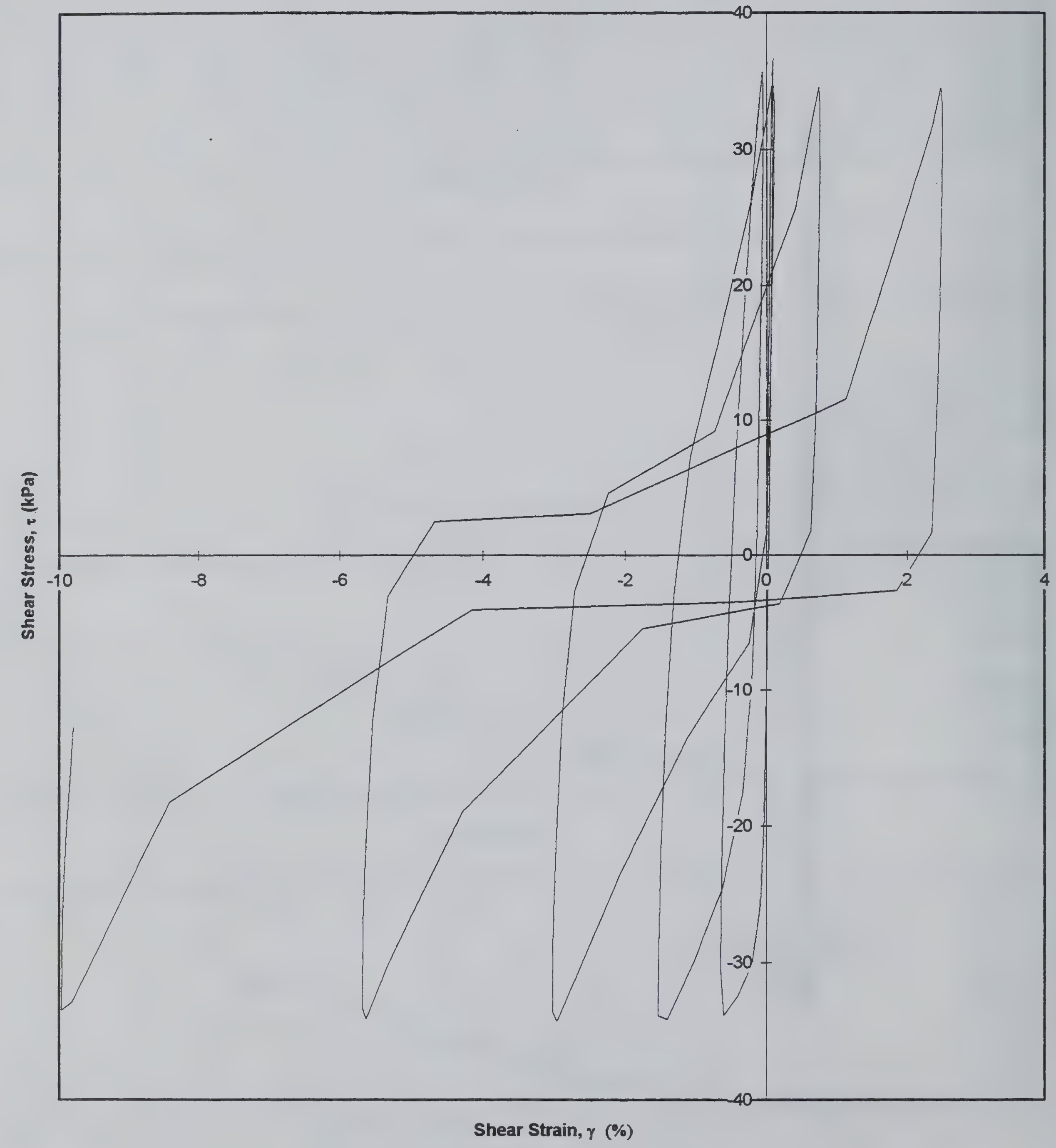

d:\nit\itp\cy_files\MONT26.XLS

8/21/96 8:58 AM

Test I.D.:	MONT30	**Controlled Parameter:**	Strain
Relative Density (%)	41.9	**Initial Effective Stress (kPa):**	100
Applied Shear Strain (%):	0.26	**Frequency (Hz):**	10

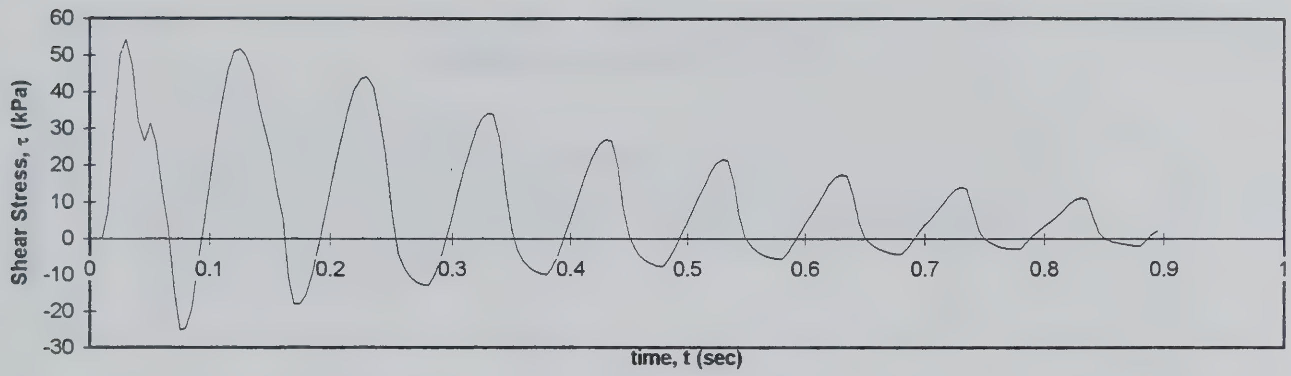

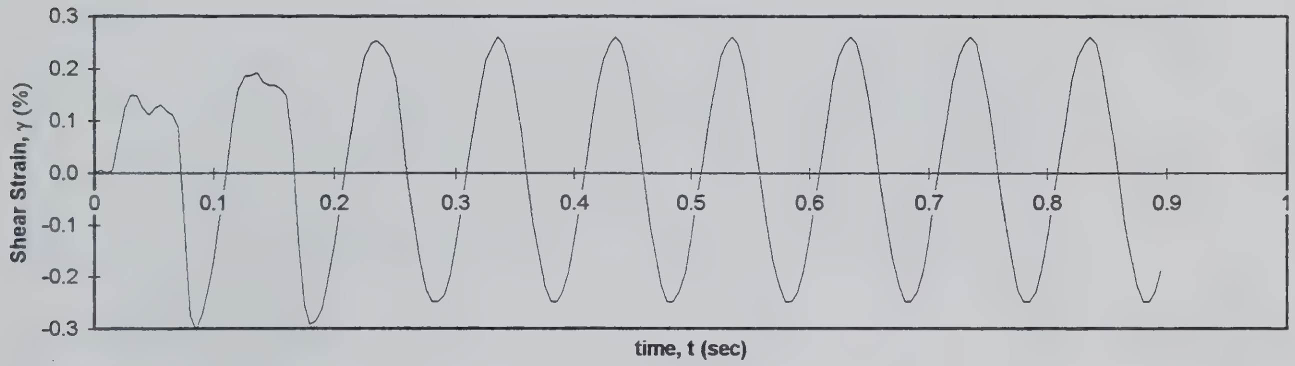

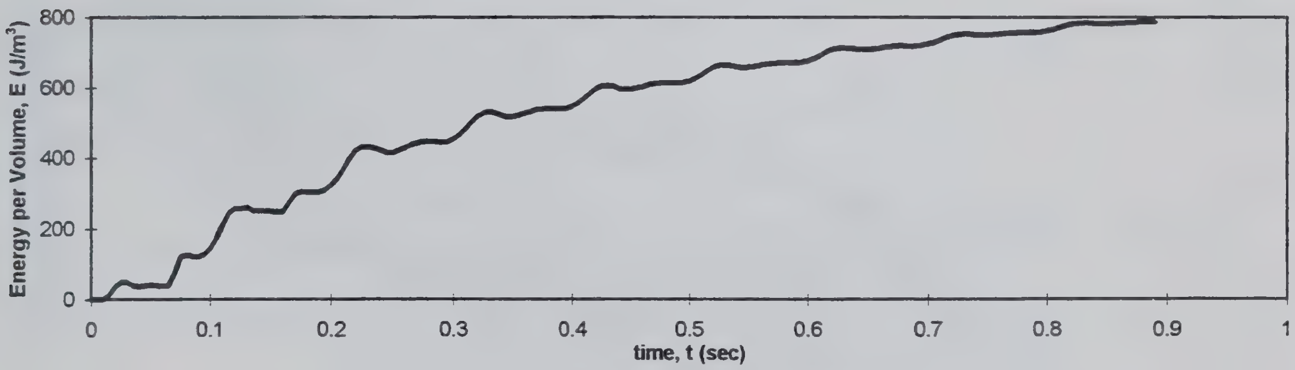

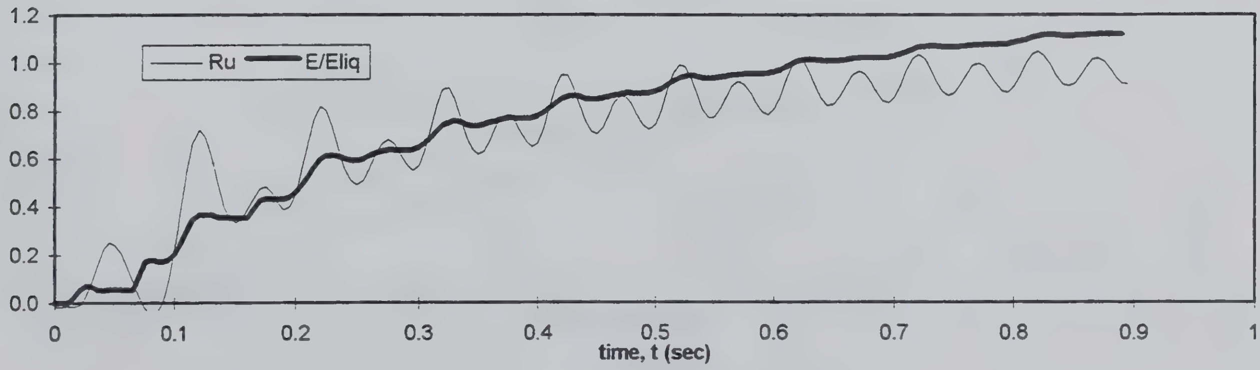

Test I.D.:	MONT30	**Controlled Parameter:**	Strain
Relative Density (%)	41.9	**Initial Effective Stress (kPa):**	100
Applied Shear Strain (%):	0.26	**Frequency (Hz):**	10

Shear Stress vs. Shear Strain

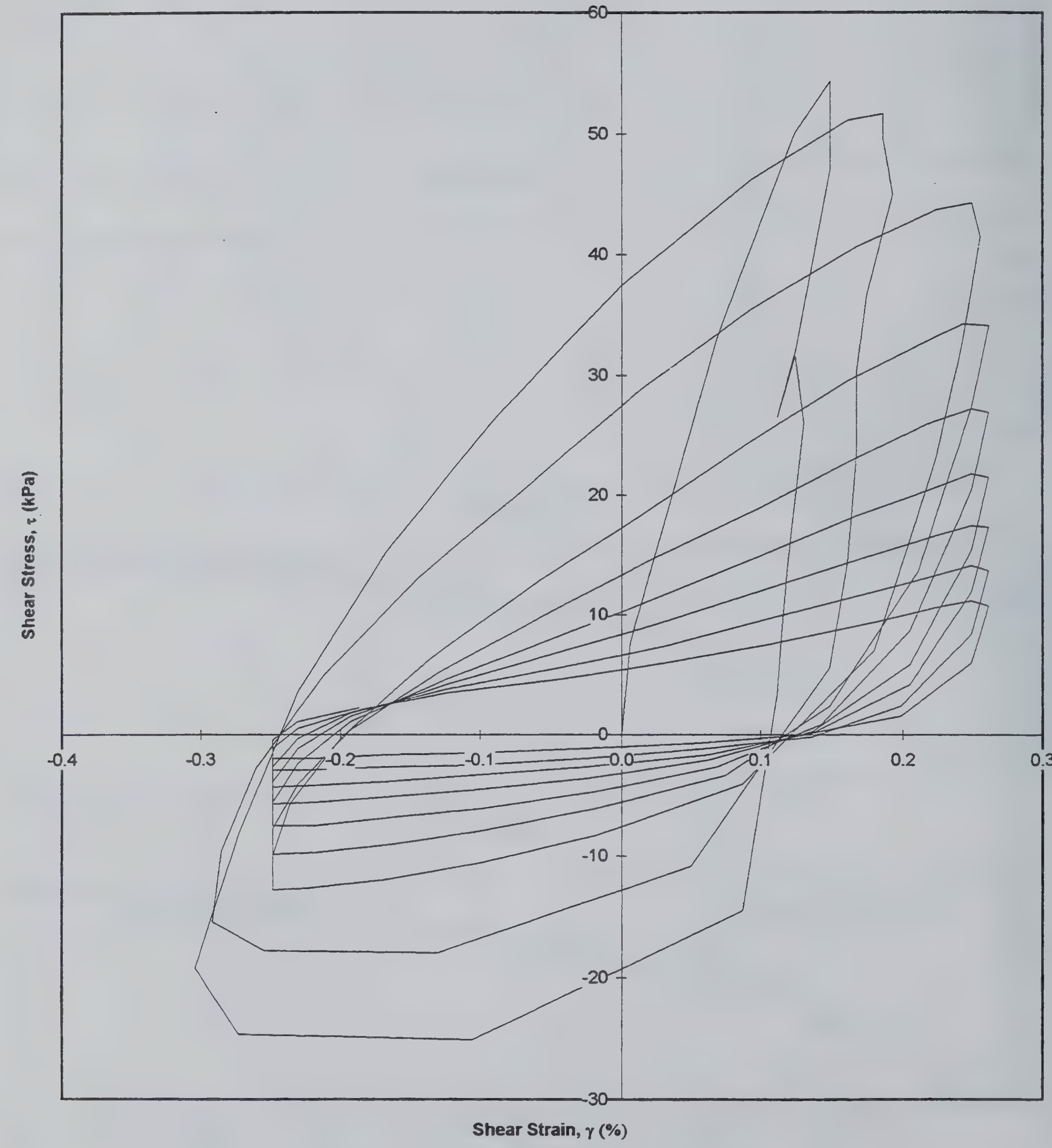

d:\nit\itp\cy_files\MONT30.XLS

8/21/96 9:08 AM

Test I.D.:	MONT33	**Controlled Parameter:**	Strain
Relative Density (%)	40.5	**Initial Effective Stress (kPa):**	100
Applied Shear Strain (%)	0.08	**Frequency (Hz):**	10

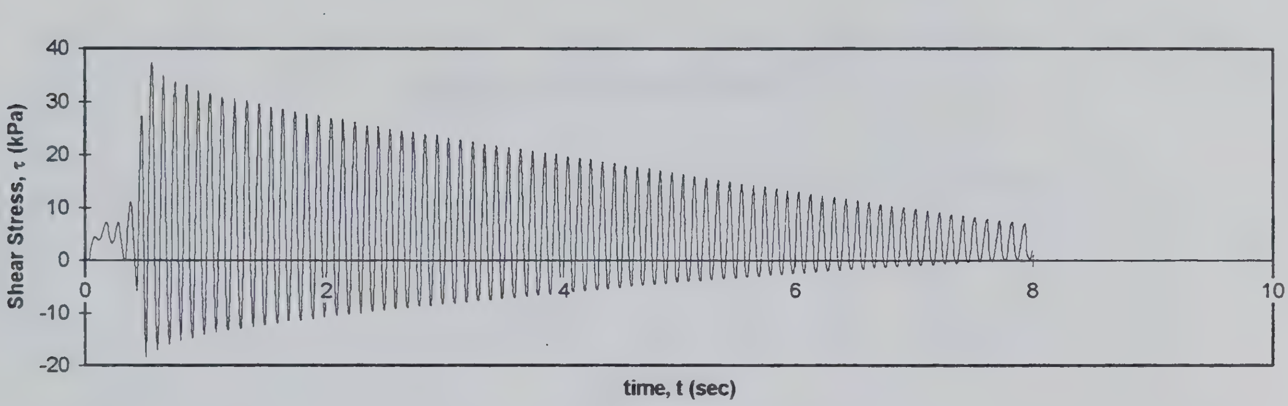

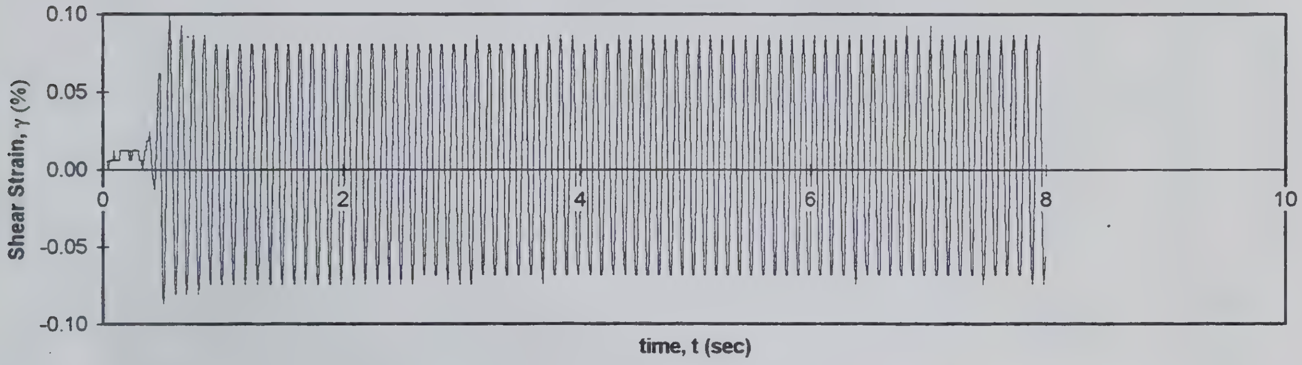

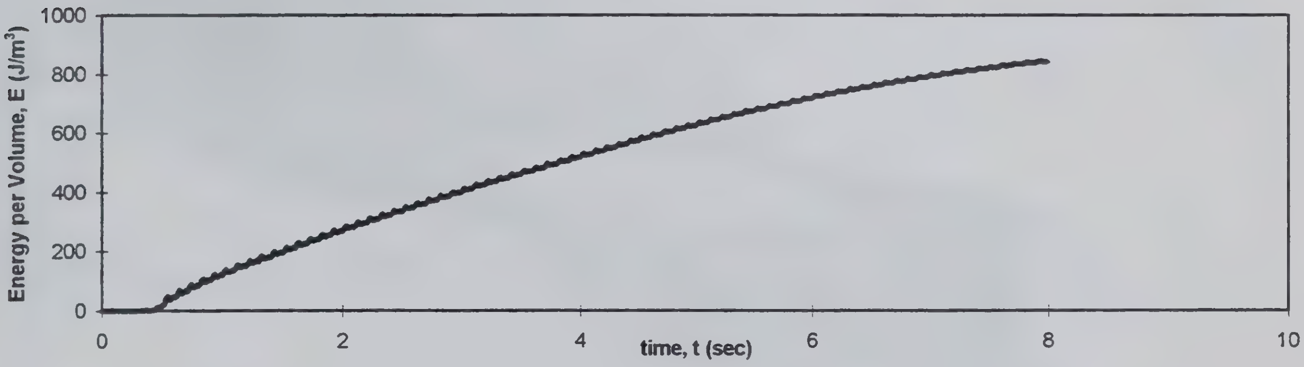

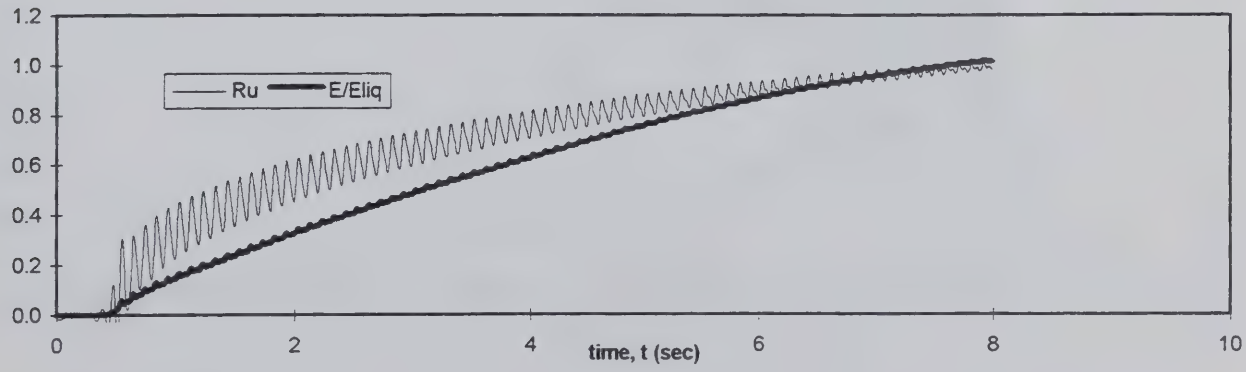

Test I.D.:	MONT33	**Controlled Parameter:**	Strain
Relative Density (%)	40.5	**Initial Effective Stress (kPa):**	100
Applied Shear Strain (%)	0.08	**Frequency (Hz):**	10

Shear Stress vs. Shear Strain

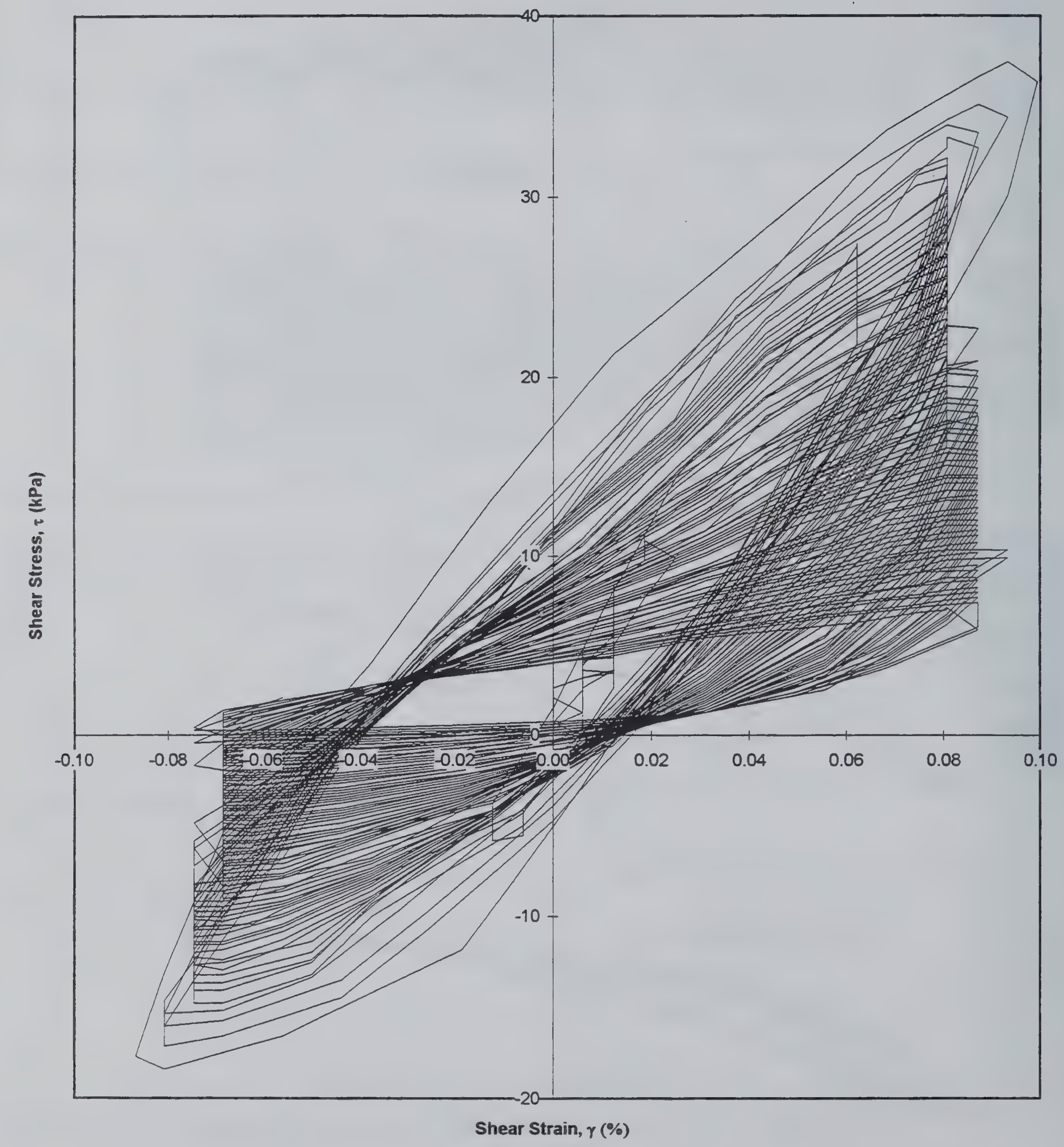

Test I.D.:	MONT35	**Controlled Parameter:**	Stress
Relative Density (%)	61.8	**Initial Effective Stress (kPa):**	100
Applied Stress Ratio:	0.35	**Frequency (Hz):**	0.1

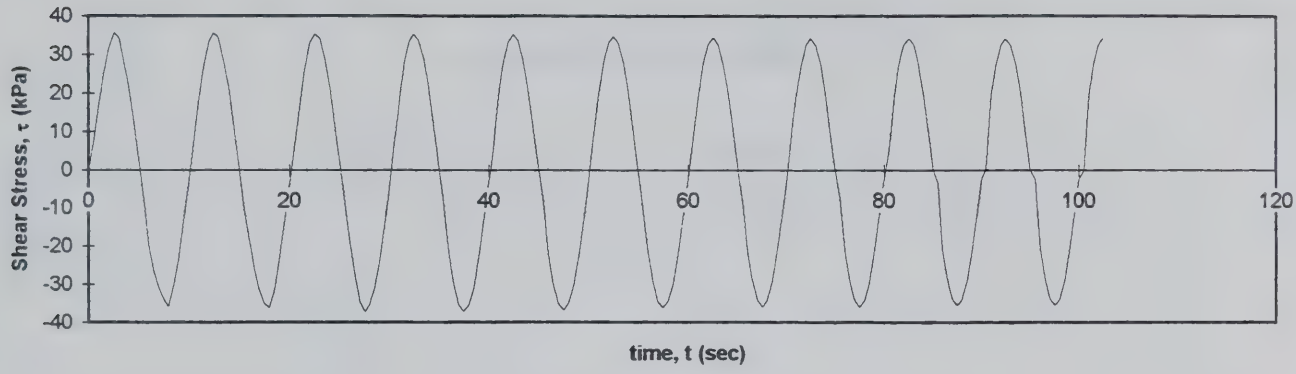

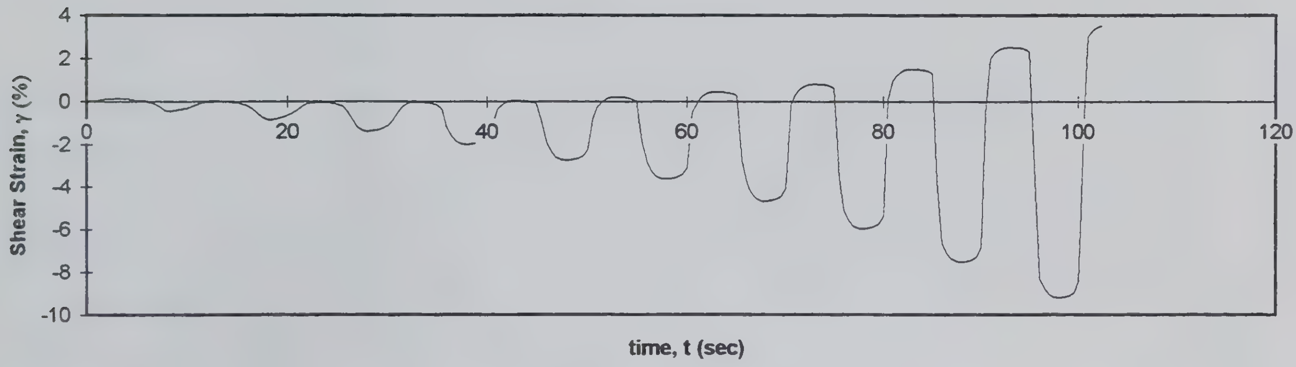

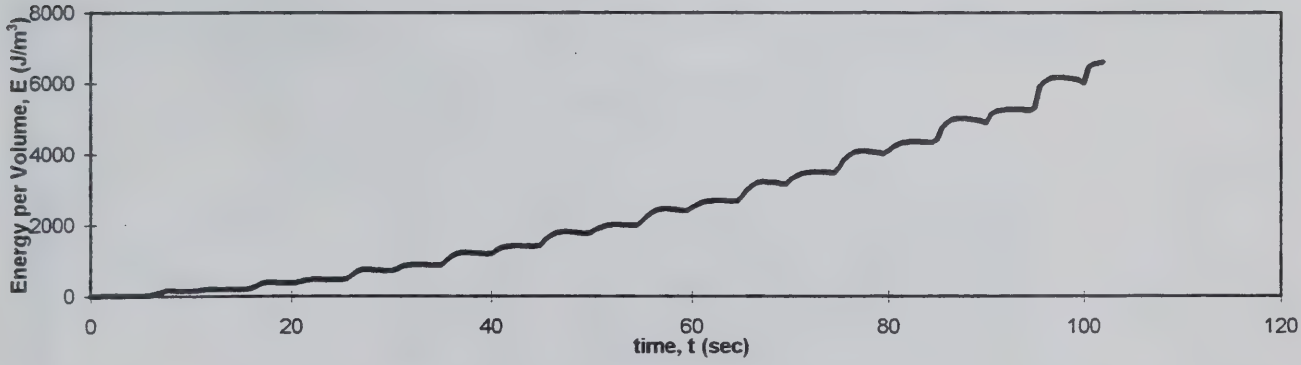

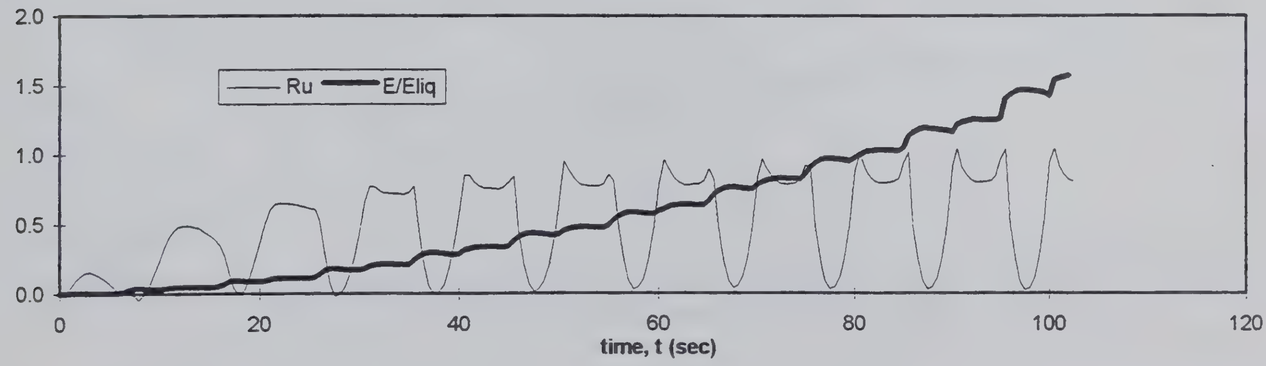

d:\nit\itp\cy_files\MONT35.XLS

8/20/96 10:42 AM

Test I.D.:	MONT35	**Controlled Parameter:**	Stress
Relative Density (%):	61.8	**Initial Effective Stress (kPa):**	100
Applied Stress Ratio:	0.35	**Frequency (Hz):**	0.1

Shear Stress vs. Shear Strain

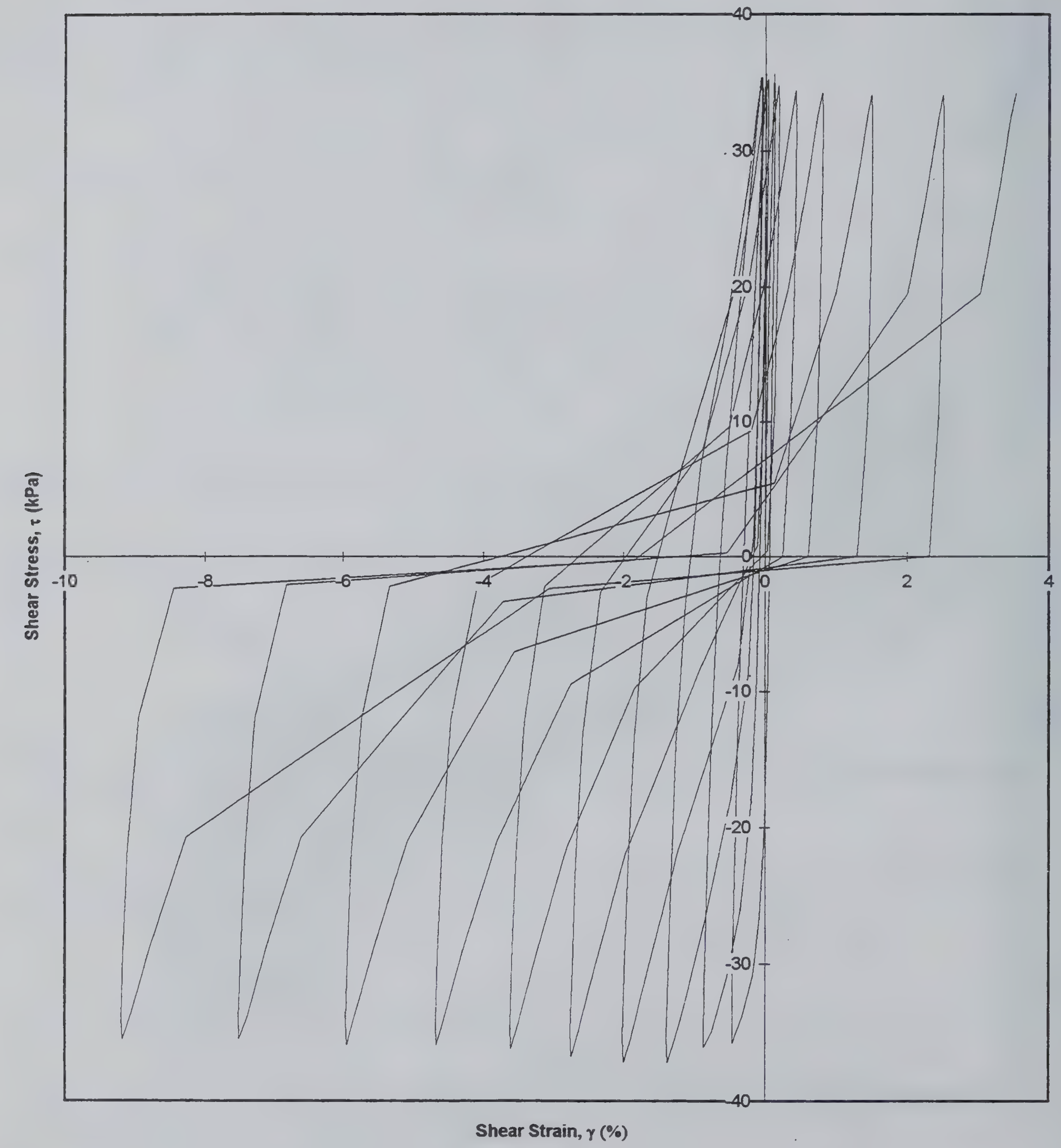

Test I.D.:	MONT37	**Controlled Parameter:**	Strain
Relative Density (%):	61.6	**Initial Effective Stress (kPa):**	100
Applied Shear Strain (%)	0.17	**Frequency (Hz):**	1

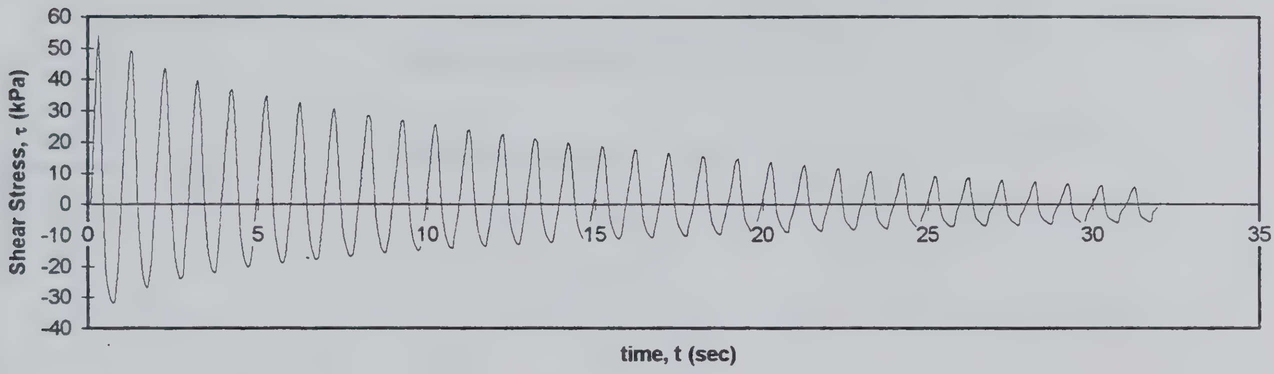

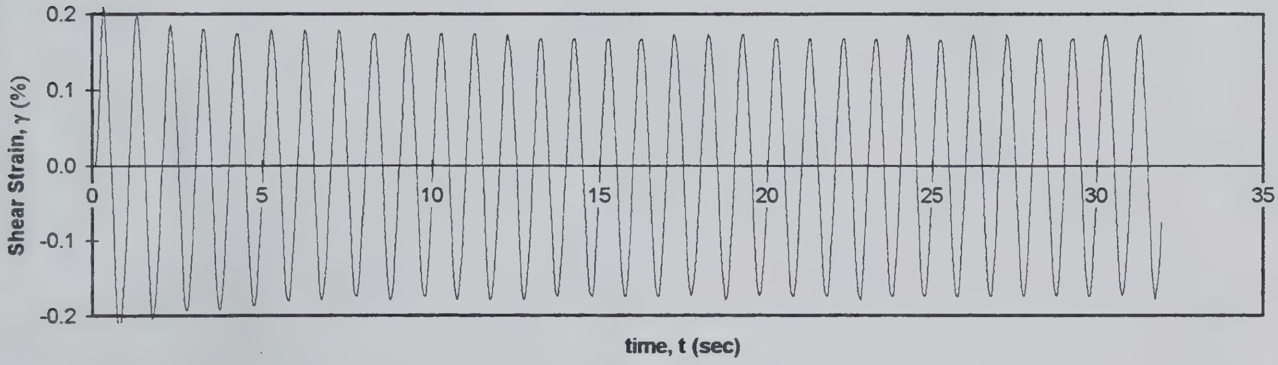

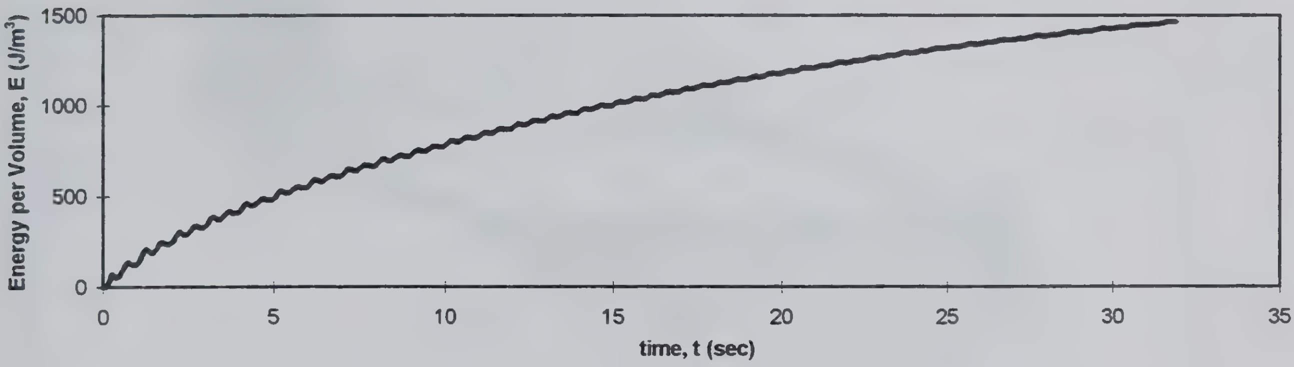

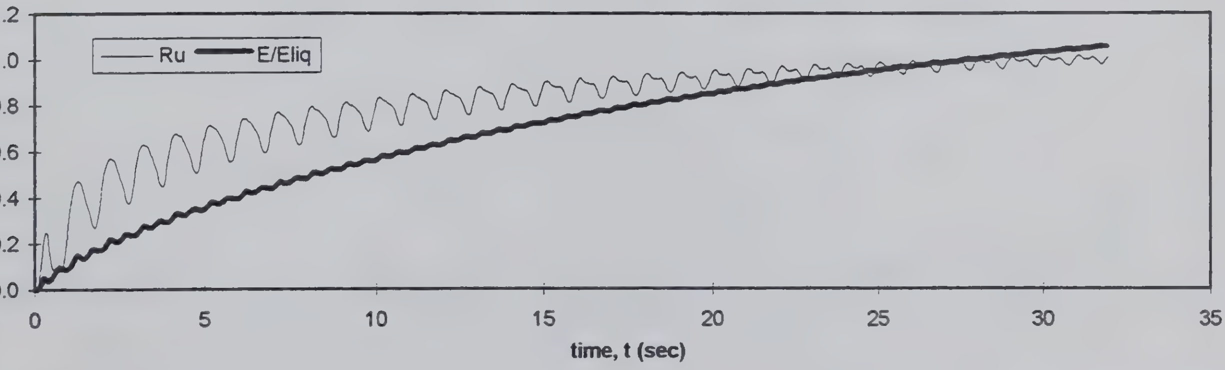

Test I.D.:	MONT37	**Controlled Parameter:**	Strain
Relative Density (%):	61.6	**Initial Effective Stress (kPa):**	100
Applied Shear Strain (%)	0.17	**Frequency (Hz):**	1

Shear Stress vs. Shear Strain

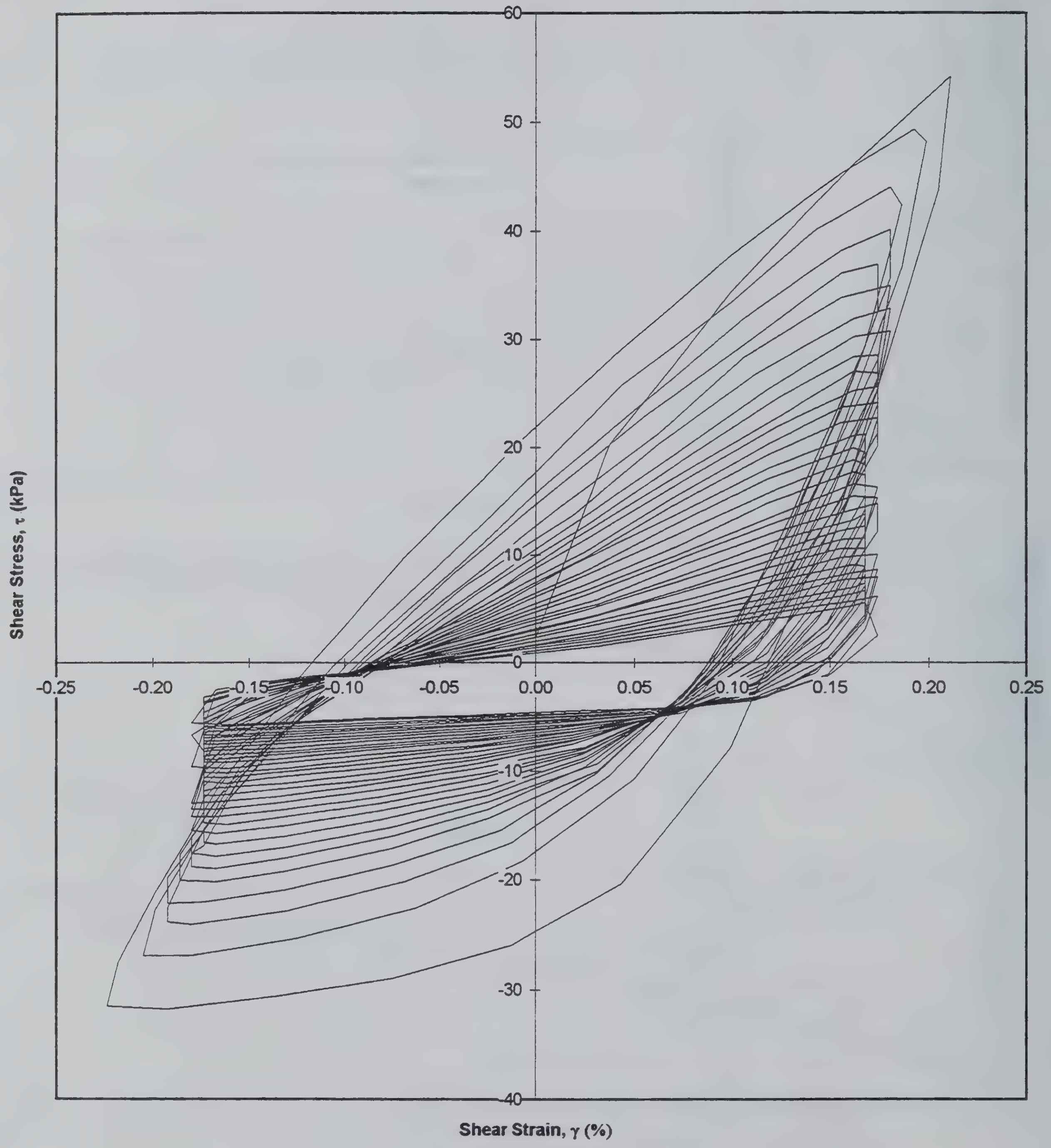

Test I.D.:	MONT38	**Controlled Parameter:**	Strain
Relative Density (%):	61.8	**Initial Effective Stress (kPa):**	100
Applied Shear Strain (%):	0.25	**Frequency (Hz):**	10

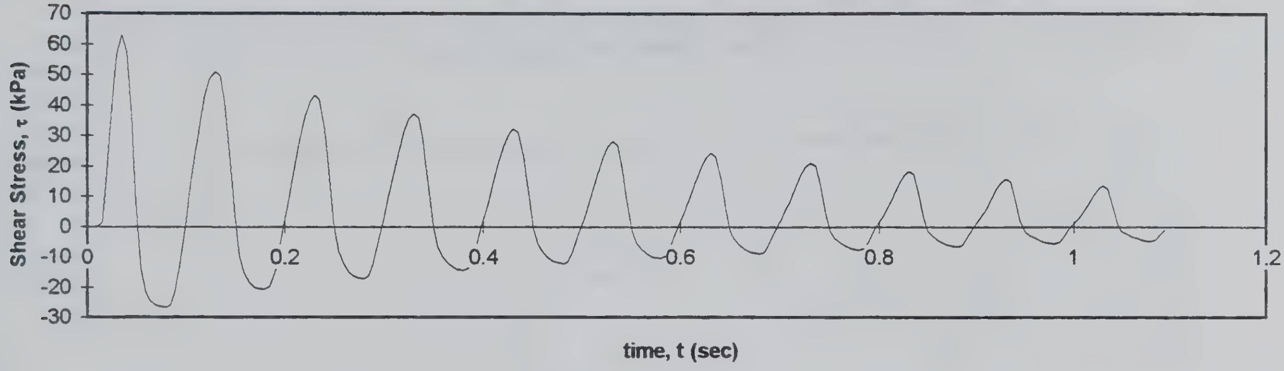

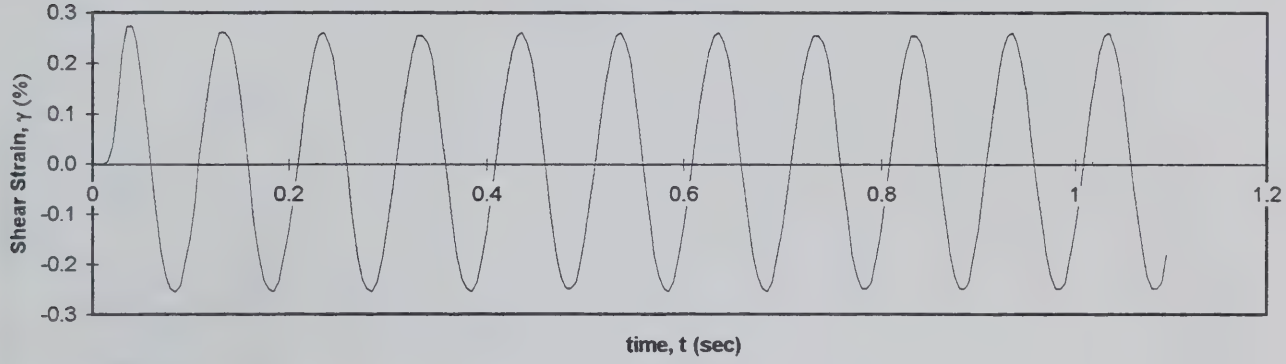

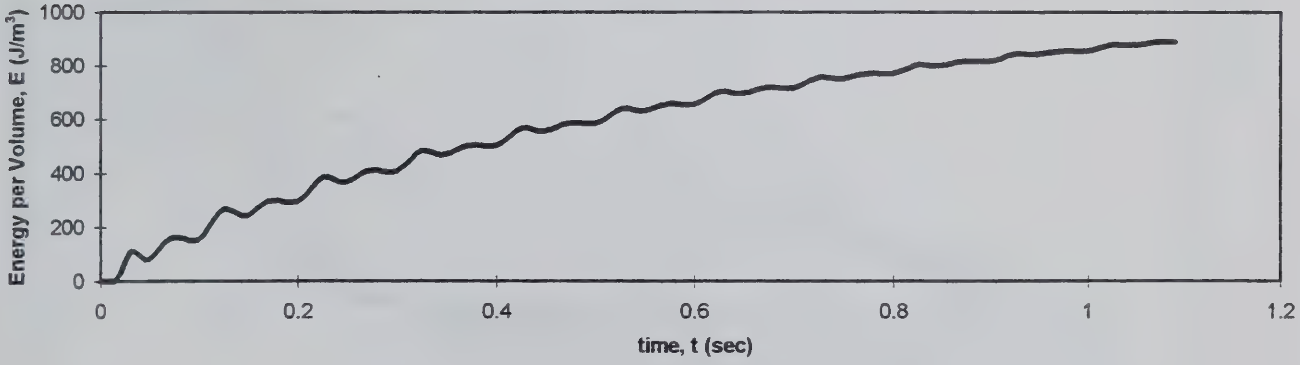

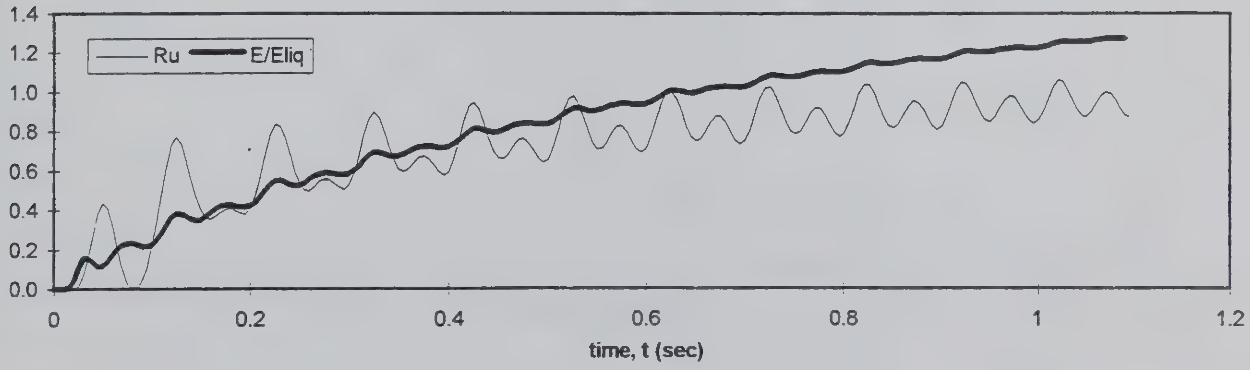

Test I.D.:	MONT38	**Controlled Parameter:**	Strain
Relative Density (%):	61.8	**Initial Effective Stress (kPa):**	100
Applied Shear Strain (%):	0.25	**Frequency (Hz):**	10

Shear Stress vs. Shear Strain

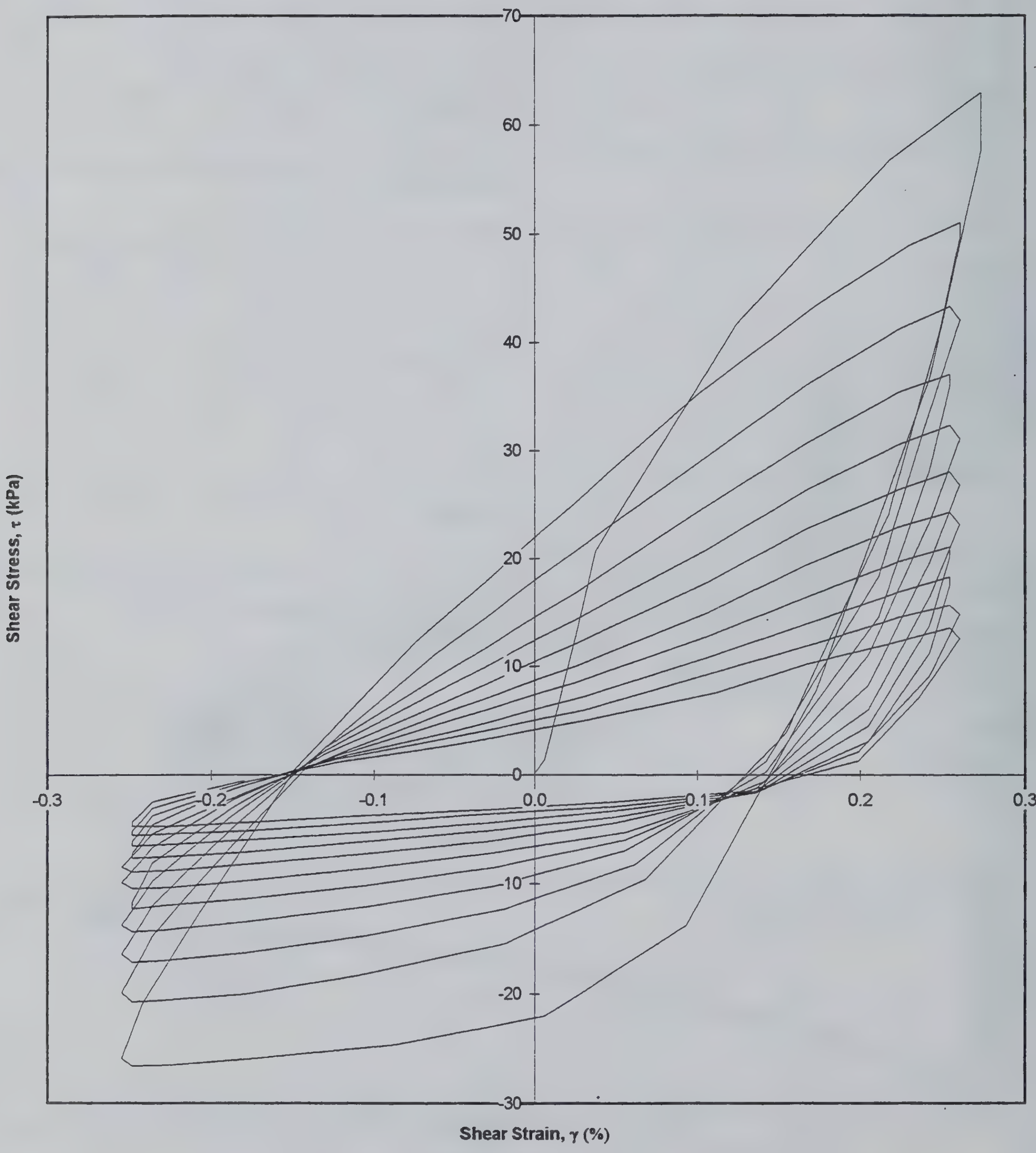

d:\nit\itp\cy_files\MONT38.XLS

8/20/96 10:54 AM

APPENDIX B

LABORATORY TESTS ON SOIL SAMPLES FROM THE SAVANNAH RIVER SITE, PERFORMED AT THE UNIVERSITY OF CALIFORNIA, BERKELEY

Table B.1 - Summary of the Cyclic Triaxial Test Data on SRS Soil Samples Performed at University of California, Berkeley

No.	Test ID	Sample	D_r(%)	E_{liq} (J/m^3)	FC (%)	γ_d (kN/m^3)	Control	σ_c' (kPa)	Freq. (Hz)	Load Shape
1	B23P2BCY	Santee	N/A	14675	33.7	16.0	Stress	400	1	Sinusoidal 2-way
2	B23P2MCY	Santee	N/A	16782	35.6	16.4	Stress	400	1	Sinusoidal 2-way
3	B23P2TCY	Santee	N/A	11402	32.6	16.8	Stress	400	1	Sinusoidal 2-way
4	B23P3BCY	Tobacco Rd.	N/A	4929	16.6	16.4	Stress	200	1	Sinusoidal 2-way
5	B23P3MCY	Tobacco Rd.	N/A	5585	18.5	15.2	Stress	200	1	Sinusoidal 2-way
6	B23P3TCY	Tobacco Rd.	N/A	2924	20.5	16.6	Stress	200	1	Sinusoidal 2-way
7	B12P5BCY	Tobacco Rd.	N/A	14918	27.0	15.8	Stress	300	1	Sinusoidal 2-way
8	B12P5MCY	Tobacco Rd.	N/A	49114	26.8	16.8	Stress	300	1	Sinusoidal 2-way
9	B12P5TCY	Tobacco Rd.	N/A	5450	22.3	18.0	Stress	300	1	Sinusoidal 2-way
10	B12P7BCY	Tobacco Rd.	N/A	7666	15.7	15.9	Stress	375	1	Sinusoidal 2-way
11	B12P7MCY	Tobacco Rd.	N/A	14482	17.0	16.3	Stress	375	1	Sinusoidal 2-way
12	B12P7TCY	Tobacco Rd.	N/A	3852	15.7	16.2	Stress	375	1	Sinusoidal 2-way
13	B2P5BCYC	Tobacco Rd.	N/A	11672	25.4	14.7	Stress	500	1	Sinusoidal 2-way
14	B2P5MCYC	Tobacco Rd.	N/A	23344	29.6	15.4	Stress	500	1	Sinusoidal 2-way
15	B2P5TCYC	Tobacco Rd.	N/A	8819	26.6	16.7	Stress	500	1	Sinusoidal 2-way
16	B23P4BCY	Tobacco Rd.	N/A	21667	11.4	14.6	Stress	750	1	Sinusoidal 2-way
17	B23P4MCY	Tobacco Rd.	N/A	36680	16.5	15.5	Stress	700	1	Sinusoidal 2-way
18	B23P4TCY	Tobacco Rd.	N/A	17968	28.0	N/A	Stress	750	1	Sinusoidal 2-way
19	B29P2TCY	Tobacco Rd.	N/A	23637	23.0	16.7	Stress	750	1	Sinusoidal 2-way
20	B2P6BCY	Tobacco Rd.	N/A	17985	18.9	16.7	Stress	725	1	Sinusoidal 2-way
21	B2P6MCY	Tobacco Rd.	N/A	19831	20.1	16.5	Stress	743	1	Sinusoidal 2-way
22	B2P6TCYC	Tobacco Rd.	N/A	14446	22.4	16.0	Stress	750	1	Sinusoidal 2-way

Test Results Following the Sequence of Test ID's are Attached.

Test I.D.:	B23P2BCY	**Controlled Parameter:**	Stress
Fines Content (%):	33.7	**Initial Effective Stress (kPa):**	400
Dry Density (kN/m³):	16.04		

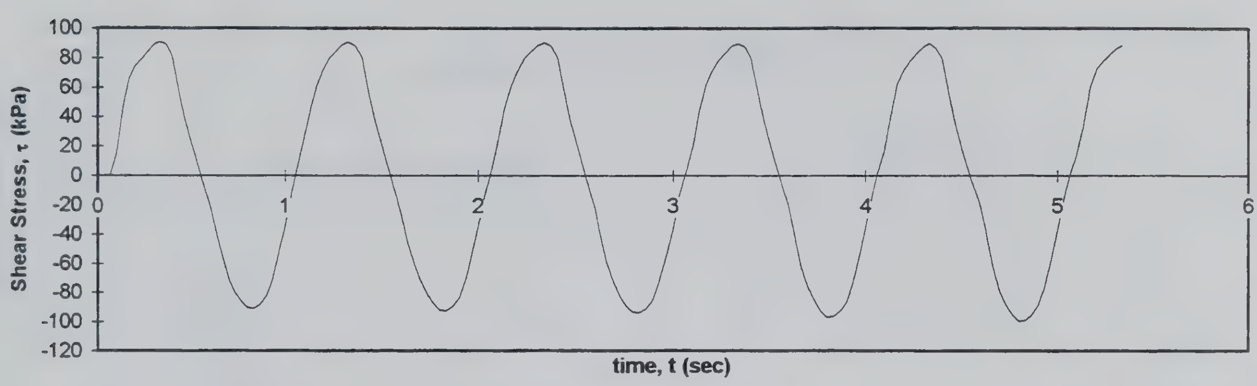

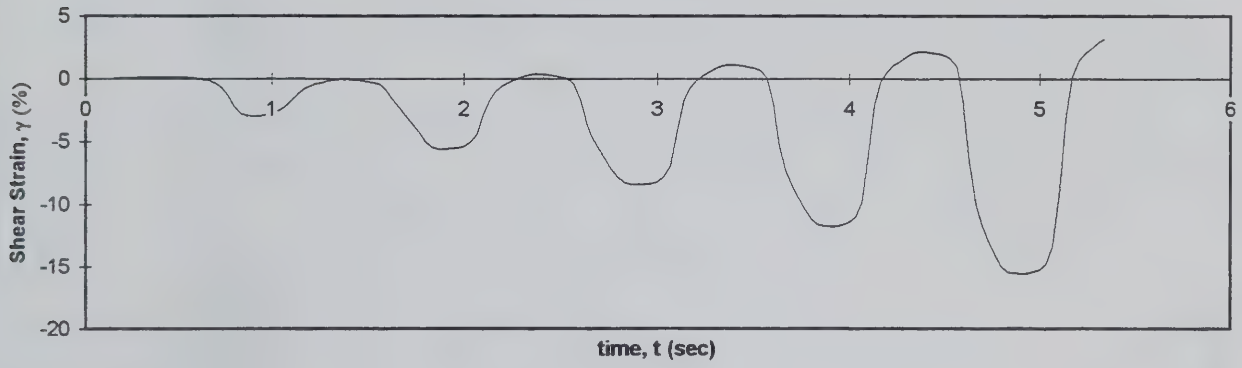

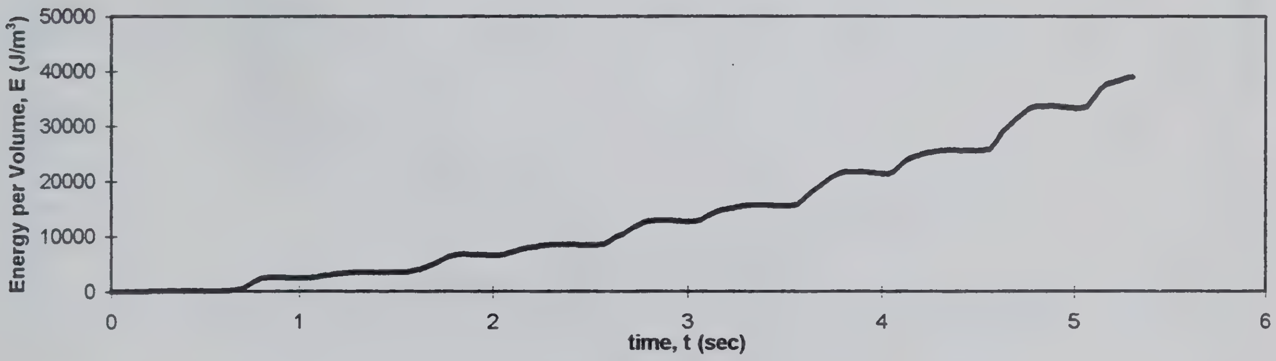

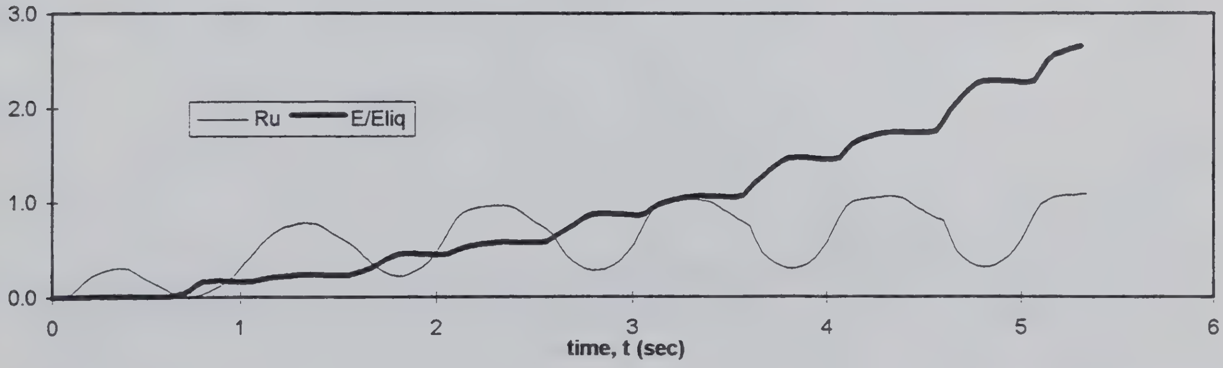

Test I.D.:	B23P2BCY	**Controlled Parameter:**	Stress
Fines Content (%):	33.7	**Initial Effective Stress (kPa):**	400
Dry Density (kN/m^3):	16.04		

Shear Stress vs. Shear Strain

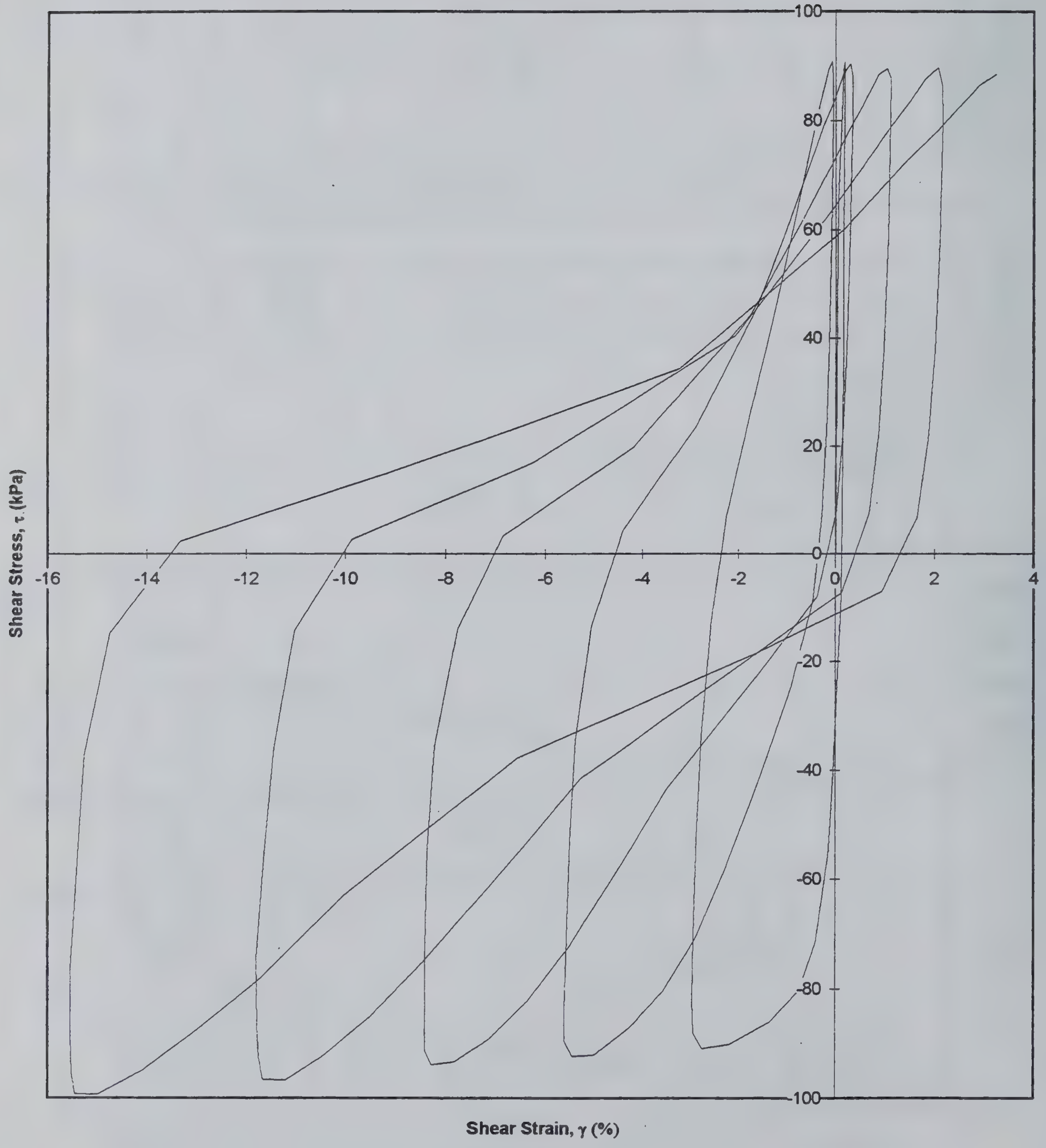

d:\nit\itp\cy_files\B23P2BCY.XLS

8/20/96 5:01 PM

Test I.D.:	B23P2MCY	**Controlled Parameter:**	Stress
Fines Content (%):	35.6	**Initial Effective Stress (kPa):**	400
Dry Density (kN/m^3):	16.43		

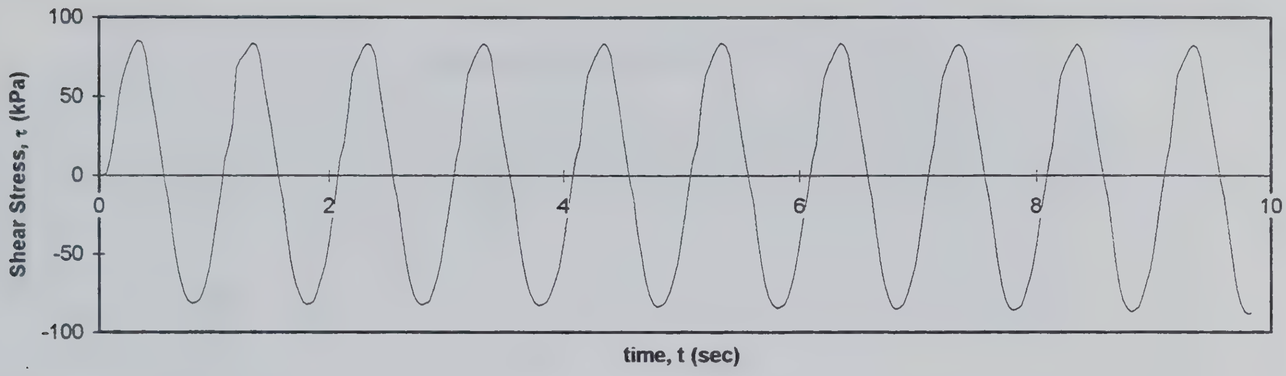

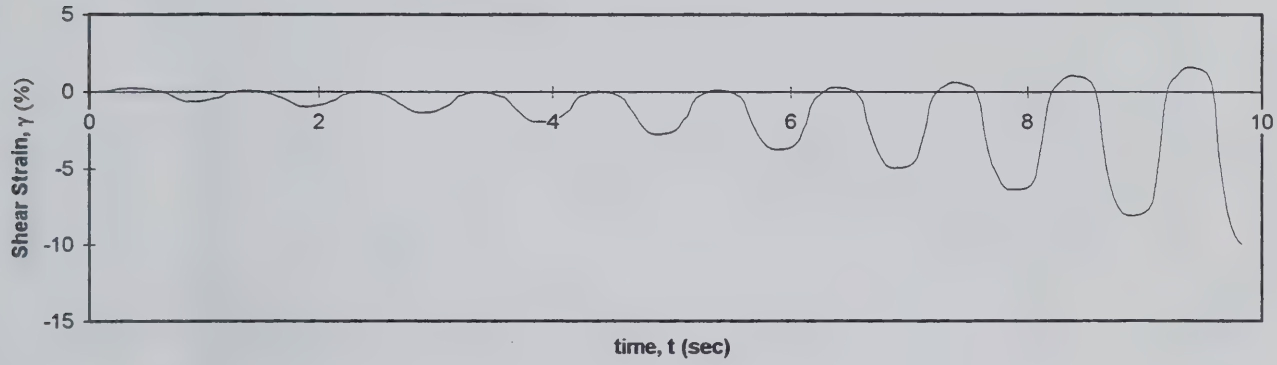

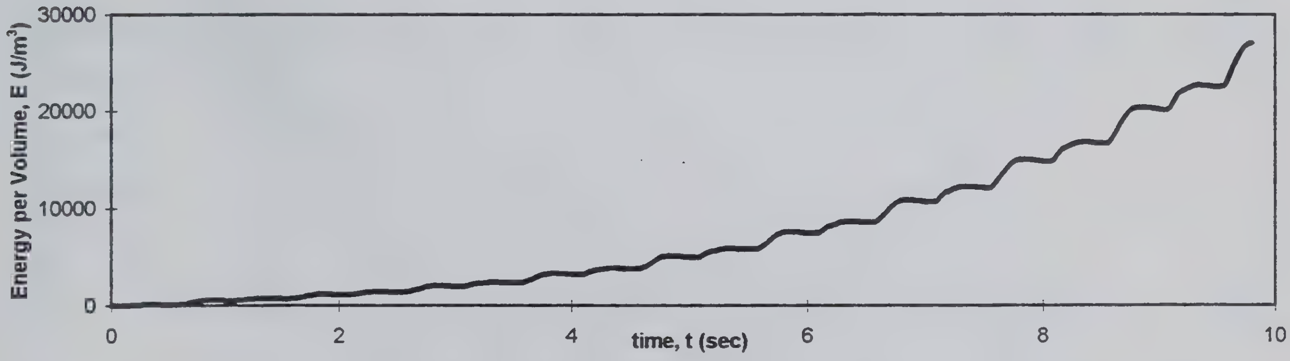

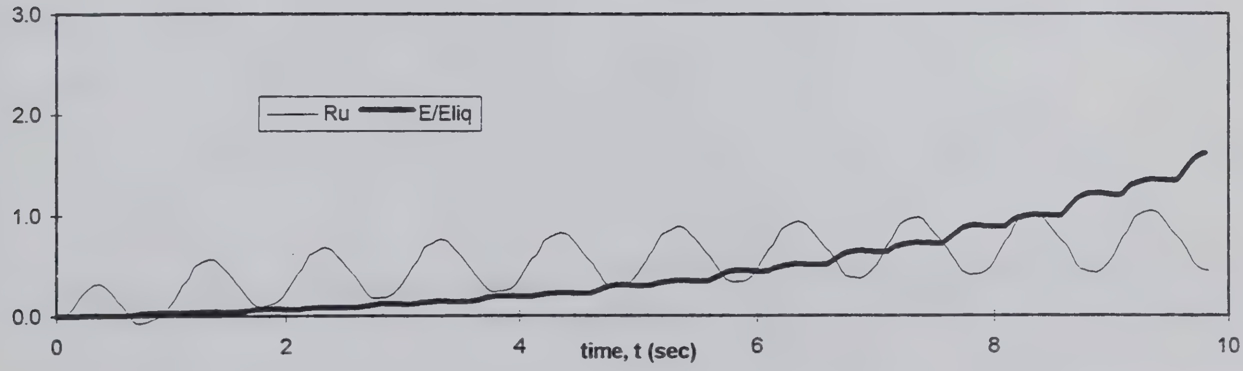

Test I.D.:	B23P2MCY	**Controlled Parameter:**	Stress
Fines Content (%):	35.6	**Initial Effective Stress (kPa):**	400
Dry Density (kN/m^3):	16.43		

Shear Stress vs. Shear Strain

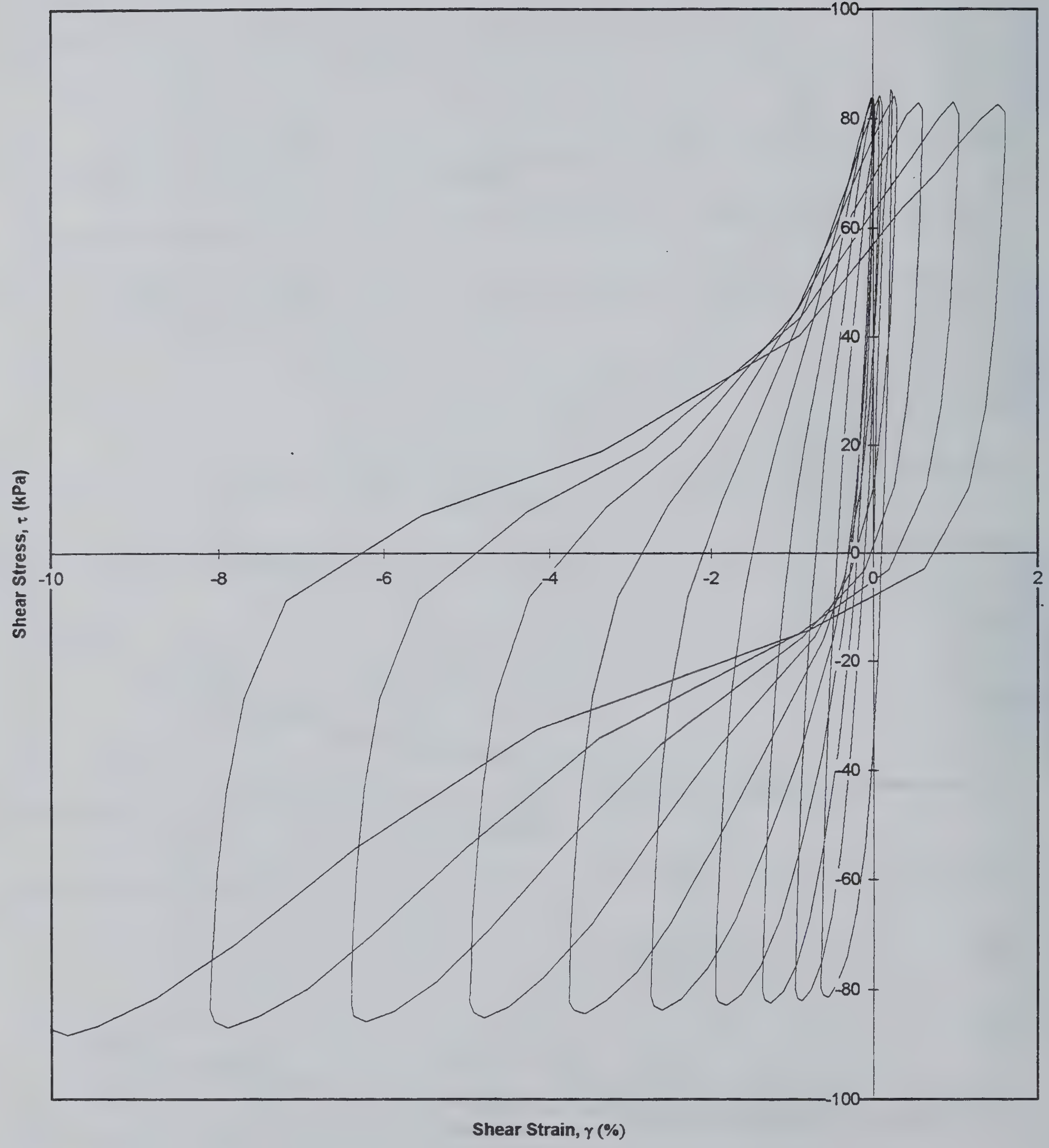

Test I.D.: B23P2TCY
Fines Content (%): 32.6
Dry Density (kN/m^3): 16.75
Controlled Parameter: Stress
Initial Effective Stress (kPa): 400

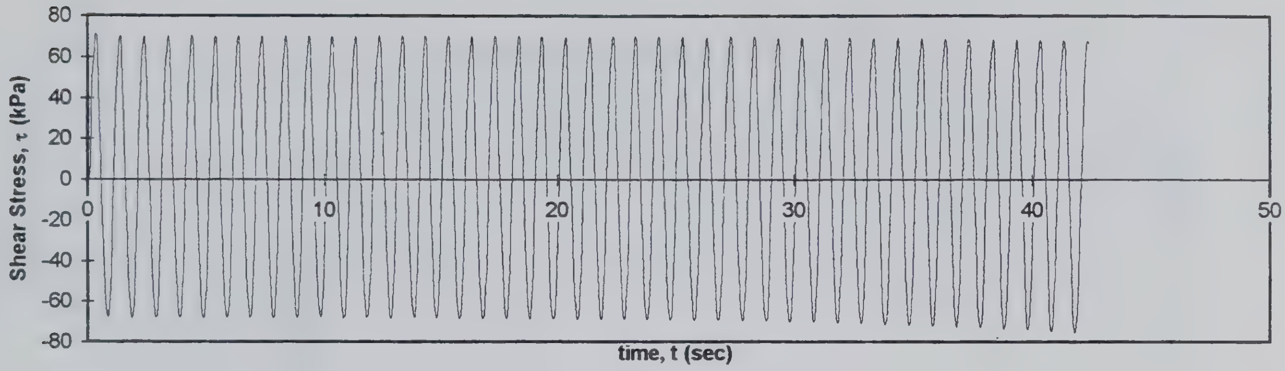

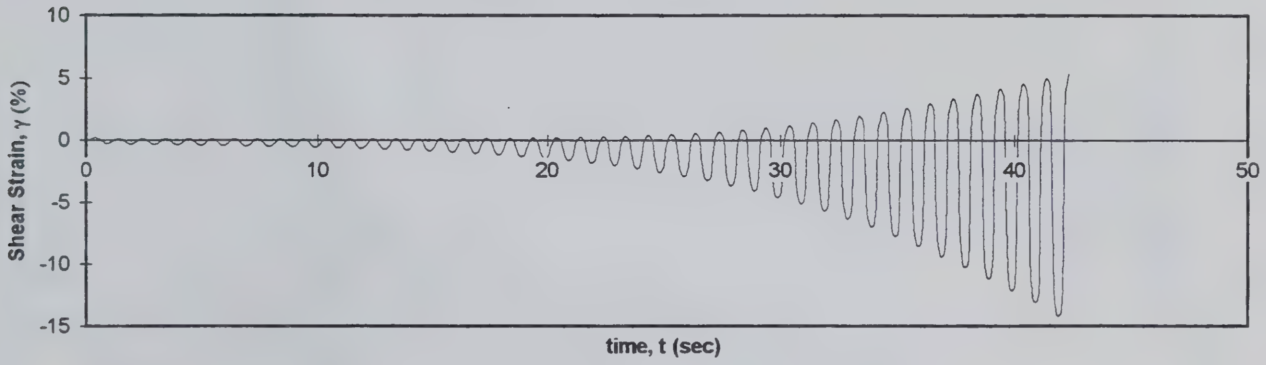

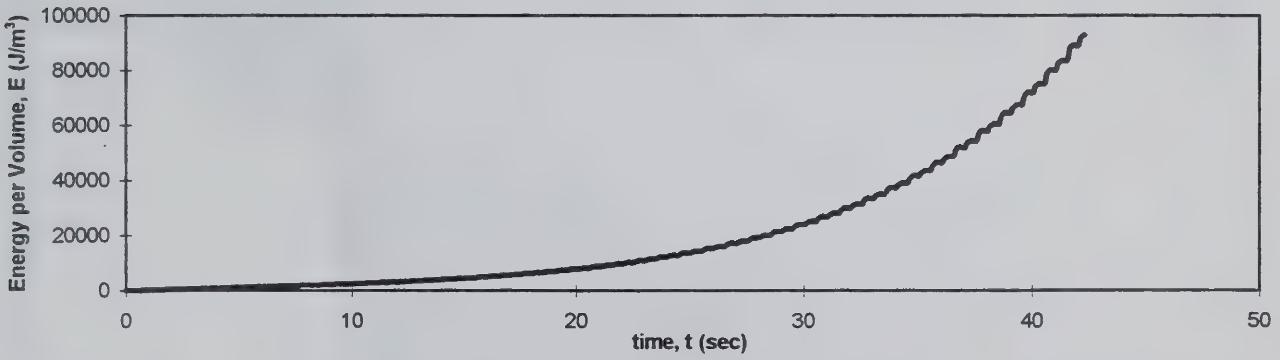

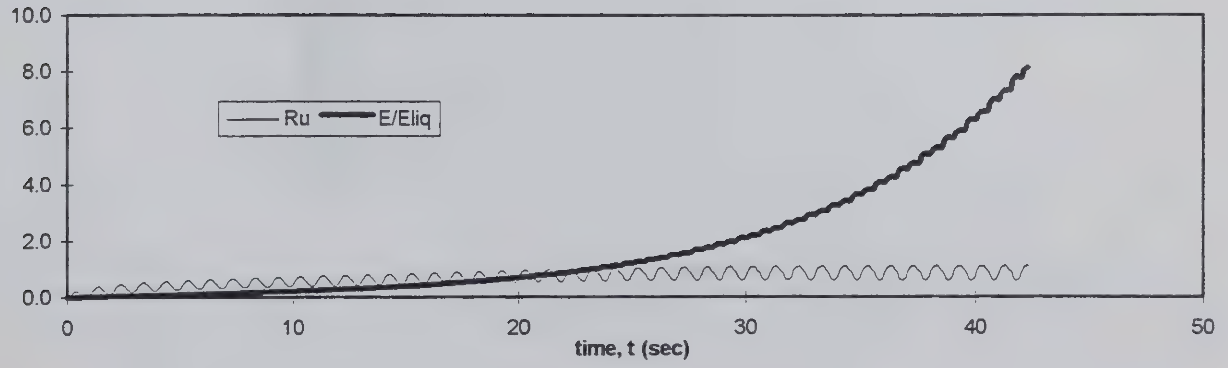

Test I.D.:	B23P2TCY	**Controlled Parameter:**	Stress
Fines Content (%):	32.6	**Initial Effective Stress (kPa):**	400
Dry Density (kN/m^3):	16.75		

Shear Stress vs. Shear Strain

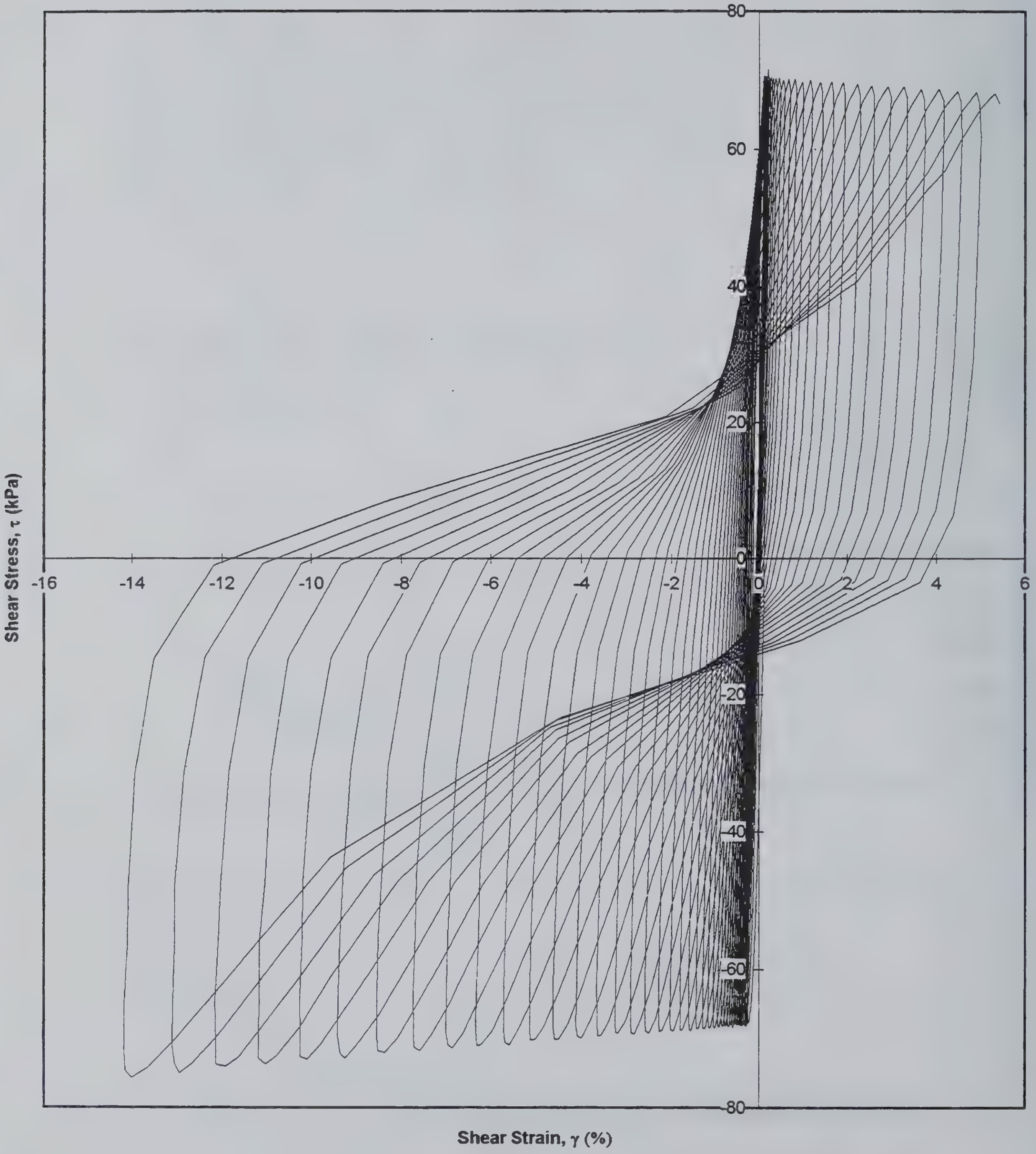

Test I.D.: B23P3BCY
Fines Content (%): 16.6
Dry Density (kN/m^3): 16.4
Controlled Parameter: Stress
Initial Effective Stress (kPa): 200

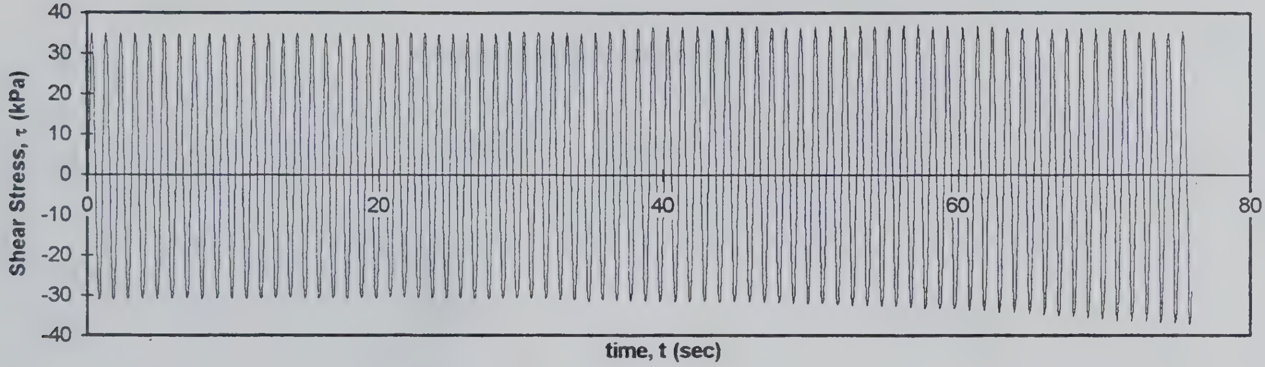

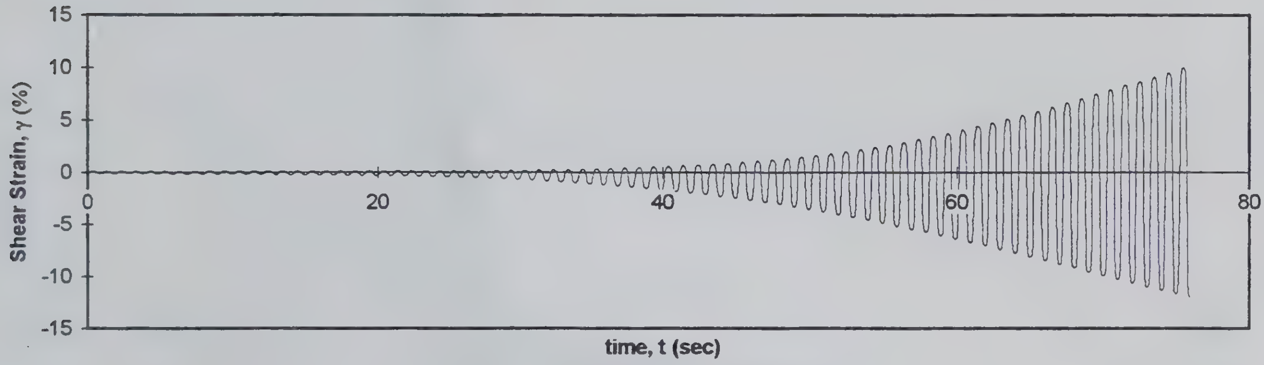

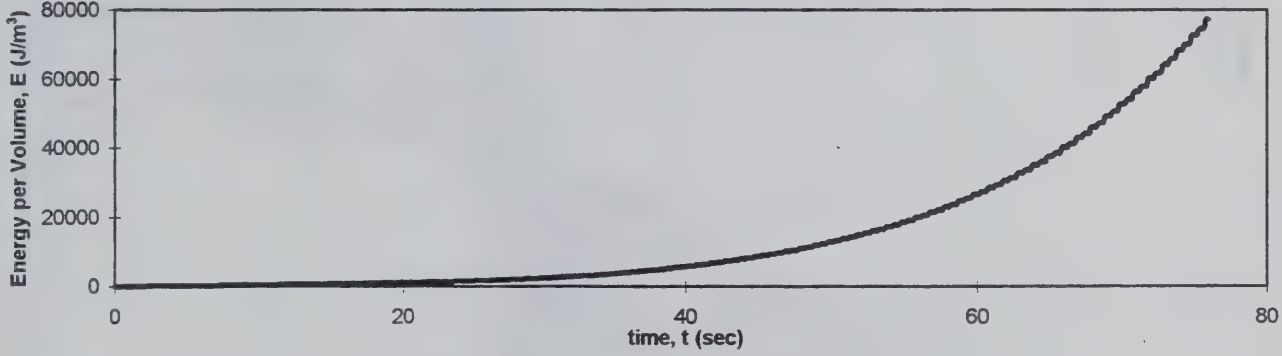

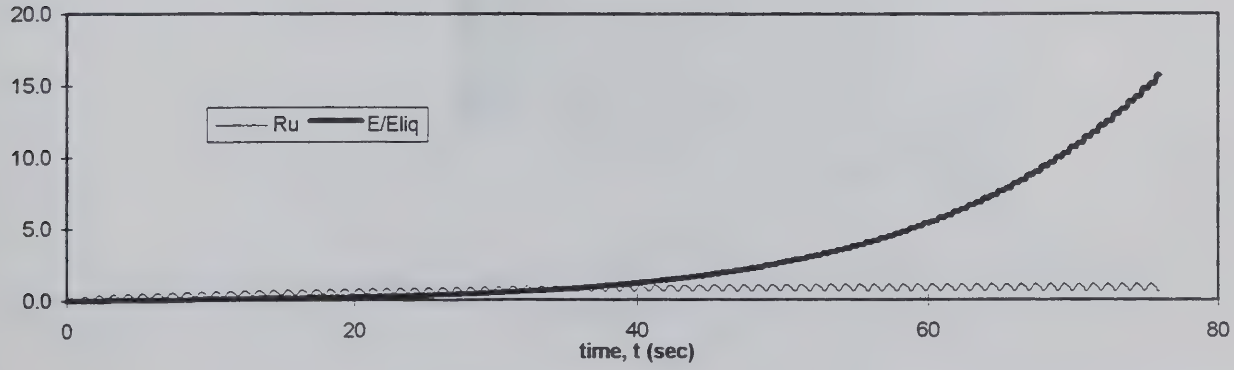

Test I.D.:	B23P3BCY	**Controlled Parameter:**	Stress
Fines Content (%):	16.6	**Initial Effective Stress (kPa):**	200
Dry Density (kN/m^3):	16.4		

Shear Stress vs. Shear Strain

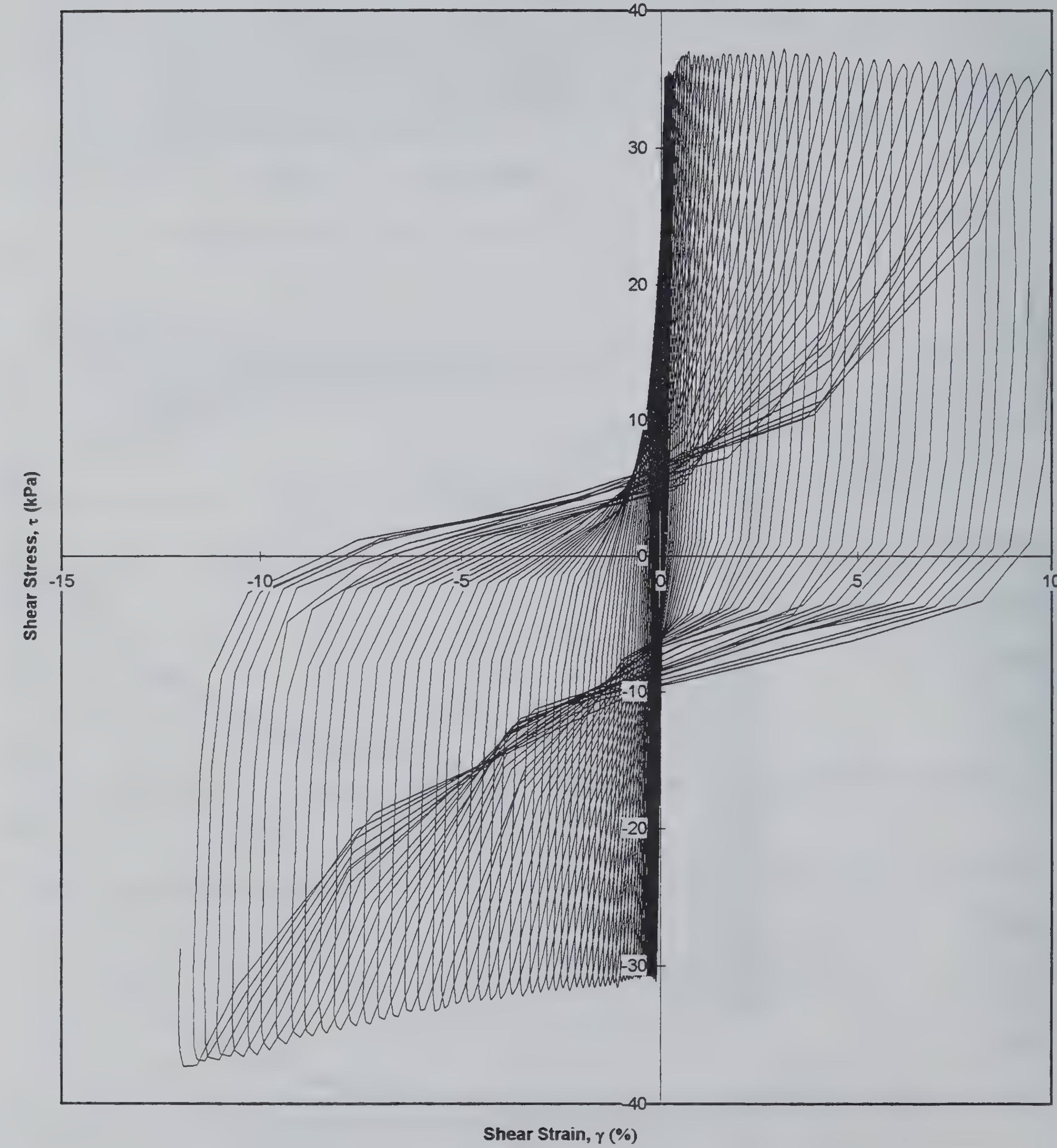

d:\nit\itp\cy_files\B23P3BCY.XLS

8/21/96 7:48 AM

Test I.D.:	B23P3MCY	**Controlled Parameter:**	Stress
Fines Content (%):	18.5	**Initial Effective Stress (kPa):**	200
Dry Density (kN/m^3):	15.22		

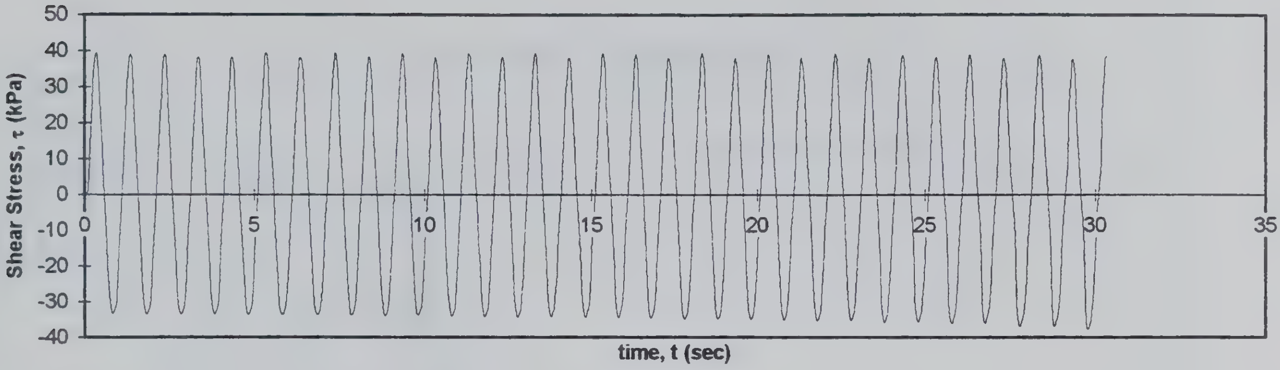

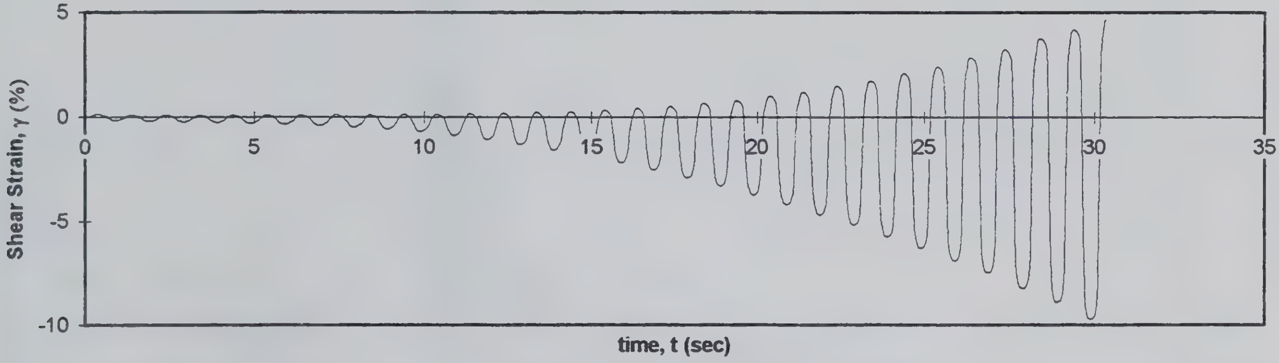

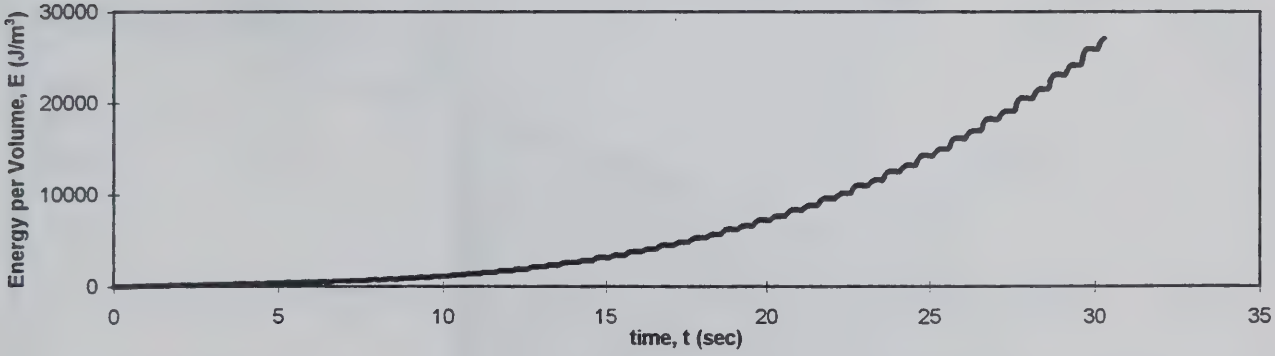

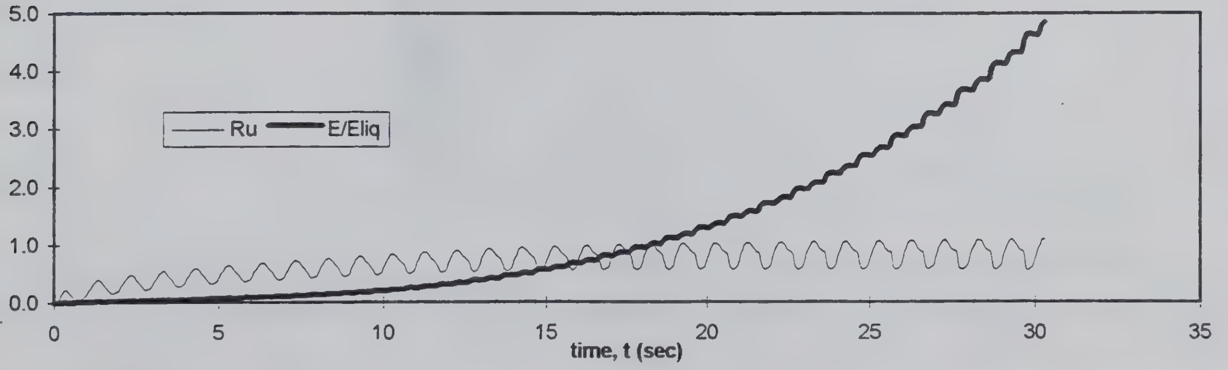

Test I.D.:	B23P3MCY	**Controlled Parameter:**	Stress
Fines Content (%):	18.5	**Initial Effective Stress (kPa):**	200
Dry Density (kN/m^3):	15.22		

Shear Stress vs. Shear Strain

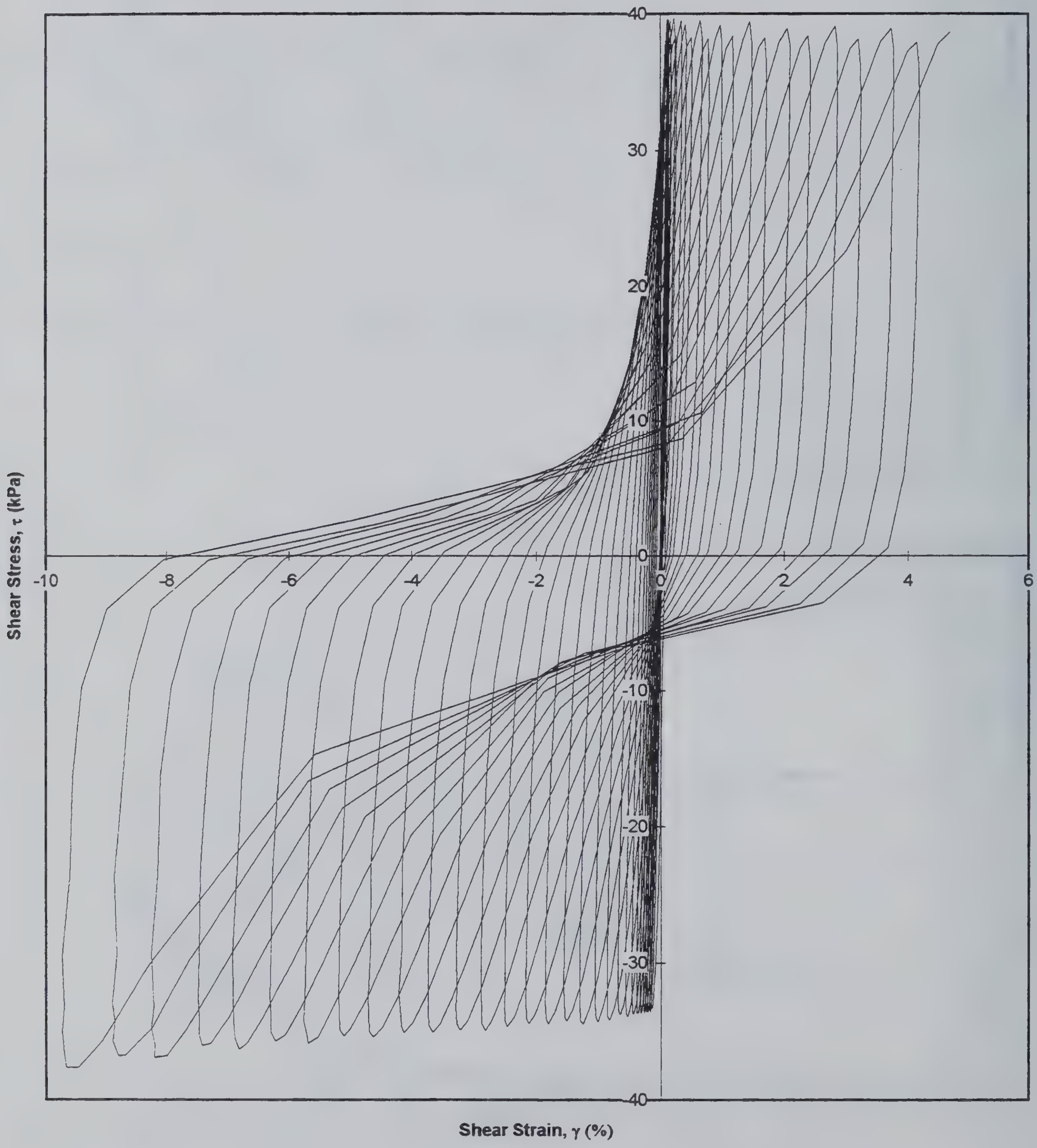

d:\nit\itp\cy_files\B23P3MCY.XLS

8/21/96 7:52 AM

Test I.D.:	B23P3TCY	**Controlled Parameter:**	Stress
Fines Content (%):	20.5	**Initial Effective Stress (kPa):**	200
Dry Density (kN/m³):	16.63		

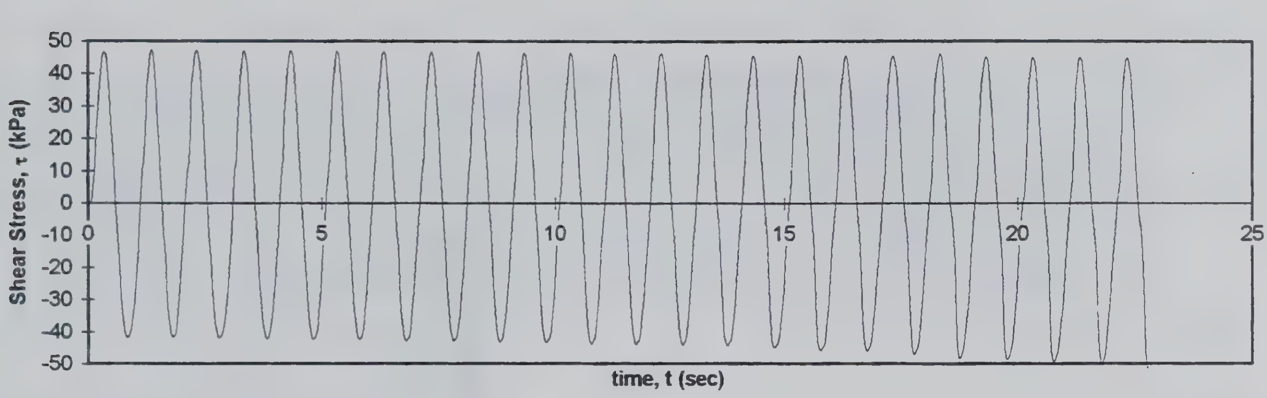

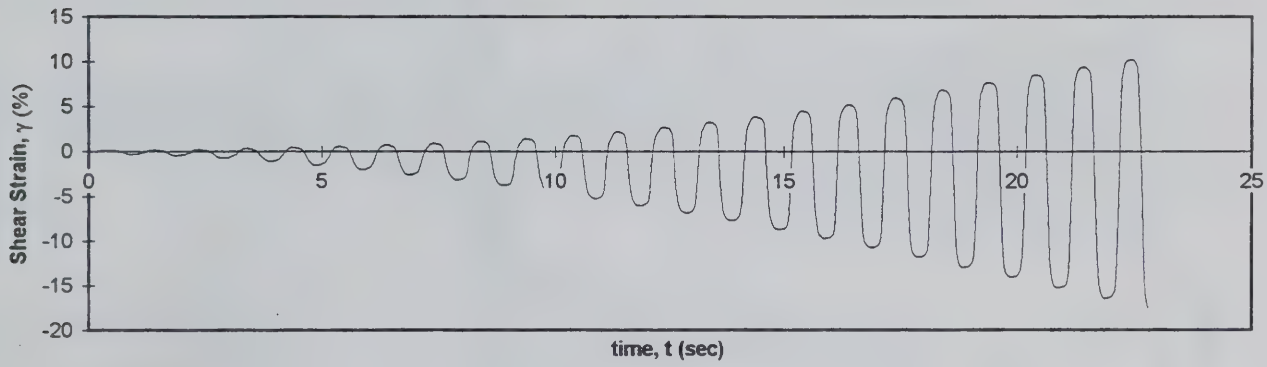

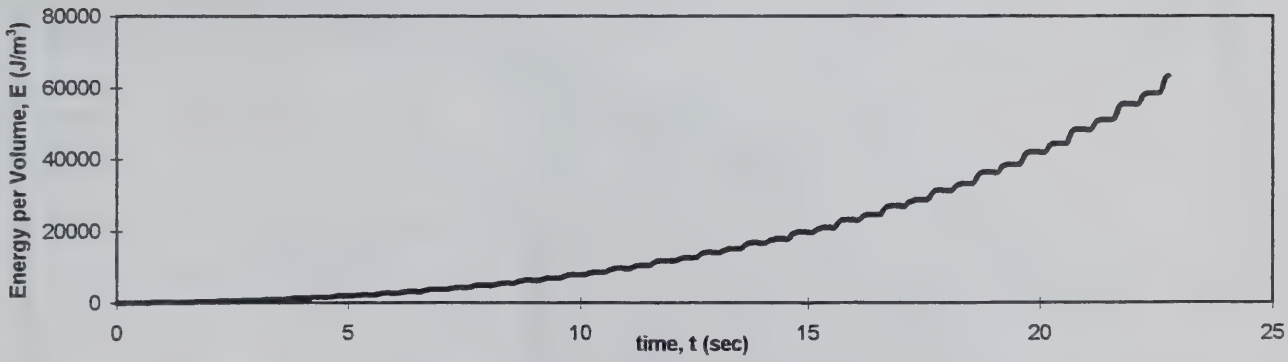

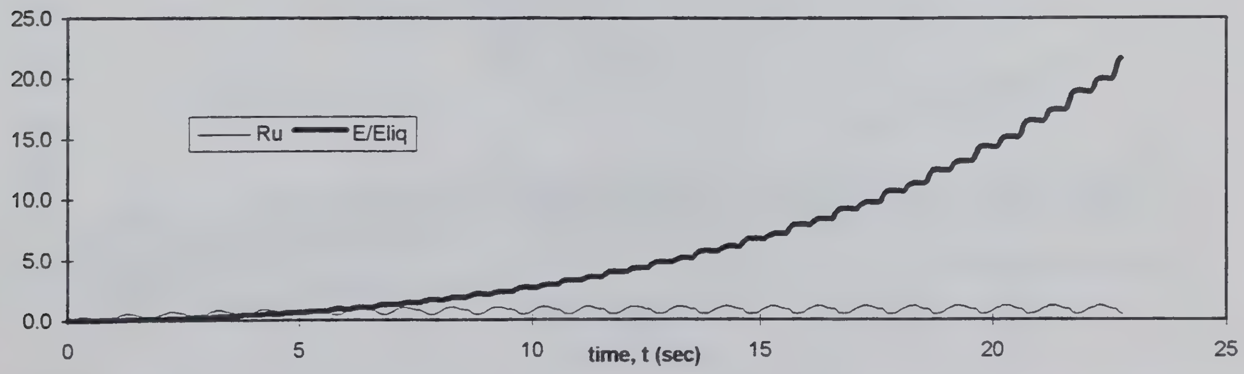

Test I.D.:	B23P3TCY	**Controlled Parameter:**	Stress
Fines Content (%):	20.5	**Initial Effective Stress (kPa):**	200
Dry Density (kN/m^3):	16.63		

Shear Stress vs. Shear Strain

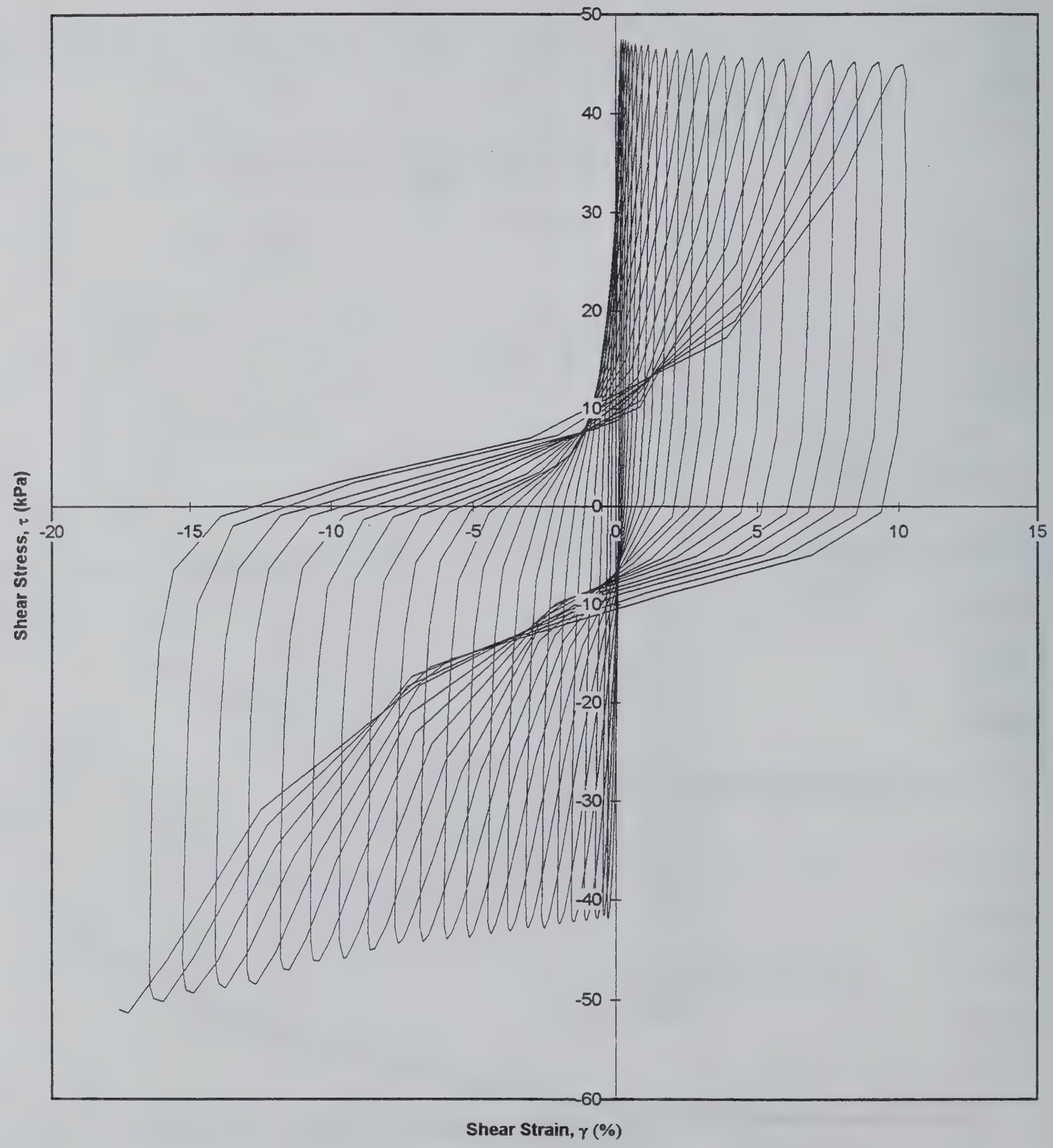

d:\nit\itp\cy_files\B23P3TCY.XLS

8/21/96 7:57 AM

Test I.D.: B12P5BCY
Fines Content (%): 27
Dry Density (kN/m^3): 15.82
Controlled Parameter: Stress
Initial Effective Stress (kPa): 300

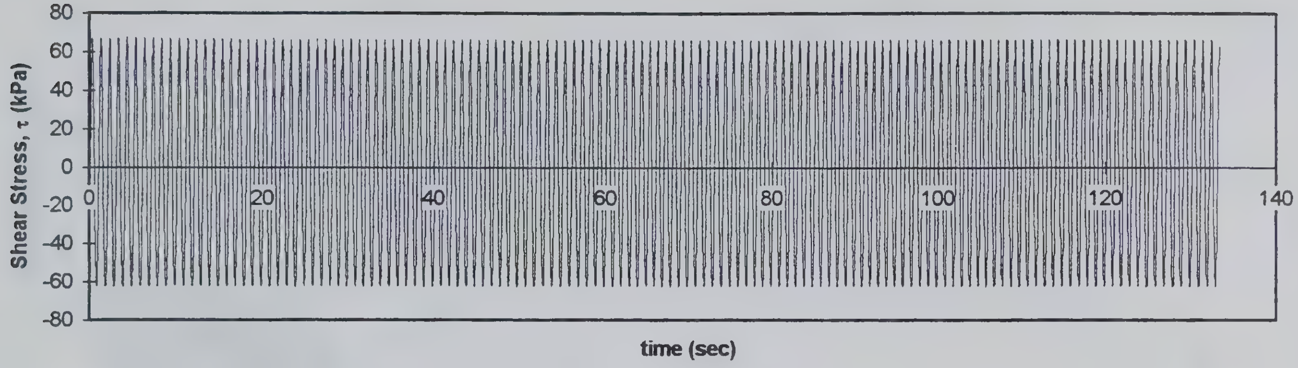

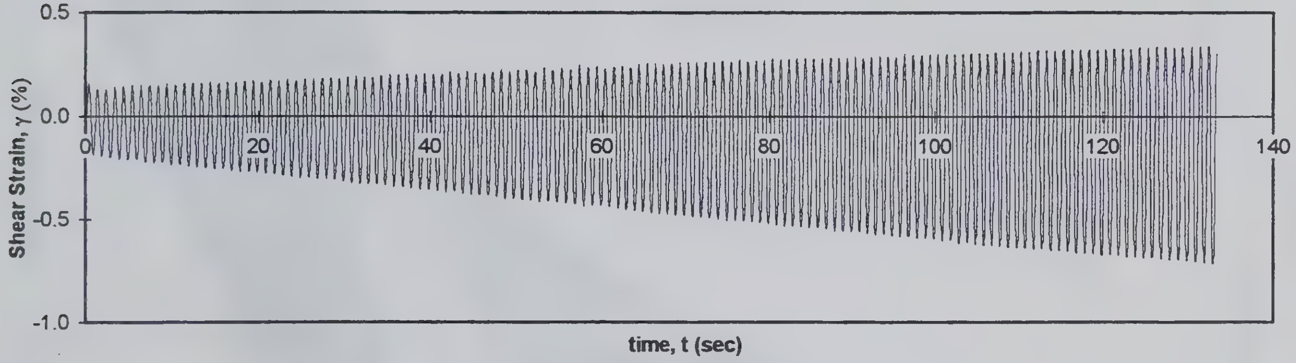

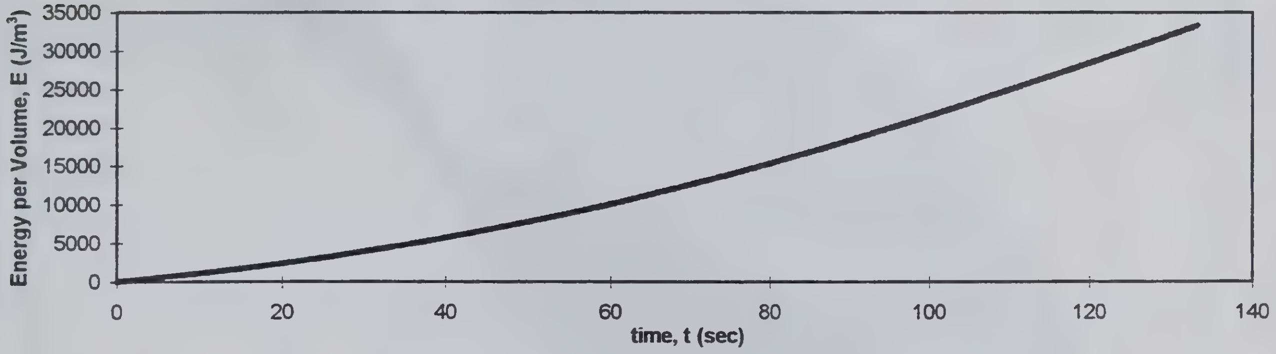

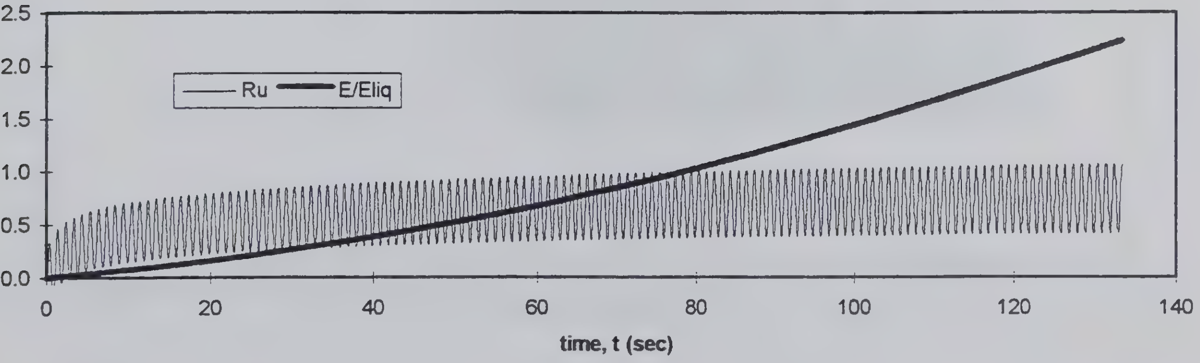

Test I.D.:	B12P5BCY	**Controlled Parameter:**	Stress
Fines Content (%):	27	**Initial Effective Stress (kPa):**	300
Dry Density (kN/m^3):	15.82		

Shear Stress vs. Shear Strain

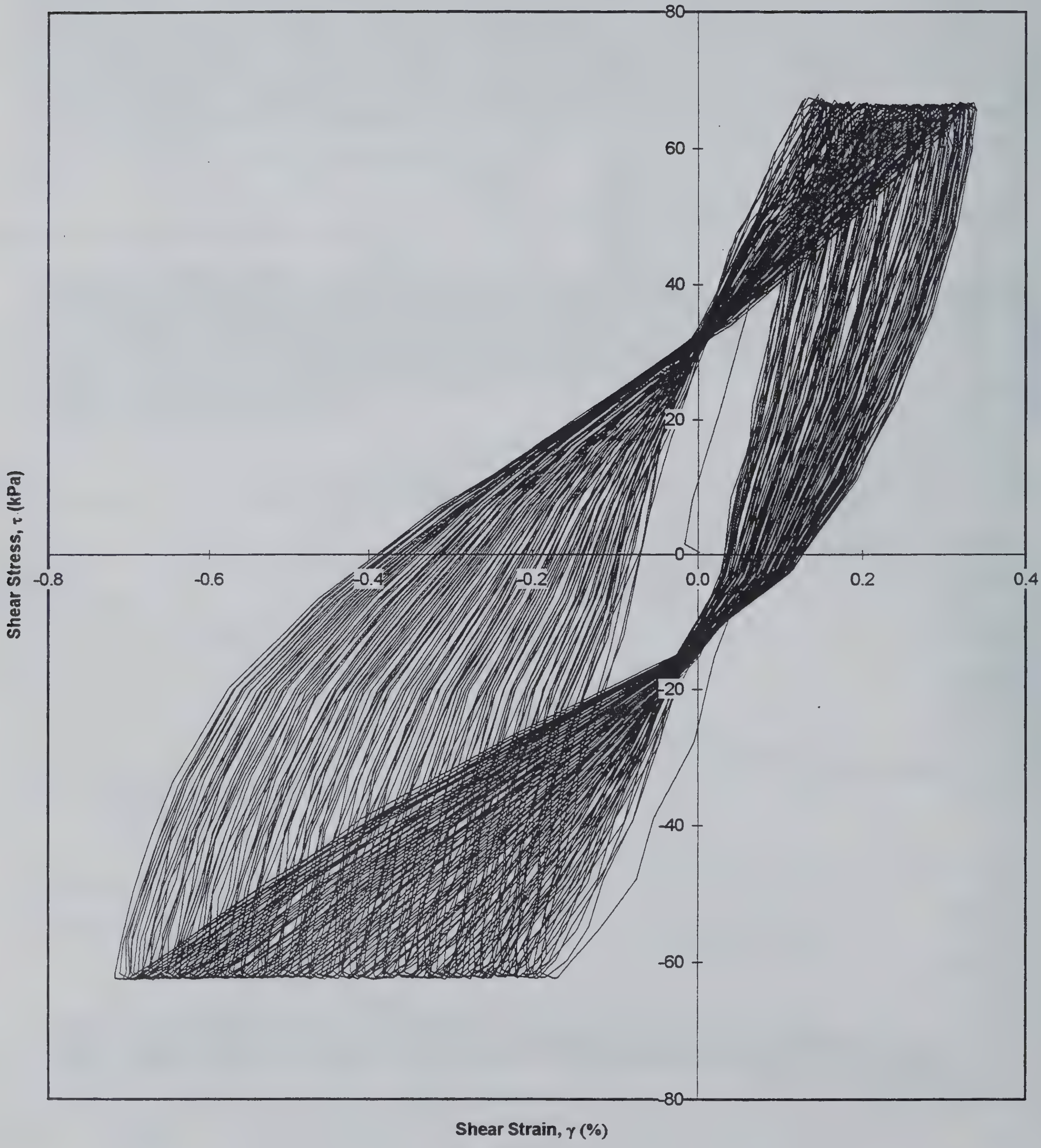

d:\nit\itp\cy_files\B12P5BCY.XLS

8/20/96 4:34 PM

Test I.D.: B12P5MCY
Fines Content (%): 26.8
Dry Density (kN/m^3): 16.78

Controlled Parameter: Stress
Initial Effective Stress (kPa): 300

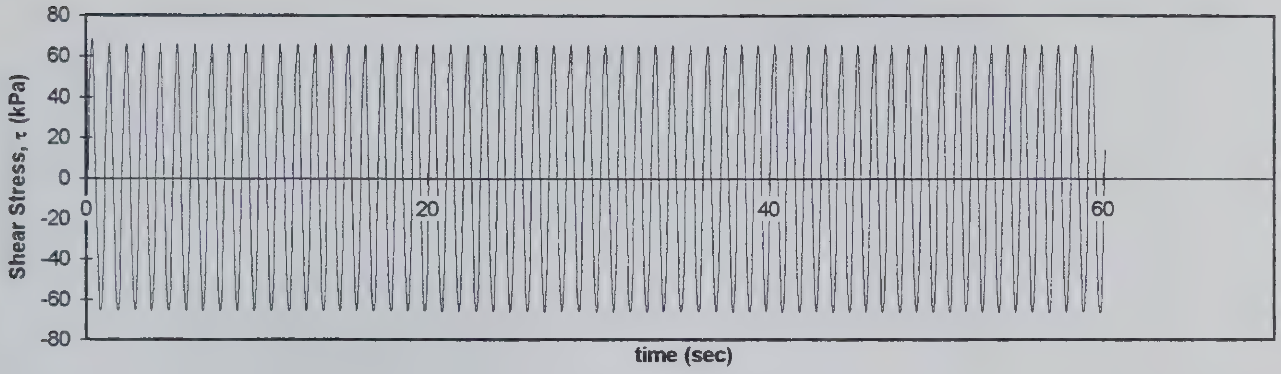

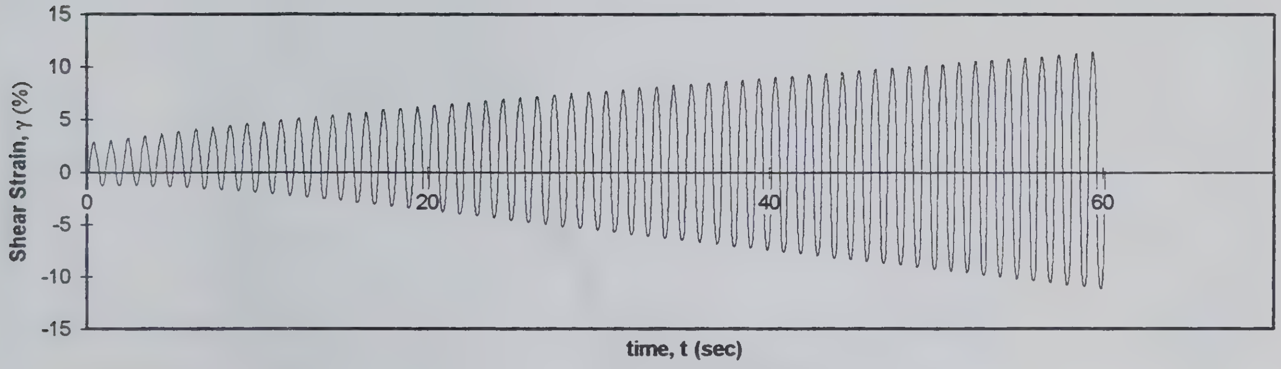

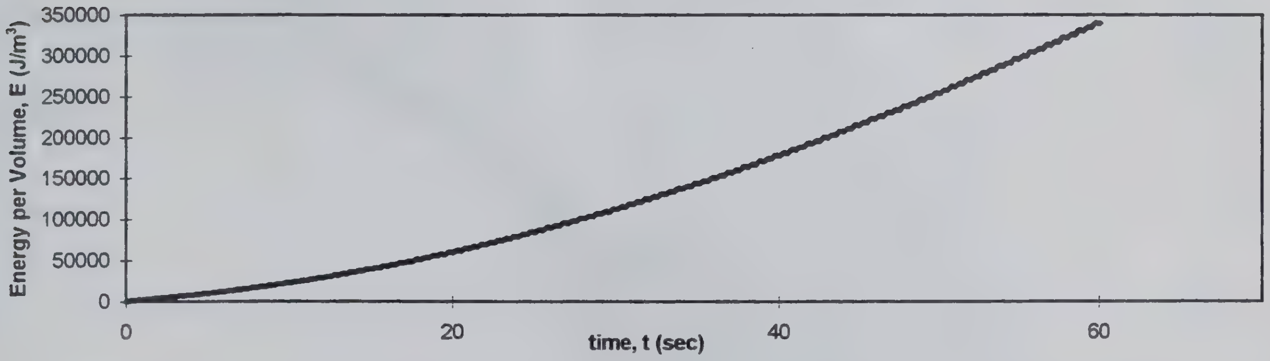

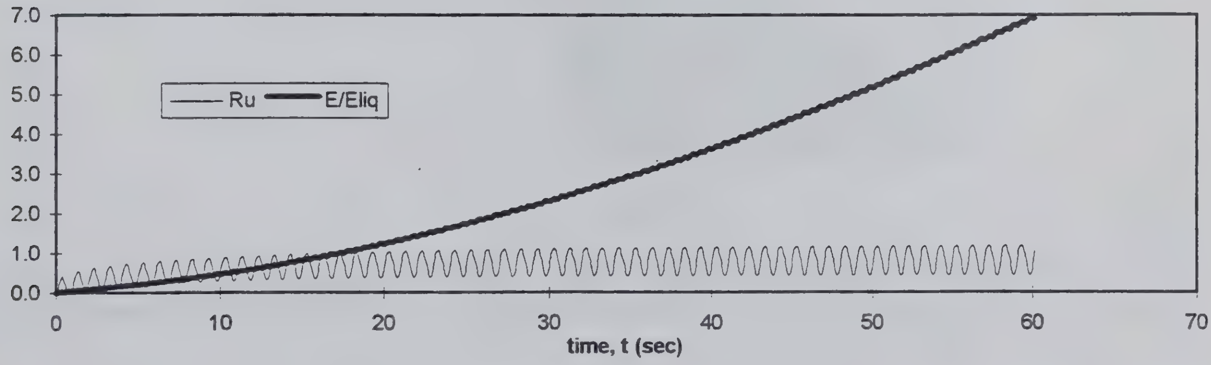

Test I.D.:	B12P5MCY	**Controlled Parameter:**	Stress
Fines Content (%):	26.8	**Initial Effective Stress (kPa):**	300
Dry Density (kN/m^3):	16.78		

Shear Stress vs. Shear Strain

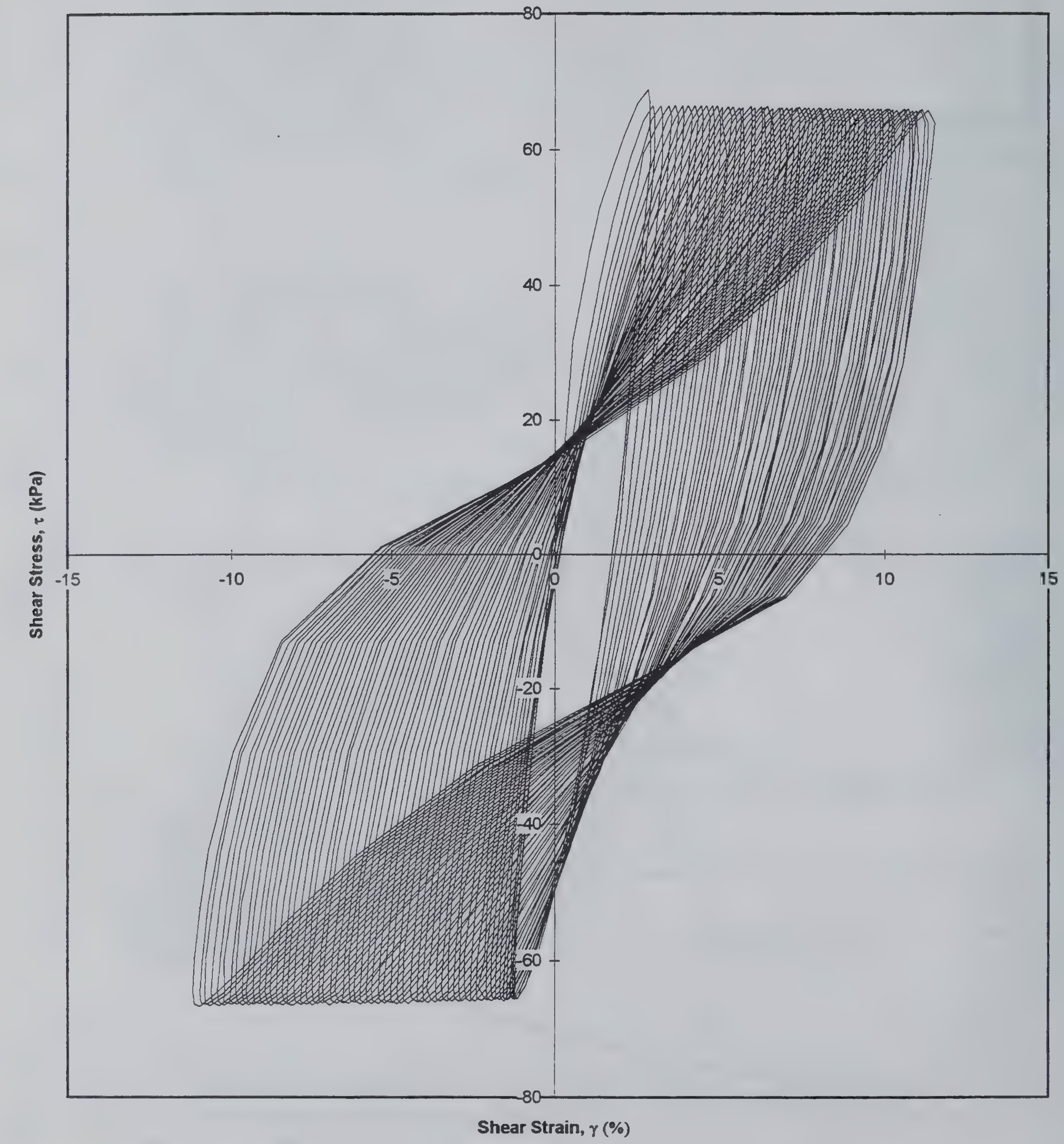

Test I.D.: B12P5TCY
Fines Content (%): 22.3
Dry Density (kN/m^3): 18.02
Controlled Parameter: Stress
Initial Effective Stress (kPa): 300

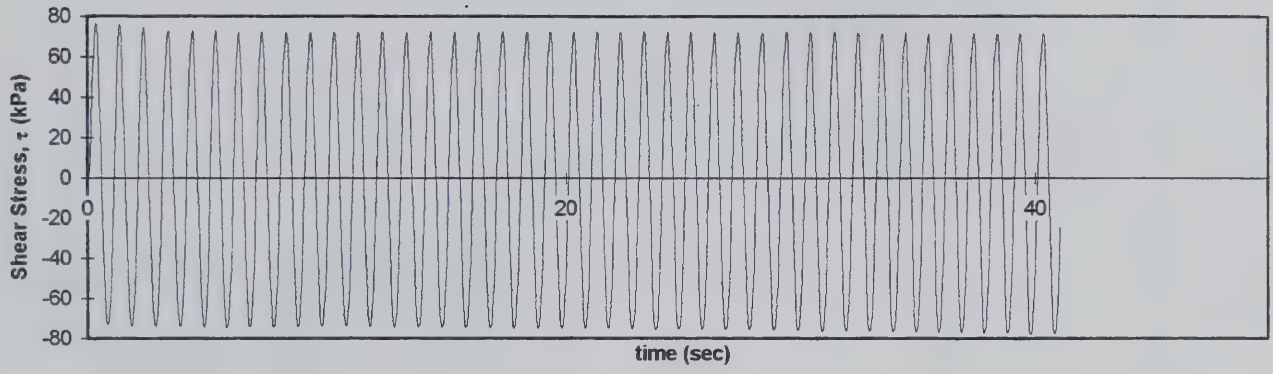

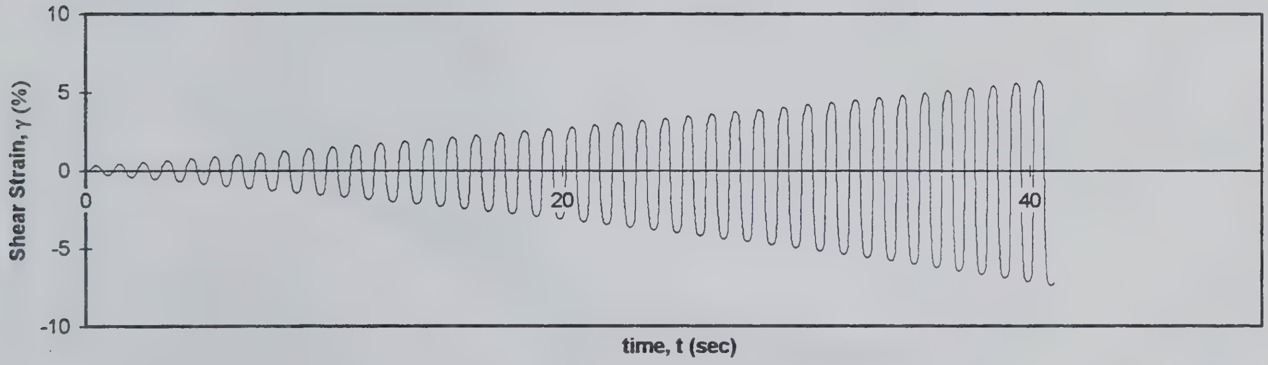

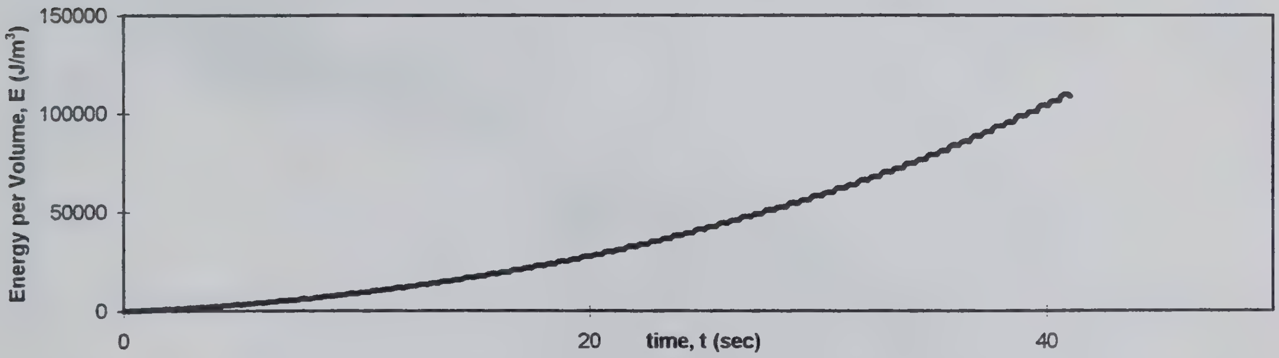

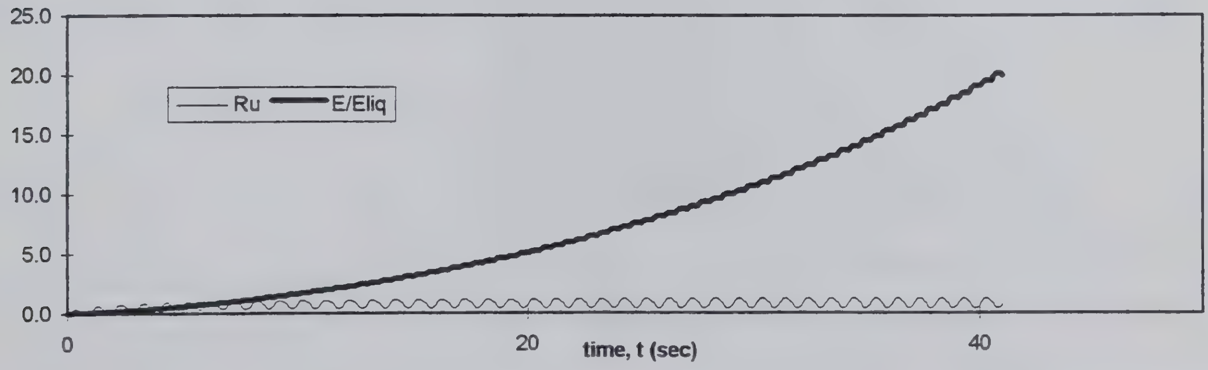

Test I.D.:	B12P5TCY	**Controlled Parameter:**	Stress
Fines Content (%):	22.3	**Initial Effective Stress (kPa):**	300
Dry Density (kN/m^3):	18.02		

Shear Stress vs. Shear Strain

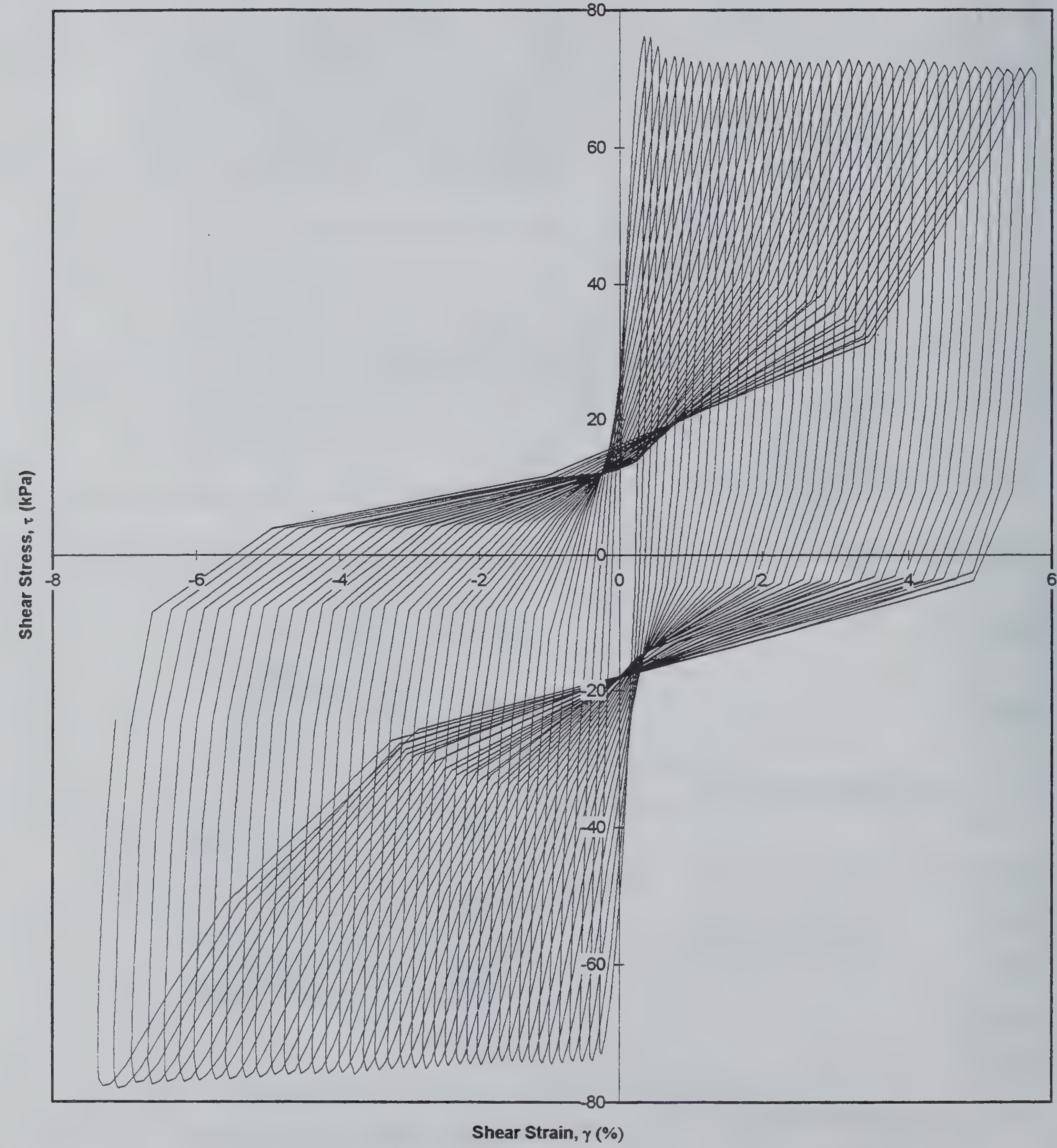

d:\nit\itp\cy_files\B12P5TCY.XLS

8/20/96 4:45 PM

Test I.D.: B12P7BCY
Fines Content (%): 15.7
Dry Density (kN/m^3): 15.91
Controlled Parameter: Stress
Initial Effective Stress (kPa): 375

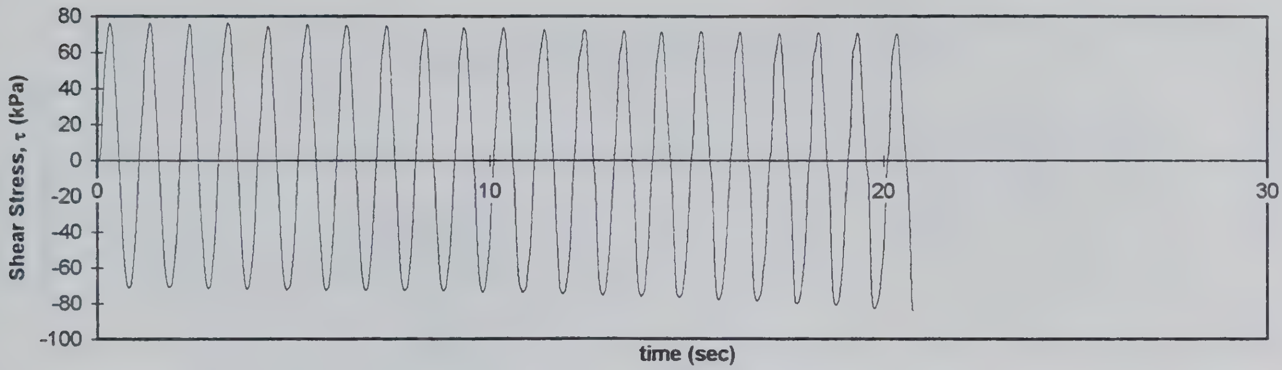

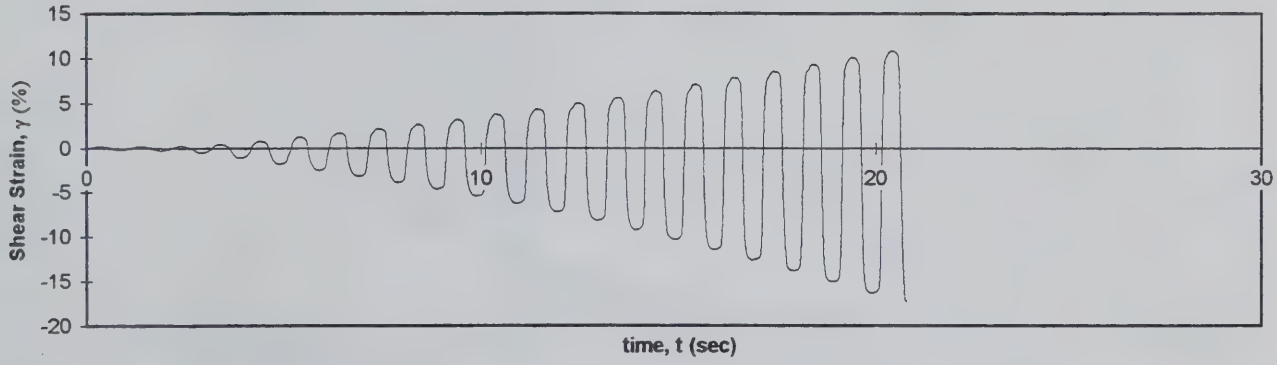

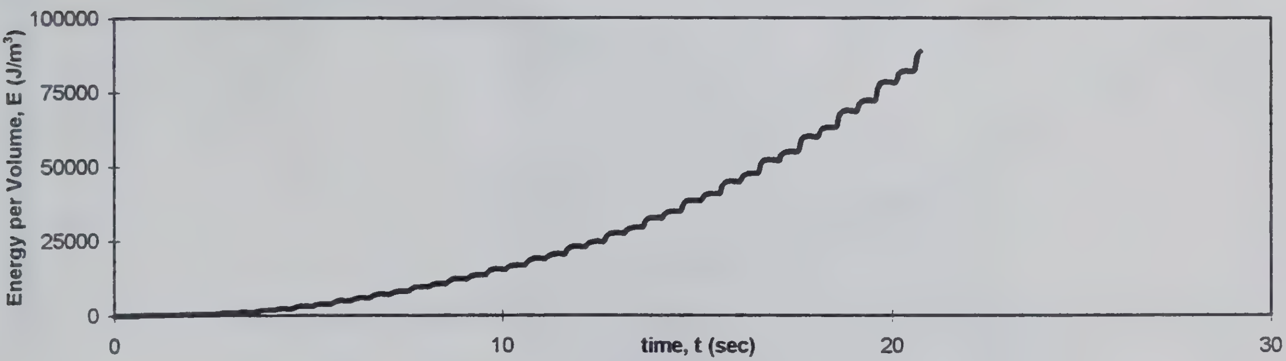

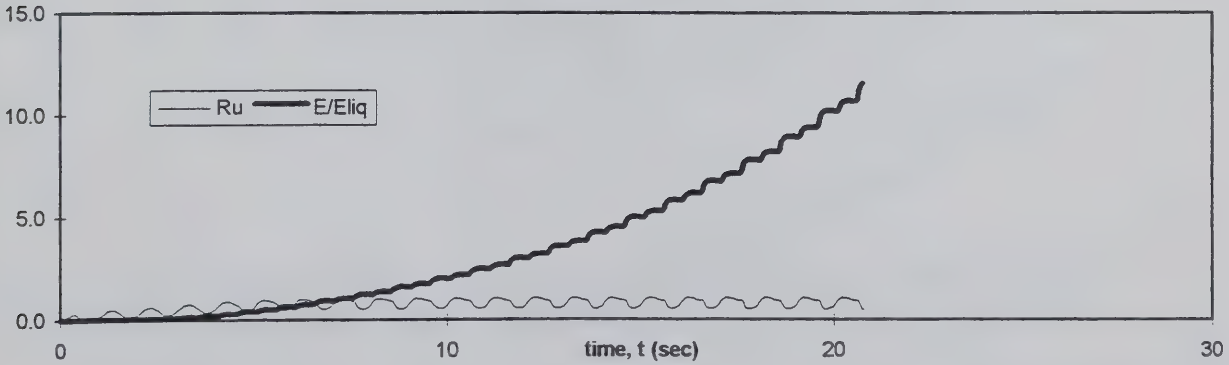

Test I.D.: B12P7BCY
Fines Content (%): 15.7
Dry Density (kN/m^3): 15.91

Controlled Parameter: Stress
Initial Effective Stress (kPa): 375

Shear Stress vs. Shear Strain

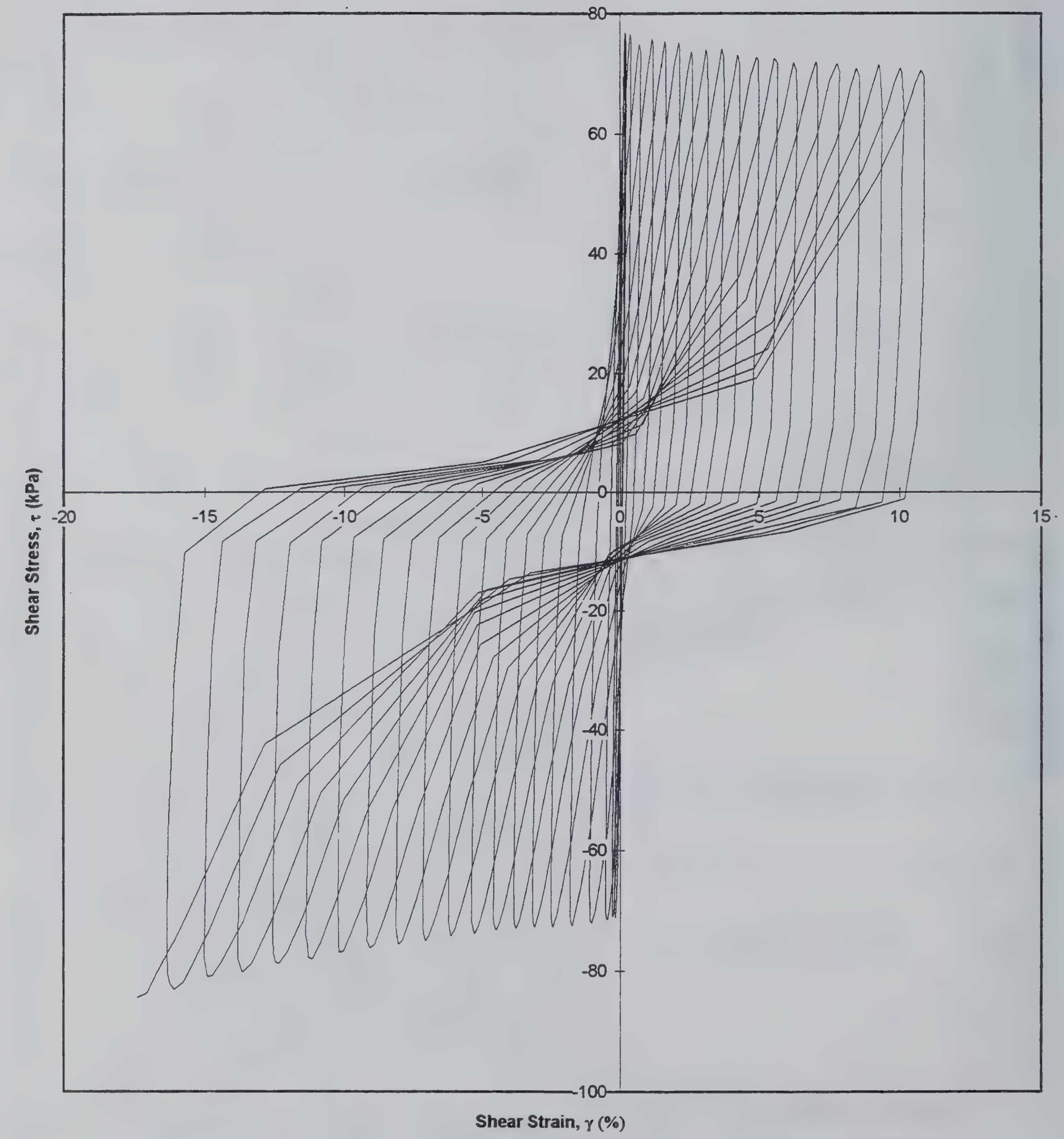

Test I.D.: B12P7MCY

Fines Content (%): 17

Dry Density (kN/m^3): 16.25

Controlled Parameter: Stress

Initial Effective Stress (kPa): 375

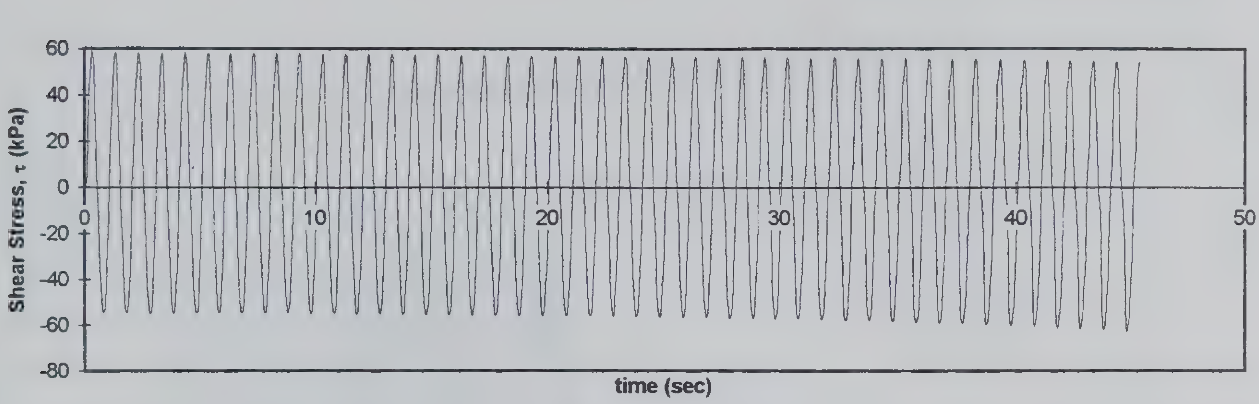

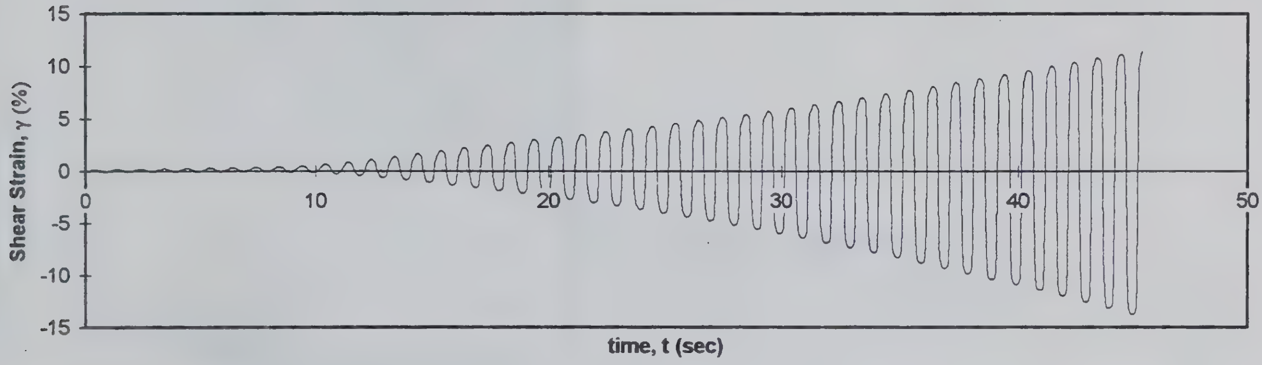

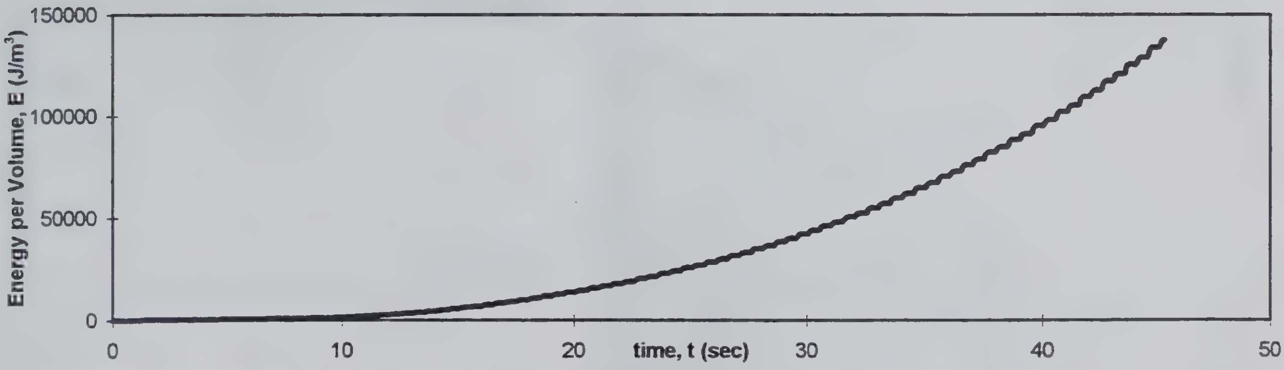

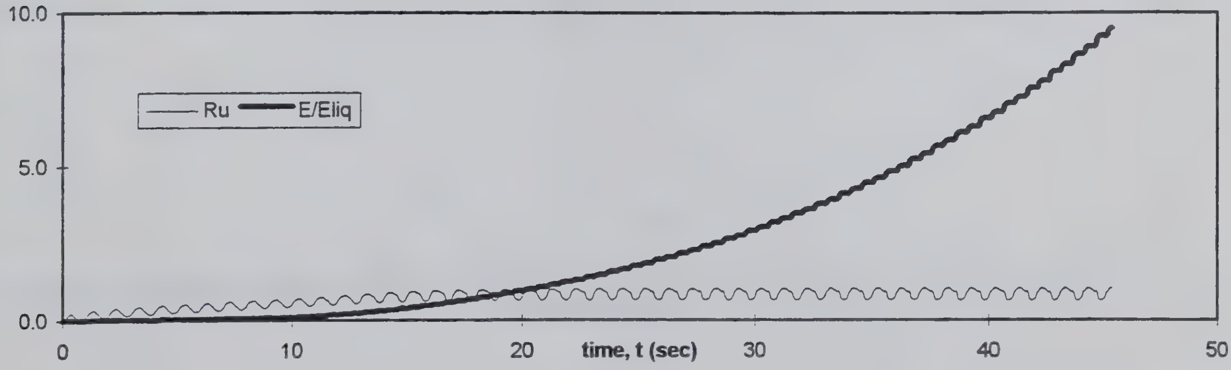

Test I.D.:	B12P7MCY	**Controlled Parameter:**	Stress
Fines Content (%):	17	**Initial Effective Stress (kPa):**	375
Dry Density (kN/m^3):	16.25		

Shear Stress vs. Shear Strain

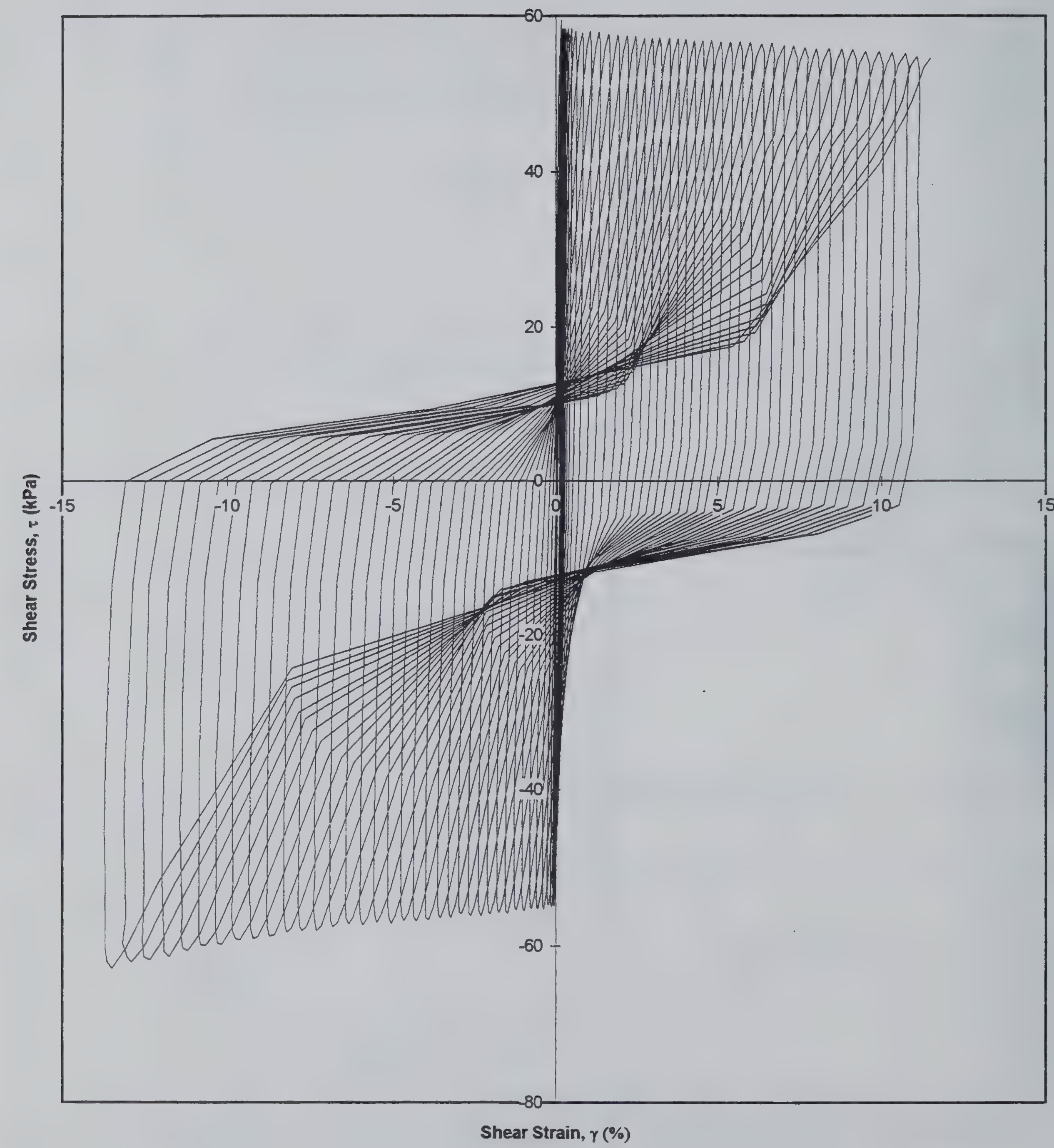

d:\nit\itp\cy_files\B12P7MCY.XLS

8/20/96 4:54 PM

Test I.D.:	B12P7TCY	**Controlled Parameter:**	Stress
Fines Content (%):	15.7	**Initial Effective Stress (kPa):**	375
Dry Density (kN/m^3):	16.24		

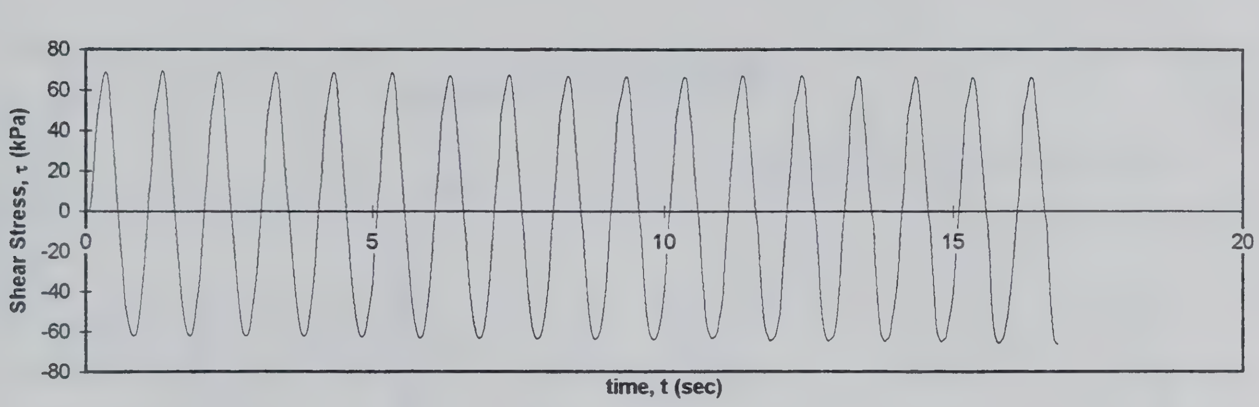

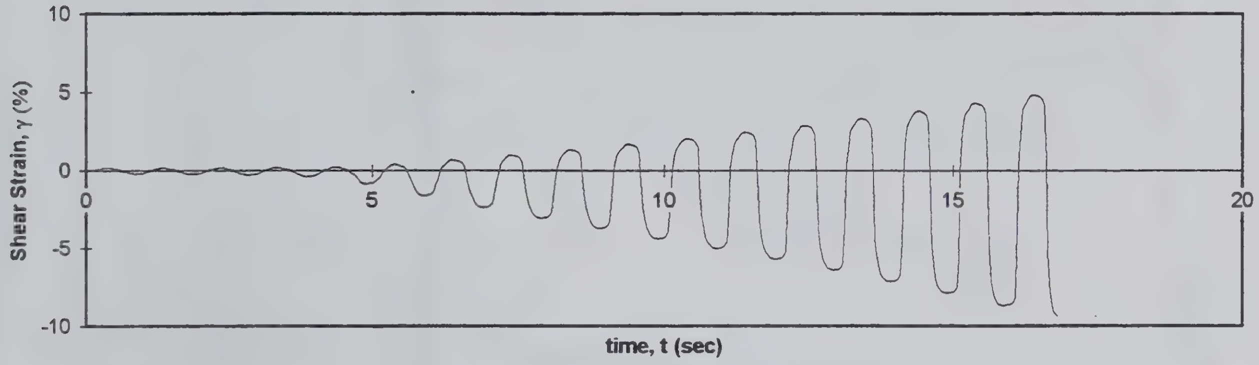

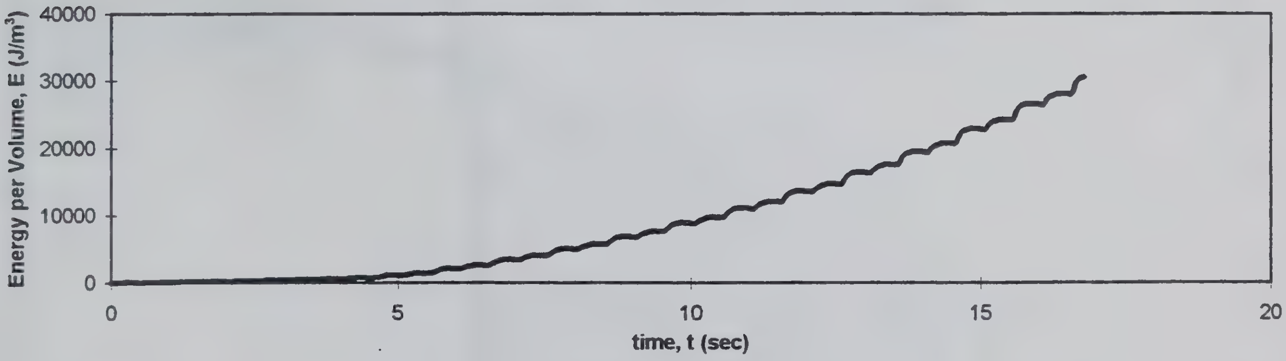

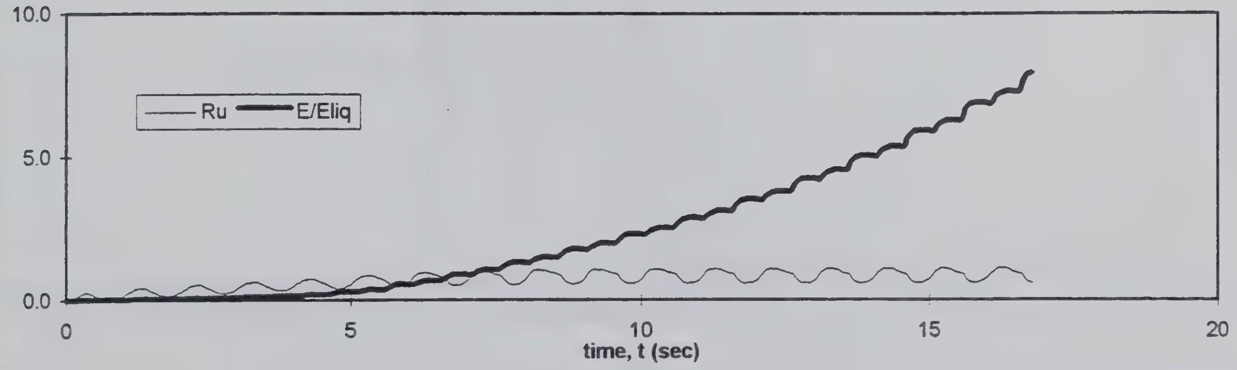

Test I.D.:	B12P7TCY	**Controlled Parameter:**	Stress
Fines Content (%):	15.7	**Initial Effective Stress (kPa):**	375
Dry Density (kN/m^3):	16.24		

Shear Stress vs. Shear Strain

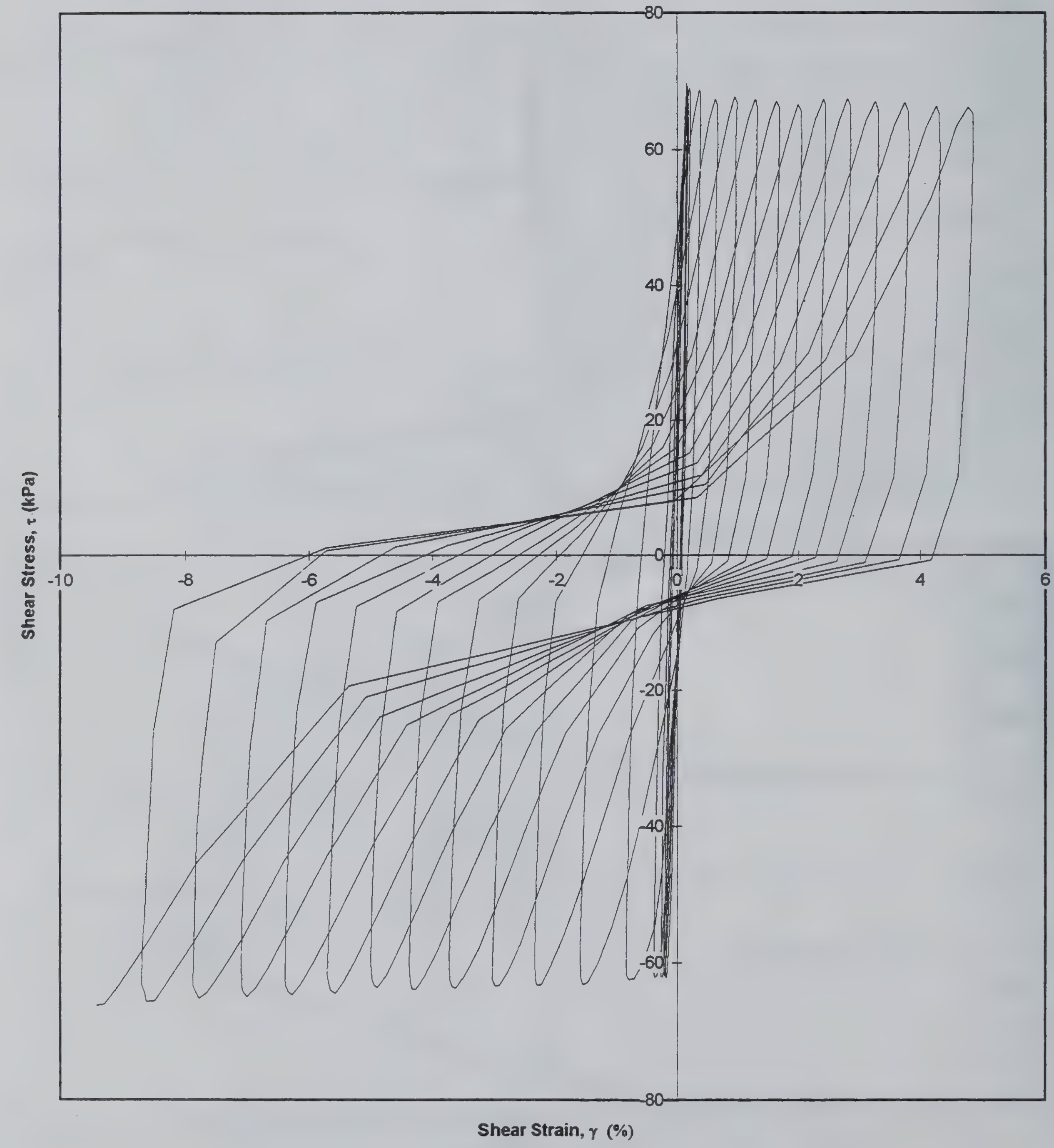

Test I.D.:	B2P5BCYC	**Controlled Parameter:**	Stress
Fines Content (%):	25.4	**Initial Effective Stress (kPa):**	500
Dry Density (kN/m^3):	14.65		

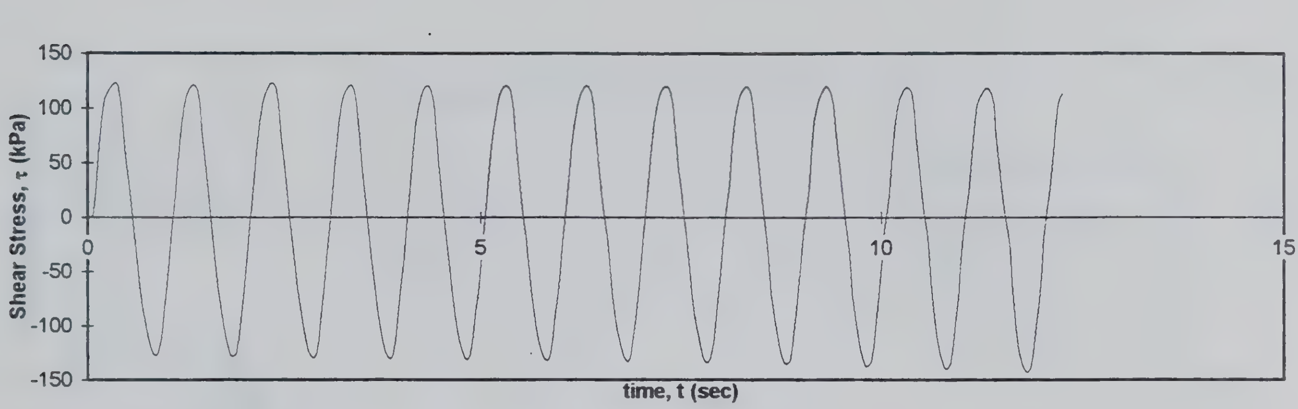

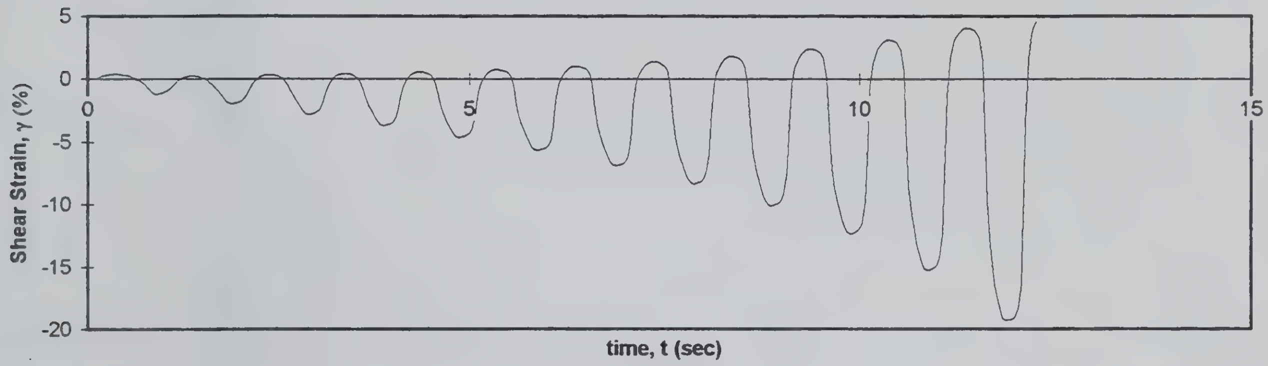

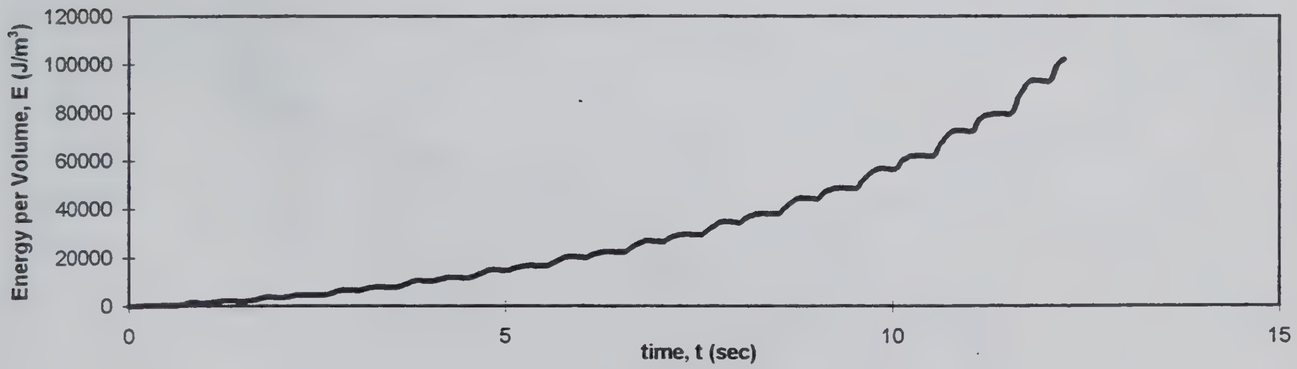

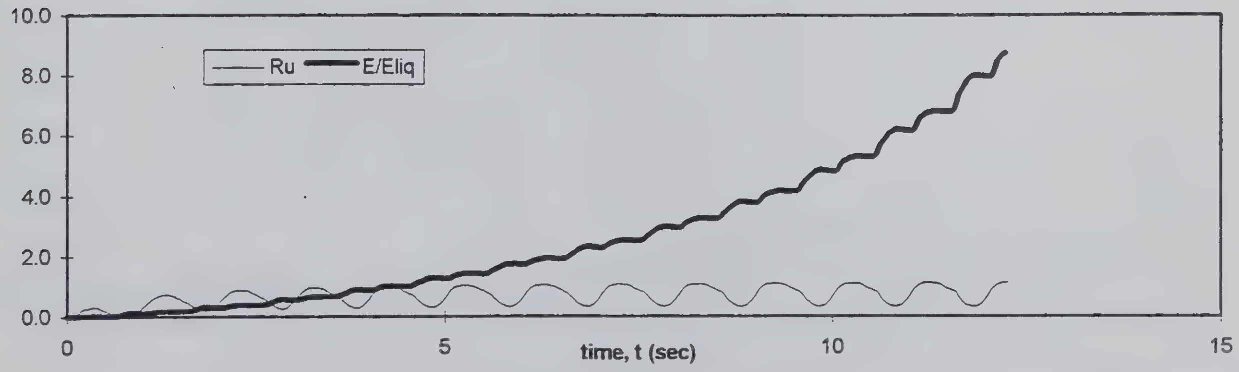

Test I.D.:	B2P5BCYC	**Controlled Parameter:**	Stress
Fines Content (%):	25.4	**Initial Effective Stress (kPa):**	500
Dry Density (kN/m^3):	14.65		

Shear Stress vs. Shear Strain

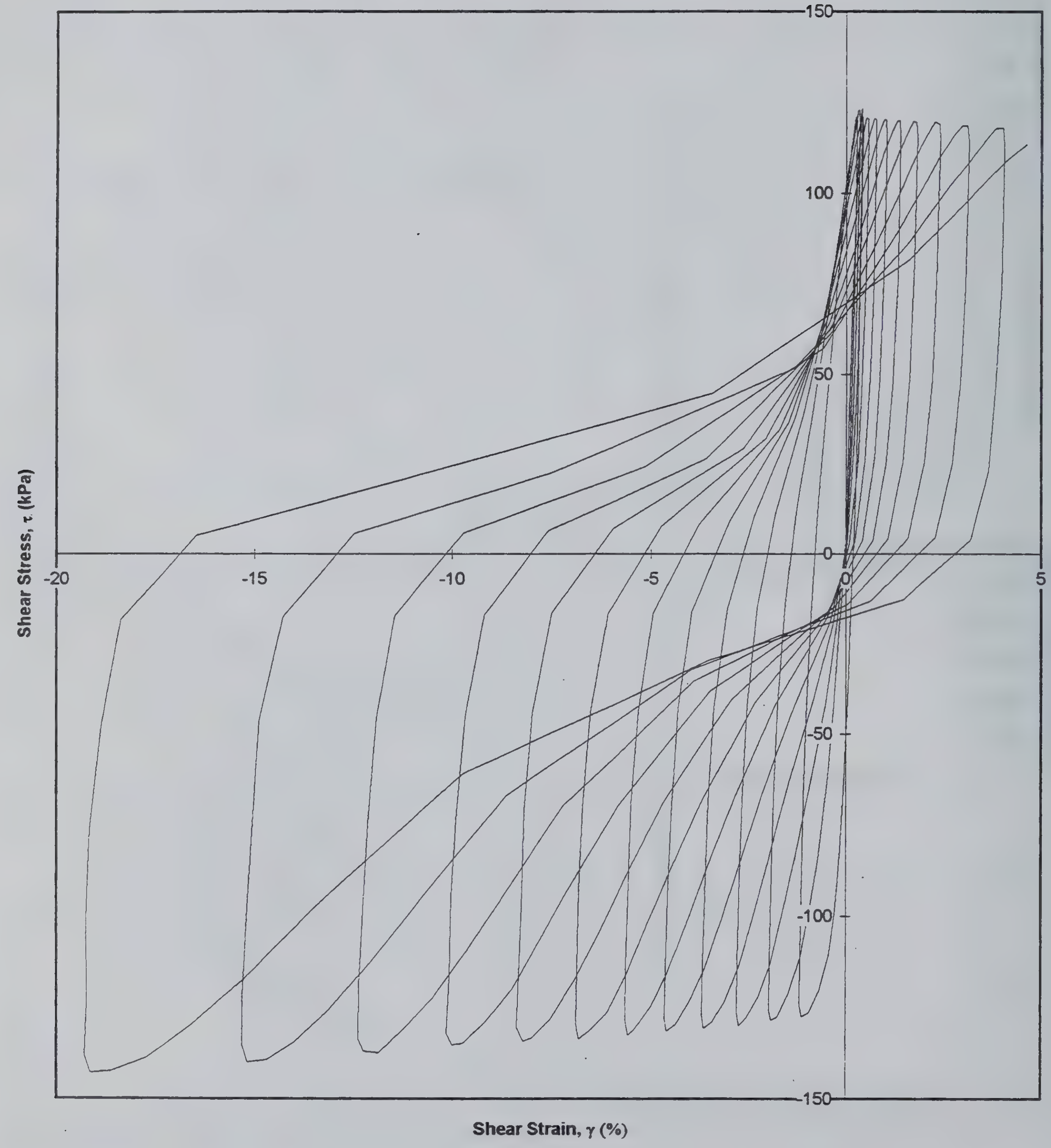

Test I.D.: B2P5MCYC
Fines Content (%): 29.6
Dry Density (kN/m^3): 15.37
Controlled Parameter: Stress
Initial Effective Stress (kPa): 500

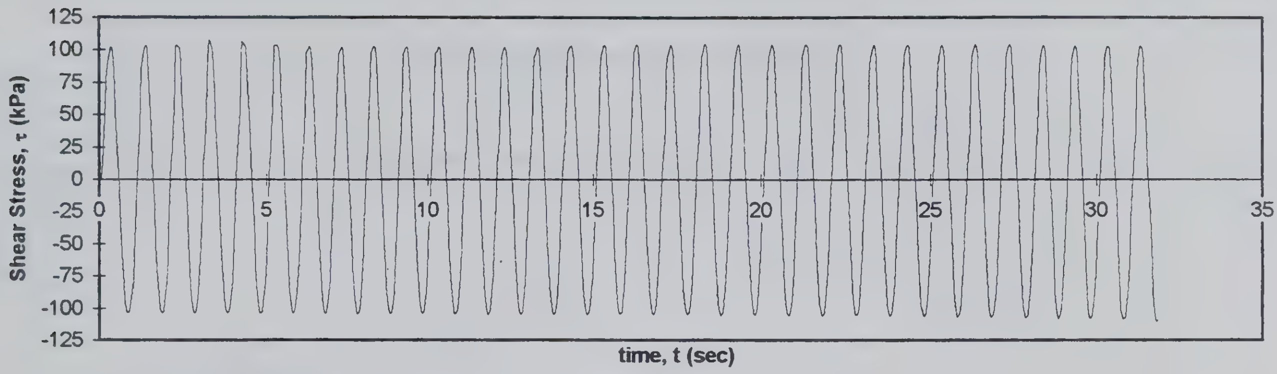

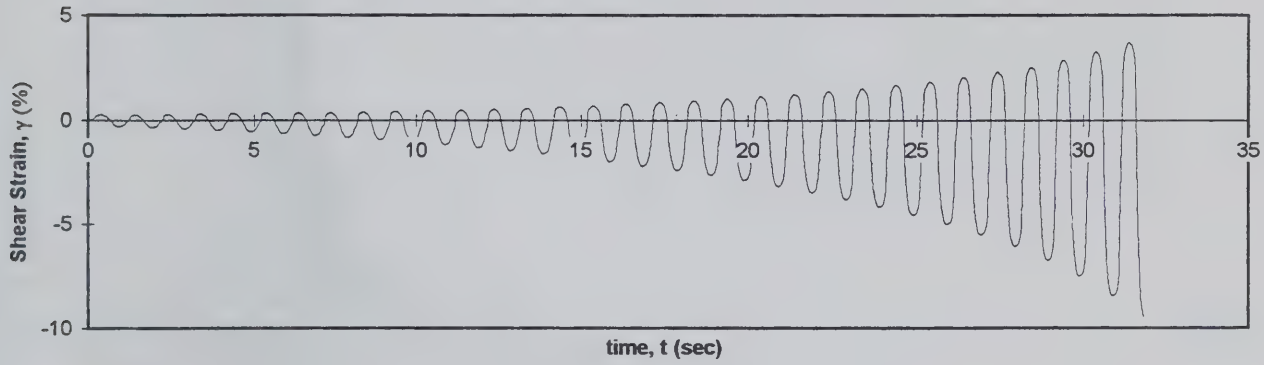

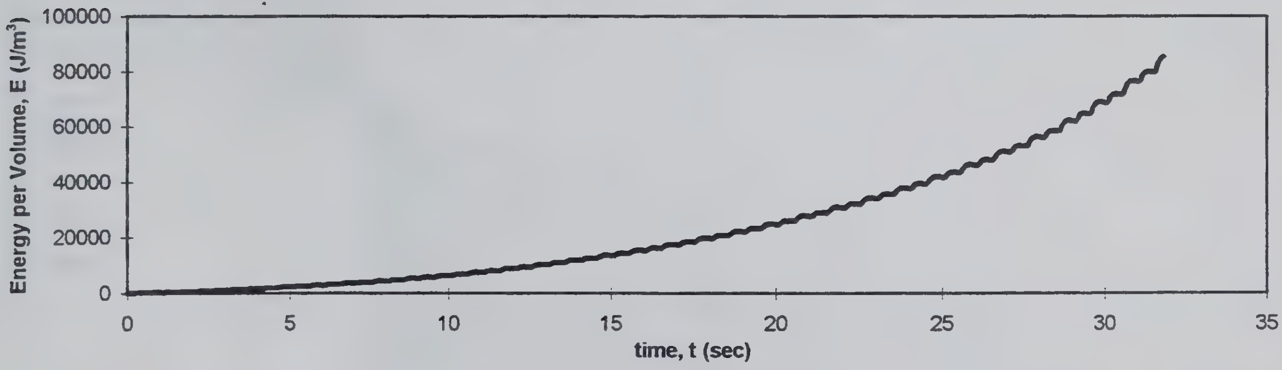

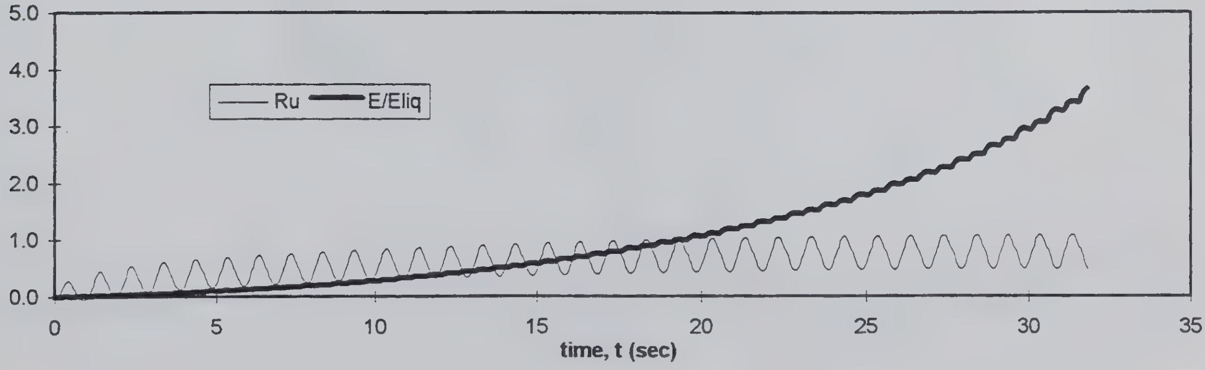

Test I.D.:	B2P5MCYC	**Controlled Parameter:**	Stress
Fines Content (%):	29.6	**Initial Effective Stress (kPa):**	500
Dry Density (kN/m^3):	15.37		

Shear Stress vs. Shear Strain

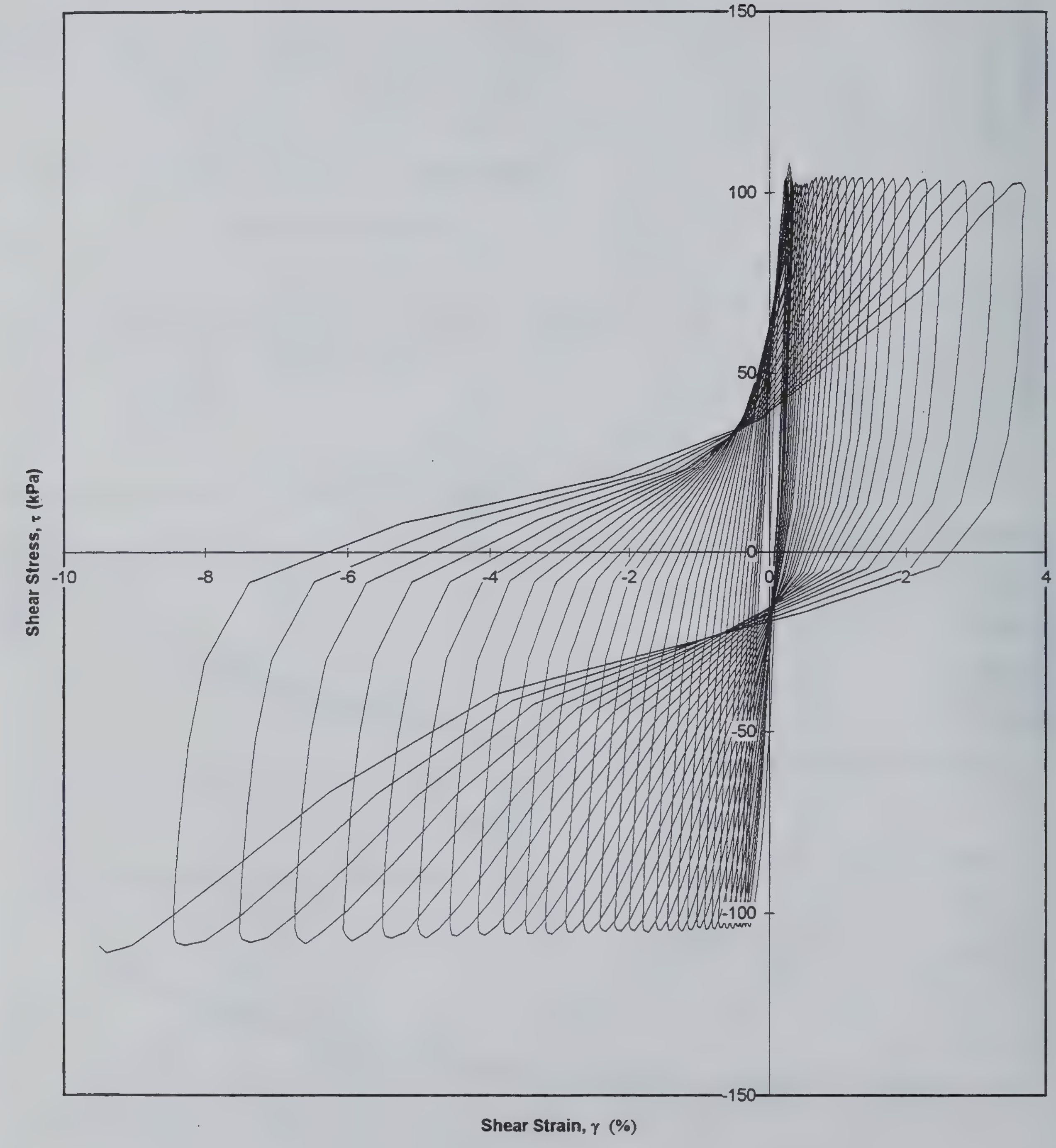

Test I.D.:	B2P5TCYC	**Controlled Parameter:**	Stress
Fines Content (%):	26.6	**Initial Effective Stress (kPa):**	500
Dry Density (kN/m^3):	16.71		

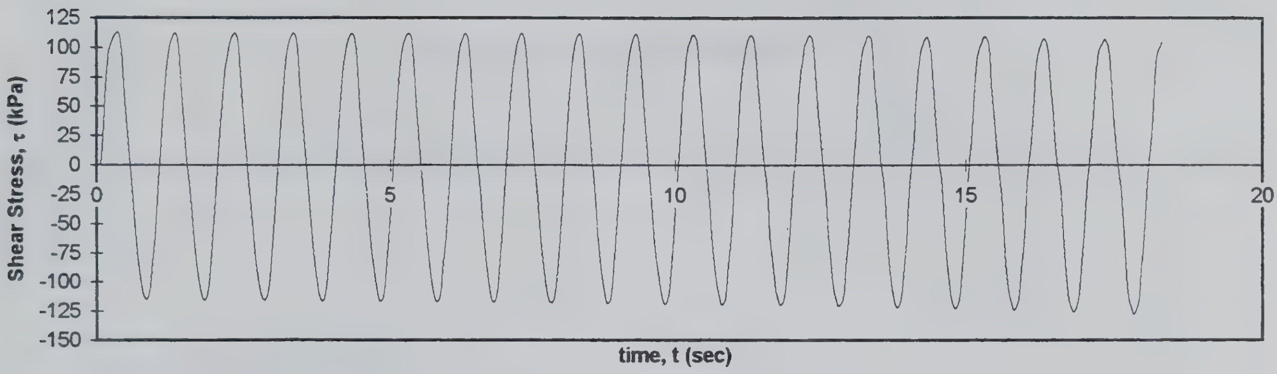

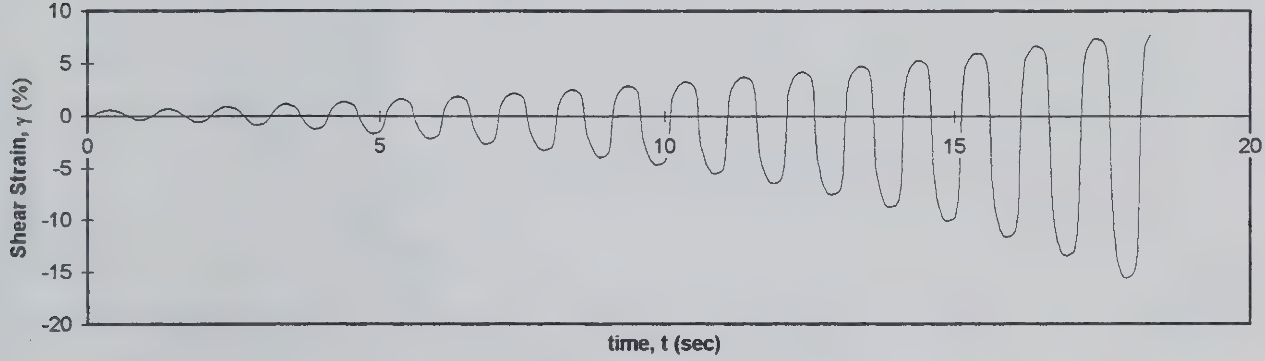

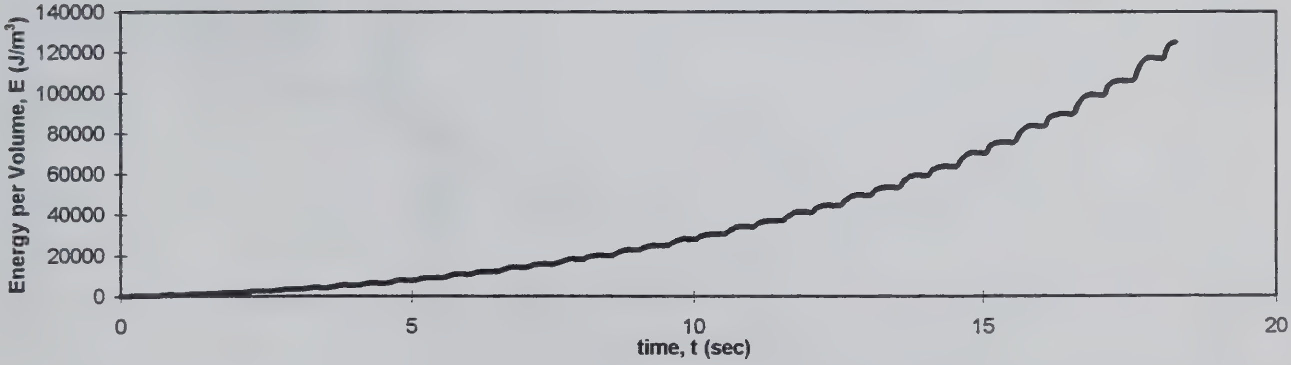

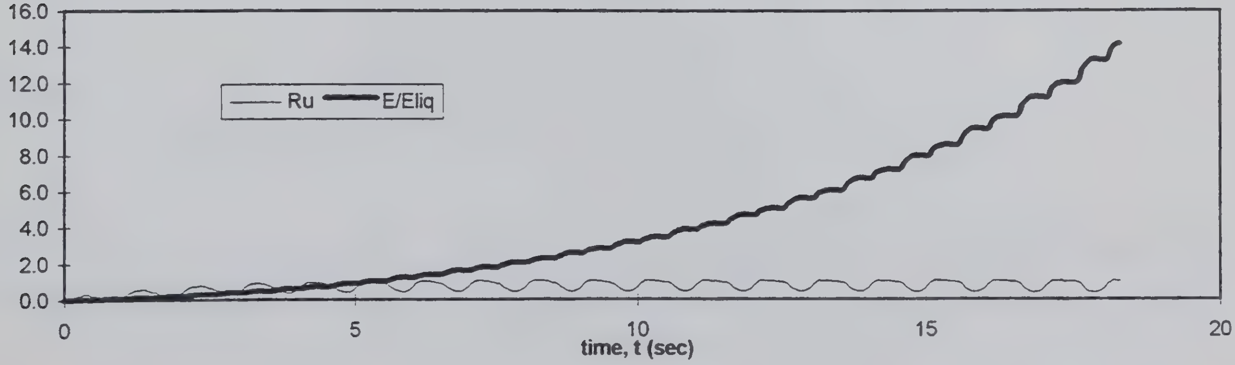

Test I.D.:	B2P5TCYC	**Controlled Parameter:**	Stress
Fines Content (%):	26.6	**Initial Effective Stress (kPa):**	500
Dry Density (kN/m^3):	16.71		

Shear Stress vs. Shear Strain

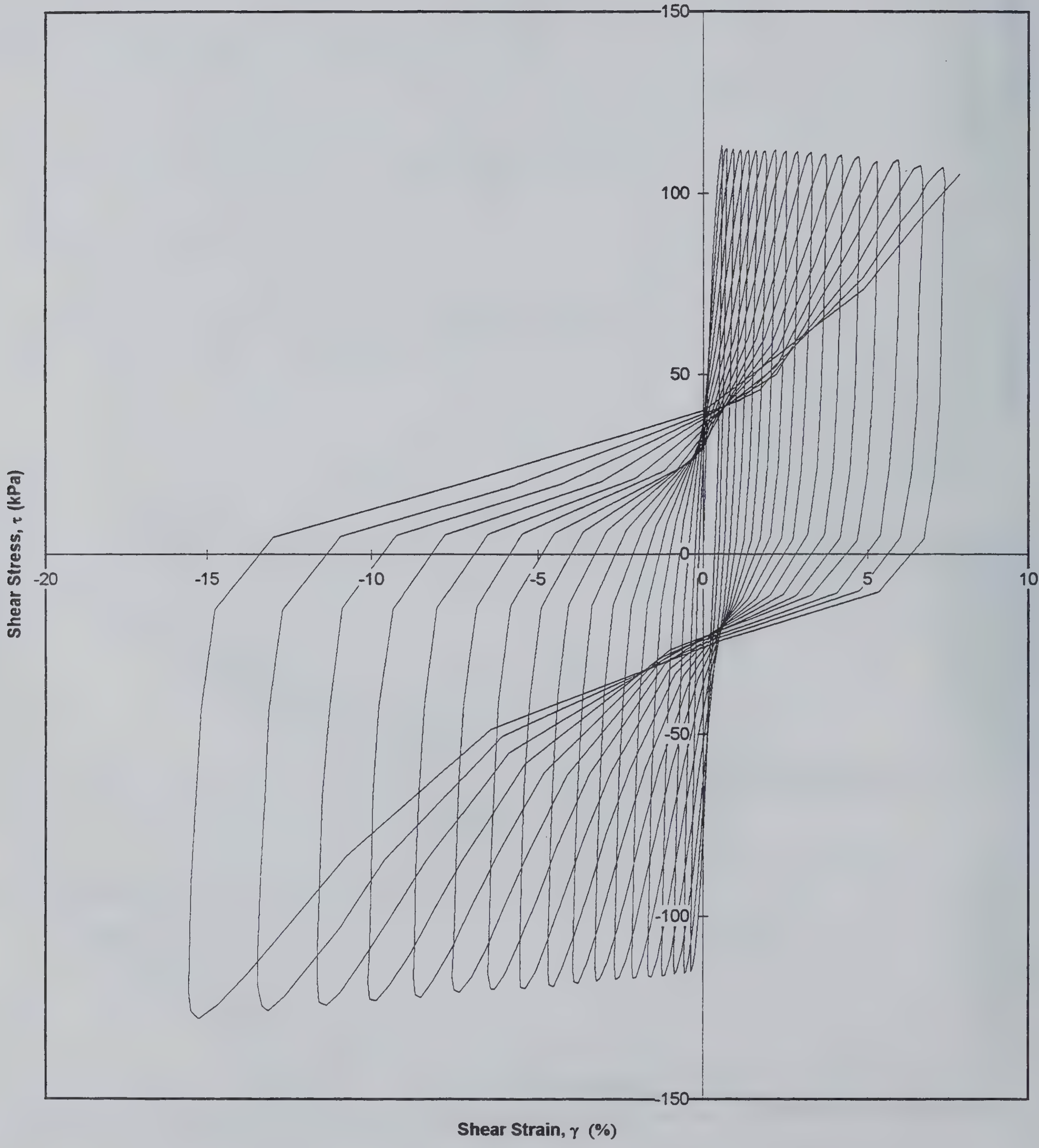

d:\nit\itp\cy_files\B2P5TCYC.XLS

8/21/96 8:25 AM

Test I.D.: B23P4BCY
Fines Content (%): 11.4
Dry Density (kN/m^3): 14.6

Controlled Parameter: Stress
Initial Effective Stress (kPa): 750

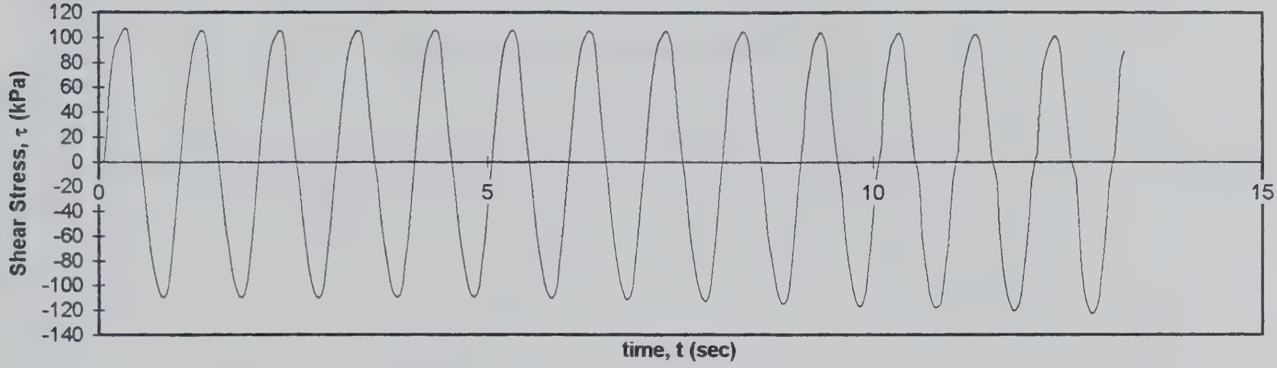

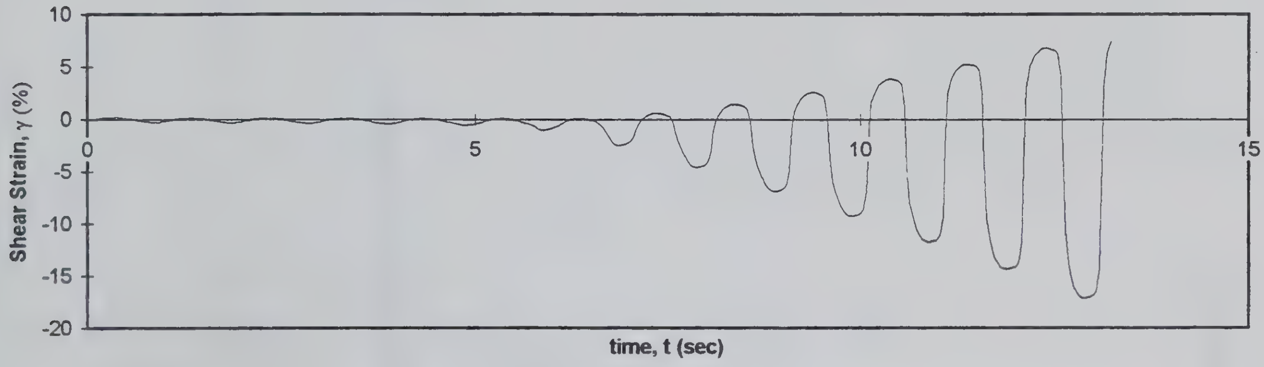

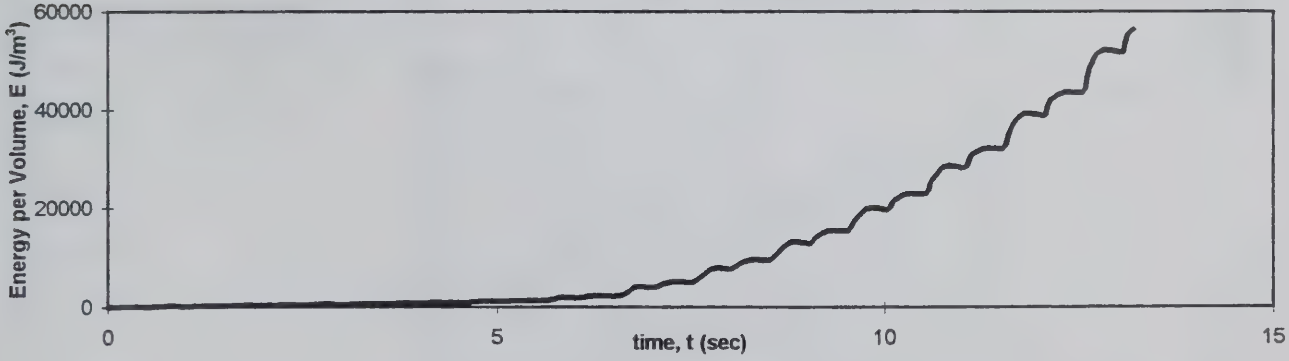

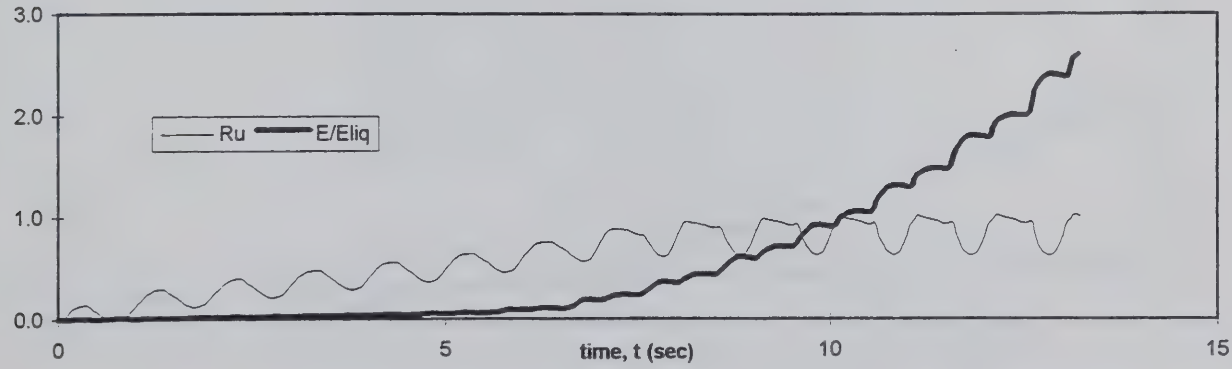

Test I.D.: B23P4BCY
Fines Content (%): 11.4
Dry Density (kN/m^3): 14.6

Controlled Parameter: Stress
Initial Effective Stress (kPa): 750

Shear Stress vs. Shear Strain

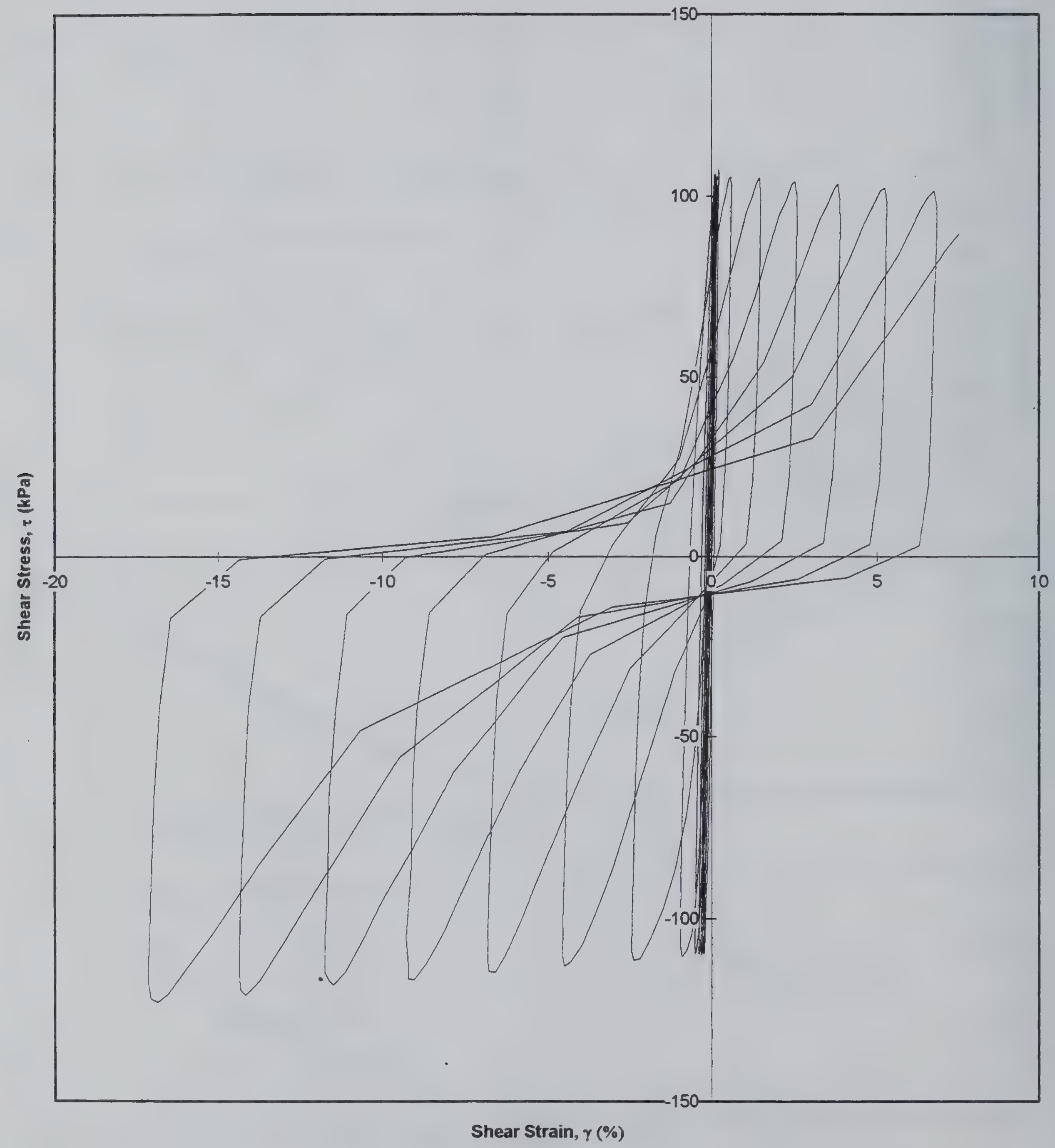

Test I.D.: B23P4MCY
Fines Content (%): 16.5
Dry Density (kN/m^3): 15.53
Controlled Parameter: Stress
Initial Effective Stress (kPa): 700

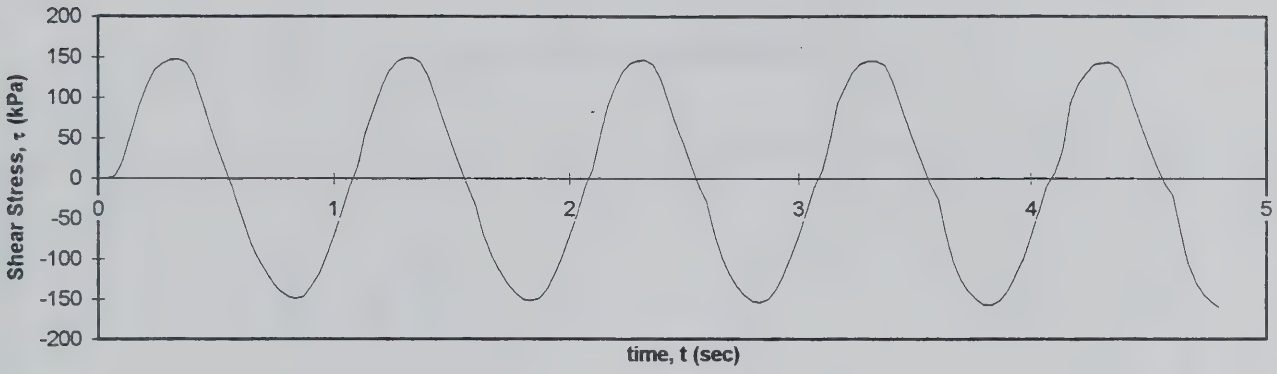

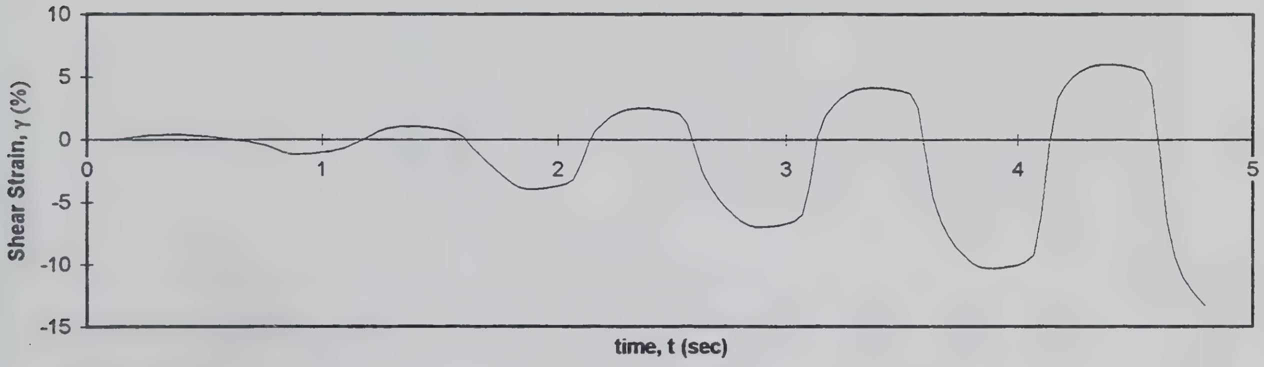

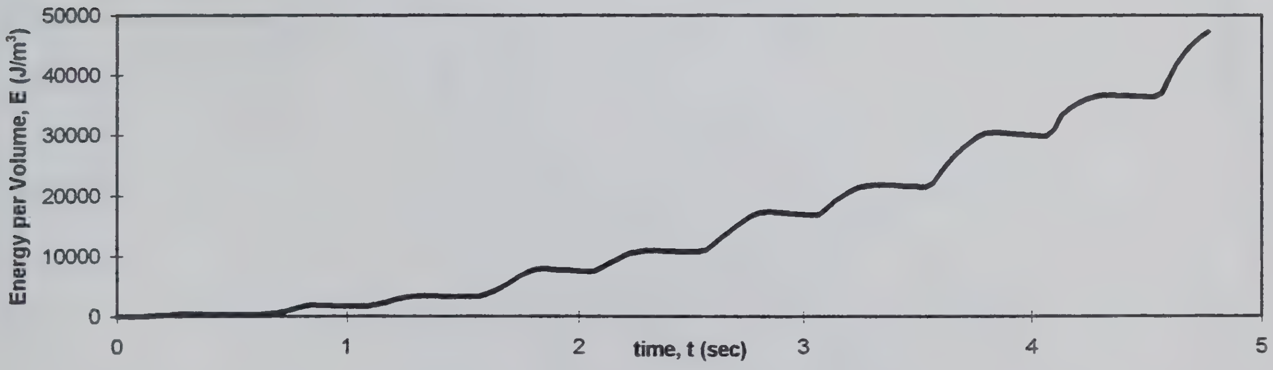

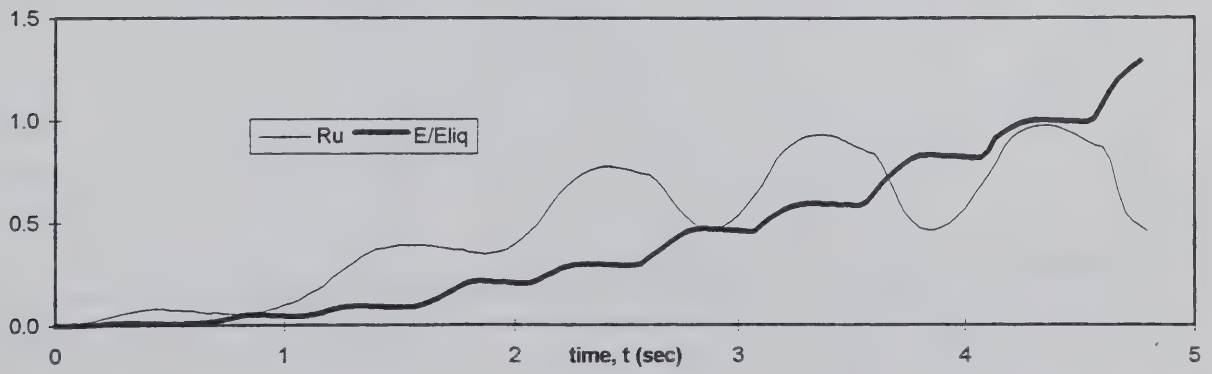

Test I.D.:	B23P4MCY	**Controlled Parameter:**	Stress
Fines Content (%):	16.5	**Initial Effective Stress (kPa):**	700
Dry Density (kN/m^3):	15.53		

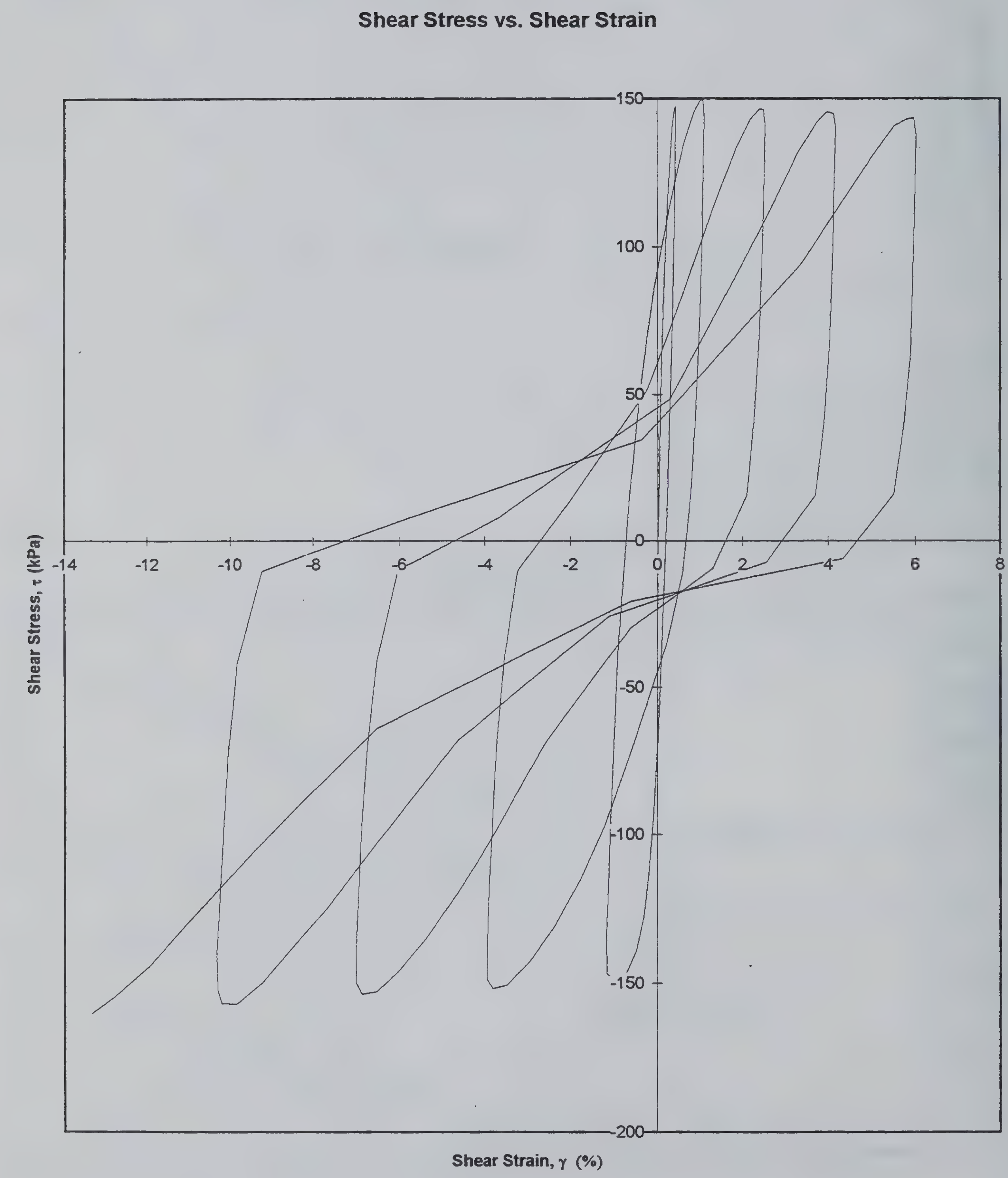

d:\nit\itp\cy_files\B23P4MCY.XLS

8/21/96 8:05 AM

Test I.D.: B23P4TCY
Fines Content (%): 28
Dry Density (kN/m^3): N/A
Controlled Parameter: Stress
Initial Effective Stress (kPa): 750

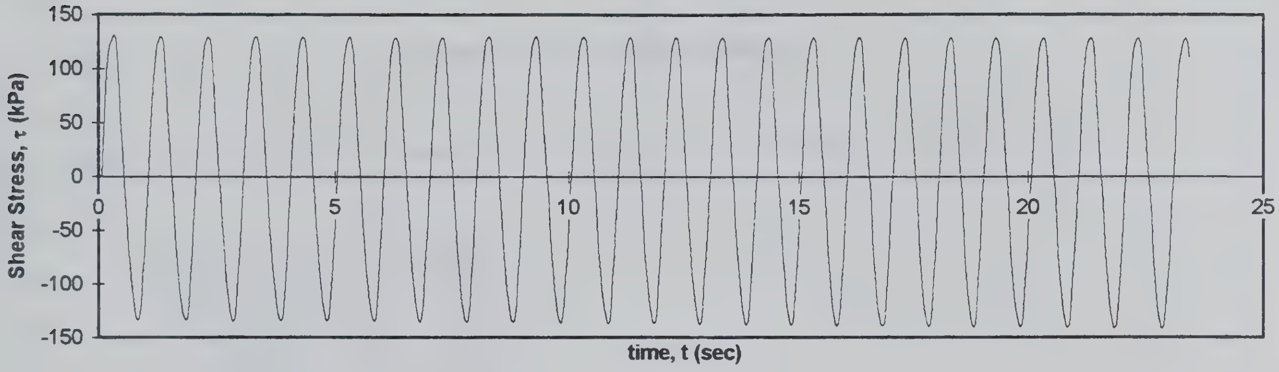

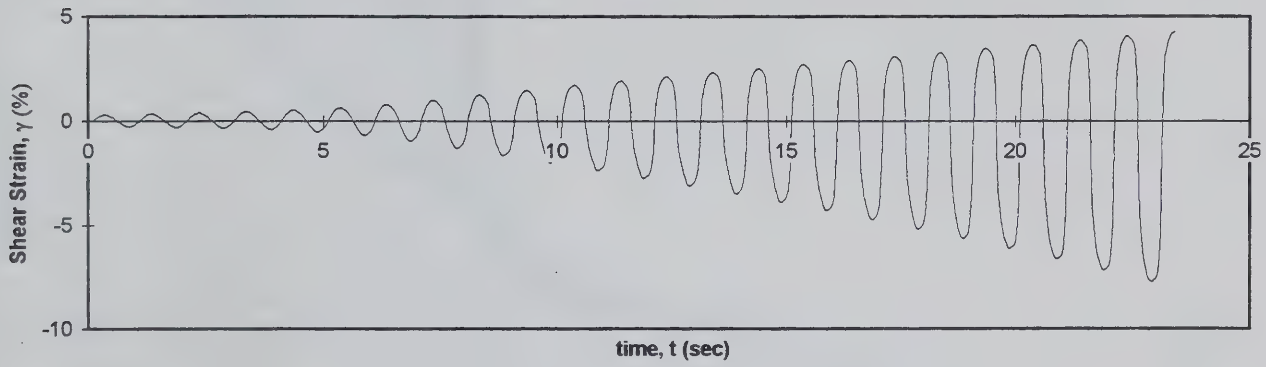

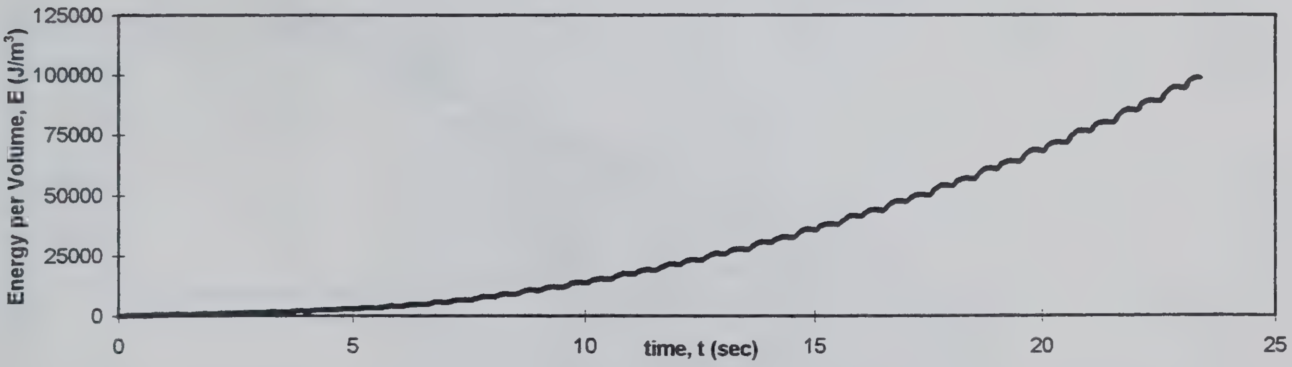

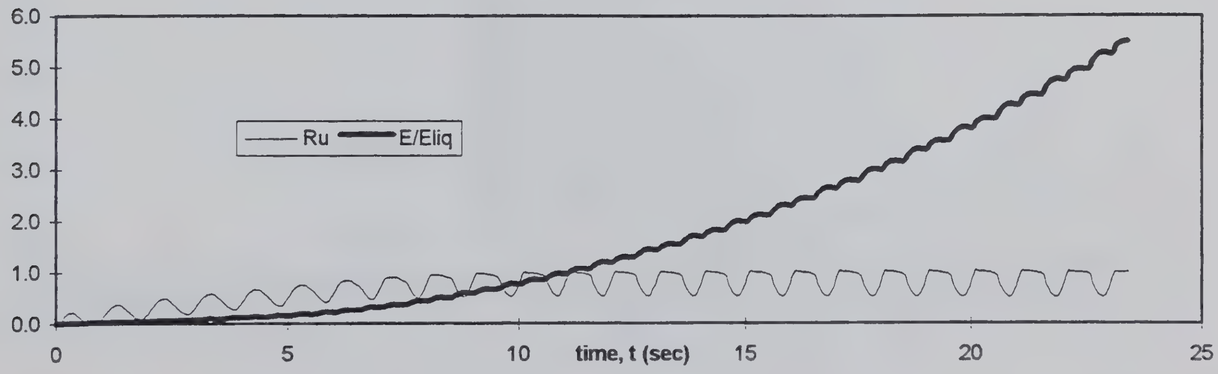

Test I.D.:	B23P4TCY	**Controlled Parameter:**	Stress
Fines Content (%):	28	**Initial Effective Stress (kPa):**	750
Dry Density (kN/m^3):	N/A		

Shear Stress vs. Shear Strain

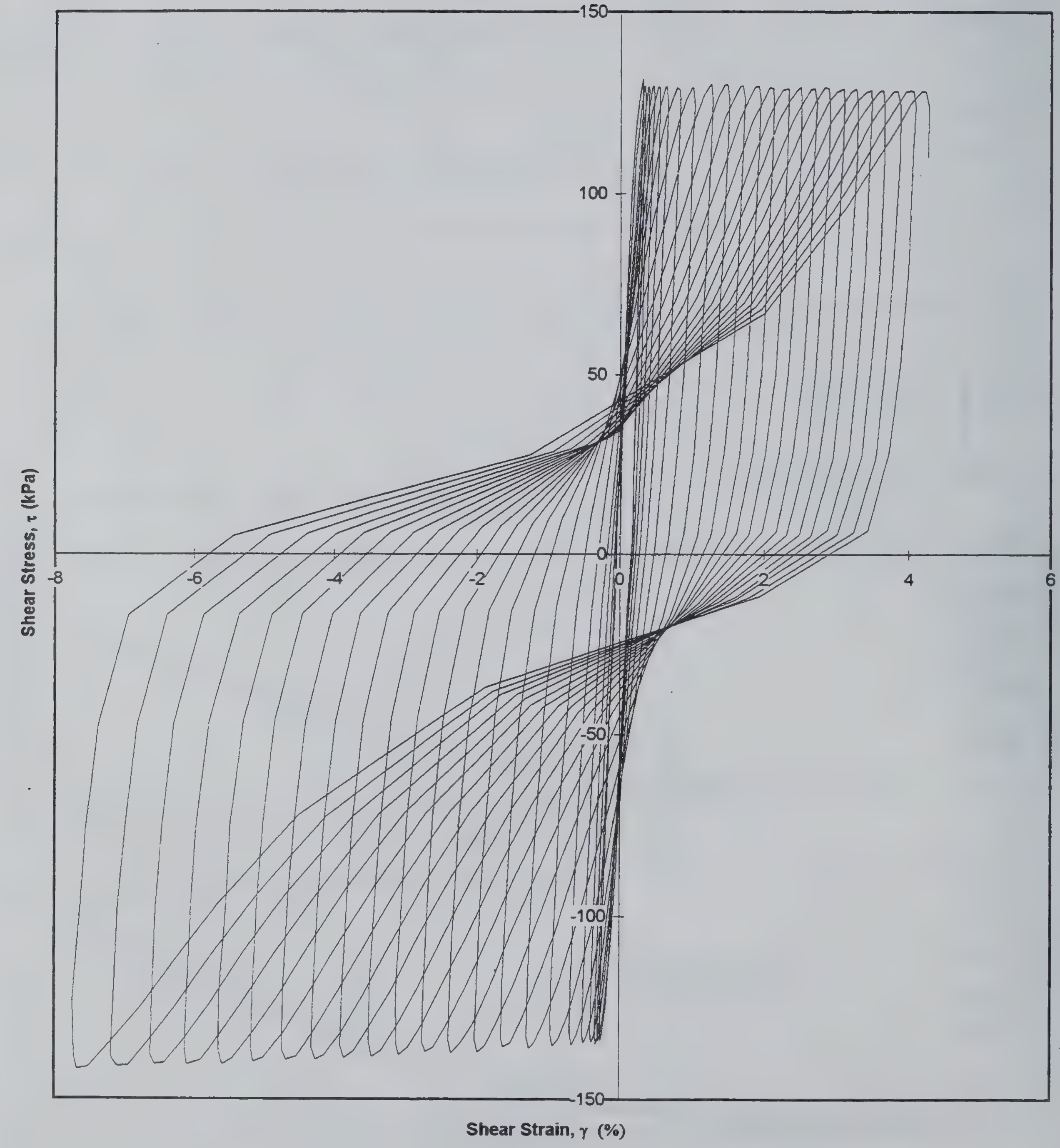

Test I.D.:	B29P2TCY	**Controlled Parameter:**	Stress
Fines Content (%):	23	**Initial Effective Stress (kPa):**	750
Dry Density (kN/m^3):	16.7		

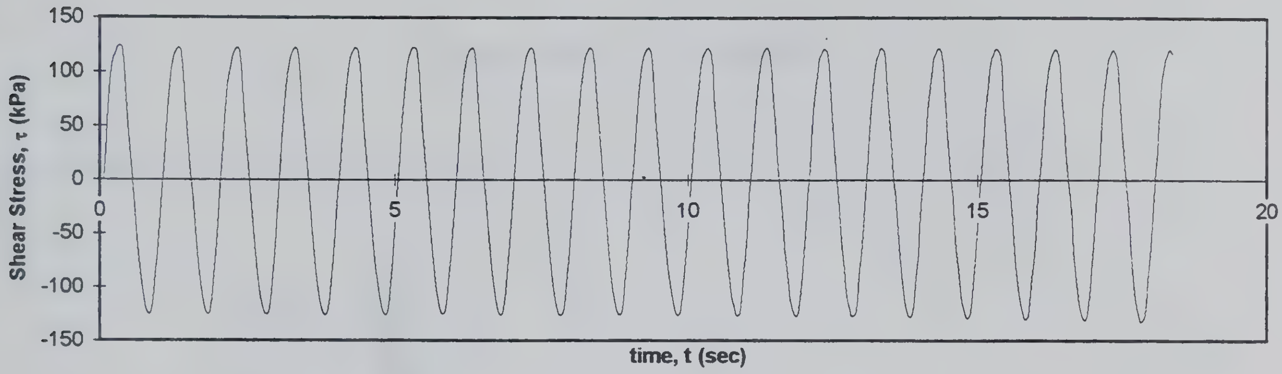

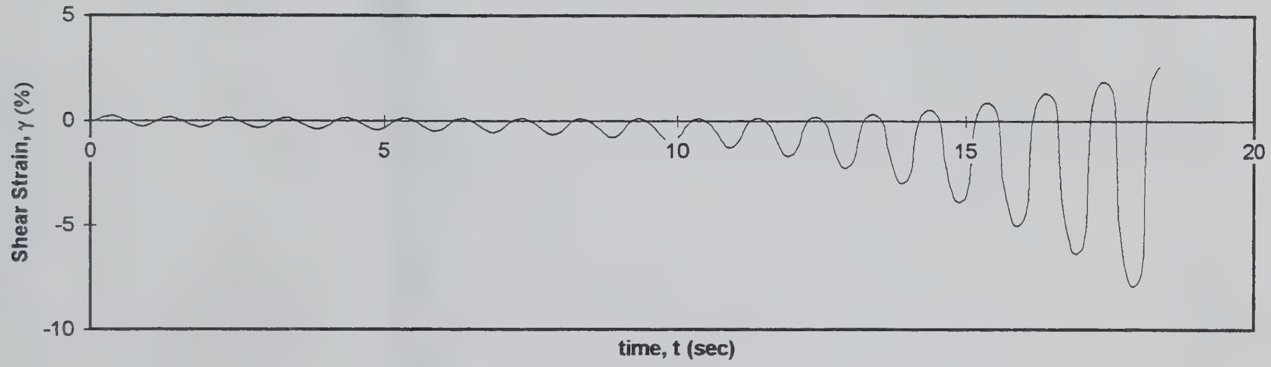

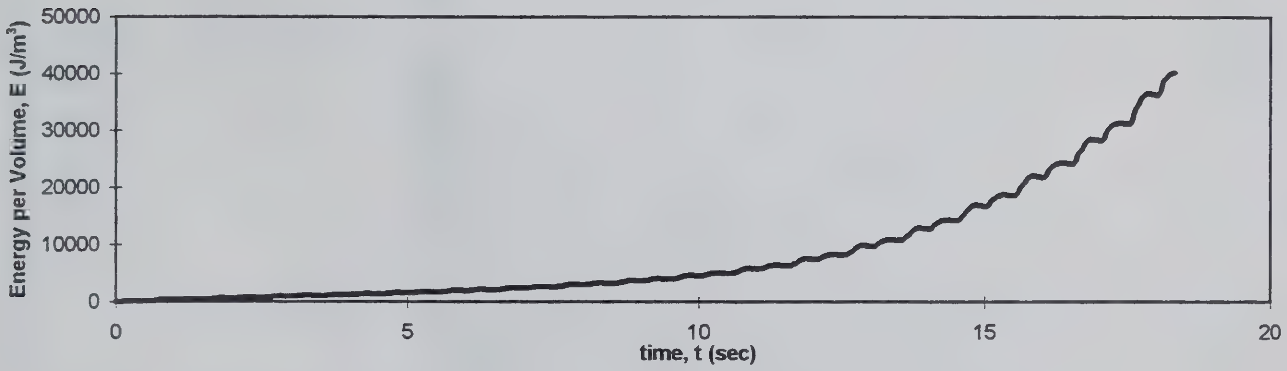

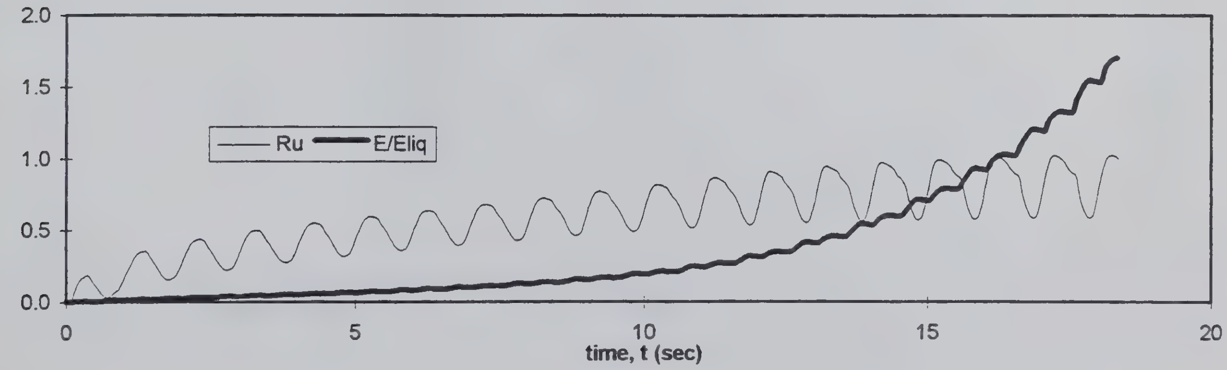

Test I.D.:	B29P2TCY	**Controlled Parameter:**	Stress
Fines Content (%):	23	**Initial Effective Stress (kPa):**	750
Dry Density (kN/m^3):	16.7		

Shear Stress vs. Shear Strain

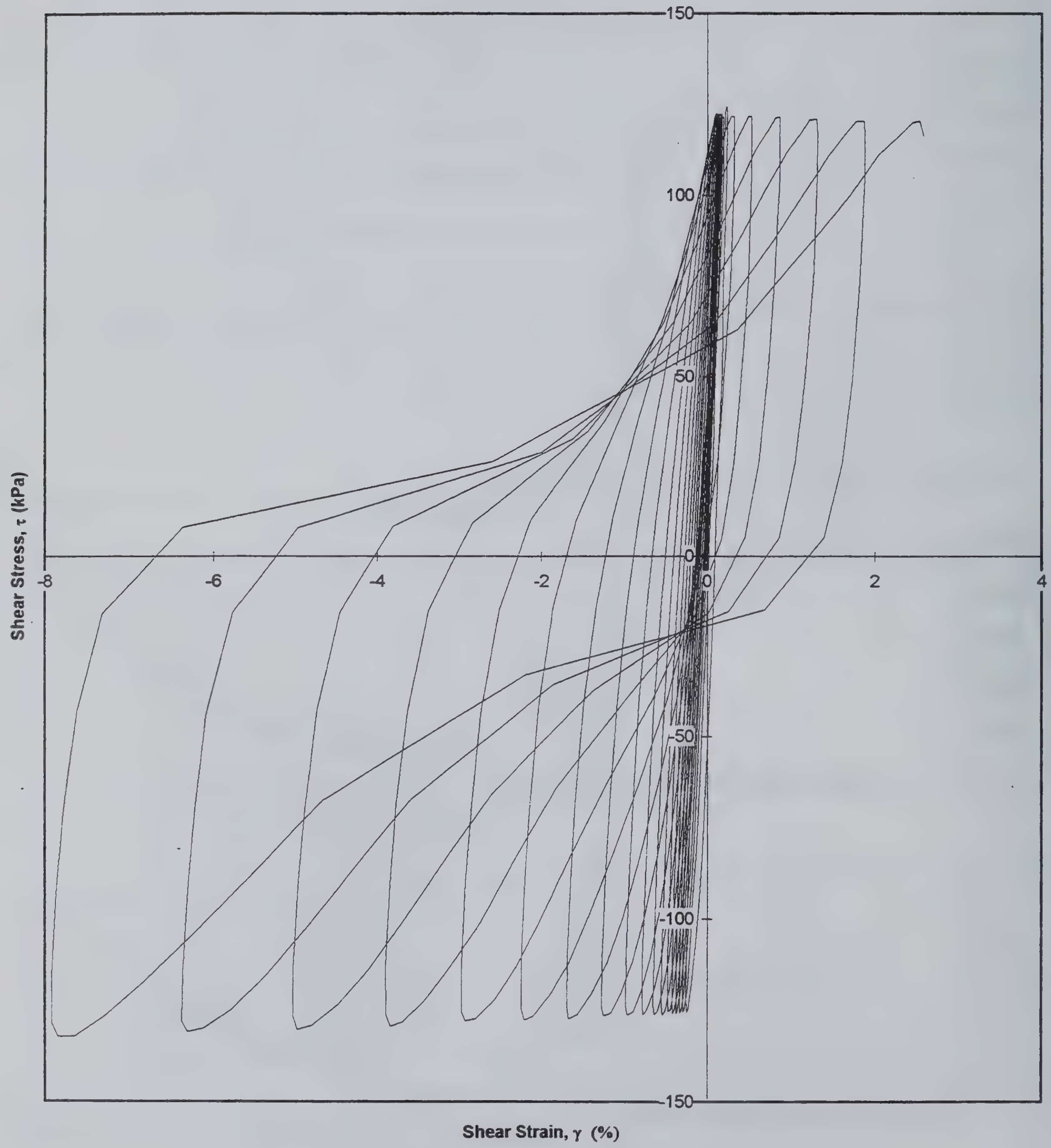

d:\nit\itp\cy_files\B29P2TCY.XLS

8/21/96 8:13 AM

Test I.D.: B2P6BCY
Fines Content (%): 18.9
Dry Density (kN/m^3): 16.73
Controlled Parameter: Stress
Initial Effective Stress (kPa): 725

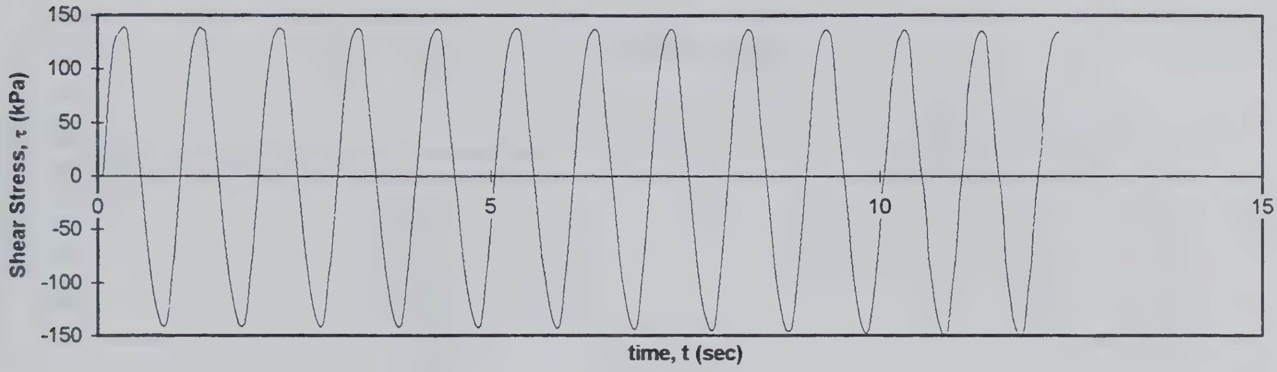

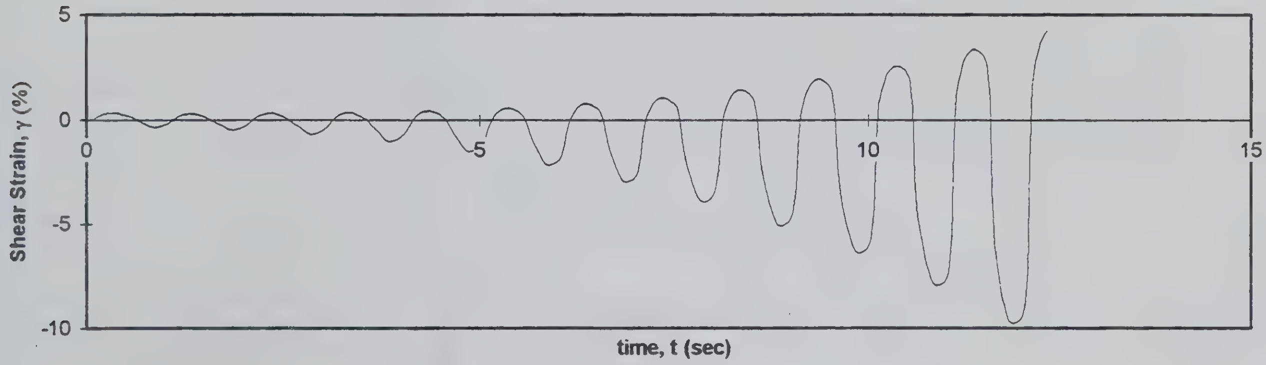

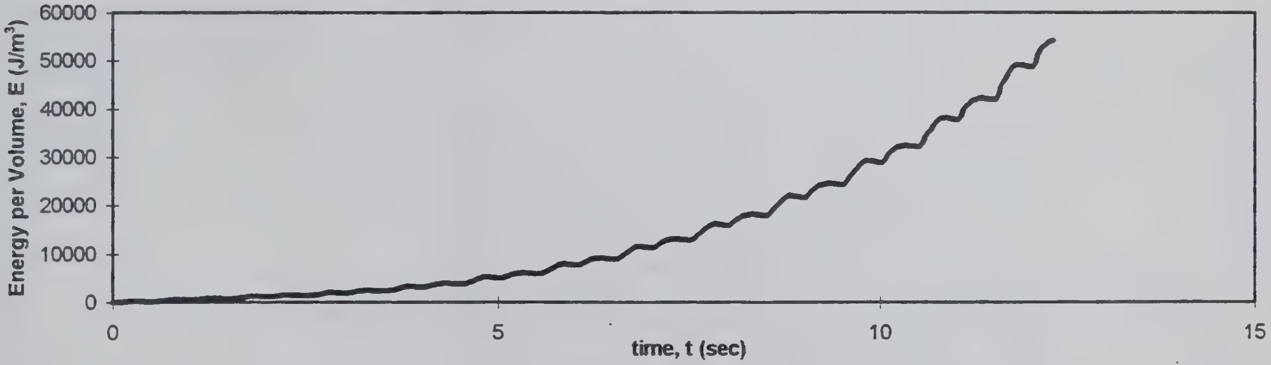

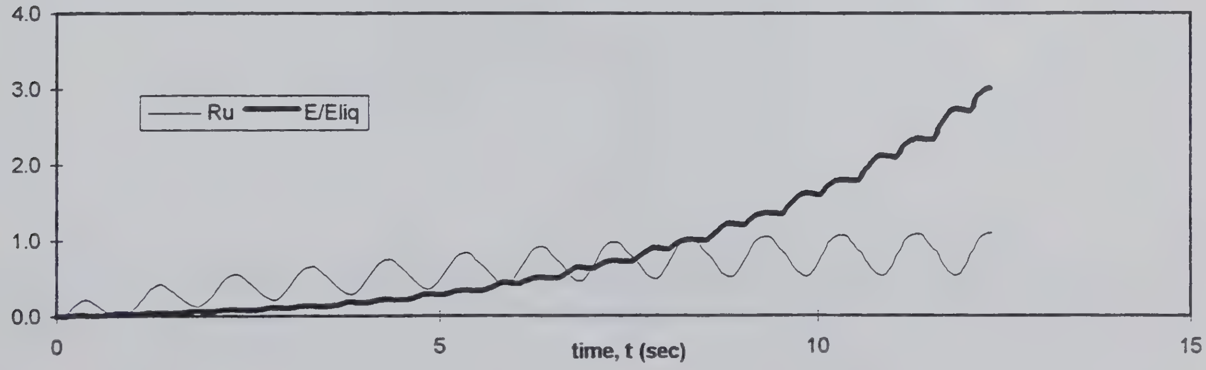

Test I.D.:	B2P6BCY	**Controlled Parameter:**	Stress
Fines Content (%):	18.9	**Initial Effective Stress (kPa):**	725
Dry Density (kN/m^3):	16.73		

Shear Stress vs. Shear Strain

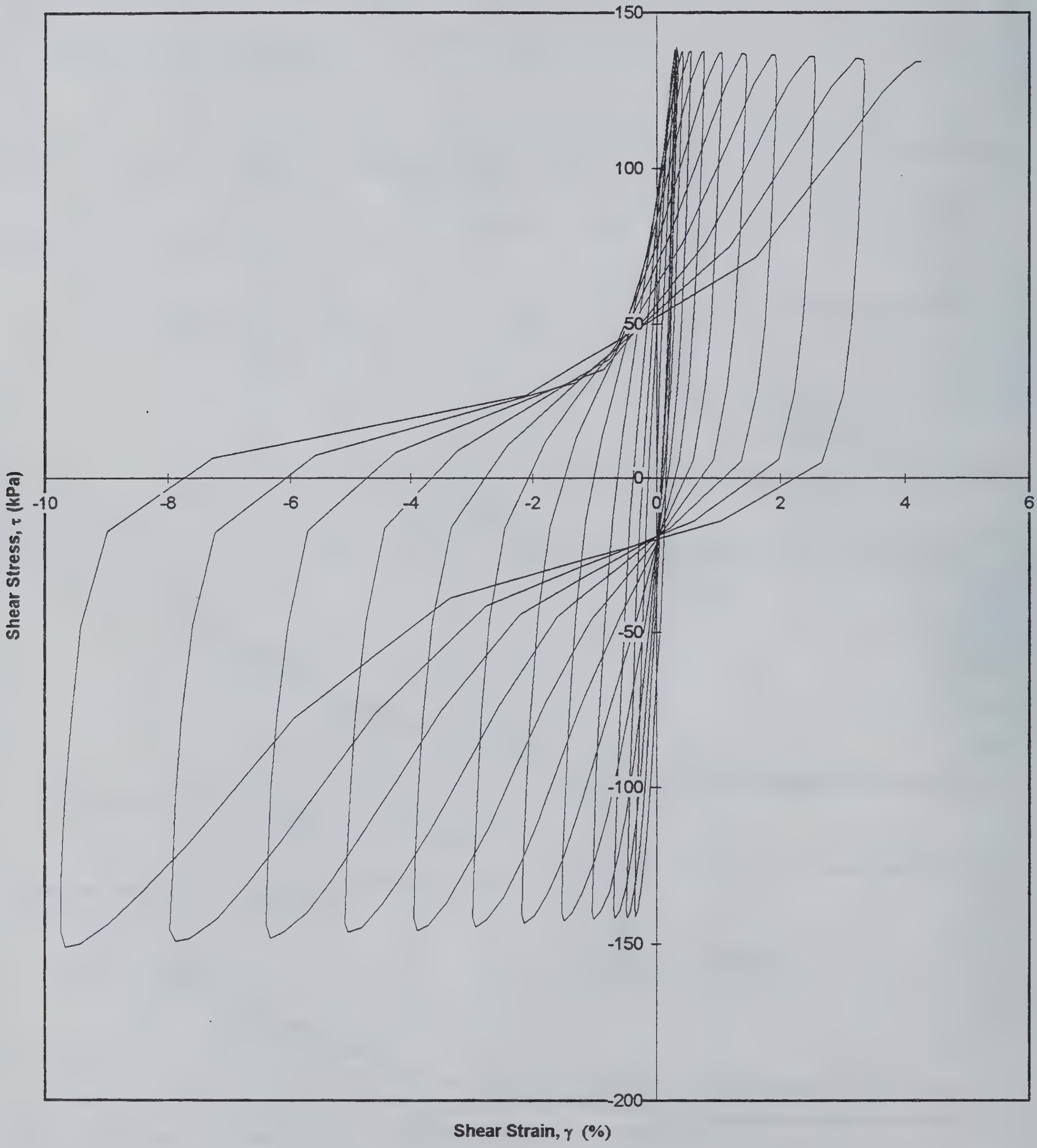

Test I.D.: B2P6MCY
Fines Content (%): 20.1
Dry Density (kN/m^3): 16.5
Controlled Parameter: Stress
Initial Effective Stress (kPa): 743

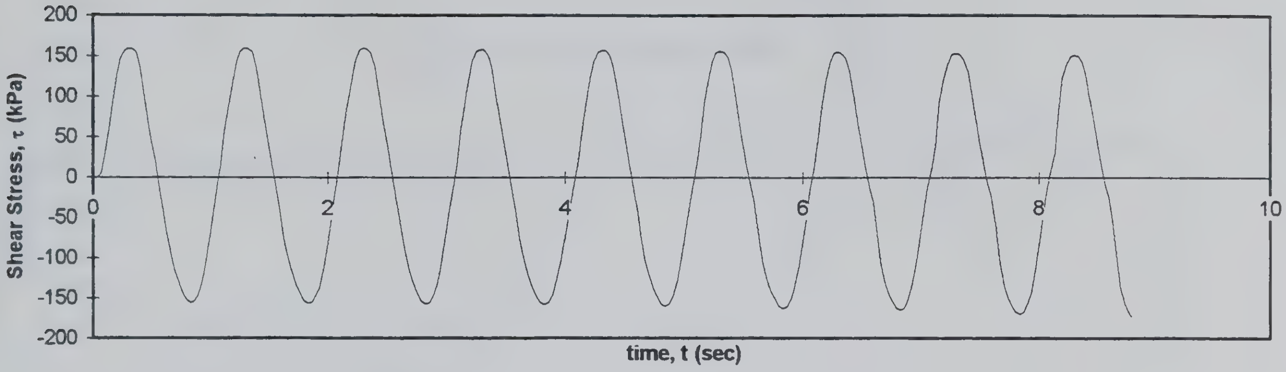

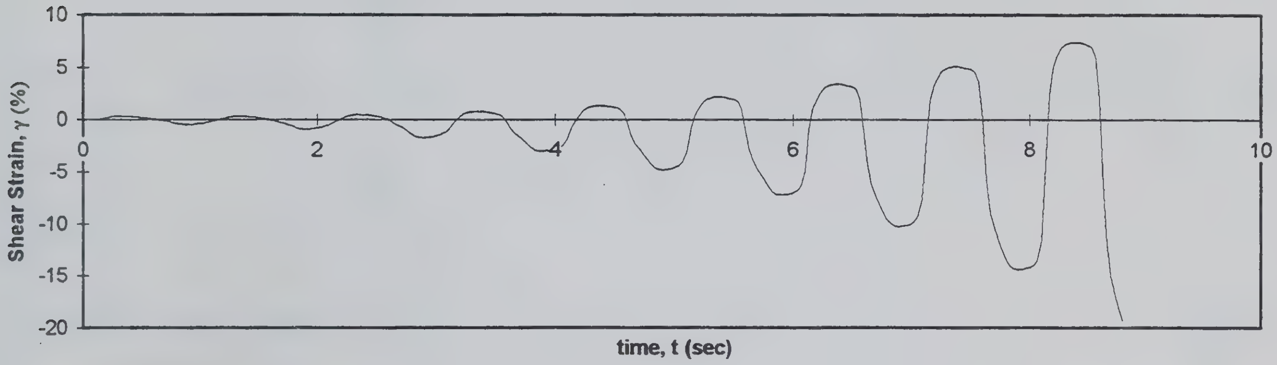

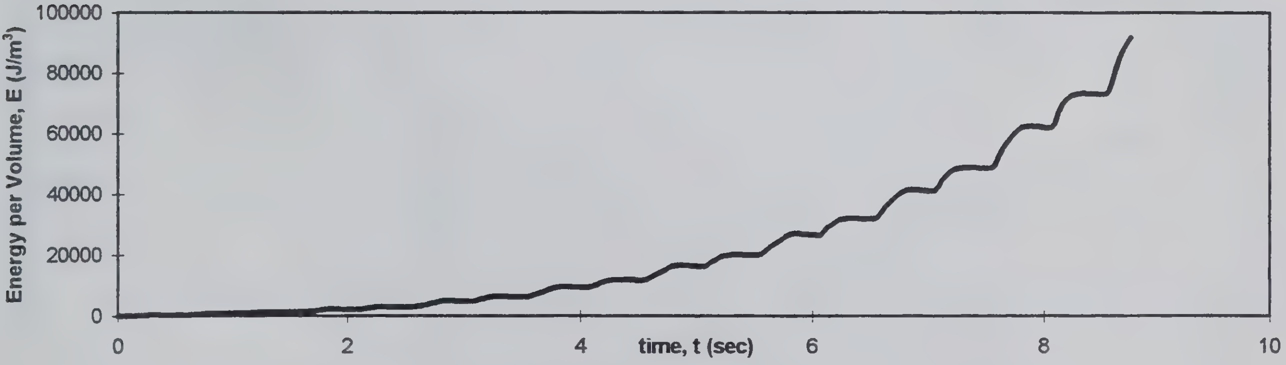

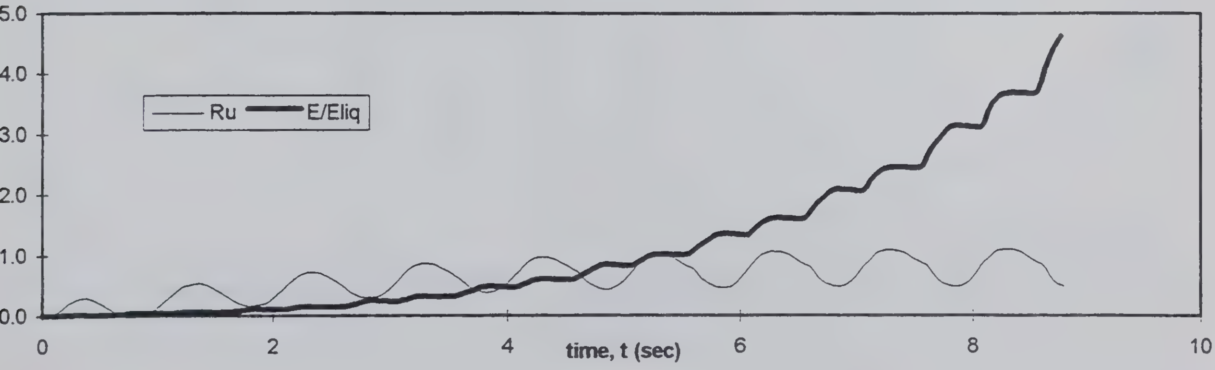

Test I.D.:	B2P6MCY	**Controlled Parameter:**	Stress
Fines Content (%):	20.1	**Initial Effective Stress (kPa):**	743
Dry Density (kN/m^3):	16.5		

Shear Stress vs. Shear Strain

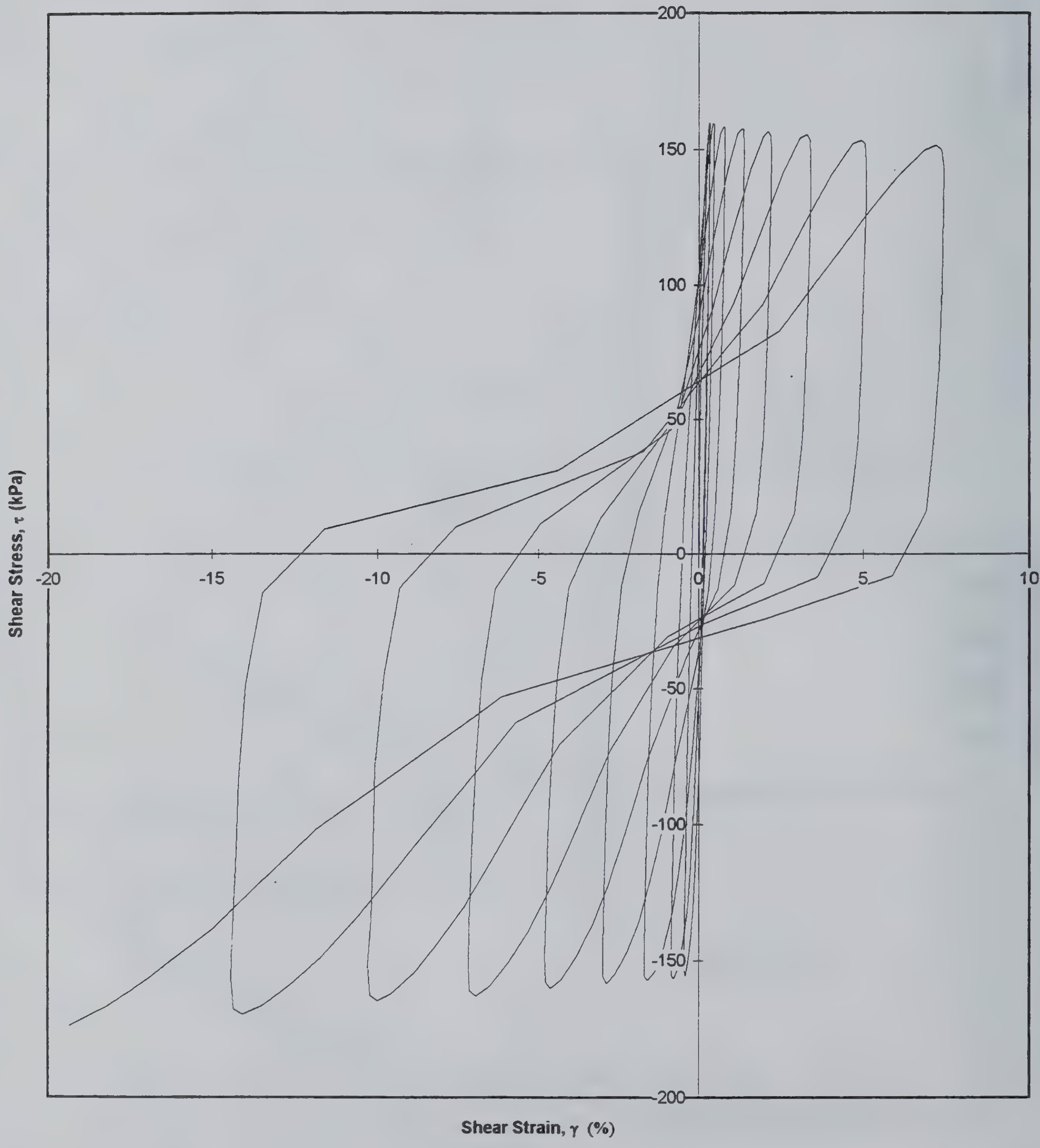

Test I.D.: B2P6TCYC
Fines Content (%): 22.4
Dry Density (kN/m^3): 16.03
Controlled Parameter: Stress
Initial Effective Stress (kPa): 750

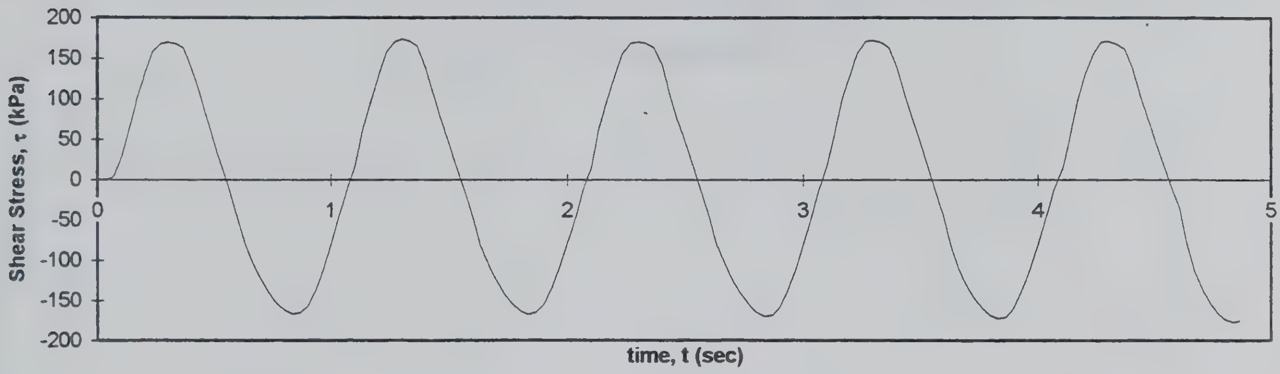

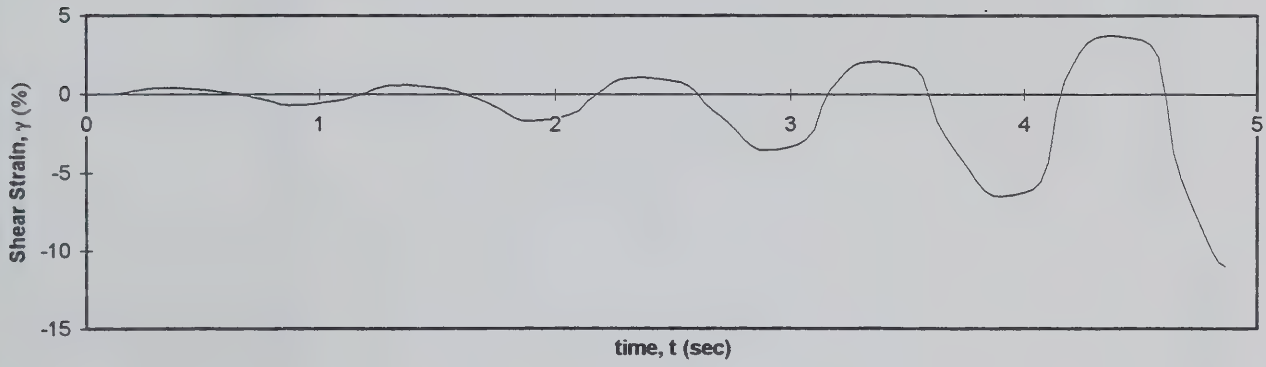

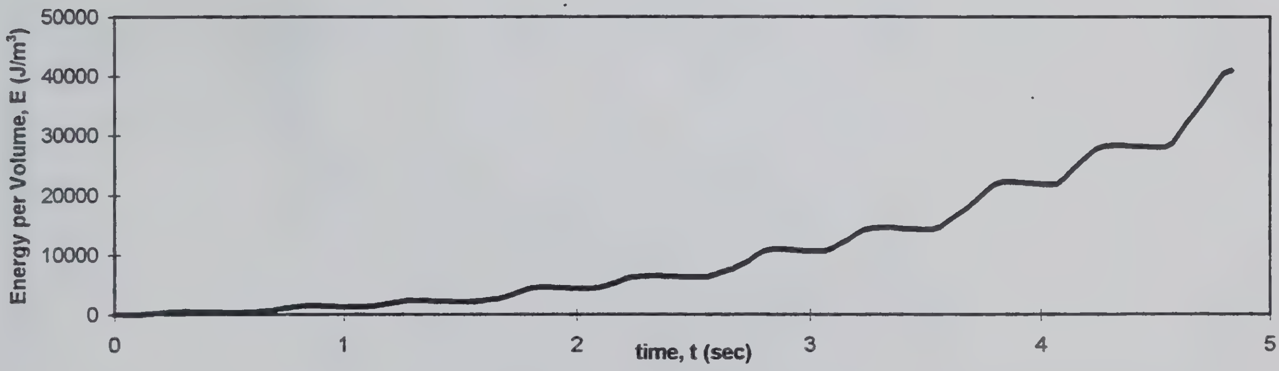

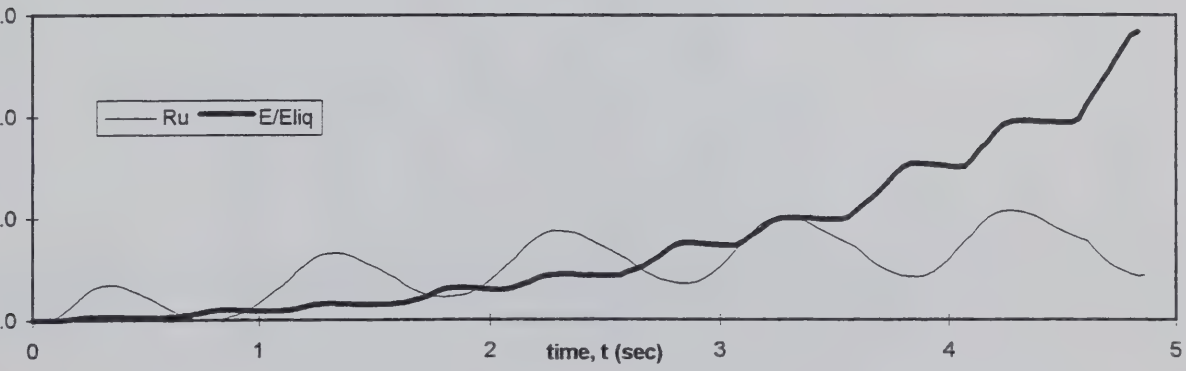

Test I.D.:	B2P6TCYC	**Controlled Parameter:**	Stress
Fines Content (%):	22.4	**Initial Effective Stress (kPa):**	750
Dry Density (kN/m³):	16.03		

Shear Stress vs. Shear Strain

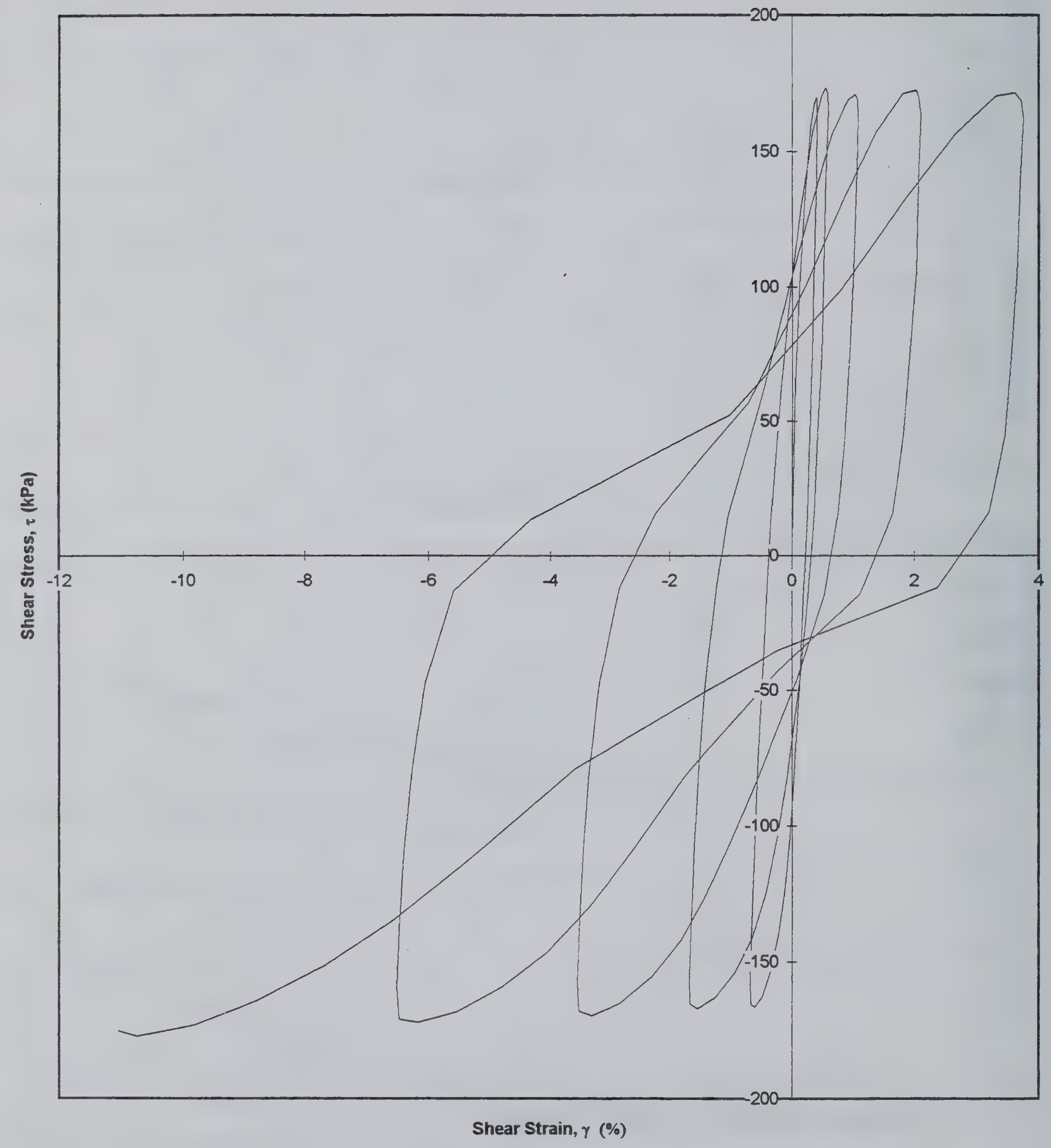

APPENDIX C

LABORATORY TESTS ON SOIL SAMPLES, PERFORMED AT THE UNIVERSITY OF COLORADO

Table C.1 - Summary of the Cyclic Torsional Test Data on Clean and Silty Sands Performed at University of Colorado

No.	Test ID	Sample	D_r(%)	E_{liq} (J/m^3)	FC (%)	γ_d (kN/m^3)	P. I.	Control	σ_c' (kPa)	Freq. (Hz)	Load Shape
1	UOFC5	F11	32.6	3728	0	14.5		Stress	199.9	0.1	Sinusoidal 2-way
2	UOFC7	F11	41.0	12495	0	14.7		Stress	204.8	0.1	Sinusoidal 2-way
3	UOFC9	F11	42.0	16997	0	14.8		Stress	304.1	0.1	Sinusoidal 2-way
4	UOFC13	F43	N/A	3450	20	15.3	10.0	Stress	299.9	0.1	Sinusoidal 2-way
5	UOFC14	F46	N/A	4753	20	15.2	25.0	Stress	199.9	0.1	Sinusoidal 2-way
6	UOFC15	F46	N/A	2485	20	15.2	25.0	Stress	201.3	0.1	Sinusoidal 2-way
7	UOFC17	F64	N/A	3427	45	16.2	15.0	Stress	203.4	0.1	Sinusoidal 2-way
8	UOFC18	F64	N/A	3993	45	16.2	15.0	Stress	190.3	0.1	Sinusoidal 2-way
9	UOFC23	F11	45.3	7437	0	14.9		Stress	199.9	0.1	Sinusoidal 2-way

Test Results Following the Sequence of Test ID's are Attached.

Test I.D.:	UOFC5	**Controlled Parameter:**	Stress
Fines Content (%):	Clean Sand	**Initial Effective Stress (kPa):**	200
Relative Density (%):	32.6		

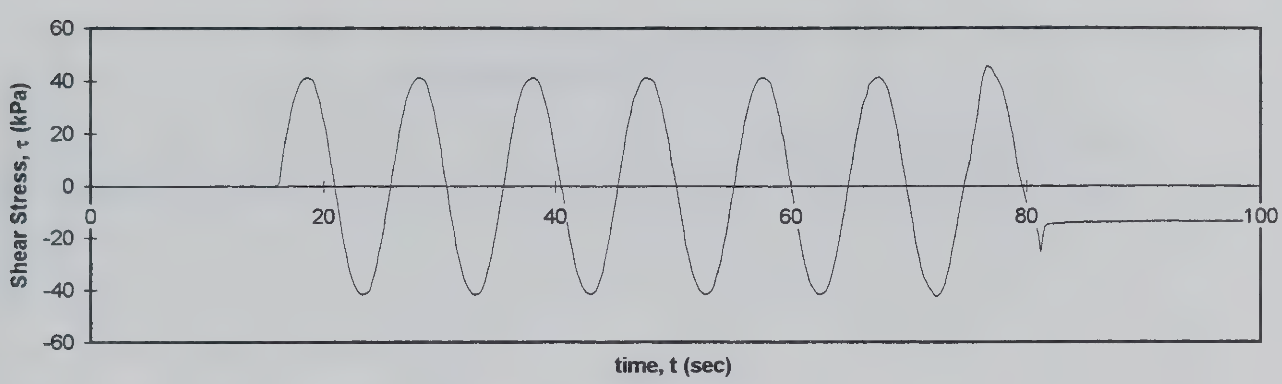

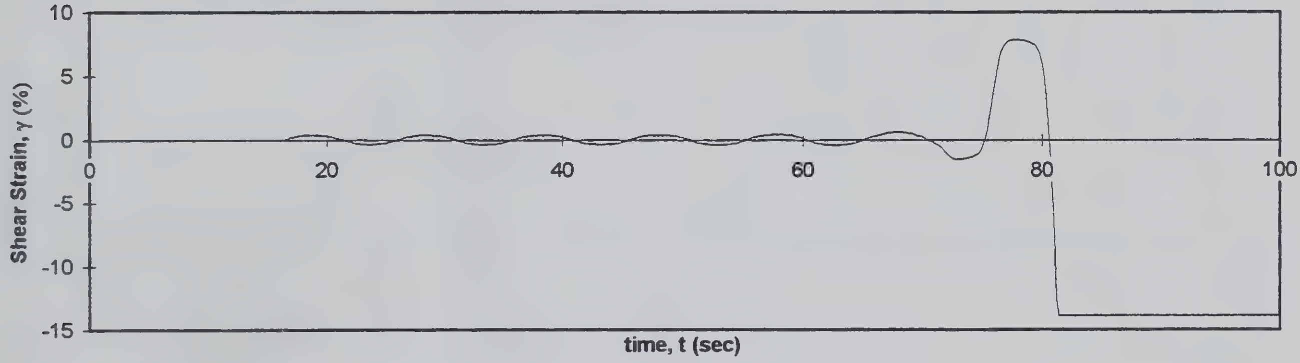

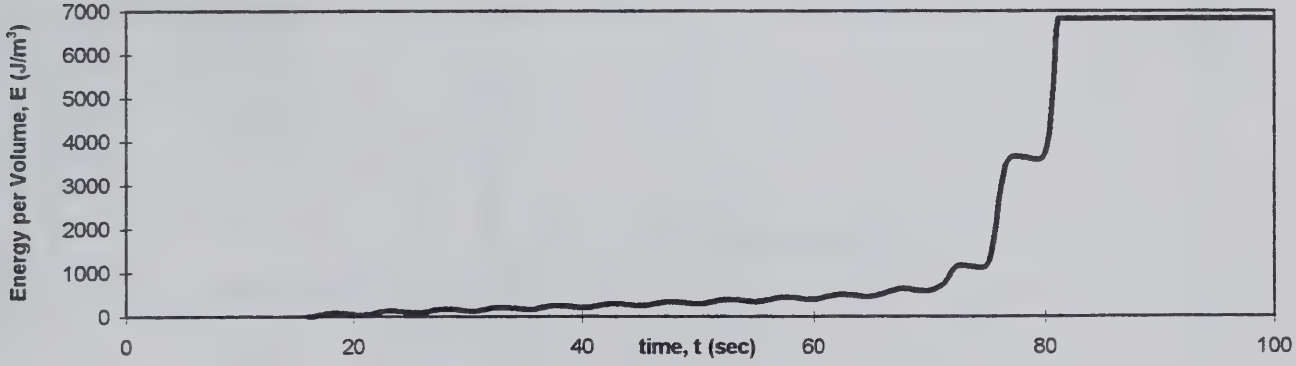

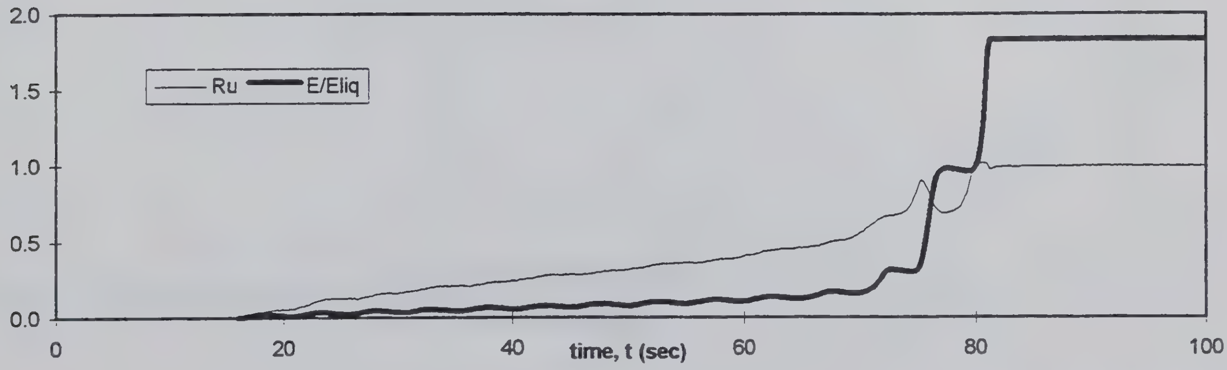

Test I.D.:	UOFC5	**Controlled Parameter:**	Stress
Fines Content (%):	Clean Sand	**Initial Effective Stress (kPa):**	200
Relative Density (%):	32.6		

Shear Stress vs. Shear Strain

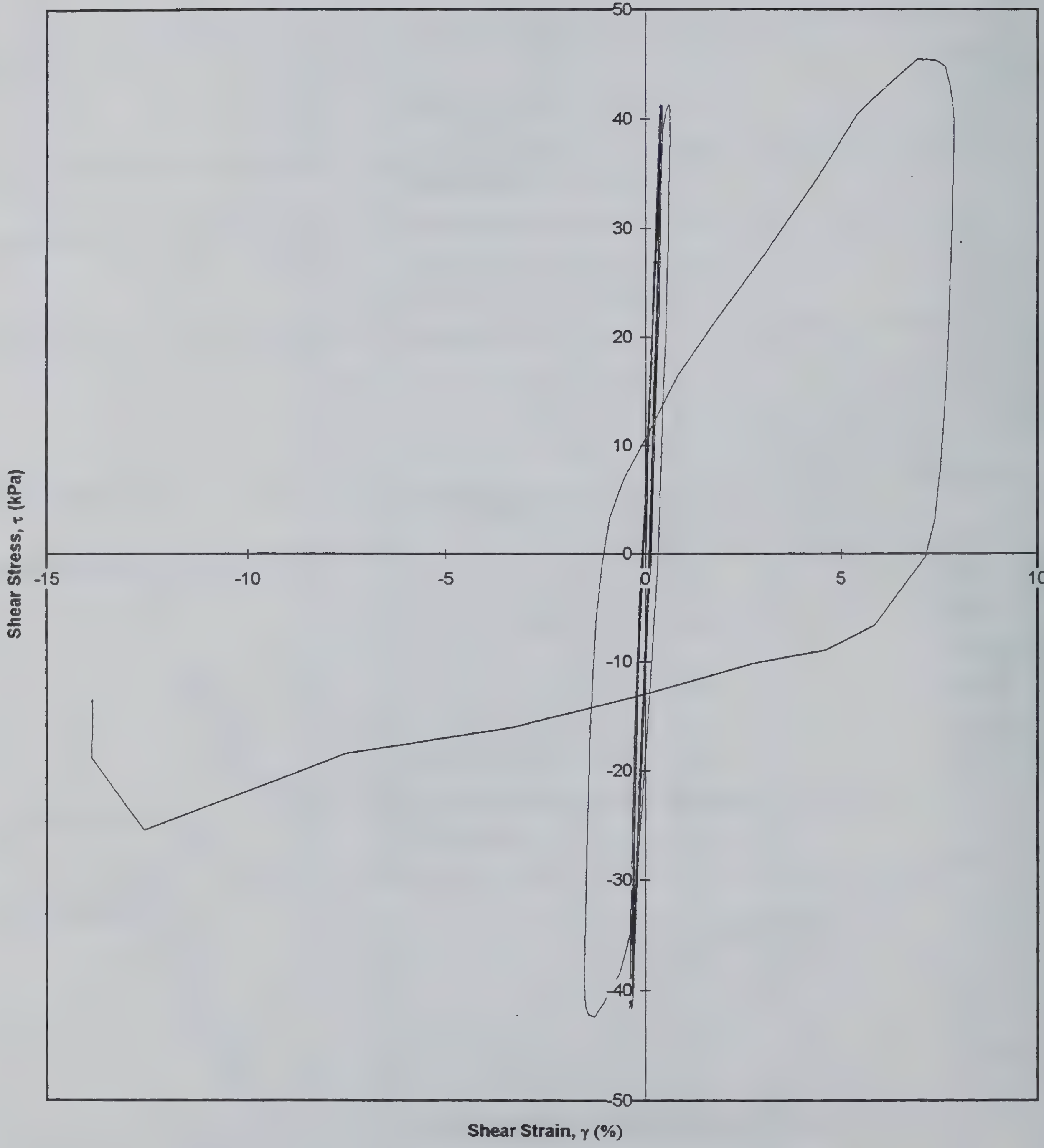

d:\nit\itp\cy_files\UOFC5.XLS

8/19/96 4:18 PM

Test I.D.: UOFC7
Fines Content (%): Clean Sand
Relative Density (%): 41
Controlled Parameter: Stress
Initial Effective Stress (kPa): 205

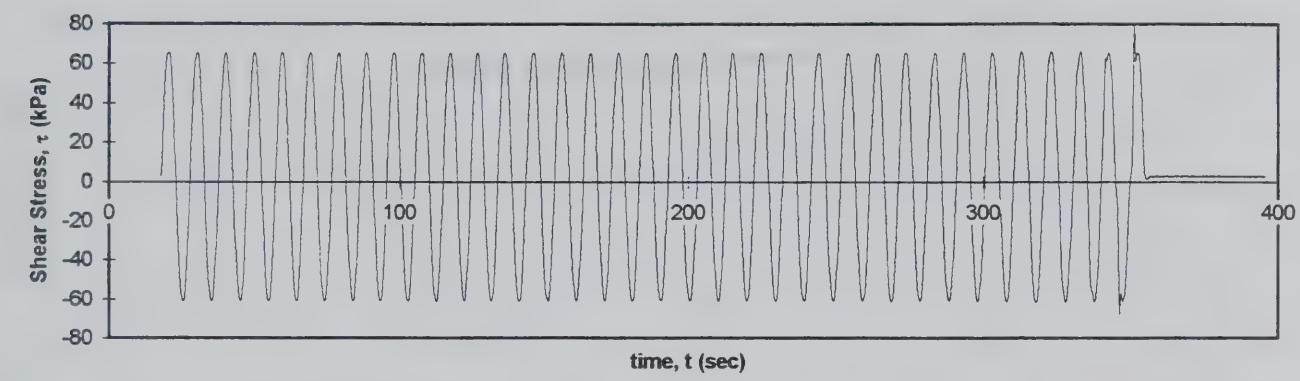

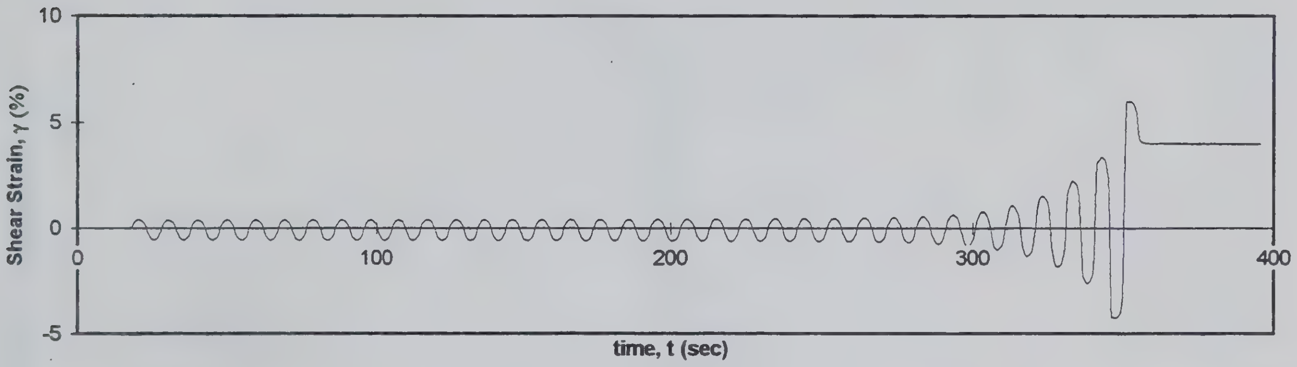

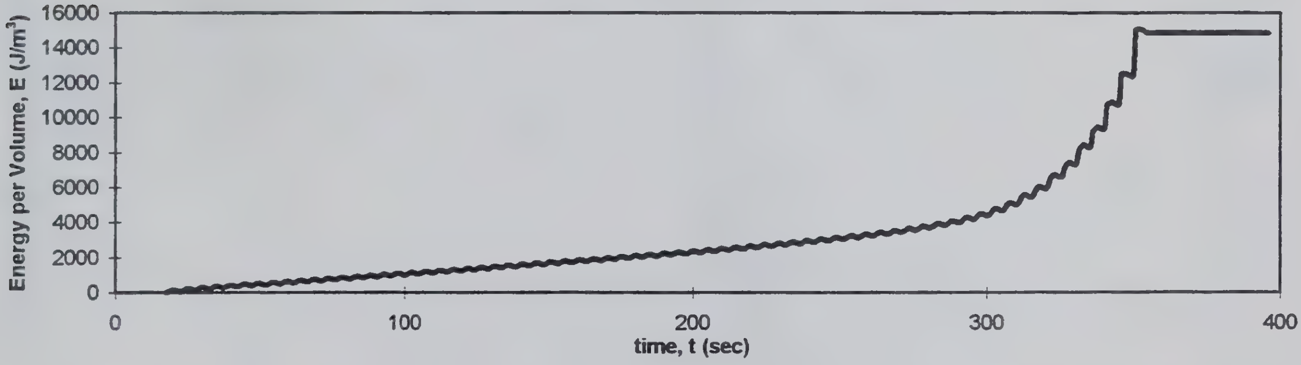

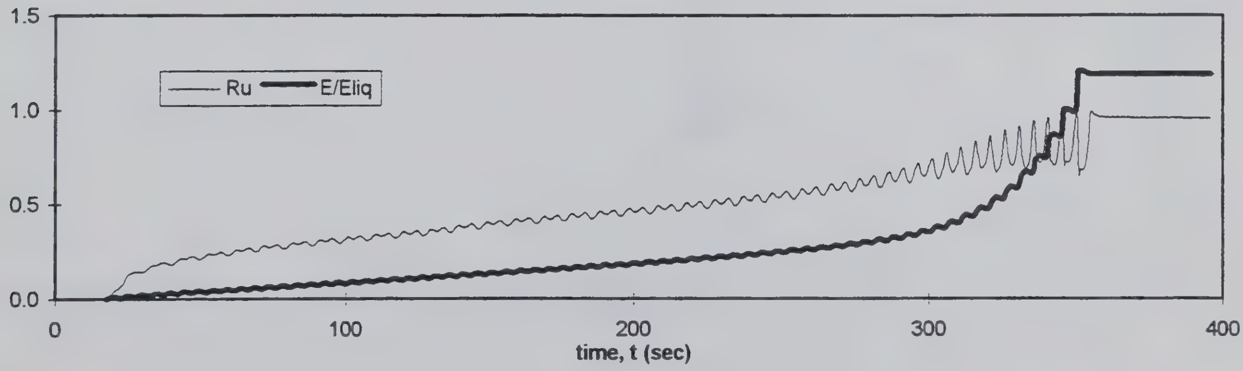

d:\nit\itp\cy_files\UOFC7.XLS

8/21/96 9:22 AM

Test I.D.:	UOFC7	**Controlled Parameter:**	Stress
Fines Content (%):	Clean Sand	**Initial Effective Stress (kPa):**	205
Relative Density (%):	41		

Shear Stress vs. Shear Strain

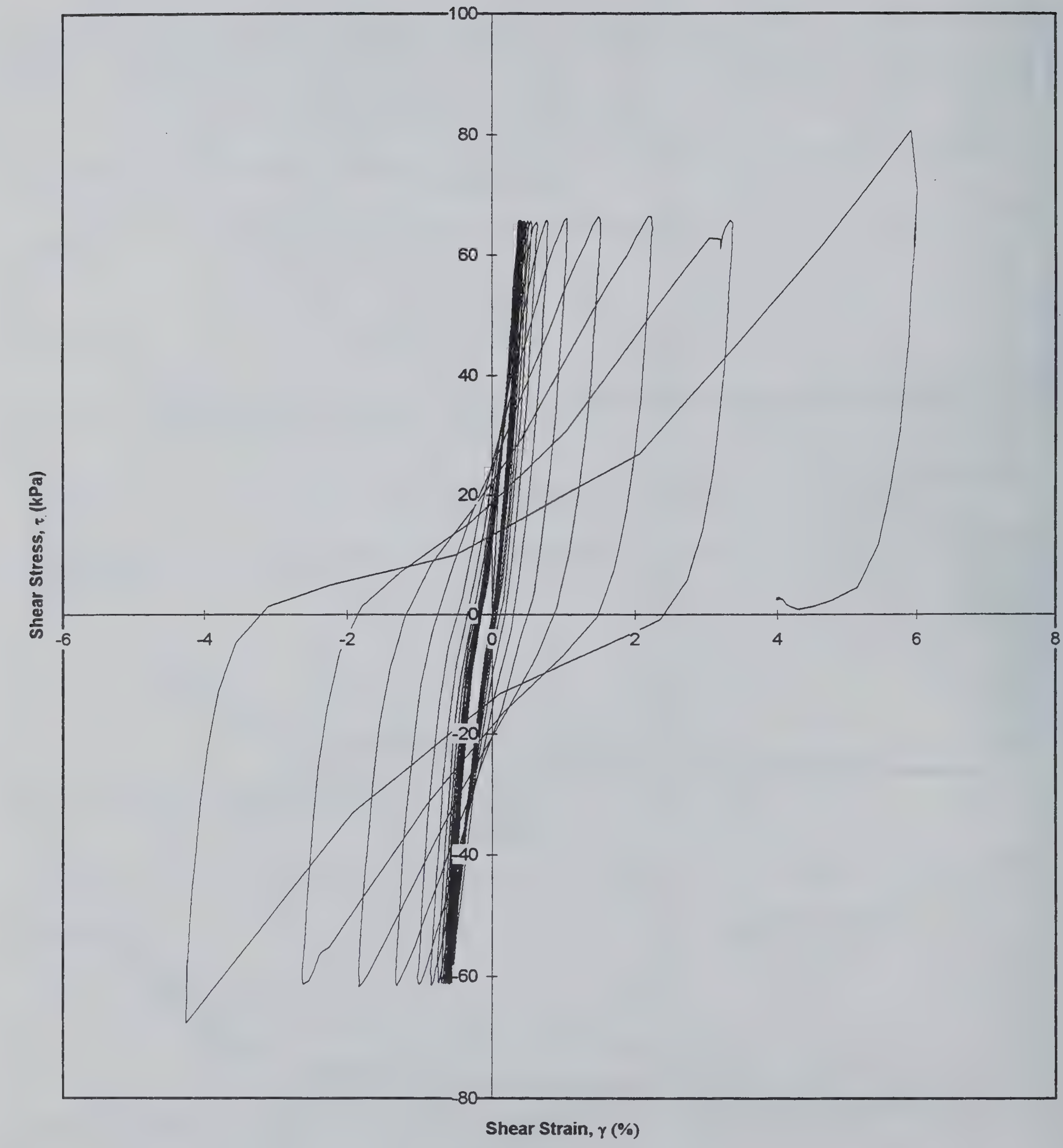

d:\nit\itp\cy_files\UOFC7.XLS

8/21/96 9:22 AM

Test I.D.:	UOFC9	**Controlled Parameter:**	Stress
Fines Content (%):	Clean Sand	**Initial Effective Stress (kPa):**	304
Relative Density (%):	42		

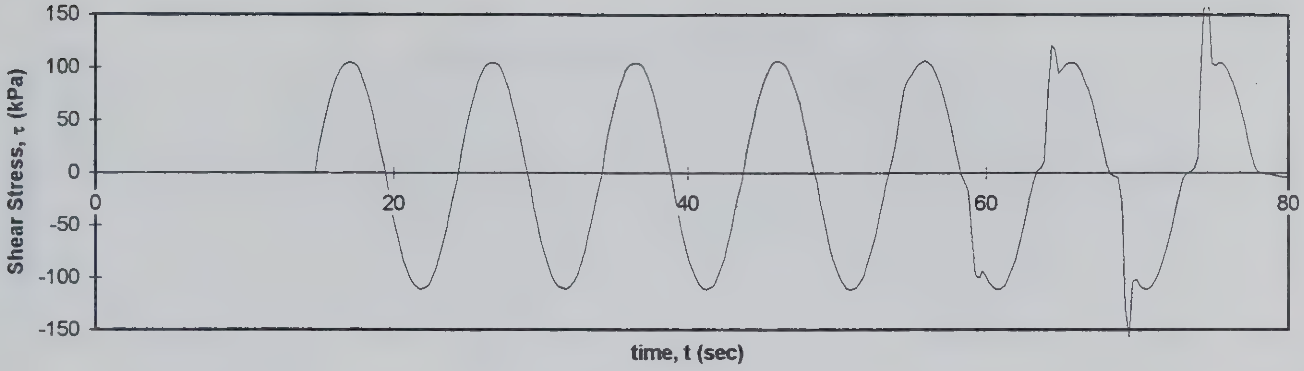

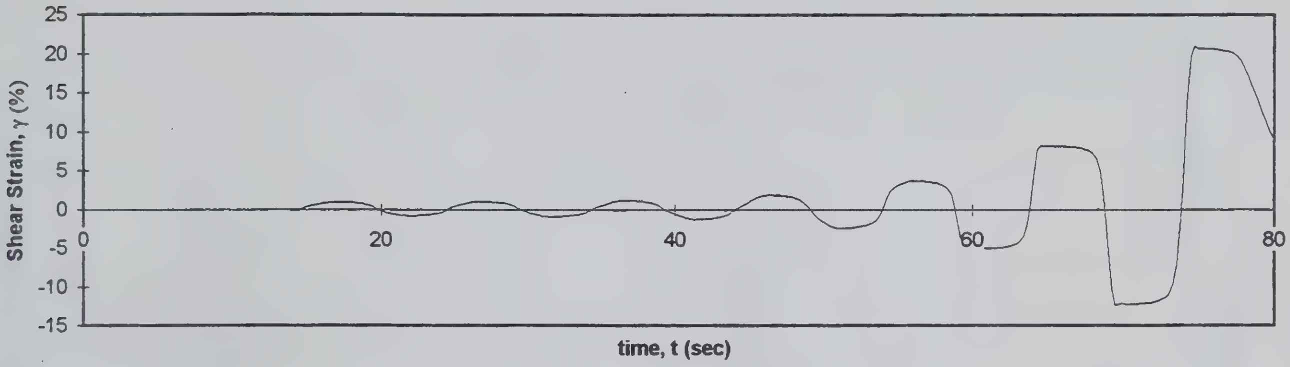

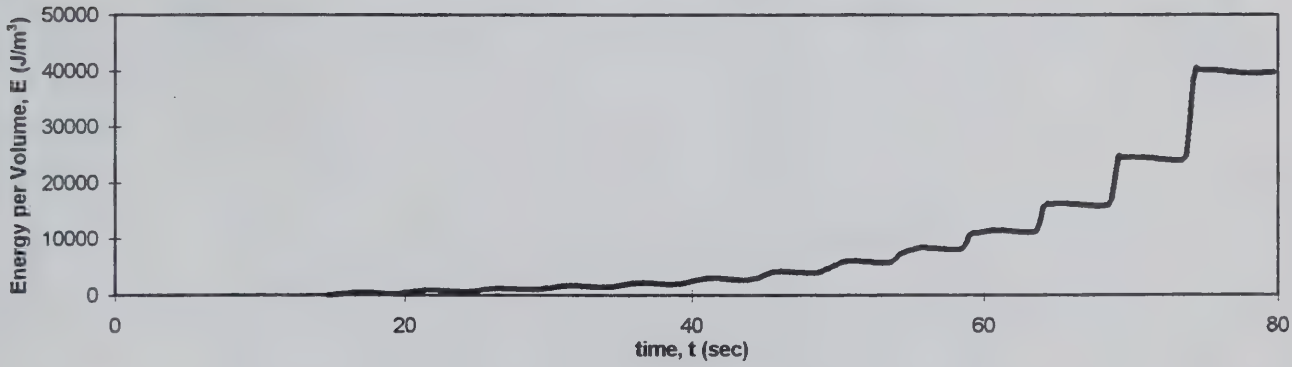

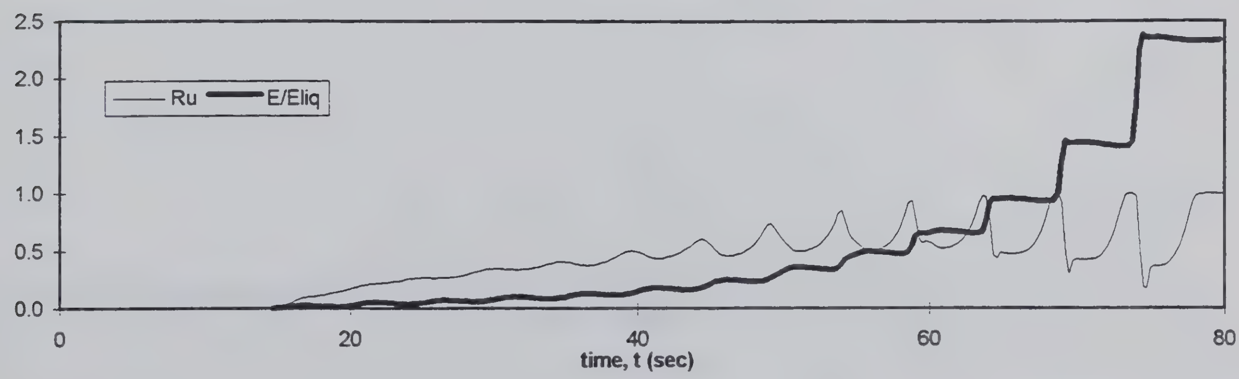

Test I.D.:	UOFC9	**Controlled Parameter:**	Stress
Fines Content (%):	Clean Sand	**Initial Effective Stress (kPa):**	304
Relative Density (%):	42		

Shear Stress vs. Shear Strain

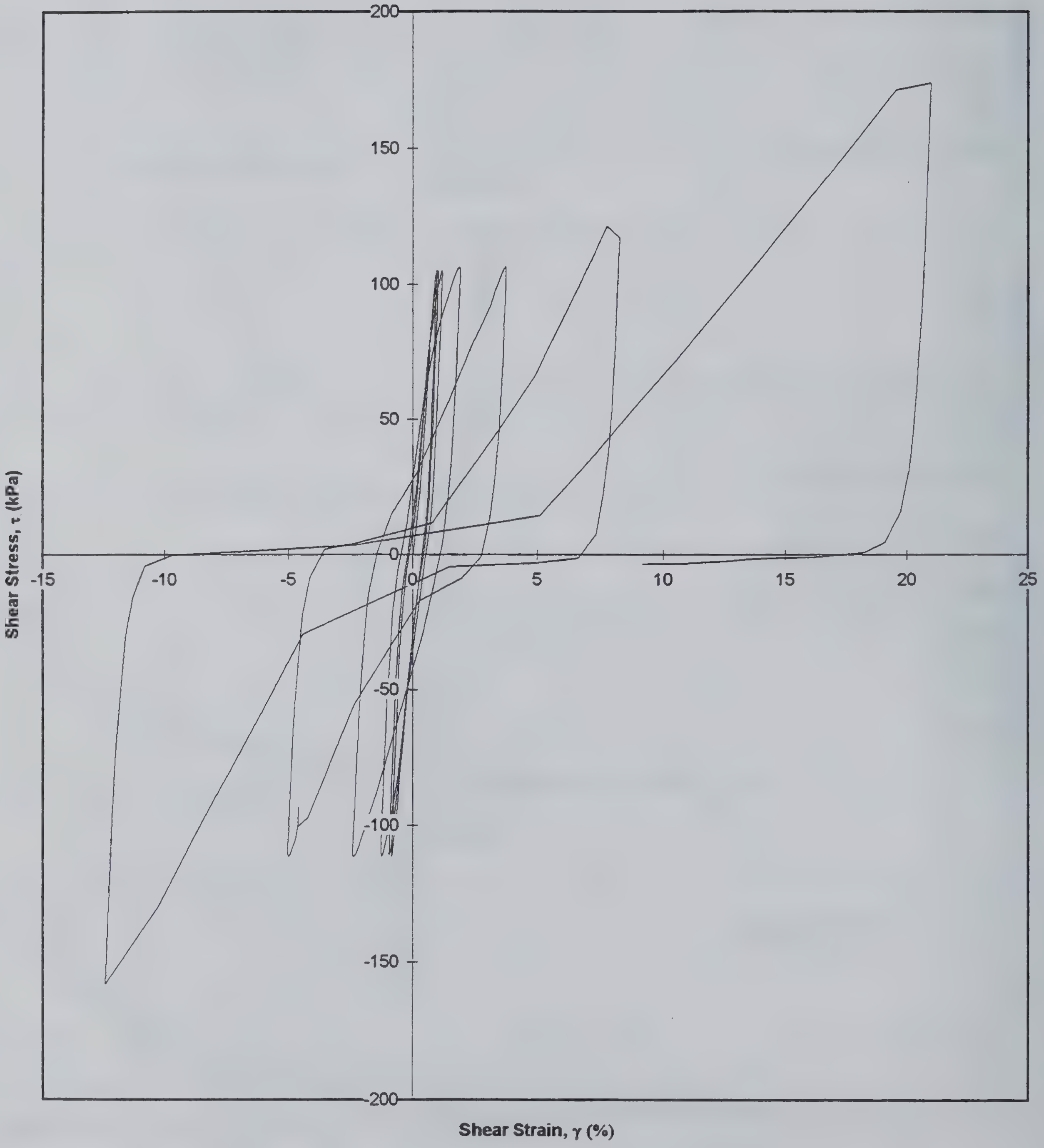

d:\nit\itp\cy_files\UOFC9.XLS

8/21/96 9:23 AM

Test I.D.: UOFC13
Fines Content (%): 20
Dry Density (kN/m^3) 15.26
Controlled Parameter: Stress
Initial Effective Stress (kPa): 300

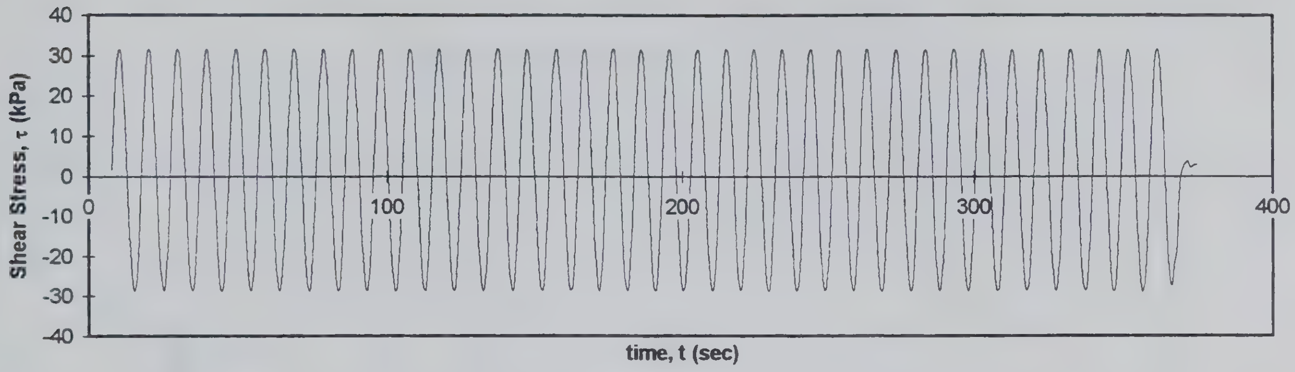

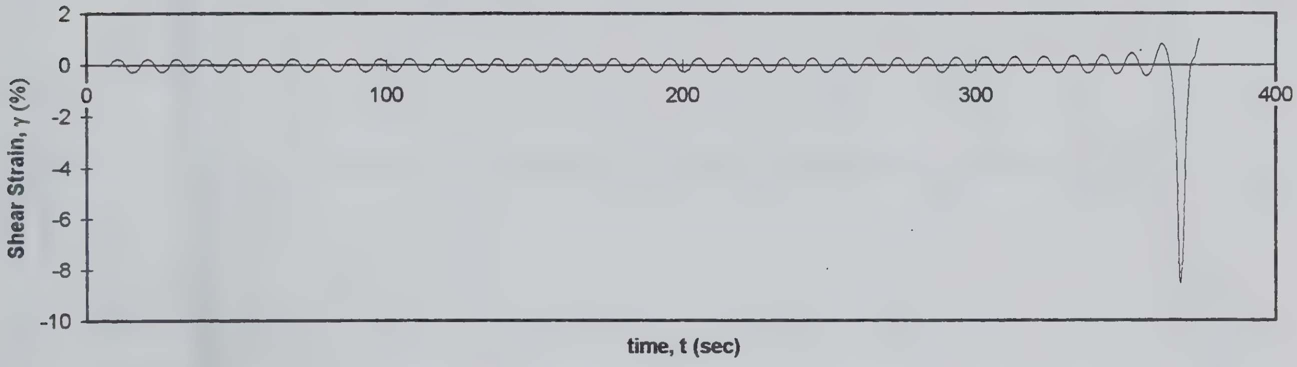

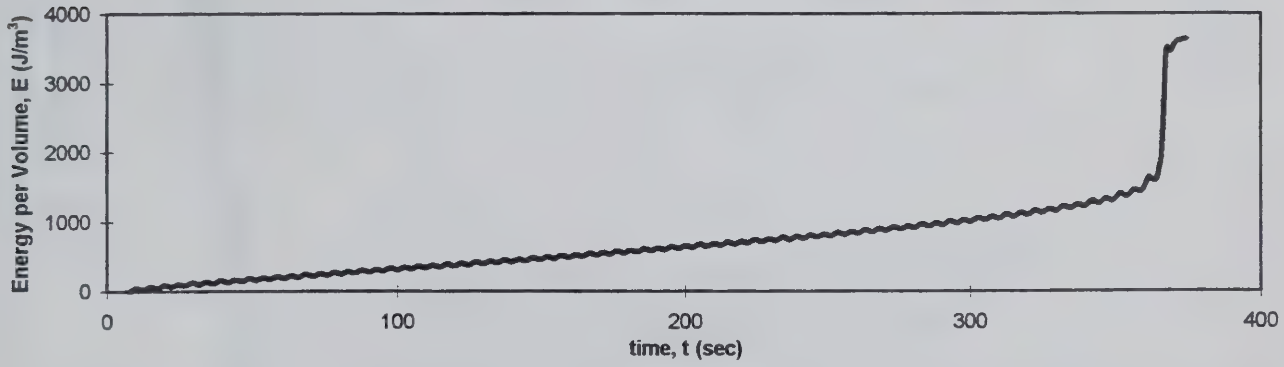

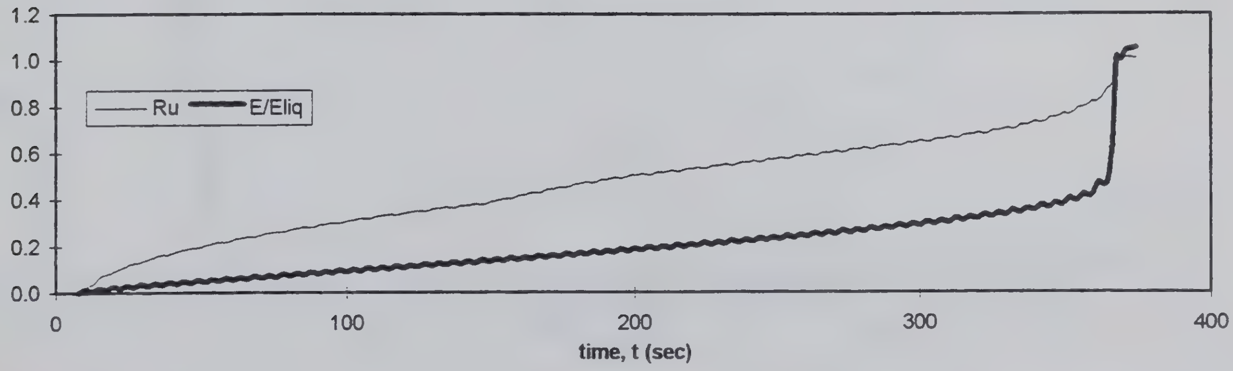

Test I.D.:	UOFC13	**Controlled Parameter:**	Stress
Fines Content (%):	20	**Initial Effective Stress (kPa):**	300
Dry Density (kN/m^3)	15.26		

Shear Stress vs. Shear Strain

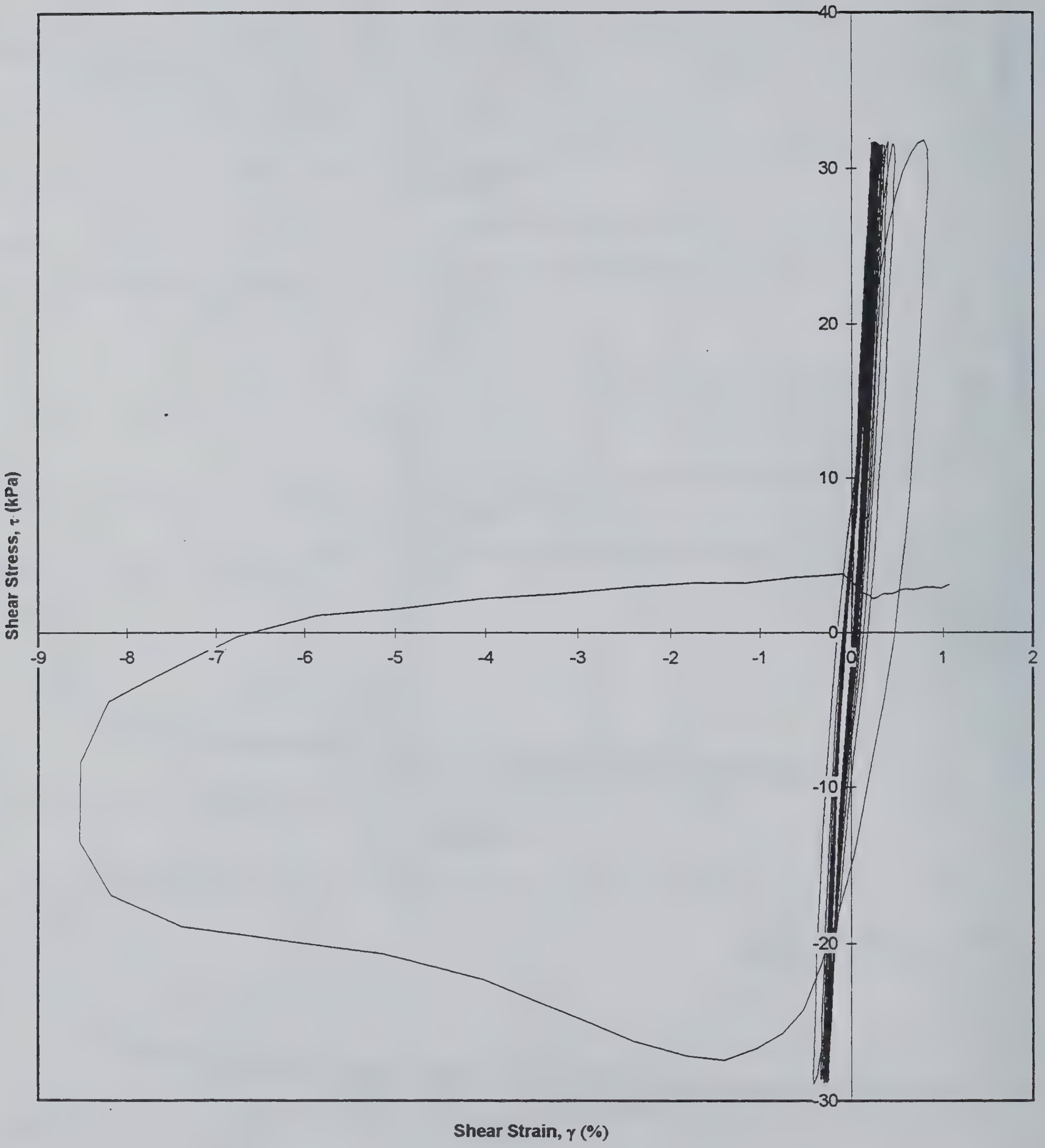

d:\nit\itp\cy_files\UOFC13.XLS

8/21/96 9:29 AM

Test I.D.:	UOFC14	**Controlled Parameter:**	Stress
Fines Content (%):	20	**Initial Effective Stress (kPa):**	200
Dry Density (kN/m^3)	15.18		

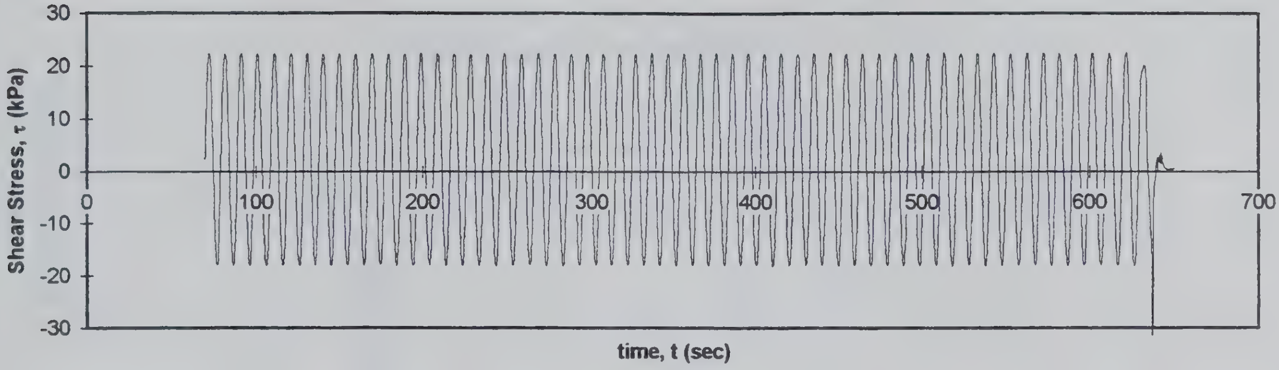

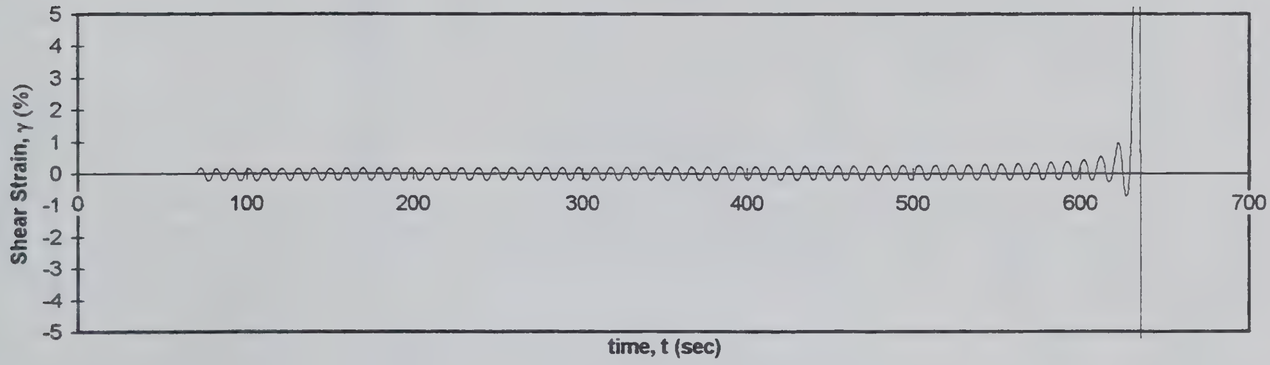

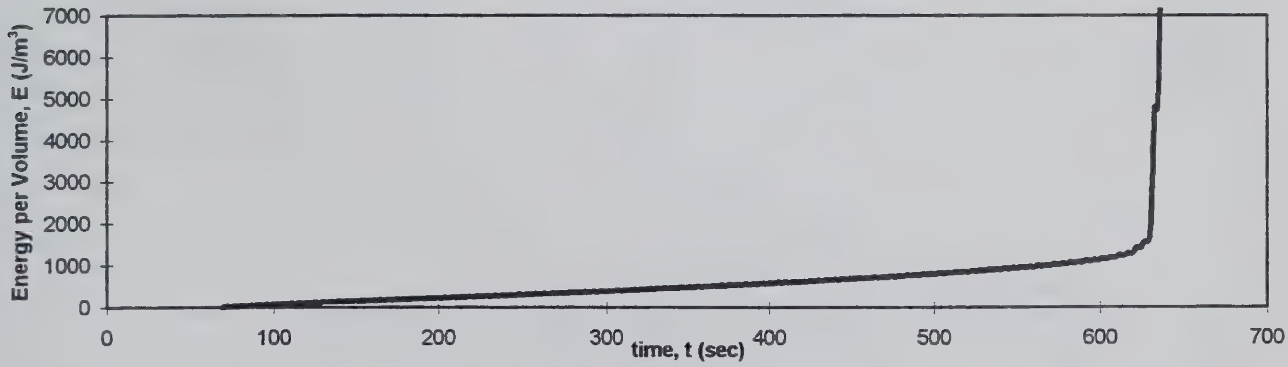

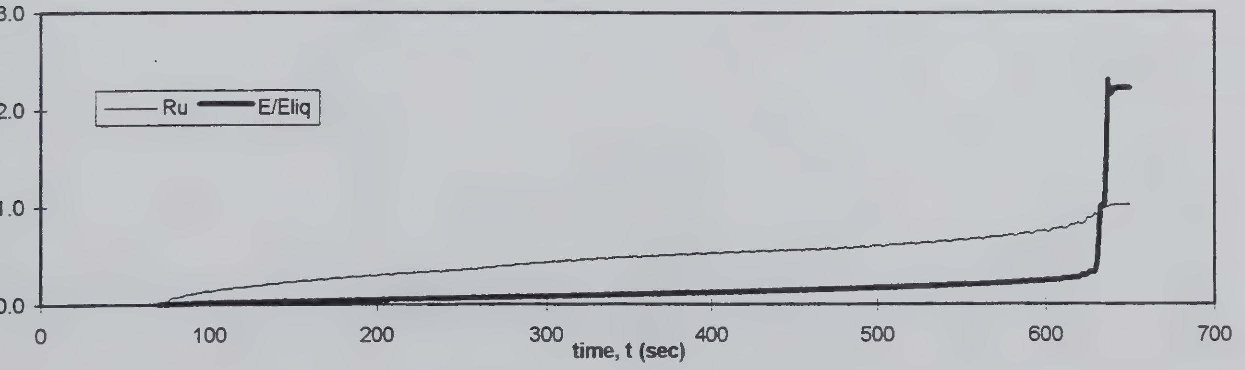

Test I.D.:	UOFC14	**Controlled Parameter:**	Stress
Fines Content (%):	20	**Initial Effective Stress (kPa):**	200
Dry Density (kN/m^3)	15.18		

Shear Stress vs. Shear Strain

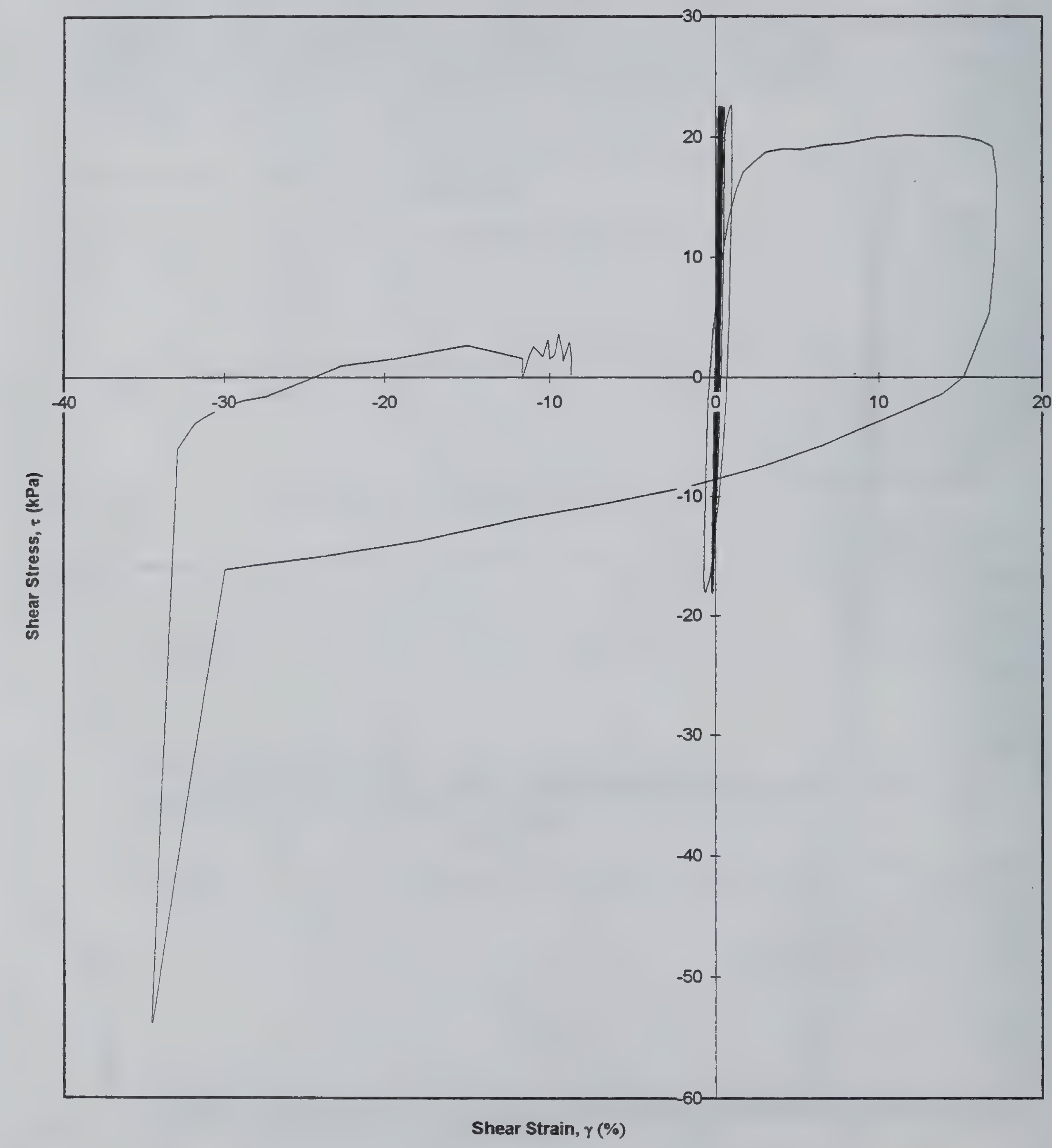

d:\nit\itp\cy_files\UOFC14.XLS

8/19/96 4:57 PM

Test I.D.: UOFC15
Fines Content (%): 20
Dry Density (kN/m^3) 15.25
Controlled Parameter: Stress
Initial Effective Stress (kPa): 200

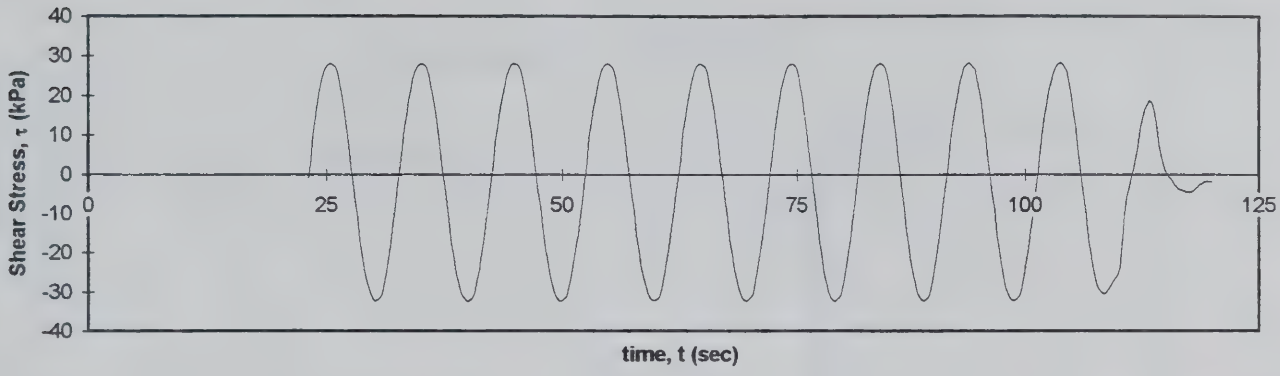

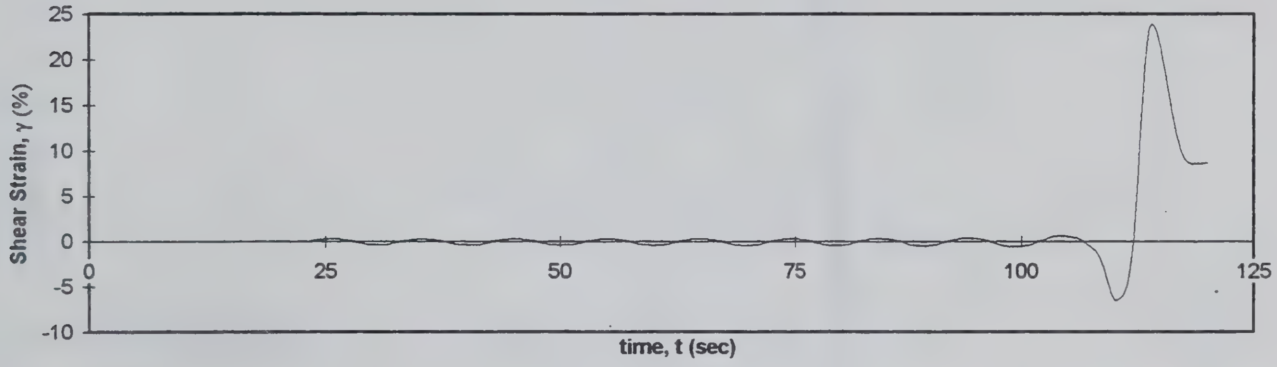

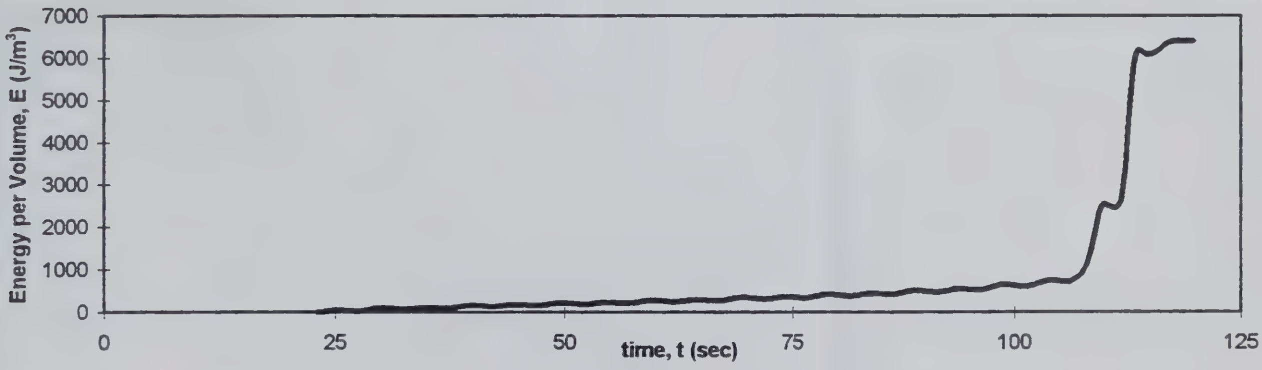

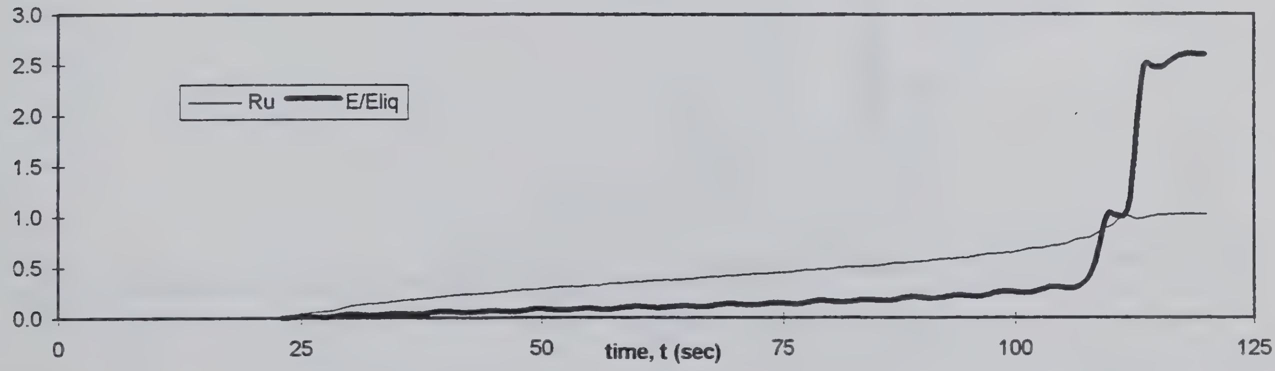

d:\nit\itp\cy_files\UOFC15.XLS

8/20/96 7:35 AM

Test I.D.: UOFC15
Fines Content (%): 20
Dry Density (kN/m^3) 15.25

Controlled Parameter: Stress
Initial Effective Stress (kPa): 200

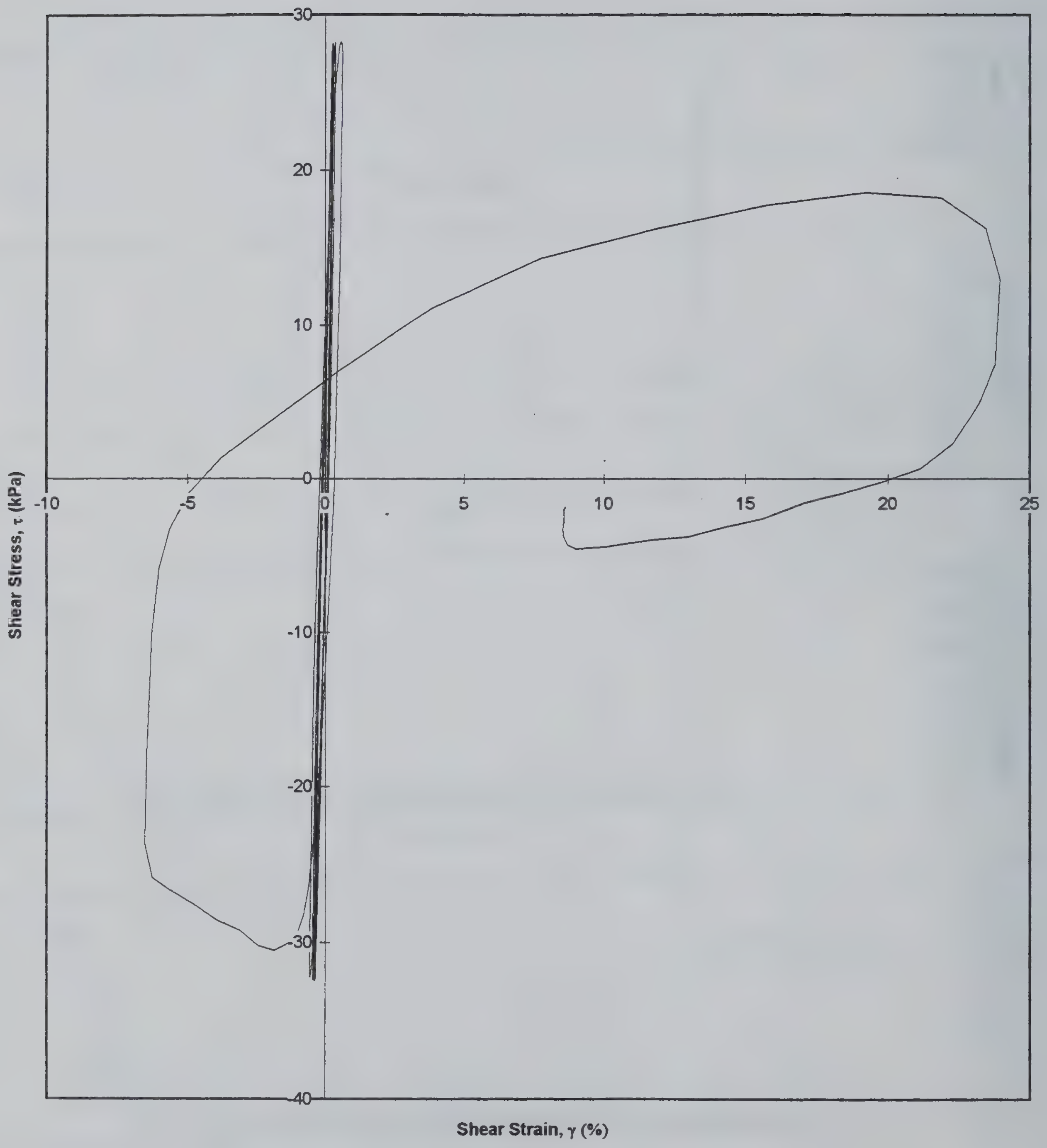

Shear Stress vs. Shear Strain

Test I.D.: UOFC17
Fines Content (%): 45
Dry Density (kN/m^3) 16.18
Controlled Parameter: Stress
Initial Effective Stress (kPa): 203.4

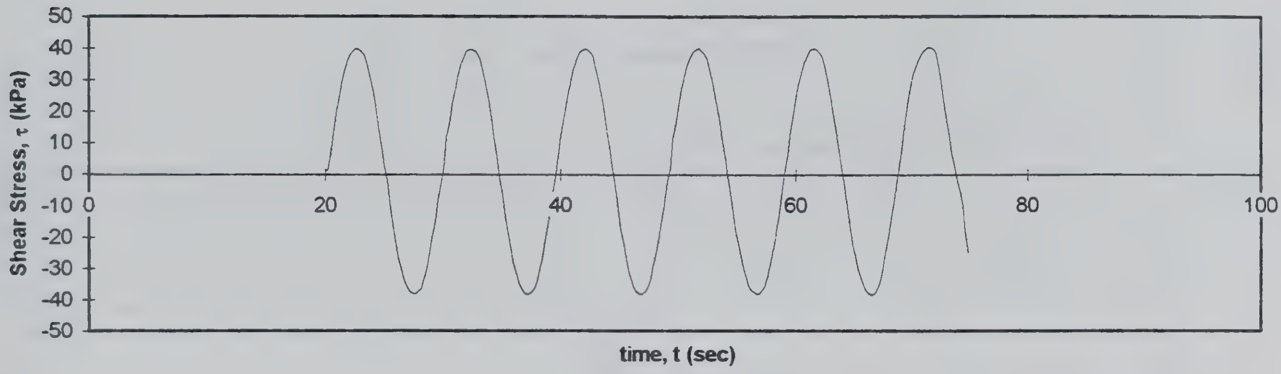

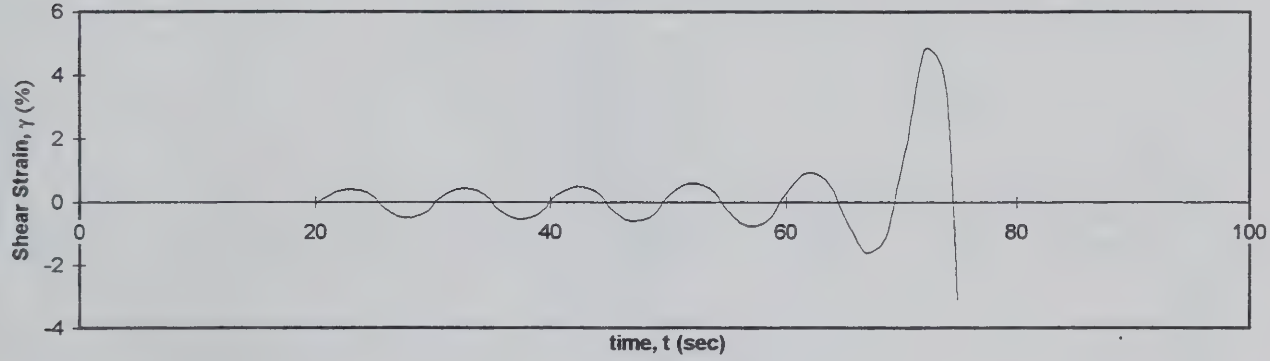

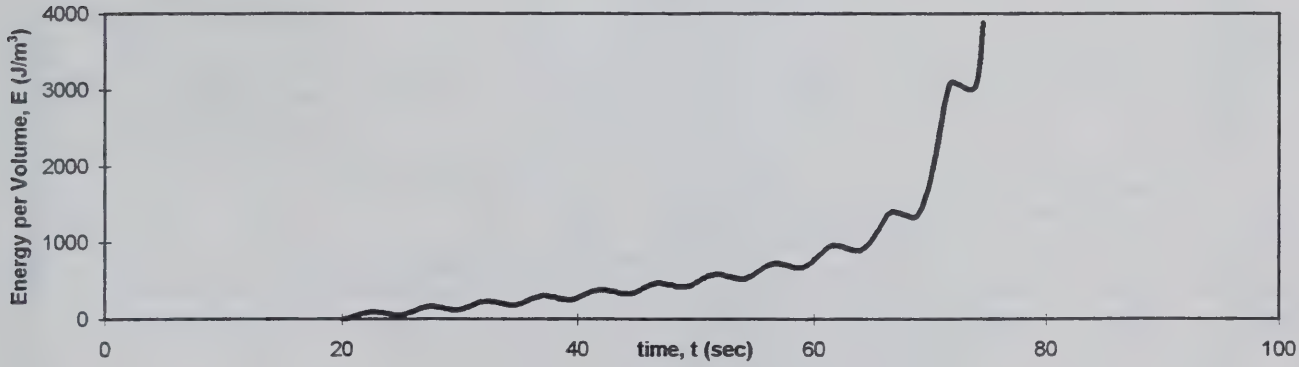

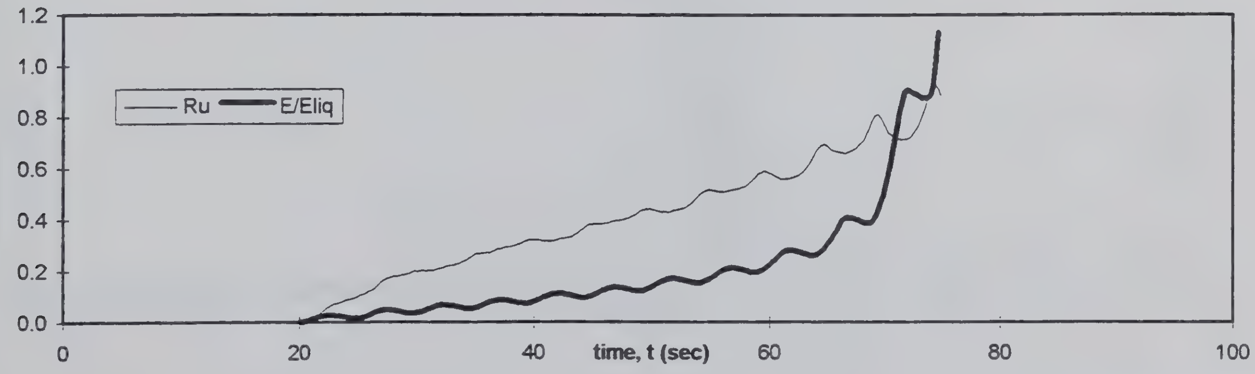

Test I.D.:	UOFC17	**Controlled Parameter:**	Stress
Fines Content (%):	45	**Initial Effective Stress (kPa):**	203.4
Dry Density (kN/m^3)	16.18		

Shear Stress vs. Shear Strain

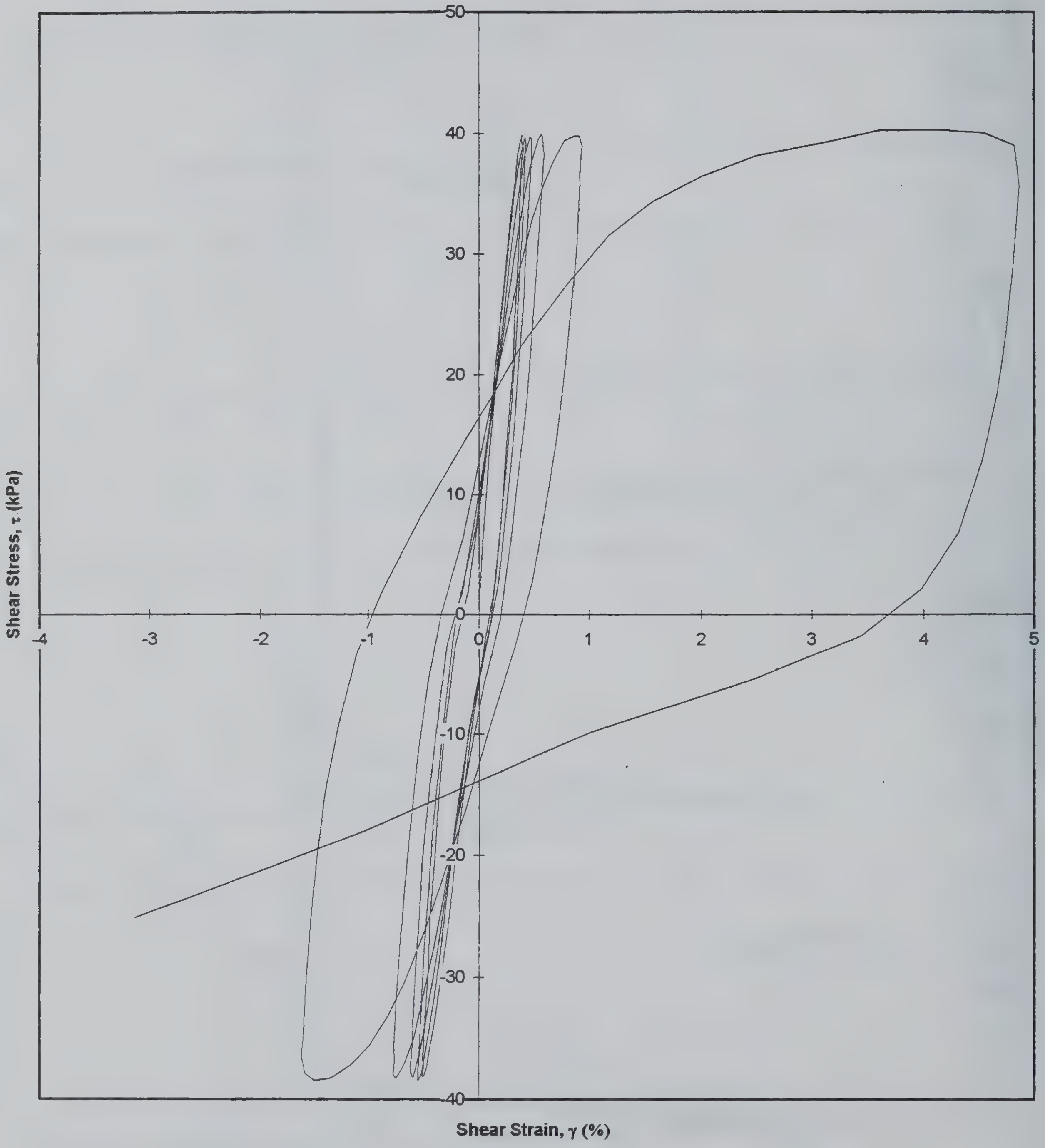

d:\nit\itp\cy_files\UOFC17.XLS

8/20/96 7:40 AM

Test I.D.:	UOFC18	**Controlled Parameter:**	Stress
Fines Content (%):	45	**Initial Effective Stress (kPa):**	190
Dry Density (kN/m^3)	16.18		

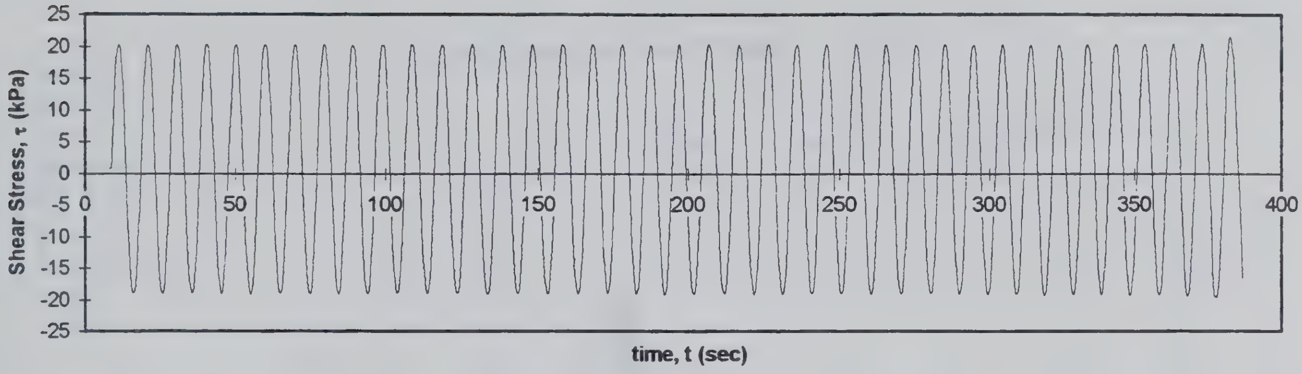

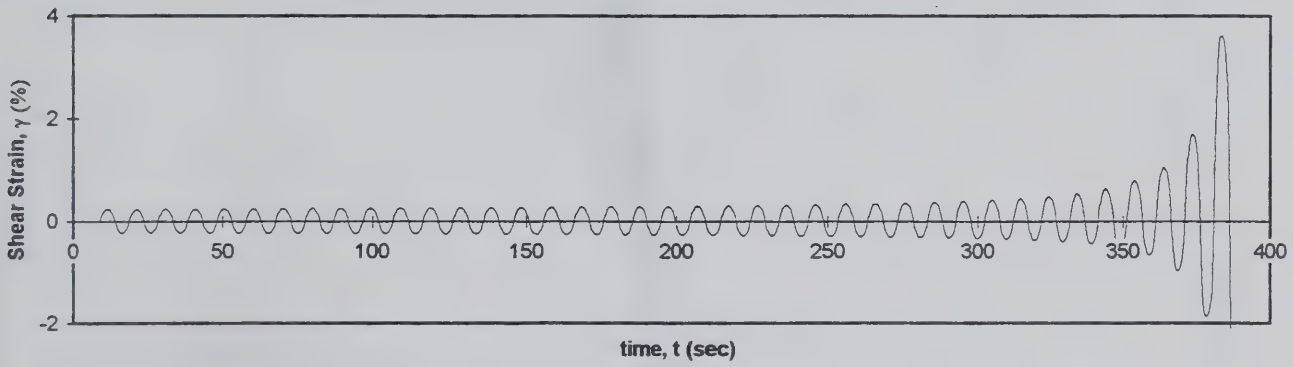

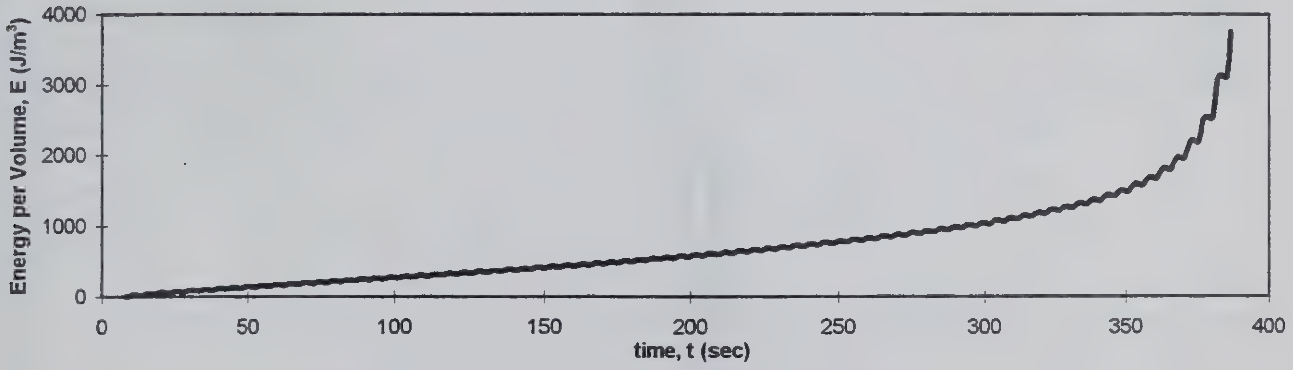

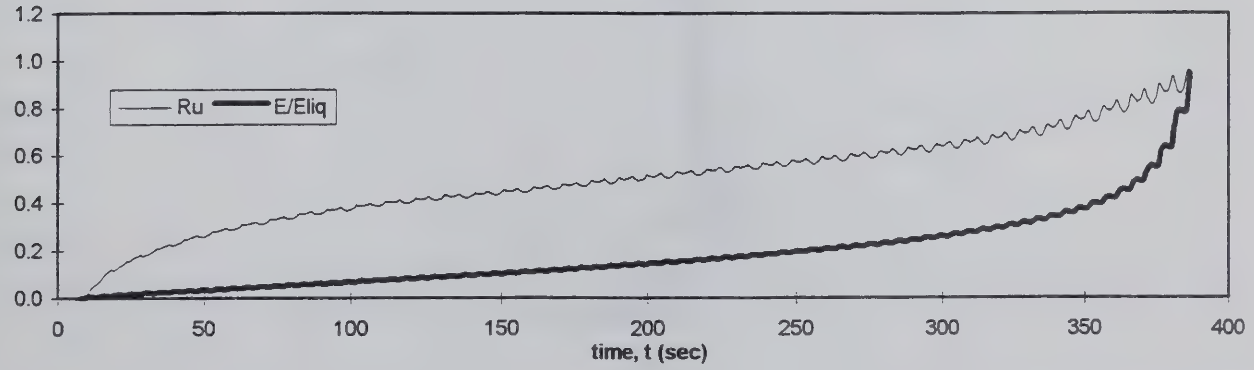

Test I.D.:	UOFC18	**Controlled Parameter:**	Stress
Fines Content (%):	45	**Initial Effective Stress (kPa):**	190
Dry Density (kN/m^3)	16.18		

Shear Stress vs. Shear Strain

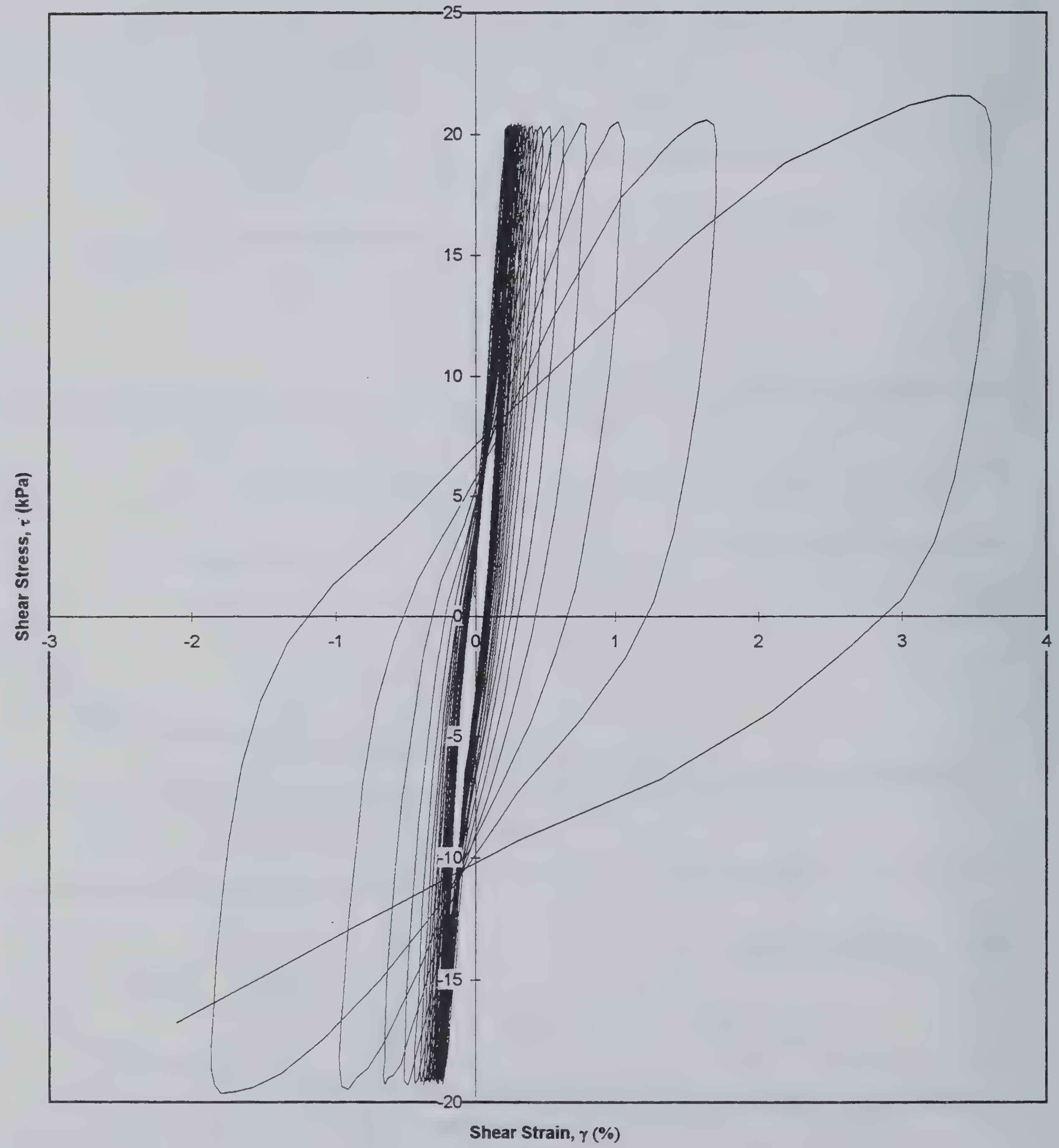

Test I.D.:	UOFC23	**Controlled Parameter:**	Stress
Fines Content (%):	Clean Sand	**Initial Effective Stress (kPa):**	200
Relative Density(%):	45.3		

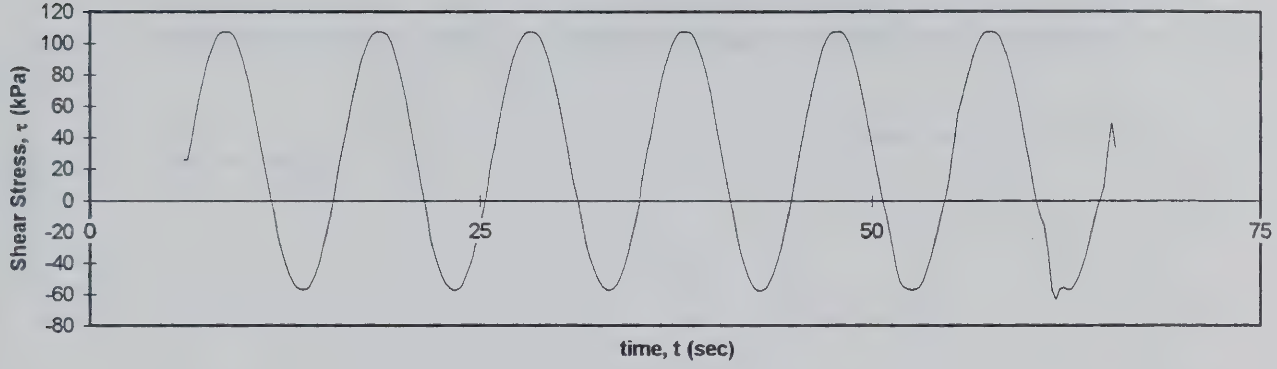

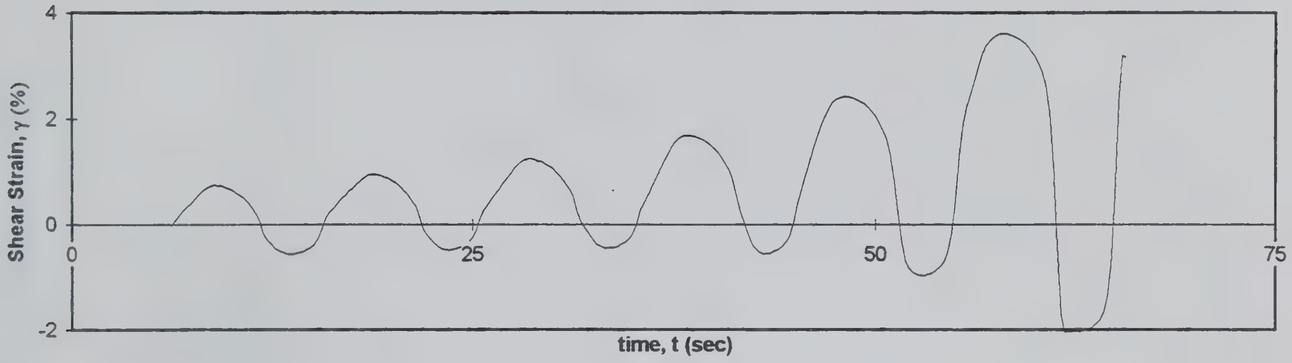

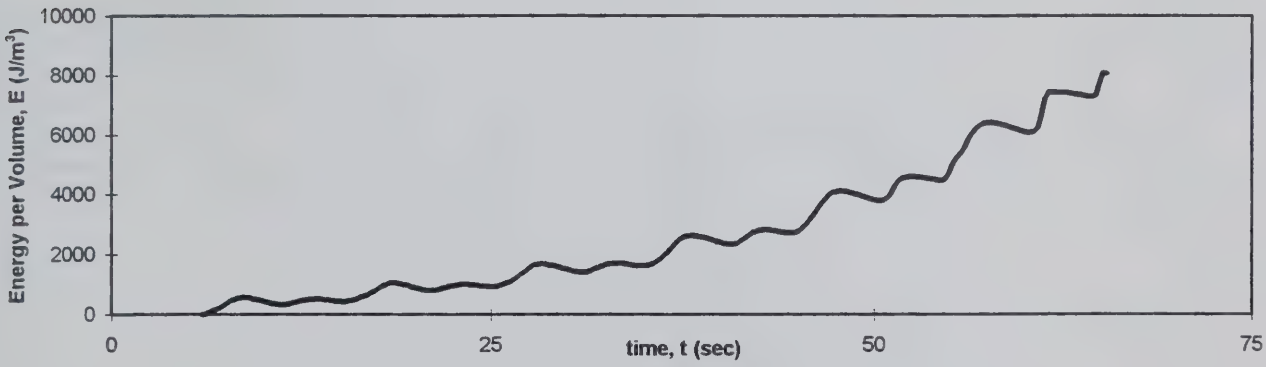

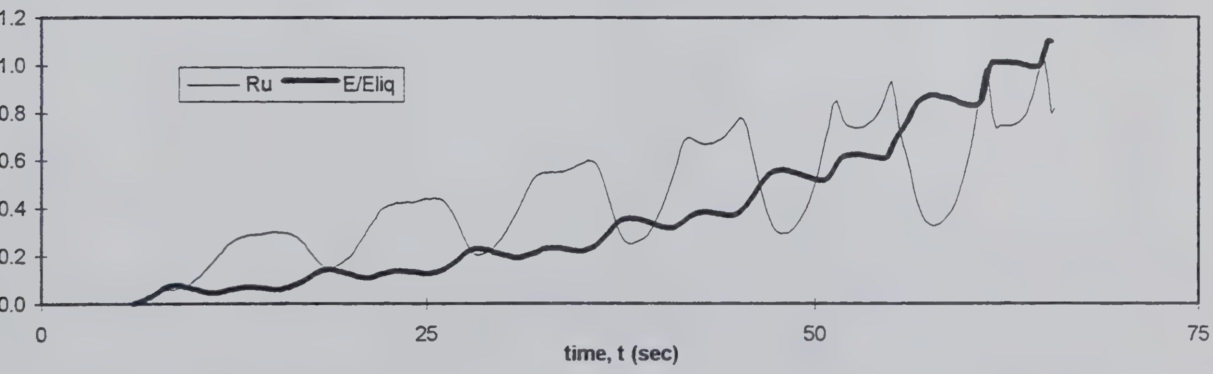

Test I.D.:	UOFC23	**Controlled Parameter:**	Stress
Fines Content (%):	Clean Sand	**Initial Effective Stress (kPa):**	200
Relative Density (%):	45.3		

Shear Stress vs. Shear Strain

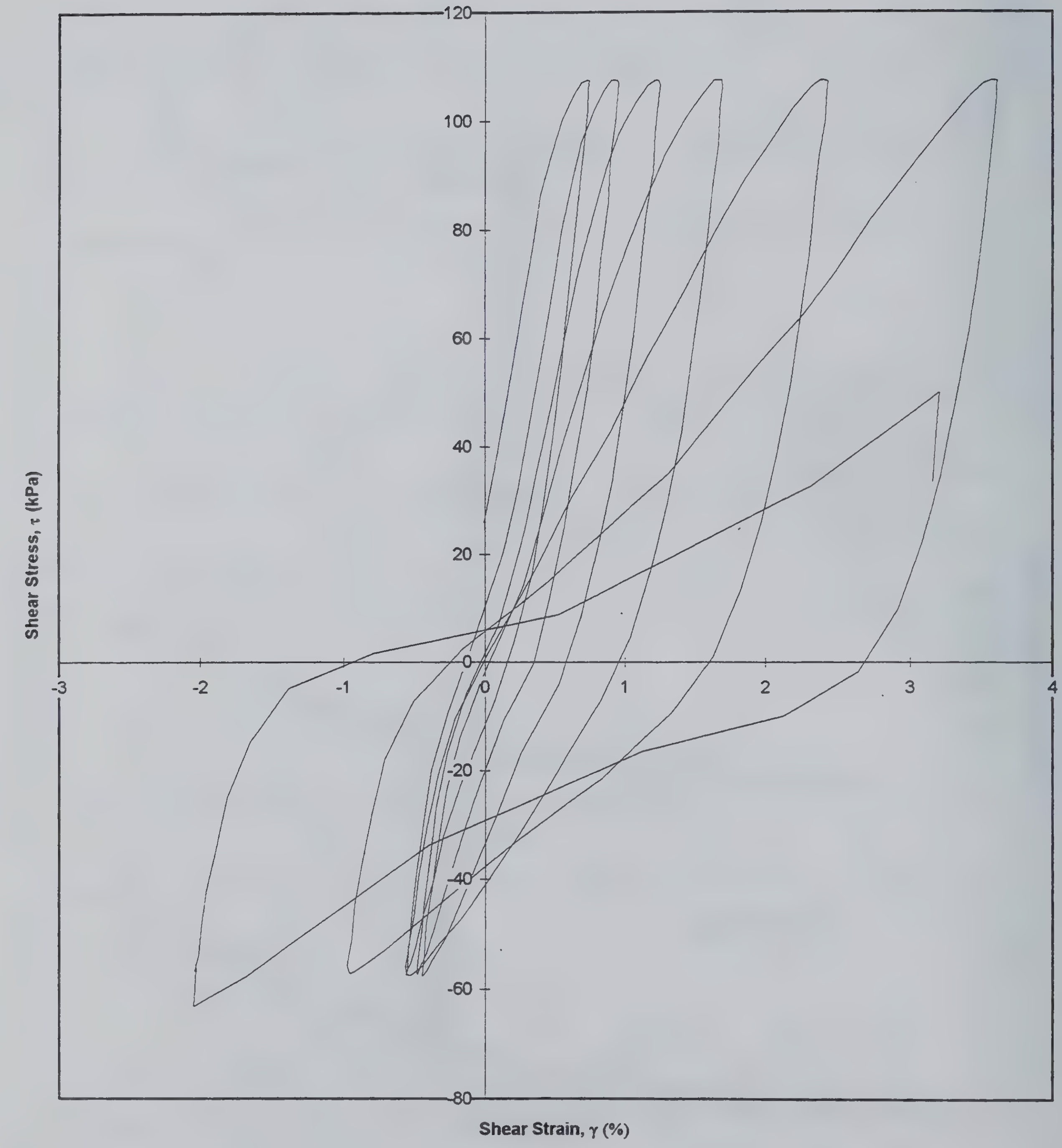

d:\nit\itp\cy_files\UOFC23.XLS

8/19/96 4:37 PM

APPENDIX D

LABORATORY DATA ON SOIL SAMPLES FROM THE NORTHRIDGE SITE, PERFORMED AT THE UNIVERSITY OF CALIFORNIA, BERKELEY

Table D.1 - Summary of the Cyclic Triaxial Test Data on Northridge Samples Performed at University of California, Berkeley

No.	Test ID	Sample	D_r(%)	E_{liq} (J/m^3)	FC (%)	γ_d (kN/m^3)	Control	σ_c' (kPa)	Freq. (Hz)	Load Shape
1	BTC2CY1	Northridge Sand	58.3	5930	5	14.5	Stress	100	1	Sinusoidal 2-way
2	BTC2CY2	Northridge Sand	78.4	2247	5	15.5	Stress	100	1	Sinusoidal 2-way
3	BTC3CY1	Northridge Sand	82.3	5146	5	15.7	Stress	100	1	Sinusoidal 2-way
4	BTC3CY2	Northridge Sand	89.9	3813	5	16.1	Stress	100	1	Sinusoidal 2-way
5	BTC3CY3	Northridge Sand	97.2	36156	5	16.5	Stress	100	1	Sinusoidal 2-way
6	BTC4CY1	Northridge Sand	93.7	7874	5	16.3	Stress	100	1	Sinusoidal 2-way
7	BTC4CY2	Northridge Sand	100.0	6647	5	16.7	Stress	100	1	Sinusoidal 2-way
8	BTC6CY1	Northridge Sand	35.2	3206	5	13.5	Stress	100	1	Sinusoidal 2-way

Test Results Following the Sequence of Test ID's are Attached.

Test I.D.: BTC2CY1
Fines Content (%): 5
Dry Density (kN/m^3) 14.51
Controlled Parameter: Stress
Initial Effective Stress (kPa): 100

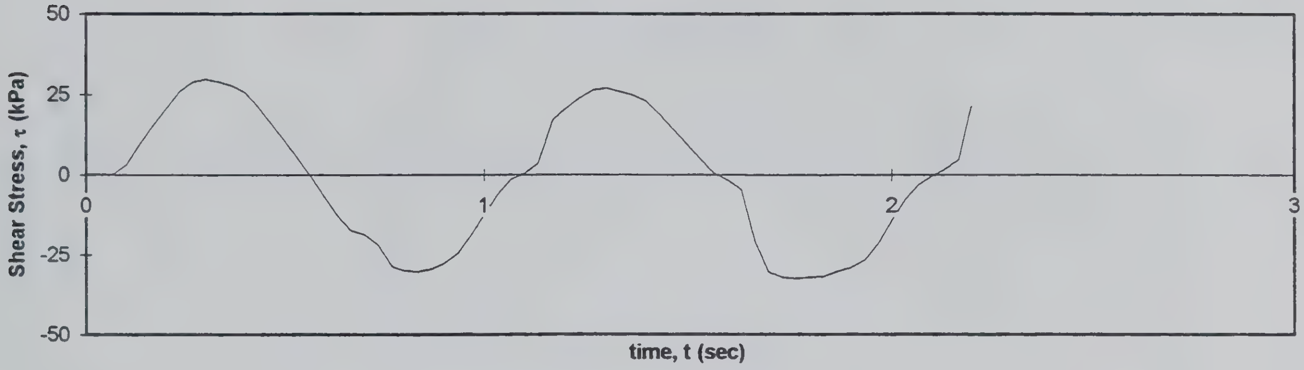

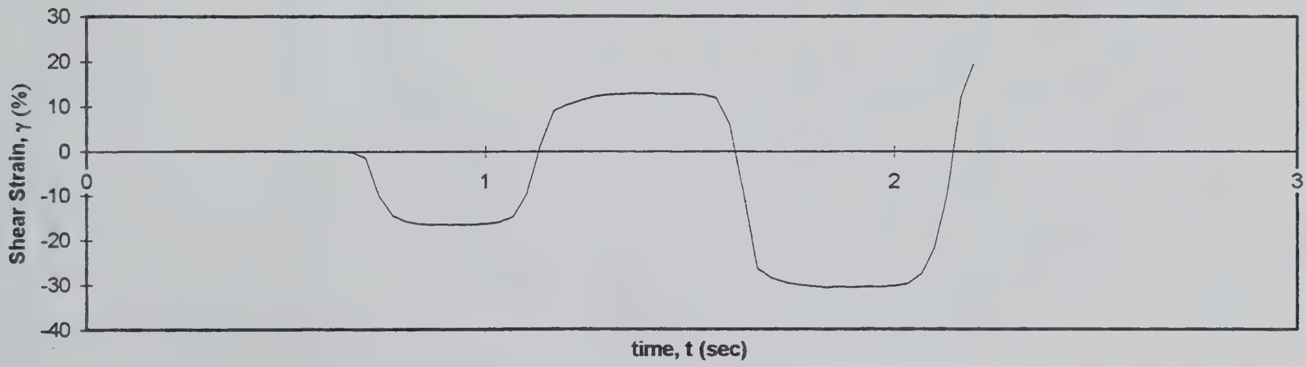

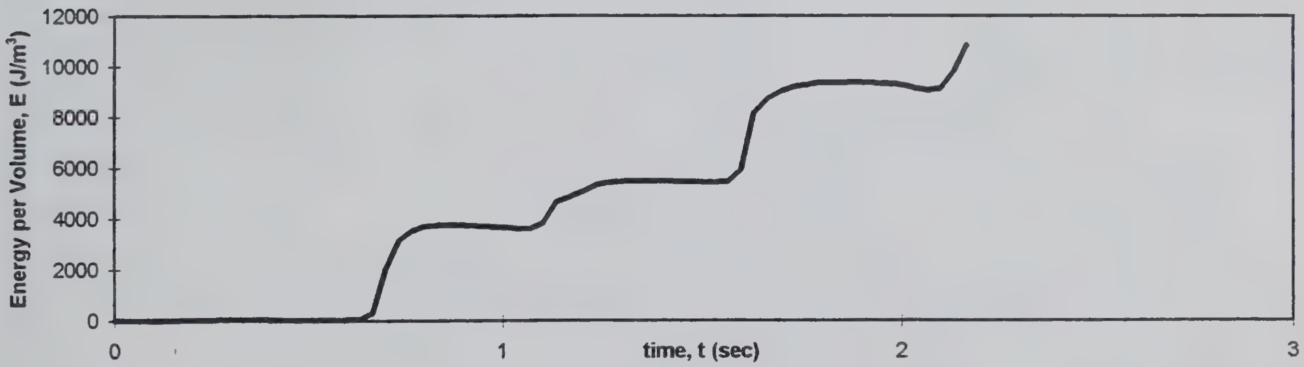

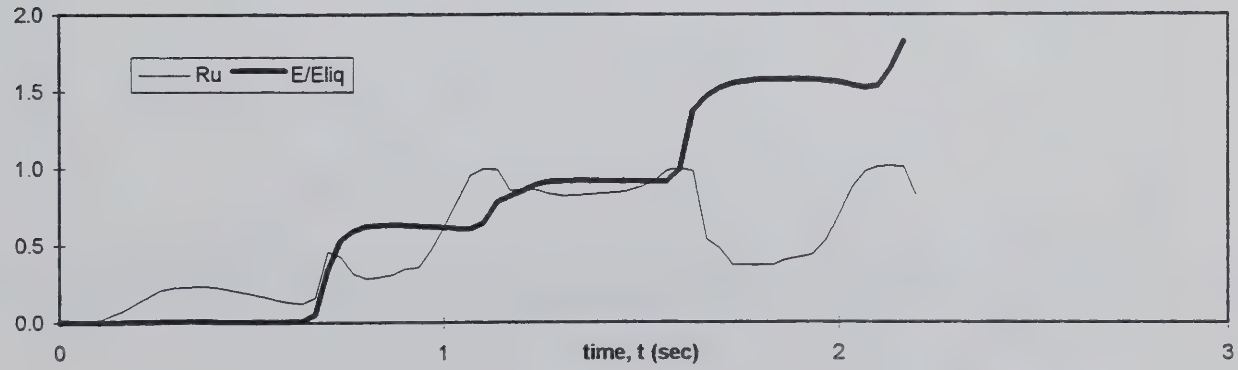

Test I.D.:	BTC2CY1	**Controlled Parameter:**	Stress
Fines Content (%):	5	**Initial Effective Stress (kPa):**	100
Dry Density (kN/m^3)	14.51		

Shear Stress vs. Shear Strain

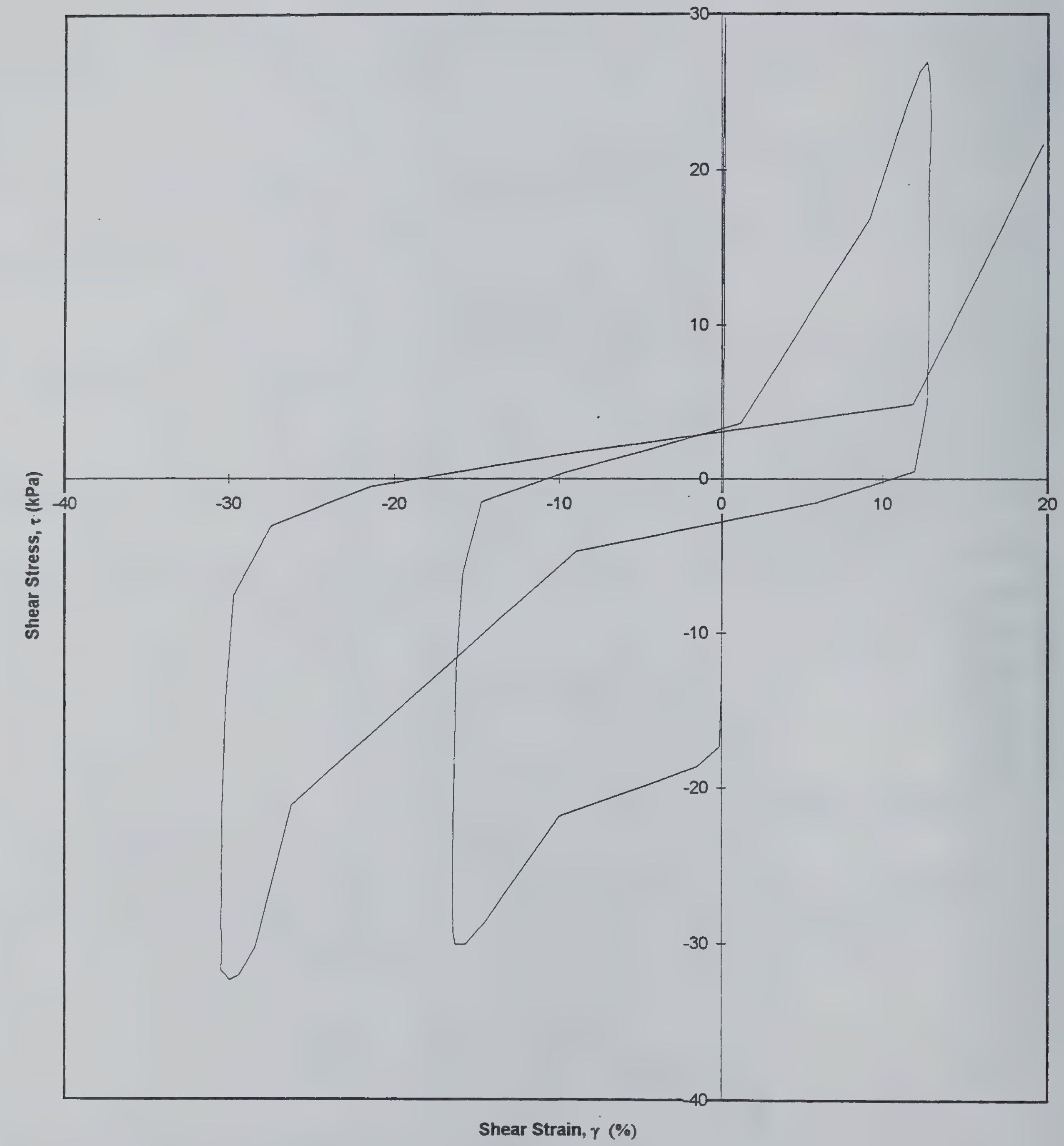

d:\nit\itp\cy_files\BTC2CY1.XLS

8/21/96 8:39 AM

Test I.D.: BTC2CY2
Fines Content (%): 5
Dry Density (kN/m^3) 15.5
Controlled Parameter: Stress
Initial Effective Stress (kPa): 100

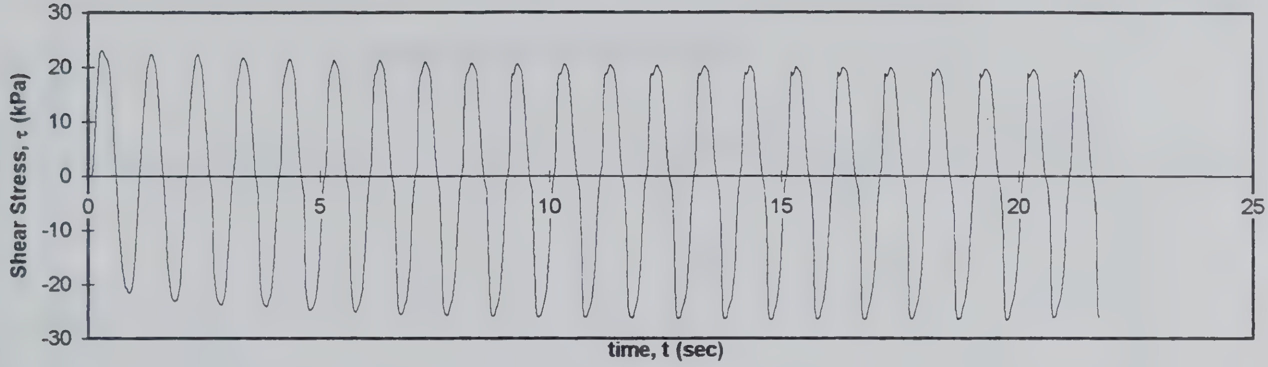

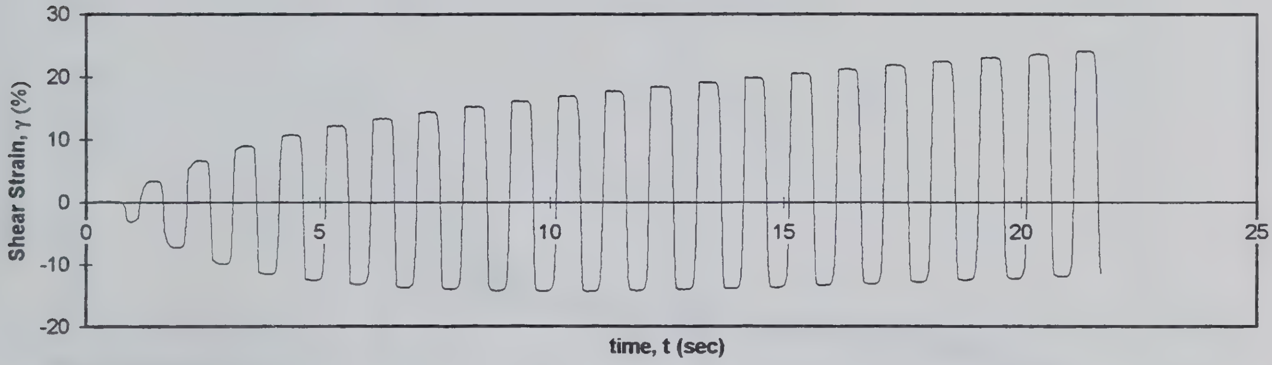

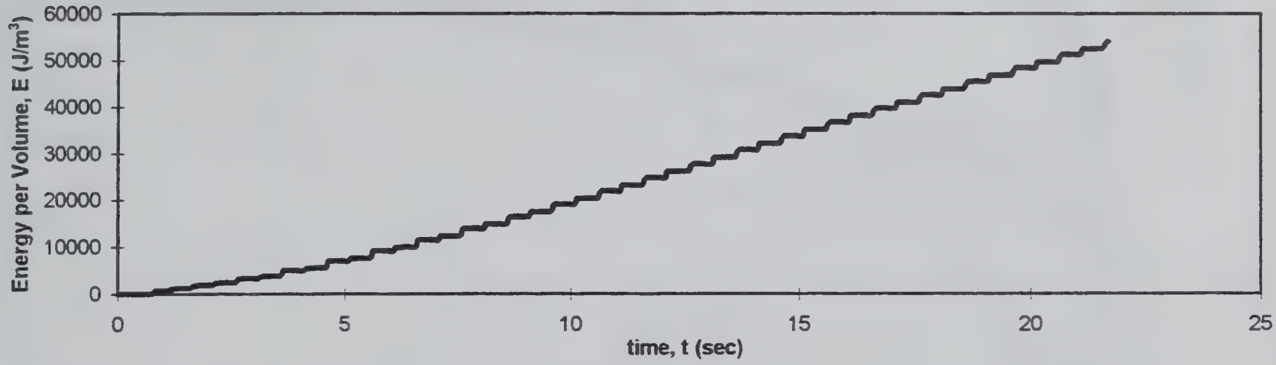

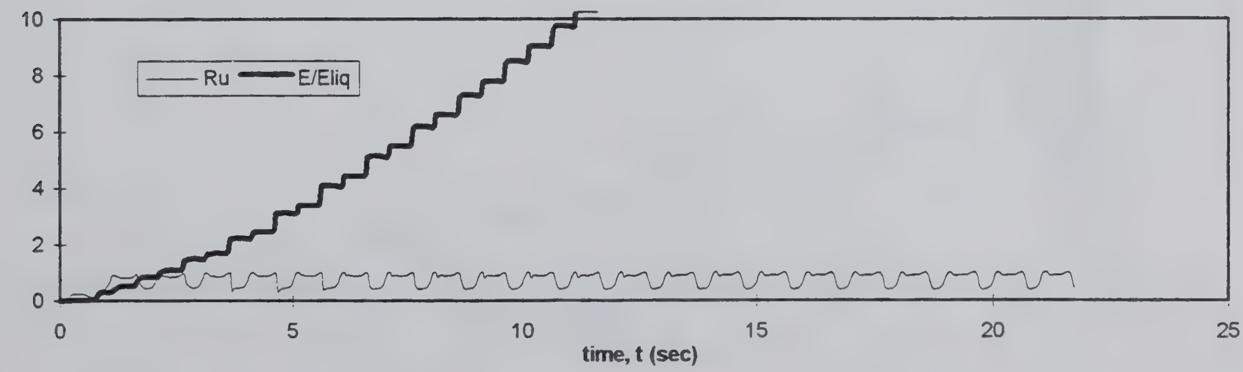

Test I.D.:	BTC2CY2	**Controlled Parameter:**	Stress
Fines Content (%):	5	**Initial Effective Stress (kPa):**	100
Dry Density (kN/m^3)	15.5		

Shear Stress vs. Shear Strain

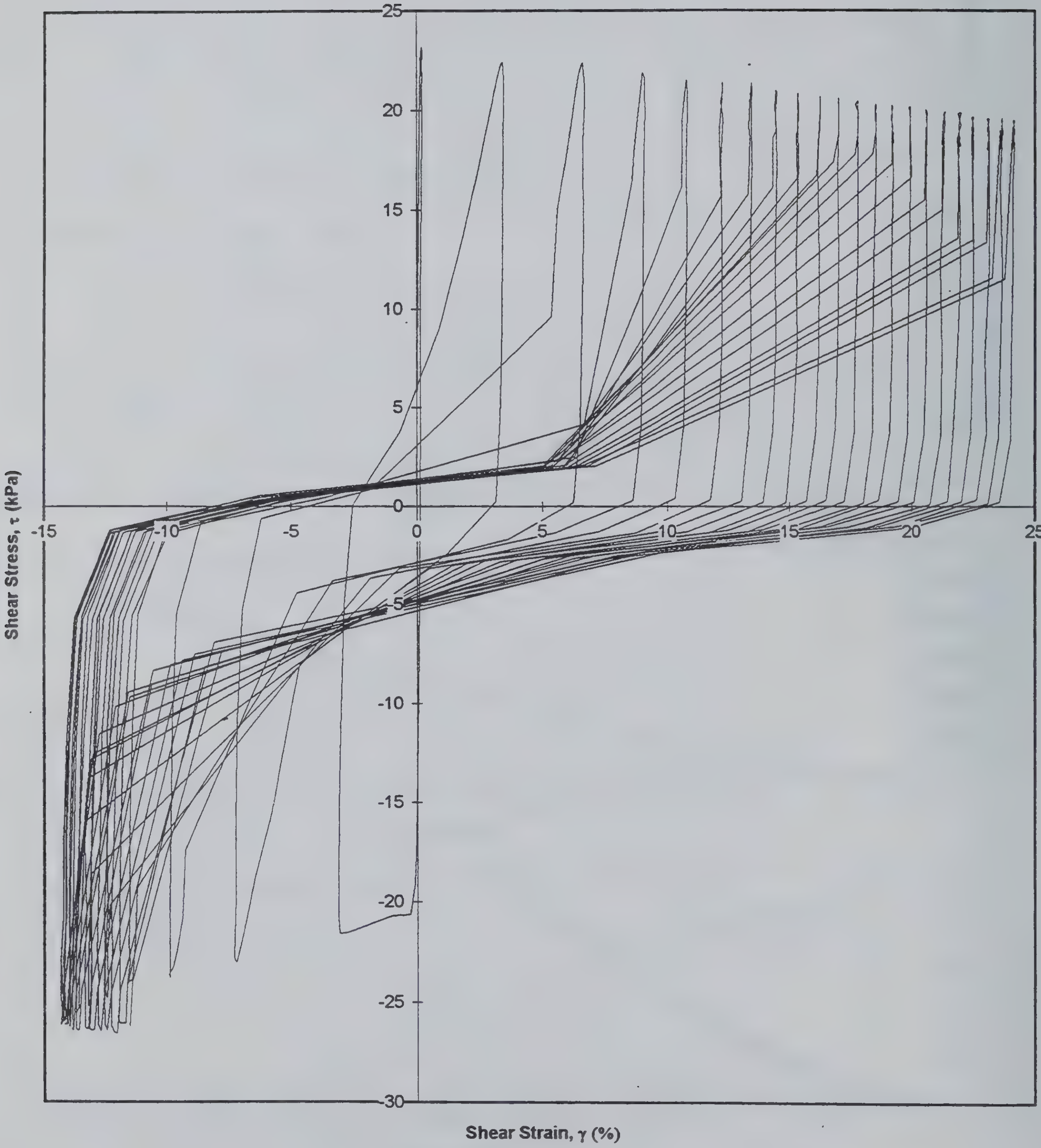

d:\nit\itp\cy_files\BTC2CY2.XLS

8/15/96 10:35 AM

Test I.D.:	BTC3CY1	**Controlled Parameter:**	Stress
Fines Content (%):	5	**Initial Effective Stress (kPa):**	100
Dry Density (kN/m^3)	15.7		

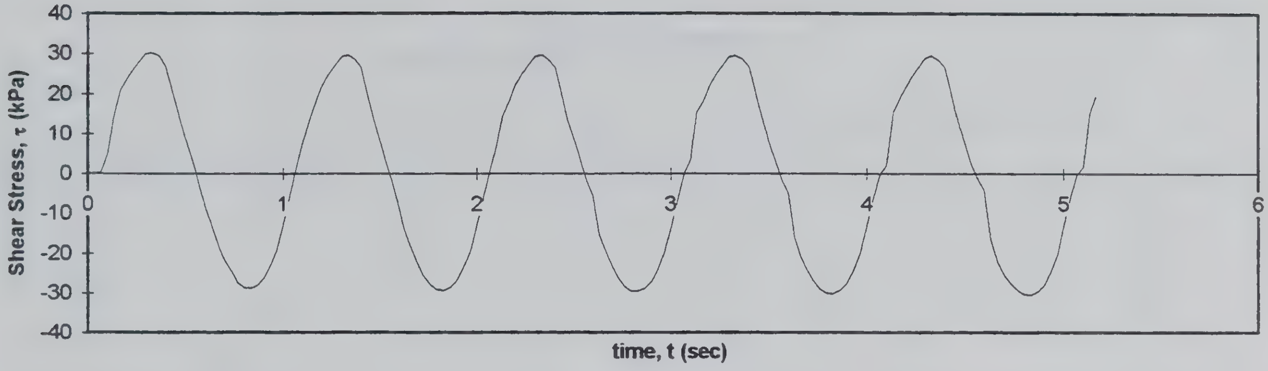

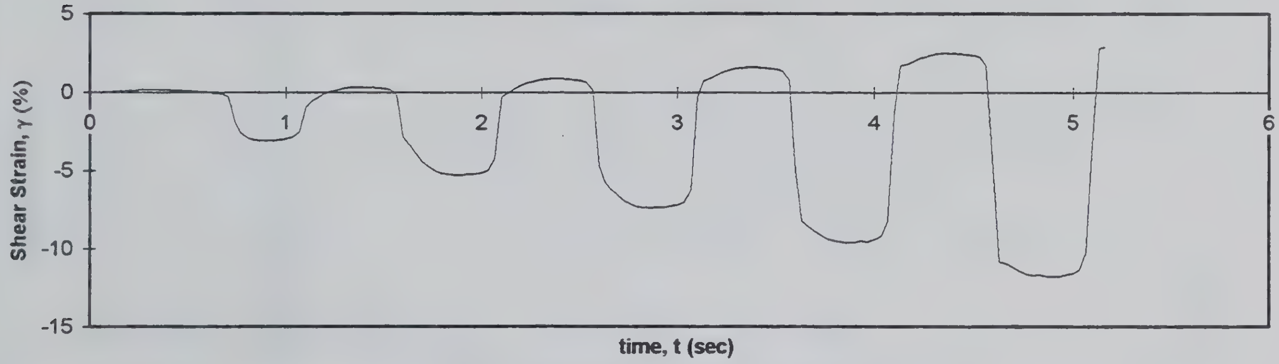

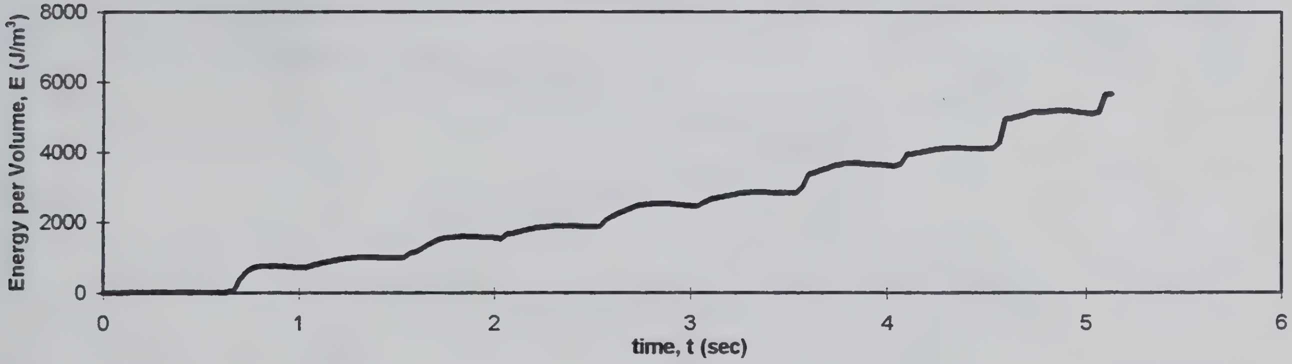

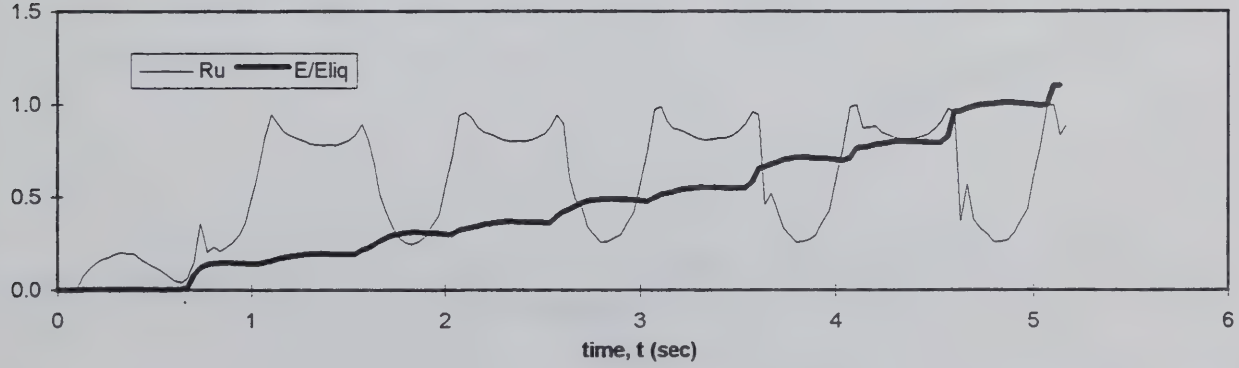

Test I.D.:	BTC3CY1	**Controlled Parameter:**	Stress
Fines Content (%):	5	**Initial Effective Stress (kPa):**	100
Dry Density (kN/m^3)	15.7		

Shear Stress vs. Shear Strain

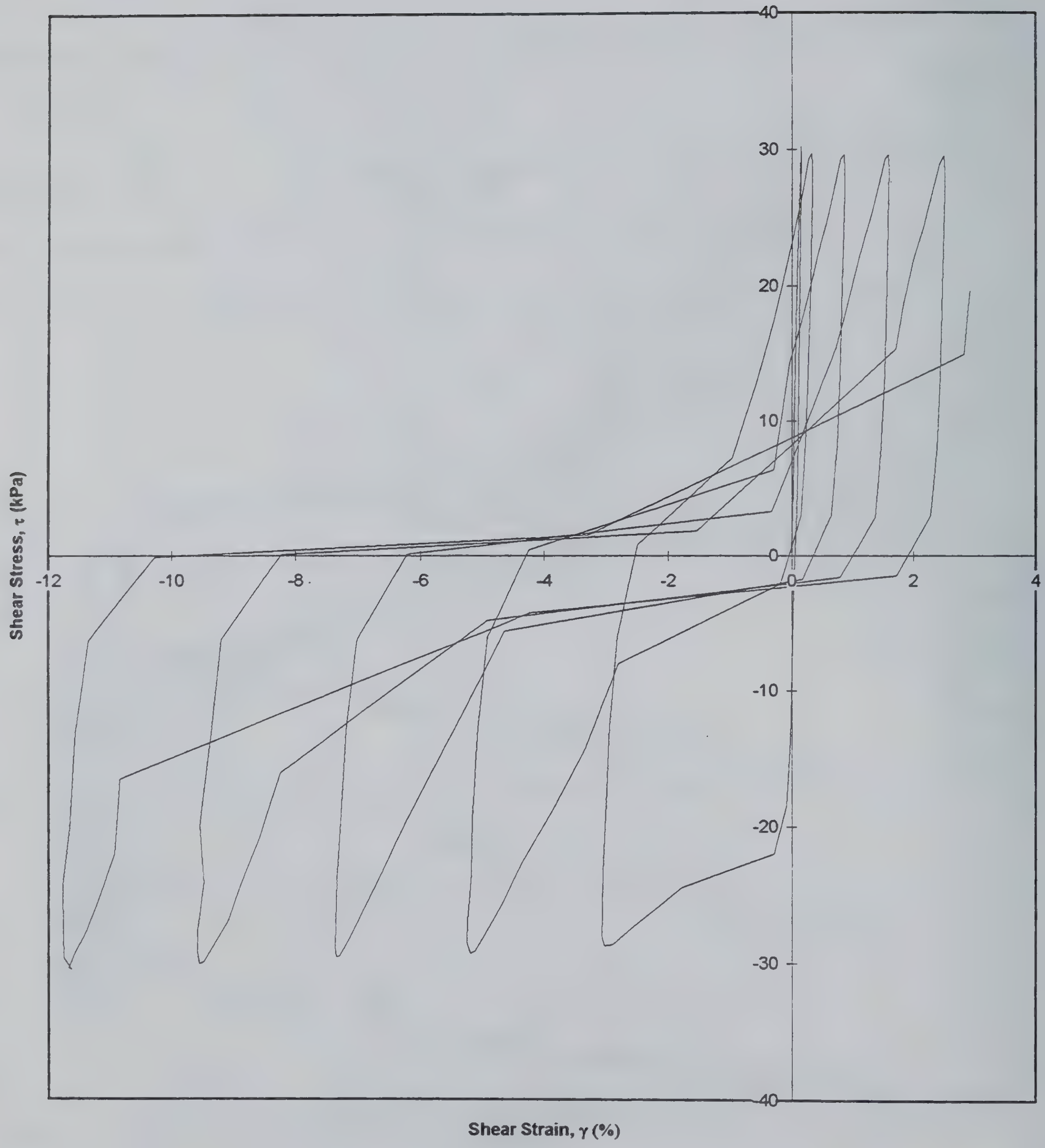

Test I.D.: BTC3CY2
Fines Content (%): 5
Dry Density (kN/m^3) 16.12

Controlled Parameter: Stress
Initial Effective Stress (kPa): 100

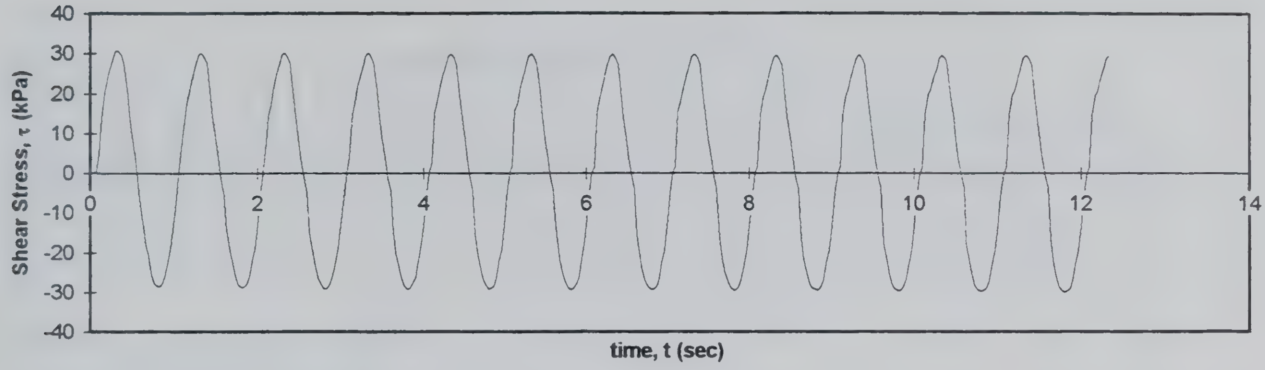

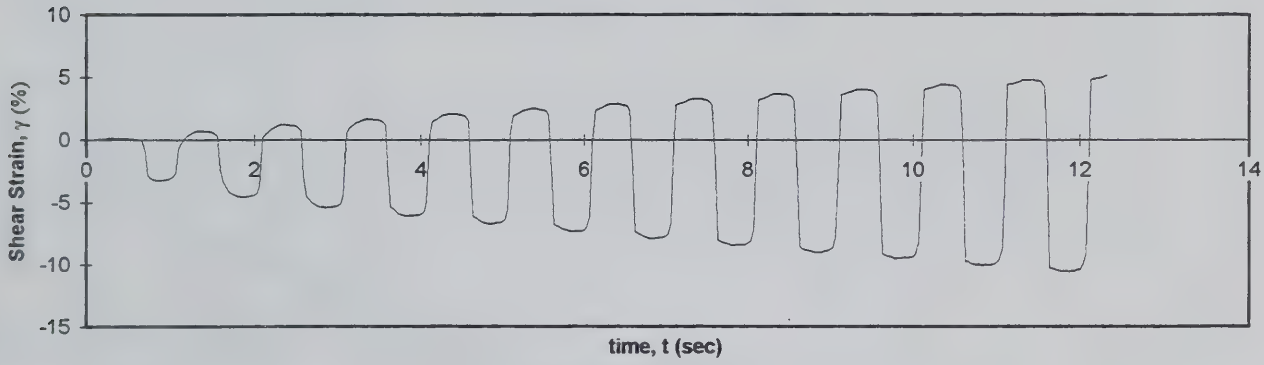

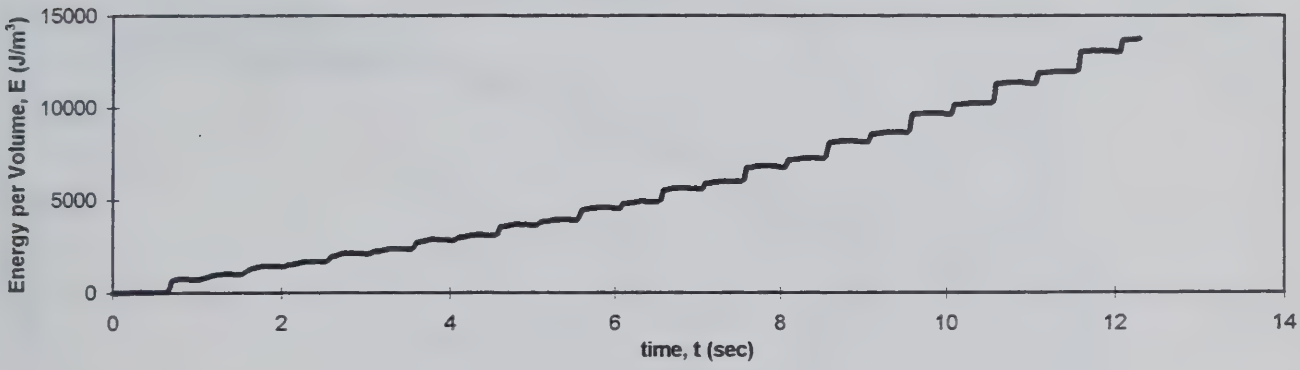

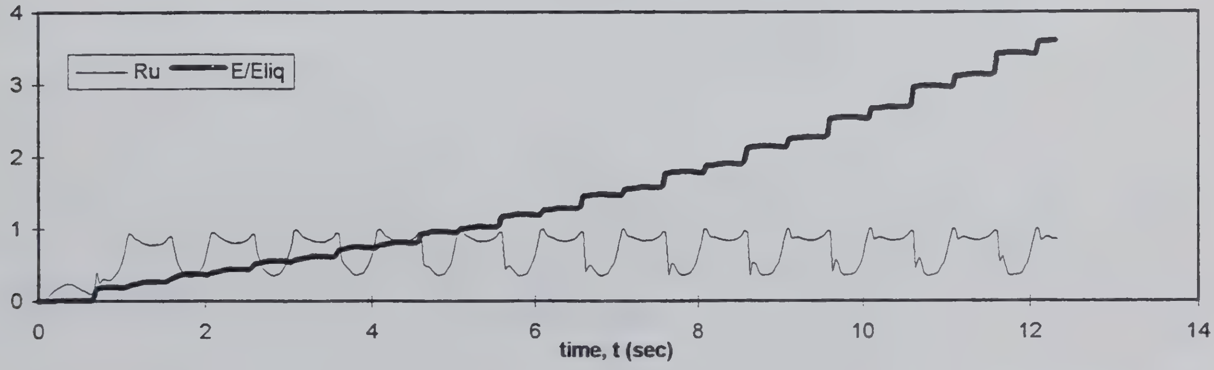

Test I.D.:	BTC3CY2	**Controlled Parameter:**	Stress
Fines Content (%):	5	**Initial Effective Stress (kPa):**	100
Dry Density (kN/m^3)	16.12		

Shear Stress vs. Shear Strain

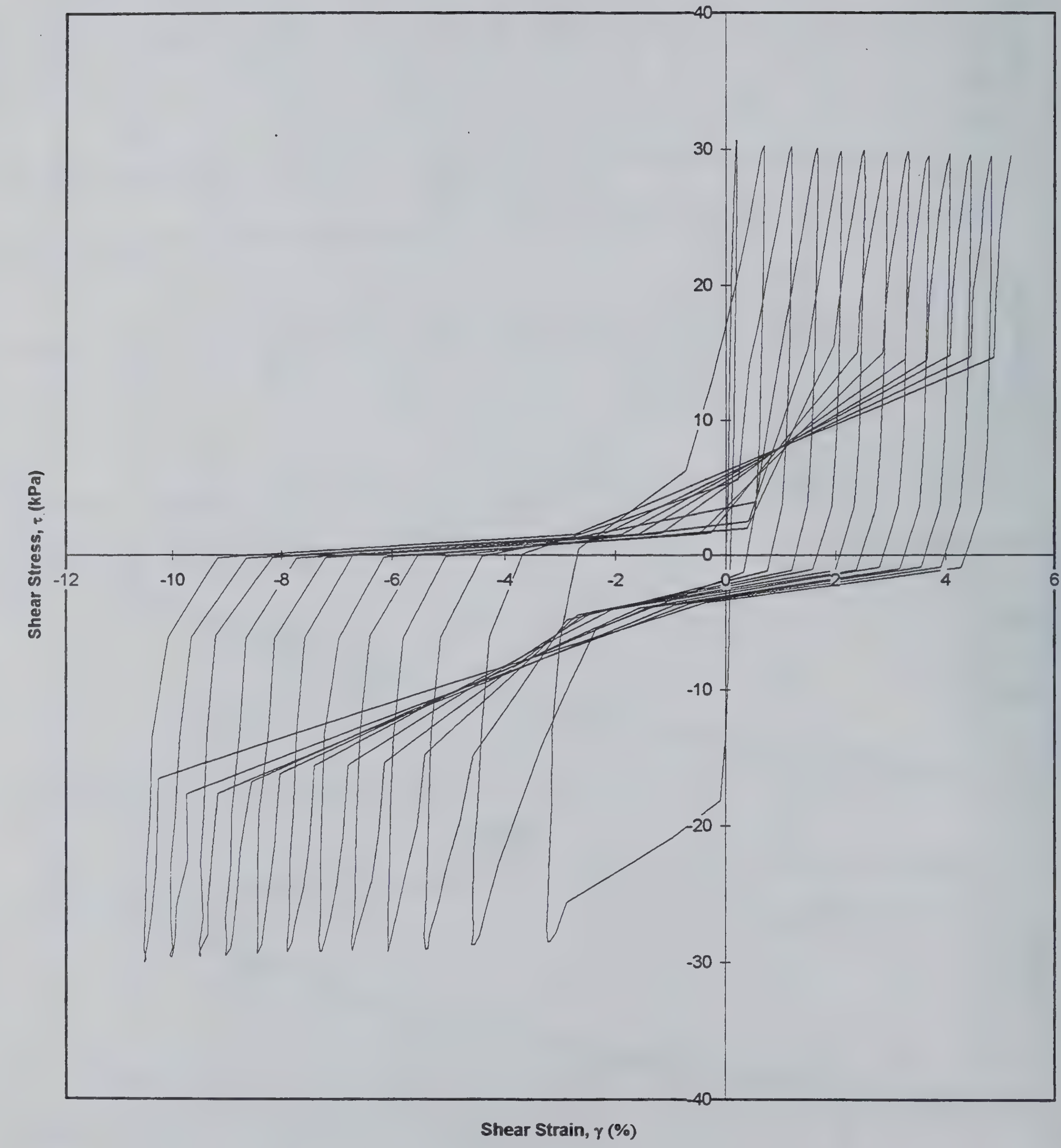

d:\nit\itp\cy_files\BTC3CY2.XLS

8/15/96 10:45 AM

Test I.D.: BTC3CY3
Fines Content (%): 5
Dry Density (kN/m^3) 16.55

Controlled Parameter: Stress
Initial Effective Stress (kPa): 100

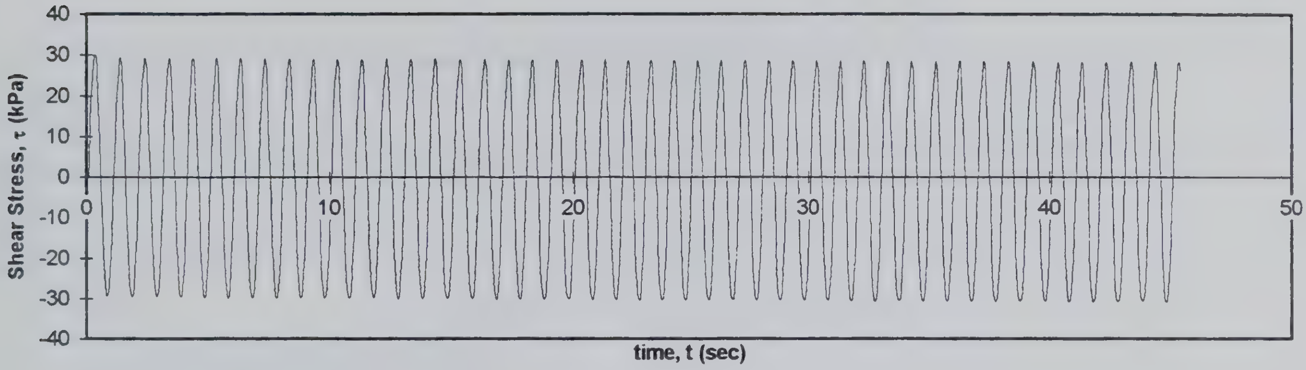

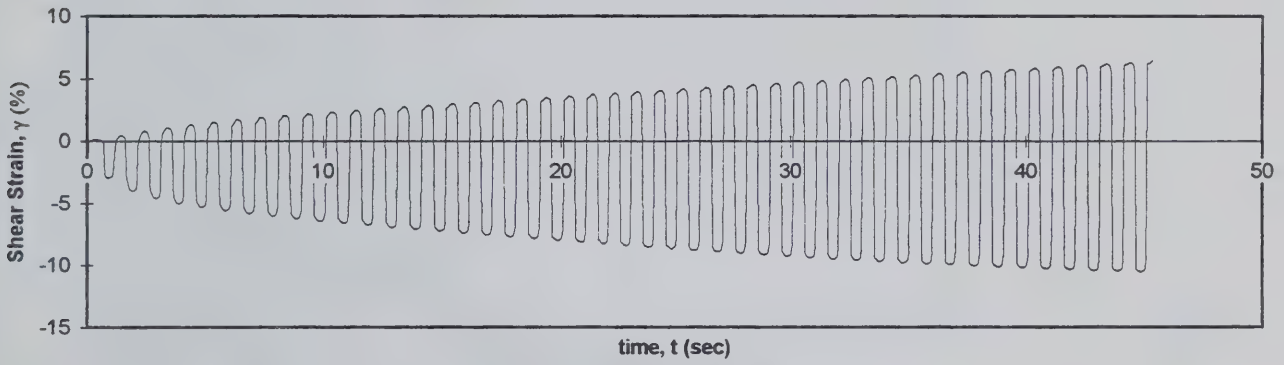

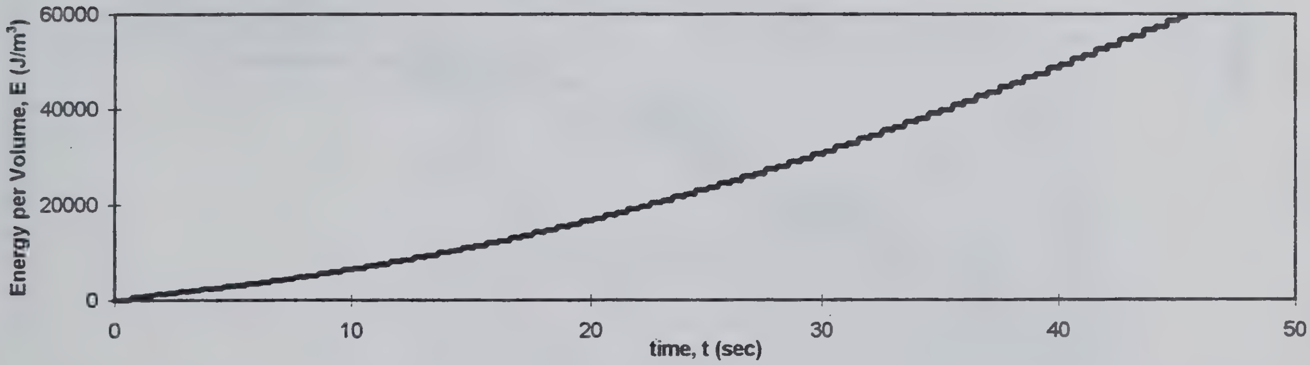

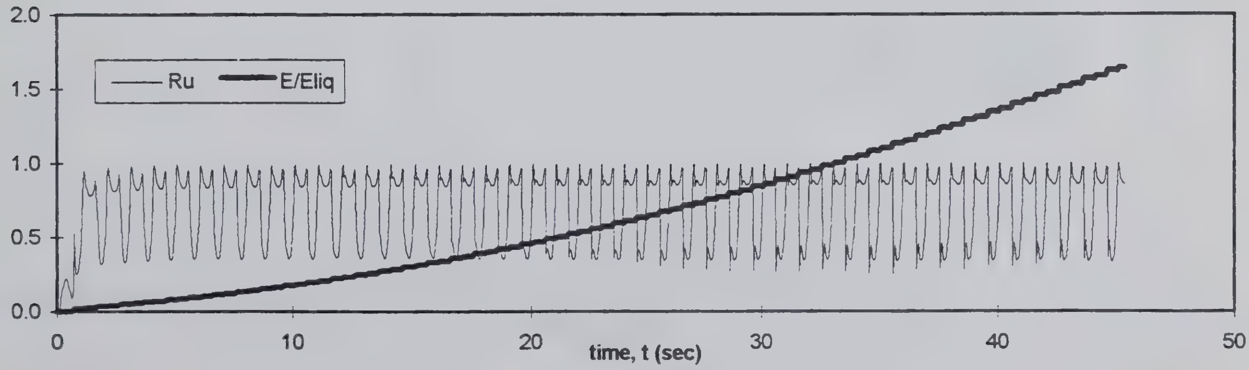

Test I.D.:	BTC3CY3	**Controlled Parameter:**	Stress
Fines Content (%):	5	**Initial Effective Stress (kPa):**	100
Dry Density (kN/m^3)	16.55		

Shear Stress vs. Shear Strain

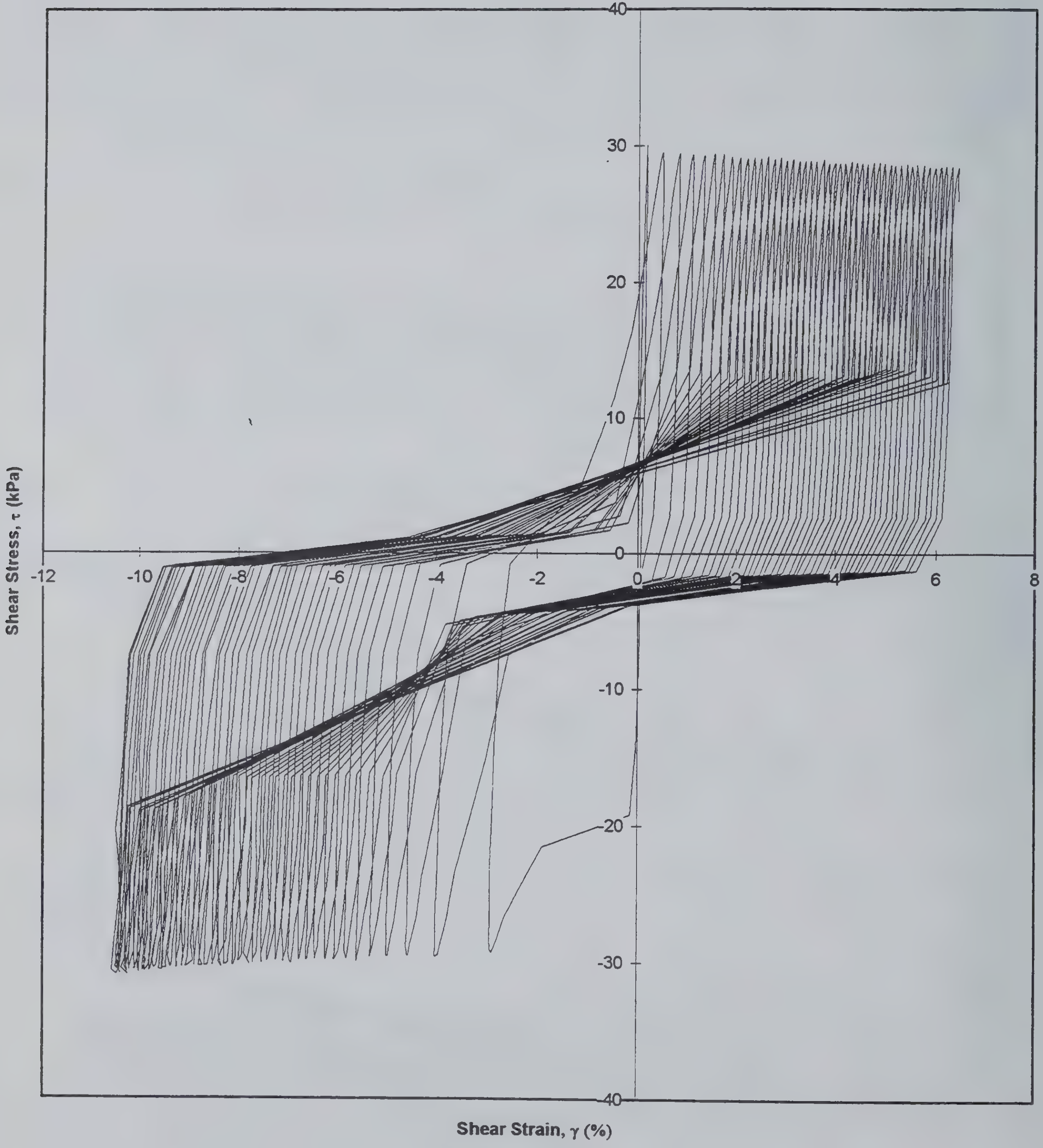

d:\nit\itp\cy_files\BTC3CY3.XLS

8/15/96 10:48 AM

Test I.D.: BTC4CY1
Fines Content (%): 5
Dry Density (kN/m^3) 16.35

Controlled Parameter: Stress
Initial Effective Stress (kPa): 100

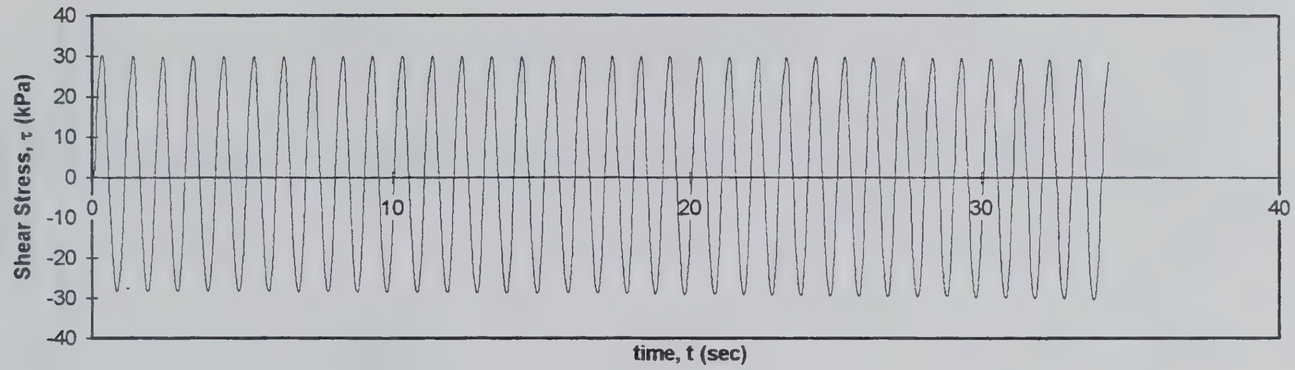

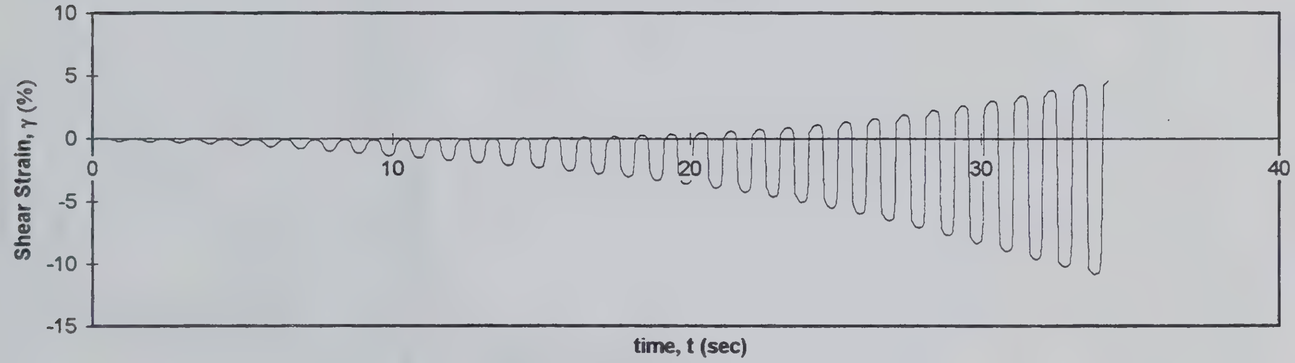

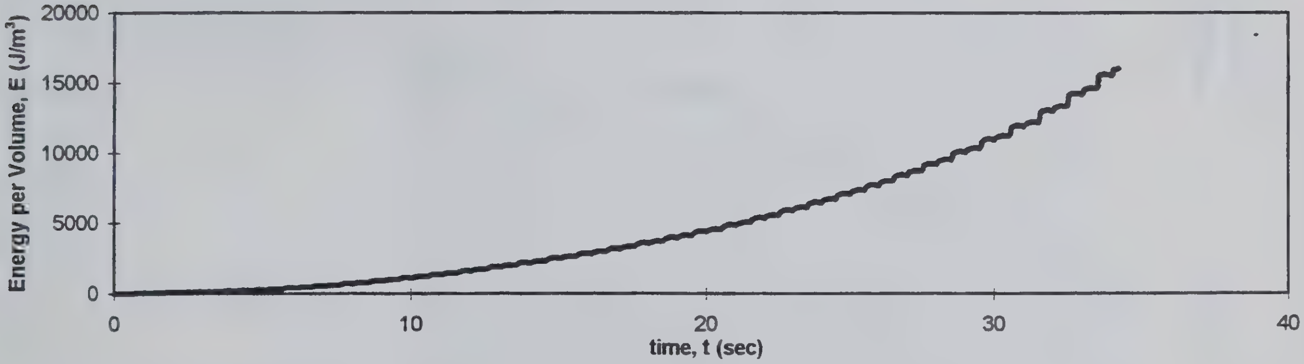

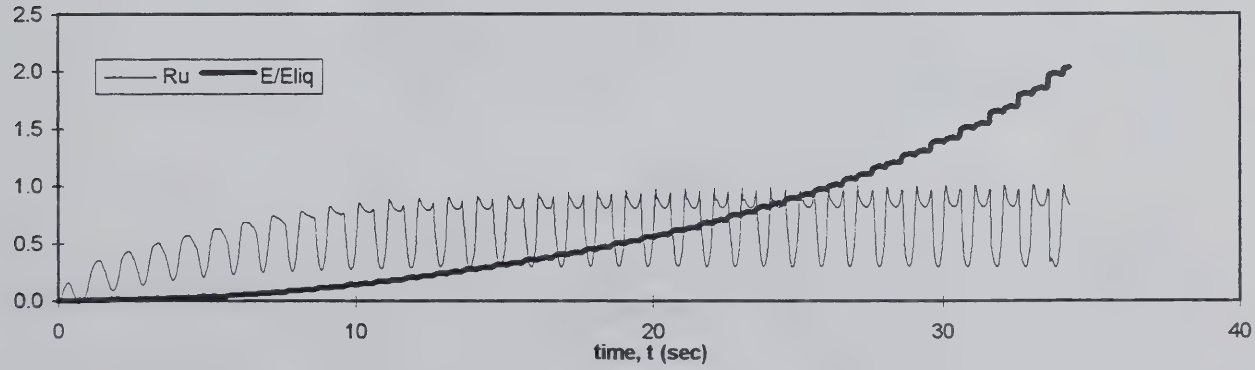

d:\nit\itp\cy_files\BTC4CY1.XLS 8/15/96 10:53 AM

Test I.D.:	BTC4CY1	**Controlled Parameter:**	Stress
Fines Content (%):	5	**Initial Effective Stress (kPa):**	100
Dry Density (kN/m^3)	16.35		

Shear Stress vs. Shear Strain

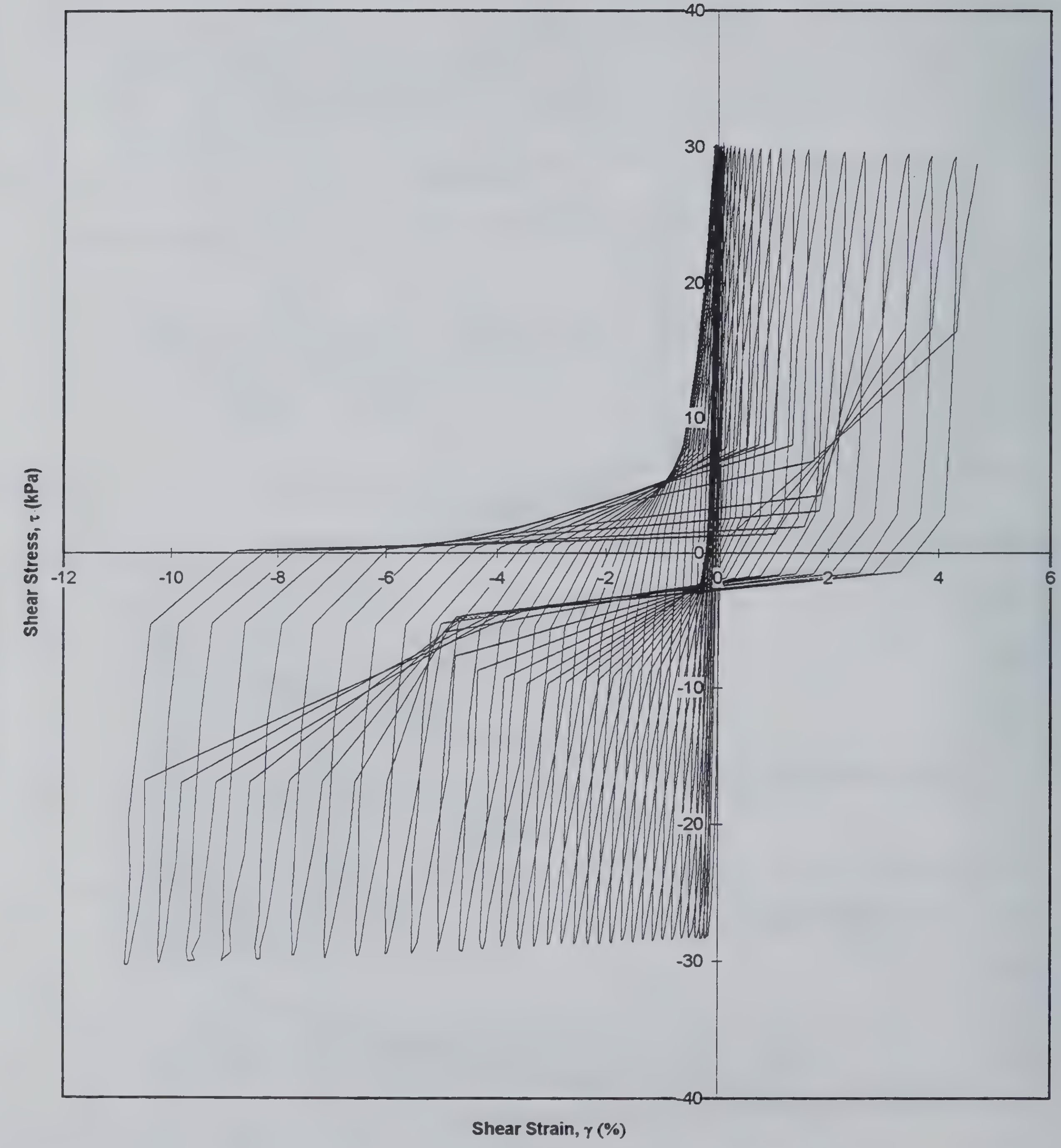

d:\nit\itp\cy_files\BTC4CY1.XLS

8/15/96 10:53 AM

Test I.D.: BTC4CY2
Fines Content (%): 5
Dry Density (kN/m^3) 16.72
Controlled Parameter: Stress
Initial Effective Stress (kPa): 100

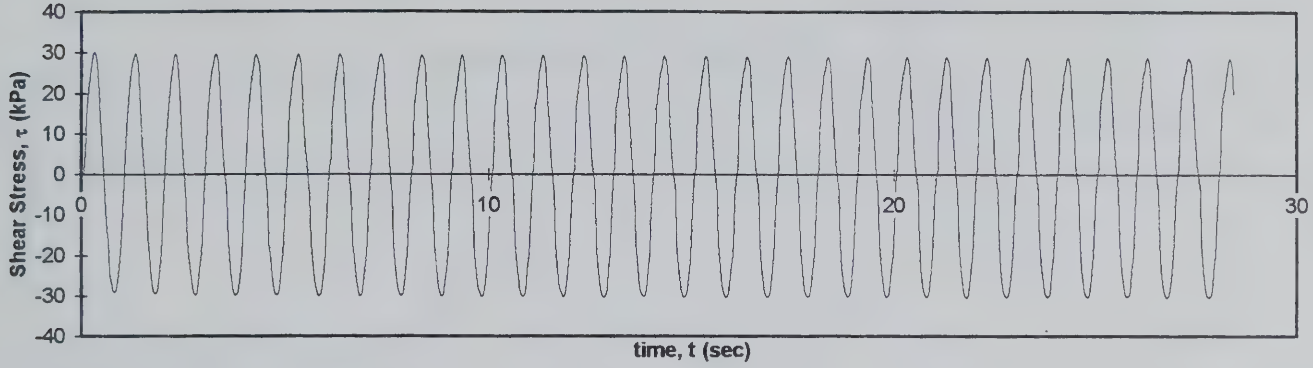

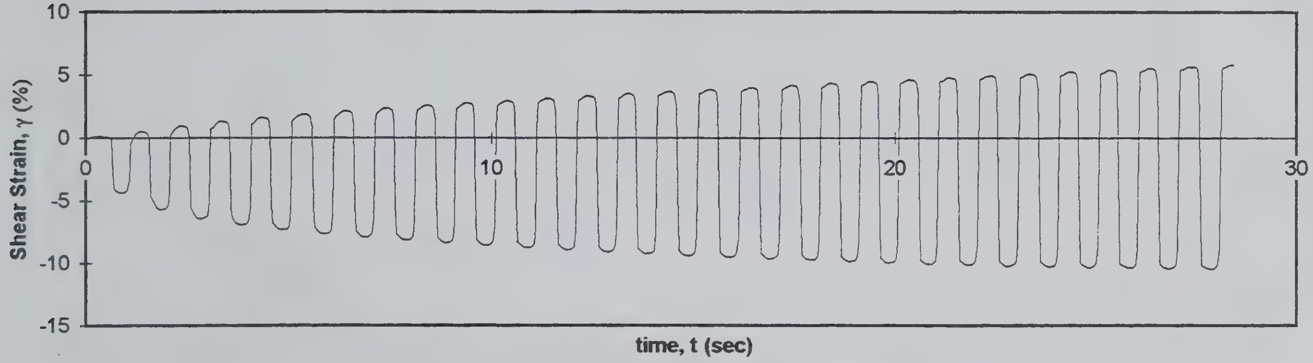

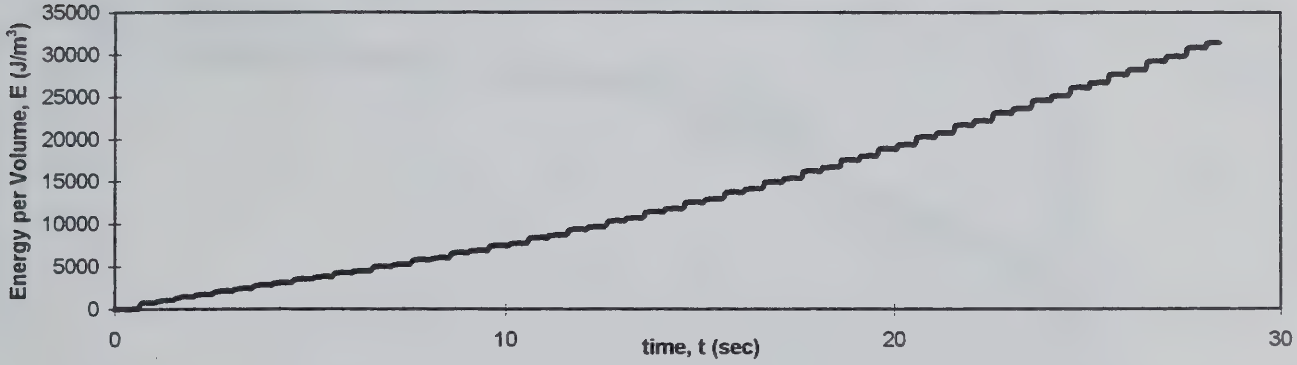

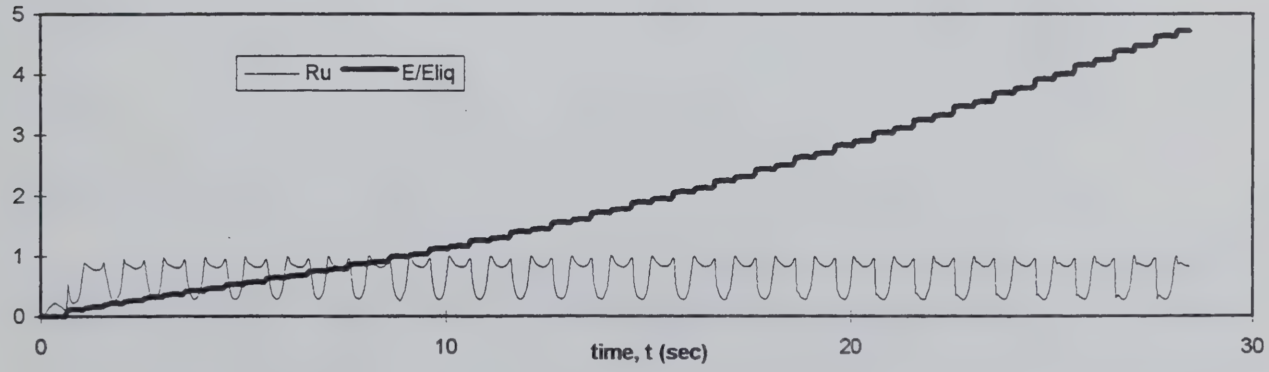

Test I.D.:	BTC4CY2	**Controlled Parameter:**	Stress
Fines Content (%):	5	**Initial Effective Stress (kPa):**	100
Dry Density (kN/m^3)	16.72		

Shear Stress vs. Shear Strain

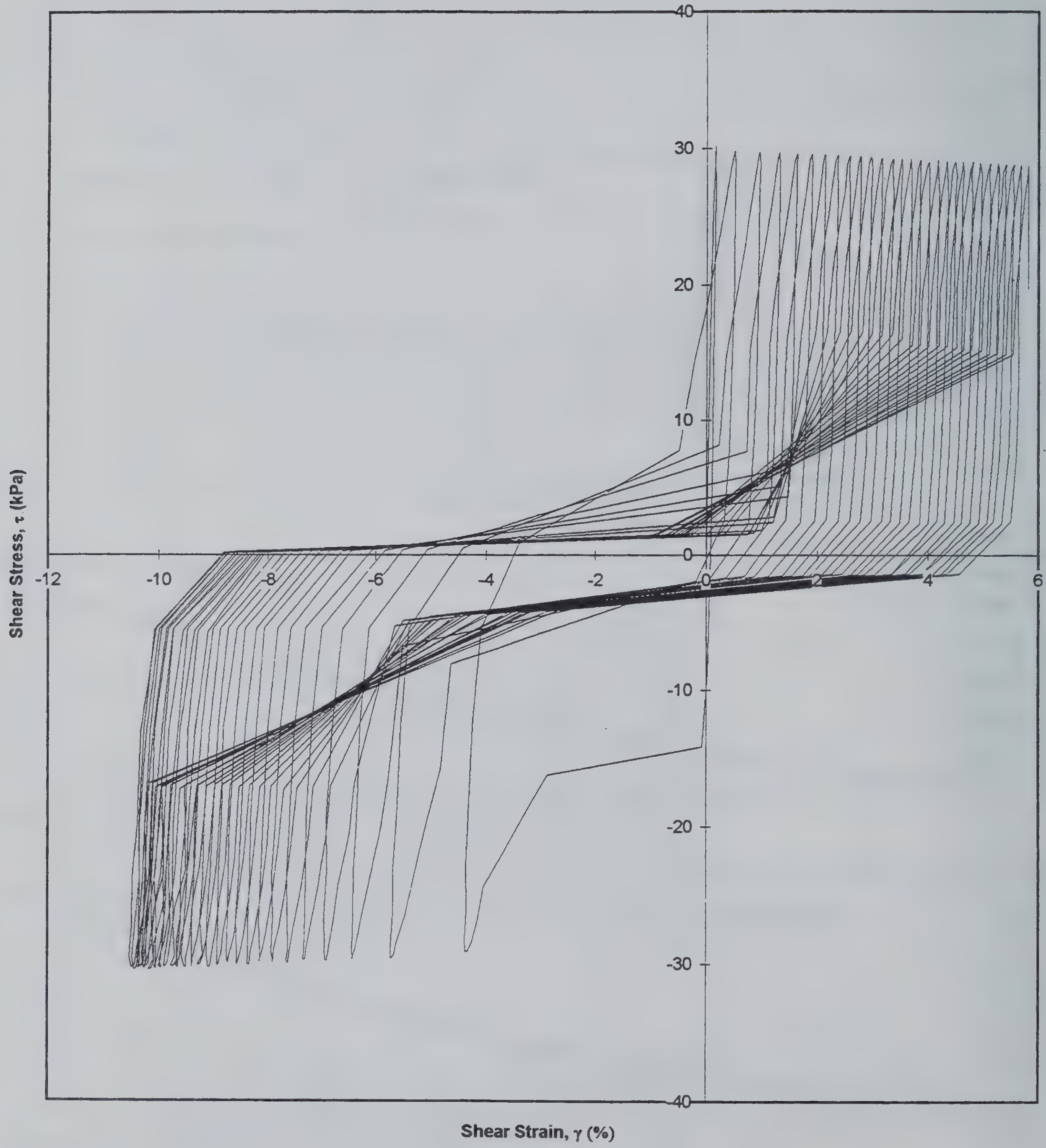

d:\nit\itp\cy_files\BTC4CY2.XLS

8/15/96 10:55 AM

Test I.D.: BTC6CY1
Fines Content (%): 5
Dry Density (kN/m^3) 13.51
Controlled Parameter: Stress
Initial Effective Stress (kPa): 100

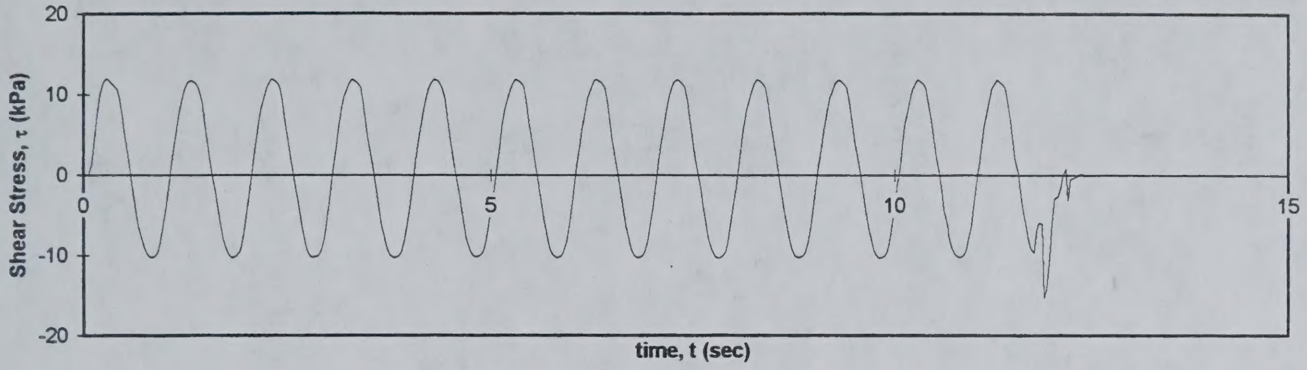

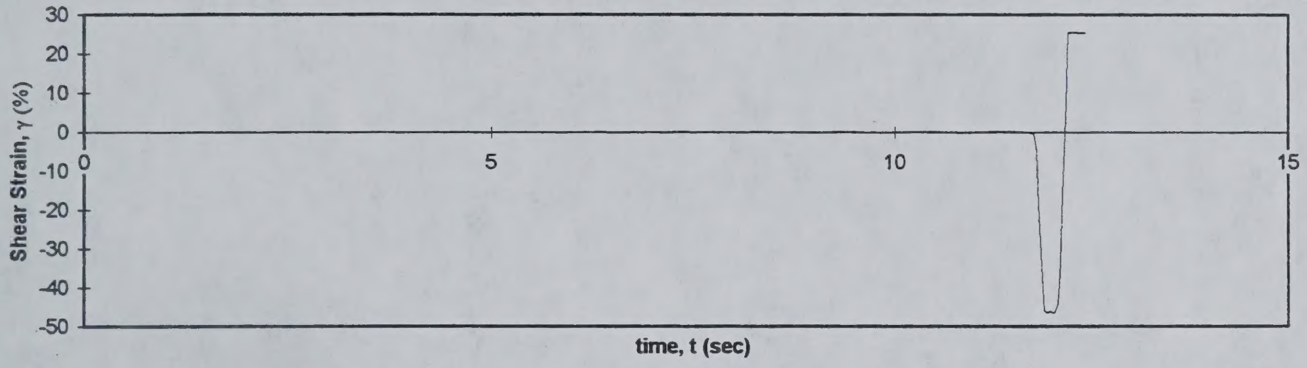

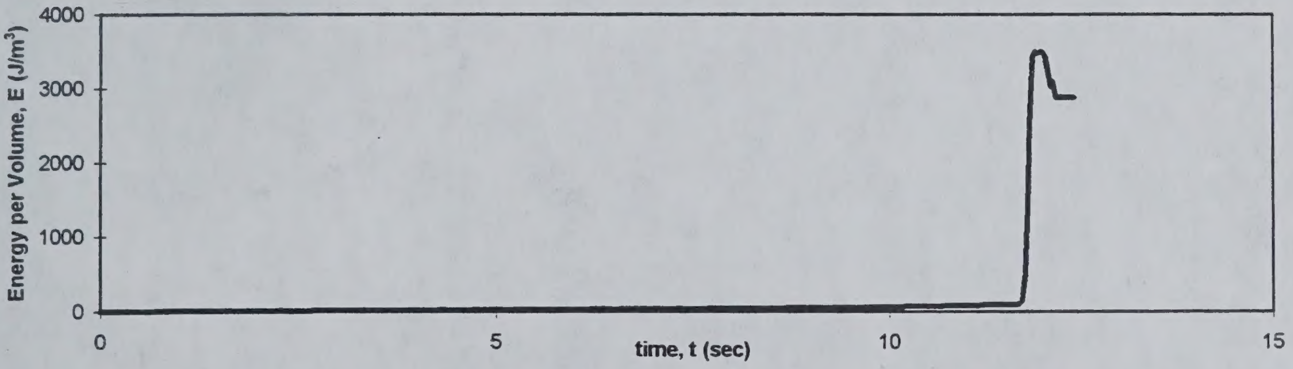

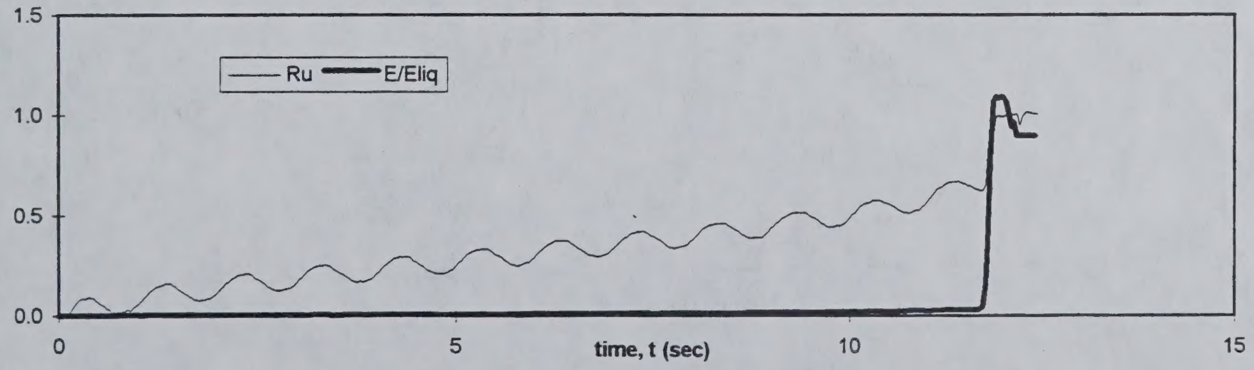

Test I.D.:	BTC6CY1	**Controlled Parameter:**	Stress
Fines Content (%):	5	**Initial Effective Stress (kPa):**	100
Dry Density (kN/m^3)	13.51